UNIVERSITY OF LEICESTER

New approaches to target cellular senescence for the amelioration of age-related pathologies.

Thesis submitted for the degree of

Doctor of Philosophy

at the University of Leicester

By

Marta Anna Pobłocka MSc

Department of Molecular and Cell Biology

College of Life Sciences

University of Leicester

May 2021

Abstract

New approaches to target cellular senescence for the amelioration of age-related pathologies.

Marta Pobłocka

Aging has been broadly defined as a functional decline that progresses with time and leads to impaired function and increased vulnerability to death. Cellular senescence is one of the main factors involved in this age-related functional decline and it has been shown that the percentage of senescent cells in tissues increases with age in different organs and in age-related disorders. Therefore, cellular senescence has been characterized as one of the hallmarks of aging. Consistent with this, elimination of senescent cells could ameliorate the negative effects of ageing, as it has already been shown in mouse models. However, the currently available methods of targeting and eliminating senescent cells lack specificity and have off-target effects. The first barrier that slows the development of anti-senescent drugs is lack of specific markers for senescence. To overcome this issue, we validated VPS26A, EBP50 and PLD3, which were recently identified in a screen of proteins specifically upregulated in senescent cells. Moreover, we propose novel approaches to target and eliminate senescent cells. Our first approach is an Antibody Drug Conjugates that specifically identifies and directly eliminates senescent cells through a marker expressed in their plasma membrane. Second, we used senoblocking, a strategy that aims to block cellular senescence before it occurs. For that purpose, we treated a progeroid mouse model with Ibrutinib, a clinically available BTK inhibitor. It has been previously shown that BTK inhibition interrupts cellular senescence. The treatment resulted in an improvement of healthspan and protection of a decline in brain and skeletal muscle performance. The third approach tested relied on the combinations of BCL-X_L inhibitors, A1331852 and 9-hydroxyellipiticine, that synergistically kill senescent cells. The results from our research introduce novel promising therapeutic interventions for the elimination of senescent cells which could find a translational application in the future.

Acknowledgements

I would firstly like to thank **Dr Salvador Macip** for being the best supervisor in the world. I feel very grateful and honoured to have had an opportunity to be a member of his research group. I appreciate his support, guidance, and encouragement during all the years of my PhD. His mentoring and leadership deserve the full admiration and respect. His outstanding knowledge, amazing personality, and passion for research have been truly inspirational and encouraged me to think outside the box and rise to new scientific challenges.

I want to express my gratitude to the members of my research committee, **Dr Sally Prigent** and **Dr Alessandro Rufini**, for their guidance and words of encouragement.
My special thanks go to **MIBTP directors**, past and present, who believed in me and supported to undertake this personal and professional journey.

Thanks to **Dr Elena Piletska** for an amazing collaboration and our work on nanoparticles. Many thanks to **Dr Chris Young** for his help and guidance with the muscle experiments. I would like to also thank **Dr Rajinder Singh** and **Dr Thong Cao** for their help with proteomics analysis. A big thank to **Dr Kayoko Tanaka** for her faith in me and personal support. Thank you to all members of University of Leicester Preclinical Research Facility for their commitment and help with animals' work.

Thanks to all of the members of the MOCAA lab, past, and present, who have helped me through my studies. Thank you for being the best team I could have ever imagine. I would like to especially thank **Mr Vinesh Dhokia** for all his support, many conversations, grammar lessons, and for being truly a friend. Big thanks to **Miss Marta Falcicchio** for her friendship, time, big heart, and kindness. Special thanks to **Dr Victoria Smith** for being a person I could always count on, her help with BH3 profiling, great knowledge, and delicious cakes. A special mention to **Dr Antonella Tabasso-Smith** for many interesting discussions and help with mass spectrometry analysis. A big thank to **Dr Akang Ekpenyong-Akiba** for helping me to take the first steps in the lab. I also want to

thank **Ms Amal Albati**, **Mr Fares Al Mansour, Miss Hannah Smith and Mr Anes Saleh** for being the best lab colleagues, big smile and all the support for this project.
I would like to also thank my personal friend, **Mr Jacek Dorosz** for his encouragement, appreciation and great support.

The most importantly, I would like to thank my family, who have been on this journey with me from the beginning till the end and gave me everything they have so that I could become the person I am today. An especially big thank you to my mother, **Ms Małgorzata Pobłocka**, for her never-falling love, constant support, believe in me, generous help and encouragement. Her dedication and no-limit kindness made me believe that nothing is impossible. An especially big thank you to my father, **Mr Przemysław Pobłocki,** for all his great love, help, never-ending encouragement and generosity. His sense of humour made this journey so much easier and had the power to chase the darkest clouds away. I would like to especially thank my grandmother, **Ms Maria Pakieser**, my late great grandmother, **Ms Helena Lorek,** and my uncle, **Mr Piotr Pakieser,** for their big hearts, selflessness and care. They have supported me every step of the way and inspired to broaden horizons. I would like to thank my brother, **Mr Tomasz Pobłocki,** for being the best big brother, always very supportive and on my side. Thanks for all his help, especially during programming lessons. I would like to thank my sister, **Mrs Wiktoria Hapka,** for being the best sister, her faith in me and being always able to count on her. Many thanks to **Mr Daniel Hapka**, **Miss Zuzanna Hapka** and **Miss Agata Hapka** for their unconditional support and for always being there for me.
I will forever owe my achievements to my dedicated, caring and thoughtful family.

My profound gratitude goes to God Almighty, to whom I owe everything.

Table of Contents

Table of Figures

List of Tables

Abbreviations

ADC	Antibody-drug conjugate
ADCC	Antibody-dependent cell-mediated cytotoxicity
ARF	Alternative reading frame AML Acute myeloid leukeamia
ARMCX3	Armadillo repeat-contatining X-linked protein 3
ATM	Ataxia telangiectasia mutated kinase
ATP	Adenosine triphosphate
AUC	Area under the curve
B2M	Beta-2 Microglobulin
BAK	BCL2 antagonist/ killer
BAX	BCL2 associated X
BCL-2	B-cell lymphoma 2
BCL-2A1	BCL2-related protein A1
BCL-X_L	B-cell lymphoma-extra large
BH	BCL2 homology
BID	BH3 interacting domain death agonist
BSA	Bovine Serum Albumin
BID	BH3 interacting domain death agonist
BSA	Bovine Serum Albumin
BTK	Bruton's tyrosine kinase
C. *elegans*	Caenorhabditis elegans
CDK	Cyclin- dependent kinase
CDKI	Cyclin-dependent kinase inhibitor
CDKN1A	Cyclin dependent kinase inhibitor 1A
CDKN2A	Cyclin dependent kinase inhibitor 2A
cDNA	Complimentary DNA
Chk1	Checkpoint kinase 1
Chk2	Checkpoint kinase 2
CI	Combination index
CLL	Chronic lymphocytic lymphoma
DAPI	4',6-diamidino-2-phenylindole

ddH_2O	double-distilled water
DDR	DNA damage response
DEP1	Density-enhanced phosphatase
DMEM	Dulbecco's Modified Eagle's medium
DMSO	Dimethyl sulfoxide
DNA	Deoxyribonucleic acid
DPP4	Dipeptidyl peptidase 4
DTT	Dithiothreitol
EDTA	Ethylene diamine tetra acetic acid
EBP50	Ezrin-radixin-moesin-binding phosphoprotein 50
EGTA	Ethylene glycol tetra acetic acid
ER	Endoplasmic reticulum
FACS	Fluorescence Activated Cell Sorting
FBS	Foetal bovine serum
FCCP	Carbonyl cyanide-p-trifluoromethoxyphenylhydrazone
FITC	Fluorescin isothiocyanate
GAPDH	Glyceraldehyde 3-phosphate dehydrogenase
H_2O_2	Hydrogen peroxide
HEPES	4-(2-hydroxyethyl)-1-piperazineethanesulfonic acid
IGF-1	Insulin-like growth factor 1
IAP	Inhibitors if apoptosis
IC_{50}	The half maximal inhibitory concentration
IHC	Immunohistochemistry
IPF	Idiopathic Pulmonary Fibrosis
IPTG	Isopropyl β-D-1-thiogalactopyranoside
JAK	Janus kinase
MAPK	Mitogen-activated protein kinase
MCL	Mantle cell lymphoma
MCL1	Myeloid cell leukaemia (sequence) 1
MEB	Mannitol experimental buffer
MEF	Mouse embryonic fibroblasts
MiMOMP	Minority mitochondrial outer membrane permeabilisation

MIPs	Molecularly imprinted polymers
miRNA	Micro RNA
MM	Multiple myeloma
MOMP	Mitochondrial outer membrane permeabilisation
mTOR	Mammalian target of rapamycin
NACWO	Named Animal Care & Welfare Officer
NanoMIPs	Molecularly Imprinted nano-polymers
NFκB	Nuclear factor kappaB
NK	Natural killer
NOTCH3	Neurogenic locus notch homolog protein-3
OD	Optical Density
OIS	Oncogene-induced senescence
OS	Overall survival
ORR	Overall response rate
P/N	Penicillin and streptomycin
PBS	Phosphate buffered saline
PBS-T	Phosphate buffered saline with 0.05% Tween-20
PCNA	Proliferating cell nuclear antigen
PD	Population Doublings
PI	Propidium Iodide
PI3K	Phosphatidylinositol 3 kinase
PIIPS	Proteasome inhibition induced premature senescence
PTEN	Phosphatase and tensin homolog
PLD3	Phospholipase D3
Rb	Retinoblastoma
RNA	Ribonucleic acid
ROS	Reactive oxygen species
SADS	Senescence-associated distension of satellites
SAHF	Senescence-associated heterochromatin foci
SASP	Senescence-associated secretory phenotype
SA-β-Gal	Senescence-associated β galactosidase
SCAPs	Senescent cell anti-apoptotic pathways

SD	Standard deviation
SDS	Sodium dodecyl sulphate
SDS-PAGE	Sodium dodecyl sulphate polyacrylamide gel electrophoresis
shRNA	Short hairpin ribonucleic acid
STAT	Signal transducer and activator of transcription
STX4	Syntaxin 4
TAF	Telomere associated foci
TEMED	Tetramethylethylenediamine
Tet	Tetracycline
TG	Thioglycerol
TGF-β	Transforming growth factor beta
TIF	Telomere dysfunction-induced foci
TPM	Transcripts per million
UV	Ultra violet
v/v	Volume per volume ratio
VDAC	Voltage dependent anion channel
VPS26A	Vacuolar protein sorting-associated protein 26A
WT	Wild type
X-Gal	5-bromo-4-chloro-3-indolyl-β-d-galactopyranoside
XLA	X linked agammaglobulinemia
ZMPSTE24	Zinc metalloproteinase STE24
ΔΨm	Loss of mitochondrial membrane potential

WT	Wild type
X-Gal	5-bromo-4-chloro-3-indolyl-β-d-galactopyranoside
XLA	X linked agammaglobulinemia
ZMPSTE24	Zinc metalloproteinase STE24
ΔΨm	Loss of mitochondrial membrane potential

1 Introduction

1.1 Cellular senescence

Cellular senescence is a response to numerous stress signals mainly characterized by an irreversible proliferation arrest. It was firstly described more than 50 years ago, when Leonard Hayflick and colleagues observed limited proliferation ability of human fibroblasts in the culture (Hayflick and Moorhead, 1961, Hayflick, 1965). Experiments showed that cell proliferation declined after several cell passages till the total loss of dividing ability. The non-proliferating cells remained metabolically active for many weeks but failed to grow even with the presence of nutrient and growth factors. The non-indefinite proliferation phenomena have been since then called 'cellular senescence' and speculated to be linked with ageing.

1.2 Features of senescent cells

Senescent cells are characterized by several hallmarks (**Figure 1.1**) (Hernandez-Segura et al., 2018). To date, some of these features have been used alone or in combination for detection of senescent cells *in vitro* and *in vivo*. However, none of these markers is exclusive to the senescent state and are often cell-type and tissue-type dependent (Rodier and Campisi, 2011a, Sikora et al., 2011, Munoz-Espin and Serrano, 2014). Nevertheless, there are several phenotypes which allow for more specific senescent cell identification, as described below.

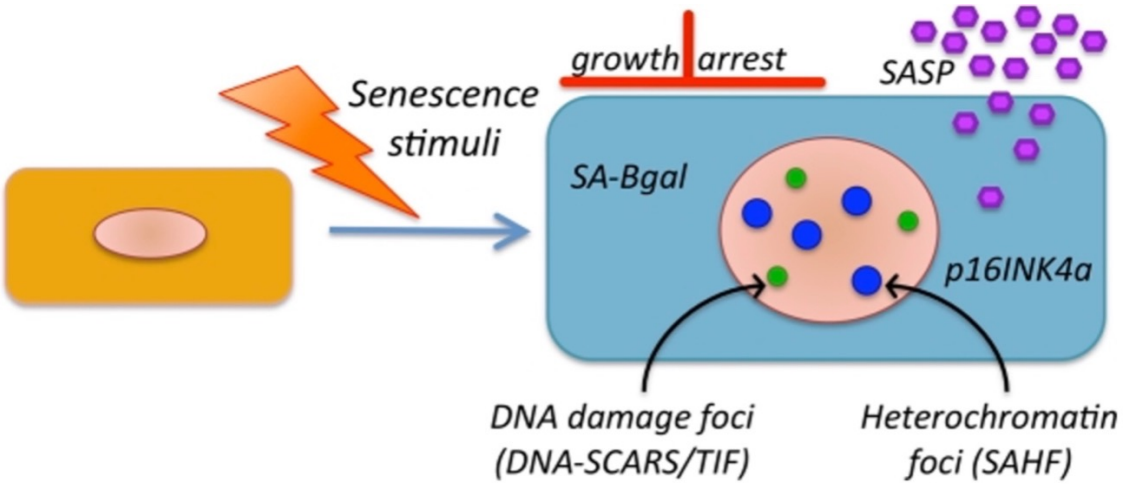

Figure 1.1. Characteristics of senescent cells.

Senescent cells are characterized by stable proliferation arrest, activation of DNA damage response and upregulation of the cell cycle inhibitors, p53, p16 and p21. In addition, senescent cells can show evidence of morphological changes, telomere shortening, epigenetic changes (such as senescence-associated heterochromatin foci), decreased level of LAMIN B1, increased lysosomal SA-ß-galactosidase activity. Another characteristic feature of many senescent cells is SASP, which among others includes different interleukins, chemokines, inflammatory factors, and growth factors. Figure adapted from (Rodier and Campisi, 2011b).

1.2.1 Morphological changes

Morphological change is one of the features of the senescent phenotype. Senescent cells are often enlarged comparing to wild type counterparts (Chen et al., 2000b). Apart from cellular enlargement, cytoskeleton-mediated shape changes and organelle alterations have been also observed. These modifications have been linked to altered expression of cytoskeletal and adhesion proteins (Wang and Gundersen, 1984, Wang, 1985, Nishio et al., 2001). However, the exact underlying mechanism responsible for morphological changes is still poorly understood.

1.2.2 Growth arrest

One of the most defining features of the senescent state is growth arrest. Unlike quiescent or terminally differentiated cells, this proliferation arrest cannot be reversed by known physiological stimuli, like mitogenic or growth factors. In the laboratory environment, researchers were able to bypass senescent-related cell-cycle arrest through genetic manipulations of Cyclin-Dependent Kinase Inhibitors (CDKi) combined with p53 inactivation (Beauséjour et al., 2003). Nevertheless, that has not been reported to happen spontaneously in physiological conditions. The proliferation arrest is caused by blocked progression through the cell cycle by the activity of cell- cycle inhibitors. In particular, senescent cells are characterized by accumulation of CDK2 inhibitor $p21^{WAF1/Clip1}$ *(CDKN1A)* and CDK4/6 inhibitor $p16^{INK4A}$ (*CDKN2A*). Activity of these inhibitors leads to persistent activation of retinoblastoma protein (RB), which in turn inhibits E2F transcript factors and consequently trigger cell-cycle arrest (**Figure 1.2**) (Gorgoulis et al., 2019).

1.2.3 Pathways involved

The establishment and maintenance of senescence growth arrest mainly relies on activation of two or one of the pathways, p53-p21 and p16-pRb (**Figure 1.2**). These pathways can interact or act independently and preferred activation of either one of them depends on cell type and triggering factors.

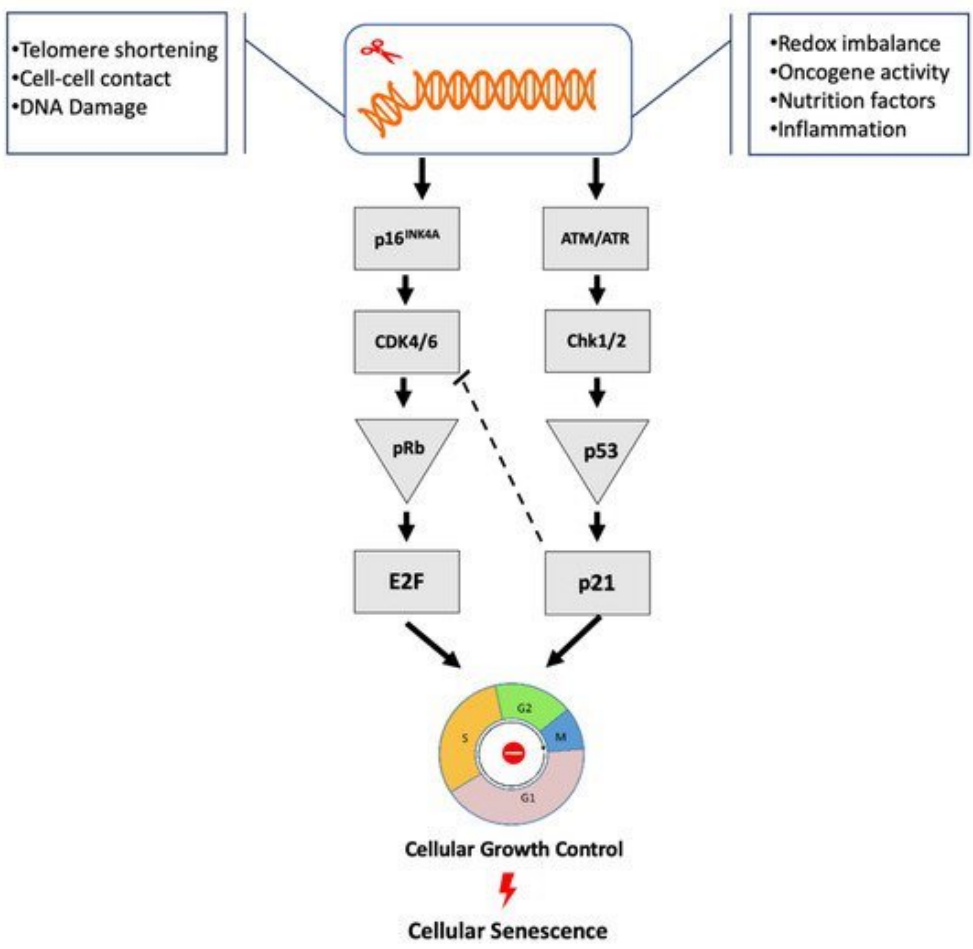

Figure 1.2. Main pathways involved in senescence growth arrest.

Senescence-inducing stimuli usually engage p53-p21 and/or p16-pRb pathways. Activation of either both or one of the pathways is dictated by cell type and triggering stimuli, such as telomere shortening, cell-cell contact, DNA damage, redox imbalance, oncogene activation, nutrition factors, inflammation. ARF negatively regulates MDM2, which facilitates degradation of p53. Active p53 induces p21, which prevents CDK2 and 4 from phosphorylating Rb. In p16-pRb signalling, p16 also prevents Rb phosphorylation by inhibition of CDKs. Hypophosphorylated active Rb halts cell proliferation through suppression of E2F activity, a crucial transcription factor that regulates expression of genes essential for cell-cycle progression. Moreover, E2F can act as a crosslink and activate p53-p21 pathway by induction of ARF. Adapted from (Mijit et al., 2020).

.

1.2.3.1 The p53/p21 axis

p53 is known as a guardian of the genome due to its multifunctional role within the cell, such as genome integrity maintenance, tumour suppression, regulation of proliferation, DNA damage response, senescence and apoptosis (Lane, 1992, Toufektchan and Toledo, 2018). A number of p53 mutations have been found in different human malignancies (Rivlin et al., 2011, Perri et al., 2016). In cellular senescence, once activated, p53 regulates a cascade of an antiproliferative transcriptional program that leads to cell cycle arrest.

p53 activation occurs as a result of myriad stressors, like DNA damage, oncogenic or oxidative stress. DNA damage leads to increased deposition of γH2Ax and 53BP1 in chromatin, which in turn activates a kinases cascade involving first ATM and ATR and later CHK1 and CHK2 and eventually resulting in activation of p53 (Campisi and d'Adda di Fagagna, 2007, Fumagalli et al., 2012). ATR negatively regulates a p53 inhibitor, the E3 ubiquitin-protein ligase HDM2 (MDM2 in mice), which facilitates degradation of p53. p53 induces transcription of cyclin-dependent kinase inhibitor $p21^{Cip1}$, which binds and blocks activity of cyclin CDK2, CDK4 and CDK6 complexes, therefore causing cell cycle arrest. Inhibition of CDKs promotes hypophosphorylation of Rb, which then bind to E2F and suppress its activity (**Figure 1.2**) (Ben-Porath and Weinberg, 2005). E2F is a transcription factor that stimulates the expression of critical genes required for DNA replication and cell-cycle progression. Interfering with p53 signalling impairs induction of cellular senescence (Shay et al., 1991, Beauséjour et al., 2003, Stewart et al., 2003).

Upregulation of p53 and p21 was detected in many senescent models (Kastan et al., 1991, Qian and Chen, 2013, Artandi and Attardi, 2005, Ben-Porath and Weinberg, 2005, el-Deiry et al., 1992). Moreover, it has also been demonstrated that p21 progressively accumulates in aging cells (Harper et al., 1993, Stein et al., 1999, Cmielova and Rezáčová, 2011). However, there are also indications that after initial upregulation of p53 and p21, when growth arrest is established, the level of p53 and p21 decrease (Stein et al., 1999). While p21 expression goes down, the level of another CDK inhibitor, $p16^{INK4}$ increases. Therefore, it has been proposed that p53 and p21 are important for induction

of senescence-related proliferation arrest, but they are not crucial for maintenance of senescent state (Chang et al., 1999). In turn, p16 has been proposed as second barrier for cell proliferation that is essential to maintain irreversibility of senescence-related arrest (Macip et al., 2002, Beauséjour et al., 2003).

Additionally, $p21^{Cip1}$ is involved in control of cell proliferation, differentiation and cell death also in a p53-independent manner (Karimian et al., 2016, Georgakilas et al., 2017). For example, p53-independent control of cell proliferation was observed in EJp21 bladder carcinoma cells, which contain a tetracycline regulatable p21-expression system. These cells are lacking functional p53 and undergo senescence upon induction of p21. That is associated with characteristic morphological changes, such as enlarged flattened shape and enlarged nuclei, reduction in CDK2 kinase activity and irreversible cell cycle arrest in G1 and G2/M (Fang et al., 1999). Moreover, p21 overexpression via retroviral vector also induced senescence in immortal Li-Fraumeni fibroblasts (Vogt et al., 1998).

Interestingly, p21 mutations are rare in cancer, however there are reports of mutation in few, such as oral, oesophageal and breast cancer (Balbín et al., 1996, Bahl et al., 2000, Ralhan et al., 2000, Keshava et al., 2002, Powell et al., 2002). Therefore, it has been proposed that p21 might also act as an oncogene due to its procancer and anti-apoptotic activities. For example, elimination of p21 in p53-deficient mice prolonged survival and decreased the rate of spontaneous thymic lymphomas (De la Cueva et al., 2006). Additionally, induction of p21 has been found in patients with rectal carcinoma, and was associated with development of resistance to radio-chemotherapy (Ohkoshi et al., 2015). This suggests a potential pro-apoptotic function of p21, although the mechanism remains unclear. It has been reported that overexpression of p21 induced both senescence and apoptosis in the same cells line and that was proposed to be mediated by Reactive Oxygen Species (ROS) (Masgras et al., 2012). Additionally, there is evidence that targeted overexpression of p21 promotes apoptosis (Gartel and Tyner, 2002). For example, p21 overexpression increases rate of apoptosis after the treatment with cisplatin in glioma and ovarian carcinoma cell lines (Kondo et al., 1996, Lincet et al., 2000). Moreover, p53-independent induction of p21 after the treatment with

genistein, a tyrosine kinase inhibitor, was associated with induction of BAX and apoptosis in breast cancer cell line MDA-MB-231 (Li et al., 1999). The mechanisms by which p21 promotes apoptosis are not yet understood.

Recently, the Bruton's Tyrosine Kinase (BTK) has been identified as important regulator of p53-p21 signalling pathway and induction of senescence-related growth arrest (Althubiti et al., 2016b, Rada et al., 2017, Rada et al., 2018a). BTK's involvement and mechanisms of action is further discussed in section 1.6.

1.2.3.2 p16-pRb axis

Stimuli that produce a DDR can also activate p16-pRb but this usually occurs secondary to engagement of the p53 pathway (Campisi and d'Adda di Fagagna, 2007). However, in some cells, senescence induction occurs preferentially through p16-pRB pathway. For instance, in culture, epithelial cells are more prone to induce growth arrest through activation of p16 than fibroblasts (Stein et al., 1999)

Rb is a crucial factor responsible for cell cycle progression through the G1 phase. Its activity is controlled by several post-translational modifications, such as phosphorylation, acetylation and ubiquitination (Campisi, 2005, Takahashi et al., 2007). The main role of $p16^{INK4a}$ is similar to $p21^{Cip1}$ as both inhibit the kinases that phosphorylates Rb. This leads to accumulation of the active, hypophosphorylated form of Rb (Herbig et al., 2004, Campisi and d'Adda di Fagagna, 2007, Xu et al., 2014b), which binds to E2F and repress its activity. *$p16^{INK4a}$* share locus *INK4a/ARF* with another tumour suppressor, ARF (Kim and Sharpless, 2006). Their upregulation promotes senescence and their accumulation has been found in many senescent cells (Lundberg et al., 2000). Both are able to regulate Rb activities. Moreover, ARF regulates p53 by blockage of its direct inhibitor, MDM2. $p16^{INK4a}$ is considered as main marker used for identification of senescent cells, as it is widely expressed in most senescent cells (Taniguchi et al., 1999, Simboeck and Di Croce, 2013, Campisi, 2011) and increases with age in different tissues, reaching 7 fold increase in some human tissues and 30 fold in mouse tissues (Krishnamurthy et al., 2004, Collado et al., 2007, Wang et al., 2009, Romagosa et al., 2011, Sherr, 2012).

1.2.4 Apoptosis resistance

During development, apoptosis is a process of programmed cell death that is used to eliminate unwanted cells. In adults, apoptosis is a response to damage or stress that acts as an important anti-tumour mechanism to eliminate unfunctional cells (Green and Evan, 2002). Many cell types are able to resist apoptosis when they become senescent. However, the apoptotic resistance depends strongly on cell type. For instance, human senescent fibroblasts can resist ceramide-induced apoptosis, in contrast to endothelial senescent cells (Hampel et al., 2004). Moreover, senescent fibroblasts are able to resist apoptosis caused by oxidative stress or abnormal activity of growth factors, although they are not able to overcome FAS-death receptor's dependent apoptosis (Chen et al., 2000a, Tepper et al., 2000). The mechanism of apoptosis resistance by senescent cells is not fully understood. It could be controlled via the p53 tumour suppressor protein, which is a crucial regulator for both senescence and apoptosis, or expression changes in apoptosis activators and inhibitors might play a key role (Childs et al., 2014).

The cell fate decisions between undergoing senescence or apoptosis are not clear. Damaged fibroblasts and epithelial cells tend to undergo senescence, but damaged lymphocytes usually undergo apoptosis (Rebbaa et al., 2003, Seluanov et al., 2001). However, most of the cells are able to undergo both responses depending on conditions. For examples, cells that usually undergoing apoptosis can switch to senescence and senescence prone cells might changeover to the process of apoptosis (Crescenzi et al., 2003). It appears that this switch between senescence and apoptosis process is partially controlled by the balance of pro- and anti-apoptotic proteins, however the exact mechanism is still poorly understood. Another hypothesis indicates importance of p53 in determination of cell fate decisions (Macip et al., 2003). Study using EJ bladder carcinoma cell line revealed that magnitude of p53 overexpression can determine the cell decision between senescence and apoptosis. Expression of p53 in EJ cell line through tetracycline-regulatable expression system induced permanent growth arrest. However, a 10- to 20-fold greater expression of p53 introduced by adenovirus vector induced apoptosis in the same cell line. Both, the growth arrest and apoptotic

responses were accompanied with ROS accumulation, of which the greater magnitude was observed in cells undergoing apoptosis. Importantly, manipulations of ROS level, were able to ameliorate accumulation of ROS and partially rescue the same cells from permanent growth arrest and correlated with decreased magnitude of apoptosis. This study suggests that the level of p53 and p53-dependent accumulation of ROS might be important players in determination of cell fate between senescence and apoptosis (Macip et al., 2003).

1.2.5 Senescence Associated β-Galactosidase (SA-β-gal)

Several human cells express a high level of lysosomal β-galactosidase upon undergoing cellular senescence (named senescence-associated β-galactosidase or SA-β-gal). The high level of enzyme β-galactosidase can be easily detected in freshly fixed cells or tissues using cytological or histochemical colorimetric stainings (Dimri et al., 1995, Munoz-Espin and Serrano, 2014), in which senescent cells are stained blue at pH=6. Although the functional implications are not clear, the SA-β-gal is thought to be a result of increased biogenesis of lysosomes, which is a common process in senescent cells (Lee et al., 2006). SA-β-Gal was originally detected in senescent fibroblasts and keratinocytes but not in immortal cells, quiescent fibroblasts or terminally differentiated keratinocytes (Dimri et al., 1995). However, despite the promising diagnostic potential of SA-β-Gal, there are indications of many false positive results. It is worth to mention, that in almost all human cells, activity of endogenous lysosomal β-galactosidase can be detected at pH=4. Additionally, in certain cell types positive staining was observed at pH=6 independently of senescent state, although with less intensity (Itahana et al., 2013). Moreover, there are other factors that might contribute to false-positive staining, such as high cell confluency for long periods, serum starvation or hydrogen peroxide (Itahana et al., 2007, Debacq-Chainiaux et al., 2009). Nevertheless, SA- β-gal is still considered as one of the best available markers of cellular senescence.

A good substitute of SA-β-gal might be Sudan Black-B (SBB), which stains the age related pigment lipofuscin, or GL13, an analogue of SBB which is coupled with biotin (Terman and Brunk, 2004, Georgakopoulou et al., 2013). An advantage over SA-β-gal is the ability to stain formalin-fixed and paraffin-embedded tissues.

1.2.6 Senescence-Associated Secretory Phenotype

Senescent cells secrete a number of factors (**Table 1.1**) including pro-inflammatory cytokines, chemokines, matrix metalloproteinases (MMPs), growth and angiogenic factors (Kuilman and Peeper, 2009, Coppé et al., 2010, Young et al., 2013, Kirkland and Tchkonia, 2017, McHugh and Gil, 2018). This phenomenon is collectively known as senescence-associated secretory phenotype (SASP) and it is one of the main hallmarks of cellular senescence (Hernandez-Segura et al., 2018).

SASP plays a different function and depending on the conditions, it might have positive or negative effects **(Figure 1.3)** (Kuilman and Peeper, 2009). The positive role of SASP is the recruitment of immune system to eliminate senescent cells via adaptive and innate immune cells, such as macrophages, neutrophils and natural killers (NK) (Xue et al., 2007, Kang et al., 2011). This function is especially important during tumour initiation, when recruitment of immune system through SASP acts as tumour suppressive mechanism. Moreover, recruitment of macrophages has a suppressive effect on fibrosis (Krizhanovsky et al., 2008). Specific SASP components have a beneficial effect on wound healing (e.g., secretion of platelet-derived growth factor AA (PDGF-AA)) (Demaria et al., 2014b).

However, SASP-mediated immune recruitment can have also a negative effect on the organism. For instance, recruitment of immature myeloid cells protected a fraction of proliferating tumour cells from senescence-related growth arrest, thus sustaining tumour growth in prostate and liver cancer (Di Mitri et al., 2014, Eggert et al., 2016).

The negative function of SASP relies mainly on the profile of secreted factors. It has been shown that secreted factors, such as vascular endothelial growth factor (VEGF), chemokine ligand 5 (CCL5), TGFβ family members, growth factor GROα, C-X-C motif chemokine-ligand 1 (CXCL1), Interleukin-8 (IL-8), interleukin-6 (IL-6) and growth factors e.g., GROα, can stimulate tumour progression by promotion of endothelial cells proliferation (Krtolica et al., 2001), increase of angiogenesis (Coppé et al., 2006b, Eyman et al., 2009), fibrosis progression (Meng et al., 2016), advance tumour cell invasion (Badache and Hynes, 2001) or formation of cancer stem cells (Ritschka et al., 2017). Moreover, the SASP-mediated autocrine reinforcement and paracrine recruitment of

senescent cells fuels aging-related disorders, through tissue disruption and changes in its structure and function (Cahu, 2013).

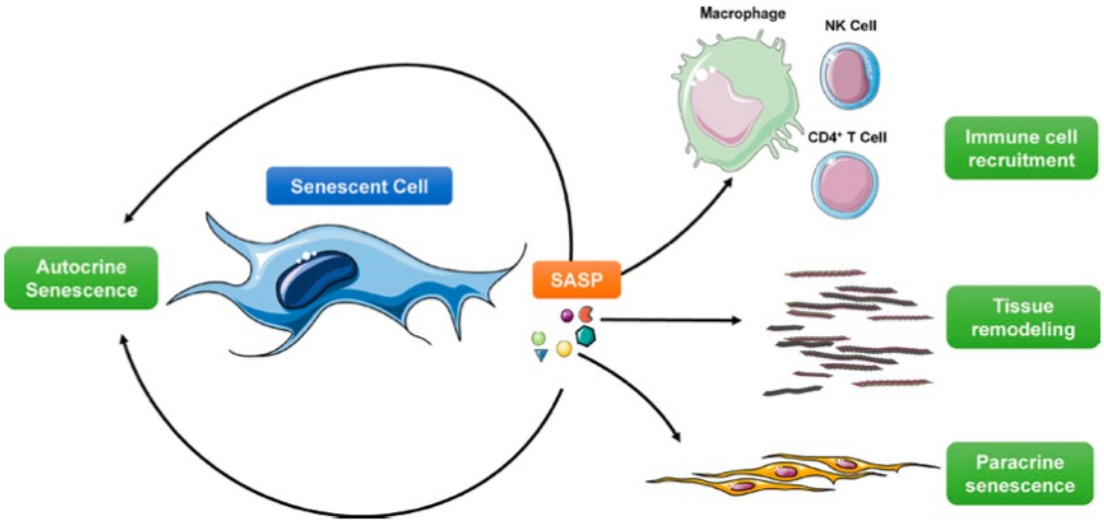

Figure 1.3. Functions of the SASP.

SASP mediates variety of functions of senescent cells. It can reinforce SASP itself through an autocrine loop but also can play a role in establishment of other senescent hallmarks such as growth arrest. SASP recruits immune cells like neutrophils, macrophages and natural killer to phagocytose or for elimination of senescent cells. It also affects surrounding tissue structure and trigger its remodelling. Moreover, in a paracrine manner, SASP can spread the senescence phenotype to surrounding cells. Adapted from (McHugh and Gil, 2018)

The mechanisms involved in the SASP induction and maintenance are not fully understood. So far, it is known that SASP does not depend on other characteristics of senescence, like enlarged morphology, SA-β-Gal, or cell cycle arrest (Laberge et al., 2015b, Herranz et al., 2015b, Wang et al., 2017a). It has been suggested that SASP is not an essential feature of cellular senescence and a senescent state can be established without production of SASP (Coppé et al., 2011). And in the other way round, SASP might develop independently of the main regulators of the senescent state, such as $p16^{INK4a}$ (Coppé et al., 2008, Coppé et al., 2011). For instance, SASP may be triggered by severe DNA damage and can be regulated by the mTOR, NF-κB, microRNAs or signalling pathways, such as cGAS/STING or JAK/STAT. Some of SASP markers can be used for identification of senescent state, especially IL-6 and IL-8 which seemed to be the most

sustained part of secretome. Although, SASP composition may vary between cells, tissues and depends on inducing stimuli (Malaquin et al., 2016, Wang et al., 2017a). The profiles of SASP composition should be then carefully analysed and could help with identification of the senescence type. Moreover, strategies developed to block or reduce expression of SASP could have a therapeutic potential in the fight against age-related diseases and cancer.

Table 1.1. Components of Senescence-Associated Secretory Phenotype (SASP)

Adapted from (Gorgoulis et al., 2019)

Class	Component
Interleukins	IL-6; IL-7; IL-1; IL-1β; IL-13; IL-15
Chemokines	IL-8; GRO- α, -β, -γ; MCP-2; MCP-4; MIP-1α; MIP-3α; HCC-4; eotaxin; eotaxin-3; TECK; ENA-78; I-309; I-TAC
Other inflammatory molecules	TGFβ; GM-CSE; G-CSE; IFN-γ; BLC; MIF
Growth factors and regulators	Amphiregulin; epiregulin; heregulin; EGF; bFGF; HGF; KGF (FGF7); VEGF; angiogenin; SCF; SDF-1; PIGF; NGF; IGFBP-2, -3, -4, -6, -7
Proteases and regulators	MMP-1, -3, -10, -12, -13, -14; TIMP-1; TIMP-2; PAI-1, -2; tPA; uPA; cathepsin B
Receptors and ligands	ICAM-1, -3; OPG; sTNFRI; sTNFRII; TRAIL-R3; Fas; uPAR; SGP130; EGF-R
Non-protein molecules	PGE2; nitric oxide; ROS
Insoluble factors	Fibronectin; collagens; laminin

1.2.7 Nuclear changes

Altered chromatin assembly is another feature of cellular senescence. Senescent cells are characterized by easy to visualize senescence-associated heterochromatin foci (SAHF) (Narita et al., 2003, Cichowski and Hahn, 2008). SAHF are highly condensed regions of heterochromatin and are prominent in oncogene-induced senescence (OIS). They can be easily identified using DAPI staining. Characteristic for SAHF is presence of repressive marks, such as histone H3 trimethylation at lysine 9 (H3K9me) and other heterochromatin proteins, such as HMGA, macroH2A and HP1γ (Salama et al., 2014, Adams, 2007, Kuilman et al., 2010). Moreover, senescent cells lack characteristic for proliferating and quiescent cells histone marks on histone H3, lysine 4 trimethylation (H3k4me3) and acetylation of histone 3 at lysine 9 (H3K9Ac). The formation of SAHF is thought to not be a result of global changes in histone methylation. Rather, the favoured explanation is spatial repositioning of pre-existing repressive marks (Chandra et al., 2012). Several senescence markers have been also linked with SAHF formation, $p16^{INK4a,}$ Rb, p53, IL-6 and C/EBPβ and interfering with signalling of these pathways affected formation of SAHF (Narita et al., 2003, Cichowski and Hahn, 2008, Kuilman et al., 2010). Due to the abundance of repressive markers, SAHF is thought to contribute to changes in gene expression observed in senescent cells (Young et al., 2013, McDuff and Turner, 2011).

Another nuclear rearrangement observed in senescent cells is loss of lamin B1. The inner surface of the nuclear envelope is lined by a lamina, which is responsible for shape, size and nucleus stability (Bridger et al., 2007, Dechat et al., 2008). In majority, lamina consists of the nuclear lamins (Krohne and Benavente, 1986), divided into two categories based on, A-type (lamin A, C) and B-type (Lamin B1, B2). Lamins A and C are alternatively spliced forms of the *LMNA* gene (Lin and Worman, 1993) and are expressed usually during differentiation. Loss of Lamin A was not crucial for HeLa cell growth (Harborth et al., 2001) and mice that does not express Lamin A but still have functional Lamin C also appears normal (Fong et al., 2006). However, mutations in *LMNA* that lead to production of misfolded or mutated form of Lamin A are linked with several disorders, called laminopathies, which include Hutchinson-Gilford progeria syndrome (HGPS) (Worman et al., 2010).

The B-type lamins arise from two different genes, *LMNB1* and *LMNB2.* It has been proposed that lamin B1 is required for brain development but not for embryonic stem cell renewal (Kim et al., 2011). Moreover, mice lacking the *LMNB1* gene die just after birth and fibroblasts from these mice has altered shape of nucleus and undergo premature senescence in culture (Vergnes et al., 2004). Importantly, many human and mice cells undergoing senescence are characterized by loss of Lamin B1 at protein and mRNA level (Freund et al., 2012). It is known that this decrease is independent of activation of reactive oxygen species, DDR signalling, MAPK or NF-κB. The exact mechanism is still not fully understood.

Additionally, there are also other chromatin-related changes that occurs during cellular senescence. One of them are DNA segments with chromatin alterations reinforcing senescence (DNA-SCARS) (Rodier et al., 2011). DNA-SCARS are nuclear structures observed after persistent DNA damage in human and mouse cells. They can form independently of p53 and pRB, although they require p53 and pRB to trigger the senescence-related growth arrest.

1.3 Types of cellular senescence and triggering stimuli

The type of cellular senescence depends strongly on induction stimuli. There are a number of senescence causes that has been identified, however this field is still not fully explored. Triggering stimuli can dictate the activation of a particular signalling pathway and senescent phenotype.

1.3.1 Replicative senescence

One of the stimuli that triggers senescence is telomere shortening. Telomeres are located at the end of chromosomes and protect them from degradation, inappropriate recombination or fusion (Wang et al., 2009). Through consecutive divisions, the erosion of telomeres occurs and triggers a type of senescence termed replicative senescence (RIS).

Human telomeric DNA consists of repetitive TTAGGG sequence followed by a specific loop- shape structure called t-loop (Blackburn, 2001, Chai et al., 2005). During the replication process, the DNA polymerase is unable to completely replicate the full chromosome. The replication failure results with loss of 50-200 base pairs of telomeric DNA after each S phase and this process is known as 'end- replication' problem (d'Adda di Fagagna et al., 2004). Telomeres shorten after every cell division till they become critically short (Harley et al., 1990, Griffith et al., 1999). The loss of telomeres is sensed by a cell as DNA damage and cell activates DNA damage response (DDR) with cell-cycle arrest and activation of the DNA-repair mechanisms, which in turn leads to a senescence-related growth arrest (d'Adda di Fagagna et al., 2003). Thus, telomeres protect genes located on chromosomes from being truncated. The lack of telomeres could result in uncontrolled cell division followed by genomic instability through chromosome breakage and a great number of mutations that eventually would lead to cancer.

Telomere shortening does not occur in cells that express telomerase, which is a reverse transcriptase that can restore telomeric sequence (Blasco, 2003, McEachern et al., 2000). In humans, such cells are rare, however the identified telomere-positive cells

include cancer, embryonic stem cells, some of adult stem cells and a few somatic cells, such as activated T cells (Blackburn, 1991, Nan-Ping and Hodes, 2000, Wright and Shay, 2000, Rodier et al., 2005, Zeng and Rao, 2007). Moreover, genetic manipulation of the p53-p21 pathway resulted in reverse of senescence-related proliferation arrest (Beauséjour et al., 2003). Human fibroblasts with low level of p16 resumed growth upon inactivation of p53, although expression of oncogenic RAS triggered back proliferation arrest. However, cells with a high level of p16 failed to resume proliferation upon inactivation of p53 and expression of oncogenic RAS did not affect established growth-arrest (Beauséjour et al., 2003). These findings highlight the importance of p16 in prevention of senescence reversal by p53 inactivation.

1.3.2 Stress induced premature senescence

Stress induced premature senescence (SIPS) is a telomere -independent type of senescence caused by a number of physical and chemical stimuli, such as oxidative stress, activation of oncogenes, chemotherapeutic drugs, ionizing radiation or DNA damage (Serrano and Blasco, 2001, Mirzayans et al., 2017). SIPS has been also known as aberrant signalling-induced senescence (STASIS) (Serrano et al., 1997, Drayton and Peters, 2002). It is thought that the main role of SIPS is a cellular protective mechanism against possible carcinogenic stimuli. Unlike RIS, which require months or years to develop, SIPS may occur within days, activating the intercellular cascade prematurely (Chen et al., 1995, Frippiat et al., 2001, Di Leonardo et al., 1994, Serrano et al., 1997, Munoz-Espin and Serrano, 2014).

All types of senescence share morphological and functional phenotype, such as growth arrest, enlarged morphology, expression of SA-β-Gal or p16 and p21 overexpression, further described above (1.2), however SIPS are not usually characterized by shortened telomeres (Campisi and d'Adda di Fagagna, 2007, Wang and Bennett, 2012). Similarly to RIS, activation of SIPS is associated with DDR, in which DNA damage sensor proteins such as ataxia telangiectasia mutated (ATM) and ataxia telangiectasia Rad 3 related (ATR) initiate the DDR response and activation of p53 and other participants in DNA repair (Bartek and Lukas, 2007). Senescent cells are also known to have a higher level of reactive oxygen species (ROS) (Sergiev et al., 2015), although low levels of ROS are

associated with lengthening of organismal lifespan (Ristow and Schmeisser, 2011). It is known, that during aging, pathological changes occur in mitochondria, which then produce higher level of ROS, than young organisms (Toussaint et al., 2000). Accumulation of ROS has been shown to be associated with p53 overexpression, which regulates expression of pro-oxidant genes (Macip et al., 2003). These *in vitro* studies showed that ROS upregulation of p53 lead to increased level of ROS, and that p21 was also able to do so (Macip et al., 2002, Macip et al., 2003). However, that was not observed after senescence induction due to p16 overexpression. Additionally, oxidative stress that can cause senescence-dependent growth arrest can be also triggered by other factors, like hypoxia or sub lethal doses of hydrogen peroxidase (H_2O_2) (Macip et al., 2003, Toussaint et al., 2000, Wang et al., 2013).

An important example of SISP is Oncogene Induced Senescence (OIS), which, as the name suggests, can be induced by oncogenic stress (Xu et al., 2014b), that can occur prematurely, independently of cells' proliferating potential. Although the activation of oncogenes is one of the main tumour-promoting event that leads to uncontrolled proliferation, it may act as stress stimulus and trigger proliferation arrest in cultured cells and tumours (Saretzki, 2010). There are many oncogenes that have been found to trigger OIS. For instance, a mutated form of *RAS* induced senescence in human primary fibroblasts IMR90 *in vitro* (Serrano et al., 1997) and in mammary epithelial cells *in vivo* (Sarkisian et al., 2007). It has been demonstrated that senescence can be also induced by other oncogenes, like $BRAF^{V600E}$, *E2F1*, *AKT*, *cyclin E*, *c-Myc,* or by inactivation of certain tumour suppressors, such as PTEN or NF1 (Courtois-Cox et al., 2008). Moreover, it has been noted that p53 and RB are the cellular main, but not the only regulators of OIS induction (Rufini et al., 2013, Rayess et al., 2012). Also, PI3K/AKT/mTOR pathway has been found to mediate OIS responses (Xu et al., 2014b). Additionally, microRNAs (miRNAs) have been reported to contribute to OIS activation. For instance, miR-34a has been shown to mediate B-RAF- senescence independently of p53, through downregulation of MYC expression (Christoffersen et al., 2010).

1.4 The physiological roles of senescence

Cellular senescence has been found to play distinct physiological roles with both beneficial and detrimental effects depending on the age of organism (Williams, 1957, Rauser et al., 2006). Therefore, senescence has been linked with term 'antagonistic pleiotropy'. Pleiotropy refers to multiple effects from single gene or process. Senescence, which can promote fitness and health of young (e.g., tumour suppression), can be also detrimental in aged organisms (e.g., cancer progression, ageing acceleration) (Rodier and Campisi, 2011b). Therefore, cellular senescence cannot be simply classified as good or bad. Senescence plays a role in both, beneficial and detrimental aspects of human life, such as development, wound healing, cancer and aging and its involvement in these processes was shortly discussed here.

1.4.1 Positive functions of cellular senescence

1.4.1.1 Tumour suppression

The role of cellular senescence in cancer has been extensively studied for many years and nowadays we know that senescence has a contrasting effect on cancer depending on the age of organism. On one hand, it might be a potential anti-tumour mechanism, through proliferation arrest. (Rodier and Campisi, 2011b).

Senescence-inducing stimuli have oncogenic potential and cancer cells must avoid senescence growth arrest. Mutations and other changes typically occur within p16-pRB and p53 pathways. For instance, cells from genetically engineered mice, that are p53-deficient, failed to induce senescence and were susceptible to spontaneous formation of tumours (Donehower et al., 1992). That has been confirmed also in cells from patients with Li Fraumeni syndrome, who are carrying a germline mutations of p53 (Malkin et al., 1990, Srivastava et al., 1990). Results revealed that those cells were more prone to overcome senescence than cells derived from healthy individuals (Iwakuma et al., 2005), and underlined a potential tumour suppressor role of senescence. Moreover, large number of senescence cells have been found in preneoplastic lesions but not in malignant ones (Braig et al., 2005, Collado et al., 2005, Chen et al., 2005, Lazzerini

Denchi et al., 2005, Michaloglou et al., 2005, Swanson et al., 2013), suggesting that senescence suppress progression to malignancy. However, it is not clear how cancer cells eventually emerge from the premalignant state. Furthermore, as main feature of cancer is abnormal proliferation, any mechanism that prevents cells from undergoing an abnormal growth theoretically can prevent cancer as well. Cellular senescence depends critically on p53 and pRB/p16, which are powerful tumour suppressors pathways (Shay et al., 1991, Hickman et al., 2002, Collins and Sedivy, 2003). Therefore, senescence can contribute to tumour regression. It has been reported that some tumour cells senesce *in vivo* in response to chemotherapy (Ewald et al., 2010, Schmitt et al., 2002) or after reactivation of p53 (Ventura et al., 2007, Xue et al., 2007). Although there is evidence that senescence might act as a potential tumour-suppressive mechanism, the complete role of cellular senescence is not fully understood.

1.4.2 Senescence in development

Senescent markers have been found in the embryos of numerous species (e.g., axolotl, mice, chick) during different stages of development (Muñoz-Espín et al., 2013, Davaapil et al., 2017, Villiard et al., 2017). The main function of senescence during development is thought to be recruitment of immune components to promote regression of transient embryonic structures. That has been observed for instance in amphibian pronephros and mammalian mesonephros, in which senescence induction starts from tubules and then spreads throughout the whole structure. Next, due to the senescence-related recruitment of monocytes or macrophages, senescent cells are cleared together with associated structural degeneration (Muñoz-Espín et al., 2013, Villiard et al., 2017). Moreover, senescent cells are thought to play a role in tissue patterning and morphogenesis. This has been observed in frog embryos, in which alterations of TGF-β signalling resulted with patterning defects in the oral and nasal cavities (Muñoz-Espín et al., 2013, Davaapil et al., 2017). Additionally, during murine limb development, two SASP-derived factors, FGF8 and FGF4, have been found to be crucial proliferating-inducing signals for the adjacent mesenchymal cells. Moreover, studies using p21 null mouse embryos revealed that loss of cellular senescence disturbed normal expression of crucial patterning genes and disrupted maintenance of apical epidermal ridge (AER),

a main signalling centre during limb development (Storer et al., 2013). Cellular senescence has been also linked with expansion of different cell populations. During inner ear development, senescence induction occurs in a subset of epithelial cells and is thought to contribute to migration of pendrin-positive cells, where pendrin is an anion exchange protein (Everett et al., 1997). Studies on p21 null mice revealed that loss of cellular senescence resulted in reduction of pendrin-positive cells and expansion of pendrin-negative cells, resulting in defects of inner ear epithelium structure (Muñoz-Espín et al., 2013).

In many cases described here, compensatory mechanisms such as apoptosis or late macrophage infiltration were able to correct developmental abnormalities (Yu and Yun, 2020). Interestingly, senescence induction during development seems to be mainly p21-dependent and occurs with absence of DNA damage. Nevertheless, members of DDR signalling pathway have been detected during developmental stages, in particular p15 in mouse endolymphatic sac and mesonephros, and p53 in axolotl pronephros.
Taken together, cellular senescence can occur in a programmed manner not only as a response to damage signals, but also to developmental clues.

Apart from embryonic development, cellular senescence plays a physiological role in a programmed manner in adult organisms. In particular, it has been found that cellular senescence is involved in maturation of megakaryocytes (Besancenot et al., 2010) and placental syncytiotrophoblasts (Chuprin et al., 2013). Mature megakaryocytes differentiate in response to thrombopoetin. In the early stages of differentiation, thrombopoetin induces proliferation of megakaryocytes, and at a later stage it triggers proliferation arrest leading to platelet production. Megakaryocytes senescence is dependent on p21 and independent of p16, p53 or p21 (Besancenot et al., 2010). In turn, in megakaryocytes from myeloproliferative disorders, such as primary myelofibrosis senescence induction was not observed and also, they do not express p21 (Besancenot et al., 2010).

Study on human syncytiotrophoblast revealed that this maternal/fetal interface at the placenta exhibited the phenotype and expressed senescence markers (Chuprin et al.,

2013). Interestingly, both, megakaryocytes and syncytiotrophoblasts are examples of cell types that undergo endoreplication, which leads to polyploidy. The occurrence of cellular senescence in cells that naturally undergo polyploidy might suggests physiological correlation. Moreover, fusion of different unrelated cell types has been associated with induction of cellular senescence, and senescence features have been found in normal and cancer cells infected with measles virus that leads to cell fusion (Chuprin et al., 2013). These findings suggest physiological role of cellular senescence also during infectious processes.

1.4.3 Wound healing and tissue repair

Tissue repair is a multistep process, compromising multiple cell types. Tissue repair consists of few mechanisms which could be sum up as haemostasis, inflammation, cell proliferation and dermal remodelling (Wilkinson and Hardman, 2017). During the first step, haemostasis, an insoluble bloc clot is formed and endothelial cells from damaged vasculature cover the injury site with temporary fibrin scaffold, with simultaneous attraction of resident skin cells and immune cells (Velnar et al., 2009). The immune cells recruitment starts with pro-inflammatory macrophages and neutrophils that remove bacteria and necrotic tissue (Young and McNaught, 2011, Wilkinson and Hardman, 2020). During later stages, there is a replacement of macrophages from pro- to anti-inflammatory, which remove remaining pro-inflammatory cells through phagocytosis and thus support healing (Korns et al., 2011). The next stage involves a mechanism called re-epithelialisation, which refers to epithelial-to-mesenchymal transition of keratinocytes, that migrates towards the wound gap in order to close it (Shaw and Martin, 2016). This highly proliferating stage is supported by an angiogenesis process that provides a sustenance (Baum and Arpey, 2005). During the last stage, fibroblasts replaced initial temporary fibrin matrix with stronger scaffold proteins, such as mature collagen fibres (Li et al., 2007). The whole wound repair mechanism requires intense cellular communication, orchestrated by a variety of growth factors, cytokines, chemokines and components of the extracellular environment (Wilkinson and Hardman, 2020). It is important to mention that these factors are closely related to the

senescent secretome. Therefore, it is reasonable to suggest that cellular senescence could significantly contribute to tissue repair and wound healing process.

Indeed, the role of senescence in tissue repair mechanism has been extensively studied and recent reports revealed its beneficial function in this process. For instance, senescence-associated fibrolytic enzyme production reduced fibrosis, which could cause tissue dysfunction, after liver damage and cutaneous injury (Krizhanovsky et al., 2008, Jun and Lau, 2010). Moreover, similar findings were reported using a model of cardiac injury. Senescence induction reduced the fibrosis and in turn, the blockage of p53 and p16 expression promoted fibrosis (Meyer et al., 2016). Furthermore, in the same model, ectopic expression of CCN1 also decreased the fibrosis progression. CCN1 is known to induce cardiac senescence and is often upregulated at sites of injury (Kim et al., 2018a). It has been reported that, in part, CCN1 is also involved in tissue repair during skin injury and liver damage through senescence stimulation in cells at injury sites (Jun and Lau, 2010, Kim et al., 2013). Interestingly, recent findings revealed that topical application of another CCN family member, CCN2, similarly stimulated senescence induction in mice and thus reduced fibrosis in cutaneous wounds (Jun and Lau, 2017). Another research confirmed that senescent fibroblasts stimulated appropriate skin repair through secretion of growth factor PDGFA (Demaria et al., 2014a) and ablation of p16 and p21 in the same mouse model impaired deposition of extracellular matrix and decreased rate of wound healing.

Although the majority of research was based on murine models, these key findings provide a clear evidence of beneficial impact of senescence during tissue repair. However, the exact mechanism remains unclear. For instance, it is still unknow if the transient senescence-induction on the site of injury arises through intrinsic or extrinsic stimuli. And how senescent cells are effectively cleared from the injury site while they are no longer required? What are the differences between the clearance of senescent cells during wound healing and in aging-related tissue damage? Additional research should be carried to answer those questions.

1.4.4 Negative functions of cellular senescence

1.4.4.1 Aging

The number of senescent cells increase with age in variety of different tissues and they have been found at sites of age-related pathologies (Munoz-Espin and Serrano, 2014). The mechanisms by which senescence might be linked to ageing includes SASP and altered gene expression. Secretion of inflammatory cytokines or growth factors might affect surrounding cells and promote tissue remodelling (Campisi, 2005). Secreted factors can alter normal function of a cell and potentially trigger chronic inflammation and pre-mature aging symptoms (Parrinello et al., 2005, Franceschi et al., 2007, Chung et al., 2009).

Furthermore, accumulation of senescent cells leads to abnormal expression of senescence-related pathways p53-p21 or/and p16-pRB, which contribute to shorten healthspan and lifespan. For example, genetically modified mice with continued chronically elevated expression of p53 have shorter lifespan and premature aging symptoms comparing to their wild type counterparts (Maier et al., 2004, Tyner et al., 2002). However, it is worth to mention that negative effect of p53 on mice lifespan was only linked with continuous expression of p53. Intermittent activation of p53 resulted with normal lifespan and no signs of premature aging (Garcia-Cao et al., 2002). Due to an extra copy of wild type p53 locus introduced into the mouse genome, the p53 expression was regulated intermittently without continued expression. The high level of p53 was induced only upon activation. Nevertheless, mentioned above highlight the pro-aging role of p53 pathway, which depends on the p53 expression level and physiological environment (de Keizer et al., 2010).

Additionally, p16-dependent senescence has been linked to three hallmarks of ageing: haematopoiesis, neurogenesis and pancreatic function (Lopez-Otin et al., 2013). Moreover, an age-related increase of p16 expression has been found in mice stem and progenitor cells of bone marrow, pancreas and brain. The increased expression of p16 suppressed proliferation of stem-cell and regeneration of above-mentioned tissues (Janzen et al., 2006, Krishnamurthy et al., 2006, Molofsky et al., 2006).

These findings suggest that the p16 tumour suppressive role might be linked to its pro-ageing activity. However, it is not yet known if p16 functions in ageing and tumour-suppression are due to senescence or due to senescence-independent growth-arrest. Nevertheless, p16 is used as the main marker of cellular senescence, as mentioned before, and its expression has been detected in variety of aging tissues (Krishnamurthy et al., 2004, Baker et al., 2016, Baker and Petersen, 2018).

Moreover, elimination of $p16^{INK4A}$-positive cells from $BubR1^{H/H}$ progeroid mouse model promoted normal function of the tissues, delayed the onset of age-related pathologies in adipose tissue, skeletal muscle and eye and delayed the onset of already established age-related diseases (Baker et al., 2011). The same research group also demonstrated that clearance of $p16^{INK4A}$-positive cells from naturally aged mice also attenuated age-related deterioration of several organs and increased lifespan (Baker et al., 2016).
These findings highlight the importance of p16 in aging and age-related disorder and indicate that elimination of p16-positive cells may be an attractive approach to extend healthy lifespan.

1.4.4.1 Promotion of cancer

Beyond its tumour suppressive function, cellular senescence can have totally opposite effect and trigger malignant transformations. A number of senescent cells increase in age in varied tissues and their accumulation has been found in many age-related disorders (Dimri et al., 1995, Krtolica et al., 2001, Campisi, 2005, Wang et al., 2009, Rufini et al., 2013, Munoz-Espin and Serrano, 2014). Cancer is an age-related disease, and the probability of malignant transformation raises approximately after age of 50 (White et al., 2014).
Importantly, a characteristic feature of senescent cells, SASP, that is responsible for secretion of inflammatory factors can stimulate phenotypes characteristic for aggressive cancers (Coppé et al., 2010, Faget et al., 2019). SASP factors can promote tumour initiation, for instance, the growth-related oncogene (GRO) secreted by senescent fibroblasts stimulates the premalignant epithelial cells proliferation (Krtolica et al., 2001, Yang et al., 2006). Moreover, when co-cultured, senescent fibroblasts can

directly promote proliferation of pre-neoplastic or neoplastic cells through paracrine mechanism (Bavik et al., 2006, Coppe et al., 2008). Further, the secretion of interleukin 6 and 8 (IL-6 and IL-8) stimulates premalignant epithelial cells invasion through basement membrane into vasculature (Bavik et al., 2006, Smith and Kang, 2013). This suggests that effectors of SASP can promote cancer metastasis. Additionally, senescent cells can also secrete matrix metalloproteinase, which is another crucial factor for cancer invasiveness (Freitas-Rodríguez et al., 2017). Moreover, SASP can drive angiogenesis by secreting vascular endothelial growth factor (VEGF) or connective tissue growth factor (CTGF), that both promote angiogenesis and tumorigenesis (Coppé et al., 2006a, Yang et al., 2005). Additionaly, in vivo observations revealed that co-injection of senescent cells with fully malignant cancer cells results in an increased rate of tumour formation in mice comparing to co-injection with non-senescent cells (Krtolica et al., 2001, Wang et al., 2020). Chemotherapy-induced senescent stromal cells promoted metastasis of breast cancer cells to the lung, indicating an involvement of SASP in cancer relapse (Demaria et al., 2017).

Taken together, senescence plays a dual role in cancer progression. For a young organism senescence might block the progression of malignant transformation, however for old organisms it can be destructive, as accumulation of senescent cells is associated with accumulation of mutation and SASP. Further tests focusing on elimination of senescent cells should be performed to understand which factors and triggers are crucial for senescence transformation from positive to negative mechanisms.

1.4.4.2 Fibrosis

Although, presence of senescent cells has been found in number of different age-related diseases, its role in these pathologies is not clear (Minamino et al., 2009, Tchkonia et al., 2010, Markowski et al., 2013, Munoz-Espin and Serrano, 2014). The antagonistically pleiotropic nature of cellular senescence has been observed in this case as well. This is particularly evident in fibrosis. Cellular senescence has been found contributing to pathogenesis of Idiopathic pulmonary fibrosis (IPF). IPF is a progressive fatal lung pathology with unknown etiology (Schafer et al., 2017a). The link between

cellular senescence and IPF was set up through the number of evidences. Different cell types have been found to undergo senescence in IPF lungs, including alveolar epithelial cells and fibroblasts (Yanai et al., 2015, Lehmann et al., 2017). Moreover, senescent cells has been detected in experimental models of lung fibrosis induced by different stimuli (Aoshiba et al., 2003, Tian et al., 2019). And importantly, pharmacological removal of senescent cells ameliorated lung fibrosis and contributed to restoration of the lung function *in vivo* (Lehmann et al., 2017, Schafer et al., 2017a).

Although, the majority of reports indicates a negative role of cellular senescence in fibrosis progression (Clements et al., 2013, Liu et al., 2012), there are some studies questioning this hypothesis. For example, studies using *CDKN2A*-null mice (gene encoding INK4 family member p16 and $p14^{ARF}$) revealed that upon loss of $p16^{INK4A}$, the expression of main senescence markers, like SA-β-Gal, was significantly reduced, concomitantly with accelerated progression of renal fibrosis (Wolstein et al., 2010). Cellular senescence has been also linked with regulation of cardiac fibrosis (Xie et al., 2017, Shimizu and Minamino, 2019). Cardiac fibrosis can be caused by myocardial infraction (Zhu et al., 2013). Myocardial infraction is associated with elevated number of senescent myofibroblasts in the heart together with overexpression of core senescence regulators like p53, p16 and p21, suggesting a negative impact of cellular senescence on heart condition. However, the knockdown of p53 via siRNA in mice significantly reduced the number of senescent fibroblasts, inflammation, matrix metalloproteinases and cytokines production, whereas increased collagen deposition. Therefore, inhibition of p53-mediated senescence could have a positive impact on cardiac condition by prevention of heart rupture after myocardial infraction via increase of reparative fibrosis (Zhu et al., 2013).

1.5 The senescent surfaceome

As mentioned above, of all characteristic changes during cellular senescence, very few of them are stably and specific enough to be considered a proper marker (Wang et al., 2009, Sharpless and Sherr, 2015). All of the markers identified so far are still insufficiently specific, with a high rate of false positive and negatives and characterized by cell-type or tissue- dependent expression. The main markers of cellular senescence play important role in other crucial biological processes, like tumour suppression, DNA damage, maintenance of genomic stability. The perfect universal marker should be specific for senescent cells and its detection should be minimal in non-senescent states. However, it seems unlikely that such a marker will ever be found. Probably, it would be expected that the panel of markers will be used to identify senescent state and the most likely there will be a panel of markers specific for particular condition, like cell, tissue or disease. However, lack of specific marker delays development of elective anti-senescence therapeutics, due to a high level of side-targeting. Therefore, it is crucial to identify novel markers of cellular senescence, which would allow for specific detection of senescent cells *in vitro* and *in vivo* with minimal rate of side effects. In the need for better markers of senescence, the surfaceome proteins have emerged as interesting alternative. The surfaceome can be defined as the group of proteins present in the plasma membrane of a given cell type with at least one extracellular amino acid residue. Among human surfaceomes we can distinguish all types of transmembrane proteins, like single or polytopic α-helical or β-sheet transmembrane proteins, which act as receptors, transporters, enzymes or channels (Bausch-Fluck et al., 2018). The cell surfaceome can be compared to a hub, which transmits information from and to outside environment therefore playing a crucial role in cell's interactions and signalling. However, the surfaceome panel might vary depending on a cell and tissue type and like other senescence markers, it is unlikely to be universal. Importantly, the presence of extracellular epitopes makes a surfaceome protein a promising diagnostic marker of cellular senescence that potentially could even be used for targeted therapies.

1.5.1 Currently known markers of the senescent surfaceome

Several proteins have been identified as members of senescent surfaceome (**Table 1.2**). NOTCH3 was one of the first proteins identified as a member of senescent surfaceome (Cui et al., 2013, Althubiti et al., 2014). It belongs to the Notch family receptors, known to have tumour suppressor functions (Rangarajan et al., 2001, Klinakis et al., 2011, Nicolas et al., 2003). NOTCH3 overexpression was found in human senescent cells activated by various senescence- inducing stimuli (Cui et al., 2013, Althubiti et al., 2014). It has been also reported, that expression of NOTCH3 was required for p21 induction in senescent cells and its downregulation delayed onset of senescence and extended replicative lifespan (Cui et al., 2013). Moreover, restoration of NOTCH3 expression in tumours impaired cell proliferation and promoted senescence activation. Another member of Notch signaling, NOTCH 1 has been also identified as surfaceome marker of cellular senescence (Hoare et al., 2016). Upregulation of NOTCH1 was confirmed *in vitro* in OIS and RIS and *in vivo* in NRAS senescent hepatocytes. In addition, authors revealed that NOTCH1 controls secretome composition and *in vivo* inhibition of NOTCH1 promoted senescence surveillance (Hoare et al., 2016).

Table 1.2. Currently characterized markers of senescent surfaceome.

Adapted from (Ekpenyong-Akiba et al., 2020b)

Surfaceome protein	Reference
NOTCH3	(Cui et al., 2013, Althubiti et al., 2014)
NOTCH1	(Hoare et al., 2016)
B2M	(Althubiti et al., 2014)
NTAL	
VAMP3	
LANCL1	
STX4	
DPP4	(Kim et al., 2017)
CD264	(Madsen et al., 2017)
SCAMP4	(Kim et al., 2018b)
uPAR	(Amor et al., 2020)

Another protein identified as a member of senescent surfaceome is CD264 (Madsen et al., 2017). CD264 is a decoy receptor for tumour necrosis factor-related apoptosis-inducing ligand (TRAIL) (Falschlehner et al., 2007) involved in the formation of death-inducing signalling complex (Pan et al., 1998, Lee et al., 1992). CD264 has been detected in premalignant tumours induced by *RAS* and its downregulation was observed in malignant lesions of *RAS*-induced tumours (Collado et al., 2005). Moreover, upregulation of CD264 was found in in stress-induced senescence of vascular smooth muscle cells but not in replicative senescence (Zhu et al., 2011). Additionally, upregulation of CD264 has been detected in human bone marrow mesenchymal stem cells and inversely correlated with proliferation and differentiation potential (Madsen et al., 2017). For all these reasons, CD264 was proposed as a biomarker of cellular aging (Madsen et al., 2017).

Many senescent surfaceome members were identified through a mass spectrometry screening of membrane fractions of senescent cell lysates in our lab (Althubiti et al., 2014). To the best of our knowledge, that was the first systematic screen of senescent surfaceome, by which more than 100 proteins were reported to be preferentially expressed in the membranes of senescent cells but not in proliferating counterparts. However, it is important to consider that that plasma membrane protein panel is only a subset of all membrane proteins within the cell detected by mass spectrometry screen. Therefore, it is necessary to provide further validation to distinguish plasma membrane proteins that partially or fully bridge over the cells surface and have present extracellular epitopes from intercellular membrane proteins (i.e. Golgi, endoplasmic reticulum), or the ones bound to the intercellular part of plasma membrane, i.e. BTK (Althubiti et al., 2016b).

For the identification of the surfaceome proteins in our lab, we used previously described genetic models of senescence, derivatives of the EJ bladder carcinoma cell line, EJp16 and EJp21(Althubiti et al., 2014). Induction of senescence in EJp16 and EJp21 occurs via regulation of tetracycline-dependent expression system for p16 or p21 respectively, which are core genes responsible for induction and maintenance of senescent phenotype. The EJ-based cell model allows for establishment of cellular 3-4 days after removal of tetracycline (Chang et al., 1999, Macip et al., 2002). It is a useful

model for pathway depended studies, due to direct activation of p53/p21 or pRb/p16 signalling without additional heterogenic effects caused by senescence stimuli seen in more physiological models. Therefore, a panel of proteins identified using these models can be directly linked to the activation of one of the main senescence-related pathways. 107 proteins were identified in plasma membrane of EJp21 and 132 in EJp16. Ten of them that had not been previously linked to cellular senescence were picked for further validation: B2M, DEP1, EBP50, VPS26A, PLD3, ARMCX3, NTAL, VAMP3, LANCL1 and STX4. Further characteristics revealed a tissue dependent specific profile. For instance, DEP1, STX4, B2M and NTAL were detected in analysis of human naevi and tissues samples of ^{V600E}BRAF lung adenoma mouse model, known to have a high percentage of senescent cells (Mercer et al., 2005, Carragher et al., 2010). However, additional validations are still needed to confirm their cellular localisation and expression pattern. Among reported markers, B2M is the most characterized so far and its overexpression was detected in aging brain and skin (Ekpenyong-Akiba et al., 2020a).

An alternative approach to surfaceome screen performed in our lab, focused on replicative senescence (Kim et al., 2017). Human diploid fibroblasts WI-38 were subjected to extensive cell division and fractions of membrane-associated proteins were analysed using mass spectrometry. Proteins were compared between proliferating cells (population doubling level (PDL)= 23) and their senescent counterparts (PDL=59). Results revealed proteins that were classified into two groups: those present in intracellular membranes (i.e. Golgi) and cell surface proteins. 118 proteins were identified at the overlap of these two groups. Authors narrowed the list down to 15, out of which, DPP4 and SCAMP4 were chosen for further validation (Kim et al., 2017, Kim et al., 2018b). DPP4 deactivates the glucose-dependent insulinotropic peptide (GIP) and glucagon-like peptide-1 (GLP-1) (Zhong et al., 2013), which are crucial hormones in diabetes. GIP and GLP-1 mediate insulin release by pancreatic β cells, thereby contributing to suppression of the glucose level in the blood after a meal (Wu et al., 2016). Expression of DPP4 was analysed using different senescent models and triggers of senescence. For instance, DPP4 overexpression was confirmed after ionizing radiation and in HRAS^{G12V} mediated oncogene-induced senescence.

The secretory carrier membrane protein 4 (SCAMP4) is thought to be involved in intercellular trafficking (Lin et al., 2005) and its membrane localization has been previously confirmed (Lee et al., 2005). SCAMP4 abundancy was tested in different senescent models (Kim et al., 2018b) and results revealed its upregulation in replicative senescence, doxorubicin-induced and oncogene-induced senescence. Moreover, authors discovered a potential involvement of SCAMP4 in SASP, since SCAMP4 silencing reduced the secretion of many SASP factors, like IL6, IL8, GDF-15, IL1B, MIF and CCL2.

uPAR is another interesting member of senescent surfaceome that has been identified recently (Amor et al., 2020) through RNA-sequencing analysis. Expression of markers was compared between three senescence models: an *in vivo* model of therapy-induced senescence, an *in vivo* model of oncogene induced senescence and an *in vitro* culture-induced senescence. uPAR was upregulated in all of them and its plasma membrane localisation was determined by UniProtKB. uPAR is receptor for urokinase-type plasminogen activator that is responsible for the extracellular matrix degradation during fibrinolysis, wound healing and cancer and promotes tumour cells invasion, motility and survival (Smith and Marshall, 2010). Interestingly, uPAR has been reported as one of SASP factors (Coppé et al., 2008) and was identified as serum biomarker for diabetes and kidney diseases (Hayek et al., 2015). Its upregulation was further confirmed in other senescence models: in replicative-senescence induced in human primary melanocytes; in oncogene senescence induced by $KRAS^{G12D}$ and $NRAS^{G12V}$, in therapy induced senescence mouse lung adenocarcinoma $KRAS^{G12D};p53^{-/-}$ (KP) cells that were subjected to MEK and CDK4/6 inhibition (Amor et al., 2020). Moreover, its expression was confirmed in tissues from patients with age-related disorders, such as osteoarthritis, diabetes, idiopathic pulmonary fibrosis, liver fibrosis or pancreatic cancer (Belcher et al., 1996, Guthoff et al., 2017, Schuliga et al., 2017, Amor et al., 2020). Importantly, uPAR has been used as a target for CAR T-mediated elimination of senescent cells, which is further explained in **section 1.7.3**

1.6 BTK

In our lab, BTK was identified in the screen of proteins preferentially expressed in membranes of senescent cells and was found to be a crucial modulator of the senescent pathway (Althubiti et al., 2016b).

Bruton's agammaglobulinemia tyrosine kinase (BTK) is a member of non-receptor tyrosine kinase family (TEC), which besides BTK includes four other members: tyrosine kinase expressed in hepatocellular carcinoma (TEC), interleukin-2-inducible T cell kinase (ITK), resting lymphocyte kinase (RLK) and bone marrow expressed kinase (BMX) (Bradshaw, 2010). The most characteristic feature of this family is the presence of a pleckstrin homology (PH) domain in their protein structure.

Activation of BTK is thought to rely on the autophosphorylation at tyrosine 223 (Pal Singh et al., 2018). The first step of BTK activation starts with BTK recruitment to the membrane from cytosol, through interaction of its PH domain with PI3K product PIP_3. Then, BTK is phosphorylated by SYK or SRC family kinases at tyrosine 551 (Y551) (Rawlings et al., 1996). Phosphorylation at Y551 promotes its catalytic activity and subsequently triggers autophosphorylation in SH domain at tyrosine 223 (Park et al., 1996) consequently further stabilizing the active conformation and activating BTK kinase activity.

1.6.1 Oncogenic activity of BTK

The activated form of BTK is essential for B cell development, differentiation and signalling (Herman et al., 2011). *BTK*-deficient B lymphocytes fail to reach the mature state and are presumably doomed to a premature death. Mutations in the *BTK* gene lead to an immunodeficiency disorder called X-linked agammaglobulinemia (XLA) in humans (Tsukada et al., 1993, Vetrie et al., 1993) and X-linked immunodeficiency (Xid) in mice (Lindvall et al., 2004, Thomas et al., 1993).

However, the role of BTK is not only limited to BCR signalling, since it has been found to be involved in various other pathways like Receptor activator of nuclear factor-κB (RANK) in osteoclasts (Shinohara et al., 2008), collagen and CD32 signalling in platelets (Oda et al., 2000) or the NLRP3 inflammasome in brain (Ito et al., 2015). Importantly, high BTK expression has been found in B cell malignancies, such as chronic lymphocytic

leukaemia, mantle cell lymphoma, and multiple myeloma. Moreover, BTK oncogenic activity has been observed also in various solid tumours (Zucha et al., 2015, Kokabee et al., 2015, Grassilli et al., 2016, Wei et al., 2016). Therefore, it was proposed that blocking BTK could act be a promising therapeutic strategy (Ekpenyong-Akiba et al., 2020a).

Ibrutinib is one of the chemical inhibitors of BTK, with the molecular formula $C_{25}H_{24}N_6O_2$, and a molecular weight of 440.5 g/mol (Honigberg et al., 2010). It forms a covalent bond with Cys481 in the BTK ATP binding domain rendering the enzyme irreversibly inactive and blocking BCR signalling pathway. However, the drug also has activity against other kinases, including ITK, TEC, BLK and JAK3, EGF and HER2 (Honigberg et al., 2010). This broad activity on one hand can be used to target oncogenic pathways other than BTK in tumour cells but on the other hand, it may have other therapeutic implications. Therefore, more selective BTK inhibitors were also introduced into the clinic, like Acalabrutinib (ACP-196) or Zanubrutinib (Witzig and Inwards, 2019, Syed, 2020).

1.6.2 Tumour suppressor role of BTK

Several papers indicate that, antagonistically to its oncogenic activity and depending on the context, BTK might contribute to tumour suppressor mechanism instead (Rada et al., 2018b). Indeed, BTK has been recently characterized as a member of p53 pathway (Althubiti et al., 2016b). After damage, BTK protein levels increase in a p53 dependent manner. Furthermore, BTK modulates p53 activity by phosphorylation at many residues, mainly at serine 15, therefore increasing its cellular responses, especially apoptosis and senescence. The importance of BTK in p53 regulation was confirmed by BTK knock-down analysis, which resulted in deregulation of p53 function. The double dependency of p53 and BTK suggests regulation of these two proteins by a positive feedback loop, with the ultimate goal of p53 stabilization in damage responses.

Furthermore, BTK also increases the protein level of MDM2, a direct p53 inhibitor and its target gene (Chène, 2003). MDM2 activity was blocked by BTK-mediated phosphorylation of MDM2. Phosphorylation of MDM2 impairs its ubiquitinating activity and leads to further stabilization of p53. However, the exact mechanisms of MDM2 phosphorylation by BTK remained unclear and further tests should be done to confirm whether it is direct or indirect phosphorylation mechanism.

Additionally, the BTK involvement in tumour suppressor mechanisms was further uncovered by its relationship with p73, another tumour suppressor involved in cell cycle regulation, and induction of apoptosis (Rada et al., 2018a). BTK regulates p73 protein level after DNA damage and induce expression of its target genes. This suggests a pro-apoptotic function of BTK independently of p53, by enhancement of p73 activity as a supplement or substitute of p53 function.

Importantly, observations on BTK tumour suppressor function led us to the hypothesis that inhibition of BTK may impair senescence induction. Indeed, inhibition of BTK via shRNA or treatment with Ibrutinib abolishes p53 expression and blocked senescence induction (Rada et al., 2017).

In summary, BTK display a pleiotropic activity, playing important but opposed functions depending on the context. Either acts as oncogene and stimulates proliferation and survival signals or plays a tumour suppressive role by induction of apoptosis and senescence.

1.7 Strategies to target cellular senescence

Aging has been defined as a gradual loss of physiological homeostasis leading to impaired function and increased vulnerability to death (Lopez-Otin et al., 2013) that exponentially increase in the last quarter of the lifespan (St Sauver et al., 2015). Among the diseases highly dependable on chronical aging are myocardial infarction and cardiovascular disorders, cancer, chronic lung diseases, diabetes, renal dysfunctions, osteoporosis, neurodegenerative disorders and many others (Munoz-Espin and Serrano, 2014, Kirkland and Tchkonia, 2017, Tchkonia and Kirkland, 2018). Moreover, during aging, physiological resilience decreases and manifests itself with an increased severity of injections, delayed recovery after infection or injury and impaired antibody development after immunization (Kirkland et al., 2016, Kirkland and Tchkonia, 2020). Taking into consideration that the aging population increases worldwide, the incidence of multiple age-related pathologies is going to have an enormous impact on public health. Therefore, the design of new therapies aiming to increase the human healthspan is an urgent need. Cellular senescence has been identified as one of the hallmarks of aging (Lopez-Otin et al., 2013) and recently, elimination of senescent cells from human body gained a lot of interests as a promising anti-aging strategy (Kirkland and Tchkonia, 2017).

The development of genetically engineered mouse models has uncovered the role of cellular senescence in a number of age-dependent disorders. Moreover, selective elimination of senescent cells has been found to delay age-related disorders and enhance both healthspan and lifespan in mice (Paez-Ribes et al., 2019). Therefore, the development of senotherapies, therapies aimed to interfere with senescent cells, is rapidly developing. Among senotherapies, three main strategies can be distinguished: development of compounds that selectively kill senescent cells (senolysis), reduce of SASP (senostasis or senomorphosis), or inhibit senescence before it occurs (senoblocking). Preclinical validations of various senotherapies confirmed that elimination of senescent cells delays and, in some cases, reverts a number of age-related pathologies. In particular, that was confirmed in cardiovascular diseases, neurological disorders, fibrosis, musculoskeletal impairments and cancer (Lewis-

McDougall et al., 2019, Ekpenyong-Akiba et al., 2020a, Schafer et al., 2017a, Jeon et al., 2017, Demaria et al., 2017). The successful *in vivo* validation advanced the senotherapy field to further steps and, currently, senolytics reached clinical trials (Hickson et al., 2019, Justice et al., 2019). However, cellular senescence is a highly heterogenous process that depends on different variables, including type of triggering stimuli, pathway response, cell-type and tissue origin. This complicates the design of therapies Moreover, currently available senotherapies exhibit markable side effects and toxicities, which limit their clinical potential. For instance, navitoclax (ABT-263) has been found to cause thrombocytopenia and neutropenia (Vogler et al., 2011). Therefore, development of more selective therapies is crucial and requires deep understanding of molecular mechanisms that drive cellular senescence. Here, we discuss the three main senotherapy strategies, senolysis, senomorphosis and senoblocking, and highlight our contribution to this field.

1.7.1 Senolysis

Senolytics are class of drugs and a powerful 'hit and run' tool to selectively clear senescent cells' burden. In preclinical models, senolytics has been shown to increase healthspan and lifespan of mice, with amelioration of age-related dysfunctions like lung fibrosis (Schafer et al., 2017a), osteoporosis and osteoarthritis (Farr et al., 2017b, Jeon et al., 2017), cardiac dysfunctions (Lewis-McDougall et al., 2019), emphysema (Mikawa et al., 2018), Alzheimer (Zhang et al., 2019) or hepatic steatosis (Ogrodnik et al., 2017b). Recently, senolytics reached clinical trials and have been shown to decrease the number of senescent cells in humans (Hickson et al., 2019) and reduce the symptoms of idiopathic pulmonary fibrosis (Justice et al., 2019). To date, several senolytics have been identified and might be classified as a first-generation (**Table 1.3**) and second-generation of senolytics (**Table 1.4**). First-generation of senolytics includes natural compounds and their derivatives, and chemical senolytics. In second-generation of senolytics, there are drug-delivery tools that directly recognize and eliminate senescent cells.

1.7.2 First generation of senolytics

1.7.2.1 Natural compounds

Many natural compounds have been used in traditional medicine or as a nutritional supplement for years. Most of them are antioxidants, which reduce oxidative damage. Among them there is quercetin (Xu et al., 2018, Zhu et al., 2017b, Hickson et al., 2019) and fisetin (Yousefzadeh et al., 2018). Both of them are a natural flavonoids, that are a group of natural substances with variable phenolic structures, found in fruits, vegetables, roots, flowers, red wine and tea (Panche et al., 2016). Quercetin shows a broad spectrum of biological activities, such as antioxidant, anti-inflammatory, anti-bacterial or anti-carcinogenic effects (David et al., 2016). Its mechanism of action and molecular target remain unknown. However, considering its antioxidant activity, quercetin has been tested *in vivo* and showed amelioration of cognitive defects in aged mice (Singh et al., 2003) and promoted longevity in *Saccharomyces cerevisiae* (Belinha et al., 2007). The first indications of its senolytic activity were reported by Dr Kirkland's group (Zhu et al., 2015a). However, its senolytic activity was moderate and cell-type dependent. Therefore, quercetin has been combined with other senolytic agent, dasatinib, and that combination exhibits a synergistic effect in killing senescent cells from different origins. Furthermore, their activity has been tested in the fast-aging mouse model *ERCC1*$^{-/\Delta}$ and revealed a significantly lower level of senescent cells number, which was accompanied by improvement of healthspan and lifespan extension (Zhu et al., 2015a). Since then, combination of quercetin and dasatinib has been widely used *in vivo* as a therapy against different age-related pathologies, such as Alzheimer's, obesity-related dysfunctions, atherosclerosis, pulmonary fibrosis, hepatic steatosis, age-related bone loss, hyperoxia-induced airway disease, cardiac dysfunctions and chronic kidney disease, among others (Zhang et al., 2019, Ogrodnik et al., 2019, Palmer et al., 2019, Roos et al., 2016, Schafer et al., 2017b, Ogrodnik et al., 2017a, Farr et al., 2017a, Xu et al., 2018, Parikh et al., 2019, Lewis-McDougall et al., 2019, Kim et al., 2019). Combination of dasatinib and quercetin is the first senolytic that reached clinical trials (Justice et al., 2019, Hickson et al., 2019). Results from clinical trials revealed that the

combination of dasatinib and quercetin was well tolerated and reduced the number of senescent cells in patients with idiopathic pulmonary fibrosis and diabetic kidney disease.

Fisetin, similarly to quercetin, has antioxidant, anti-inflammatory, neuroprotective and anti-tumour effects (Pal et al., 2016, Khan et al., 2013, Sundarraj et al., 2018). Interestingly, fisetin exhibited tumour-suppressive function by inhibition of proliferation or induction of apoptosis in different cancer cells, with insignificant effect on normal cells (Lall et al., 2016). Its senolytic activity is cell-specific, in particular fisetin selectively killed senescent human umbilical vein endothelial cells, but not IMR-90 or primary human preadipocytes (Zhu et al., 2017b). *In vivo* treatment of progeroid and naturally aged mice revealed a significant improvement in healthspan and increase of maximum lifespan (Yousefzadeh et al., 2018).

Another natural senolytic is piperlongumine and its analogs, an extract from Piper species (Bezerra et al., 2013). It can effectively kill various types of cancer, for instance leukaemia, skin, breast, lung, renal and prostate cancers with a little effect on normal cells (Bezerra et al., 2007, Bezerra et al., 2013, Piska et al., 2018). It has been shown that it can suppress cancer through modulation of different pathways, including the mitochondrial apoptosis pathway, extracellular signal-regulated kinases (ERK1/2) and RAF-1 and it can induce production of ROS in cancer cells through regulation of GSTp1 and CRB1, enzymes involved in the oxidative stress response. The senolytic activity of piperlongumine has been confirmed in irradiated senescent WI-38 fibroblasts, replicative senescence, chemically-induced senescence and OIS triggered by overexpression of oncogene *RAS* (Wang et al., 2016b). Moreover, combination of piperlongumine with navitoclax synergistically killed senescent cells (Wang et al., 2016b). The exact mechanisms by which piperlongumine kills senescent cells remain unknown. Although it has the ability to kill cancer cells through induction of ROS, it cannot induce ROS production in senescent cells. However, it has been discovered that OXR1, an important antioxidant protein that is overexpressed in some senescent models, is one of piperlongumine targets (Zhang et al., 2018). These observations provided a new insight of how the senescent cells response to oxidative stress might be controlled. Moreover, it highlights a senolytic potential for future OXR1 inhibitors. Nevertheless, piperlongumine and its analogues have to be firstly tested *in vivo* to

provide more information about its senolytic activity and potential effect on healthspan and lifespan.

Another type of natural senolytic is curcumin and its analogues. Curcumin is a hydrophobic polyphenol extracted from herb *Curcuma longa* that exhibit strong free radical scavenging activity (Sharma, 1976). Its beneficial activity on humans healthspan was confirmed in different biological aspects. For instance, curcumin has been found to ameliorate the onset of atherosclerotic disease, skin aging, Alzheimer and cancer (Grill et al., 2018, Yang et al., 2017a, Cole et al., 2005, Takano et al., 2018). Moreover, its anti-aging activity has been tested in *Caenorhabditis elegans* and *Drosophila melanogaster,* in which it extended both healthspan and lifespan (Liao et al., 2011, Chandrashekara et al., 2014). However, despite high therapeutic potential, curcumin is characterized by low potency and poor bioavailability (Shoba et al., 1998). Therefore, many analogues have been developed, including EF24 (Adams et al., 2005, He et al., 2018), 2-HBA (Dinkova-Kostova et al., 2007), HO-3867 (Selvendiran et al., 2009), dimethoxycurcumin (DIMC) (Tamvakopoulos et al., 2007) and among them EF24 exhibits the strongest senolytic activity (Li et al., 2019a). EF24 selectively reduced the viability of different senescent models, including irradiated cells, replicative senescence and oncogene-induced senescence. Although, EF24 is able to kill cancer cells through induction of ROS production, it has been shown that its senolytic activity is ROS-independent. Instead, it was hypothesized that the senolytic activity of EF24 might be linked to a concomitant decrease of BCL-X_L and MCL-1 levels in treated senescent cells but not in proliferating cells (Li et al., 2019a).

Recently, ouabain and digoxin have been identified as promising senolytics due to their broad-spectrum senolytic potential (Guerrero et al., 2019a, Triana-Martínez et al., 2019a). Ouabain and digoxin are cardiac glycosides (CGs), a family of compounds that derived from the foxglove plant. Their mechanism of action is thought to depend on inhibition of the plasma membrane Na^+/K^+ ATPase, which leads to disturbance of ions concentrations, NA^+, K^+ and H^+, causing acidification of the cells. Senescent cells seem to be more susceptible to ion unbalance than proliferating cells, due to basal partial depolarization of their plasma membrane and higher concentration of H^+ (Guerrero et al., 2019a, Triana-Martínez et al., 2019a). CGs senolytic activity has been confirmed in a variety of *in vitro* senescent models and in tissues of different origin, and *in vivo*. For

instance, ouabain and digoxin selectively decreased the burden of senescent cells in liver, pituitary and lung despite different senescence-triggering stimuli, such as oncogenes or irradiation (Guerrero et al., 2019a). Elimination of senescent cells resulted in fibrosis reduction and improvement of various physiological functions, including the reduction of tumour growth after treatment with chemotherapeutic agents in a lung and breast cancer xenograft mouse model (Triana-Martínez et al., 2019a). These data indicate therapeutic potential of cardiac glycosides for the treatment of age-related diseases and as adjuvant therapy for cancer.

1.7.2.2 Chemical senolytics

Various senolytics have been identified by repurposing already existing drugs used for inhibition of the uncontrolled growth and proliferation of cancer cells. Among them, was dasatinib, which was introduced as senolytic for the first time in 2015 (Zhu et al., 2015a). Dasatinib is a tyrosine kinase inhibitor used to treat chronic myelogenous leukaemia (CML) and Philadelphia-chromosome positive acute lymphoblastic leukaemia (ALL) (Kantarjian et al., 2006). It has been shown that dasatinib reduced viability of senescent human preadipocytes but for other models, such as senescent HUVECs, its senolytic activity was less effective (Zhu et al., 2015a). However, combination with quercetin revealed a synergistic activity of the drugs and since then, this combination has been widely used to clear senescent cells in variety of *in vitro* and *in vivo* models (Kirkland and Tchkonia, 2017, Paez-Ribes et al., 2019) (as discussed earlier in 1.7.2.1).

Another class of chemotherapeutics that has been found to effectively kill senescent cells are HSP90 inhibitors. HSP90 is a molecular chaperone that plays important function in the regulation of protein stability and it is upregulated in many types of cancers (Whitesell and Lindquist, 2005, Solárová et al., 2015). Interestingly, survival of senescent cells seems to be more HSP90-dependent than non-senescent cells, which has been shown using HSP90 inhibitors. For example, 17-DMAG treatment of *ERCC1*$^{-/\Delta}$ progeroid mice diminished the burden of senescent cells in tissues and ameliorated the onset of age-related phenotypes (Fuhrmann-Stroissnigg et al., 2017a). The exact mechanism of HSP90 inhibitors remain unknown, however, it has been shown that they can affect

interactions between phosphorylated AKT and HSP90, which leads to destabilization of the AKT active form that is important for senescence induction and survival of senescent cells (Nogueira et al., 2008).

Additional approaches tested so far interfere with the interactions between p53 and FOXO4 (FOXO4-DRI peptides) (Baar et al., 2017) or between p53 and MDM2 (e.g. UBX0101, nutlin-3a) (Jeon et al., 2017, Efeyan et al., 2007). FOXO4 upregulation has been reported in senescent human fibroblasts induced by irradiation (Rodier et al., 2011). FOXO4 is a member of Forkhead box O (FOXOs) family, which has been previously linked with aging (de Keizer et al., 2011, Eijkelenboom and Burgering, 2013, Martins et al., 2016). Overlapping function of FOXOs and p53 lead to the hypothesis that they might interact with each other. Indeed, growing evidence highlights several links between p53 and FOXOs signalling. For instance, p53 and FOXO share several downstream targets, such as p21, WIF1, FASLG, GADD45 (Seoane et al., 2004, Tran et al., 2002, Bourgeois and Madl, 2018). Moreover, SGK1, a downstream target of p53 involved in cell survival mediates FOXOs phosphorylation and translocation from the nucleus to the cytoplasm (Brunet et al., 2001). Inhibition of FOXO4 using shRNA resulted in reduced viability and density of senescent cells but not their control counterparts (Baar et al., 2017). Therefore, authors designed FOXO4-DRI peptide that selectively induced apoptosis in senescent cells through perturbations in the FOXO4-p53 interactions. That lead to p53 nuclear exclusion and induction of apoptosis. *In vivo*, treatment affected doxorubicin-induced chemotoxicity and ameliorated negative impacts of renal aging in fast aging and wild-type mice (Baar et al., 2017).

Senolytic activity has been also found in agents interfering with p53-MDM2 interactions. MDM2 is direct inhibitor of p53, which promotes p53 degradation through a ubiquitin-dependent pathway (Shay et al., 1991, Muñoz-Espin and Demaria, 2020). Inhibition of the interactions between MDM2 and p53 can then increase p53 activity and protein level. UBX0101 is an MDM2 inhibitor that selectively eliminated senescent cells in vitro. Moreover, treatment with UBX0101 decreased the number of senescent cells in mice with post-traumatic osteoarthritis (Hsu et al., 2020). However, it is worth to mention that MDM2 inhibitor has been found to cause gastrointestinal toxicity and substantial

hematopoietic suppression and it remains unknown if adverse effects are results of on- or off-target toxicity (Tisato et al., 2017).

1.7.2.2.1 BCL-2 family inhibitors

One of the main features of senescent cells is their resistance to apoptosis. Various senescent cells may depend on different Senescent Cells Anti-Apoptotic Pathways (Kirkland and Tchkonia, 2017)(SCAPs) to survive . The BCL-2 protein family includes both pro- and anti-apoptotic proteins (Youle and Strasser, 2008). All proteins within the family share at least one of four characteristic domain known as BCL-2 homology (BH) and interact with each other via hydrophobic interactions (Kale et al., 2018). The anti-apoptotic BCL-2 family members share the homology of all BH1-4 domains and consist of BCL-2, BCL-X_L, BCL-W, MCL-1, BCL2A1 (Hata et al., 2015). The pro-apoptotic proteins are divided into two groups. First, sharing homology of multi-BH domains (1-4), BAK and BAX; and pro-apoptotic that share only the BH3 domain with each other, BIM, BID, BAD, BIK, BMF, NOXA, PUMA and HRK. During cellular stress, the pro-apoptotic BH3-only protein are upregulated, inhibit the anti-apoptotic proteins and activate the effectors BAK and BAX. Activation of BAK and BAX induces their oligomerization and formation of the macropores that induce mitochondrial outer membrane permeabilization (MOMP). Then, MOMP causes the irreversible release of cytochrome C from mitochondria to cytoplasm, which binds to apototic protease-activating factor 1 (APAF1) to form apoptosome. Apoptosome formation activates caspases cascade that leads to apoptosis. The balance ratio and interactions between pro- and anti-apoptotic proteins seems to dictate the cell fate decision (Shamas-Din et al., 2013).

Among BCL-2 anti-apoptotic proteins, BCL-X_L and BCL-W have been found overexpressed in senescent cells. Therefore, it is thought that apoptotic resistance of senescent cells mainly relies on them. Dual inhibitors, such as ABT737 and ABT263 (Navitoclax), which target BCL-2, BCL-X_L and BCL-W are known to be effective senolytics (Chang et al., 2016a, Yosef et al., 2016a, Zhu et al., 2016). ABT737 has the ability to induce apoptosis in many cancer types, such as different leukaemia's and lymphomas, multiple myeloma, glioblastoma and small cell cancer cell lines (Oltersdorf et al., 2005, Chauhan et al., 2007, Tagscherer et al., 2008, Tahir et al., 2007). Senolytic activity of

ABT737 has been confirmed *in vitro* and *in vivo,* for instance, in lung DNA-damage induced senescence caused by whole body irradiation and in senescent skin of p53-dependent transgenic mouse model (Yosef et al., 2016a). However, ABT737 is not orally bioavailable and its poor aqueous solubility makes delivery of this drug challenging (Tse et al., 2008). That led to discovery of navitoclax, which is orally bioavailable and quickly became one of the crucial drugs in senescent field (Zhu et al., 2016). Senolytic activity of navitoclax has been confirmed in variety of senescent cells, for instance in HUVEC and IMR90, but not in human preadipocytes (Zhu et al., 2016). Interestingly, despite being highly effective in killing a culture cell model of lung fibroblasts, it was less potent against senescent primary human fibroblasts isolated from patients (Schafer et al., 2017a). Moreover, ABT263 can effectively clear senescent cells *in vivo* from various mouse models, leading to a decrease in expression of senescence markers, including $p16^{INK4a}$, $p21^{CIP1}$, SASP factors and SA-β-Gal activity (Zhu et al., 2015a, Chang et al., 2016a). Moreover, clearance of senescent cells was associated with improved healthspan of treated mice. In particular, navitoclax treatment rejuvenated aged hematopoietic stem cells and hematopoietic system in progeria mice (Chang et al., 2016a), ameliorated age-related pathologies such as dementia (Bussian et al., 2018), atherosclerosis (Childs et al., 2016b) and pulmonary fibrosis (Pan et al., 2017). Although, navitoclax exhibits strong senolytic potential, it causes a high level of off- and on-target toxicity. For instance, it has been found that navitoclax causes thrombocytopenia (Vogler et al., 2011), trabecular bone loss and impaired osteoprogenitor function (Sharma et al., 2020).

ABT-737 and ABT-263 targets three anti-apoptotic proteins, BCL-2, BCL-W and BCL-X_L. There are currently studies to identify which of them is the crucial player responsible for apoptotic resistance in senescent cells. Direct inhibition of BCL-X_L alone by A1331852 and A1155463 had a strong senolytic effect on some but not all human and murine cells (Kirkland and Tchkonia, 2017, Zhu et al., 2017b, Leverson et al., 2015, Moncsek et al., 2018). It is unknown if direct inhibition of BCL-W would have a similar effect, as there is no BCL-W specific inhibitor available yet. However, TW-37, a drug which inhibits both BCL-2 and BCL-W but not BCL-X_L does not appear to be senolytic (Zhu et al., 2016). Moreover, a specific inhibition of other anti-apoptotic proteins, BCL-2 and MCL-1 had weak or no effect on survival of senescent cells (Chang et al., 2016a, Yosef et al., 2016a).

This supports hypothesis that BCL-X_L is the key player in senescence-associated apoptotic resistance.

The exact mechanism of BCL-X_L role in cellular senescence is not fully understood. However, one of the hypotheses highlights importance of the ratio of pro- and anti-apoptotic proteins (Childs et al., 2014). During cellular senescence, the pro-apoptotic proteins, such as BAK can be upregulated as a result of persistent stress (Chang et al., 2016a). To counteract the abundance of pro-apoptotic proteins, senescent cells express higher-level of anti-apoptotic proteins, like BCL-X_L. Therefore, inhibition of BCL-X_L release cell death mediators, such as BIM, that can further activate BAK and BAX, cell death executors.

1.7.2.2.1.1 BCL-X_L

The *BCL2L1* gene has two splice variants: the anti-apoptotic BCL-X_L and the pro-apoptotic BCL-X_S (Boise et al., 1993). The mRNA level of BCL-X_S is highly expressed in cells that undergo a high rate of turnover, such as developing lymphocytes, whereas a BCL-X_L mRNA has been detected in long-lived postmitotic cells, such as adult brain (Boise et al., 1993). The favour of splice variants seems to be condition-dependent and has been found to change after exposure to DNA-damage signals (Shkreta et al., 2011).

Apart of its role in cell death regulation, BCL-X_L has been found to regulate Ca^{2+} flux when localized to endoplasmic reticulum by which it contributes to maintenance of intracellular homeostasis (Eno et al., 2012). Moreover, it is thought to be involved in neuronal signalling through regulation of mitochondrial biomass, fission and fusion, which are important for synaptic activity in healthy neurons (Berman et al., 2009). Moreover, BCL-X_L is also involved in regulation of autophagy through binding and inhibition of evolutionarily conserved autophagy protein, Beclin-1 (Pattingre et al., 2005). Interestingly, The BCL-X_L role in regulation of autophagy has been linked to expression of BAX and BAK. In the absence of BAX and BAK, BCL-X_L had no effect on autophagy or cell death of myeloid or fibroblasts cell line. However, with active BAX and BAK, inhibition of BCL-X_L not only stimulated autophagy, but was also associated with increased cell death. These results indicate that in addition of BCL-X_L regulation of

Beclin-1, its function in autophagy could be also indirectly mediated through interactions with BAX/BAK (Lindqvist et al., 2014, Lindqvist and Vaux, 2014).

BCL-X_L is thought to play a dual role in cellular senescence. Some studies indicate its positive and some a negative correlation with survival of senescent cells. For instance, BCL-X_L was upregulated in $CD41^+$ megakaryocyte differentiation and subsequently senescence was reduced (Sanz et al., 2001). Moreover, overexpression of BCL-X_L in MEFs and primary cultured lymphocytes downregulated senescence-pathway markers, $p16^{INK4a}$, $p14^{ARF}$, $p21^{CIP}$ and SA-β-Gal (Borras et al., 2016). Mentioned above are examples of negative correlation between senescence and BCL-X_L expression.

In contrast, there are also evidences of BCL-X_L positive functions in cellular senescence. For instance, overexpression of BCL-X_L has been detected in several triple-negative breast cancer (TNBC) cell lines after induction of senescence through exposure to inhibitors of bromodomain and extra-terminal protein (BETi) (Gayle et al., 2019). In many cancer cells, response to BETi exposure vary and cells either undergo senescence or apoptosis. Authors revealed that in six tested human TNBC cell lines, the terminal cellular response to BETi is dictated by BCL-X_L expression level. In the cells that started to senesce, BCL-X_L level was higher than in those that underwent apoptosis. Moreover, forced overexpression of BCL-X_L in cells that normally undergo apoptosis shift them to senescence. In turn, inhibition of BCL-X_L induced apoptosis also in cells that were already senescent. Another study, on human lymphoma cell lines revealed that following DNA damage, BCL-X_L can translocate to the nucleus and binds to CDK1 during the G2/M cell-cycle checkpoint and its overexpression stabilizes senescence-like growth arrest. Arrested cells exhibited high level of SA-β-Gal activity and were unable to synthesize new DNA (Schmitt et al., 2007).

Interestingly, there is evidence of BCL-X_L contributing to aging. Transcriptomic studies of human peripheral blood mononuclear cells (PMBC) compared gene expression level between centenarians, septuagenarians and young people. Data revealed that centenarians had a high mRNA level of BCL-X_L (Borras et al., 2016). Centenarians have presumably higher numbers of senescent cells and high expression of BCL-X_L could contributes to successful elimination of surplus, thereby restoring the pre-damage status of the tissue (Serrano, 2017).

Moreover, authors performed longevity analysis using *C. elegans* with a gained function of Ced-9, ortholog of human BCL-X_L (Borrás et al., 2020). Data revealed that overexpression of Ced-9 promoted significant increase in mean and maximum lifespan. These data indicate potential involvement of BCL-X_L in longevity and healthy aging.
Moreover, throughout life, BCL-X_L expression is maintained in adult brain (González-García et al., 1995), whereas expression of other members of BCL-2 family gradually decline during development (Krajewska et al., 2002), which support the previous reports of BCL-X_L importance in mature neurons function (Li et al., 2008, Li et al., 2013).
Inhibition of BCL-X_L is considered as potential senotherapy. Indeed, BCL-X_L knock-down with siRNAs affected survival of senescent cells but not proliferating human abdominal subcutaneous preadipocytes (Zhu et al., 2015a). Moreover, treatment with senolytics, Dasatinib and Quercetin, significantly reduced level of BCL-X_L in the tissues of treated mice (Zhu et al., 2015a). The joined inhibition of BCL-X_L, BCL-W and BCL-2 by ABT-263 or ABT-737 showed strong senolytic potential (Zhu et al., 2016, Chang et al., 2016a, Zhu et al., 2017b) and that was further confirmed by specific inhibition of BCL-X_L using A1331852 and A1155463 (Zhu et al., 2017b). However, BCL-X_L inhibition is associated with side effects as thrombocytopenia and it should be tested if a single inhibition of BCL-X_L is less cytotoxic than mutual inhibition of BCL-X_L, BCL-2, BCL-W.

Taken together, BCL-X_L is involved in the three interconnected main defence responses of the cell: autophagy, senescence and apoptosis, which depending on the circumstances can be both beneficial and detrimental (Borrás et al., 2020). Presumably, the decision could be dependent on several factors, such as cell type, genetic background, type and level of stress, and the influence of surrounding microenvironment. Involvement of BCL-X_L in healthy aging can be related to its contribution to keep the energy balance through regulation of ATP synthesis in mitochondria (Alavian et al., 2011). During healthy aging, BCL-X_L may control cells survival manly through autophagy and apoptosis, therefore longevity can be associated with high level of BCL-X_L, such as in the case of centenarians (Borrás et al., 2020). That also suggests that certain number of senescent cells is required for successful aging. However, during ordinary or chronic aging, an inefficient immune system fails to eliminate the surplus of senescent cells and in that scenario, BCL-X_L might be a ‘double

player', which actually contributes to accumulation of senescent cells. Nevertheless, further studies are needed to confirm mentioned above hypotheses, and to elucidate BCL-X_L dual behaviour it is crucial to fully understand its biological function.

1.7.3 Second generation of senolytics

Second generation of senolytics consist of drug-delivery approaches that selectively target and eliminate senescent cells. Second generation of senolytics represents a class of drugs that mechanism of action can be linked with targeted therapies in which, senescent cells act as a target **(Table 1.4**). These therapies, although not without adverse effects, aims to inhibit a molecule of interest with a minor effect on neighbouring microenvironment (Walter and Ahmed, 2017, Ke and Shen, 2017). Targeted therapies have been primarily developed as anti-cancer strategies. However, they have been tested in other diseases as well (Florence and Lee, 2011, Daste et al., 2016, Pauliah et al., 2018). Paul Ehrlich, a German physician was the first person who introduced the concept of using a selective vehicle to deliver a cytotoxic drug to a tumour (Ehrlich, 1906, Perez et al., 2014). Since then, targeted therapies have been continuously studied and improved. Targeted therapies can be more specific and more effective than traditional approaches due to the lower rate of offsite targeting and cytotoxicity.

The usage of targeted therapies in the context of cellular senescence seems to be a promising approach. The goal will be to eliminate senescent cells more specifically than standard senolytics treatment based on chemotherapy for cancer. Several approaches using targeted therapies are under development and will be shortly discussed here. Some of them exploit senescent surfaceome based on the presence of extracellular epitopes but there are also others against intercellular targets. Among them, we can distinguish therapies based on nanoparticles, monoclonal antibodies and the immune system (***Figure* 1.4**).

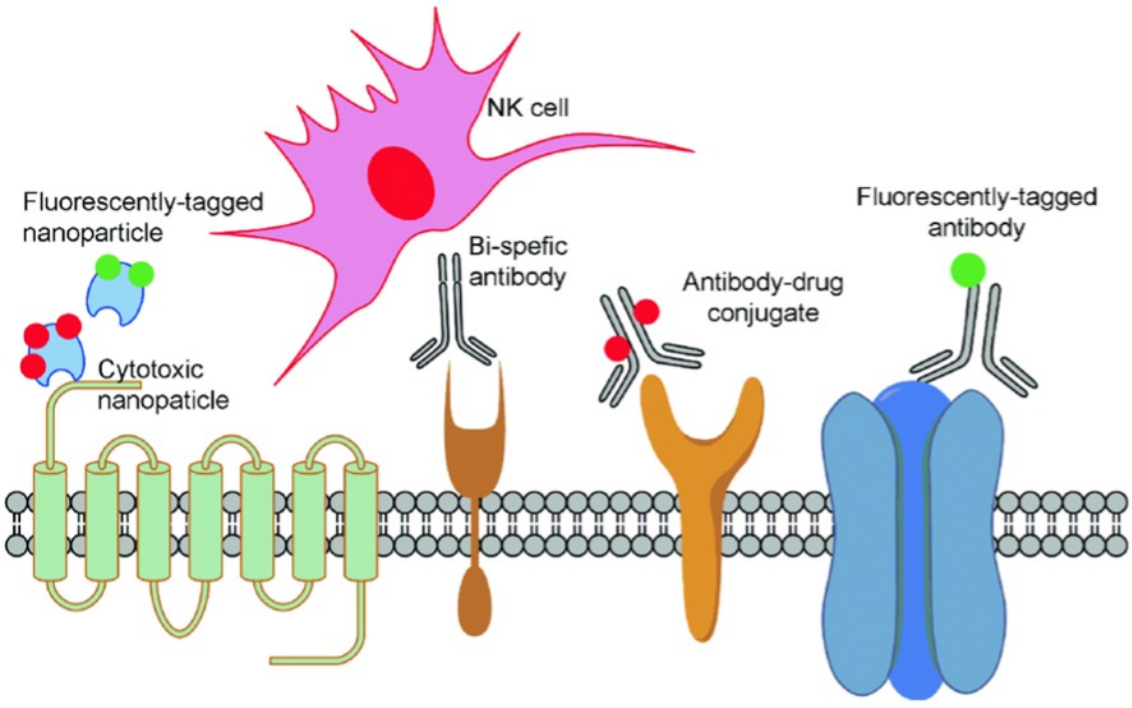

Figure 1.4. Summary of targeted senolysis therapies based on the senescent surfaceome.

Schematic representation of different approaches to targeted senolysis using surfaceome proteins. Presented strategies are further described in this chapter. Adapted from (Ekpenyong-Akiba et al., 2020b)

1.7.3.1 Nanoparticles

The first published usage of nanoparticles applied to target senescent cells was based on senescence-associated β-galactosidase activity (Munoz-Espin et al., 2018). After internalization by endocytosis, galactosidase-encapsulated drugs trafficked to lysosomes for digestion and the drug or fluorescent cargo was released. Due to high level of lysosomal β-galactosidase, senescent cells were able to lyse the galactosidase coat, while the cargo was protected in the other cells (Agostini et al., 2012, Muñoz-Espín et al., 2018b). This system of drug delivery was shown to work *in vivo* using tumour xenografts and bleomycin-induced pulmonary fibrosis mouse model (Muñoz-Espín et al., 2018b). In both cases, senescent cells burden was decreased by nanoparticles treatment and disease progression reduced. Moreover, the same research group designed Nav-Gal, a pro drug generated by galacto-conjugation of navitoclax and its activity was tested in wide range of cell type (González-Gualda et al., 2020b). Nav-Gal selectively induced apoptosis in senescent cells with reduced toxicity in nonsenescent

cells, when compared to Navitoclax. Moreover, combination of Nav-Gal with cisplatin efficiently reduced lung tumour growth *in vivo*. Additionally, treatment with Nav-Gal revealed reduced platelet toxicity compared to Navitoclax, which indicates that galacto-conjugated Navitoclax can act as effective senolytic *in vivo* with reduced level of its associated toxicities.

A similar concept has been used by another group which designed galactose-modified duocarmycin derivatives (GMD) and tested their senolytic activity *in vitro* and *in vivo (Guerrero et al., 2020)*. Among the GMDs, the authors tested JHB75B, JHB76B and JHB35B with all of them able to preferentially kill senescent cells in an oncogene-induced senescence cell model ER:RAS IMR90. JHB75B, named as prodrug A, has been further tested *in vivo*. Results revealed that prodrug A reduced the presence of senescent cells in mice lung after irradiation and preferentially eliminated preneoplastic senescent cell clusters in a mouse model of pituitary paediatric tumour.

Senescence-specific killing compound 1 (SSK1) is another example of a prodrug that has been found to selectively eliminate senescent cells (Cai et al., 2020). SSK1 consists of galactose-modified gemcitabine and its senolytic activity was confirmed using mouse and human cellular models of replicative, oncogene and stressed-induced senescence. Additionally, SSK1 decreased the number of senescent cells in bleomycin-induced lung-injured mice. Similar results were observed after the SSK1 treatment of aged mice, together with decreased expression of SASP-associated genes in aged livers and kidneys. Moreover, SSK1 treatment has been found to improve physical function of aged mice as measured by rotarod, treadmill and grip strength performance (Cai et al., 2020).

The SA- β-galactosidase activity was used in other study as well, where authors used enzyme-instructed peptide self-assembly (EISA). EISA triggers formation of nanofibers and hydrogels specifically in cells of interest, in this case in senescent cells. Formation of nanostructures inhibit the expression of core senescence regulators p53, p21 and p16 and lead to induction of apoptosis (Xu et al., 2019).
Another example of usage β-galactosidase enzymatic activity was presented by (Thapa et al., 2017b). Authors used porous calcium carbonate nanoparticles coated with

conjugate of lactose and loaded with mTOR and SASP inhibitor, rapamycin. To increase specificity, authors tagged them to monoclonal antibody against CD9. CD9 is a glycoprotein receptor of tetraspanin family that regulates cellular growth, activity and motility (Maecker et al., 1997, Thapa et al., 2017b). These nanomolecules were tested in human fibroblasts subjected to extensive culture and results confirmed their senolytic activity through targeted drug delivery to senescent cells mediated by CD9 receptor.

An alternative approach taking advantage of nanotechnology would be the use of Molecularly Imprinted NanoPolymers (nanoMIPs). They are synthetic antibody-like molecules characterized by high stability, cost effectiveness, long shelf time and no need for animal usage during production (Sellergren and Allender, 2005, Piletsky et al., 2006, Vasapollo et al., 2011b, Canfarotta et al., 2016a, Canfarotta et al., 2016b). NanoMIPs consists of a matrix synthetised from methacrylic or acrylic polymer specific by a shape to template target molecule. The production of nanoMIPs relies on the immobilization of a template molecule on a solid surface, like glass beads. Immobilized template is incubated with mixture of monomers and by the process of polymerisation, the polymer nanoparticles are formed (Vasapollo et al., 2011a). Next, remaining monomers and low-affinity polymers are removed together with the template molecule. The final product is nanoMIP cavity complementary to target's shape and functional groups (**Figure 1.5**).
The advantage of this approach is that nanoMIPs possess high affinity and specificity toward the targets. These "plastic antibodies" have been tested as potential detection tools in different cancers (Sengupta and Sasisekharan, 2007, Voigt et al., 2014, Tyagi et al., 2016, Cecchini et al., 2017b) and drug delivery systems (Sellergren and Allender, 2005, Cunliffe et al., 2005, Puoci et al., 2011, Tieppo et al., 2012, Kempe et al., 2015, Luliński, 2017).
Therefore, it could be beneficial to repurpose nanoMIPs and use them for detection of senescent cells or as drug delivery tool against an extracellular senescent surfaceome marker for nanoparticles to bind.

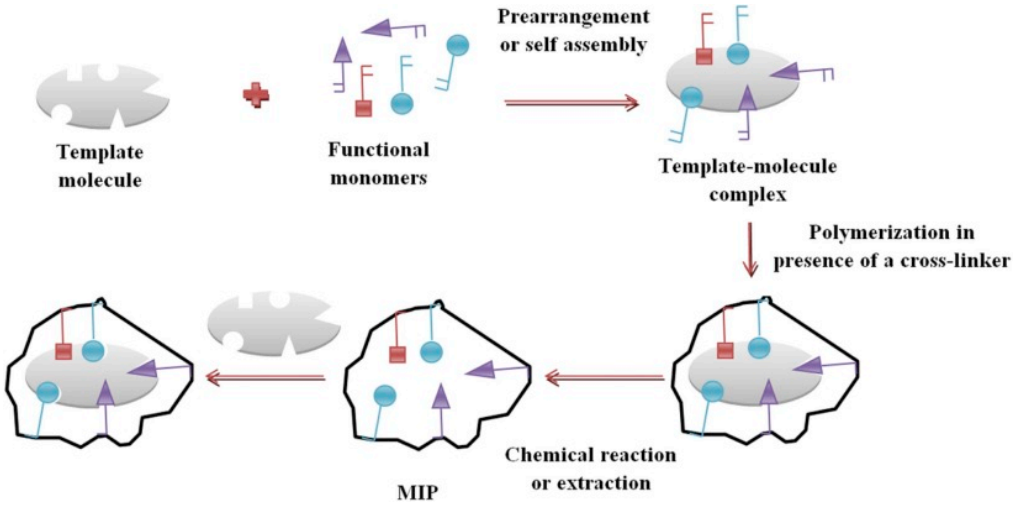

Figure 1.5. Schematic representation of molecular imprinting

Image adapted from (Płotka-Wasylka et al., 2015).

In our lab, nanoMIPs were produced against one of the previously identified surfaceome marker, β2-Microglobulin (B2M) (Ekpenyong-Akiba et al., 2019). These nanoMIPs were fluorescently tagged and their selectivity for senescent cells was confirmed *in vitro*. For that purpose, EJp16 bladder cancer cell line was used. EJp16 contains tetracycline(tet)-regulatable p16 expression system, upon activation of which these cells senesce. Senescent and control cells were incubated with fluorescently tagged B2M nanoMIPs and data revealed preferential accumulation of nanoparticles in the membrane of senescent cells (**Figure 1.6**). Thus, confirmed that nanoMIPs were able to selectively target senescent cells through surfaceome marker.

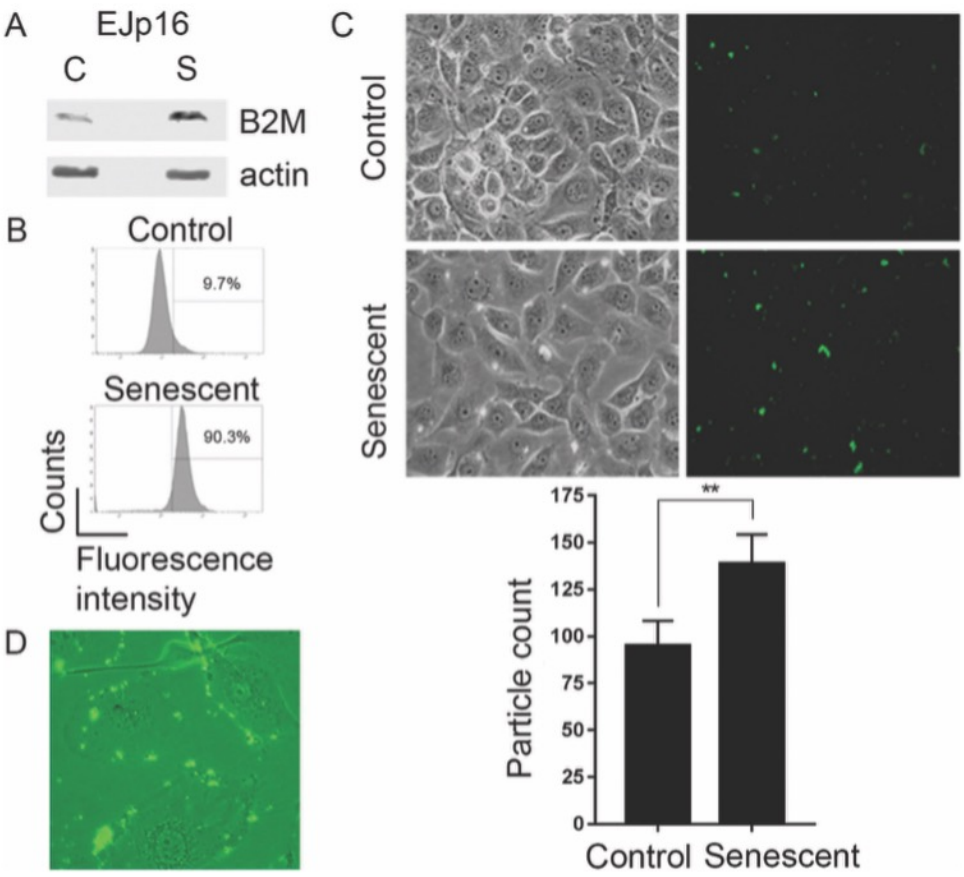

Figure 1.6. Fluorescent nanoMIPs selectively bind to senescent cells.

*Figure adapted from (Ekpenyong-Akiba et al., 2019).[A] Representative Western blot showing B2M expression in EJp16 proliferating and senescent cells 4 days after senescence induction. β-actin was used as a loading control. [B] FACS analysis of proliferating and senescent EJp16 incubated with fluorescent B2M nanoMIPs. Numbers show the percentage of cells postivie for green fluorescence above background levels, which is indicative of cells to which the nanoMIPs attached. [C] Representative fluorescent microscopy images of EJp16 cells taken 4 hours after incubation with nanoMIPs. Fluorescent particles in each microscopic field were quantified using Image J software. Results show mean ± SD of triplicate independent experiments. **p < 0.005 (unpaired t-test). [D] Representative fluorescent microscopy images from the same cells showing that nanoMIPs bind to the membranes of senescent EJ16 cells.*

Next, B2M nanoMIPs were conjugated with a senolytic, dasatinib and their selectivity in elimination of senescent cells was tested using the same cell line (**Figure 1.7**). Results showed that treatments of dasatinib-conjugated B2M nanoMIPs significantly reduced viability of senescent EJp16 cells, when compared with proliferating counterparts. Of note, treatment of clear B2M nanoMIPs (not conjugated to the drug) had no effect on viability of treated cells, demonstrating that nanoMIPs had no cytotoxic effect on their own. This supported the hypothesis that nanoparticles could be used to successfully deliver the drug into senescent cells, minimizing the impact on other cells.

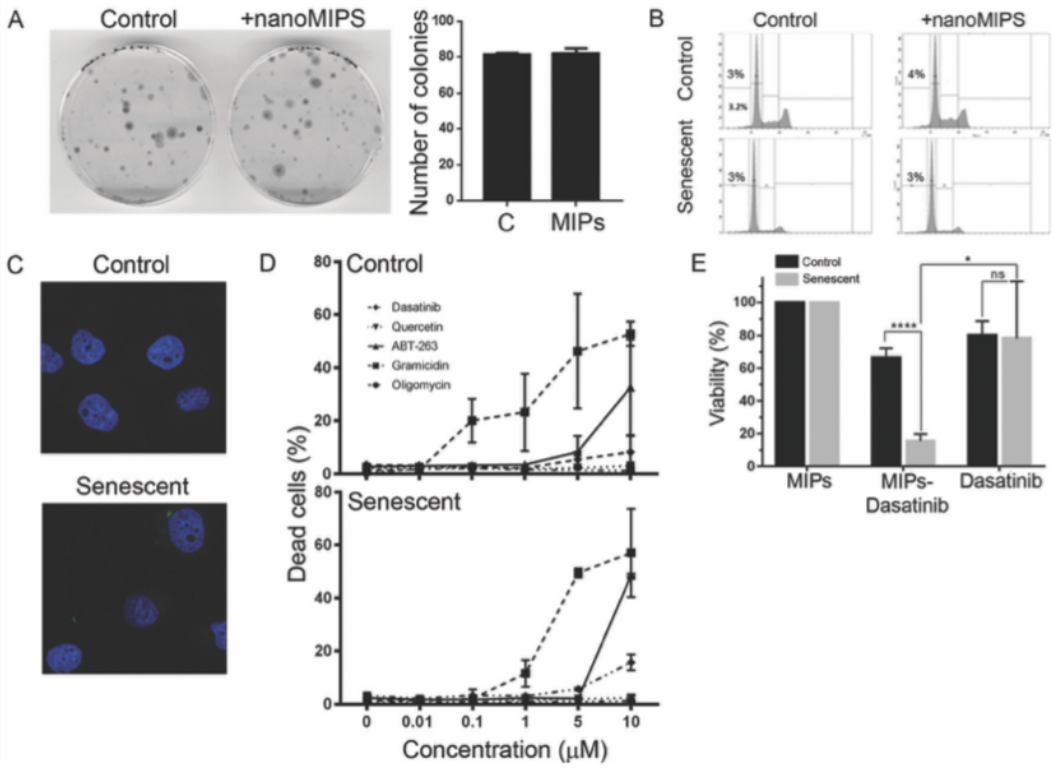

Figure 1.7. Targeted delivery of drugs into senescent cells by nanoMIPs.

*Figure adapted from (Ekpenyong-Akiba et al., 2019). [A] Representative images of colony formation assays of control EJp16 (cultured in the presence of tet) incubated with nanoMIPs. Experiment was performed twice in duplicate. Graph shows the mean ± SD. [B] Representative FACS cell cycle analysis of PI-stained EJp16 cells incubated with B2M nanoMIPs for 24 hours. Percentages of cell death (subG1 populations) are indicated. [C] Representative confocal microscope images of control and senescent EJp16 fixed with formalin and stained with DAPI 24 hours after incubation with B2M nanoMIPs at 37 1C. [D] Percentage of cell death, as measured by PI staining, of control and senescent EJp16 treated with different concentrations of oligomycin, gramicidin, ABT-263, quercetin and dasatinib for 48 hours. Results represent the average of three independent experiments. Error bars show standard deviation. [E] Cell viability measured by an MTS assay of proliferating and senescent EJp16 (4 days after tet removal) treated with B2M nanoMIPs, 10 mM Dasatinib-conjugated B2M nanoMIPs or 10 mM Dasatinib for 24 hours. Results show average ± SD of four replicates. *p < 0.05; ****p < 0.0005; ns: not significant (two-tailed paired t tests).*

Further, ability of B2M nanoMIPs to recognize senescent cells was tested *in vivo* and these data are presented in the **Chapter 4.1.**

1.7.3.2 Antibody- based therapies

An antibody-based drug delivery system could be an alternative to nanoparticles. Antibody-drug conjugates (ADCs) are biopharmaceutical drugs designed as a targeted therapy, especially for cancer treatment. Nowadays, several ADCs has been tested in clinical trials to target different cancers, such as breast cancer (Trail et al., 1993, Kolodych et al., 2017, Trail et al., 2018), ovarian cancer (Jiang et al., 2016), lung and colon cancers (Trail et al., 1993). Moreover, there are three ADCs already approved by the USA Food and Drug Administration (FDA), two of them for treatment of haematological cancers: Mylotarg® and Adcetris®, and Kadcyla® for the treatment of breast cancer.

ADCs consists of monoclonal antibodies conjugated to cytotoxic compounds through a chemical linker (Strohl and Strohl, 2012, Casi and Neri, 2012, Perez et al., 2014, Gébleux and Casi, 2016, Kumar et al., 2017). During the design of the ADC, a crucial role play an internalization rate, linker stability, the drug to antibody ratio (DAR) and payload potency (Sievers and Senter, 2013, Perez et al., 2014, Gébleux and Casi, 2016, Kolodych et al., 2017, Trail et al., 2018). All of these factors can be used as determinants of ADCs efficacy.

Because of their well-known therapeutic potential, ADCs might be used as another drug delivery tool to target and eliminate senescent cells from the body. In our lab, we explored the usage of ADCs which targeted extracellular epitopes of the surfaceome, and the outcomes of this study are described in results chapter (**Chapter 4: 4.1.2**).

Another example of antibody's usage in targeted therapies is antibody-dependent cell-mediated cytotoxicity (ADCC). This method guides natural killer (NK) cells to eliminate a target (Lo Nigro et al., 2019). This approach has been already tested in the context of cellular senescence. For that purpose, a DPP4, a senescent surfaceome marker mentioned above, has been used as a target (Kim et al., 2017). First, human peripheral blood mononuclear cells were used for isolation of NK cells and then, NK cells were added to condition media of WI-38 proliferating and senescent cells previously incubated with anti-DPP4 antibody. Results revealed a significant reduction in senescent

cell viability comparing to proliferating controls. In this way, results confirmed that NK cells were attracted to DPP4-expressing senescent cells.

1.7.3.1 Other cellular approaches

Another approach that can be classified as second generation of senolytics are CAR T, which were used against the recently identified senescent surfaceome marker uPAR (Amor et al., 2020). Chimeric antigen receptors (CARs) are synthetic receptors that target and reprogram T cells specificity and function (Sadelain et al., 2017). Authors designed uPAR-specific CAR T cells and tested its specificity in elimination of senescent cells *in vivo* (Amor et al., 2020). Results revealed reduced number of senescent cells, significantly prolonged survival of treated mice, reduced collagen deposition in liver fibrosis and decreased level of ALT and AST, enzymes commonly used as markers of liver damage (Nyblom et al., 2006). These data provide a first indication of CAR T therapeutic potential in age-related pathologies.

Second generation of senolytics represents targeted delivery of drugs specifically to senescent cells. They could be an attractive approach as an anti-senescence therapy. Especially, targeted senolytics could increase effectivity and reduce the range of side effects. However, this area of research is still in early stages and more works should be done to explore this field. For both, first generation and second generation of senolytics (**Figure 1.8**) it is crucial to define *in vivo* safety profile including pharmacodynamics of each potential anti-senescence candidate, appropriate dose, length of the treatment or possible side-effects. It will be also essential to identify potential synergism when used in combination with other medications and determine contradictions or antagonistic events.

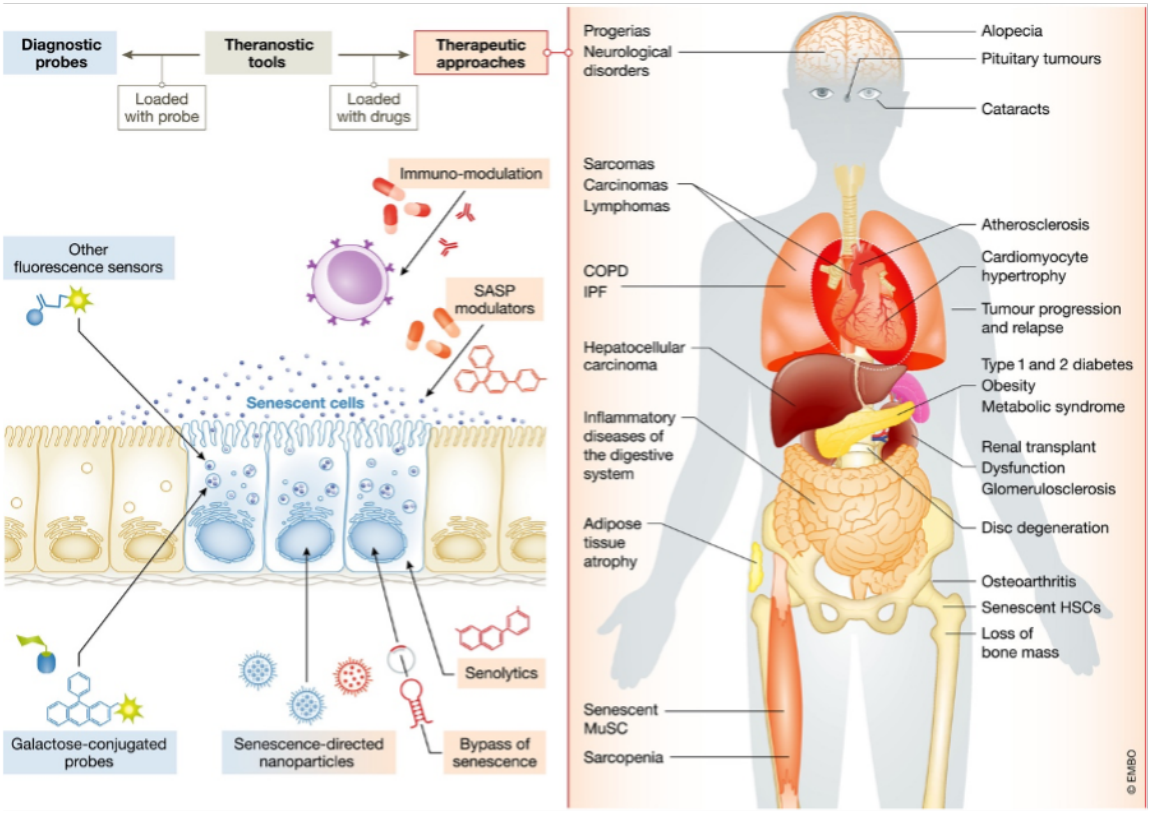

Figure 1.8. Therapeutic approaches in senescence-associated disorders.

Cellular senescence is associated with multiple pathological disorders (right). Clearance of senescent cells or reduction of senescent phenotype acts as potential approach for diagnostic and targeted senotherapeutic interventions (left). Among senotherapies there are compounds that blocks negative senescent phenotype, such as SASP modulators (senostatics, senomorphics), prevent accumulation of senescent cells before they emerge (senoblockers) or eliminate senescent cells that are already present in the tissue (senolytics). Discovery of senolytics offers a therapeutic potential for monitoring of senescent cells burden in the clinic. To date, senolysis therapies compromise identification of first-generation senolytics that combine natural and chemical compounds, and development of second generation of senolytics, that selectively detect senescent cells and specifically deliver the drug into them. Second generation of senolytics includes galactose-conjugated probes, senescence surfaceome-directed nanoparticles, immuno-modulators and others. Image adapted from (Paez-Ribes et al., 2019)

1.8 Senoblocking

One type of senotherapies focuses on preventing the accumulation of senescent cells before they emerge. Therefore, it is called senoblocking as, it prevents cellular senescence before it is triggered. Any therapy which abrogates either p53-p21 or p16-pRb pathways may class as a senoblocking agent. However, to date only one study has looked at the effects of senoblocking in mice, which were treated throughout their lives, starting from 8 weeks of age till the human end points were reached (Ekpenyong-Akiba et al., 2020a) **(Figure 1.9**). Mice were treated with Ibrutinib, a BTK inhibitor. Previously published *in vitro* data showed that BTK inhibition, (further described in **1.6.1**), prevents stabilization of p53 (Althubiti et al., 2016b). As BTK cannot phosphorylate p53 and MDM2, MDM2 successfully ubiquitinate p53 for degradation and senescence-relate growth arrest is blocked (Rada et al., 2017). Thus, it was reasoned that BTK inhibition could prevent accumulation of senescent cells *in vivo*. Therefore, prematurely aged mice (**2.13.1**), in which progeria phenotype is partly mediated by pathological increase in p53 signalling (Varela et al., 2005), were given 10 mg/kg of Ibrutinib or vehicle (DMSO and water) as a control. Data revealed no significant changes in average lifespan of treated mice when compared to control (**Figure 1.9A**). However, there was a significant increase in maximum lifespan (from 202 to 230 days) (**Figure 1.9A**). Moreover, these mice were assessed for signs of clinical frailty (**Figure 2.2**). In the first 4 months after initial start of the treatment, there were no major differences between treated and control group of mice. However, after that point the health of control animals started to deteriorate, while in Ibrutinib-treated mice it was preserved (**Figure 1.9B,C**). Importantly, there were no visible tumours in tested animals, which could result from the inhibition of core tumour suppressor, as p53. These data showed that prolonged treatment of Ibrutinib ameliorated negative effects of aging in *ZMPSTE24*$^{-/-}$ mice by reduction of frailty and increase of their maximum lifespan.

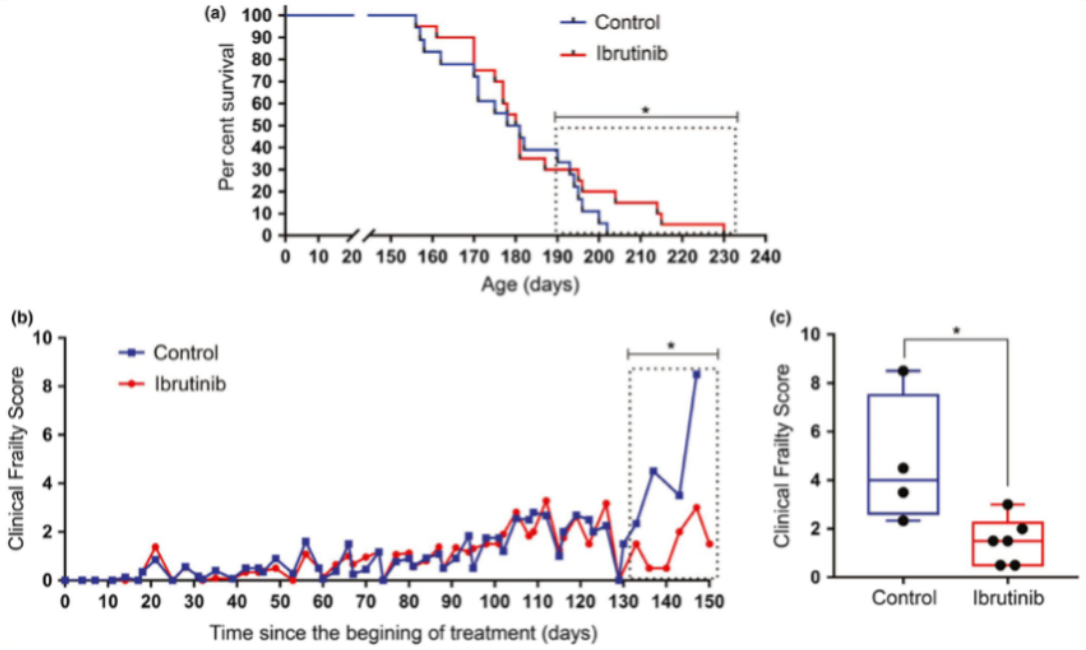

Figure 1.9. Effect of Ibrutinib on lifespan and healthspan of progeroid mice.

*Adapted from (Ekpenyong-Akiba et al., 2020a). [A] Kaplan-Meier survival curve for ZMPSTE24$^{-/-}$ mice treated with 10 mg/kg Ibrutinib or vehicle (control). There were no significant differences in median lifespan between control and treated mice (log-rank Mantel-Cox test, p=0.2813). However, the maximum lifespan of the longest-lived mice (boxed area) differed significantly. [B] Clinical Frailty Score in the same experiment. See (**Figure 2.2**) for parameters used. Each parameter is scored as absent (0), mild (0.5), or severe (1) and the total sum of values is presented. Data are presented as mean of the values. [C] Late life clinical frailty scores of the boxed area in [B], each dot represents one mouse. Data show median, upper and lower quartiles (box) and lowest and highest values (error bars) Analysis in boxed area performed using unpaired t-test, *p=0.0248. For each of the graphs: n=18 (control) and 20 (Ibrutinib).*

To further determine the effect of Ibrutinib treatment on the healthspan, tissue specific analysis was performed. Results revealed that BTK expression increased in brains of old wild-type animals, when compared with young concomitantly with p16 expression (**Figure 1.10**), which is a known marker of senescent cells (Baker et al., 2011)

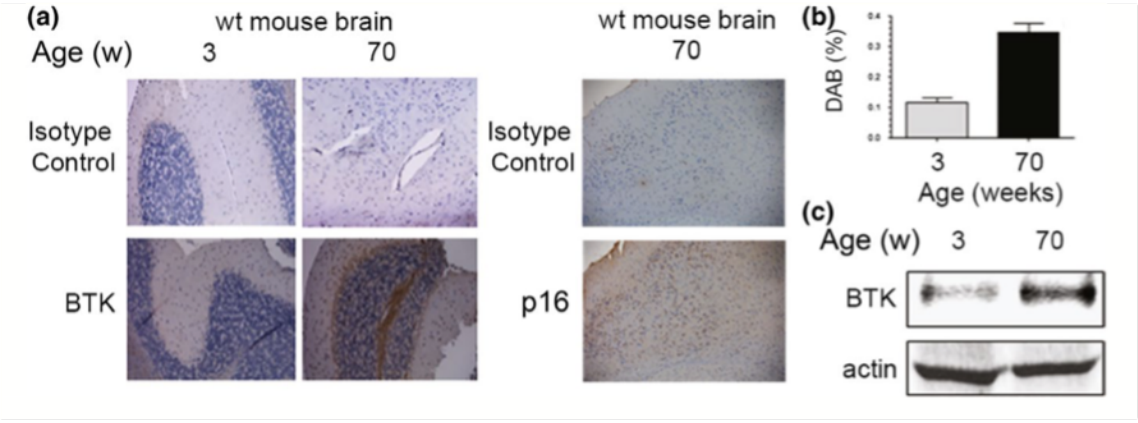

Figure 1.10. BTK expression increased with age in mouse brains

[A] Representative pictures of Immunohistochemical staining of wild-type young (3 weeks) and old (70 weeks) mice brains compared to isotype control and p16 antibody as aging positive control [B] Quantification of samples in [A] from 3 mice per group. Graphs represents mean ± SD. [C] Representative Western blot of whole brain lysates from the same mice showing expression level of BTK. ß-actin was used as a loading control

Further biochemistry analysis of the brain tissues was performed to determine if BTK inhibition prevent the age-dependent accumulation of senescent cells. Analysis of this experiment are described later in the results chapter (**Chapter V: 5.1.1**).

Moreover, data revealed differences in anxiety-like behaviour of treated animals, which has been strongly associated with aging (Perna et al., 2016). This was tested using Elevated Plus Maze (EPM). The EPM is widely used behavioural assay for rodents. The test assembly consist of elevated platform with two open and two enclosed arms (**Figure 1.11A**) (Pellow et al., 1985, Treit et al., 1993). The model was designed to test animal's aversion to open spaces and tendency to be thigmotaxic, a preference to remain in enclosed spacer or close to the edges of a bounded space. The more time mice spend on the open arm indicates lower level of anxiety. Data revealed that at the beginning of the treatment, both groups, Ibrutinib treated and control mice entered to open arms and spent similar time in open space. However, with time, when animals got older, control mice were not keen to explore the open arms, while Ibrutinib-treated mice still examined them (**Figure 1.11B**). These data exposed that inhibition of BTK was able to partially reduced anxiety-like behaviour in tested mouse model.

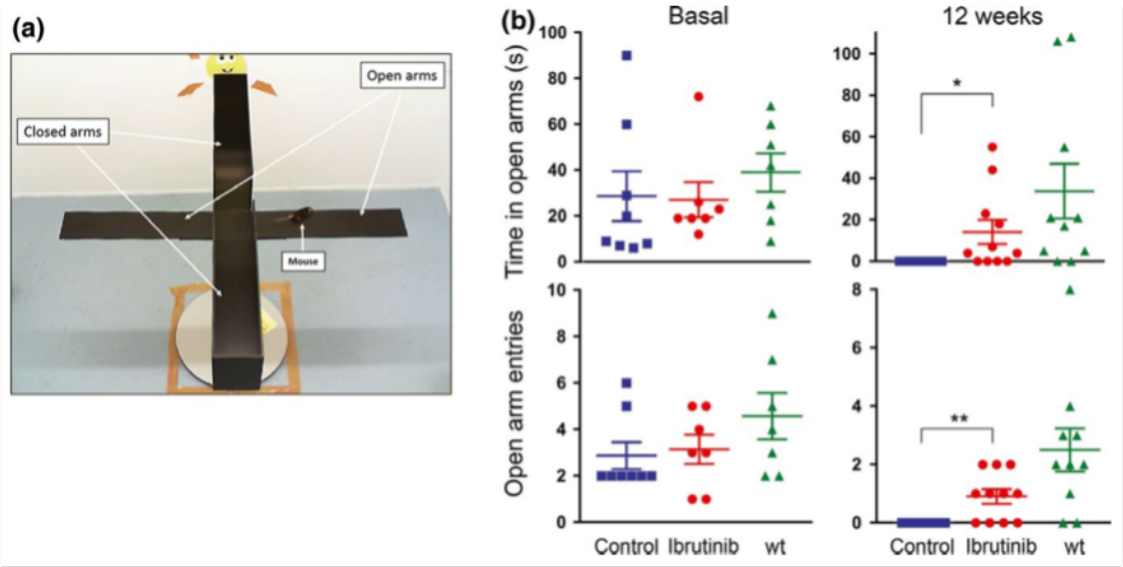

Figure 1.11. BTK inhibitor reduce anxiety-like behaviour in progeria mice.

*The anxiety-like behaviour was compared between ZMPSTE24$^{-/-}$ mice treated with 10mg/kg Ibrutinib and vehicle-treated controls and untreated wild-type mice using the elevated plus maze [A]. [B] Quantification of average entries and time spent by animals in the open arm of an Elevated plus maze. Experiment performed 12 weeks after beginning of treatment. Each dot represents single mouse. Error bars show SD. n=10 for each group. Statistical significance measured using one-way ANOVA and unpaired t-test (*p=0.03, **p=0.003).*

Moreover, treatment with Ibrutinib preserved age-related memory decline in treated animals. These data are presented and explained in results **Chapter 5.1.1.**

Mentioned above are the first indications of continuous senoblocking therapy. Some of the data presented further in the results chapter were used in this publication (Ekpenyong-Akiba et al., 2020a).

1.9 Senomorphics

Among senotherapies, a group of drugs, that can interfere with SASP, are called senomorphics (**Table 1.5**). SASP is the main feature of senescence, that is responsible for its detrimental function. It can accelerate cancer and aging and trigger mutagenesis in surrounding microenvironment. SASP composition might be cell and tissue specific and dependent on inducing stimuli. To fully understand function of SASP it is essential to tease apart its elements and focus on the key regulator responsible for its beneficial or detrimental role. Therefore, the majority of senomorphics target one or a group of SASP factors and simultaneously might or might not affect other features of cellular senescence, such as cell cycle arrest (Picallos-Rabina et al., 2020). Among senomorphics there are inhibitors of NFκB (e.g., metformin, resveratrol, simvastatin). NFκB has been identified as a master regulator of SASP (Chien et al., 2011). Suppression of NFκB *in vitro* resulted with immune system failure to recognize senescent cells and changes in SASP composition. *In vivo* studies using a mouse lymphoma model, revealed that NFκB inhibition bypasses chemically induced senescence, promotes drug resistance and reduce survival. These data demonstrate that NFκB controls both intrinsic and extrinsic aspects of cellular senescence, including SASP (Chien et al., 2011).

Another crucial regulator of SASP is mTOR and its inhibitor has been tested in the context of senotherapies (e.g., rapamycin) (Wang et al., 2017b). Inhibition of mTOR revealed decreased cancer invasiveness through reduced epithelial-mesenchymal transition (EMT) elicited by condition media derived from senescent cells (Herranz et al., 2015a). Also, inhibition of mTOR reduced the paracrine induction of senescence mediated by SASP factors present in condition media. Moreover, co-injection of tumour cells with senescent cells that promoted tumour growth was reduced after mTOR silencing through shRNA.

Bromodomain containing 4 (BRD4) is another important player regulating the SASP (Tasdemir et al., 2016). It is a member of bomodomain and extra terminal domain (BET) family, which is consist of important transcriptional regulators (Hajmirza et al., 2018). BRD4 inhibition led to elimination of senescent cells but also disruption of immune

surveillance through decreased SASP and changes in senescence paracrine activity, macrophage polarization and impaired NK cytotoxic activity (Tasdemir et al., 2016).

Although the senomorphic strategy is in its infancy, the beneficial effect of senomorphics is quite clear. However, inhibition of SASP can carry risk of on-target side effects, especially in processes where short-term SASP might be beneficial, such as promotion of tumour immune surveillance, tissue remodelling and repair retardation (Muñoz-Espin and Demaria, 2020).

Each of the three strategies, senolysis, senoblocking and senomorphosis have potential to prevent age-related diseases and contribute to improved healthspan (Kirkland and Tchkonia, 2017, Childs et al., 2017, Ekpenyong-Akiba et al., 2020a). They all have beneficial and negative aspects. Senolysis seems to be the most attractive strategy to combat aging and age-related diseases, as it requires less drug exposure to eliminate senescent cells. Even if the clearance of senescent cells burden is not permanent, the restoration of senescent cells number is not happening rapidly but requires time. That helps to avoid multiple treatments within a short period of time and thus decreases drug toxicity and can lead to a more durable effect than senomorphic inhibition of SASP or senoblocking treatment throughout long periods of time. Prolonged inhibition of p53 or pRB pathways, as it is in senoblocking, might accelerate progression of tumours as the main tumour suppressors pathways are continuously blocked. However, currently available senolytics are still characterized by high level of on- and off- target cytotoxicity. Their specificity should be first extensively tested across a range of primary cells, as cultured-cell lines are usually acclimated strains with abnormal genes expression and also carefully tested *in vivo* to assess the true impact of the drug in tissue heterogenic environment. Therefore, it is difficult to contend that any particular candidate senolytic drug would be universally effective for all senescent cells' types. Therefore, next generation of senolytics should involve targeted senolytics, which specifically deliver a drug into senescent cells, and combination therapies that would be more specific and characterized by reduced level of side effect.

Table 1.3. Summary of main first-generation senolytics.

Compounds	Targets	Validation Models	Clinical Trials	References
First-generation senolytics				
Dasatinib	Pan-receptor tyrosine kinases (including ephrin B1)	- Irradiated human preadipocytes, - human lung fibroblasts, - MEFs, mouse preadipocytes (adipose-derived stem cells) - Mice whole body irradiation, progeria (*Ercc1*−/Δ) and chronological aging - atherosclerosis ($ApoE^{-/-}$)	**D+Q:** - Phase II, (NCT02848131) for chronic kidney disease, - phase II (NCT04313634) for skeletal health, - phase I/II (NCT04063124) for Alzheimer disease	(Zhu et al., 2015b)
Quercetin	Numerous (including PI3K)	- HUVECs, human lung fibroblasts (IMR-90), mouse bone marrow-derived stem cells, MEFs	**D+Q:** - Phase II NCT02848131) for chronic kidney disease, - phase II (NCT04313634) for skeletal health, - phase I/II (NCT04063124) for Alzheimer disease	(Zhu et al., 2015b)

Fisetin	PI3K/AKT/mTOR	- Senescent cells and SASP in progeroid and aged mice in vivo;	- Phase I/II (NCT04210986) for osteoarthritis of the knee, - phase II (NCT04313634) for skeletal health	(Zhu et al., 2017a, Yousefzadeh et al., 2018)
ABT-737	BCL-2, BCL-X_L and BCL-W	- Senescent IMR90, - Senescent cells in lungs and epidermis of mice	Preclinical animal models	(Yosef et al., 2016b)
ABT-263 (navitoclax)	BCL-2, BCL-X_L and BCL-W	- Senescent HUVECs, human fibroblasts and MEFs, - Senescent hematopoietic stem cells and muscle stem cells in aged and irradiated mice,	- Phase I/II (NCT00445198), - Phase II (NCT02591095), - Phase I (NCT02520778), - Phase II (NCT02079740) for various cancers	(Chang et al., 2016b, Demaria et al., 2017, Childs et al., 2016a, Bussian et al., 2018, Kim et al., 2017)
A-1331852	BCL-X_L	- Senescent HUVEC and senescent human lung fibroblasts	Preclinical models of senescence in vitro	(Zhu et al., 2017a)
A-1155463	BCL-X_L	- Senescent HUEVEC and senescent human lung fibroblasts -	Preclinical models of senescence in vitro	(Zhu et al., 201

EF24	Proteosomal degradation of BCL-2 family proteins	- Senescent human fibroblasts (WI-38, IMR90), epithelial cells (HUEVEC and HREC), preadipocytes	Preclinical models of senescence in vitro	(Li et al., 2019b)
Cardiac glycosides (including oubain and digoxin)	BCL-2, BCL-X_L and BCL-W (prosurvival proteins) Na^+/K^+ ATPase	- Senescent A549, primary fibroblasts and osteoarthritic chondrocytes. - Enhanced the effect of chemotherapy against xenografts in mice, - Senescent cells and fibrosis in mouse model of lung fibrosis	Preclinical animal models	(Guerrero et al., 2019b, Triana-Martínez et al., 2019b)
Azithromycin and Roxithromycin	Autophagy, metabolic	- Senescent MRC-5 and BJ fibroblasts	Preclinical models of senescence in vitro	(Ozsvari et al., 2018)
UBX0101	MDM2 and p32	- Human primary chondrocytes - p16-3MR transgenic mouse model with post-traumatic osteoarthritis -	Phase II (NCT04129944) for osteoarthritis of the knee	(Jeon et al., 2017)
Panobinostat	HDAC	- Chemotherapy-induced senescent NSCLC and HNSCC cells	Approved for multiple myeloma	(Samaraweera et al., 2017)

Geldanamycin, Tanespimycin, Alevspimycin 17-DMAG	HSP90	- *Ercc1*−/− MEFs	Preclinical models of senescence in vitro	(Fuhrmann-Stroissnigg et al., 2017b)
Piperlongumine (and analogues)	OXR1 (unknown)	- Irradiated human lung fibroblasts (WI-38)	Preclinical models of senescence in vitro	(Wang et al., 2016a, Liu et al., 2018)
BET protein degrader	Bromodomain and extraterminal domain family protein	- Senescent hepatic stellate cells	Preclinical animal models	(Wakita et al., 2020)

Table 1.4. Summary of main second-generation senolytics and senoblockers.

Second-generation senolytics				
Compounds	**Targets**	**Validation Models**	**Clinical Trials**	**References**
Galactose-conjugated nanoparticles	Lysosomal activity of senescent cells	- palbociclib-induced senescence in a human melanoma cell line (SK-Mel-103), - xenographs in mice, bleomycin mice model of lung fibrosis	Preclinical animal models	(Muñoz-Espín et al., 2018a)
Galactose-modified cytotoxic agents	Lysosomal activity of senescent cells	ProdrugA: - Senescent human fibroblasts and epithelial cells, senescent cells in mice lung after irradiation, preneoplastic senescent cells in mouse pituitary tumour, NavGal: - senescent human adenocarcinoma, melanoma, colorectal carcinoma cell line, senescent human lung	Preclinical animal models	(Guerrero et al., 2020, González-Gualda et al., 2020a, Cai et al., 2020)

		fibroblasts, senescent mouse breast cancer and mouse lung fibroblasts, xenografts and orthotopic models of NSCLC - SSK1: - Senescent mouse new born derma fibroblasts, senescent mouse embryonic and lung fibroblasts, senescent human embryonic fibroblasts and umbilical vein endothelial cells and preadipocytes. - Bleomycin mice model of lung fibrosis and - Senescent cells in aged mice		
nanoMIPs	B2M	- Senescent bladder carcinoma cells (EJp16)	Preclinical models of senescence in vitro	(Ekpenyong-Akiba et al., 2019)
CAR-T	uPAR	- Senescent lung cancer cells - Senescent hepatocytes in vivo, senescent cells from lung adenocarcinoma and CCl4-dependent liver fibrosis mouse model	Preclinical animal models	(Wakita et al., 2020)

Senoblockers				
Ibrutinib	BTK, ITK, TEC, BLK, JAK3, EFG, HER2	EJp53, ZMPSTE24$^{-/-}$ progeria	Preclinical animal models	(Althubiti et al., 2016a, Ekpenyong-Akiba et al., 2020a)

Table 1.5. Summary of main senomorphics.

Compounds	Targets	Validation Models	Clinical Trials	References
Senomorphics				
Rapamycin	mTOR	- p16/p21-induced senescence in rodent and human cells in vitro; - senescence in progeroid human fibroblasts ex vivo; - senescence in human primary keratinocytes and epithelial stem cells in vitro; - radiation-induced mucositis in mice; - SASP in human fibroblasts and breast epithelial cells in vitro; - senescence and SASP in mouse fibroblasts in vitro;	Approved for immunosuppression	(Harrison et al., 2009, Herranz et al., 2015a, Laberge et al., 2015a, Thapa et al., 2017a)

		- SASP and senescent cells in serum and fat tissues of mice; - number of senescent Ercc1$^{-/-}$ murine embryonic fibroblasts in vitro		
Metformin	IKK and/or NF- κB	- SASP in human senescent lung fibroblasts in vitro; - ceramide-induced senescence in myoblasts in vitro; - human senescent lung fibroblasts in vitro	Approved for type 2 diabetes	(Oubaha et al., 2016, Maruthur et al., 2016, Moiseeva et al., 2013, Noren Hooten et al., 2016)
Apigenin and Kaempferol (Naturally occurring flavonoid)	NF-κB p65 subunit and IκB	- Bleomycin induced senescence in BJ fibroblasts	Preclinical models of senescence in vitro	(Lim et al., 2015)
SB203580	P38 MAPK	- SASP in human fibroblasts in vitro	Preclinical models of senescence in vitro	(Freund et al., 2011)
Ruxolitinib	JAK	- SASP in human primary preadipocytes and HUVECs in vitro;	Approved for graft-versus-host disease	(Xu et al., 2015)

		- inflammation and improvement of physical function in aged mice		
KU-60019	ATM	- Functional recovery of senescent fibroblasts through lysosomal-mitochondrial axis	Preclinical animal models	(Kang et al., 2017)
Nordihydroguaiaretic acid (NDGA)	HSP90 Naturally occurring antioxidant	- Senescence murine embryonic fibroblasts	Preclinical models of senescence in vitro	(Harrison et al., 2014, Fuhrmann-Stroissnigg et al., 2017b)
Simvastatin	IL-6, IL-8, MCP1	- Senescent human fibroblasts - Prevents invasion of breast cancer cells	Preclinical models of senescence in vitro	(Liu et al., 2015b)
Cortisol	IL-6 secretion	- Senescent human fibroblasts - Prevents invasion of breast cancer cells	Steroid hormone	(Laberge et al., 2012)

1.10 Aims and objectives

1.10.1 Aim of research

Accumulation of senescent cells leads to multiple age-associated dysfunctions and selective elimination of senescent cells has been shown to have great therapeutic potential (Kirkland and Tchkonia, 2017). However, currently available approaches to eliminate senescent cells are limited and characterized by lack of specificity. Therefore, the aim of this research is to propose novel therapeutical strategies to prevent the accumulation of senescent cells.

1.10.2 Objectives

1. To identify new approaches to target and eliminate senescent cells:
    - Identification of novel senolytics and synergistic combinations
    - Targeting senescent cells *in vivo* using molecularly imprinted polymers
    - Clearance of senescent cells *in vitro* using antibody-drug conjugates
2. To characterize the effects of BTK inhibition by Ibrutinib in the context of preventing senescent cell accumulation.
    - Assessment of cognitive functions and muscle strength of animals treated with Ibrutinib.
    - Testing the presence of senescence markers after the Ibrutinib treatment in different tissues.
3. To validate expression profiles of novel markers of cellular senescence:
    - Testing the presence of VPS26A, EBP50 and PLD3 in different models of senescence.

2 Materials and Methods

2.1 Cell culture and passaging

Three bladder carcinoma cell models were used in this study: EJp53, EJp21 and EJp16, together with the fibrosarcoma cell line HT1080-p21-9. Two non-small cell lung carcinoma (NSCLC) cell lines were also used throughout the project: A549 and H522. Furthermore, human pulmonary fibroblasts were provided by the Leicester Respiratory Biomedical Research Unit (BRU), Department of Infection Immunity and Inflammation, University of Leicester and were isolated from Idiopathic Pulmonary Fibrosis (IPF) patients and non-fibrotic control (NFC) individuals. All cells were cultured using a Thermo HeraCell 240 incubator at 37°C and 5% CO_2. The culture media used varied between cell lines used (**Table 2.1**)

To prevent overgrowth, cells were passaged upon reaching 70% confluency. Old media was first aspirated, and cells washed twice with 1x Phosphate Buffered Saline (PBS). Cells were then detached using 0.25% Trypsin–EDTA (GIBCO) and kept at 37°C for 5 minutes (min). Cells were then collected using 5ml of appropriate growth medium and centrifuged at 300 g for 3 min. The pellet was then resuspended in 1 ml of media and cells counted using a BioRad TC20 automated cell counter according to the manufacturer's instructions and re-plated at the desired density.

Table 2.1. Cell lines used

Cell line	Culture conditions
EJp53 and EJp21	- DMEM with 10% v/v Foetal Bovine Serum (FBS) - penicillin–streptomycin (50 unit/ml) - hygromycin (100 μg/ml) - geneticin (750 μg/ml).
EJp16	- DMEM with 10% FBS - penicillin–streptomycin (50 unit/ml) - hygromycin (100 μg/ml) - puromycin (2 μg/ml)
HT1080-p21-9, A549, Primary fibroblasts	- DMEM with 10% FBS - penicillin–streptomycin (50 unit/ml)
H522	- RPMI with 10% FBS,) - penicillin–streptomycin (50 unit/ml)

Table 2.2. Cell culture reagents and supplements

Reagent/ Supplement	Supplier	Product No.
Dulbecco's Modified Eagle's medium (DMEM)	Gibco	61965026
Roswell Park Memorial Institute 1640 Medium (RPMI)	ThermoFisher	11875085
Foetal Bovine Serum (FBS)	Gibco	10500064
Penicillin-streptomycin	Gibco	15140122
Dulbecco's Phosphate Buffered Saline (PBS)	Gibco	20012019
Trypsin-EDTA (0.25% Phenol red)	Gibco	25200056
Hygromycin B (50 mg/mL)	Gibco	10687010
Geneticin™ Selective Antibiotic (G418 Sulfate) (50 mg/mL)	Gibco	10131035
Puromycin dihydrochloride	Sigma-Aldrich	P8833-10MG
Tetracycline hydrochloride	Sigma-Aldrich	T8032-20MG
Isopropyl β-D-1-thiogalactopyranoside (IPTG)	Sigma-Aldrich	I5502-1G
Dimethyl Sulfoxide (DMSO)	Sigma-Aldrich	D8418-100ML

2.2 Induction of Senescence

The EJ bladder cancer cell lines (EJp53, EJp21 and EJp16), utilise a tetracycline (tet)- off gene expression system (Sugrue et al., 1997a, Fang et al., 1999, Macip et al., 2002), which allows overexpression of p53, p21 or p16, respectively, in the absence of tetracycline. These cells become senescent 3-4 days after tetracycline removal, thus making them a highly useful model of genetically induced senescence.

To keep EJp53, EJp21 and EJp16 cells proliferating, 1 µM of tetracycline was added to the culture media, which was replaced every three days. To induce senescence, tetracycline was removed. First cells were detached by trypsinisation and then washed with 1 x PBS followed by centrifuging at 300 x g for 3 min. This washing step was repeated 3 times.

The HT1080-p21-9 is a derivate of the HT1080 fibrosarcoma cell line (Chang et al., 2013, Demidenko et al., 2005) with a β-D-1-thiogalactopyranoside (IPTG)-dependent regulation of p21 expression. To induce p21 expression, 50 µM of IPTG was added to the media and the cells left for up to five days to induce senescence.

2.3 Cell counting

To confirm senescence-related growth arrest, senescence was induced and two 6 cm dishes with $5x10^5$ cells were plated for each cell line. Cells were then incubated for 15 days with regular counting. Every third day, cells were trypsinised as previously described **(2.1).** The cell suspension was then mixed with 0.4% Trypan blue solution (Gibco) in a 1:1 ratio to determine the percentage of viable cells with 10 µl of the mixture placed in a counting slide (BIO-RAD). The slide was then inserted into a TC20 BIO-RAD automated counter and the readings recorded. After counting, cells were split when needed to prevent overgrowth. The total cell number was then multiplied by each split factor each time the cells were split.

2.4 Long term storage of cell lines

For long-term storage, cells were cryopreserved regularly to ensure a low as possible passage number of cell stocks. When cells reached 90% confluency, the media was aspirated, and cells washed 2 times with 1 x PBS then trypsinised and incubated for 5 min at 37°C and 5% CO_2. When fully detached, cells were collected in media and centrifuged at 300 x g for 3 min. The supernatant was removed, and cells counted and re-suspended in complete growth media supplemented with 10% v/v DMSO (Sigma-Aldrich, #D5879). Approximately $1x10^6$ cells/ml were transferred into a Cryovial which was immediately placed in an isopropanol freezing container (Nalgene Mr Frosty, Sigma Aldrich) and kept at -80°C for 24- 48 hours (h) before being transferred to liquid nitrogen storage tanks.

2.5 Gene overexpression

2.5.1 Bacterial Transformation

Bronze α-select competent (BIO-85025) bacteria cells were used to amplify plasmid DNA. 50 µl of thawed competent cells were mixed with 100 ng of plasmid and incubated for 20 min on ice. Next, cells were heat shocked for 1 min at 42°C and placed back onto ice. Then, using aseptic techniques, 950 µl of Lysogeny broth (LB) and the mixture were incubated at 37°C with shaking for 1 h. Samples were then centrifuged for 1 min at 7500 x g and the pellet resuspended with SOC (Super Optimal broth with Catabolite repression, Invitrogen). The suspension was placed in 10% and 90% dilutions on Agar plates supplemented with the appropriate selection antibiotic (resistance determined by the plasmid) using CoilRollers plating beads (Novagen) followed by overnight incubation at 37°C. Next day, single colonies were picked and transferred into fresh LB media supplemented with the appropriate selection antibiotic and incubated overnight at 37°C with 150 x g shaking. The following day, glycerol stocks were prepared mixing 500 µl of the bacterial culture with 50% glycerol in 1:1 ratio and stored in -80° for future usage. For DNA purification, a pipette tip was used to scrape the top of the glycerol stock and incubated in LB with appropriate selection antibiotic overnight at 37°C with 150 x g shaking. Next day, a QIAGEN Miniprep kit was used to purify the plasmid

according to the manufacturer's instructions. DNA was diluted in 100 µl of ddH20 and stored at -20°C. The concentration was measured using a Nanodrop spectrophotometer (ThermoScientific).

2.5.2 Plasmid Transfection

Lipofectamine 2000 (Invitrogen) was used to transfect the plasmids. The day prior to transfection, EJp16 and EJp53 cells were split into 60 mm plates in order to reach 70-80% confluency. On the day of transfection, media was replaced with serum-free media. Further, for each plate, two Eppendorfs with 500 µl of serum-free media were prepared; one mixed with 1 µg of plasmid DNA (B2M cDNA ORF clone-OriGene RC207587) and the other, mixed with 5-10 µl Lipofectamine 2000. Both tubes were left for 5 min to settle. Next, the diluted Lipofectamine 2000 was combined with the diluted plasmid and incubated for 20 min at room-temperature (RT). Afterwards, the mixture was added dropwise to each plate and the cells incubated at 37°C. After 6 h, the serum-free medium was changed, and the cells left for 24 h. Antibiotic selection was performed every three days for 12 days to create single colonies which were picked and expanded to create stable cell lines.

2.6 Cell viability assay

To assess cell viability after treatment with senolytics, Cell Titer-Glo (Promega) luminescent cell viability assay (CTG) was used to detect metabolically active cells. The luminescent output is directly relative to the amount of adenosine triphosphate (ATP) present and represents the number of viable cells present and their rate of metabolism (Hannah et al., 2001). First, cells were plated in duplicates in 96-well plates with a final density of 6 x 10^3 cells in each well. The following day, cells were treated with increasing drug concentrations either as a single agent or in combination (0, 0.001, 0.01, 0.1, 1, 10 µM) and left to incubate at 37°C and 5% CO_2 for 72 h. A dimethyl sulfoxide (DMSO) control was used for the 0 µM concentration. Then, to measure cell viability 5% v/v of CellTiter-Glow reagent (Promega, G7570) was added to each well and incubated in the dark at room temperature (RT) for 10 min. Luminescence was then measured using a Hidex Sense plate reader. Data were normalised to control samples. Viability was calculated using Microsoft Excel according to the formula:

$$\%\ Cell\ Viability = \frac{Sample\ signal}{Control\ signal} * 100\%$$

Table 2.3. Compounds used for Cell Viability assay.

Compound	Target	Supplier
ABT-737	BCL-2, BCL-X_L, BCL-W	Selleck Chemicals (S1002)
ABT-199	BCL-2	Selleck Chemicals (S8048)
A1331852	BCL-X_L	Selleck Chemicals (S7801)
S63845	MCL-1	AppexBio (A8737)
GQC-05	BCL-X, MYC, MCL-1	Prof. Ian C. Eperon, Dr. Cyril Dominguez
9-hydroxyellipticine	BCL-X_L	Dr. Cyril Dominguez
SPHINX	VEGF-A	Prof. Ian C. Eperon
FC-A	p53/14-3-3σ stabilisation	Dr. Richard Doveston
WR-1065	p53/14-3-3σ stabilisation	Dr. Richard Doveston

The half-maximal inhibitory concentration (IC_{50}) of drugs were calculated in GraphPad Prism using a nonlinear regression (variable slope) based on cell viability data with lower and upper constraints set to 0 and 100%.

Combination indexes calculated using Calcusyn via the Chou-Talalay method were used to describe the effect of drug combination as additive, antagonistic or synergistic (Chou and Talalay, 1984, Chou, 2010). Output values below 0.9 are considered synergistic, values between 0.9-1.1 are additive and antagonistic are values above 1.1 (**Table 2.4**).

Table 2.4. Combination index values and their outcomes.

Combination Index (CI) represents classification of synergism in drug combination based on the Chou-Talalay method. Adapted from (Chou, 2008)

Combination Index (CI) value	Outcome
< 0.1	Very strong synergism
0.1-0.3	Strong synergism
0.3-0.7	Synergism
0.7-0.85	Moderate synergism
0.85-0.9	Slight synergism
0.9-1.1	Nearly additive
1.1-1.2	Slight antagonism
1.2-1.45	Moderate antagonism
1.45-3.3	Antagonism
3.3-10	Strong antagonism
>10	Very strong antagonism

2.7 Senescence-associated ß-galactosidase (SA-ß-gal) assay

Senescence-associated ß-galactosidase (SA-ß-gal) assay is a cytochemical method described in 1995, which utilises enzymatic activity of β-galactosidase (Dimri et al., 1995). β-galactosidase is present and detectable at pH=4.0 in all the cells, however only in senescent cells can it be detected at pH=6.0. The assay uses the chromogenic substrate 5-bromo-4-chloro-3-indoyl β-D-galactopyranoside (X-gal), which yields an insoluble blue compound when cleaved by β-galactosidase.

To detect SA-ß-gal, two 6 cm dishes with 5 x 10^5 of each cell line or 25 µg pieces of fresh tissues were used. First, samples were washed twice with 1x PBS and fixed for 5 min (cells) or 10-15 min (tissues) with 10% Neutral Buffered Formalin (Sigma-Aldrich). Following fixation, cells were washed again twice with 1x PBS to remove formalin. Next, the PBS was aspirated and replaced with staining solution (**Table 2.5**) and cells incubated at 37°C. The blue staining was detected 15-24 h later depending on the cell or tissue type. Images were taken using a Leica DMi1 microscope with Leica MC170 HD camera and analysed using ImageJ cell-counter plug-in.

Table 2.5. Components of ß-galactosidase staining solution

Reagent	Stock concentration	Volume	Final concentration	Supplier
*** Citric acid/Sodium phosphate buffer pH=6**	0.2 M	4 ml	40 mM	N/A
Potassium ferrocyanide	100 mM	1 ml	5 mM	Sigma-Aldrich, P9387
Potassium ferricyanide	100 mM	1 ml	5 mM	Sigma-Aldrich, 244023
Sodium chloride	5 M	600 µl	150 mM	Sigma-Aldrich, S9888
Magnesium chloride	1 M	40 µl	2 mM	Sigma Aldrich, M8266
ddH_2O	N/A	12.36 ml	N/A	Millipore
X-gal in dimethylformamide	20 mg/ml	1 ml	1 mg/ml	Sigma-Aldrich, B4252
*** The Citric acid/ Sodium phosphate buffer was prepared using 3.7 ml 0.1 M citric acid (Fluka Analytical, 27488) and 6.3 ml 0.2 M sodium phosphate (Sigma Aldrich, S2554).**				

2.8 Flow Cytometry

Flow Cytometry is a frequently used technique to analyse the characteristics of cells or particles and allows for cells to be sorted in a heterogenous cell population. The technique predominantly relies on the detection of fluorescence intensity produced by fluorescently labelled agents detecting proteins, or ligands that specifically bind to cell-associated molecules (Ormerod and Imrie, 1990).

2.8.1 Cell-cycle analysis

Propidium Iodide (PI) is fluorescent DNA intercalating dye, commonly used to detect dead cells within a population of live cells (Boulos et al., 1999). PI stains dead cells as a result of a porous membrane and is impermeable to live cells.

Proliferating and senescent cells were seeded in 12-well plates and allowed to attach overnight. Then, cells were treated with different drug concentrations and incubated at 37°C for 24-72 h. Next, the conditioned media was collected into 15ml falcon tubes, cells washed with 1 x PBS and 0.25% Trypsin added. After 5 min incubation at 37°C, cells were collected into their respective falcon tubes and centrifuged for 3 min at 300 x g. Next, the supernatant was discarded, and the pellets resuspended in 1 x PBS and centrifuged again. Supernatant was once again discarded, and the pellets resuspended in ice-cold 70% Ethanol for fixation. Samples were stored at -20°C for at least 2h. After the required time, ethanol from the samples was removed by centrifuging then washed with 5 ml of PBS and centrifuged again for 3 min at 200 x g. The supernatant was discarded and the pellets resuspended in 400 µl of PI staining solution (50 µg/ml Propidium iodide (Sigma Aldrich), 10 µg/ml RNase A (Sigma Aldrich) in 1 x PBS), vortexed and transferred to polystyrene round – bottom FACS tubes (Falcon). The tubes were incubated for 30 min in the dark followed by analysis using a BD FACSCanto II (Becton Dickenson Biosciences). Cells were gated using forward and side scatter to exclude debris with 10000 events per sample being detected and quantified using the 580/30 nm wavelength filter. Analysis was performed using FACS DivaTM 6.1.3 software (BD Bioscience) and GraphPad Prism 7.0 software.

2.9 BH3 profiling

This method was adapted from (Ryan and Letai, 2013). BH3 profiling is an assay to predict cell fate decisions by measuring the integrated function of the mitochondrial apoptotic pathway. To measure permeabilization of the outer mitochondrial membrane, known concentrations of the panel peptides mimicking BH3 domains are used and the release of cytochrome c is measured. This can be used to predict cell responses to chemical agents that target the BCL-2 family of proteins which share one or more BH homology domains.

All steps were performed at room temperature. Proliferating and senescent cells were collected in 15 ml falcon tubes and centrifuged for 3 min at 300 x g. Cell pellets were washed with 1 x PBS and resuspended in 1 x MEB buffer (**Table 2.6**) and seeded at $5x10^5$ cells per 100 µl/well in a 96-well black plate or $5x10^4$ cells per 10 µl/well in a 384-well black plate. Cell concentration was optimised for cell lines and was determined using titration experiments to allow for maximal fold change between control values (DMSO and carbonyl cyanide-p-trifluoromethoxyphenylhydrazone (FCCP) treatments) whilst preventing large hyperpolarisations which result in overloading of the cells. The proper peptides (**Table 2.7**) were added into their respective wells with 0.1-10 µM concentrations. 10 µM of FCCP (Sigma C2920) was used as a positive control and an equal volume of DMSO was used as a negative control. 100 µl (96-well plate) or 10 µl (384-well plate) of freshly made 2 X staining solution (25 µM oligomycin (Sigma O4876), 0.005% w/v digitonin (Sigma D5628), 4 µM JC-1 (VWR 89166-014) and 10 µM β-mercaptoethanol in MEB) was added to each well immediately prior to analysis. Fluorescence intensity (ex. 545 nm, em. 590 nm both +/- 10 nm) was measured at 30°C with intermittent agitation using a HidexSense plate reader. Measurements were taken every 5 min for 2 h. The fluorescent signal intensity is proportional to mitochondrial membrane integrity. The area under each response curve (AUC) was calculated and normalised to the controls (DMSO and FCCP) based on the following formula:

$$Depolarisation = 1 - \frac{AUC_{Sample} - AUC_{FCCP}}{AUC_{DMSO} - AUC_{FCCP}}$$

Table 2.6. The MEB buffer components

Reagents (stock)	MW	Final Concentration (mM)	Final Volume (L)	Mass (g)
150 mM Mannitol	182	0.15	0.5	13.65
10mM HEPES-KOSH pH= 7.5	238.3	0.01	0.5	1.19
50 mM KCl	74.55	0.05	0.5	1.86
0.02 mM EGTA	380.35	2×10^{-5}	0.5	20 µl
0.02 mM EDTA	292.24	2×10^{-5}	0.5	20 µl
0.1% BSA	66.463	0.1	0.5	0.5
5 mM Succinate	118.09	0.005	0.5	0.295

Table 2.7. BH3 profiling peptides.

Synthetic peptides previously designed and published specifically for BH3 profiling [1-(Deng et al., 2007), 2- (Foight et al., 2014), 3- (Dutta et al., 2015), 4- (Jenson et al., 2017)].

Peptide	Sequence	Binding partners
BIM[1]	Ac-MRPEIWIAQELRRIGDEFNA- NH_2	All
BAD[1]	Ac-LWAAQRYGRELRRMSDEFEGSFKGL-NH_2	BCL-2/W/X_L
MS1[2]	Ac-RPEIWMTQGLRRLGDEINA-NH_2	MCL-1
XXa1_Y4Ek[3]	Ac-RPEIWYAQGLKRFGDEFNAYKAR-NH_2	BCL-X_L
w-HRK[1]	Ac-SSAAQLTAARLKALGDELHQY-NH_2	BCL-X_L
FS2[4]	Ac-QWVREIAAGLRRAADDVNAQVER-NH_2	BCL-2A1

2.10 RNA analysis

2.10.1 RNA extraction from cells and tissues

RNA extraction from cells (Promega, Z6011) and frozen mouse tissues (Promega, Z6111) was performed using ReliaPrep RNA miniprep system, according to manufacturer instructions. 0.25-20 mg of tissue grinded in pre chilled pestle and mortar or 1 x 10^6 cells were collected, and pellets were firstly washed with 1 x PBS and centrifuged at 300 g for 5 min. Then, pellets were resuspended in cold BL + TG buffer and passed through a 20-gauge needle 6-7 times in order to shear DNA. Then, isopropanol was added, and samples were mixed by flicking and then centrifuged for 30 s at 14000 x g. Next, supernatant was transferred to supplied minicolumns placed in a collection tubes and centrifuged again for 30 sec at 14000 x g. The minicolumns were then washed with RNA Wash Solution and centrifuged for 30 sec at 14000 x g. Next, the DNase I incubation mix (Yellow Core Buffer, $MnCl_2$, DNase I enzyme) was added to the minicolumns and samples were incubated for 15 min at RT. Then, columns were washed first with Column Wash Solution and followed by RNA Wash Solution, each time centrifuging at 14000 g for 30 sec. For a final wash, 300 µl of RNA Wash Solution was used and samples were centrifuged at 14000 x g for 2 min. The RNA was eluted by addition of 30 µl of nuclease-free H_2O and centrifugation at 14000 x g for 1 min.

RNA extraction from Formalin Fixed Paraffin Embedded (FFPE) mouse tissues was performed using a ReliaPrepTM FFPE Total RNA Miniprep System Kit (Promega, Z1002) following the manufacturer's protocol. Extraction from FFPE tissues was similar to the one described above however involved deparaffinization step using Xylene and decreasing concentrations of Ethanol. The concentration and yield (A_{260}/A_{280} ratio) of eluted RNA regardless of the starting material was assessed and recorded using a Nanodrop spectrophotometer (ThermoScientific). Only samples with an A_{260}/A_{280} ratio value between 1.8-2.1 were used for further analysis.

2.10.2 Reverse Transcription

Complimentary DNA or cDNA synthesis was performed using Superscript II reverse transcriptase system (Invitrogen, 18064). Equal concentrations of RNA, within a range of 0.5 – 2 µg, from all samples were used for the reaction. First, 1 µl of Random Primers (Thermo Scientific, SO142) and 1 µl of 10 mM dNTP mix (Thermo Scientific, RO191) were mixed with RNA in a microcentrifuge tube with RNase-free water used to make up the volume to 13 µl. Then, samples were transferred to a Techne Prime thermal cycler (5PRIME/02) and heated to 65°C for 5 min to allow for primer annealing. Next, the temperature was cooled to 10°C for one 1 min and 7 µl of master mix was added to the samples and gently mixed. The Master mix consisted of 4 µl of 5 x First-Strand Buffer, 1 µl of 0.1M dithiothreitol (DTT), 1 µl of SuperScript II reverse transcriptase and 1 µl of RNaseOUT (Invitrogen 1077-019). Samples were given a short spin and returned to the thermocycler. Next, samples were heated to 25°C for 5 min following heating to 50°C for 1h. Lastly, samples were heated to 70°C for 15 min before being held at 4°C. The cDNA was either used immediately or stored at -20°C.

2.10.3 Quantitative polymerase chain reaction (qPCR)

Each reaction was performed in triplicate using a white 96-well plate (LightCycler® 480 Multiwell Plate 96, Roche). Glyceraldehyde 3-phosphate dehydrogenase (GAPDH) was used as an internal control. cDNA was diluted at a ratio of 1:5 using nuclease-free water. 5 µl of cDNA was mixed with the freshly prepared reaction mix, which contained 10 µl of SensiMix SYBR NO-ROX (Invitrogen, QT650-05) and 100nM of each primer pair (**Table 2.8**, **Table 2.9**). Then the plate was sealed with Thermal Seal RTTM Sealing Film (Alpha Laboratories) and briefly centrifuged for 1 min. The reaction was performed using a Lightcycler 480 Real Time PCR (Roche) using the following conditions: 95°C for 10 min followed by 40 cycles of denaturation for 15 s at 95°C and 1 min of annealing and elongation at 60°C. Lastly, a melting curve analysis was obtained to test the specificity of the primers. The background values were excluded by manual adjustment of the baseline threshold for the amplification plots. Relative expression of the target genes was quantified based using the delta delta Ct method as shown below:

$$\Delta Ct = Ct_{target\ gene} - Ct_{housekeeping\ gene}$$

$$\Delta\Delta Ct = \Delta Ct_{treated} - \Delta Ct_{experimental\ control}$$

$$Fold\ change = 2^{-\Delta\Delta Ct}$$

Table 2.8. Primers used for qPCR- human samples.

Target Gene	**Primer sequence (5'- 3')**	**Harvard Primer bank ID**
GAPDH	F: TCT CTG CTC CTC CTG TTC R: GCC CAA TAC GAC CAA ATC C	N/A
CDKN2A (p16)	F: GAT CCA GGT GGG TAG AAG GTC R: CCC CTG CAA ACT TCG TCC T	17738298a1
CDKN1A (p21)	F: TGT CCG TCA GAA CCC ATG C R: AAA GTC GAA GTT CCA TCG CTC	310832423c1
TP53 (p53)	*F: CAG CAC ATG ACG GAG GTT GT* *R: TCA TCC AAA TAC TCC ACA CGC*	371502118c1
PLD3	F: AAG CCT AAA CTG ATG TAC CAG GA R: GCC TCA ATC TCA TTC ATG GGC	166197682c1
B2M	F: GAG GCT ATC CAG CGT ACT CCA R: CGG CAG GCA TAC TCA TCT TTT	37704380c1
SLC9A3R1 (EBP50)	F: GG CTG GCA ACG AAA ATG AGC R: TGT CGC TGT GCA GGT TGA AG	381214354c1
VPS26A	*F: TTC AGG AAA GGT AAA CCT AGC CT* *R: ATT GGC ACC GAT GTA AGA TTC AT*	78482612c1
IL-6	F: ACT CAC CTC TTC AGA ACG AAT TG R: CCA TCT TTG GAA GGT TCA GGT TG	224831235c1
IL-1B	F: ATG ATG GCT TAT TAC AGT GGC AA R: GTC GGA GAT TCG TAG CTG GA	27894305c1
PTPRJ (DEP1)	F: AGT ACA CAC GGC CCA GCA AT R: GAG GCG TCA TCA AAG TTC TGC	N/A
BTK	F: TCT GAA GCG ATC CCA ACA GAA R: TGC ACG GTC AAG AGA AAC AGG	N/A
ARMCX3	F: TCT GGG GCC AGG TAT AAT GAC R: GGA AGC CCG TTT CTG GAC A	47578120c1
ANGPTL2	F: GAA CCG AGT GCA TAA GCA GGA R: GTG ACC CGC GAG TTC ATG TT	N/A
BCL2	F: GGT GGG GTC ATG TGT GTG G R: CGG TTC AGG TAC TCA GTC ATC C	72198345c1

BCL2L1 (BCL-X)	F: GAG CTG GTG GTT GAC TTT CTC R: TCC ATC TCC GAT TCA GTC CCT	20336333c1
BCL2L2 (BCL-W)	F: GCG GAG TTC ACA GCT CTA TAC R: AAA AGG CCC CTA CAG TTA CCA	315360667c1
MCL1	F: GTG CCT TTG TGG CTA AAC ACT R: AGT CCC GTT TTG TCC TTA CGA	11386165a2
BAK1 (BAK)	F: ATG GTC ACC TTA CCT CTG CAA R: TCA TAG CGT CGG TTG ATG TCG	109698605c2
BAX	F: CCC GAG AGG TCT TTT TCC GAG R: CCA GCC CAT GAT GGTTCT GAT	163659849c1
BCL2L11 (BIM)	F: TAA GTT CTG AGT GTG ACC GAG G R: GCT CTG TCT GTA GGG AGG TAG G	323362951c1
BAD	F: CCC AGA GTT TGA GCC GAG TG R: CCC ATC CCT TCG TCG TCC T	10835069a1
BBC3 (PUMA)	F: GAC CTC AAC GCA CAG TAC GAG R: AGG AGT CCC ATG ATG AGA TTG T	15193488a1
PMAIP1 (NOXA)	F: ACC AAG CCG GAT TTG CGA TT R: ACT TGC ACT TGT TCC TCG TGG	21595743a1

Table 2.9. Primers used for qPCR- mouse samples

Target Gene	**Primer sequence (5'- 3')**	**Harvard Primer bank ID**
GAPDH	F: GTTGTCTCCTGCGACTTCA R: GGTGGTCCAGGGTTTCTTA	
CDKN2A (p16)	F: CCCAACGCCCCGAACT R: GCAGAAGAGCTGCTACGTGAA	
CDKN1A (p21)	F: GGCAGACCAGCCTGACAGAT R: TTCAGGGTTTTCTCTTGCAGAAG	
TRP53 (p53)	*F: CCCCTGTCATCTTTTGTCCCT* *R: AGCTGGCAGAATAGCTTATTGAG*	*187960038c1*
PLD3	F: CTGAGGAACCGGAAGCTGT R: GGAAAGGGGTGGTCCTGA	
BTK	F: ACAGATTCCGAGGAGAGGTGAGG R: GGTCCTTCATCATATACAACCTGGAATGG	
SLC9A3R1 (EBP50)	F: AGTGCAAAGTGATCCCATCC R: GAGGGCTCTGTGGAAACTTG	
VPS26A	*F: CTGGAAAGAGGCTAGAGCATCA* *R: AGGCAAGGCTAGTTCCTTCAC*	164518902c1
IL-6	F: CCACTTCACAAGTCGGAGGCTTA R: GCAAGTGCATCATCGTTGTTCATAC	
IL-1B	F: TCCAGGATGAGGACATGAGCAC R: GAACGTCACACACCAGCAGGTTA	
PTPRJ (DEP1)	F: GCAGTGTTTGGATGTATCTTTGGT R: CTTCATTATTCTTGGCATCTGTCCTT	N/A
ARMCX3	F: CTGGAGCCTGCTATTGCATTT R: TCAGACCAGTCATTATACCTGGC	21311833a1
B2M	F: GCT ATC CAG AAA ACC CCT CAA R: CAT GTC TCG ATC CCA GTA GAC GGT	

2.11 Protein extraction and analysis

2.11.1 Whole cell lysate

The culture media were aspirated, cells washed 2 times with 1 x PBS and trypsinised. After 5 min, cells were collected and centrifuged at 300 x g for 3 min. Pellets were collected, washed with 1 x PBS and kept on ice. Pellets were re-suspended in Radio immunoprecipitation assay buffer (RIPA)-50 mM Tris HCl, 1% v/v NP40, 0.5% w/v SDS, 150 mM NaCl, 2 mM EDTA, 50 mM NaF, pH=7.4) supplemented with Phosphatase Inhibitor (Sigma Aldrich) and Protease Inhibitor Cocktail Set III, (Calbiochem) in a 1:100 ratio. Then samples were vortexed and incubated on ice for 20 min. After incubation, cells were ruptured by passing the cell suspension through a 27 Gauge needle (5-7 times) followed by centrifugation at 20000 x g for 15 min at 4°C. The supernatant was transferred into fresh Eppendorf's and the protein concentration was estimated using a Bradford assay. 4X loading buffer (8% w/v SDS, 20% v/v 2- mercaptoethanol, 40% v/v glycerol, 0.4% w/v bromophenol blue, 200 mM Tris HCl pH=6.8) was added in a 1:4 ratio. This was followed by boiling the sample at 95°C and loading onto an SDS-Polyacrylamide gel. Alternatively, lysates were stored at -80°C. for future use.

2.11.1.1 Bradford assay

To determine the concentration of proteins in prepared lysates, a Bradford assay was performed. 1 µl of sample was mixed with 200 µl of Pierce Coomassie plus assay reagent (Thermo Fisher, 23236) and the absorbance measured using a HidexSense plate reader at A595 nm. To calculate the protein concentration, a standard curve was generated using known concentrations of bovine serum albumin mixed with Coomassie reagent.

2.11.2 Total protein extraction from Formalin-Fixed Paraffin-Embedded (FFPE) tissues

Tissues were collected post-mortem from WT and ZMPSTE24$^{-/-}$ mice, fixed with 10% Neutral Buffered Formalin (Sigma-Aldrich) for 24-48 h and sent to the University of Leicester Histopathology Department to be embedded in paraffin. Extraction of total protein from the formalin-fixed paraffin-embedded mouse tissues was performed using a Qproteome FFPE Tissue Kit (QIAGEN) according to manufacturer protocol. Extraction involved tissue deparaffinization with xylene and decreasing percentages of ethanol. For extraction samples were incubated in the mixture of Extraction Buffer EXB Plus and β-mercaptoethanol and incubated for 2 h at 80°C with gentle agitation. After extractions, samples were centrifuged at 4°C at 14000 x g and concentration of eluted proteins was quantified using Bradford assay. After extraction, 4 x Laemmli buffer was added to the protein extracts in a ratio of 1:4 and the samples stored at -20°C for future use.

2.11.3 Protein extraction from frozen tissues

After collection, tissues were snap frozen in liquid nitrogen and stored at -80°C for future use. To extract proteins, tissues were grinded in a pre-chilled (-80°C overnight) pestle and mortar with 50 mg of tissues being used for each extraction. The amount of 3 x extraction buffer (187.5 mM Tris-HCL pH=6.8, 9% SDS, 30% Glycerol, 10% 2-Mercaptoethanol) was determined according to the formula:

$$Volume\ of\ 3\ x\ extraction\ buffer(\mu l) = \big(2\ x\ weight\ of\ the\ tissue(mg)\big) * 10$$

Extraction buffer was added together with Phosphatase Inhibitor, Sigma Aldrich and Protease Inhibitor Cocktail Set III, Calbiochem, both in a ratio of 1:100. Samples were then homogenized on wet ice in a Dounce Homogenizer for around 50 passes. Following homogenization, samples were centrifuged in 1.5 ml Eppendorfs at 4°C at 600 x g for 1 min to remove any debris and then transferred to fresh Eppendorfs and passed through a 27-Gauge needle attached to a 1 ml syringe for 10 passes to break up the DNA. After extraction, protein concentration was estimated using a Bradford assay and 4 x Laemmli

buffer was added to extracts in a ratio of 1:4. Lastly, the samples were stored at -20°C for future use.

2.11.4 Sodium dodecyl sulfate- polyacrylamide gel electrophoresis (SDS-PAGE) and Western Blot

Bio-Rad gel casting apparatus was used to prepare polyacrylamide gels together with Mini-PROTEAN® Spacer Plates. The polyacrylamide gel percentages used were determined by the size of the proteins being detected. Polyacrylamide gels were prepared by assembly of two parts: a stacking upper gel and resolving/separating lower gel (**Table 2.10**). The lower gel was poured into the casting cassette, covered with 70% ethanol and left to polymerize for 45 min at RT. Next, the ethanol was poured out with the excess removed using Whatman filter paper. The upper gel was poured on top of the lower gel and a 1.5 mm 15 -well Mini-PROTEAN comb was inserted before polymerization of the stacking gel. After 30 min incubation, gels were set and 20-50 µg of protein was loaded onto the gels next to 4 µl of PageRuler Plus Prestained protein ladder (Thermo Scientific). Electrophoresis was carried out using a Mini- PROTEAN Tetra cell electrophoresis module apparatus (Bio-Rad) filled with 1 x Running Buffer, at 100 V for around 1 h until the resolving gel was completely separated.

Table 2.10. Resolving and stacking gels for SDS-PAGE

Resolving/ Separating/ Lower Gel	**7%**	**10%**	**12%**	**15%**	**Stacking/ Upper Gel**	**4%**
Bis Acrylamide (40%)	4.2 ml	6 ml	7.2 ml	9 ml	Bis Acrylamide (40%)	875 µl
1.5M Tris-HCl (pH 8.8)	6 ml				0.5M Tris-HCl (pH=6.8)	1.75 ml
10% SDS	240 µl				10% SDS	70 µl
10% APS	120 µl				10% APS	70 µl
TEMED	12 µl				TEMED	7 µl
ddH_2O	13.3 ml	11.5 ml	10.3 ml	8.5 ml	ddH_20	4.325 ml

Then, proteins were transferred onto a nitrocellulose membrane (Amersham; GE) at 350 mA constant current (PowerPac 300 Electrophoresis Power Supply) for 90 min using a Bio-Rad Mini Trans-Blot Cell filled with 1 x Transfer Buffer. After transfer, membranes were incubated in Blocking Buffer at room temperature for 1 h. Next, membranes were incubated in primary antibody (**Table 2.12**) for 2 h at RT or overnight at 4°C. Then, membranes were washed 3 times for 10 min with 1 x PBST (0.1% Tween-20 in PBS) and incubated with secondary antibodies (**Table 2.12**) for 1 h in RT. Following incubation, membranes were washed 2 times with 1 x PBST for 10 min and once with 1 x PBS. Membranes were visualized using an Odyssey CLx infrared Imaging System (Li-COR) with analysis performed using Image Studio Lite Software (Li-COR).

Table 2.11. List of buffers used for WB

Name	Ingredients
10 x Running Buffer (1 L)	30.3 g Tris Base, 144 g Glycine, 10 g SDS
1 x Running Buffer (1 L)	100 ml 10 x Running Buffer, 900 ml ddH_2O
10 x Transfer Buffer (1 L)	33 g Tris Base, 144 g Glycine
1 x Transfer Buffer (1 L)	100 ml 10 x Transfer Buffer, 200 ml Methanol (Fisher Scientific), 700 ml ddH_2O
PBST (1 L)	100 ml 10 x PBS, 900 ml ddH_2O, 1 ml Tween-20
Blocking Buffer	5 g BSA, 100 ml 1 x PBST

Table 2.12. Primary and Secondary Antibodies used for WB and IHC

Name	Source	Clonality	Application	Dilution	Supplier / Product No.
β-actin	Rabbit	Polyclonal	WB	1:5000	Abcam, Ab8227
β-actin	Mouse	Polyclonal	WB	1:5000	
VPS26A	Rabbit	Polyclonal	WB, IHC	1:500, 1:100	GeneTex, GTX106297
PLD3	Rabbit	Polyclonal	WB, IHC	1:500, 1:100	Biorbyt, orb312786
ARMCX3	Rabbit	Polyclonal	WB	1:500	Abcam, Ab98938
BTK	Rabbit	Monoclonal	WB, IHC	1:500, 1:100	Cell Signaling, (D3H5) #8547S
p16	Mouse	Monoclonal	WB, IHC	1:500	Abcam, Ab54210
p21	Mouse	Monoclonal	WB	1:200	Santa Cruz, sc-53870
p53	Mouse	Monoclonal	WB	1:500	Santa Cruz, sc-126
p53	Rabbit	Polyclonal	WB, IHC	1:500, 1:100	Santa Cruz, sc-6243
IL-6 mouse samples	Rabbit	Polyclonal	WB	1:1000	Boster, PB9034
IL-6 for human	Rabbit	Polyclonal	WB, IHC	1:1000 1:400	Abcam, AB6672
IL-1B for mouse and human	Rabbit	Polyclonal	WB, IHC	1:1000 1:100	Thermo Scientific, P420B
ARMCX3	Rabbit	Polyclonal	WB	1:500	Abcam, Ab98938
B2M	Rabbit	Polyclonal	WB, IHC	1:500, 1:100	Abcam, Ab87483
B2M	Mouse	Monoclonal	WB	1:500	LifeSpan BioSciences, LS-B2200
BCL-2	Mouse	Monoclonal (4D7)	WB	1:1000	Oncogene (OP91)
BCL-X_L	Rabbit	Polyclonal	WB	1:1000	Abcam (ab32310)
MCL-1	Rabbit	Polyclonal	WB	1:1000	Santa Cruz (SC-819)

BCL-2A1	Rabbit	Polyclonal	WB	1:1000	Abcam (ab75887)
BCL-2	Rabbit	Monoclonal (31HE)	WB	1:1000	Cell signalling (2724)
BAK	Rabbit	Monoclonal (D4E4)	WB	1:1000	Cell signalling (12105)
BAX	Rabbit	Polyclonal	WB	1:1000	Abcam (ab7977)
NOXA	Mouse	Monoclonal	WB	1:1000	Abcam (ab13654)
PUMA	Rabbit	Polyclonal	WB	1:1000	Abcam (ab9643)
Name	**Specification**		**Application**	**Supplier**	
Mouse IgG	IR Dye-800 CW		WB	Li-COR #926-33210	
Rabbit IgG	IR Dye-680 RD		WB	Li-COR #926-68071	

2.12 Proteomics

Tissues were collected post-mortem from *ZMPSTE24*$^{-/-}$ fast aging mice treated with Ibrutinib or vehicle as a control. Mice tissues were firstly homogenized, and lysates prepared as previously described (**2.11.3**).

2.12.1 Filter Aided Sample Preparation

To prepare samples for mass spectrometry (MS), a Filter Aided Sample Preparation (FASP) method adapted from (Wisniewski et al., 2009) was utilised. This is an essential step prior to mass spectrometry as FASP allows for detergent depletion and preparation of peptides released by proteases from undigested material.

First the concentration of protein in each sample was estimated using a Bradford assay (2.11.1.1) and equal amounts (100 µg) of proteins were transferred to Microcon Centrifugal Filter units (Milipore) previously placed in 1.5 ml collection tubes (Milipore). Subsequently, RapiGest SF surfactant (Waters) (0.1% final concentration) was added to each filter and samples were incubated at 80°C for 45 min. Then, 15 mM 1,4-Dithiothreitol (DTT) (Sigma Aldrich) was added and samples were incubated at 60°C for 30 min. Next, 20 mM Ioadoacetamide (IAA) (Thermo Fisher) was added at RT and incubated for 30 min in the dark. In the meantime, the 1 µg/µl working concentration of MS grade Pierce Trypsin Protease (Thermo Fisher) was prepared and added to the

samples in a 1:25 ratio to protein content of the sample and incubated at 35°C overnight. Next day, 1% formic acid (FA) was added to deactivate the trypsin and samples centrifuged at 14,000 x g for 30 min. Then, filters were washed two times with 50 µl of 50 mM Ammonium Bicarbonate (ABC) (Honeywell) and centrifuged for 20 min at 14,000 g. The flow-through was collected of which 10 µl was combined with 10 µl of 100 fmol/µl Alcohol Dehydrogenase (ADH) protein digestion standard in 32 mm glass screw neck vials (Waters) and labelled. Prepared samples were transferred to our collaborators in **the Department of Genetics and Genome Biology**, **University of Leicester** where samples were run on a Liquid chromatography–mass spectrometry (LC-MS) for 75 min gradient by **Dr. Raj Singh** and raw data were analysed by **Dr. Antonella Tabasso.**

2.12.2 LC-MS

The samples were run on LC-MS by **Dr. Raj Singh** from **the Department of Genetics and Genome Biology at University of Leicester**. Samples were analysed using Water Nano Acquity Ultra Performance Liquid Chromatography (UPLC) system.

2.12.3 Bioinformatics analysis

The raw data from LC-MS was analysed using a variety of bioinformatics tools.

2.12.3.1 Progenesis QI

At first, data was processed using Progenesis QI for Proteomics by Nonlinear Dynamics 2.0 software. Progenesis allows for the conversion of raw peptides to protein expression data by alignment with the Uniprot reference mouse genome. Software allows for quantification of proteins abundance and comparison between tested conditions. Therefore, proteins expression patterns were compared between Ibrutinib and Control groups and filtered according to fold change and statistical significance. Proteins which exhibited more than a 2x fold change and an ANOVA $p < 0.05$ were selected for further analysis.

2.12.3.2 Pathway analysis

The first pathway analysis tool was Reactome (ELIXIR) software (**htpp://www.reactome.org**) used to assign detected proteins to signalling pathways and visualize the number of pathways affected by treatment.

The second tool used for pathway analysis was Panther Classification System (**http://www.pantherdb.org).** Panther allows for classification according to the class of protein, molecular function, cellular component, biological function and signalling pathway.

2.13 Histological analysis

2.13.1 *ZMPSTE24*$^{-/-}$ mice model

ZMPSTE24$^{-/-}$ is a mouse model for Hutchinson-Gilford progeria syndrome (HGPS) (Bergo et al., 2002b).

ZMPSTE24 is a metalloproteinase which allows the maturation of LAMIN A (LMNA) (Pendás et al., 2002). LMNA is an essential component of the nuclear envelope, involved in nuclear shape, DNA replication and transcription, cell division, and chromatin organization (Chen et al., 2003). It has been shown that alterations in nuclear envelope formation drives premature aging (Varela et al., 2005).

Under normal conditions, ZMPSTE24 is responsible for the cleavage of the precursor of LAMIN A, PRELAMIN A. The de novo point mutation in the *LAMIN A* gene in exon 11 on chromosome 1 is the cause of the vast majority of the HGPS cases (Eriksson et al., 2003). This mutation alters *ZMPSTE24* activity which leads to the introduction of a novel splice donor site which produces a mutant LAMIN A protein, termed 'PROGERIN' (Varela et al., 2005). In *ZMPSTE24*$^{-/-}$, a mutated form of PRELAMIN A is stuck in a permanently farnesylated form. The phenotype is equivalent to patients with HGPS syndrome.

ZMPSTE24$^{-/-}$ mice are characterized by nuclear abnormalities and histopathological defects which results in an aged phenotype. At the age of ~ 5-6 months, symptoms of aging start to develop: alopecia, loss of fur colour, kyphosis, tremor, declined forelimb grip strength, cataracts or corneal opacity, eye discharge, malocclusions, penile prolapse, piloerection and weight loss, (Reddy and Comai, 2012).

2.13.2 Mouse ear snips genotyping

Genotyping was performed to distinguish animals with a homozygous (-/-) or heterozygous (+/-) deletion of *ZMPSTE24* from those with a wild type gene (+/+). Ear snips were taken in the Preclinical Research Facility (PRF) by a qualified technician and placed in 1.5 ml Eppendorf's. Samples were kept at -20°C before use. First, to extract DNA from the ear snips, samples were covered with 200 µl of freshly prepared lysis buffer (**Table 2.13**). Additionally, 1 µl of 20 mg/ml Proteinase K was added to each sample and ear snips were incubated on a heating block (Stuart Equipment) at 55°C for 2 h. During incubation, samples were flicked by hand twice to dissolve the tissue in the lysis buffer. Then, samples were centrifuged at 14,000 x g for 2 min and the supernatant transferred into a fresh Eppendorf containing 200 µl of 100% Isopropanol (Fisher Scientific) and flicked by hand for DNA precipitation. Samples were centrifuged again at the same speed for 2 min, the supernatant aspirated, and pellets washed with 200 µl of 70% Ethanol. Samples were centrifuged at 14,000 x g for 2 min, the supernatant aspirated and pellets left to air dry at RT for 20 min. Then, pellets were resuspended in 50 µl of ddH_2O, the DNA concentration and yield measured using a Nanodrop spectrophotometer (Thermo Scientific) and the DNA kept at -20°C for future use.

Table 2.13. Tail Lysis Buffer components.

Values given for a final volume of 4 ml.

Reagent	Dilution	Volume	Final concentration
Tris HCl pH=8.0	1:10	400 µl	100 mM
EDTA 0.5M	1:100	40 µl	5 mM
10% SDS	1:50	80 µl	0.2%
NaCl 5M	1:25	160 µl	200 mM
ddH_2O		3320 µl	

2.13.2.1 PCR

To amplify the region of interest, Polymerase Chain Reaction (PCR) was used. First, 2 µl of extracted DNA (around 0.1 µg) was mixed with freshly prepared Master mix. Master mix contained 10 µl of 2 x MyTaq Red Mix (Bioline, BIO-25043), 1 µl of each primer (Forward: 5' GCT ACA TAG TGA ACA CCA GGC CA 3', Reverse: 5' GTC TGG TTG TTT GAT TAG ATG GGT C 3') and 6 µl of ddH_2O. The negative control contained 2 µl of ddH_2O (instead of DNA) mixed with 18 µl of Master mix. Samples were briefly centrifuged and placed in a Techne Prime thermal cycler (5PRIME/02) using a protocol developed by the Mutant Mouse Resource and Research Centre (MMRRC), University of California: 5 min of initiation at 95°C followed by denaturation for 1 min at the same temperature. Next, 40 cycles of annealing at 60°C for 30 sec each and elongation at 72°C for 1 min followed by 5 min of amplification at the same temperature. At the end, PCR products were held at 4°C and directly used for agarose gel electrophoresis or stored in -20°C for future use.

2.13.2.2 Agarose gel Electrophoresis

A 1.5 % agarose gel was prepared by dissolving 0.6 g of Agarose (Fisher Scientific) in 40 ml of 1 x Tris-Borate-EDTA (TBE) buffer. The mixture was microwaved in intervals for 1 min to fully dissolve the agarose and 0.8µl of 1% Ethidium Bromide (VWR Chemicals) was added to the mixture under a fume hood. The mixture was poured into a tank and the combs inserted with the gel left to solidify under a fume hood for 30 min. After solidification, the gel was placed in an electrophoresis tank filled with 1 x TBE and the comb removed. 6 µl of the sample was loaded on the gel next to 4 µl of PCR Ranger 100bp DNA Ladder (Norgen Biotek) and run for 40 min at 100 V. To visualise DNA bands, the gel was imaged using a Molecular Imager Gel DocTM XR System (Bio Rad) and captured with Image Lab software version 4.1. **Figure 2.1** shows an example of ear snip mouse genotyping results on an agarose gel, where the bands display either the wild type gene at 300 base pairs (bp), the mutant gene at 220 bp, or both genes.

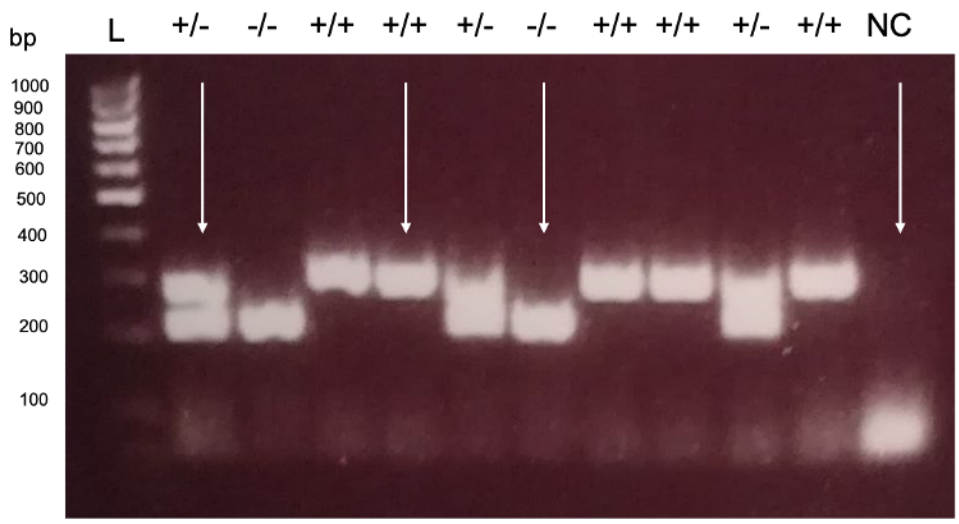

Figure 2.1. Genotyping results for ZMPSTE24$^{-/-}$ mice.

Representative image of an agarose gel supplemented with ethidium bromide for visualisation. PCR Ranger 100bp DNA Ladder (L) was used for estimating the size of the PCR products. Arrows points to examples of bands representing animals with either homozygous ($^{-/-}$), heterozygus ($^{+/-}$) or wild-type ($^{+/+}$) ZMPSTE24 gene. Distilled water was used as negative control (NC).

2.13.3 Slide subbing

Slides were placed in plastic racks and soaked in hot water with 5% Decon solution overnight. Next day, slides were washed in hot water for 30 min and rinsed with distilled water 3-4 times. Then, slides were dried at 60°C for 2 h. Further, slides were submerged in Subbing solution (2% 3-Aminopropyltriethoxysilane in Acetone), 2 times in Acetone and 2 times in ddH_2O for 2 min each. After incubations, slides were dried at 60°C overnight.

2.13.4 Hematoxylin and Eosin staining (H&E)

Samples were deparaffinised by incubating in Xylene, 100% Ethanol (2 times 10 min each) and then in 90% Ethanol and 70% Ethanol (10 min each). Next, samples were rinsed under running water for 3 min, immersed in Hematoxylin for 5 min and rinsed again with running water. Then, samples were submerged in 1% Acid alcohol for 10 seconds (sec), rinsed with running water, counterstained with Eosin for 1 min and rinsed with running tap H_2O. This was followed by incubation in 70% Ethanol for 30 sec and twice in 100% Ethanol for 5 min each. At the end, samples were cleared with Xylene (2 times for 5 min) and mounted on a slide using DPX.

2.13.5 Immunohistochemistry

The dissected tissues were washed 3 times with cold 1 x PBS and fixed in 10% formalin for 24 h. Afterwards, formalin was replaced with 70% ethanol and samples were given to the University of Leicester Histology Facility, where Formalin-Fixed Paraffin-Embedded Blocks (FFPE) were prepared. 5 µm sections of FFPE Paraffin blocks were cut using a LEICA RM2235 microtome. In order to eliminate distortion and wrinkles in the tissue, sections were stretched in a water bath (42°C) and then picked up on a slide (Superfrost plus). Prepared slides with tissue sections were deparaffinised first in Xylene, then in 100% Ethanol 2 times for 10 min each following incubation for 10 min in 90% Ethanol and 70% Ethanol. Next, slides were incubated in 30% H_2O_2 solution in 100% Methanol for 10 min to block endogenous peroxidase activity. For antigen retrieval, slides were incubated for 10 min in 10 mM citrate buffer pH=6.0 at 95°C using a pressure cooker and microwave and next, left to cool down at RT. Further, slides were washed 2 times for 10 min in 1 x PBS. Afterwards, tissue sections were marked with a Pap pen and blocked with 5% swine or goat serum in 1 x PBS and incubated in a humid chamber for 1-2 h at RT. Then, primary antibodies were applied on the tissue sections and slides were incubated overnight at 4°C. The next day, slides were washed 2 times with 1 x PBS for 10 min. Further, a biotinylated secondary antibody was applied and incubated for 1 h at RT. Then, samples were incubated with Streptavidin- peroxidase (Steptavidin, Horseradish Peroxidase, Vector-SA-5004) for 30 min at room temperature. Next,

samples were washed 2 times with 1 x PBS for 10 min and Peroxidase substrate (DAB Peroxidase HRP, Vector-SK4100) was applied for 5 min. Slides were rinsed with H_2O and counterstained with hematoxylin for 15 sec and rinsed again with H_2O. Dehydration was performed by incubating in gradual changes of ethanol (70%, 90%, and 2 times 100%) for 10 min each and slides were cleared by incubating twice in Xylene for 5 min each. Finally, sections were mounted on slides using DPX (Sigma, 44581).

Images of all slides were taken using a Nikon TE300 inverted microscope at 40 times magnification and results analysed using Immunoratio online tool (**http://153.1.200.58:8080/immunoratio/**).

Table 2.14. Reagents for immunohistochemistry

Reagent	Supplier	Product number
Eosin	Raymond Lamb	LAMB/100-D
Hematoxylin	Sigma Aldrich	GHS132-1L
Swine Serum (Normal)	Dako	X0901
Goat Serum (Normal)	Dako	X0907
Polyclonal Swine Anti-Rabbit IgG Biotinylated	Dako	E0353
Polyclonal Goat Anti-Rabbit IgG Biotinylated	Dako	E0433
Hydrogen Peroxide Solution (30% w/w in H_2O)	Sigma Aldrich	H1009
R.T.U. Horseradish Peroxidase Streptavidin	Vector Labs	SA-5704
DAB Substrate Kit	Vector Labs	SK-4100
M.O.M Immunodetection Kit	Vector Labs	BMK-2202
DPX	Sigma Aldrich	06522

2.14 nanoMIPs *In vivo* analysis

2.14.1 *In vivo* toxicity measurements

In order to assess the in vivo toxicity of B2M-targeted MIPs, 8 animals were divided into 4 groups of 2. Each group were given B2M-targeted MIPs (0.4 mg/ml) tagged with DyLight 800 NHS Ester via different routes of injection: intravenously (5 ml/kg), intraperitoneally or by oral gavage (10 ml/kg). Data were compared to untreated controls. Routine health and distress symptoms (**Table 2.15**) checks were carried out daily for 2 weeks including, weight change, skin and body appearance, natural behaviour, muscle tone, locomotion, hydration status, water and food intake. At the end of the study, mice were sacrificed, and blood samples collected through exsanguination via caudal vena cava.

Table 2.15. Distress scoring sheet to assess the impact of nanoMIPs on mouse health

Parameters		Score
Appearance	- Normal - Slight piloerection - Marked piloerection - Changes from normal to signs of deterioration of coat and skin	0 1.5 3 4-6
Natural behaviour	- Normal - Minor changes - Less mobile and isolated - Restless or very still	0 1 2 3-6
Food and water intake	- Normal - Body weight loss <5% - Body weight loss <10% - < 20%	0 3 4-6
Hydration status	- Normal - Abnormal skin pinch test - Very Abnormal skin pinch test	0 2.5 2.5-6
Body changes	- Normal - Backbones visible - Backbones very visible - Tachypnoea (fast breathing) - Dyspnoea (difficult breathing)	0 3 6 3 6
Locomotion	- Slightly abnormal gait/posture - Markedly abnormal gait/posture	0-1.5 3-6
Muscle tone	- Muscle groups have normal tone or mass - Muscle mass slightly soft -Muscle mass less firm, abdomen slightly soft - Muscle mass very thin, soft, undefined - Muscle mass has no tone or definition	0 2 3 4 5-6
Specific Indicators	- Tumour size >1.0cm^3 - Tumour impeding movement	6 6

2.14.1.1 Serum preparation

Blood was collected through exsanguination via vena cava by a University of Leicester Preclinical Research Facility (PRF) technician. After collection of the whole blood, the blood was left undisturbed to clot at RT for 30 min- 1 h. Next, the clot was removed by centrifuging at 1000 x g for 15 min. Supernatant was transferred into a new tube, snap frozen in liquid nitrogen and stored at -80°C. Serum samples were used for analysis within 2 weeks from collection.

2.14.1.2 Blood Urea Nitrogen (BUN), Alanine Transaminase (ALT) and Aspartate Transaminase (AST) analysis

Colorimetric determination of Blood Urea Nitrogen (BUN), Alanine Transaminase (ALT) and Aspartate Transaminase (AST) enzyme levels were performed as follow: BUN (Kit No. EIABUN, Invitrogen, Carlsbad, CA), AST (K753-100, Biovision, Minneapolis, MN, USA) and ALT (Kit No. 700260, Cayman chemicals, Michigan, USA). Procedures were performed as described by the manufacturer. Every serum sample was assayed in triplicate for all tested enzymes.

2.14.2 *In vivo* fluorescent imaging

All *in vivo* fluorescent imaging was performed by **Dr. Michael Kelly** and **Justyna Janus** in **University of Leicester Preclinical Imaging Facility (PIF).**

Wild type C57/BL6J mice and ZMPSTE24$^{-/-}$ fast aging mice of different ages (from 2 to 24 months) were anaesthetised and injected with 1.9 mg/kg of B2M-targeted MIPs (tagged with DyLight 800 NHS Ester or with Alexa Fluor 647) via tail vein 2 hours prior to imaging. Animals were shaved from the back (hair clippers and depilatory cream) and sterile eye lubricant applied to the animal's eyes. Further, mice were imaged using an IVIS Spectrum imaging system (PerkinEmler Inc) and a range of excitation and emission filters were chosen to reduce background signal. Analysis was performed using LivingImage software (version 4.5.2, PerkinElmer Inc). The IVIS Spectrum and Quantum FX micro-CT scanner (PerkinElmer Inc.) was used for 3D fluorescence imaging tomography (FLIT) and whole-body micro CT images taken for a subset of representative

animals. Mice remained anaesthetised for the whole imaging process and were culled before awakening.

2.15 Healthspan assessments

2.15.1 Experimental design

The aim of the study was to test the effect of senostatic (Ibrutinib) on the health-span of *ZMPSTE24*$^{-/-}$ mice. This mouse model is characterized by a short lifespan and multiple age-related disorders (Bergo et al., 2002a). For that reason, Home Office regulations allow animals to be kept for a maximum age of 8 months. To be used in any study, animals need to have reached 2 months of age. To assess the effect of Ibrutinib, treatment started in mice aged 2-3 months. Routine health checks and clinical frailty indices (**Figure 2.2**) were used to monitor and evaluate the welfare of animals to minimise and prevent any suffering. Animals were placed into experimental groups treated either with Ibrutinib or vehicle as a control. Animals were paired in cages according to their experimental group, matched by sex and age. All drug administrations were performed by a qualified PRF technician.

Animals were treated twice a week with 10 mg/kg of Ibrutinib (PCI-32765) via oral gavage with the volume not exceeding 10 ml/kg. Treatment started after weaning, when animals reached around 2-3 months of age and continued until the end of their life. Ibrutinib doses were prepared as follows: 140 mg of Ibrutinib dissolved in 560 µl of 100% DMSO and vortexed until completely dissolved. Then, 10 µl of the mixture was aliquoted into glass tubes and stored at -80°C until needed. To prepare the working doses, 2,490 µl of sterile water was added into a 10 µl aliquot of the dissolved drug and vortexed. The working concentration of the drug was 1 mg/ml and the administration volume were adjusted based on the weight of the animals according to the formula below (e.g. a 20 g mouse received 200 µl of the drug).

$$Dose\ volume(ml) = \frac{Weight\ (kg)\ x\ Dose\ (mg/kg)}{Working\ concentration\ (mg/ml)}$$

For the control (vehicle) group of animals, 10 µl of Ibrutinib was replaced with 10 µl of 100% DMSO and prepared the same as the experimental (Ibrutinib) group (10 µl of DMSO mixed with 2,490 µl of sterile water) and also administered via oral gavage according to the animal's body weight.

2.15.2 Health span evaluations

2.15.2.1 Clinical Frailty Score

Clinical Frailty Score was adapted from (Whitehead et al., 2014) and used to score the welfare of experimental animals. Assessment was performed mainly by physical examination and morphological changes such as hair loss, changes in coat condition or loss of whiskers. Hearing loss assessment was performed using a clicker pen. Forelimb grip strength test was performed by placing the mouse on a cage grid and encouraging the mouse to hold the grid by gentle tugging of its tail. A variety of parameters were tested and scored based on severity levels as follow: 0= Absent, 0.5= Mild, 1= Severe (**Figure 2.2**).

Table 2. Mouse Frailty Assessment Form©

Date: _____

Mouse #: _____ **Date of Birth:** _____ **Sex:** F M

Body weight (g): _____ **Body surface temperature (°C):** _____

Rating: 0 = absent 0.5 = mild 1 = severe

				NOTES:
➢ **Integument:**				
❖ Alopecia	**0**	**0.5**	**1**	_____
❖ Loss of fur colour	**0**	**0.5**	**1**	_____
❖ Dermatitis	**0**	**0.5**	**1**	_____
❖ Loss of whiskers	**0**	**0.5**	**1**	_____
❖ Coat condition	**0**	**0.5**	**1**	_____
➢ **Physical/Musculoskeletal:**				
❖ Tumours	**0**	**0.5**	**1**	_____
❖ Distended abdomen	**0**	**0.5**	**1**	_____
❖ Kyphosis	**0**	**0.5**	**1**	_____
❖ Tail stiffening	**0**	**0.5**	**1**	_____
❖ Gait disorders	**0**	**0.5**	**1**	_____
❖ Tremor	**0**	**0.5**	**1**	_____
❖ Forelimb grip strength	**0**	**0.5**	**1**	_____
❖ Body condition score	**0**	**0.5**	**1**	_____
➢ **Vestibulocochlear/Auditory:**				
❖ Vestibular disturbance	**0**	**0.5**	**1**	_____
❖ Hearing loss	**0**	**0.5**	**1**	_____
➢ **Ocular/Nasal:**				
❖ Cataracts	**0**	**0.5**	**1**	_____
❖ Corneal opacity	**0**	**0.5**	**1**	_____
❖ Eye discharge/swelling	**0**	**0.5**	**1**	_____
❖ Microphthalmia	**0**	**0.5**	**1**	_____
❖ Vision loss	**0**	**0.5**	**1**	_____
❖ Menace reflex	**0**	**0.5**	**1**	_____
❖ Nasal discharge	**0**	**0.5**	**1**	_____
➢ **Digestive/Urogenital:**				
❖ Malocclusions	**0**	**0.5**	**1**	_____
❖ Rectal prolapse	**0**	**0.5**	**1**	_____
❖ Vaginal/uterine/penile prolapse	**0**	**0.5**	**1**	_____
❖ Diarrhoea	**0**	**0.5**	**1**	_____
➢ **Respiratory system:**				
❖ Breathing rate/depth	**0**	**0.5**	**1**	_____
➢ **Discomfort:**				
❖ Mouse Grimace Scale	**0**	**0.5**	**1**	_____
❖ Piloerection	**0**	**0.5**	**1**	_____
❖ **Temperature score:** _____				
❖ **Body weight score:** _____				

Total Score/ Max Score:

© Susan E. Howlett, 2013

Figure 2.2. Clinical Frailty Indices used to assess the welfare of animals.

Adapted from (Whitehead et al., 2014)

2.15.2.2 Barnes Maze

To determine the effect of treatment on the animals' health span, a variety of tests were used. To assess the cognitive function of the mice after the Ibrutinib treatment, a Barnes Maze was used (Barnes, 1979, Barnes et al., 1980) and performed by **Dr. Akang Ekpenyong-Akiba** and **Dr. Gabriella Kocsis-Fodor**. My contribution involved video analysis as one of the blind observers and data analysis. The Barnes Maze was placed 1 meter above the ground and consists of a circular platform with 20 equidistant holes around it (**Figure 2.3B**). One of the holes (target hole) had a black escape box attached underneath it, while all other 19 holes were sealed with a black rubber tape to imitate a similar appearance to the target hole. The assembly of the box was necessary to create a stress-free shelter for animal to hide in. The hole opposite the target was labelled "O" and the surrounding holes were numbered. Numbers + 1 to +9 (positive) were assigned to holes from the right-hand side of the target hole and left-hand side holes were tagged with -1 to -9 numbers (negative). The experiment was performed in a designated room inside the Preclinical Research Facility (PRF), University of Leicester. The room was equipped with a speaker as a source of white noise, desktop computer, source of bright light and visual cues placed on the walls for easier identification of the target hole by the animal. Throughout the study, the position of the visual cues was kept constant and the maze was wiped with 70% industrial methylated spirit (IMS) after each animal. The experiment was carried for 14 days and involved four stages: Adaptation, Acquisition, Probe Trail and Recall (**Figure 2.4**). Each stage was recorded using a Microsoft LifeCam HD-3000 webcam and SharpCap 2.9 video software and the data obtained was manually analysed by two blind observers.

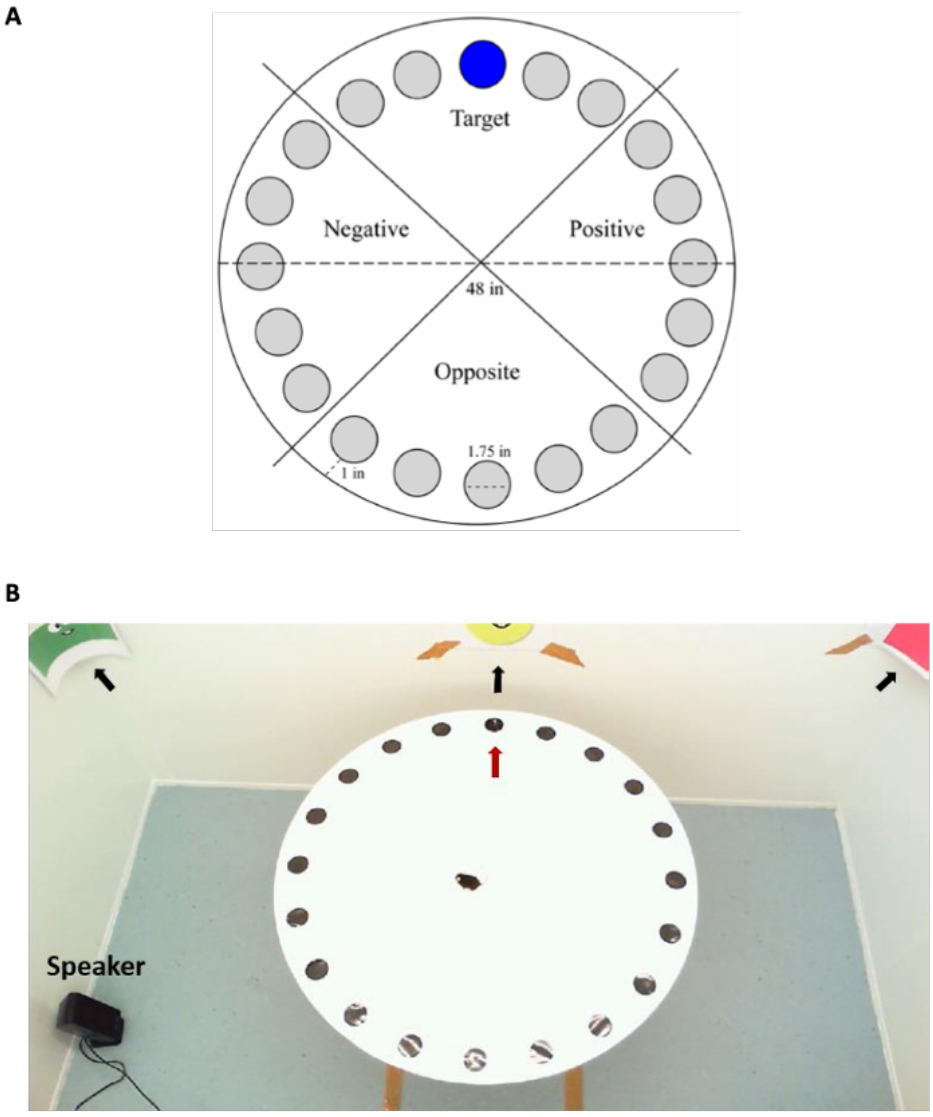

Figure 2.3. Barnes Maze set up for cognitive function test.

[A] Diagram of the Barnes Maze. Picture adapted from (Attar et al., 2013). [B] The set-up of experimental room adapted from (Ekpenyong-Akiba, 2018). The red arrow indicates the position of the target hole with the escape box placed underneath it. The visual cues placed on the walls of the experimental room are indicated by black arrows. A speaker was placed in the experimental room to provide white noise.

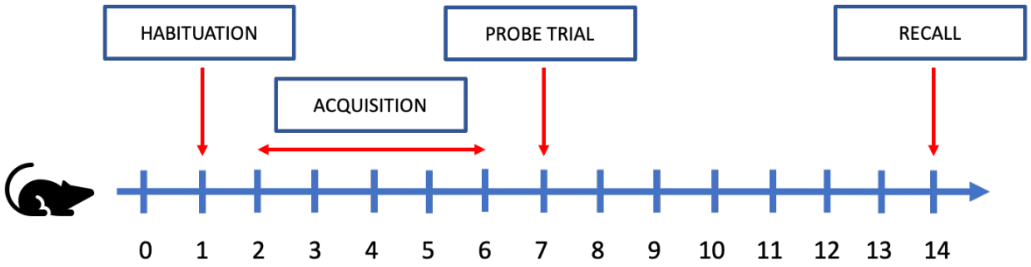

Figure 2.4. The experimental design of cognitive function test.

The Barnes Maze was used to compare the cognitive function in ZMPSTE24$^{-/-}$ mice treated with Ibrutinib or vehicle as a control group. The experiment consists of four parts. Habituation, Acquisition, Probe Trial and Recall and lasts 14 days in total.

The first stage, Adaptation, lasted one day and was aimed at familiarizing the mice with the experimental environment, the escape box, visual cues and surrounding mild stressors (white noise, bright light). Mice were placed in the middle of the maze and gently guided into the escape box, where the mice were left for 30 sec to familiarize with the safe space. As soon as mice entered the escape box, the white noise was switched off.

The Acquisition stage lasted between study day 2 and 6, where mice were given 3 min of training to locate the target hole and enter the escape box. Training was carried out in three intervals with 20 min breaks between trainings. The presence of a bright light and white noise created extra motivation for the animal to escape. The end of training was set once the mouse fully entered the box on its own. In the case of an animal unable to locate the target hole, training finished when 3 min elapsed, and the animal was gently guided into the escape box. For analysis, the latency (the time that the animal needed to reach the escape box for the first time during each round) and the number of errors made were recorded.

The third stage, Probe Trial, was on study day 7. The escape box was taken out of the maze and the target hole was sealed with the same tape as all the remaining holes. The mice were placed on the maze and allowed to locate the target hole (without the escape

box underneath it). The latency, number of errors and number of times the mice poked the target hole with their nose was recorded.

The last stage, Recall, was set 7 days after Probe Trial (study day 14). The Recall stage was conducted in the same manner as Probe Trial, also without the escape box underneath the target hole. The latency and number of errors were recorded and analysed later by two blind observers.

2.15.2.3 Kondziella's inverted screen test

To assess the effect of Ibrutinib and A1331852 treatments on muscle strength, a modified Kondziella's inverted screen test (Kondziella, 1964) was performed in the PRF using an Animal Transfer Station (ATS). The test was carried out once a week. The procedure was adapted from (Deacon, 2013) and used to test the time that the animal was able to support its own body weight. For that purpose, the mouse was placed in the middle of the square grid (**Figure 2.5**). The grid was flipped over and the time that the animal was able to hold the grid was measured. To prevent potential injuries, a fleece bedding material or a soft pillow was placed in the working station below the grid ensuring a safe base in case the mouse fell down. The duration (time a mouse was able to hold the grid) was recorded and scored 1-4 depending on the performance (**Table 2.16**). In order to normalize the results, the assigned scores were divided by a difference of animal weight and age as follow:

$$Normalized\ strength\ score = Kondziella\ Score\ /\ Weight$$

The study was divided into two parts: pilot and main study. During the pilot study 15 animals were used of which 5 knockdowns (*ZMPSTE24*$^{-/-}$) were treated via oral gavage with 20mg/kg Ibrutinib, and 4 knockdowns received vehicle via the same route of injection and additionally, 4 wild-types (*ZMPSTE24*$^{+/+}$) and 2 heterozygous (*ZMPSTE24*$^{+/-}$) were used as controls. During main study, 38 *ZMPSTE24*$^{-/-}$ animals were used and 20 of them received 10mg/kg Ibrutinib (oral gavage) and 18 were given vehicle.

Table 2.16. Kondziella's Inverted Test scoring system

Duration on the Grid (seconds)	Score
0 - 10	1
11 – 25	2
26 – 60	3
> 60	4

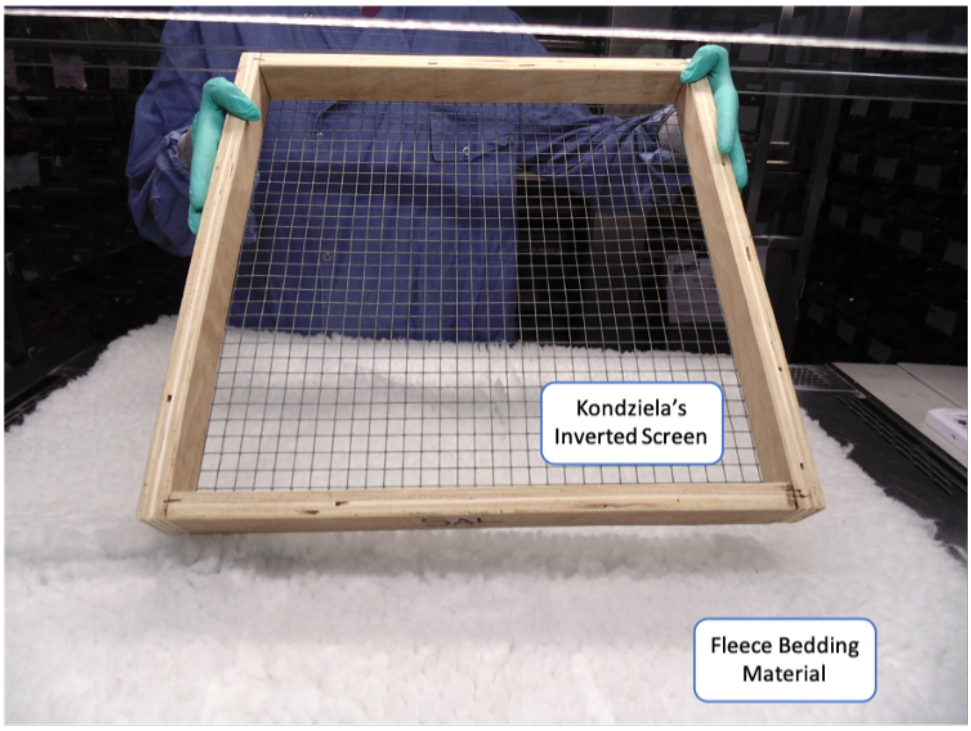

Figure 2.5. Kondziella's inverted Screen test

Assembly of the Kondziella's inverted screen test involved the Animal Transfer Station, Kondziella's Inverted Screen and Fleece Bedding Material or a Pillow.

2.16 Statistics

Statistical analysis of cells and animals' work was done using GraphPad Prism version 8 and Microsoft Excel. All results are presented as mean ± standard deviation (SD) except when stated. The Gaussian distribution of data were performed in GraphPad Prism using D'Agostino & Pearson normality tests. Statistical significance of the data was determined using paired and unpaired t-test.

3 Discovery of new senolytics

3.1 Senolytics

Elimination of senescent cells has a therapeutic potential in anti-cancer therapies and in aging-related diseases. However, availability of senolytics is limited and they are characterized by lack of specificity and presence of side effects (Kirkland and Tchkonia, 2017). Therefore, there is a strong need for further validation of already existing senolytics and more importantly development of new ones. In here, we explore potential new senolytics that could be used either alone or in combination.

3.1.1 Induction of cellular senescence in EJp53, EJp21 and EJp16 cell lines

To test effectivity of potential senolytics in killing senescent cells, we used a well-established senescence cell line models EJp53, EJp16 and EJp21, which are derivatives of bladder carcinoma (EJ) cell line with tetracycline regulatable expression systems for p53, p16, and p21, respectively (Sugrue et al., 1997b, Macip et al., 2002, Fang et al., 1999). With the removal of tetracycline from condition media, the expression of p53, p16 and p21 is induced and an irreversible senescent state is established after 3-4 days (**Chapter 2, section 2.2**). EJ-based models allow for the establishment of a senescent state due to the prolonged-expression of core proteins from the main pathways responsible for cellular senescence induction and maintenance (Campisi and d'Adda di Fagagna, 2007). Thus, the proposed panel of surfaceome proteins can be linked with the activation of p53-p21 and/or pRb-p16 pathways and could help determine in which of two pathways the candidate markers are preferentially activated.

At first, senescence was induced, and the establishment of the senescent state was confirmed (**Figure 3.1**) using a variety of methods, starting with a cell counting experiment to ensure proliferation arrest. Then, 4 days after removal of tetracycline, the induction of senescence was tested subsequently with analysis of SA-ß-gal activity. In all the cell lines, proliferation arrest was established before day 5 (**Figure 3.1A**) and the SA-β-gal activity was significantly higher after removal of tetracycline (**Figure 3.1B**). The difference in cell morphology was also observable. Cells were flattened and

enlarged comparing to proliferating controls (**Figure 3.1C**). The analysis of p53, p21 and p16 proteins expressions also revealed expected upregulation after removal of tetracycline (**Figure 3.2**). Taken together, our data confirmed successful induction of cellular senescence in EJp53, EJp21 and EJp16 cell lines.

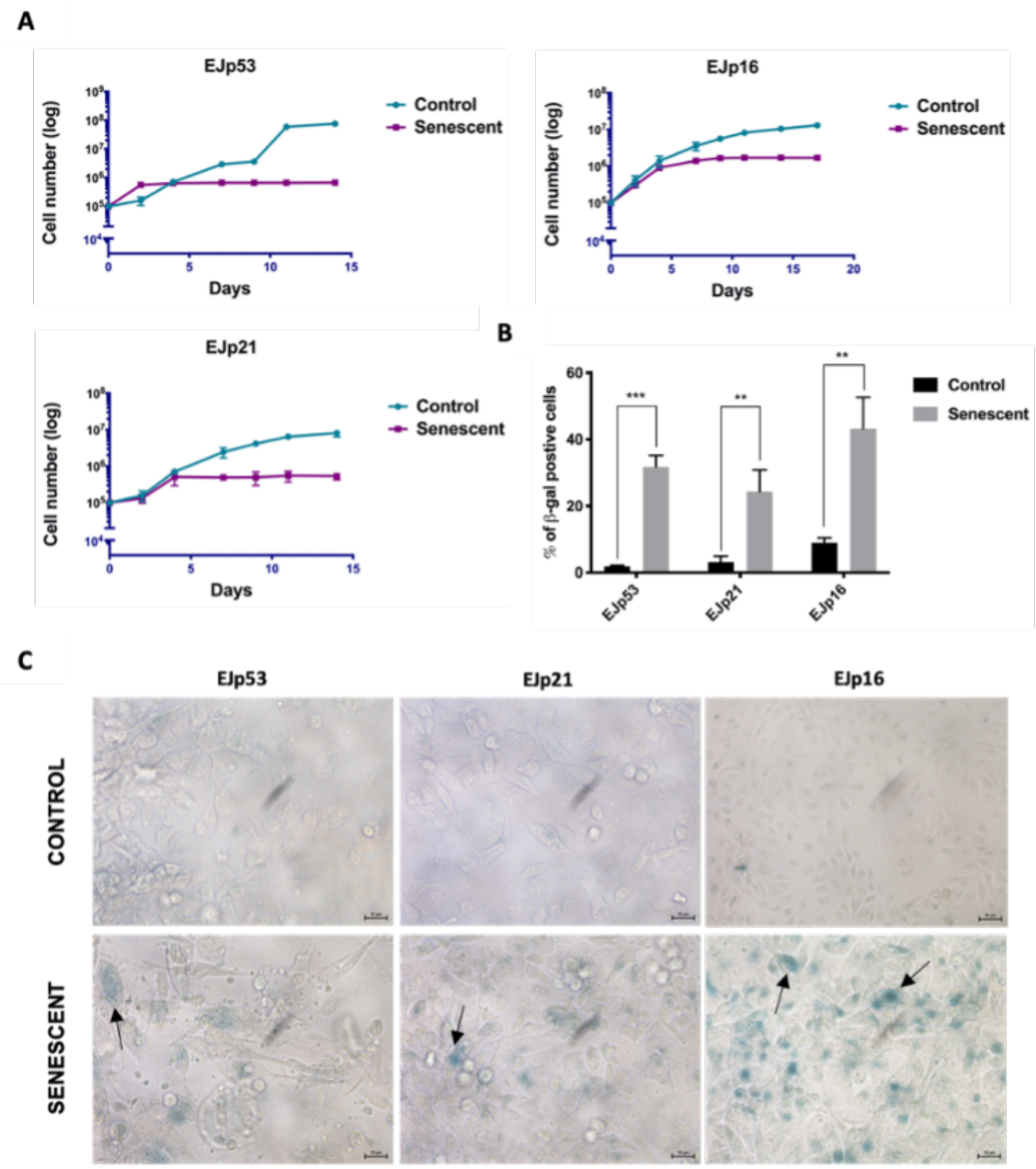

Figure 3.1. Induction of cellular senescence in EJ-based cell lines.

*[A] Cell counting experiment confirming proliferation arrest in EJp53, EJp21 and EJp16 cell lines. [B] Summary of SA-β-Galactosidase assay (4 days after removal of tetracycline) showing the % of B-gal positive cells in the tested models. [C] Representative pictures of the SA-βgal staining. Images shows changes in cell morphology and black arrows indicate positive staining (20x magnification). Bars represents the mean values ± SD, n=2. Statistical analysis performed using paired t-test (ns: not-significant, * p<0.05, ** p<0.01, *** p<0.001).*

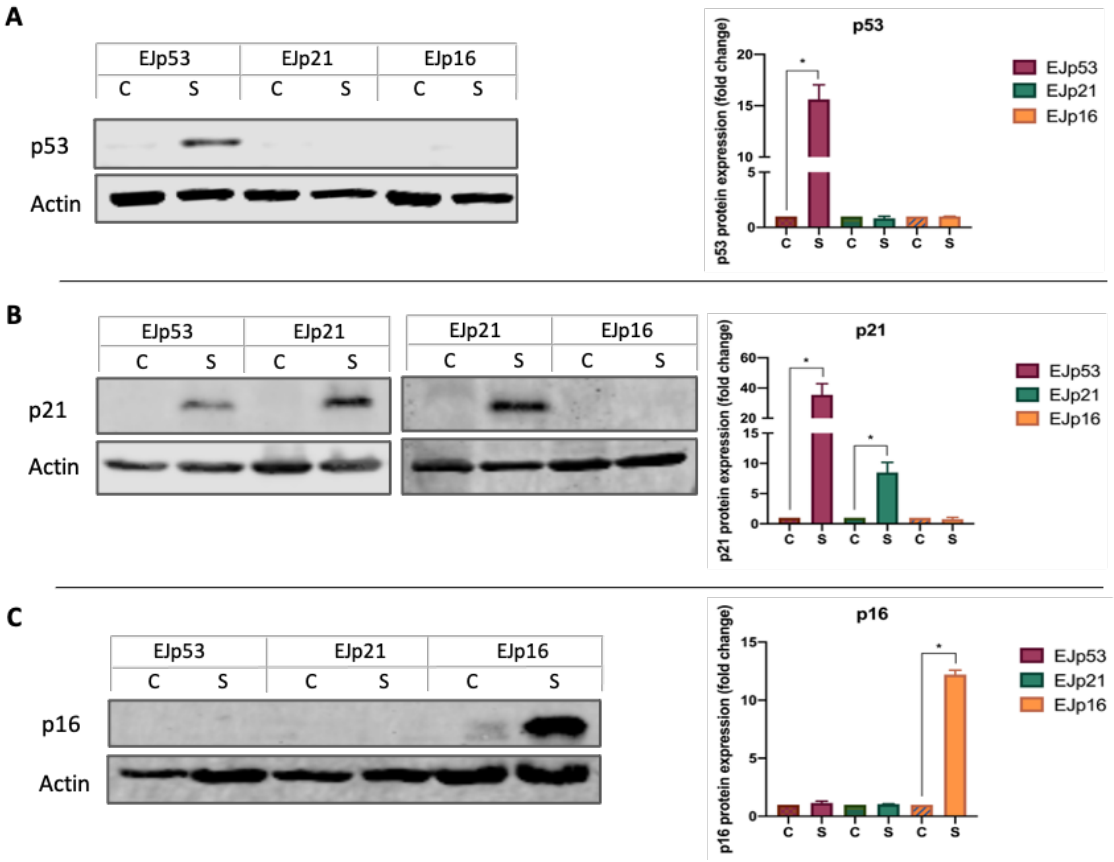

Figure 3.2. Characteristics of senescence induction in EJ-based cell lines

*Western blot analysis indicates the upregulation of p53, p21 and p16, 4 days after removal of tetracycline in corresponding EJ-models. "S" indicates senescent cells and "C" proliferating controls. Actin was used as loading control. Bars represents the mean values of the fold change calculated against proliferating counterparts ± SD, n=3. Statistical analysis between senescent and proliferating cells were performed using paired t-test (ns: not-significant, * p<0.05).*

3.1.2 Senescence induction in the HT1080-p21-9 cell line

Further, we decided to investigate senolytics effectivity in the cell line emerging from a different origin, and for that purpose, the HT1080-p21-9 cell line was used. HT1080-p21-9 is a derivative from the fibrosarcoma cell line HT1080. The model contains a p21 expression plasmid with an Isopropyl β-D-1-thiogalactopyranoside (IPTG) on-system. To induce p21 expression, 50 µM of IPTG was added to the culture media (Porter et al., 2012) and induction of cellular senescence was confirmed by cell counting, SA-β-gal staining and western blot (**Figure 3.3**). The number of SA-β-gal positive cells was significantly higher in cells treated with IPTG than in untreated controls **(Figure 3.3A**). The proliferation arrest was established within 3 days of IPTG addition (**Figure 3.3B**) and p21 level significantly increased (**Figure 3.3C**).

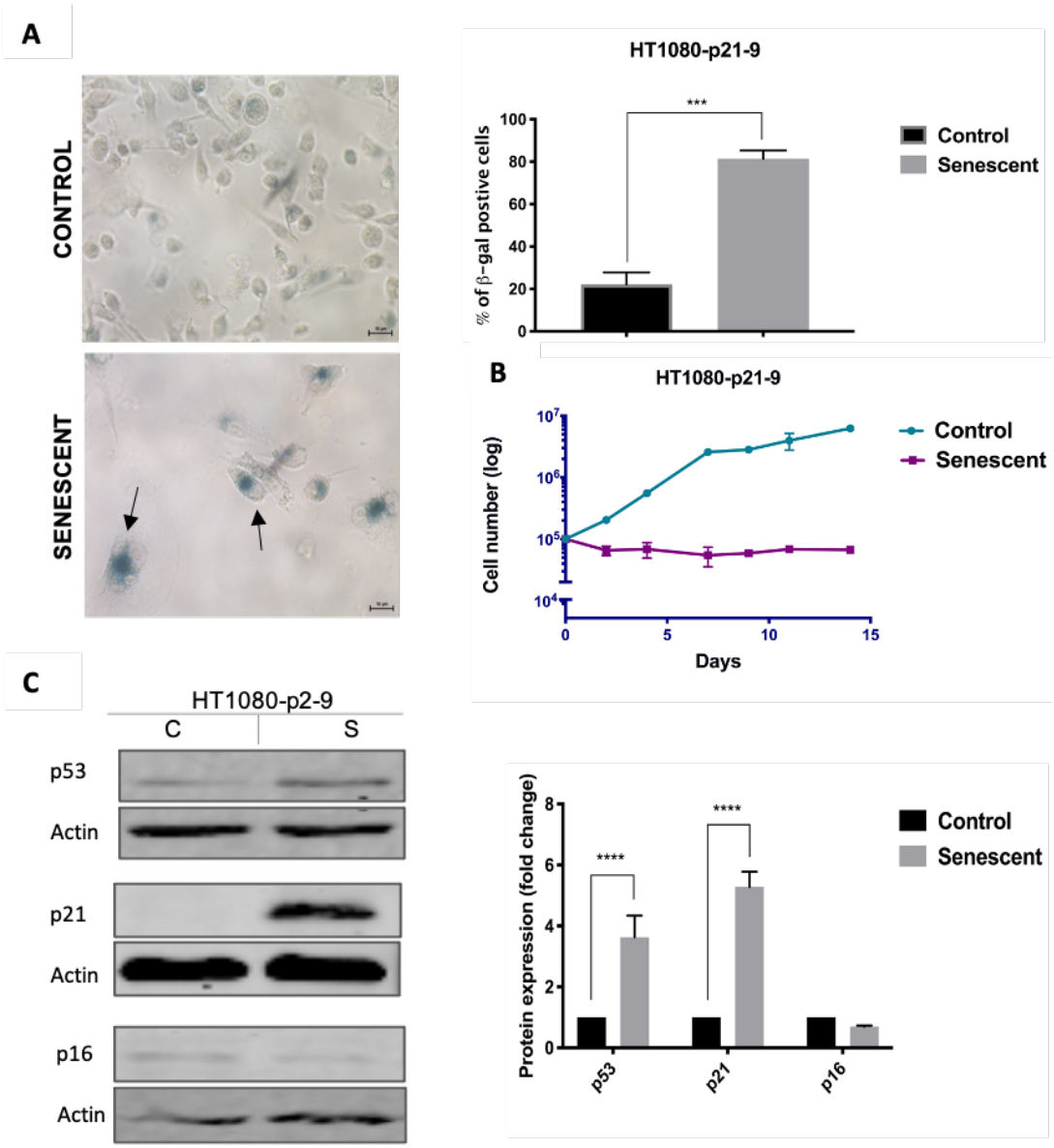

Figure 3.3. Senescence induction in HT1080-p21-9 cell line

Graph represents the assessment of senescence markers between proliferating HT1080-p21-9 controls and their senescent counterpart's. Western blot and SA-β-gal analysis performed 4 days after addition of IPTG to culture media. [A] SA-β-galactosidase assay showing the increase number of SA-β-gal positive cells (black arrows) in the cells treated with IPTG (20x magnification), n=2. [B] Cell counting analysis showing the proliferation arrest of HT1080-p21-9 cell line after addition of IPTG, n=2. [C] Western blot of p53, p21 and p16 proteins level between proliferating "C" and senescent cells "S", n=2. Actin was used as loading control. Bars represents the mean values ± SD. Statistical analysis between senescent and proliferating cells were performed using paired t-test (ns: not-significant, p<0.05, ** p<0.01, *** p<0.001, **** p<0.0001).*

3.1.3 Small-molecule p53 stabilators.

Protein-protein interactions (PPI) play important functions in many biological processes and diseases. In the last years, modifications of PPIs with small molecules have gained a lot of interests in biomedical research and has been consider a new therapeutic strategy (Falcicchio et al., 2020). Many studies focus on tumour suppressor p53 and its positive and negative interactions (Lane, 1992). The majority of small molecule-based strategies for activating wild-type p53 function has been focusing on p53 interaction with its primary negative regulator, MDM2 (Chène, 2003). A high number of compounds that interfere with p53-MDM2 interactions have been tested and some of them, such Nutlin-3a exhibited senolytic activity. Nutlin 3a stabilizes p53 through MDM2 inhibition and suppression of NF-κB, a core SASP regulator (Wiley et al., 2018). Thus, Nutlin-3a treatment of human fibroblasts decreased secretion of certain SASP factors.

We explored an alternative strategy although with the same goal, to stabilize p53, and test if pushing p53 out of the balance will be sufficient to induce apoptosis in senescent cells, hence achieving senolysis. We tested the senolytic potential of stabilization of p53 interactions with its positive regulator, 14-3-3σ. Interactions between these two proteins and their stabilization strategy has not been broadly investigated so far. 14-3-3σ is a member of 14-3-3 adapter proteins family that consists of 28-33 kDa acidic polypeptides conserved in all eukaryotic species (Hermeking and Benzinger, 2006). In humans, the 14-3-3 family consists of seven isoforms beta (β), epsilon (ε), eta (η), gamma (γ), tau (τ), sigma (σ) and zeta (ζ). Through PPI, 14-3-3 proteins are involved in many biological processes, such as metabolism, signal transduction, transcription, cell-cycle control, apoptosis, stress responses malignant transformations (Falcicchio et al., 2020). The 14-3-3σ can directly bind to p53 thus stabilizing its level (Yang et al., 2003) and also prevents p53 degradation mediated by MDM2.

We tested if small molecule stabilizers of p53-14-3-3σ interactions exhibited senolytic activity. We used two small molecule stabilizers, Fusicoccin A (FC-A) and the cytoprotective aminothiol, WR-1065. FC-A is a diterpene glycoside extracted from phytopathogenic fungus *Phomopsis Amygdali* and is known to cause peach and almond canker (Ballio et al., 1964). The exact mechanism how FC-A stabilizes p53-14-3-3σ PPI is poorly understood and there are ongoing studies to understand this process.

WR-1065 has been found to covalently bind to p53 leading to its activation and promotion of p53-14-3-3σ interactions (Pluquet et al., 2003). WR1065 also activates p53 its target genes, including p21 and Mdm2 **(Dziegielewski et al., 2008)**.

In order to test whether FC-A and WR-1065 are senolytics, a cell viability assay was performed using EJ-cell model of cellular senescence (**Figure 3.1**, **Figure 3.2**). Additionally, HT1080-p21-9 was also used (**Figure 3.3**). Cells were treated for 72h with increasing concentrations (0, 0.001, 0.01, 0.1, 1 and 10µM) of FC-A and/or WR-1065 5 days after senescence induction. Results revealed no changes in cell viability after the treatment with FC-A in both proliferating and senescent cells of all tested models (**Figure 3.4**). Similar results were observed after the treatment with WR-1065 (**Figure 3.5**). These data shows that neither FC-A nor WR-1065 exhibit senolytic activity when used as a single drug.

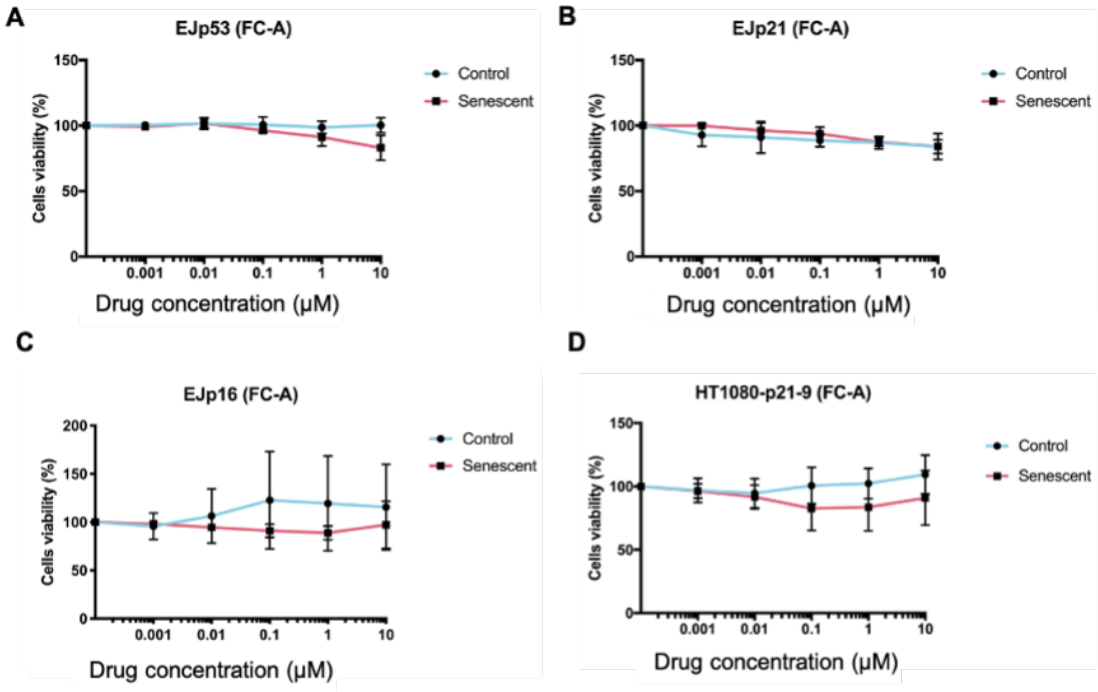

E

Cell line	EJp53		EJp21		EJp16		HT1080-p21-9	
Condition	Control	Senescent	Control	Senescent	Control	Senescent	Control	Senescent
IC50 (µM)	>50	>50	>50	>50	>50	>50	>50	>50

Figure 3.4. Cell viability of EJ and HT1080-p21-9 proliferating and senescent cells after treatment with FC-A.

Cell viability assay of proliferating and senescent (5 days after induction) EJp53, EJp21, EJp16 and HT1080-p-21-9 cells treated with increasing concentrations (0, 0.001, 0.01, 0.1, 1, 10 µM) of FC-A for 72h. [E] IC50 estimations based on cell viability results calculated using GraphPad Prism. Data were normalized to DMSO treated control. Data are expressed as mean and ± SD (EJp53 and EJp21 n=4, EJp16 n=3, HT1090-p21-9 n=2).

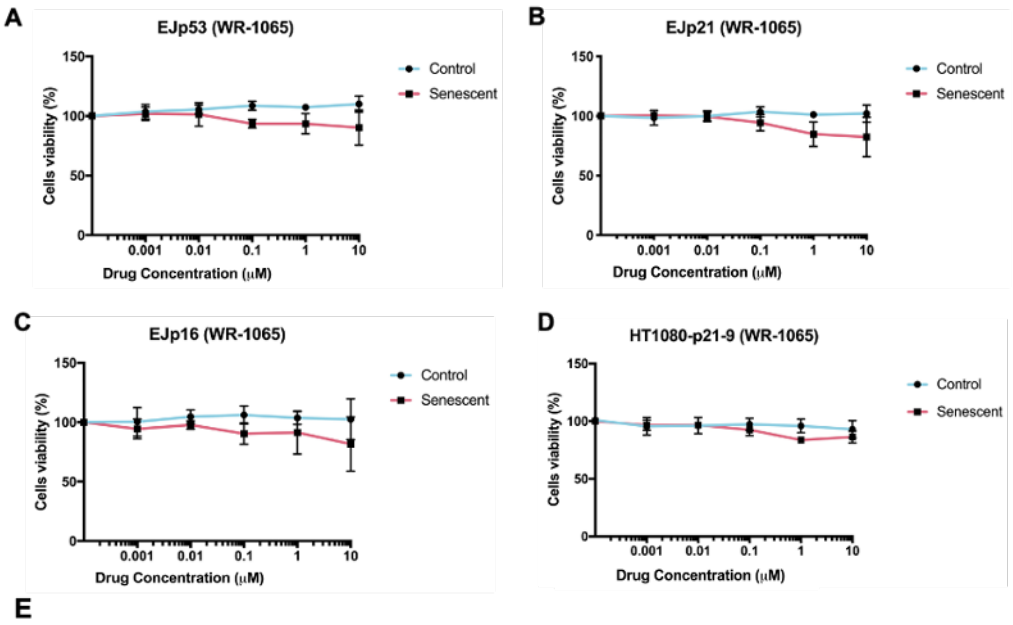

E

Cell line	EJp53		EJp21		EJp16		HT1080-p21-9	
Condition	Control	Senescent	Control	Senescent	Control	Senescent	Control	Senescent
IC50 (μM)	>50	>50	>50	>50	>50	>50	>50	>50

Figure 3.5. Cell viability of EJ and HT1080-p21-9 proliferating and senescent cells after treatment with WR-1065.

Cell viability assay of proliferating and senescent (5 days after induction) EJp53, EJp21, EJp16 and HT1080-p-21-9 cells treated with increasing concentrations (0, 0.001, 0.01, 0.1, 1, 10μM) of WR-1065 for 72h. [E] IC50 estimations based on cell viability results calculated using GraphPad Prism. Data were normalized to DMSO treated control. Data are expressed as mean and ± SD (EJp53 and EJp21 n=4, EJp16 and HT1090-p21-9 n=3).

Next, we tried the combination of both drugs, where we used the stable concentration (1μM) of one of the drugs together with increasing concentrations of the second drug. At first, we tried 1μM of FC-A and increasing concentrations of WR-1065. The combination experiment showed slight effect in majority of the cell lines, reaching up to 20% decrease in cell viability of senescent but not proliferating EJp53 cells when treated with 1 μM of FC-A and 10μM of WR-1065 (**Figure 3.6A**). A similar effect was observed in EJp16 and HT1080-p21-9, in which viability of senescent cells decreased for 15% when treated with 1 μM of FC-A and 10μM of WR-1065 (**Figure 3.6C-D**). Observed changes of EJp16 and HT1080-p21-9 cells might indicate an additional, p53-independent

functions of FC-A and WR10-65, which should be investigated further. There was no difference in viability between proliferating and senescent EJp21 cells.

Next, we used increasing concentrations of FC-A together with 1 µM of WR-1065. Results revealed a significant 30% decrease in cell viability of senescent EJp53 cells but not proliferating when treated with 10 µM of FC-A and 1 µM of WR-1065 (**Figure 3.7A**). In the other senescent cell models, the difference between proliferating and senescent cells viability was not clear. These results indicate a slight senolytic potential of FC-A and WR-1065 when used as a combination.

Taken together, our data shows no effect on viability of tested senescent models when FC-A and WR-1065 used alone. Moreover, our results showed a small difference in senescent cells viability when the combination of these drugs were used. However, the difference is minimal, and its biological impact is unclear. Further investigation using other senescence models and a wider range of concentrations of both drugs should be taken to confirm the potential synergistic effect on senescent cells. Moreover, further examinations should be taken to confirm cell death.

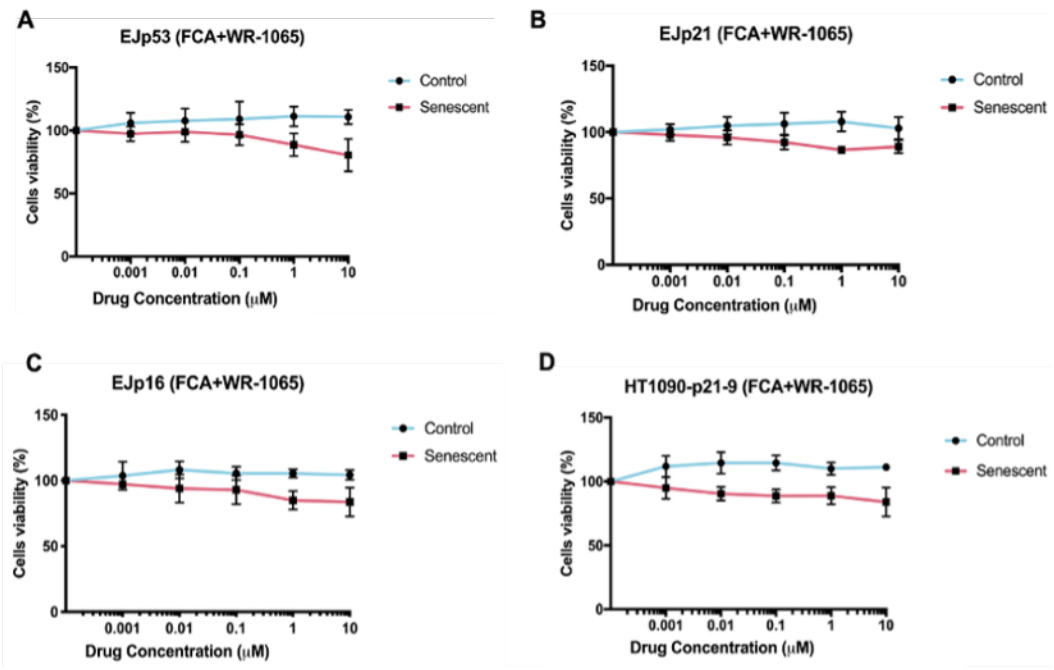

E

Cell line	EJp53		EJp21		EJp16		HT1080-p21-9	
Condition	Control	Senescent	Control	Senescent	Control	Senescent	Control	Senescent
IC50 (μM)	>50	>50	>50	>50	>50	>50	>50	>50

Figure 3.6. Combination of FC-A and WR-1065 in EJ and HT1080-p21-9 senescence models.

Cell viability assay of proliferating and senescent (5 days after induction) EJp53, EJp21, EJp16 and HT1080-p-21-9 cells treated for 72h with 1 μM of FC-A and increasing concentrations (0, 0.001, 0.01, 0.1, 1, 10 μM) of WR-1065. [E] IC50 estimations based on cell viability results calculated using GraphPad Prism. Data were normalized to DMSO treated control. Data are expressed as mean and ± SD (EJp53 and EJp21 n=4, EJp16 n=3, HT1090-p21-9 n=2).

.

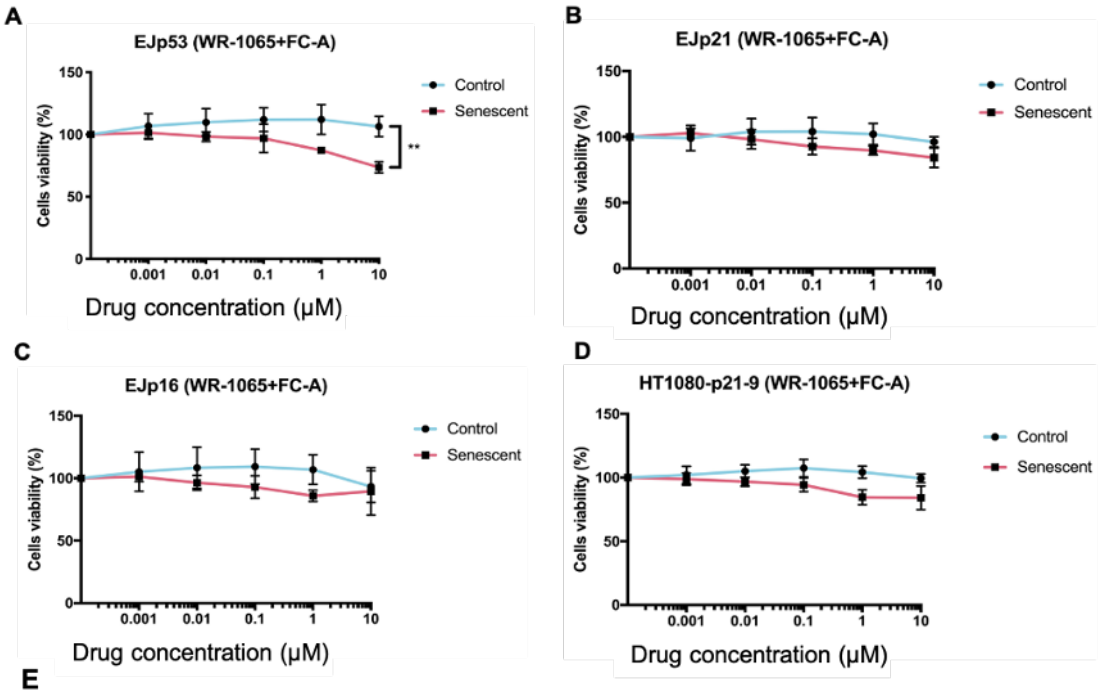

E

Cell line	EJp53		EJp21		EJp16		HT1080-p21-9	
Condition	Control	Senescent	Control	Senescent	Control	Senescent	Control	Senescent
IC50 (µM)	>50	34.15	>50	>50	>50	>50	>50	>50

Figure 3.7. Combination of WR-1065 and FC-A in EJ and HT1080-p21-9 senescence models.

*Cell viability assay of proliferating and senescent (5 days after induction) EJp53, EJp21, EJp16 and HT1080-p-21-9 cells treated for 72h with 1 µM of WR-1065 and increasing concentrations (0, 0.001, 0.01, 0.1, 1, 10 µM) of FC-A. [E] IC50 estimations based on cell viability results calculated using GraphPad Prism. Data were normalized to DMSO treated control. Data are expressed as mean and ± SD (EJp53, EJp21, HT1080-p21-9 n=4, EJp16 n=3). Statistical analysis performed using paired t-test (ns: not-significant, * p<0.05, ** p<0.01).*

3.1.4 GQC-05 and 9-Hydroxyellipticine.

We next tested GQC-05 and 9-hydroxyellipticine. Both drugs are chemical compound that shift splicing from the dominant anti-apoptotic BCL-X_L isoform to the pro-apoptotic BCL-X_S isoform (Weldon et al., 2018) and have never been tested in senescent cells, despite the fact that the BCL-2 protein family is a target of many known senolytics. Our analysis started with cell viability assay. EJp53, EJp16, EJp21 and HT1080-p21-9 were subjected to increasing concentrations of GQC-05 for 72h. Results revealed high cytotoxicity of GQC-05. The viability of both proliferating and senescence cells started to decrease after the treatment with 0.01µM in the majority of tested models (**Figure 3.8**). However, in EJp53 cells, treatment with low concentrations revealed significant changes in response between proliferating and senescent cells (**Figure 3.8A**). The treatment with 0.1µM caused 50% decrease of senescent cells viability, while for proliferating the drop was less than 10% (**Figure 3.8B**). It is worth to mention that there was a difference in IC50 values between senescent (IC50=0.3677 µM) and proliferating (IC50=0.08806 µM) EJp53 cells. In EJp16, the difference between senescent and proliferating cells was not significant. IC50 analysis of EJp21 and HT1080-p21-9 revealed that proliferating cells were more sensitive for the drugs than senescent cells and that was observed with a greater effect in HT1080-p21-9 than EJp21 cells (**Figure 3.8F**).
These data exposed a senolytic activity of GQC-05 when used at higher concentrations.

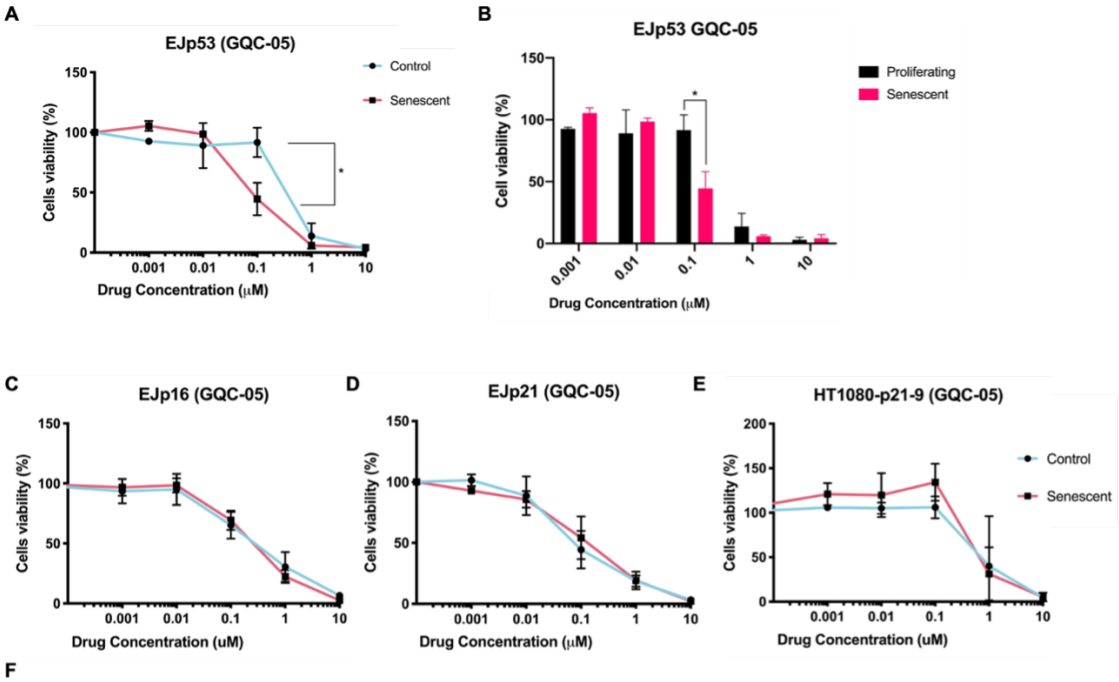

F

Cell line	EJp53		EJp21		EJp16		HT1080-p21-9	
Condition	Control	Senescent	Control	Senescent	Control	Senescent	Control	Senescent
IC50 (μM)	0.3677	0.08806	0.09498	0.1238	0.2793	0.2529	0.4608	0.8893

Figure 3.8. Cell viability of EJ and HT1080-p21-9 proliferating and senescent cells after treatment with GQC-05.

*Cell viability assay of proliferating and senescent (5 days after induction) [A-B] EJp53, [C] EJp21, [D] EJp16 and [E] HT1080-p-21-9 cells treated for 72h with increasing concentrations (0, 0.001, 0.01, 0.1, 1, 10 µM) of GQC-05. [F] IC50 estimations based on cell viability results calculated using GraphPad Prism. Data were normalized to DMSO treated control. Data are expressed as mean ± SD (EJp53 and HT1080-p21-9 n=3, EJp21 and EJp16 n=4). Statistical analysis performed using paired t-test (ns: not-significant, * p<0.05, ** p<0.01).*

The PI staining supported cell viability findings confirming higher level of cell death in senescent EJp53 when treated with concentrations such as 1 µM (**Figure 3.9A**). However, data revealed a constant percentage of cell death in all senescent cells including negative controls (0 µM). More concentrations should be added into analysis to confirm these findings. In EJp21 data revealed a strong difference between proliferating and senescent cells when treated with 1 µM. Although EJp21 analysis were performed just once and therefore should not be considered as reliable. In EJp16 there

was significant difference in the percentage of cell death between proliferating and senescent cells when treated with 1 µM (**Figure 3.9C**) which is contradictory to cell viability data.

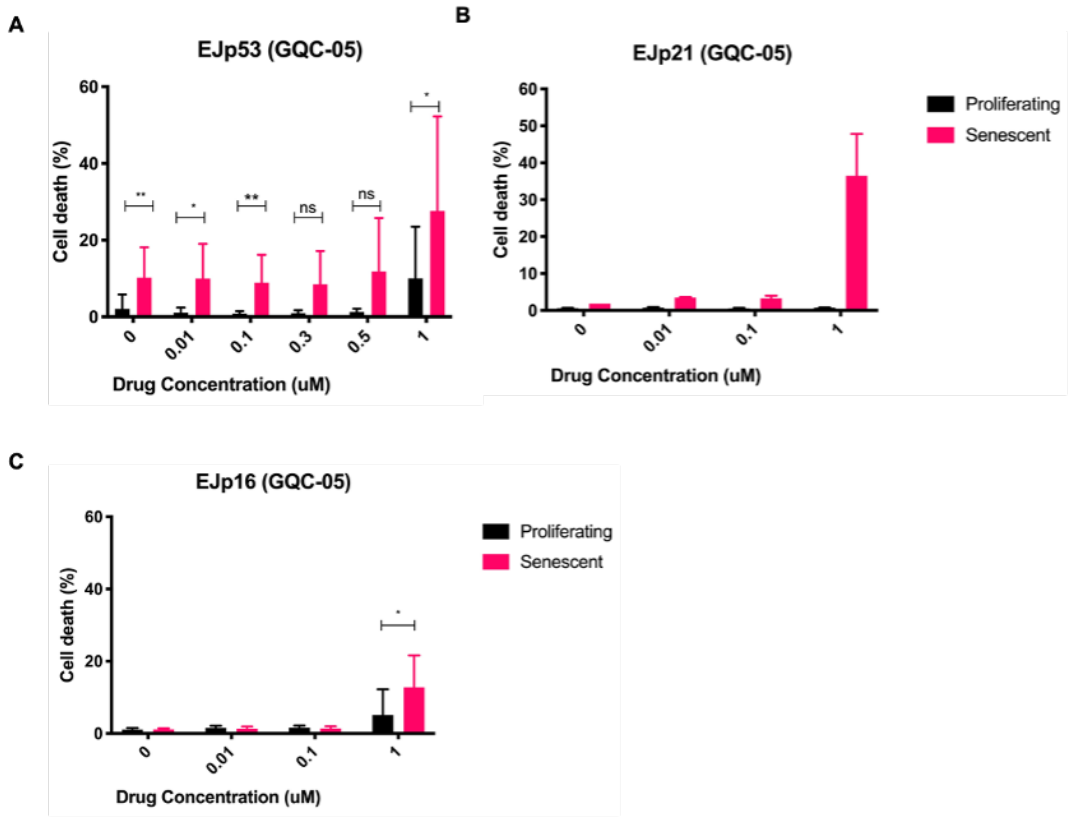

Figure 3.9. Cell death of EJp53, EJp21 and EJp16 cell lines after treatment with GQC-05.

*EJp53, EJp21 and EJp16 proliferating and senescent (5 days after induction) were incubated for 72h with selected concentrations (0, 0.01, 0.1, 0.3, 0.5 and 1 µM) of GQC-05. Cell death was analysed using PI staining measured by flow cytometry. DMSO was used as time matched control (0 concentration). Data are expressed as mean ± SD (EJp53 n=3, EJp16 n=3, EJp21 n=1). Statistical analysis performed using paired t-test (ns: not-significant, * p<0.05, ** p<0.01).*

We next tested the senolytic activity of 9-hydroxyellipticine, which has been shown to also shift splicing towards BCL-X_L favour although with lower effect than GQC-05 (Weldon et al., 2018). Cell viability data revealed no difference between proliferating and senescent cells in neither of the senescence models tested (**Figure 3.10**). Moreover, similarly to GQC-05, 9-hydroxyellipticine was also equally toxic to proliferating and

senescent cells when used in higher concentrations than 0.1 µM. Our results suggests that 9-hydroxyellipticine does not exhibit senolytic activity in the tested models of cellular senescence.

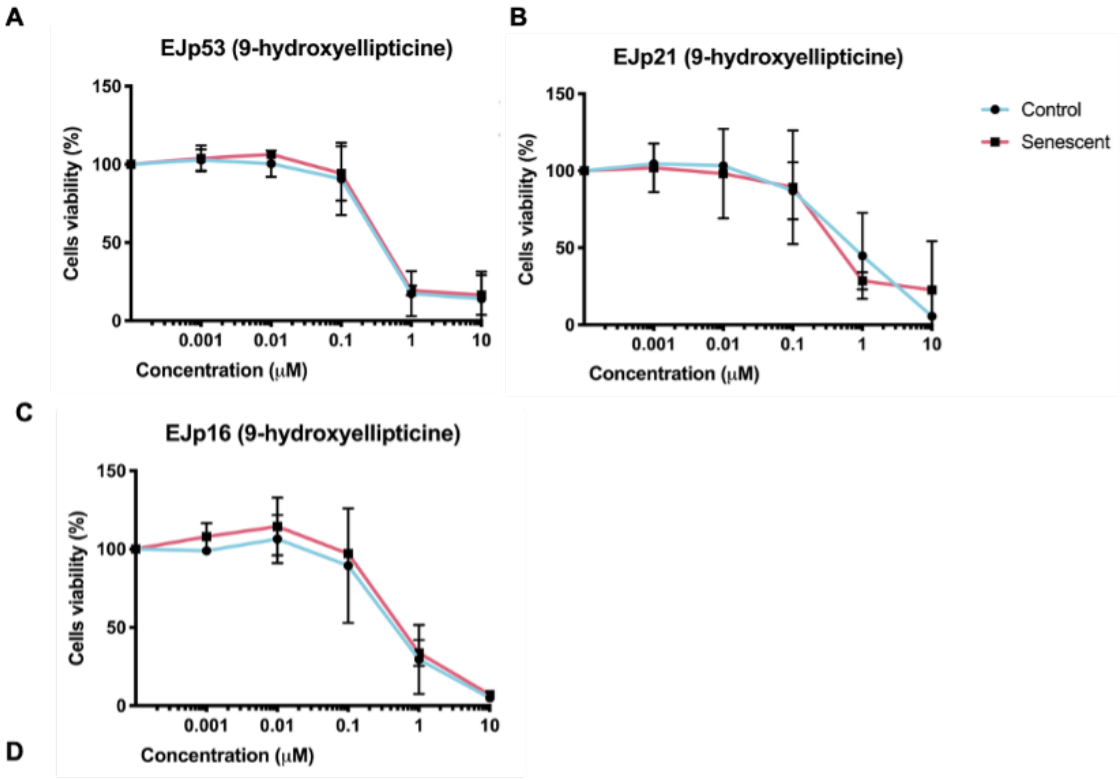

Cell line	EJp53		EJp21		EJp16	
Condition	Control	Senescent	Control	Senescent	Control	Senescent
IC50 (µM)	0.2399	0.2433	0.8367	1.244	0.4559	0.5014

Figure 3.10. Cell viability of EJp53, EJp21 and EJp16 proliferating and senescent cells after treatment with 9-hydroxyellipticine.

Cell viability assay of proliferating and senescent (5 days after induction) [A-B] EJp53, [C] EJp21, [D] EJp16 and [E] HT1080-p-21-9 cells treated for 72h with increasing concentrations (0, 0.001, 0.01, 0.1, 1, 10µM) of 9-hydroxyellipticine. [F] IC50 estimations based on cell viability results calculated using GraphPad Prism. Data were normalized to DMSO treated control. Data are expressed as mean ± SD (EJp53, EJp21 n=3, EJp16 n=2).

3.1.5 BH3 mimetics

Senescent cells have been reported to be resistant to extrinsic and intrinsic pro-apoptotic stimuli (Gorgoulis et al., 2019). While the mechanisms driving senescence are well studied, understanding the mechanisms preventing apoptosis is limited. However, it is well known that the BCL-2 protein family plays a central role in cell death regulation by diverse mechanisms, including apoptosis and autophagy (Youle and Strasser, 2008). The BCL-2 family consists of both pro-apoptotic proteins (e.g., BAX, BAK, BAD, and BIM), which activate the apoptotic program, and anti-apoptotic proteins (e.g., BCL-2, BCL-X_L, and BCL-W), which inhibit the execution of apoptosis.

Many pro-apoptotic members of the BCL-2 family play an important tumour suppression role in both mouse and human cancer models and many of them are repressed in different cancers (Aird et al., 2019, Barille-Nion et al., 2012, Barrott et al., 2017). On the other hand, the overexpression of the anti-apoptotic BCL-2 family proteins has been found in certain mouse and human cancers (Barille-Nion et al., 2012) and are a target of many senolytics (Paez-Ribes et al., 2019). Therefore, it was of our interest to further explore how the inhibition of BCL-2 family members affects the viability of senescent cells and we set out to test different BCL-2 family inhibitors on the viability of EJ senescence models.

3.1.5.1 Senescent cells upregulate BCL-2 family protein in p53-dependent manner.

To examine the dependence on BCL-2 family proteins of senescent cells, we used the EJ and HT1080-p21-9 senescent cell models. First, we assessed the transcript levels of BCL-2 family genes and compared them between senescent and proliferating cells. Results revealed statistically significant upregulation of *BCL-X$_L$*, *BCL-W* and *MCL-1L* (but not *MCL-1S*) and downregulation of *BCL-2* mRNA after p53 induction in EJp53 (**Figure 3.11**). However, that was not the case when senescence induction was triggered by upregulation of p21 without the presence of p53: In EJp21 cells there was no difference in genes expression between senescent and control cells. In turn, p16 driven senescence also indicated upregulation of *BCL-X$_L$* but downregulation of *BCL-W*. HT1080-p21-9 mRNA analysis showed significant downregulation of *MCL-1L* and *MCL-1S* but no changes in other genes.

Further, we performed analysis of expression of chosen BCL-2 pro-apoptotic members (**Figure 3.12**). In p53-driven senescence, two- fold upregulation was observed for *NOXA*, *PUMA*, *BAX* and *BAK* mRNA. In p16-dependent senescence, *BIM* and *PUMA* mRNA level significantly decreased when compared with proliferating cells. The rest of the genes remained unaffected by senescence induction. In HT1080-p21-9 cells there was no significant difference in mRNA level of any of tested pro-apoptotic members of BCL-2 family.

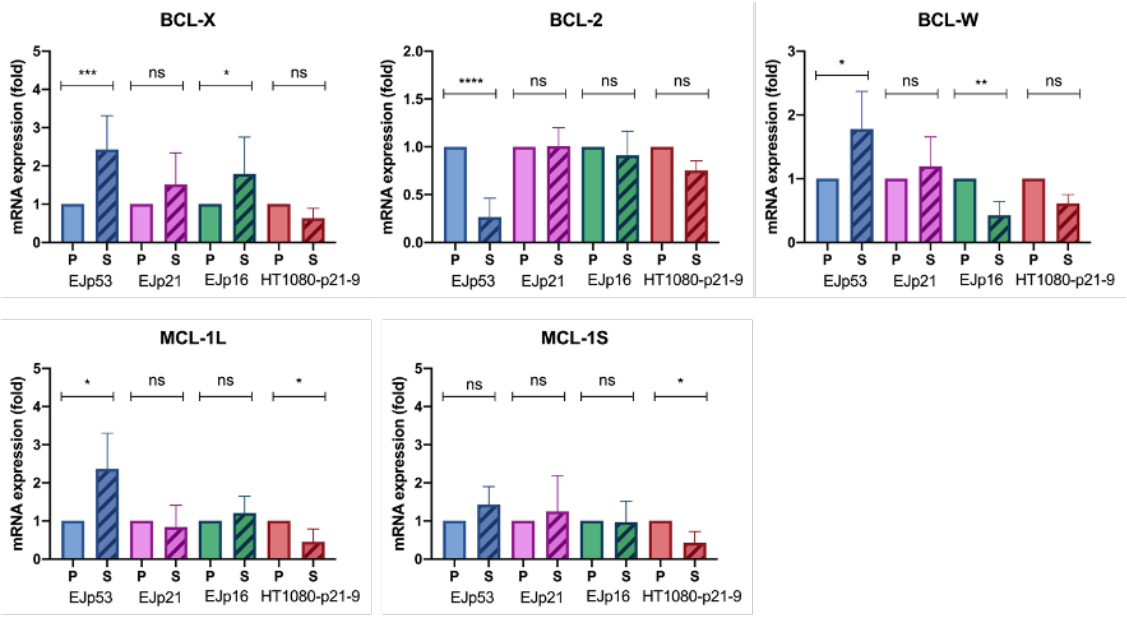

Figure 3.11. mRNA level of selected anti-apoptotic BCL-2 family members after senescence induction.

*qPCR data showing mRNA level of selected anti-apoptotic BCL-2 family members in EJp53, EJp21, EJp16 and HT1080-p21 proliferating and senescent cells (5 days after induction). GAPDH was used as internal reference control gene. Data were normalized against untreated proliferating counterparts. Bars represents the mean values ± SD, n=3 Statistical analysis performed using paired t-test (ns: not-significant, * p<0.05, ** p<0.01, *** p<0.001, **** p<0.0001).*

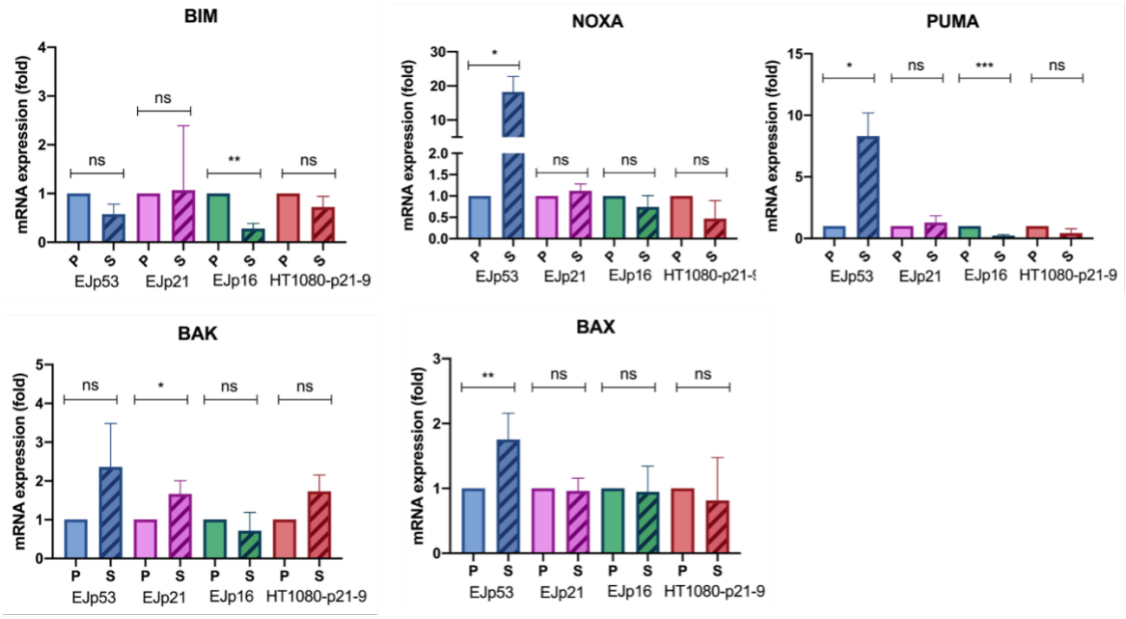

Figure 3.12. mRNA level of selected pro-apoptotic genes after senescence induction.

*qPCR data showing mRNA level of selected pro-apoptotic BCL-2 family members in EJp53, EJp21, EJp16 and HT1080-p21 proliferating and senescent cells (5 days after induction). GAPDH was used as internal reference control gene. Data were normalized against untreated proliferating counterparts. Bars represents the mean values ± SD, n=3 Statistical analysis performed using paired t-test (ns: not-significant, * p<0.05, ** p<0.01, *** p<0.001).*

Taken together, analysis of mRNA expression level of different pro- and anti-apoptotic members of BCL-2 family revealed differences in their expression depending on activation of senescence-inducing pathway.

Next, we performed WB analysis to investigate expression changes in protein level of selected members of BCL-2 family upon senescence induction (**Figure 3.13**, **Figure 3.14**). EJp53 senescent cells had an upregulation of BCL-X_L, BCL-W as well as BAX, BAK, NOXA and PUMA when compared to proliferating cells. Other markers tested, BCL-2 and MCL-1, did not change upon senescence induction. In EJp21, we observed downregulation of MCL-1, NOXA and PUMA (**Figure 3.13**, **Figure 3.14**) and no changes in other markers after senescence induction. Further, analysis of senescent EJp16 cells showed a decrease of BCL-2, BCL-W, MCL-1, BAX, BAK, NOXA and PUMA after senescence induction (**Figure 3.13**, **Figure 3.14**). There was also no difference in BCL-X_L protein level when compared with proliferating counterparts. Additionally, in HT1080-p21-9, the majority of markers were decreased after senescence induction.

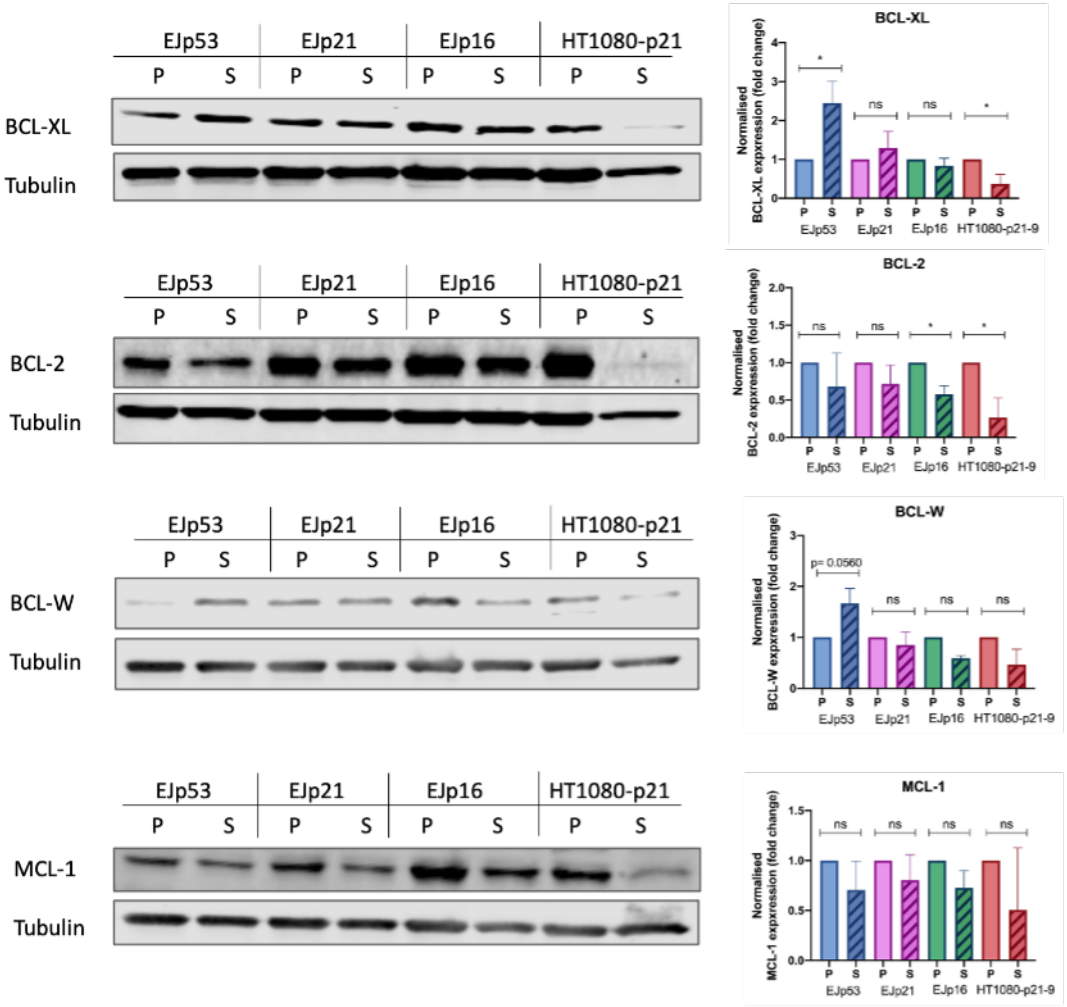

Figure 3.13. Western blot analysis of anti-apoptotic BCL-2 family members after senescence induction.

Western blot analysis showing protein level of anti-apoptotic BCL-2 family members in EJp53, EJp21, EJp16 and HT1080-p21 proliferating and senescent cells (5 days after induction). Tubulin was used loading control. Data were standardized against tubulin and compared with proliferating counterparts. Bars represents the mean values ±SD, n=3 (Further blots available in appendix ***Figure 9.1***). *Statistical analysis performed using paired t-test (ns: not-significant, * p<0.05, ** p<0.01)*

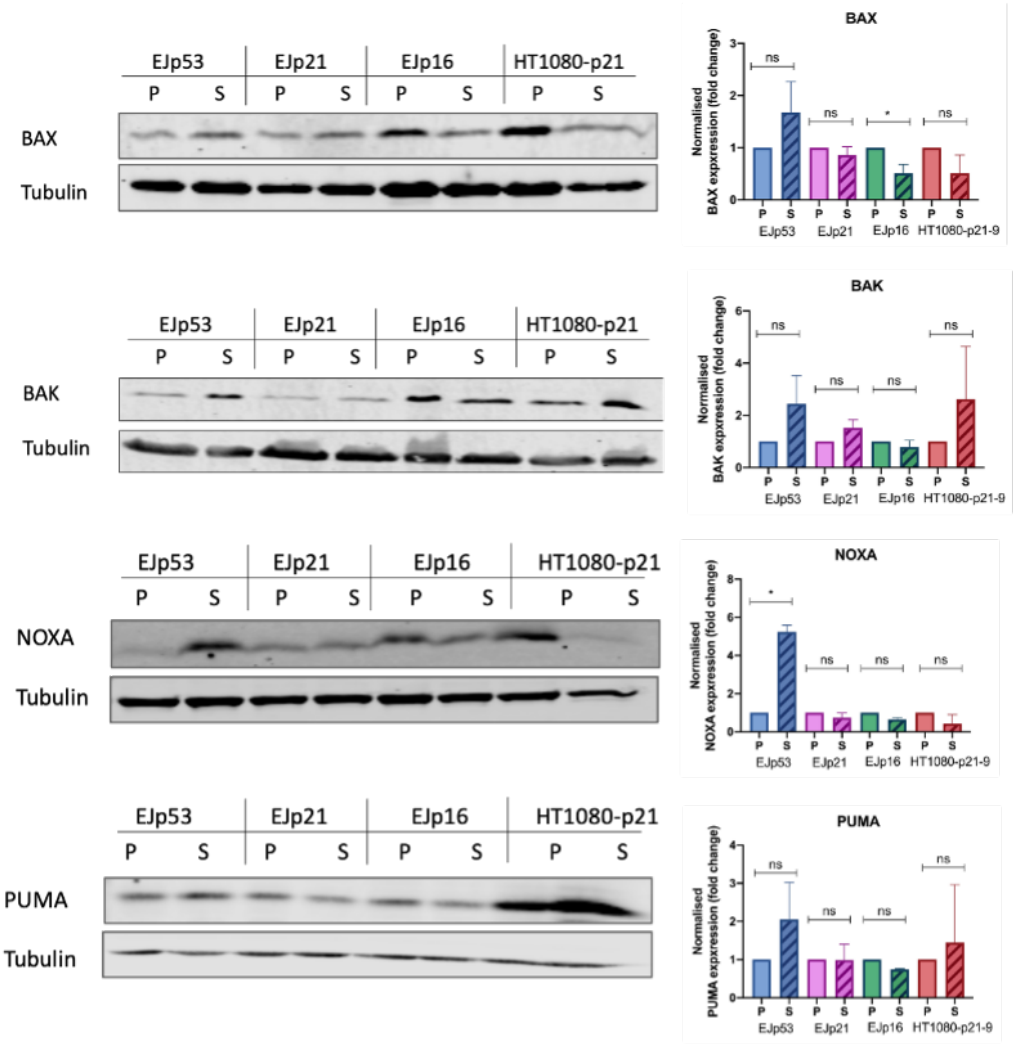

Figure 3.14. Western blot analysis of selected pro-apoptotic BCL-2 family member proteins after senescence induction.

Western blot analysis showing protein level of selected pro-apoptotic markers in EJp53, EJp21, EJp16 and HT1080-p21 proliferating and senescent cells (5 days after induction). Tubulin was used loading control. Data were standardized against tubulin and compared with proliferating counterparts. Bars represents the mean values ± SD, n=3. **(Further blots available in appendix *Figure 9.2*)**. *Statistical analysis performed using paired t-test (ns: not-significant, * p<0.05, ** p<0.01).*

Taken together, analysis of mRNA and protein level revealed similar patterns of expression (**Table 3.1**). Data revealed p53-dependent upregulation of BCL-X_L, BCL-W, BAX, BAK, NOXA and PUMA at both protein and mRNA level during senescence. BCL-X_L upregulation was also detected in p16-driven senescence, and BAX and BAK expression did not change significantly in p21-driven senescence. Interestingly, BCL-2 protein expression decreased in each of the tested models upon senescence induction albeit, its mRNA significantly decreased only in EJp53 senescent cells. In EJp21, BCL-X_L and BCL-W expression of markers did not change upon senescence induction. In EJp16 cells, majority of tested markers were downregulated except BCL-X_L. Analysis of HT1080-p21-9 senescent cells showed downregulation of all the markers except BAK, which was upregulated.

These findings revealed different expression of pro- and anti-apoptotic members of BCL-2 family depending on senescence-inducing pathway. High expression of BCL-X_L in p53-driven but not in p21 or p16-dependent senescence is interesting in the matters of previous findings. High level of BCL-X_L has been also found in two triple-negative breast cancer cell lines (MDA-MB-231 and HCC1143) that survived exposure to oncogenic suppressors by induction of cellular senescence, and inhibition of BCL-X_L in these cells has been shown to change the cell fates from senescence to apoptosis (Gayle et al., 2019). Of note, both cell lines have a high level of mutant p53 (Hui et al., 2006, Gazdar et al., 1998). The actual role of BCL-X_L in cellular senescence remains unknown. There are also indications that BCL-X_L upregulation reduced cellular senescence. In particular, overexpression BCL-X_L with a plasmid resulted in downregulation of senescence markers, such as p16 and p21 and SA-ß-galactosidase (Borras et al., 2016). This might indicate pleiotropic role of BCL-X_L in cellular senescence and regulation of cell fate decisions depending on the simultaneous expression of other factors, such as p53.

Table 3.1. Summary of BCL-2 family members expression level in senescent models in vitro.

Table presents expression level of BCL-2 family members in senescent cells when compared with proliferating counterparts. Analysis were performed using qPCR and Western blot of EJp53, EJp21, EJp16 and HT1080-p21-9 cells, 5 days after senescence induction. G- shows mRNA level of a markers, P- protein level. MCL-1 mRNA analysis includes MCL-1_L (L) and MCL-1_S (S) isoforms. BCL-X_L isoform was tested only at protein level. (N/T: not tested, —: no change, ↓: less than two-fold downregulation, ↓↓: two-fold and higher downregulation, ↑: less than two-fold upregulation, ↑↑: two-fold and higher upregulation).

	Cell line							
	EJp53		**EJp21**		**EJp16**		**HT1080-p21-9**	
Name of the marker	G	P	G	P	G	P	G	P
BCL-X	↑↑	L↑↑	↑	L—	↑	L ↑	—	L↓↓
BCL-W	↑	↑↑	—	—	↓↓	↓↓	↓	↓
BCL-2	↓↓	↓↓	—	↓	—	↓↓	—	↓↓
MCL-1	L↑ S—	↓	L— S—	↓	L— S—	↓	L↓↓ S↓↓	↓↓
BCL-2A1	N/T	—	N/T	↓	N/T	↓	N/T	↓↓
BAX	↑	↑	—	↑	—	↓↓	—	↓↓
BAK	↑↑	↑↑	↑	↑	—	—	↑	↑↑
BIM	↓	N/T	—	N/T	↓↓	N/T	—	N/T
NOXA	↑↑	↑↑	—	—	—	↓	↓	↓↓
PUMA	↑↑	↑	↑	↓	↓↓	↓	↓↓	—

3.1.5.2 Dependency of senescent cells on anti-apoptotic proteins.

Further, we decided to test senescent cells dependency on BCL-2 family anti-apoptotic proteins. For that reason, we used BH3 profiling. As discussed previously (**Chapter 2, section: 2.9**), BH3 profiling is an assay proposed to predict anti-apoptotic protein dependency and sensitivity to BH3 mimetics (Certo et al., 2006). It relies on gentle permeabilization of cells and addition of synthetic peptides that specifically target the anti-apoptotic proteins. If the cell survival is dependent on these proteins, then apoptosis will be induced. As an output, mitochondrial depolarisation is measured as an early step of intrinsic apoptosis.

We used BH3 profiling on EJp53, EJp21 and EJp16. BH3 profiling was performed with help of **Dr Victoria Smith**. All cell lines had a loss of mitochondrial membrane potential after treatment with different concentrations of BIM peptide (10 μM, 1 μM, 0.1 μM), that was used as a positive control due to its ability to bind to all anti-apoptotic proteins (Dutta et al., 2015). A dose-dependent response to the BIM peptide indicated that all three cell lines tested have a functional BAK and BAX (**Figure 3.15**, **Figure 3.16**, **Figure 3.17**). In EJp53, there was a significant difference between proliferating and senescent cells in response to the BAD peptide, which targets three anti-apoptotic proteins: BCL-2, BCL-X_L and BCL-W (**Figure 3.15**). After the treatment with BAD peptide, senescent cells had a higher rate of relative loss of mitochondrial potential, which suggest that they were more primed for death than proliferating cells. There was also a difference although not statistically significant in response to the MS1 peptide, that targets MCL-1. Importantly, a significant change in dependency of senescent EJp53 cells was observed in response to XXa1 peptide, that specifically targets BCL-X_L. There was no difference between senescent and control cells in response to the FS2 peptide, which targets BCL-2A1. Interestingly, significant differences between proliferating and senescent cells were observed only in EJp53 cell line but not in EJp21 and EJp16, in which none of the tested peptides induced a senescent-specific loss of mitochondrial membrane potential. Our data suggests that p53-driven senescence might be dependent on BCL-X_L expression, and that was not observed in p21- and p16-induced senescence.

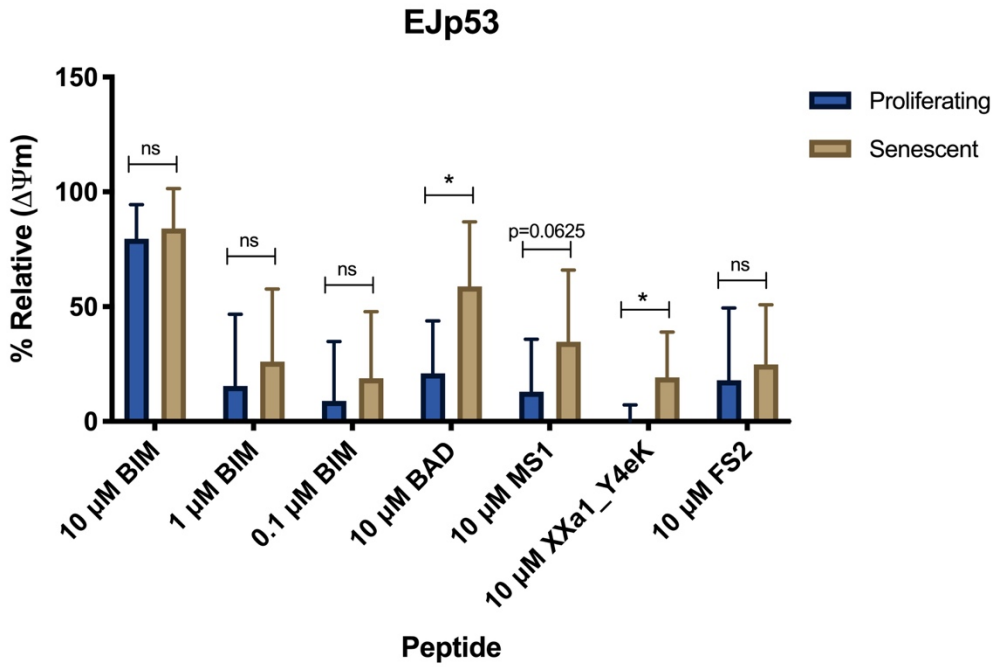

Figure 3.15. BH3 profiling of EJp53 cell line.

*5 days after senescence induction, senescent and proliferating EJp53 cells were gently permeabilised, treated with synthetic peptides and immediately before analysis stained with JC-1, a mitochondrial membrane potential probe. Plot shows the percentage of relative loss of mitochondrial membrane potential (ΔΨm), which was determined by normalising the data to DMSO (negative control). Synthetic peptides used: BIM (all anti-apoptotic proteins), BAD (BCL-2, BCL-W, BCL-X_L), MS1 (MCL-1), XXa1_Y4eK (BCL-X_L), FS2 (BCL-2A1). Bars represents the mean values ±SD, n=5. Statistical analysis performed using paired t-test (ns: not-significant, * p<0.05).*

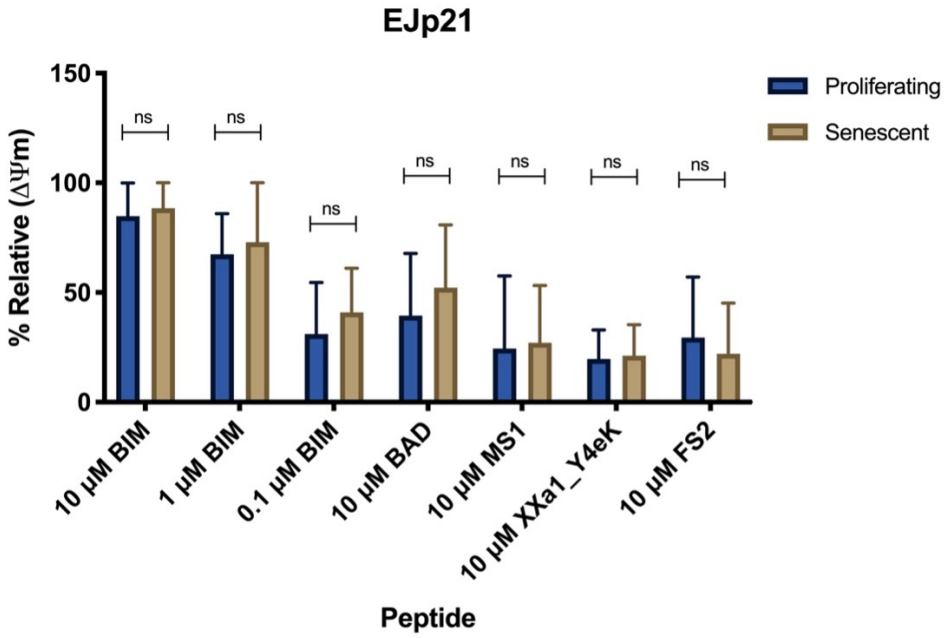

Figure 3.16. BH3 profiling of EJp21 cell line.

*5 days after senescence induction, senescent and proliferating EJp21 cells were gently permeabilised, treated with synthetic peptides and immediately before analysis stained with JC-1, a mitochondrial membrane potential probe. Plot shows the percentage of relative loss of mitochondrial membrane potential (ΔΨm), which was determined by normalising the data to DMSO (negative control). Synthetic peptides used: BIM (all anti-apoptotic proteins), BAD (BCL-2, BCL-W, BCL-X_L), MS1 (MCL-1), XXa1_Y4eK (BCL-X_L), FS2 (BCL-2A1). Bars represents the mean values ±SD, n=3. Statistical analysis performed using paired t-test (ns: not-significant, * p<0.05).*

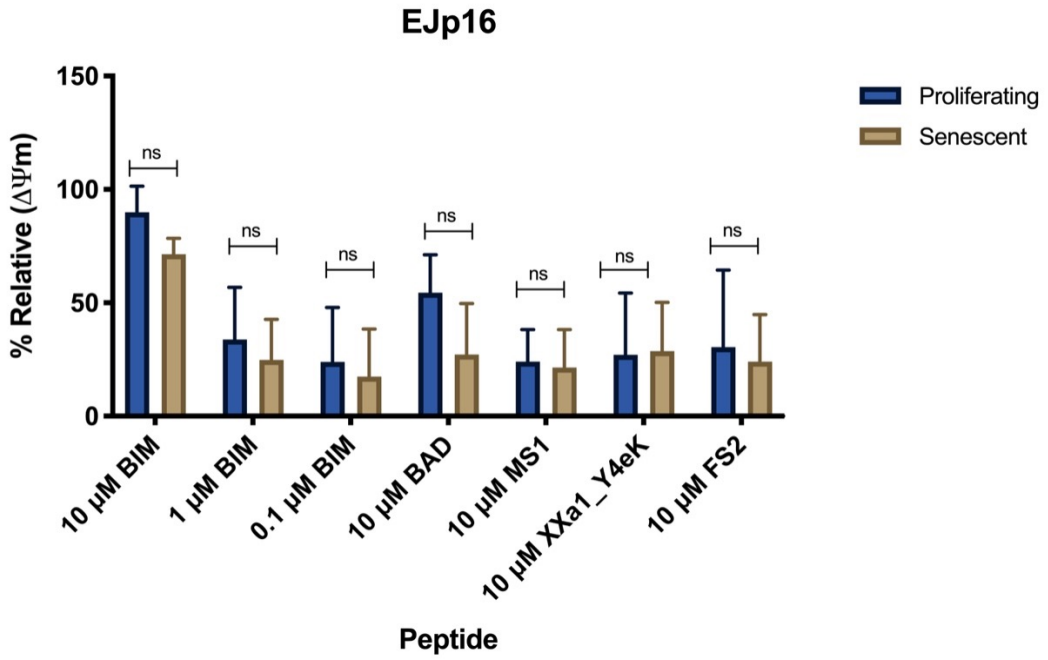

Figure 3.17. BH3 profiling of EJp16 cell line.

*5 days after senescence induction, senescent and proliferating EJp16 cells were gently permeabilised, treated with synthetic peptides and immediately before analysis stained with JC-1, a mitochondrial membrane potential probe. Plot shows the percentage of relative loss of mitochondrial membrane potential (ΔΨm), which was determined by normalising the data to DMSO (negative control). Synthetic peptides used: BIM (all anti-apoptotic proteins), BAD (BCL-2, BCL-W, BCL-X_L), MS1 (MCL-1), XXa1_Y4eK (BCL-X_L), FS2 (BCL-2A1). Bars represents the mean values ±SD, n=3. Statistical analysis performed using paired t-test (ns: not-significant, * p<0.05).*

Taken together, analysis of the EJ cell lines revealed pathway-dependent expression of BCL-2 family members in tested senescent models. In p53-driven senescence, the most distinct expression pattern was observed for BCL-X_L and BCL-W. Due to the lack of a specific BCL-W peptide, we were unable to verify how important is BCL-W for cell fate decisions. However, BH3 profiling analysis revealed a significant difference between senescent and proliferating cells in response to peptides that targets BCL-X_L. That was not observed in p53-independent senescent cell models, EJp21 and EJp16, in which none of the tested peptides induced a senescent-specific response. That is consistent with WB and qPCR analysis of BCL-2 family members expression, as none of the tested anti-apoptotic markers reached two-fold or higher upregulation in senescent EJp21 and EJp16 when compared with proliferating counterparts. Our data suggests that p53 might play an important role in senescent cells sensitivity for BCL-X_L specific inhibitors.

3.1.5.3 BCL-XL inhibitors exhibit a senolytic activity in p53-driven senescent cells.

Characteristics of the cell lines revealed that p53-driven senescent cells might be sensitive for specific inhibition of BCL-X_L protein. To test this hypothesis, we used a range of BCL-2 anti-apoptotic family inhibitors.

We started our analysis with ABT-737, which is a derivative of the senolytic Navitoclax. ABT-737 is a potent small-molecule inhibitor of BCL-2, BCL-X_L and BCL-W and it specifically induces apoptosis in senescent cells (Chauhan et al., 2007). Further, it has been reported that treatment of mice with ABT-737 efficiently eliminated the burden of senescent cells induced in the lungs through DNA damage, and in the skin, in which accumulation of senescent cells were formed in the epidermis by activation of p53 through transgenic $p14^{ARF}$ (Yosef et al., 2016).

In order to investigate upon activation of which senescence pathway ABT737 senolytic activity is the most efficient, we performed cell viability assay on HT1080-p21-9 and EJ-models of cellular senescence. Senescence was induced in EJp53, EJp21, EJp16 and HT1080-p21-9 cells, and 5 days after induction, proliferating and senescent cells were treated with increasing concentrations of ABT737 (0, 0.001, 0.01, 0.1, 1 and 10μM) for 72 h. Results supported previous findings of ABT737 senolytic activity and revealed a

significant loss of cell viability in senescent EJp53 and HT1080-p21-9 cells treated with 10 μM ABT737 (**Figure 3.18A-D**). Additionally, IC50 analysis revealed a great difference in EJp53 cells with more than 50 μM for proliferating and 0.5283 μM for senescent cells. For EJp21 and EJp16 cell lines, ABT737 seems to not have a strong effect, with IC50 higher than 50 μM for both proliferating and senescent cells. Analysis of HT1080-p21-9 revealed IC50=16.37 μM for proliferating and IC50=2.739 μM for senescent cells (**Figure 3.18G**). Taken together, our findings confirmed senolytic activity of ABT737, however only in cell lines with functional p53.

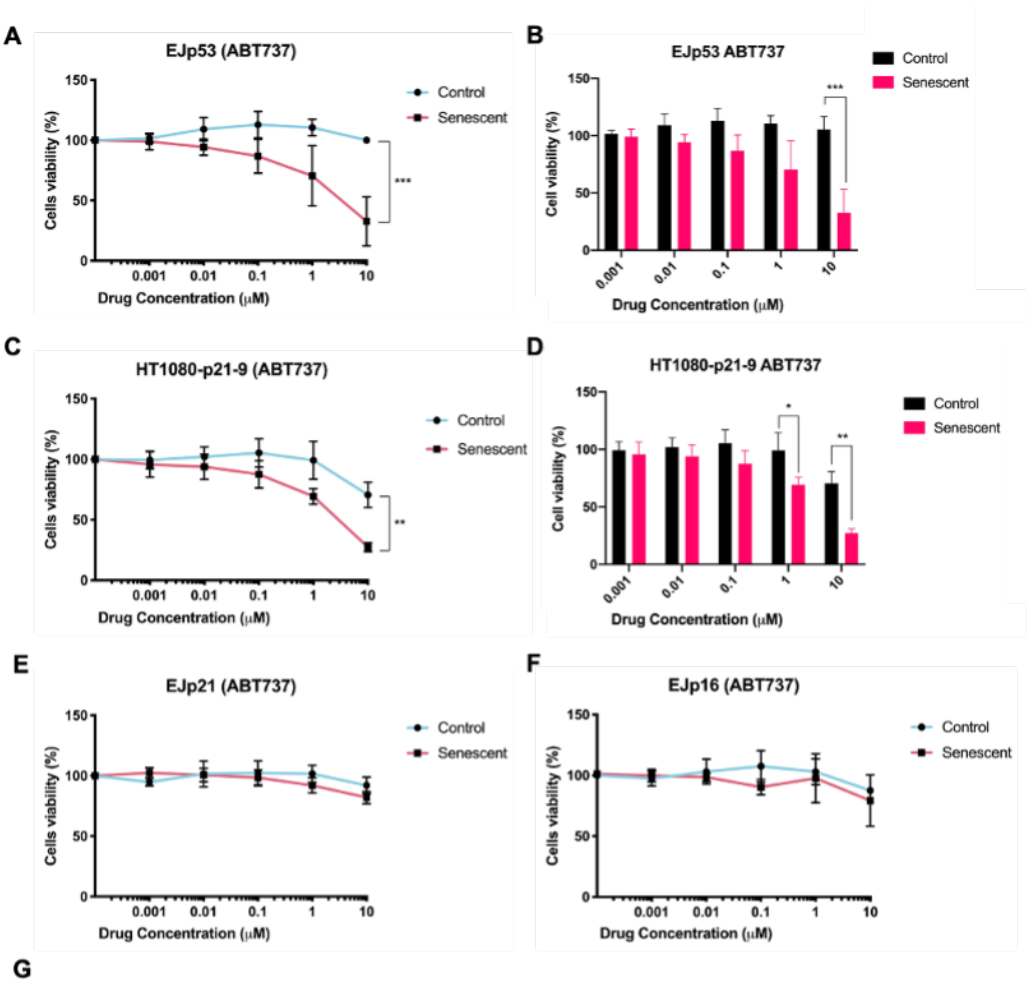

G

Cell line	EJp53		EJp21		EJp16		HT1080-p21-9	
Condition	Control	Senescent	Control	Senescent	Control	Senescent	Control	Senescent
IC50 (µM)	>50	0.5283	>50	>50	>50	>50	16.37	2.739

Figure 3.18. Cell viability of EJ and HT1080-p21-9 proliferating and senescent cells after treatment with ABT737.

*Cell viability assay presented as line or bar chart of proliferating and senescent (5 days after induction) [A-B] EJp53, [C-D] HT1080-p21-9, [E] EJp21 and [F] EJp16 cells, treated for 72h with increasing concentrations (0, 0.001, 0.01, 0.1, 1, 10 µM) of ABT737. [G] IC50 estimations based on cell viability results calculated using GraphPad Prism. Data were normalized to DMSO treated control. Data are expressed as mean ± SD (n=3). Statistical analysis performed using paired t-test (ns: not-significant, * p<0.05, ** p<0.01, *** p<0.001).*

Further, we performed PI staining and FACS to determine the percentage of cell death in EJ cell lines treated with ABT737. Data were consistent with cell viability findings and revealed more than 20% of death cells in EJp53 senescent cells when treated with 3 µM of ABT737 (**Figure 3.19A**). However due to high error bars this should not be consider as reliable. There was a slight difference in EJp21 cells when treated with 0.1 µM. Although, this experiment was performed only once and should be repeated. There was no difference in the percentage of cell death between senescent and proliferating EJp16 when treated with 0.01, 0.1 and 1 µM of ABT737 (**Figure 3.19B-C**). This highlights the importance of the p53 pathway and BCL-2 family proteins in cell fate decision in senescent cells.

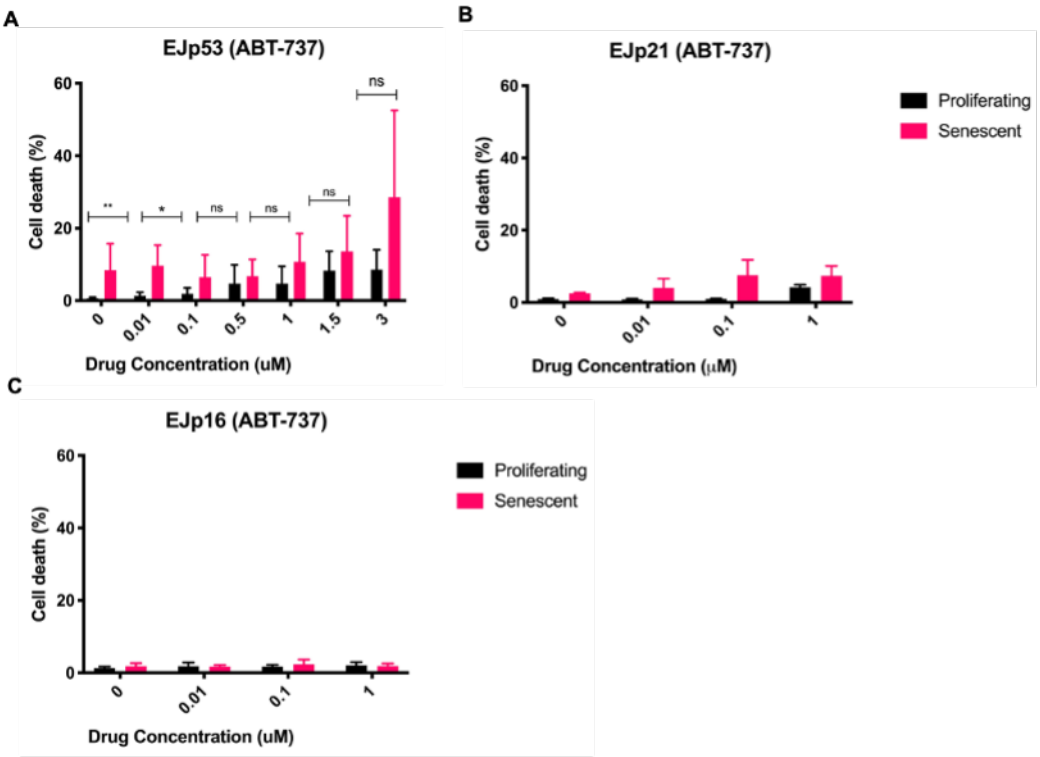

Figure 3.19. Cell death of EJp53, EJp21 and EJp16 cell lines after treatment with ABT737.

*EJp53, EJp21 and EJp16 proliferating and senescent (5 days after induction) were incubated for 72h with selected concentrations (0, 0.01, 0.1 and 1 µM) of ABT737. Cell death was analysed using PI staining measured by flow cytometry. DMSO was used as time matched control (0 concentration). Data are expressed as mean ± SD (EJp53 n=3, EJp16 n=3, EJp21 n=1). Statistical analysis performed using paired t-test (ns: not-significant, * p<0.05, ** p<0.01).*

Our data showed that ABT737 effectively kill senescent cells in two of tested by us *in vitro* models. However, ABT737 inhibits three proteins, BCL-2, BCL-W and BCL-X_L. We decided to use available inhibitors of these proteins and target each of them separately to determine if single inhibition of one of them will be sufficient to induce apoptosis in senescent cells. However, our analysis excluded BCL-W due to lack of an available inhibitor.

At first, we tested ABT199, a BCL-2 inhibitor on the same cell lines as above. EJp53, EJp21, EJp16 and HT1080-p21-9 proliferating and senescent cells were treated with different concentrations of ABT199 and a cell viability assay was performed. Results showed that ABT199 had no effect on majority of tested cell lines. Both senescent and proliferating cells remained viable even when treated with the highest concentrations (**Figure 3.20**). However, there was a 20% drop of cell viability in EJp53 senescent cells when treated with 10 μM of ABT199, although that was not statistically significant when compared with viability of proliferating cells treated with the same concentration of the drug (**Figure 3.20A**). Cell death analysis confirmed cell viability data: there was no effect of ABT199 on tested cell lines when treated with low concentrations (**Figure 3.21**).

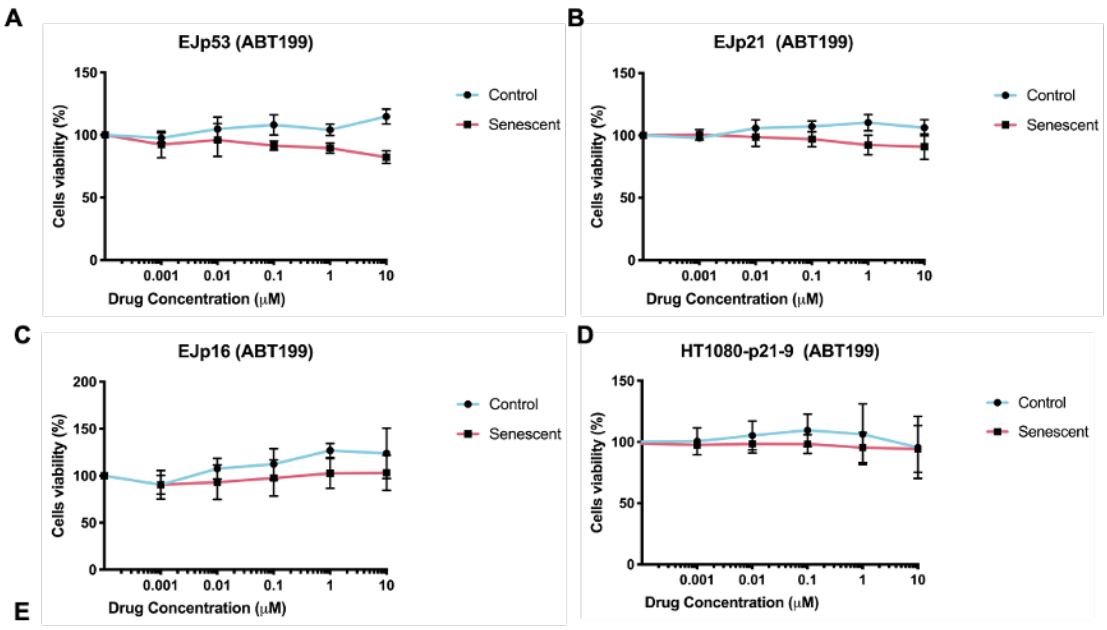

Cell line	EJp53		EJp21		EJp16		HT1080-p21-9	
Condition	Control	Senescent	Control	Senescent	Control	Senescent	Control	Senescent
IC50 (µM)	>50	>50	>50	>50	>50	>50	>50	>50

Figure 3.20. Cell viability of EJ and HT1080-p21-9 proliferating and senescent cells after treatment with ABT199.

*Cell viability assay of proliferating and senescent (5 days after induction) [A] EJp53, [B] HT1080-p21-9, [C] EJp21 and [D] EJp16 cells treated for 72h with increasing concentrations (0, 0.001, 0.01, 0.1, 1, 10 µM) of ABT199. [E] IC50 estimations based on cell viability results calculated using GraphPad Prism. Data were normalized to DMSO treated control. Data are expressed as mean ± SD (n=4). Statistical analysis performed using paired t-test (ns: not-significant, * p<0.05, ** p<0.01, *** p<0.001).*

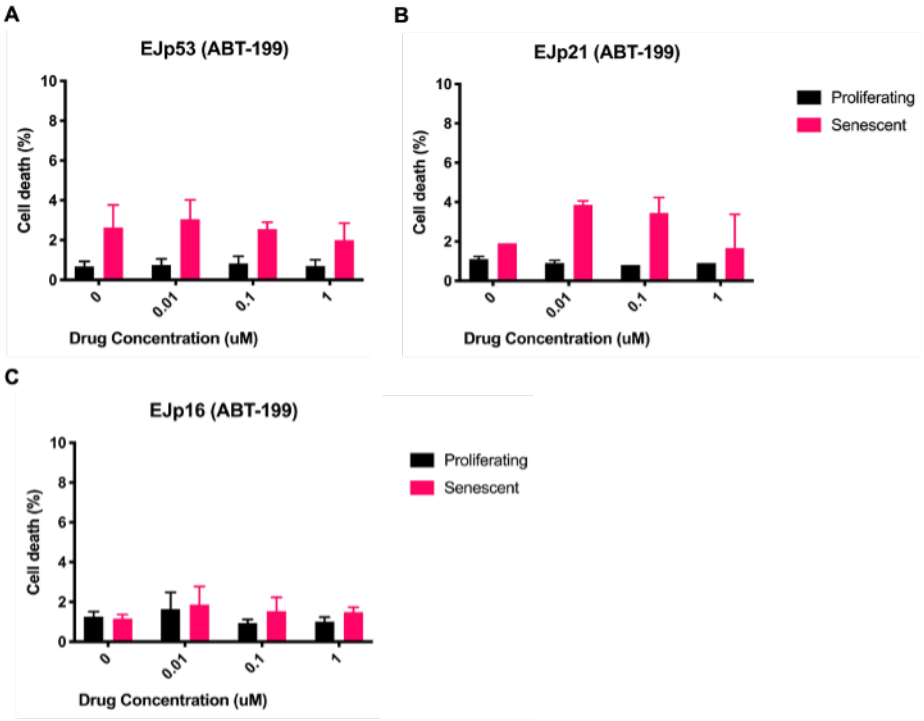

Figure 3.21. Cell death of EJp53, EJp21 and EJp16 cell lines after treatment with ABT199.

EJp53, EJp21 and EJp16 proliferating and senescent (5 days after induction) were incubated for 72h with selected concentrations (0, 0.01, 0.1 and 1 µM) of ABT199. Cell death was analysed using PI staining measured by flow cytometry. DMSO was used as time matched control (0 concentration). Data are expressed as mean ± SD (EJp53 n=2, EJp16 n=3, EJp21 n=1).

Next, we treated the same cell lines with A1331852, a BCL-X_L inhibitor. Cell viability revealed a significant decrease of EJp53 when treated with concentrations higher than 0.01 µM (**Figure 3.22A**). That was further confirmed with cell death assay that showed significant changes in the percentage of cell death between proliferating and senescent EJp53 cells when treated with 0.1 and 1 µM of A1331852 (**Figure 3.23A**). IC50 values for EJp53 proliferating cells was 13.64 µM and 0.1283 µM for senescent cells. Similarly to results from ABT737, A1331852 showed no difference in in cell viability (**Figure 3.22B-C**) and percentage of cell death (**Figure 3.23B-C**) between proliferating and senescent EJp21 and EJp16 cells. Analysis of HT1080-p21-9 revealed differences in viability of senescent and control cells, although the difference was not statistically significant (**Figure 3.22D**). IC50 analysis showed a big difference between proliferating (IC50= 3.618

µM) and senescent cells (IC50= 0.007 µM), although because of big error bars seen on a graph these data are vague (**Figure 3.22E**).

Taken together, our data showed that A1331852 has a strong senolytic activity on EJp53 senescent cells.

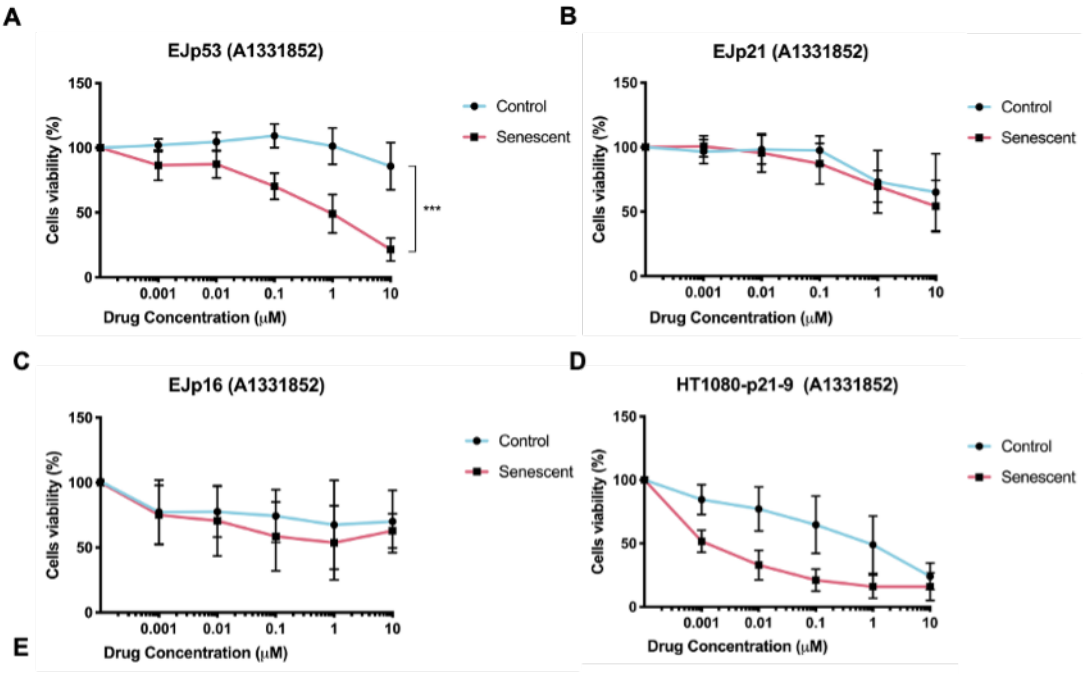

E

Cell line	EJp53		EJp21		EJp16		HT1080-p21-9	
Condition	Control	Senescent	Control	Senescent	Control	Senescent	Control	Senescent
IC50 (µM)	13.64	0.1283	>50	>50	>50	>50	3.618	0.00701

Figure 3.22. Cell viability of EJ and HT1080-p21-9 proliferating and senescent cells after treatment with A1331852.

*Cell viability assay of proliferating and senescent (5 days after induction) [A] EJp53, [B] HT1080-p21-9, [C] EJp21 and [D] EJp16 cells treated for 72h with increasing concentrations (0, 0.001, 0.01, 0.1, 1, 10 µM) of A1331852. [G] IC50 estimations based on cell viability results calculated using GraphPad Prism. Data were normalized to DMSO treated control. Data are expressed as mean ± SD (n=4). Statistical analysis performed using paired t-test (ns: not-significant, * p<0.05, ** p<0.01, *** p<0.001).*

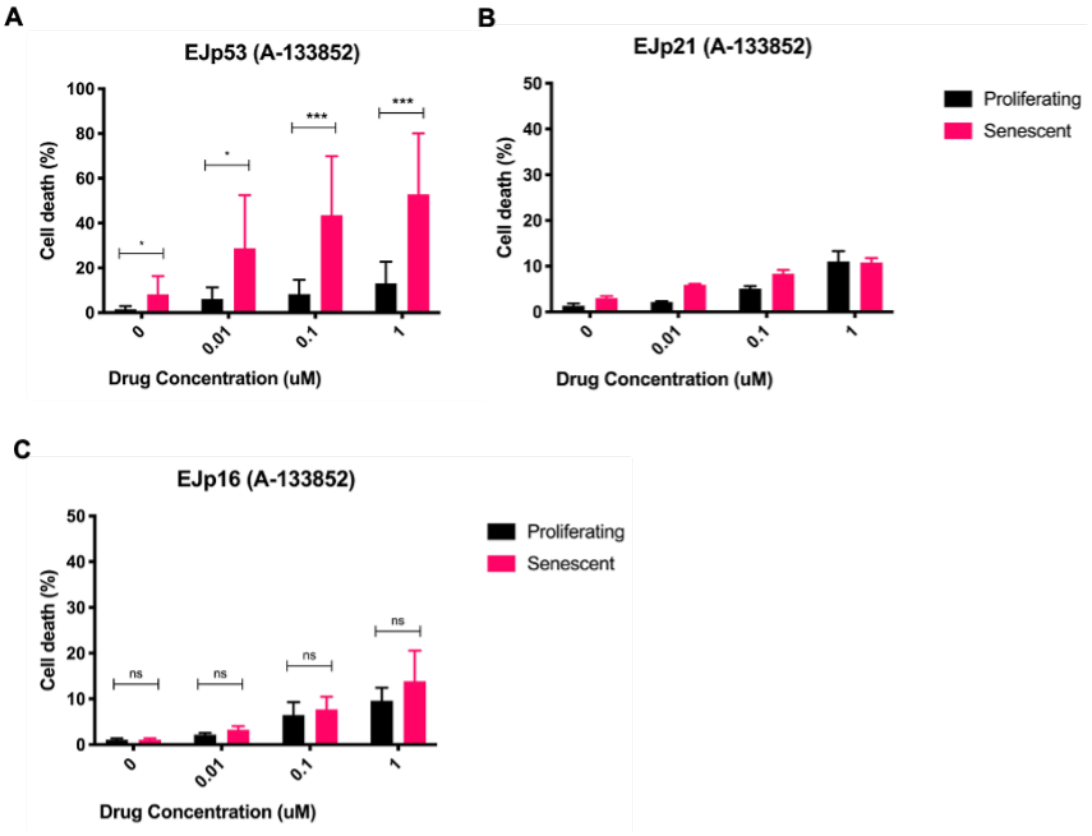

Figure 3.23. Cell death of EJp53, EJp21 and EJp16 cell lines after treatment with A1331852.

*EJp53, EJp21 and EJp16 proliferating and senescent (5 days after induction) were incubated for 72h with selected concentrations (0, 0.01, 0.1 and 1 µM) of A1331852. Cell death was analysed using PI staining measured by flow cytometry. DMSO was used as time matched control (0 concentration). Data are expressed as mean ± SD (EJp53 and EJp16 n=3, EJp21 n=1). Statistical analysis performed using paired t-test (ns: not-significant, * p<0.05, ** p<0.01, *** p<0.001).*

Next, we analysed the dependency on another BCL-2 family protein, MCL-1. S63845 is MCL- 1 specific inhibitor and its effect on senescence cells has not been fully explored. As previously, cells were treated with the drug for 72 hours. Data revealed no difference between senescent and control cell viability after the treatment with S63845 in all cell models tested (**Figure 3.24**). Of note, high concentration of the drug (10 µM) was equally toxic for proliferating and senescent cells and decreased cell viability in all tested models (**Figure 3.24E**). The PI staining analysis revealed minimal amount of cell death (less than 6%) when low concentrations of the drug were used (**Figure 3.25**). Taken together, our results indicate that MCL-1 is not a senolytic target.

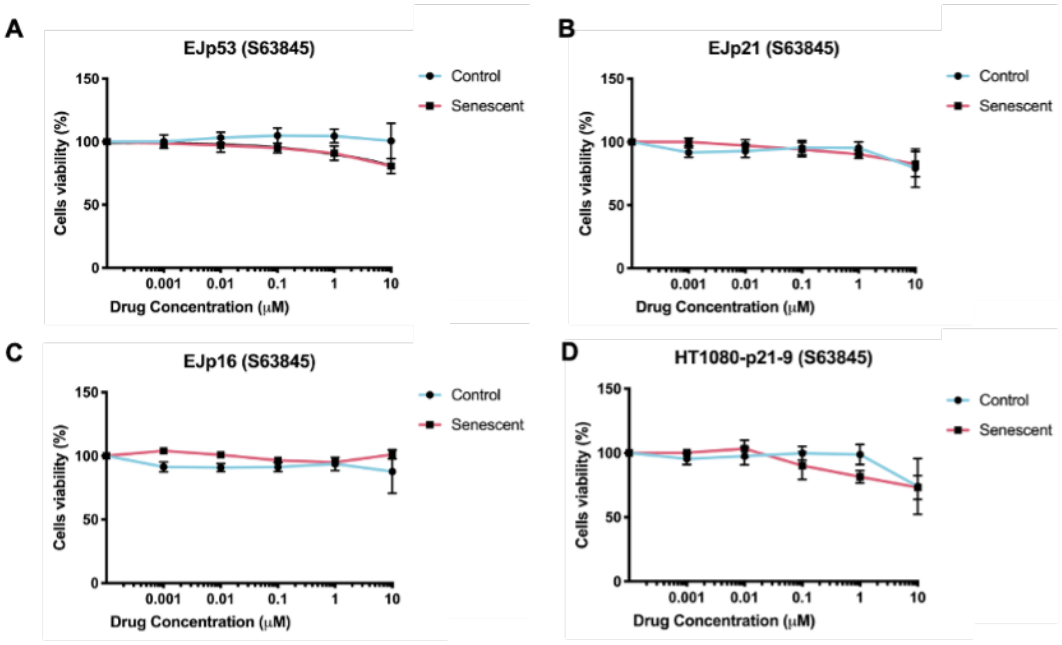

E

Cell line	EJp53		EJp21		EJp16		HT1080-p21-9	
Condition	Control	Senescent	Control	Senescent	Control	Senescent	Control	Senescent
IC50 (μM)	>50	>50	>50	>50	>50	>50	>20	>20

Figure 3.24. Cell viability of EJ and HT1080-p21-9 proliferating and senescent cells after treatment with S63845.

Cell viability assay of proliferating and senescent (5 days after induction) [A] EJp53, [B] HT1080-p21-9, [C] EJp21 and [D] EJp16 cells treated for 72h with increasing concentrations (0, 0.001, 0.01, 0.1, 1, 10 μM) of S63845. [G] IC50 estimations based on cell viability results calculated using GraphPad Prism. Data were normalized to DMSO treated control. Data are expressed as mean ± SD (n=4).

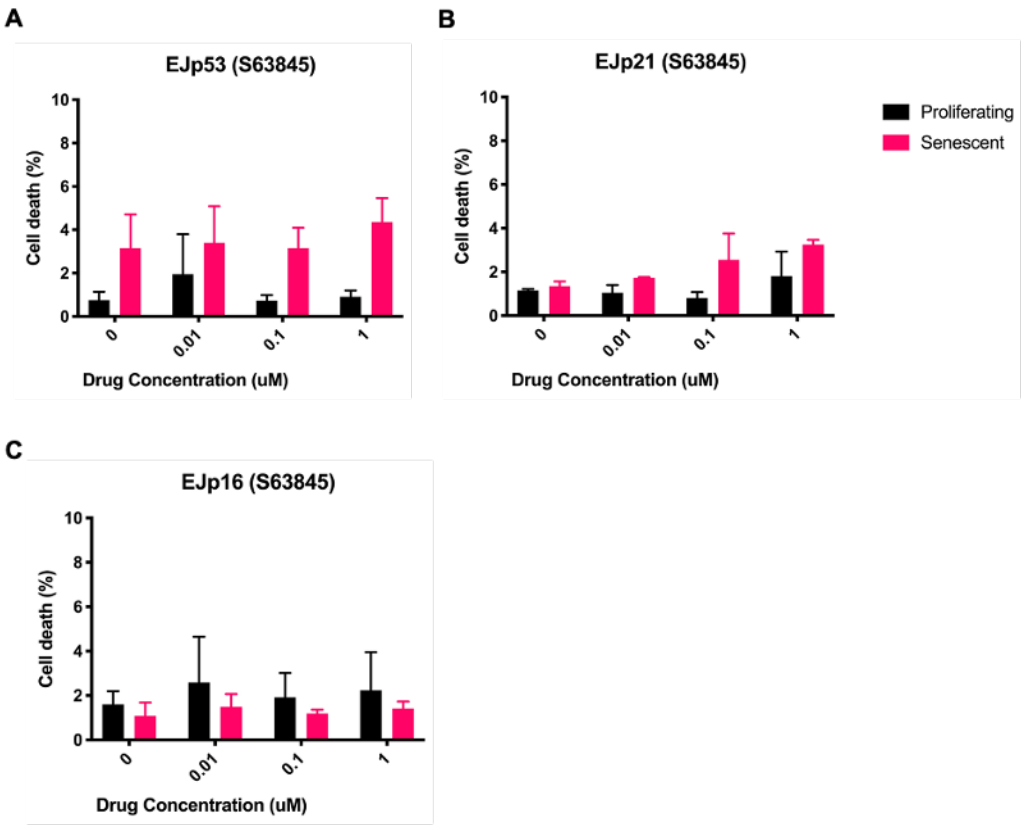

Figure 3.25. Cell death of EJp53, EJp21 and EJp16 cell lines after treatment with S63845.

EJp53, EJp21 and EJp16 proliferating and senescent (5 days after induction) were incubated for 72h with selected concentrations (0, 0.01, 0.1 and 1 µM) of S63845. Cell death was analysed using PI staining measured by flow cytometry. DMSO was used as time matched control (0 concentration). Data are expressed as mean ± SD (n=2).

Taken together, collected data revealed a senolytic activity of A1331852, ABT737 (BCL-X_L inhibitors) on senescent EJp53 and HT1080-p21-9 cells (**Table 3.2**). Moreover, our data showed some senolytic activity of GQC-05 when used in certain concentrations. This was not observed in the cell lines lacking p53, EJp21 and EJp16. None of the tested drugs exhibited senolytic potential for senescent EJp21 and EJp16 cells. Our data suggests that senolytics like Navitoclax are likely to work the most efficiently in p53-induced senescence and with a slighter effect in other cells that express wt p53, such as HT1080-p21-9.

Table 3.2. Summary of senolytics effectivity in senescent models in vitro.

Table presents effectivity of tested senolytics that targets different BCL-2 family anti-apoptotic members in tested senescent cells: EJp53, EJp21, EJp16, HT1080-p21-9, Non-Fibrotic Control fibroblasts (NFC) and Idiopathic Pulmonary Fibroblasts (IPF). Analysis performed based on cell viability data. ***V****: indicates strong senolytic activity,* ***V?****: vague senolytic activity, —: no senolytic activity.*

	Target							
	BCL-X_L				BCL-W		BCL-2	MCL-1
Cell line	A1331852	ABT737	GQC-05	9-OH ellipticine	ABT199	ABT737	ABT737	S63845
EJp53	**V**	**V**	**V?**	—	—	**V**	—	—
EJp21	—	—	—	—	—	—	—	—
EJp16	—	—	—	—	—	—	—	—
HT1080-p21-9	**V?**	**V**	—	—	—	**V**	—	—

3.1.6 Combination therapy

To further investigate the senolytic potential of BCL-X_L inhibition we assessed sensitivity of senescent EJp53, EJp21 and EJp16 cells to specific drug combinations. As previously, proliferating and senescent cells were treated for 72 hours, 5 days after senescence induction. To measure if combinations of drugs had a synergistic effect, we used combination index (CI) which was calculated using Calcusyn software. CI <1indicate synergism, CI=1 additive effect and CI >1 indicates antagonism (**Chapter 2: Table 2.4**).
We first combined ABT737, a BCL-2, BCL-W and BCL-X_L inhibitor, with BCL-X alternative splicing regulator, 9-hydroxyellipticine. Data revealed that combination of the drugs was synergistic for EJp53 proliferating (CI=0.79), but not senescent cells (CI=1.63) (**Figure 3.26A**). For EJp21, combination of ABT737 and 9-hydroxyellipticine was antagonistic and in high concentrations had a slightly stronger effect on viability of proliferating cells than senescent. Analysis of EJp16 cell line revealed moderate synergism (CI=0.83) in senescent but not in proliferating cells (CI=2.80). These data suggest senolytic potential of ABT737 combination with 9-hydroxyellipticine in EJp16 cells, although viability of both senescent and proliferating cells was not significantly affected by the treatment in the lower concentrations (0.001-0.1 μM). When EJp16 senescent cells were treated with 0.1 μM of both drugs, viability decreased by 26% in senescent cells. Further tests should be performed using wider range of concentrations between 0.1 and 10 μM to explore the therapeutic window for this combination.

Next, we tested if senolytic activity observed in combination of ABT737 with 9-hydroxyellpiticine might be due to MCL-1 inhibition by combining ABT737 with a MCL-1 inhibitor, S63845. Data revealed no synergy in both senescent EJp53 and EJp21 cells (**Figure 3.27**). For EJp16, CI values were not calculated due to low n number (n=2). Therefore, EJp16 analysis should be repeated.

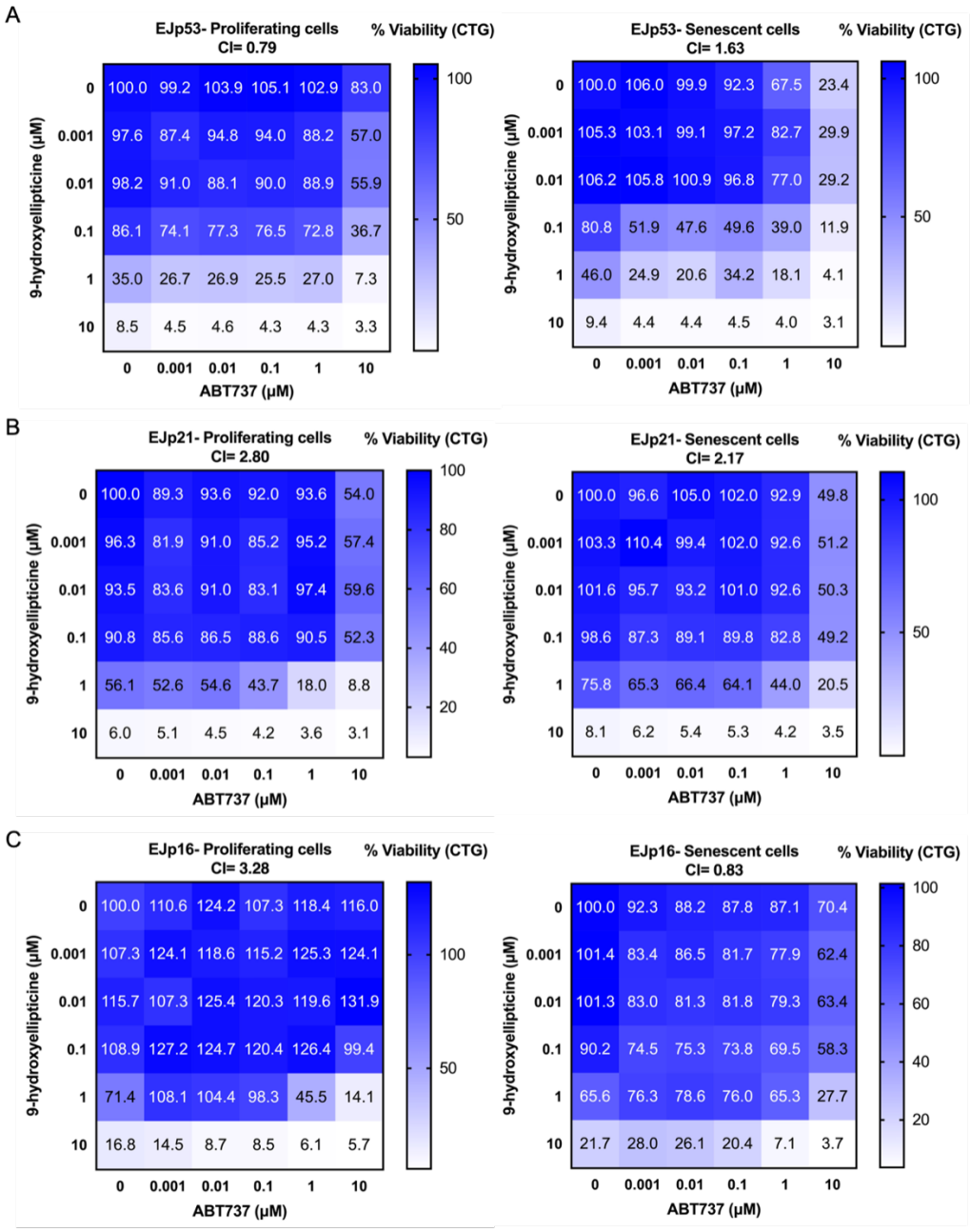

Figure 3.26. Combination of ABT737 with 9-hydroxyellipticine in EJ-cell lines.

5 days after senescence induction, [A] EJp53, [B] EJp21 and [C] EJp16 senescent and proliferating cells were treated with increasing concentrations (0, 0.001, 0.01, 0.1, 1, 10 µM) of [A] ABT737 (BCL-2, BCL-W, BCL-X_L inhibitor) and 9-hydroxyellipticine (BCL-X splicing shift) for 72 hours and cell viability was determined using CellTiter-Glo assay. Data show mean values of the percentage of viable cells. EJp53 n=4, EJp21 n=3, EJp16 n=3. Combination Index (CI) was calculated using Calcusyn and CI values <1 indicate synergy.

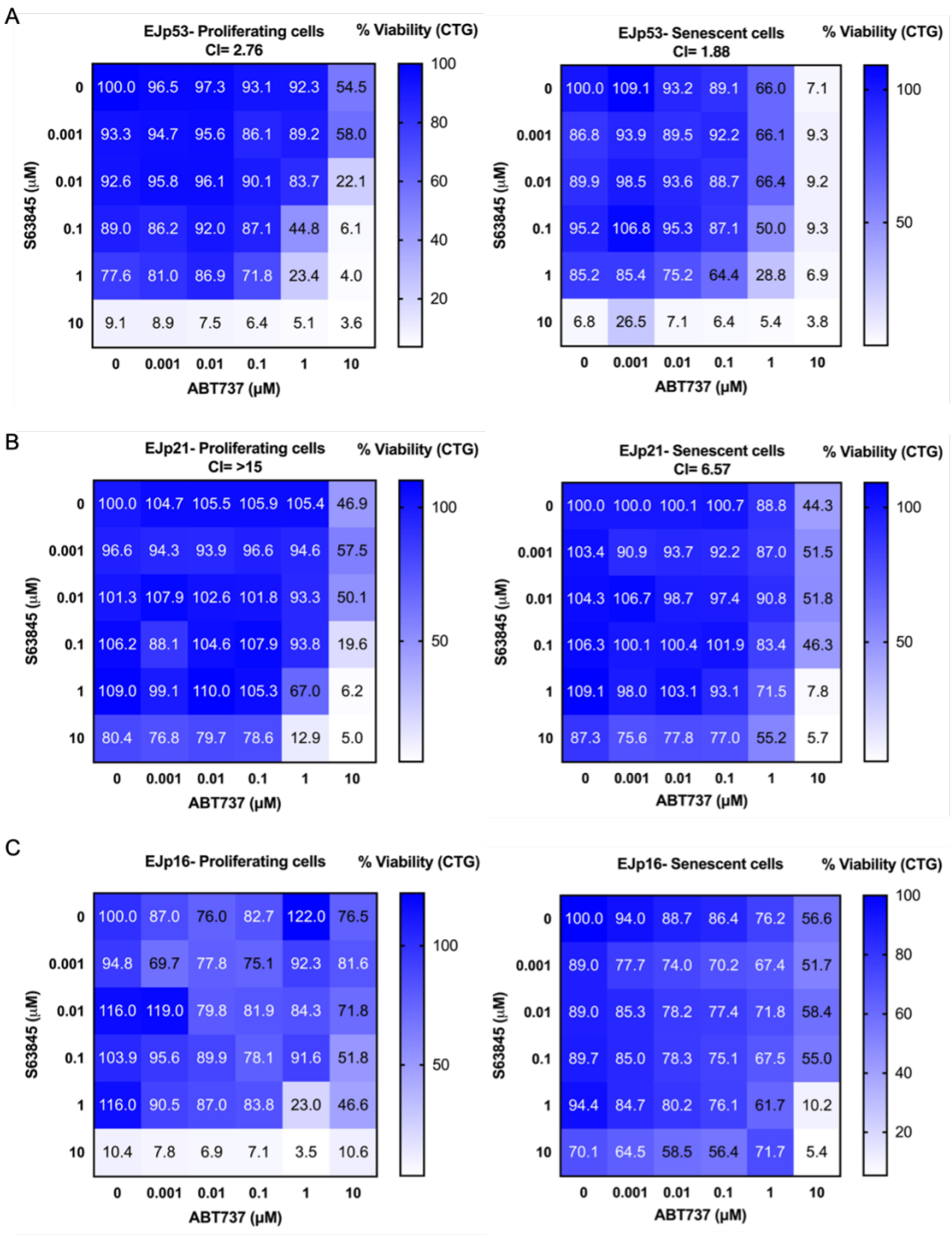

Figure 3.27. Combination of ABT737 with S63845 in EJ-cell lines.

5 days after senescence induction, [A] EJp53, [B] EJp21 and [C] EJp16 senescent and proliferating cells were treated with increasing concentrations (0, 0.001, 0.01, 0.1, 1, 10 μM) of [A] ABT737 (BCL-2, BCL-W, BCL-X_L inhibitor) and S63845 (MCL-1 inhibitor) for 72 hours and cell viability was determined using CellTiter-Glo assay. Data show mean values. EJp53 n=4, EJp21 n=3, EJp16 n=2. Combination Index (CI) was calculated using Calcusyn and CI values <1 indicate synergy.

Then, we have decided to use A1331852, a more specific BCL-X_L inhibitor that in previous analysis has shown strong senolytic activity on EJp53 senescent cells (**Figure 3.22**). We combined it with 9-hydroxyellipiticine and measured cell viability. Results revealed a synergistic effect in EJp53 senescent cells (CI=0.52) but not in their proliferating counterpart's, in which CI value indicated antagonistic effect with CI=4.53 (**Figure 3.28A**). Analysis of EJp16 cell lines revealed that combination of the drugs was also strongly synergistic for senescent (CI= 0.05) and strongly antagonistic for proliferating EJp16 cells (CI= 11.4) (**Figure 3.28C**). Wider range of concentrations should be used to fully explore its senolytic activity in EJp16 cells. In EJp21, the combination was antagonistic for both proliferating and senescent cells (**Figure 3.28B**). These data highlighted a strong senolytic potential of A1331852 combination with 9-hydroxyellipticine.

Next, we combined A1331852 with the MCL-1 inhibitor, S63845. Results revealed synergism for both EJp53 proliferating (CI=0.07) and senescent cells (CI=0.73), although greater effect on cell viability was observed in senescent cells (**Figure 3.29A**).
Similar results were observed in EJp21 cell line, in which drug combination had synergistic effect also for both proliferating (CI= 0.17) and senescent cells (CI=0.86) (**Figure 3.29B**). Despite synergistic effect of drugs combination, that was not accompanied by significant differences between senescent and proliferating cells viability. Therefore, this combination is not a suitable senolytic for EJp21 senescent cells. Combination of A1331852 and S63845 was also found synergistic for EJp16 senescent (CI= 0.57) but not proliferating cells (CI= 1.13) (**Figure 3.29C**). Although we also observed slight changes in cell viability between senescent and control cells, more test will be needed to confirm its senolytic potential. In summary, data revealed that combination of A1331852 and S63845 exhibit a senolytic activity in both, EJp53 senescent and proliferating cells, therefore suggesting a high level of off-target cytotoxicity.

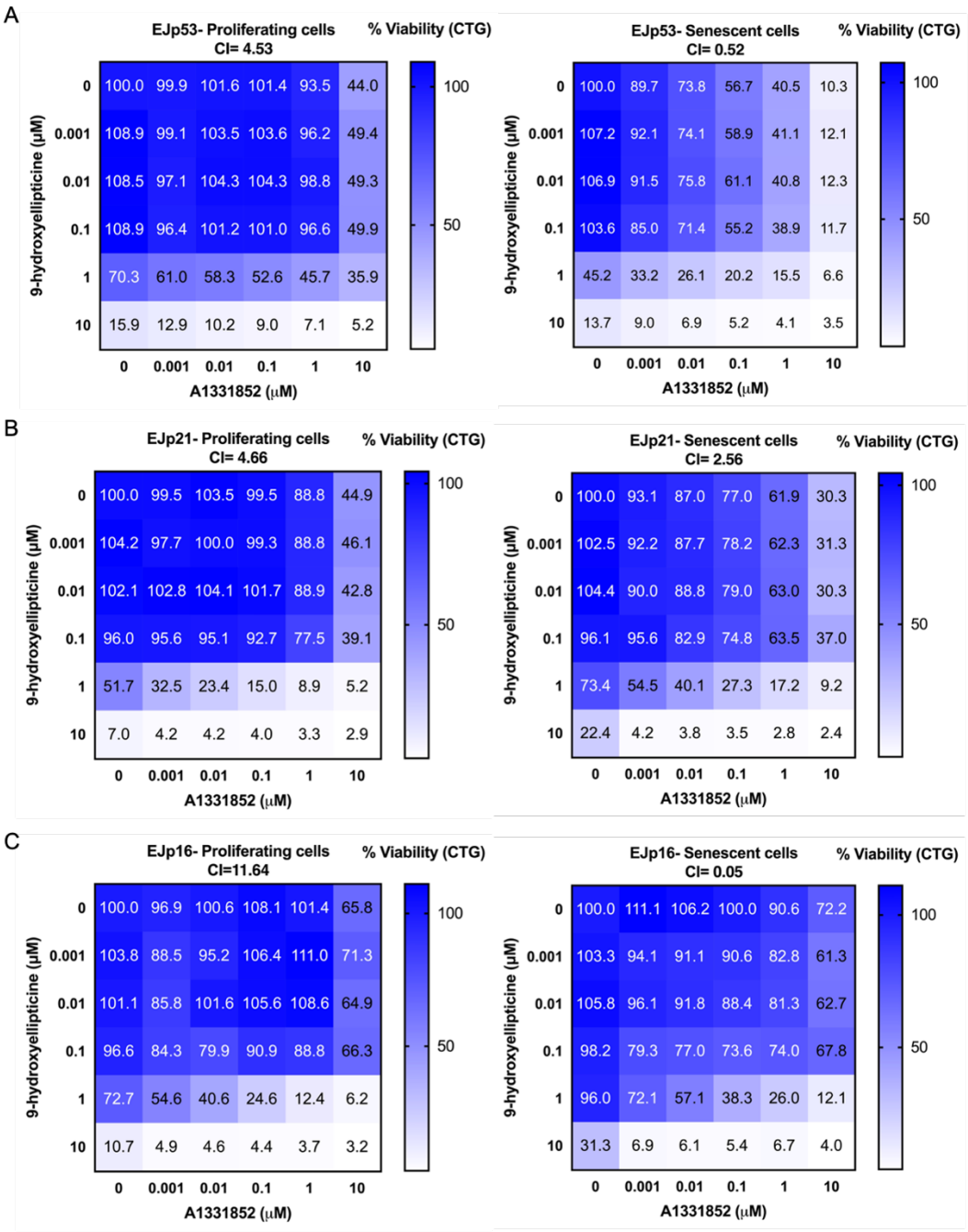

Figure 3.28. Combination of A1331852 with 9-hydroxyellipticine in EJ-cell lines.

5 days after senescence induction, [A] EJp53, [B] EJp21 and [C] EJp16 senescent and proliferating cells were treated with increasing concentrations (0, 0.001, 0.01, 0.1, 1, 10 µM) of A1331852 (BCL-X_L inhibitor) and 9-hydroxyellipticine (BCL-X splicing shift) for 72 hours and cell viability was determined using CellTiter-Glo assay. Data show mean values. EJp53 n=4, EJp21 n=3, EJp16 n=3. Combination Index (CI) was calculated using Calcusyn and CI values <1 indicate synergy

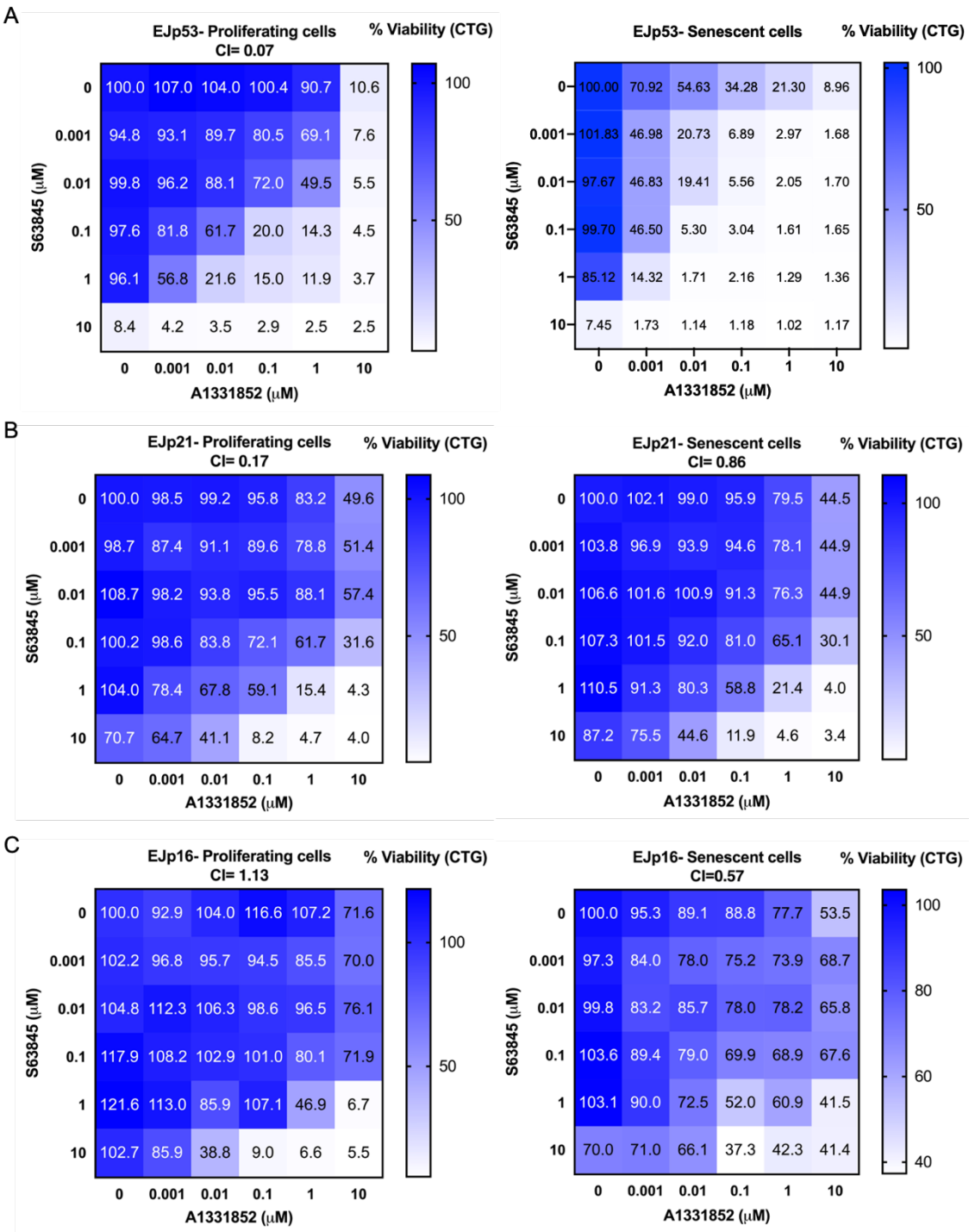

Figure 3.29. Combination of A1331852 with S63845 in EJ-cell lines.

5 days after senescence induction, [A] EJp53, [B] EJp21 and [C] EJp16 senescent and proliferating cells were treated with increasing concentrations (0, 0.001, 0.01, 0.1, 1, 10 µM) of A1331852 (BCL-X_L inhibitor) and S63845 (MCL-1 inhibitor) for 72 hours and cell viability was determined using CellTiter-Glo assay. Data show mean values. EJp53 n=4, EJp21 n=3, EJp16 n=3. Combination Index (CI) was calculated using Calcusyn and CI values <1 indicate synergy

Taken together, results showed that combination of BH3 mimetics with BCL-X alternative splicing regulators have a distinct effect depending on the cell line used. Synergic effect was observed in different combinations on both proliferating and senescent cells. In EJp53 cell line, few combinations had a synergistic effect on treated cells although only one was specific for senescent cells, A1331852 with 9-hydroxyellipticine. This combination caused synergistic decrease in senescent but not proliferating cells viability (**Table 3.3**) and that was further examined by visual detection of dead cells in condition media, 8 hours after the treatment. Results revealed that there was a higher number of cell death in senescent cells treated with 0.1 µM A1331852 and 0.1 µM 9-hydroxyellipticine, than in proliferating cells. Moreover, the higher level of cell death was seen in senescent cells treated with 0.1 µM A1331852 and 0.1 µM 9-hydroxyellipticine than in the same concentrations of ABT737 combination with 9-hydroxyellipticine (**Figure 9.3**). A synergistic effect in EJp53 cell line was also observed when A1331852 was combined with S63845. That was also further examined and 8 hours after the treatment a large amount of cell death was observed in both proliferating and senescent cells (**Figure 9.4**). This indicates that combination of A1331852 with S63845 is equally toxic for both proliferating and senescent cells and that excludes it from potential usage in senotherapies. Moreover, in EJp53 senescent cells A1331852 alone exhibit stronger effect then in previous replicates, therefore it cannot be trusted and should be repeated (**Figure 3.29A**).
In summary, the best combination that indicates a senolytic potential and that should be further validated on different senescent models is A1331852 and 9-hydroxyellipticine.

In EJp21 majority of combinations had antagonistic effect. Although data revealed that combination of A1331852 and S63845 had a synergistic effect on EJp21 senescent cells, the same findings were confirmed in their proliferating counterparts. Therefore, none of the tested combinations is a suitable senolytic for EJp21 senescent cells. The greatest senolytics potential was observed in EJp16 senescent cells, in which three different combinations of the drug turned to be synergistic only for senescent cells. Interestingly, when used as a single agent, these drugs were the most effective in p53-driven

senescent cells and there were no significant changes between senescent and control EJp16 cells viability after the treatment. However, combination of drugs was found to have synergistic effect. Further analysis should be performed to clarify if that is reflected by significant reduction of senescent cells.

Summarized results suggest that subsequent treatment with inhibitors that act at both BCL-X_L protein and mRNA level might have a therapeutic potential in the clearance of senescent cells.

Table 3.3. Summary of drug combinations in EJ-cell lines.

Summary of drug combinations together with Combination Index (CI) values that corresponds classification of synergism in drug combination based on the Chou-Talalay method (Chou, 2008). Green colour represents synergism, orange colour represents antagonism. Colour shades indicate how strong the effect is.

	EJp53		**EJp21**		**EJp16**	
	P	S	P	S	P	S
ABT737 + 9-ellipticine	Moderate Synergism (CI= 0.79)	Antagonism (CI= 1.63)	Antagonism (CI= 2.80)	Antagonism (CI= 2.17)	Antagonism (CI=3.28)	Moderate Synergism (CI=0.83)
ABT737 + S63845	Antagonism (CI= 2.76)	Antagonism (CI= 1.88)	Very strong Antagonism (CI>15)	Strong Antagonism (CI=6.57)	Not tested	
A1331852 + 9-ellipticine	Strong Antagonism (CI= 4.53)	Synergism (CI= 0.53)	Strong Antagonism (CI=4.66)	Antagonism (CI=2.56)	Very strong Antagonism (CI=11.64)	Very Strong Synergism (CI=0.05)
A1331852 + S63845	Very strong Synergism (CI= 0.07)	Not clear	Strong Synergism (CI=0.17)	Slight Synergism (CI=0.86)	Slight Antagonism (CI=1.13)	Synergism (CI=0.57)
S63845 + 9-ellipticine	Synergism (CI=0.7)	Synergism (CI=0.61)	Not tested			

3.2 Discussion

Since senescence has been strongly established to be one of the main causes of aging (López-Otín et al., 2013) and elimination of senescent cells burden has been shown to delay and ameliorate several age-related pathologies (Paez-Ribes et al., 2019), it is critical to seek new approaches to target senescence for enhancing healthspan/lifespan. Although nowadays a great emphasis has been put on discovery of new senolytics, their availability remains limited due to lack of specificity. Therefore, we decided to perform *in vitro* validation of eight drugs and five drug combinations to better understand which pathways are critical for senescent cell sensitivity to drugs and find the more specific senolytic in our senescent models. Our data revealed that the senolytic potential of ABT737 (BCL-2, BCL-W and BCL-X_L inhibitor) or A1331852 (BCL-X_L inhibitor) might depend on functional p53. Our results indicate that drugs such as Navitoclax might be highly effective senolytics in p53-driven models of cellular senescence, but also to some extend in other cells with functional p53, such as HT1080-p21-9. These findings might be important for future choice of senolytics based on the previous determination of p53 levels.

ABT737 and Navitoclax are inhibitors of three BCL-2 family proteins, BCL-2, BCL-X_L and BCL-W. To clarify which of these targets is crucial for ABT737 senolytics potential and thus avoid unwanted side effects brought by the unnecessary inhibition of important pathways, we characterized the expression profiles of anti- and pro-apoptotic BCL-2 family proteins based on the activation of crucial senescence-inducing pathways, p53-p21 or p16-pRB. Our studies indicated that in p53-driven senescence there was a higher level of BCL-X_L and BCL-W, two of the three ABT737 targets, compared with controls. Moreover, our BH3 profiling results supported the importance of BCL- X_L and showed that cell fate decisions in p53-driven senescence partially depends on functioning BCL-X_L. Inhibition of BCL-2 by ABT-199 showed that BCL-2 is not a crucial factor for survival of senescent cells in p53-driven senescence. In turn, inhibition of BCL- X_L using A1331852 revealed a significant decrease of senescent cell viability when compared to proliferating controls. However, that effect was observed only in p53-dependent senescent cells. Therefore, we hypothesised that BCL-X_L inhibitors are the most effective senolytics in senescent cells with functional p53. Our data reinforce also the concept

that senolytics could be used as a promising adjunct to treat cancer. That could be effective with a p53-dependent senescence-inducing chemotherapies that would be followed with a BCL-X_L targeting senolytic. The clearance of senescent cancer cells could prevent the progression of tumours by mitigation of SASP that fuels cancer progression. It is worth to mention that many cancer cells have inactivated p53 pathway. In this case, clearance of senescent cells in neighbouring tissues would also have a beneficial effect through establishment of SASP-free microenvironment.

There are few study limitations, such as lack of expression profiles analysis of BCL-2 pro- and anti-apoptotic members after the treatment with each drug and combination. Due to lack of the time, this analysis has not been finished. That could bring useful information on how inhibition of one anti-apoptotic protein affects others depending on the senescence-pathway involved. Another limitation was lack of a BCL-W inhibitor that would exclude its potential involvement in senescent cells survival. This drug does not yet exist. It would be also essential to test other BCL-X_L inhibitors, such as WEHI-539 or A1155463, to confirm our results. Moreover, different senescence models should be used, such as replicative senescence or oncogene-induced senescence, with a careful consideration of p53 levels. Additionally, all cell viability experiments should be cultured with low percentage of FBS in order to prevent proliferation, as it might result in differences with senescent cells that are not related to different responses to the drug, but because of the different cell numbers.
Moreover, our data showed that combination of A1331852 with BCL-X splicing regulator 9-hydroxyellipticine synergistically induce cell death in p53-driven senescent cells. However, it would be important to check if 9-hydroxyellipticine indeed changes the splicing of BCL-X towards its pro-apoptotic variant BCL-X_S. Due to technical limitations and lack of the time, this analysis has not been finished.

In the future, it would be interesting to test combination of these drugs on p53-driven *in vivo* models of aging, such as *ZMPSTE24*$^{-/-}$ progeria mouse model. It will be extremely interesting to check if combination of A1331852 with 9-hydroxyellipticine reduce the number of senescent cells *in vivo* and affect the healthspan and lifespan of treated animals. However, careful studies will be needed to assess toxicity of mentioned drugs

in vivo, especially due to on-target related side effects, such as thrombocytopenia and neutropenia, that has been found as a result of BCL-X_L inhibition. Combination of A1331852 with 9-hydroxyellipticine provides a double BCL-X_L inhibition by acting at gene and protein level (Ashkenazi et al., 2017). Moreover, the exact function of BCL-X_L in cellular senescence in not yet well understood, therefore careful monitoring of BCL-X_L inhibitions would be necessary, as BCL-X_L targeting might turn to be a "double -edge sword". Further studies will be essential to validate the scale of on- and off-target side effect.

4 Second generation of senolytics.

Senolytics have shown to be effective *in vitro* and *in vivo* (Kirkland and Tchkonia, 2017, Paez-Ribes et al., 2019), with the first clinical trials showing successful results (Hickson et al., 2019, Justice et al., 2019). However, the currently available senolytics are repurposed non-specific drugs and therefore have numerous side effects. Thus, there is a need to design improved second generation senolytics with higher specificity to improve their clinical potential. To this end, we focused on the exploration of the strategy of combining cytotoxic compounds and a specific drug delivery system. The concept relies on the delivery of the drug to the cell of interest via a target-specific carrier.

In order to achieve that, nanoparticles (nanoMIPs) and antibody drug conjugates (ADCs) were designed to target epitopes of the senescent surfacome and the validations of their therapeutic potential are presented in this chapter. Of note, all nanoMIPs data were published in (Ekpenyong-Akiba et al., 2019).

4.1 nanoMIPs detect senescent cells *in vivo*.

Targeting cellular senescence is one of the major challenges in the field of aging and cancer. The goal of clearing senescent cells from the body is to delay, prevent or reverse age-related diseases. The first method used by us to directly target senescent cells relies on the application of nanomolecules. Nanomedicine is an innovative field of science, which can be used as a leading-edge approach based on the biomarker-specific cargo delivery. In here, molecularly imprinted nanoparticles (nanoMIPs) were designed against B2M, a surfaceome protein identified in a mass spectrometry screen (Althubiti et al., 2014). NanoMIPs are polymeric particles with the binding site specific for their target molecule, in this case B2M. The production of nanoMIPs relies on the immobilization of a template molecule on a solid surface, like glass beads. Immobilized template is incubated with mixture of monomers and by the process of polymerisation

the polymer nanoparticles are formed (Vasapollo et al., 2011a). Remaining monomers and low-affinity polymers are removed together with the template molecule, leaving the polymer matrix, which is the final form of nanoMIPs. NanoMIPs possess high affinity and specificity toward the targets (**Chapter 1: Figure 1.5**).

4.1.1 B2M as a marker of senescence and target for nanoMIPs and ADCs.

To develop new targeted senolytic strategies, we hypothesized that surfaceome proteins could be used to specifically deliver cytotoxic compound into senescent cells. Therefore, to test this hypothesis, we designed nanoMIPs that target beta-2-microglobulin (B2M), a component of MHC class I molecules and one of the surfaceome proteins identified and validated by us (Althubiti et al., 2014, Ekpenyong-Akiba, 2018, Ekpenyong-Akiba et al., 2019). The upregulation of B2M in different senescence models has been previously reported by Althubiti et al., 2014 and Ekpenyong-Akiba et al., 2018 and further validated here. Previously, we found age-related increase of B2M protein level in mice brain and skin (Ekpenyong-Akiba, 2018, Ekpenyong-Akiba et al., 2019). This highlights the B2M potential to be used as a target for the clearance of senescent cells from age-related pathologies that manifest in these organs. Therefore, to further explore the specificity of B2M expression in senescent models, we used the EJ bladder carcinoma cell lines with a tetracycline regulatable expression system (for p53, p21 or p16) and the HT1080-p21-9 cell line with IPTG dependent expression of p21 (**Chapter 2, section 2.2**). EJ cells undergo senescence upon tetracycline removal and HT1080-p21-9 upon addition of IPTG. These cell lines are well characterized cellular models of senescence and allow for activation of main senescence pathways without interference of any other factor. Our data revealed more than 4-fold upregulation of *B2M* mRNA in senescent EJp53 cells and nearly 2-fold increase in EJp16 senescent cells, relative to proliferating counterparts (**Figure 4.1**). Moreover, analysis of B2M protein expression confirmed qPCR findings and showed significant overexpression in both senescent EJp53 and EJp16 cells (**Figure 4.1B**). There was no change in B2M levels when senescence was induced by p21 overexpression in both EJp21 and HT1080-p21-9. These

data confirm that B2M is induced in senescence in response to p53 and p16 activation, albeit at different levels.

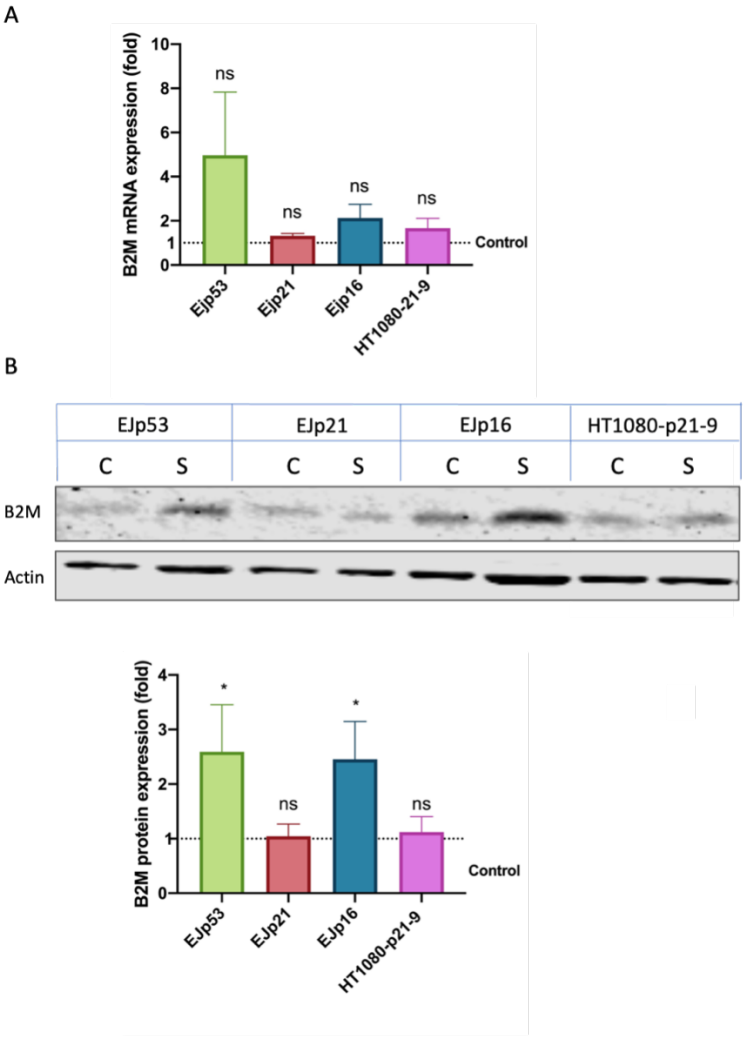

Figure 4.1. B2M expression in genetically induced senescence models.

[A] RT-qPCR and [B] western blot analysis of B2M expression level in EJp53, EJp21, EJp16 and HT1080-p21-9 cells between proliferating (C) and senescent cells (S). The protein expression was normalized against loading control and compared to proliferating counterparts. The graphs represent mean values ±SD, n=3. Statistical analysis performed using paired t-test (p<0.05, ** p<0.01, *** p<0.001, **** p<0.0001).*

4.1.1.1 *In vivo* assessment of nanoMIPs toxicity.

The *in vitro* analysis of nanoMIPs specificity to target senescent cells was performed by Dr. Akang Ekpenyong-Akiba and have been already published (Ekpenyong-Akiba et al., 2019). The specificity of B2M nanoMIPs was tested using EJp16 cells. As mentioned above, B2M is overexpressed in these cells upon expression of p16 and thus senescence induction (**Figure 4.1**). Cells were incubated with fluorescein-tagged B2M nanoMIPs and results showed a significant difference in the accumulation of nanoMIPs with a specific preference to the membrane of senescent cells over proliferating cells (**Chapter 1: Figure 1.6**) (Ekpenyong-Akiba et al., 2019). Further, after binding to B2M on the surface, nanoMIPs internalized and accumulated in the cytosol. Importantly, long exposure to the B2M nanoMIPs did not affect viability of treated cells, either control or senescent cells. Then, B2M nanoMIPs were conjugated with dasatinib, a senolytic drug (Kantarjian et al., 2006) and results showed successful elimination of senescent cells when treated with 10 μM of B2M nanoMIPs (**Chapter 1, Figure 1.7**). Of note, B2M nanoMIPs conjugated with dasatinib were more effective in clearance of senescent cells than dasatinib alone (Ekpenyong-Akiba et al., 2019). These *in vitro* findings revealed that nanoMIPs can selectively target senescent cells and effectively deliver a cytotoxic compound into them.

We decided to further validate these findings and test nanoMIPs specificity *in vivo* using wild type and fast aging *ZMPSTE24*$^{-/-}$ mice.

First, we analysed the short-term effects of B2M-targeted MIPs on mouse health. Animals were given B2M nanoMIPs tagged with DyLight 800 NHS Ester via different routes of injection, intravenously (iv), intraperitoneally or in oral gavage. Routine health and distress symptoms checks were carried for two weeks. Distress symptoms checked included appearance abnormalities like piloerection or coat and skin changes, behavioural differences, food and water intake and hydration status, visibility of backbones, presence of tachypnea, dyspnea, locomotion problems and muscle tone assessment (**Chapter 2, Table 2.15**). All study animals scored negative (score 0) for distress symptoms throughout whole study.

Moreover, drop of weight is one of the most frequent and earliest signs of adverse health outcomes in laboratory mice (Burkholder et al., 2012), therefore weight changes were monitored and scored on a daily basis. As shown on the **Figure 4.2A** the administration of B2M targeted nanoMIPs did not affect the weight of mice, which remained stable through whole study. Furthermore, we performed evaluations of mice kidney and liver functions by measurement of Blood Urea Nitrogen (BUN), Alanine aminotransferase (ALT), and Aspartate aminotransferase (AST) levels, which are commonly used indices of kidney and liver damage (Gowda et al., 2010, McGill, 2016). Results revealed no changes of BUN, ALT and AST levels between treated mice and control mice in all of the tested routes of injections. However, the levels of AST and ALT were elevated comparing to the standards for normal mice (Sher and Hung, 2013). This can be due to advance age of used animals, as the high level of liver markers were present also in untreated animals and due to the genetic background of *ZMPSTE24*$^{+/-}$ animals. Taken together, data showed that B2M nanoMIPs had no important effect on general health of mice during 14-days follow-up after treatment. Our findings are consistent with previous reports that nanoMIPs delivered intravenously were safe and cleared from the blood (Hoshino et al., 2010).

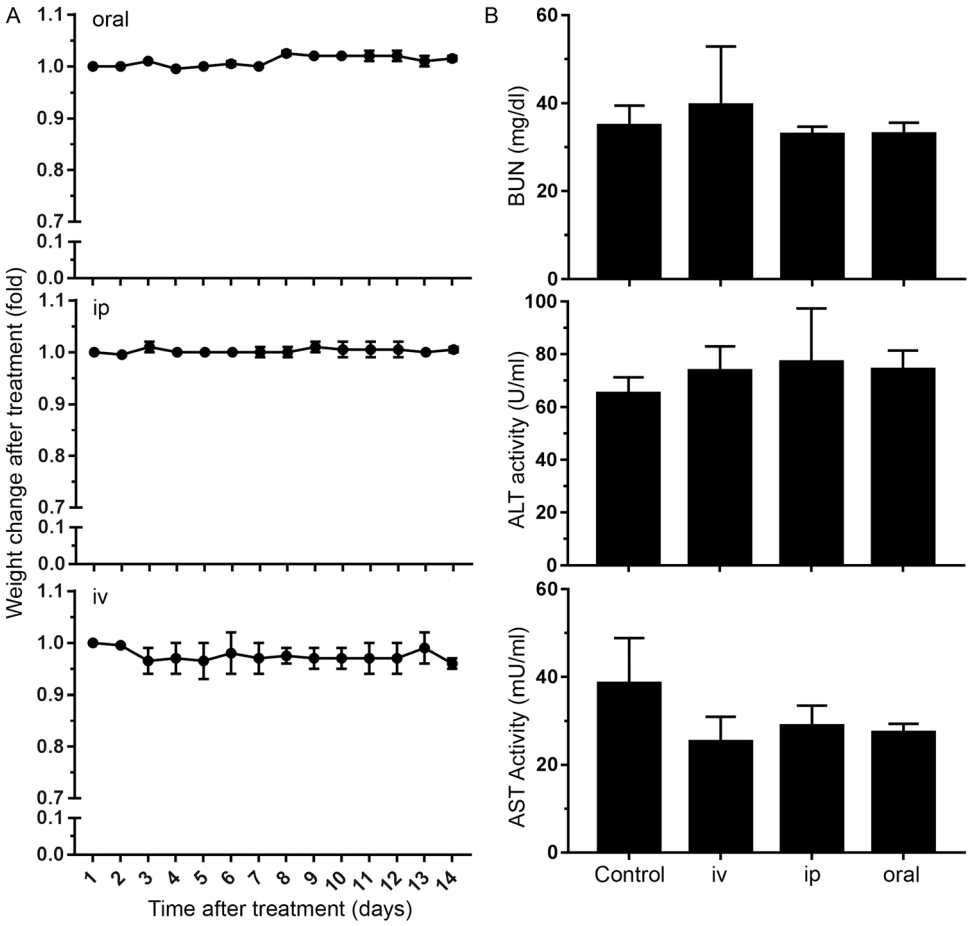

Figure 4.2. Evaluations of B2M nanoMIPs toxicity in vivo.

Six ZMPSTE24+/- mice were exposed to B2M nanoMIPs (0.4mg/ml) via 3 different roads of injection: intravenously (5ml/kg body weight), intraperitoneally and by oral gavage (both 10mg/kg). [A] Body weight changes of mice 14 days after B2M nanoMIPs injection presented as a fold change. The weight of animals has been measured and recorded daily for a period of 2 weeks and normalised to the weight on day 0. Error bars show ± SEM [B] Blood Urea Nitrogen (BUN), Alanine aminotransferase (ALT), and Aspartate aminotransferase (AST) levels detected in serum samples from two mice per group 14 days after injection of B2M nanoMIPs. Blood samples were collected through exsanguination via caudal vena cava and serum samples were analysed within 2 weeks of collection. Every serum sample was assayed in triplicates for all tested enzymes. The data represent the mean ± SEM. The statistical analysis revealed nonsignificant difference between the groups (One-way ANOVA, p>0.05).

4.1.1.2 B2M nanoMIPs detects senescent cells *in vivo.*

To test whether B2M nanoMIPs will be sufficient for recognition of senescent cells in vivo we conjugated them with different fluorescent agents. Since the B2M epitope is well conserved between human (**RV**N**HV**TLSQ**PK**I**V**K**W**GK) and mouse (**RV**K**HV**SMAE**PK**T**V**Y**W**DR) we utilized the same B2M nanoMIPs used for *in vitro* tests (**Chapter 1, section 1.7.3.1**).

Therefore, B2M-targeted nanoMIPs were conjugated with DyLight 800 NHS Ester and injected intravenously into two young (2months) and two old (11 months) C57/BL6J wild type mice. One young and one old untreated mouse were used as a control. Two hours after treatment, animals were imaged in order to localize MIPs inside the body. 2D epi-fluorescent images were taken in prone position (**Figure 4.3**). Results revealed a higher fluorescent signal in old mice than in young animals. Moreover, there was no signal from untreated mice (**Figure 4.3A**). Furthermore, 3D best-case registration to micro-CT and organ atlas (**Chapter 2, section 2.14.2**) was performed for one of the old mice, which exhibited the highest fluorescent signal (**Figure 4.3, Figure 4.3B**). The signal concentrated in the right side of abdominal area, in the intestine, preferentially jejunum. This might or might not be related to increased presence of senescent cells in gastrointestinal track of old mice (Saffrey, 2014). However, the exact location of MIPs should be further confirmed by analysis of the tissues.

After imaging at prone position, animals were humanly culled and quickly open through dissection to reveal internal organs and imaged again in supine position. The fluorescent signal from tested animals was quantified and presented as total radiant efficiency. Results revealed significant difference between old and young mice treated with B2M nanoMIPs (**Figure 4.4A**). However, specific control nanoMIPs should be used in the future alongside B2M-nanoMIPs, such as nanoMIPs that do not target any senescence or aging related protein, or non-targeting nanoMIPs. Further, we performed *ex vivo* imaging of post-mortem dissected organs, such as lung, liver and kidneys. However, results showed the same intensity of the signal in all of the tested groups and tissues (**Figure 4.4B**).

All image analyses and 3D reconstructions were performed with help of **Dr. Michael Kelly** and **Justyna Janus**, of the Univeristy of Leicester Preclinical Imaging Unit, Centre for Core Biotechnological Services (CBS).

Taken together, our results suggest that B2M nanoMIPs accumulate in older animals, which might be reflected by the higher number of senescent cells. Therefore, further analysis should be performed to fully characterize localization of nanoMIPs within the body and validate the use of B2M nanoMIPs as a marker for aged tissues. In here, nanoMIPs accumulated in abdominal area, presumably in the in the intestine, preferentially jejunum. It is unclear why nanoMIPs accumulate in the intestine but not in the other tissues. This should be further investigated. One of the limitations of this study is a low number of biological replicates. Moreover, different routes of injections should be tested and time-specific analysis to assess how fast B2M nanoMIPs are cleared from the body.

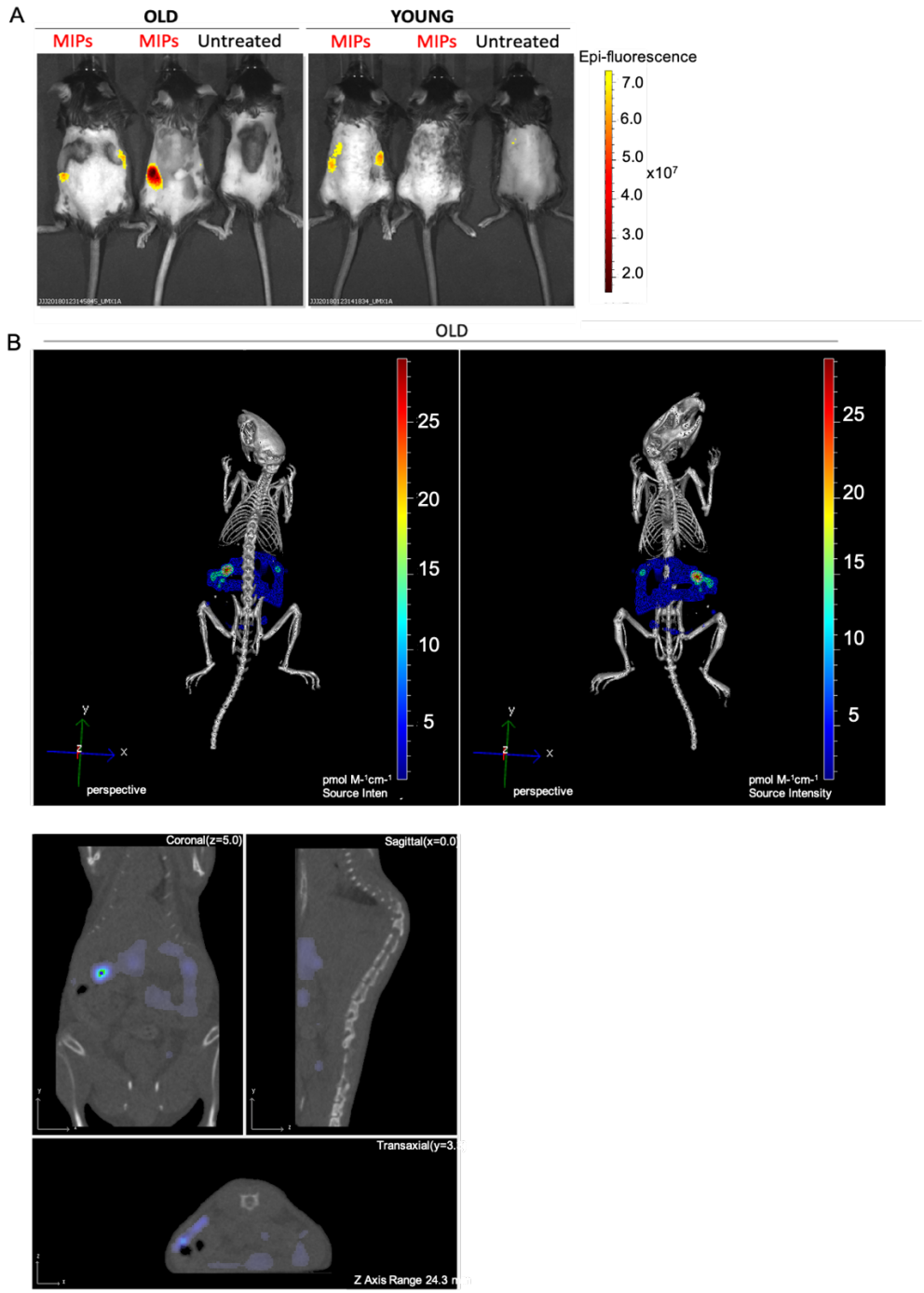

Figure 4.3. In vivo and ex vivo imaging of B2M-positive cells by fluorescent nanoMIPs.

[A] Representative 2D epi-fluorescent images of young (2 month) and old (11 month) mice in prone position injected intravenously with B2M nanoMIPs conjugated with DyLight 800. Untreated mice from the same group of age were used as negative control. [B] Representative 3D registration and signal abdominal cavity localization of B2M nanoMIPs conjugated with DyLight 800 in a 11-month-old mouse.

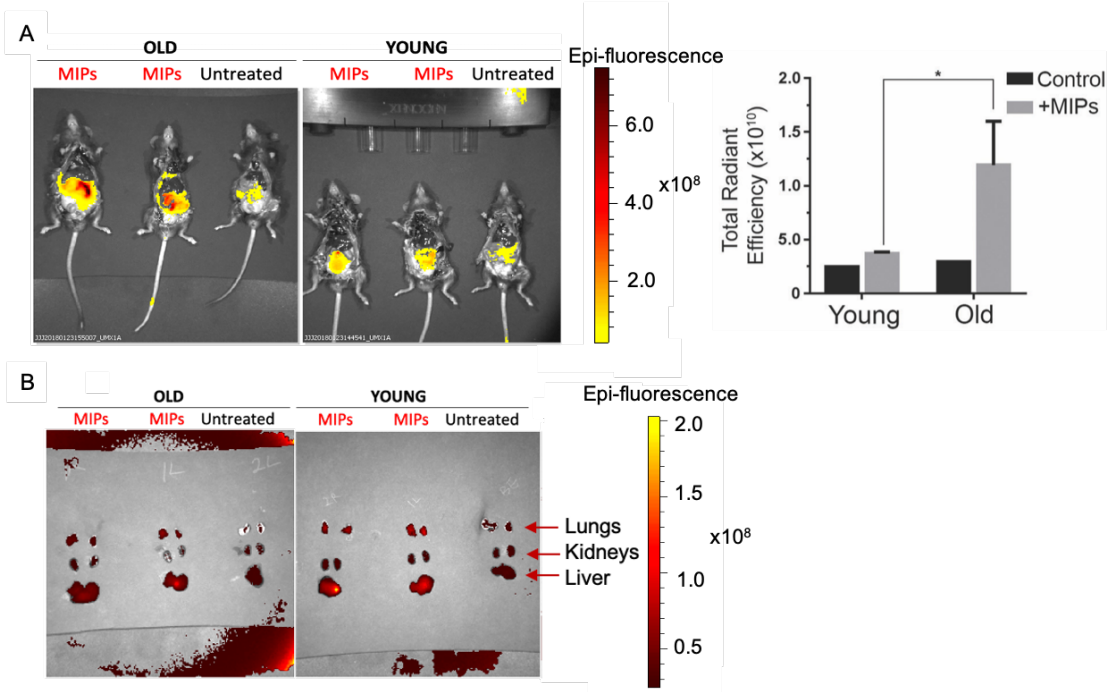

Figure 4.4. Mice imaging after the treatment with B2M nanoMIPs.

[A] Representative 2D epi-fluorescent images of young (2 month) and old (11 month) mice in [A] supine position injected intravenously with B2M nanoMIPs conjugated with DyLight 800. Untreated mice from the same group of age were used as negative control. Graph presents quantification of the fluorescent signal expressed as total radiant efficiency. Bars represents mean value ± SD. Statistical significance determined using unpaired t-test (p<0.05).*

[B] Ex vivo imaging of dissected organs: lungs, kidneys and liver from the same mice as above.

4.1.2 Antibody-drug conjugates

ADCs are biopharmaceutical drugs designed as a targeted therapies, especially for cancer treatment (Zolot et al., 2013). Antibodies track a cell expressing a specific marker and then get internalized by the targeted cell. After internalization, the conjugated cytotoxic compound is released which results in the death of the cell of interest (**Figure 4.5**).

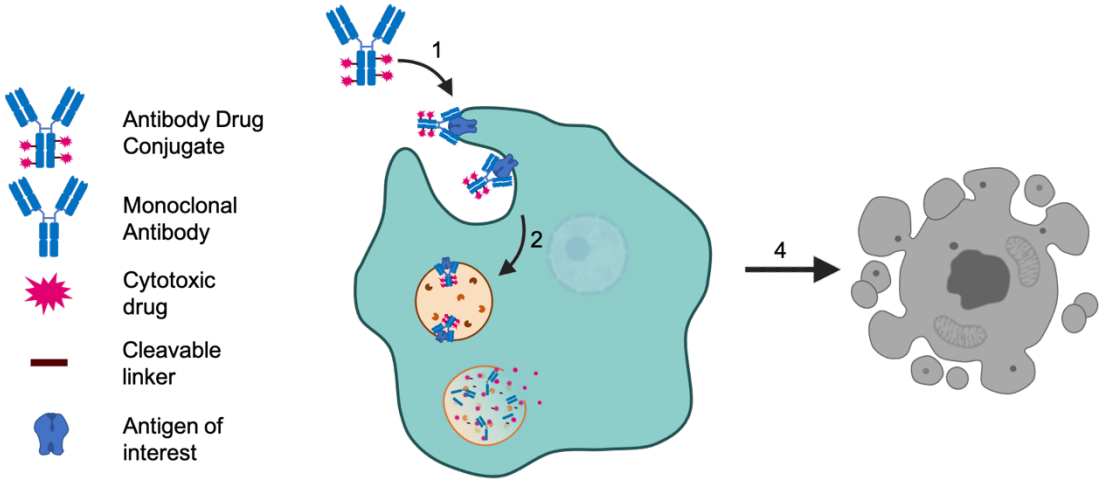

Figure 4.5. Schematic representation of ADCs.

Left panel of the figure represents the ADCs components and right side presents the mechanism of ADCs action: ADCs recognize antigen of the surfaceome protein (1). Complex is internalized and traffics to lysosome (2). The ADCs are disintegrated, and the cytotoxic payload is released (3) leading to apoptotic-mediated cell death (4).

4.1.2.1 B2M as a marker of senescence and target for ADCs

To develop new targeted senolytic strategies, we hypothesized that the senescent surfaceome could be used to specifically deliver cytotoxic compound into senescent cells. To test this hypothesis, we designed ADCs to target B2M, component of MHC class I molecules and one of the surfaceome protein identified and validated by us (Althubiti et al., 2014, Ekpenyong-Akiba, 2018, Ekpenyong-Akiba et al., 2019). and previously used B2M as a target for nanoMIPs (**Chapter 4, section 4.1.1.2**).

4.1.2.2 Development of B2M-ADCs and their specificity in senescent cells clearance.

To further explore whether targeted senolysis could have a clinical potential, we designed senolytic ADC. There are five classes of human antibodies (G,A, D, E and M). Among them, the IgG isotype has been shown to have the lowest immunogenicity potential (Parks and Weigle, 1980). Therefore, IgG isotype, predominately the IgG1, has been used for the most of immunotherapeutics approved in the clinic.

Prior the production of ADCs, we picked a commercially available B2M IgG1 monoclonal antibody (BioSciences Cat nr: LS-B2200) and tested its internalization specificity. Internalization CypHer assay was performed by Dr Mohammad Althubiti. The CypHer assay uses pH-sensitive cyanine dye derivative, termed, CypHer™ 5, which is non-fluorescent at pH 7.4 and is maximally fluorescent at pH 5.5. Therefore, it has been used to report the molecule movement from the cell surface (pH= 7.0-7.4) into internal acidic endosomes (pH= 6.0-4.5). Results revealed successful internalization of B2M antibody with the highest internalisation rate achieved after 120 minutes (**Figure 4.6**). Based on the results from successful internalization, the monoclonal B2M-Antibody was sent to our commercial partner, ABZENA, for the production of B2M-targeting ADCs conjugated with duocarmycin.

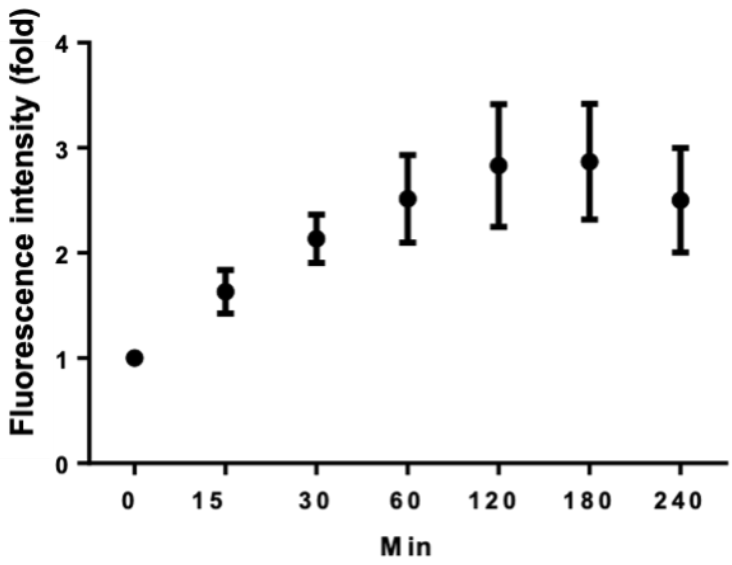

Figure 4.6. Internalization rate of B2M antibody

Internalization rate of the unconjugated B2M antibody in control EJp16 cells as measured by CypHer5E fluorescence in a FACS analysis. Results show mean ± SD of three independent experiments. Experiment performed by Dr Mohammad Althubiti.

Duocarmycin is an irreversible DNA alkylating agent commonly used in ADCs (Dokter et al., 2014, van der Lee et al., 2015) and was chosen as a cytotoxic conjugate following company recommendation based on conjugation properties. The conjugation was established using a cleavable pH-sensitive linker, which initiates hydrolysis of the acid-sensitive group within the linker upon internalization to endosomes (pH=5-6) and lysosomes (pH=4.8). Of note, the similar concept was used during assessment of B2M IgG1 monoclonal antibody internalization, which further support specificity potential of designed ADCs. The final concentration of B2M-ADCs was 1.16 mg/ml with average drug/ antibody rate (DAR) of 2.02 (**Figure 4.7C**). Additionally, an isotype IgG1 ADCs conjugated with duocarmycin was also generated and used as control. The concentration of IgG1-ADCs had similar characteristic to B2M-ADCs, with 1.36 mg/ml concentration and 2.46 DAR average.

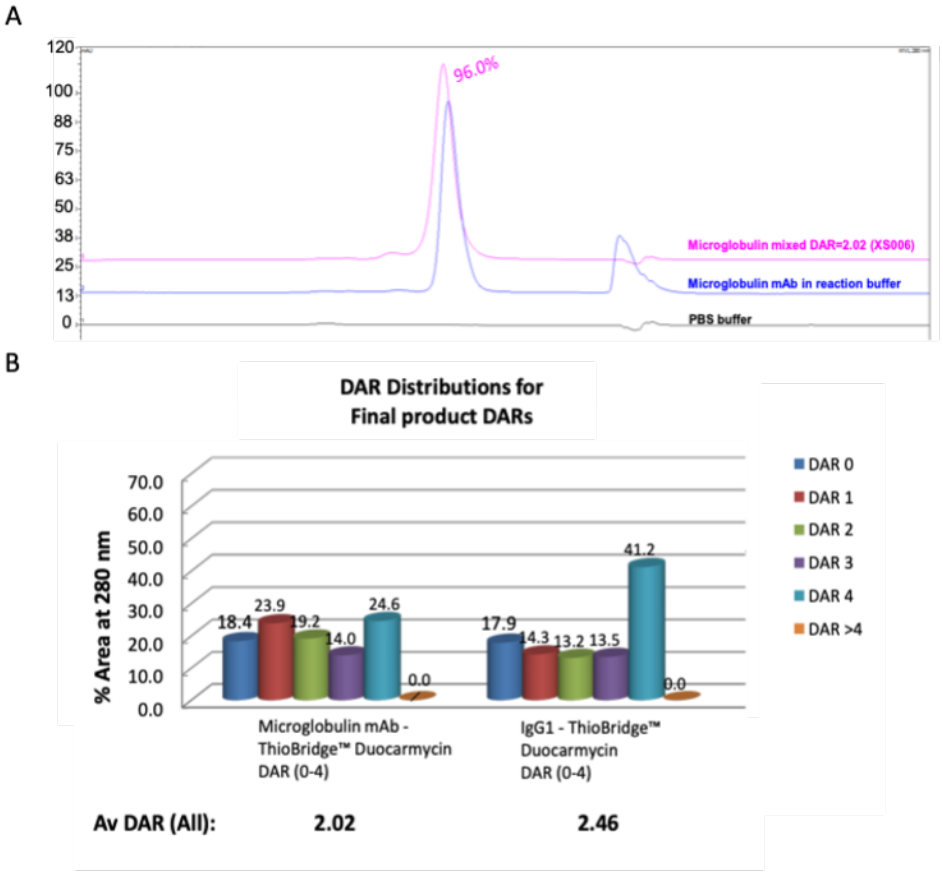

Figure 4.7. Characteristics of B2M-ADCs.

All experiments presented here were performed by Abzena. [A] Size-Exclusion Chromatography characterization of the purity of the final ADC mix, compared to pure antibody and PBS.

(B) Quantitation of Drug-Antibody Ratios (DAR) of the B2M conjugated antibodies. Numbers indicate percentages of each DAR population in the mixture. Average DAR: 2.02.

Next, the specificity of the ADCs in clearance of senescent cells was validated using cell-viability assay. Senescence was induced in EJp53 and EJp21 cells (**Chapter 3: Figure 3.2, Figure 3.3**). Additionally, proliferating EJp53 cells were transfected with B2M cDNA as a positive control. For negative control, unspecific for B2M IgG1-ADCs conjugated with duocarmycin were used. Expression of B2M in tested models was confirmed by western blot (**Figure 4.8**). Consistently with **Figure 4.1** B2M was strongly expressed in response to p53 but not by p21. High level of B2M in positive control confirmed successful transfection. (**Figure 4.8**)

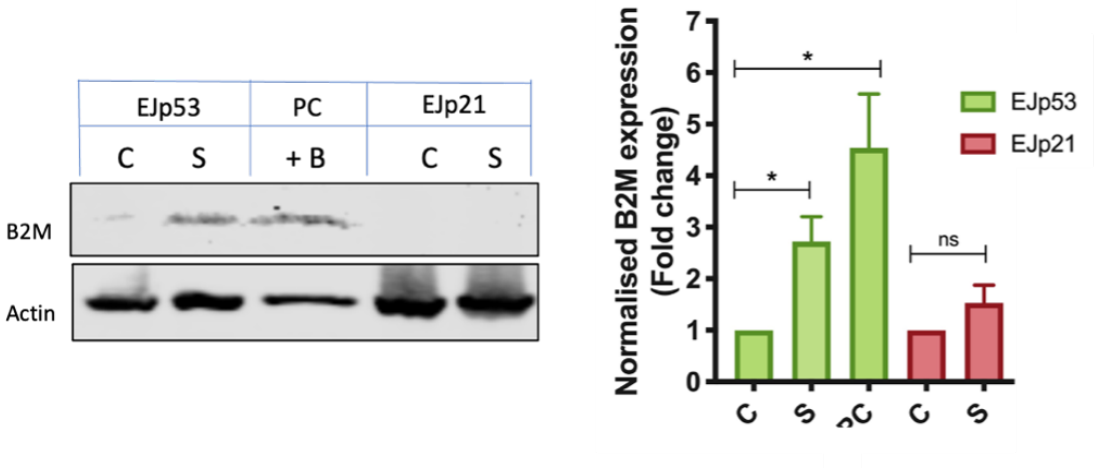

Figure 4.8. B2M expression in tested models.

Representative western blot and bands quantifications showing B2M expression level in EJp53 and EJp21 cells just before the treatment with ADCs. B2M level was compared between proliferating controls (C) and senescent cells (S). Proliferating EJp53 cells transfected with B2M-cDNA were used as a positive control (P). Data were normalized against loading control β-actin and the fold change was calculated in comparison to proliferating counterparts of each cell line. Bars represents mean value ± SD, n=2. Statistical analysis performed using paired t-test (p<0.05, ** p<0.01, *** p<0.001, **** p<0.0001).*

Following confirmation of B2M expression, an equal number of cells was seeded in a 96-well plate and both proliferating and senescent cells were incubated with the B2M-ADCs or isotype control for 72 hours. To determine the number of viable cells, Cell-Titer Glo assay was used. Results revealed significant changes between proliferating and senescent cells treated with B2M-ADCs in the cells where B2M expression was high after induction of senescence, EJp53 and positive control (**Figure 4.8**). In senescent EJp53, the significant difference in cell viability was observed between B2M-ADCs and control IgG1-ADCs already at nanomolar level, with the highest difference at 0.05μM (63% to 87% viability) (**Figure 4.9**). Similar difference was observed in B2M-transfected positive cells, although the difference was stronger when treated with high concentrations of B2M ADCs. This confirms that toxicity of generated ADCs in this cell line was dictated by B2M expression. In EJp21 cells there was no difference in viability between proliferating and senescent cells treated with B2M ADCs (**Figure 4.9B**). However, analysis of EJp21 cell line revealed that there was a similar drop in cells viability of proliferating and senescent cells when treated with higher concentrations, such as 0.05μM B2M ADCs. This suggests B2M-unrealated off-target cytotoxic effects of the ADCs when treated with high dosage.

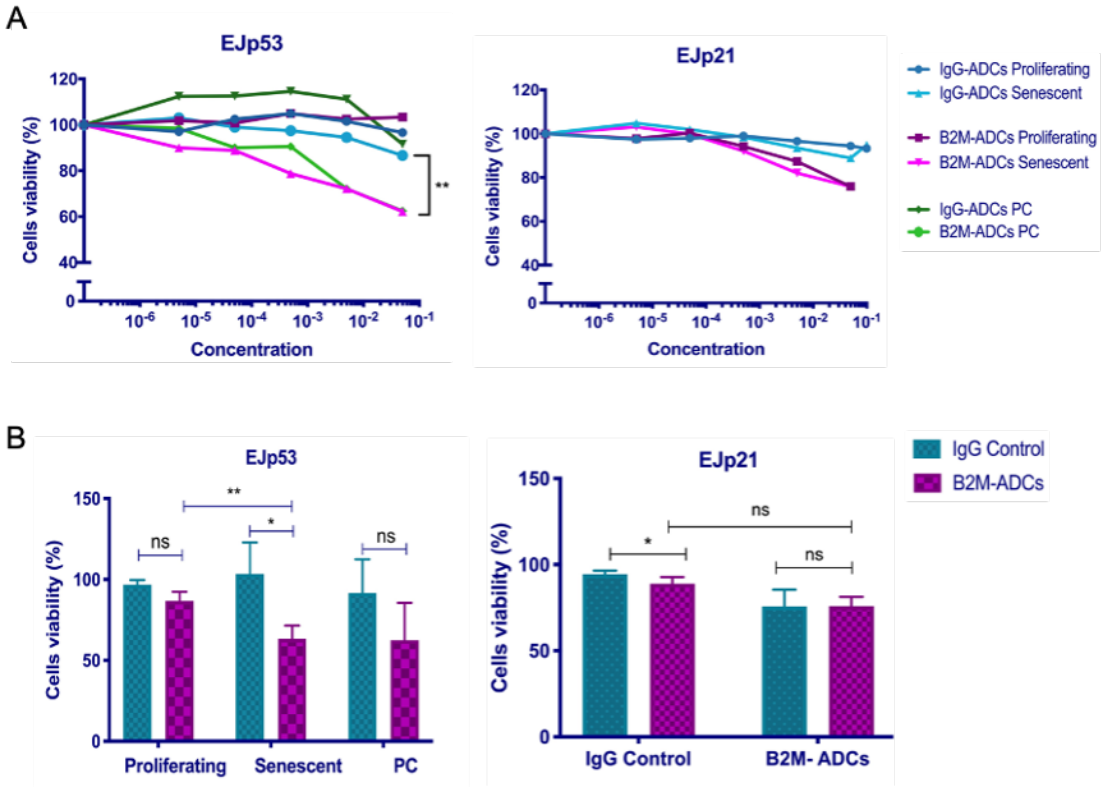

Figure 4.9. Cell viability of senescent EJp53 and EJp16 cells after the treatment with *B2M-ADCs. [A] Cell viability of proliferating and senescent EJp53, EJp21 cells 72h after the treatment with increasing concentrations (0, 0.00005, 0.0005, 0.005, 0.05 and 0.1 µM) of B2M-ADCs or control IgG-ADCs. Proliferating EJp53 cells transfected with B2M-cDNA were used as a positive control (PC). [B] Cell viability, as measured by Cell Titre Glo, of proliferating and senescent (4 days after induction) EJp53 and EJp21 cells 72h after the treatment with 0.05 µM of B2M-ADCs or isotype control. Bars represents mean value ± SD. EJp53 n=5, PC and EJp21 n=3 for all the panels. Statistical analysis performed using paired t-test (* p<0.05, ** p<0.01).*

To further validate if the drop of senescent cells viability after the B2M-treatment was caused by the increased amount of cell death, PI staining and FACS were performed (**Figure 4.10**). The data were consistent with the drug assays findings (**Figure 4.9**). There was considerable difference in EJp53 senescent cells treated with B2M-ADCs and IgG1-ADCs. However, there was also a high level of cell death detected in proliferating cells after the treatment with B2M ADCs. The treatment of EJp21 cells did not show significant changes in the percentage of cell death between senescent cells treated with ADC B2M and IgG1 B2M. However, around 10% of cell death was observed in both proliferating and senescent cells treated with 0.05μM B2M ADCs. Also, analysis of positive control cells revealed a difference in percentage of cell death between the treatment with B2M-ADCs and IgG1-ADCs with a p value on the border of statistical significance (p=0.0590, paired-t test).

Taken together, these results show that B2M ADC indicates senolytics properties and can selectively kill senescent cells although not without side effects. Further experiments are needed to determine the level of off-target cytotoxicity.

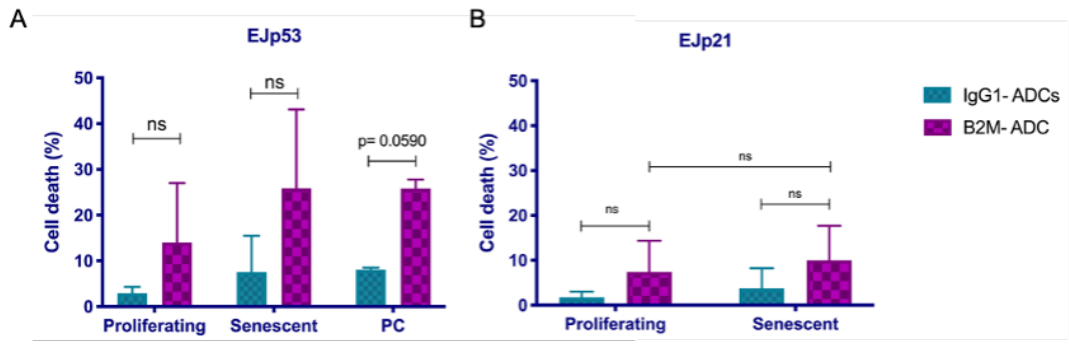

Figure 4.10. B2M ADCs selectively kill senescent cells.

*Percentage of cell death, as measured by PI staining of proliferating and senescent (4 days after induction) in EJp53 and EJp21 cells incubated with 0.05μM of the B2M ADCs or IgG1 ADC for 72 hours. Bars represents mean value ± SD, EJp53 and EJp21 n=3, PC n=2. Statistical analysis performed using paired t-test (ns: not-significant, * p<0.05, ** p<0.01, ***p<0.001).*

4.2 Discussion.

One of the concepts to improve senolytic that has recently evolved is designing a novel class of drugs, a second-generation of senolytics that would specifically recognize senescent cells and deliver the drug to the cell of interests, thus being more specific than already existing first-generation drugs.

In this chapter, we presented the validation of two approaches that represent a second generation of senolytics. Our approaches detect and/or eliminate senescent cells burden by delivery of cytotoxic compound through specific recognition of a senescent surfaceome marker. Our data provides a pre-clinical validation that the specific pattern of the senescent surfaceome could be used to detect and eliminate senescent cells through advanced technology, such nanoparticles and antibody drug conjugates. In the current study we tested the potential use of nanoparticles that take advantage of the senescent surfaceome to locate senescent cells *in vivo*. Targeting surfaceome has an advantage over intracellular targets that there is no need to cross the cell membrane and penetrate into the cell to access intracellular targets. We developed a nanomaterial that recognizes B2M, a protein that was previously identified as a membrane marker of senescent cells (Althubiti et al., 2014). Our results show that fluorescently tagged B2M nanoMIPs had no short-term side effects when injected *in vivo*. Our experiment of fluorescently tagged nanoMIPs provide a basis for a future diagnostic potential. Next, multiple and subsequent dosages should be tested with consideration of different injection routs and time needed for nanoMIPs to be cleared from the body. Our proof-of principle study could act as a basis for design of more specific nanoparticles that could work as diagnostic tool. Moreover, it would be important to test this approach against other senescent surfaceome markers and characterize its specificity and effectivity *in vivo* not only in aging animals but also in the mouse model of age-related diseases. In the future, it would be also interesting to load B2M-nanoMIPs or nanoMIPs that recognize different and more specific senescent surfaceome markers with senolytics. A direct delivery of the drug to senescent cells could reduce the global cytotoxicity and reduce the amount of off-target side effects. Therefore, second-generation of senolytics

have an advantage over the first-generation of senolytics that are characterized by lack of specificity and high level of side effects. This concept has been already tested by different research group, which designed Nav-Gal, a pro-drug created by galacto-conjugation of Navitoclax (González-Gualda et al., 2020b). Treatment of Nav-Gal reduced the number of senescent cells and, most importantly, exhibited a lower rate of off-target toxicity over Navitoclax. NanoMIPs and Nav-Gal present a new class of diagnostic and drug delivery tools. A big advantage of nanotechnology is no need for animal use, lower production costs and longer shelf time than antibodies. The properties and capabilities of nanoMIPs have been extensively studied, for example as a replacement of antibodies in different assays, such as ELISA. Moreover, nanoMIPs have been already successfully applied as imaging tool *in vivo*, which further support their diagnostic potential (Cecchini et al., 2017a). However, despite increasing evidence of nanotechnologies in preclinical models, there are few crucial limitations preventing their full transition to clinic. To start, not much is known about nano-bio interactions, bio-distribution, potential toxicities and clearance of nanoparticles from the body. Moreover, other limitations from technical and economic aspects may occur when the nanoparticles production will need to be scaled up for clinical use. Further studies related to biosafety will be crucial before nanoparticles could be used in humans.

We also presented the first indications of *in vitro* elimination of senescent cells using ADCs as drug delivery tool. The results of the ADCs to target an extracellular epitope on the senescent cells surfaceome is another example of second-generation senolytics and targeted senolysis strategy. Although this is a novel approach in the field of cellular senescence, a similar concept has been already widely characterized and validated as a cancer treatment (Thomas et al., 2016). Despite the fact that production of ADCs is expensive and require the usage of animals, we show that it could be promising new approach for elimination of senescent cells. Our results showed that B2M ADCs selectively induced cell death in EJp53 senescent cells that express B2M. However, we also saw a toxic effect in senescent cells that do not express B2M when treated with high dose of ADCs. Therefore, further studies should be taken to establish therapeutic window for the treatment and more cell lines should be tested in the future. Of note, B2M is a protein widely expressed in most cell types, therefore it is unlikely that it would

be the universal target of choice. It might be still used in tissues in which its expression significantly increases with age, such as brain and skin. However, *in vivo* experiments will be needed to determine if and to what degree the background expression of B2M is an obstacle to use such ADC in humans. Additionally, in our study we conjugated ADCs with duocarmycin, a DNA alkylating agent. To solidify our findings, additional experiment is needed to check the effect of duocarmycin alone on tested cell lines. Further, to increase specificity of ADCs it would be important to conjugate ADCs with a senolytic drug, such as navitoclax. During ADCs production, a conjugation method of ADCs with the drug is highly important. It is crucial for a drug to remain stable during preparation, storage and circulation in the blood. Unstable linkage with cytotoxic payloads may result with premature release of the drug before full internalization of ADCs.

Taken together, our preliminary experiment acts as a proof of concept for use of targeted senolytics as a novel class of senotherapeutic. They could be an efficient detection system and drug delivery tool that could eliminate senescent cells with minimal side effects. Further studies will be needed to discover the best target, evaluate safety and determine effectivity of proposed approach.

5 Characterization of the effects of BTK inhibition in senescence *in vitro* and *in vivo.*

Senoblocking is one of the approaches to prevent the accumulation of senescent cells and their detrimental effects on tissue function. This can be achieved by blocking the senescence-inducing pathways and thus preventing the emergence of the phenotype, or reversing it once it has been established. Although, the reversing approach so far was achieved only in laboratory conditions e.g. by enforced telomerase activity (Pellegrini et al., 2004). However, the first approach relies on the strategy to stop the activation of one or both core senescence pathways, p53-p21 and p16-pRB.

Previous studies performed by our group identified Bruton's tyrosine kinase (BTK) (Althubiti et al., 2014) as one of the proteins overexpressed in senescent cells and revealed that its inhibition results in the blockage of cellular senescence (Rada et al., 2017, Althubiti et al., 2016b). BTK is a nonreceptor tyrosine kinase mutated in the inherited immunodeficiency X-linked agammaglobulinemia (Vetrie et al., 1993). It is expressed in different leukaemias and lymphomas (Herman et al., 2011) and plays a role in B-cell development (Rawlings et al., 1996). Surprisingly, opposite to its oncogenic role in B cells, BTK has been found to be activated in response to damage and contribute to the tumour suppressor mechanisms regulated by p53 (Althubiti et al., 2016b). BTK expression increases the stability of p53 and increases the binding of p53 to the promoters of its target genes after genotoxic stress, which results in higher levels of expression of both proapoptotic and proarrest signals (Althubiti et al., 2016b). Moreover, BTK is also acting on MDM2, a p53 target gene and direct inhibitor (Rada et al., 2017). BTK expression increases the protein levels of MDM2 and impaired its ubiquitination activity, which results in further stabilization of p53 protein level. Conversely, the inhibition of BTK reduced the level of p53 after DNA damage in several models of p53 induction, which resulted in impaired cellular responses like apoptosis and cellular senescence (Althubiti et al., 2016b).

All these findings underscore the importance of BTK in the regulation of p53 pathways and highlights its physiological relevance in the context of tumour suppression and cellular senescence. Inhibition of BTK affects the expression of p53 target genes, which results in altered senescent responses (Althubiti et al., 2016b). This led to the hypothesis that BTK inhibitors could prevent the accumulation of senescent cells and thus ameliorate ageing phenotypes by acting as senoblockers.

Indeed, we showed that Ibrutinib, a covalent BTK inhibitor approved for the treatment of certain leukaemias (Akinleye et al., 2013, Aalipour and Advani, 2014, Masso-Valles et al., 2016, Walter et al., 2017), could increase the lifespan and healthspan of the *ZMPSTE24*$^{-/-}$ Hutchinson-Gilford progeria mouse model (Ekpenyong-Akiba et al., 2020a). These results underscore the importance of BTK in the regulation of p53-dependent cell fate decisions and highlight the physiological relevance of BTK inhibitors in the context of aging, which still needs to be fully characterized. Therefore, the effects of BTK inhibition in senescence was characterized in this chapter to investigate if BTK can be used as a potential preventor of senescence.

5.1 The *in vivo* effect of BTK inhibition on *ZMPSTE24*$^{-/-}$ mice.

Since BTK inhibitors are commercially available and widely used in the clinic (Akinleye et al., 2013), we decided to test its effect on cellular senescence *in vivo*. As the p53 pathway is one of the core pathways involved in the induction and maintenance of cellular senescence, we decided to investigate the effect of BTK inhibition on aging using *ZMPSTE24*$^{-/-}$ mouse model. The *ZMPSTE24*$^{-/-}$ is the mouse model for Hutchinson- Gilford progeria syndrome (HGPS) (Bergo et al., 2002b) and *ZMPSTE24*$^{-/-}$ mice are characterized by nuclear abnormalities and histopathological defects of aging phenotype that results at least in part by pathological increase of p53 signalling (Varela et al., 2005). At the age of ~ 4-6 months, the aging symptoms start to develop: alopecia, loss of fur colour, kyphosis, tremor, declined forelimb grip strength, cataracts or just corneal opacity, eye

discharge, malocclusions, penile prolapse, piloerection, weight loss, etc (**Chapter 2, section 2.13.1**).

38 *ZMPSTE24*$^{-/-}$ mice were selected for the study. 20 of them were treated with the BTK inhibitor Ibrutinib (10mg/kg), and 18 received a vehicle (sterile water with appropriate volume of DMSO). The treatment was held continuously (twice a week by oral gavage) starting from 2 months of age up till the end of their life, as determined by the humane endpoints allowed in the Project Licence. Several features of aging were investigated (**Figure 2.4, Figure 5.1**).

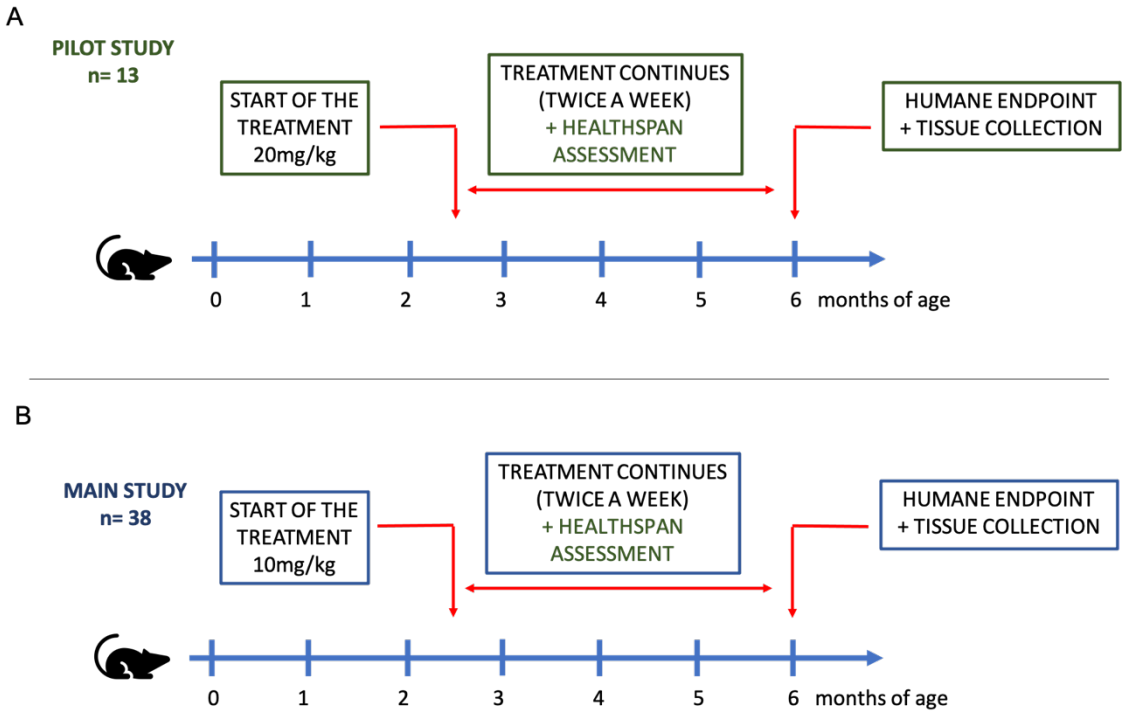

Figure 5.1. The experimental design of in vivo experiments.

Treatment with Ibrutinib (10mg/kg for pilot study) and (20mg/kg for main study) started after weaning, when animals reached around 2-3 months of age. Treatment, together with healthspan assessment, continued twice a week until the end of animal's life.

5.1.1 Ibrutinib treatment ameliorates age-related decline of brain function in the *ZMPSTE24*$^{-/-}$ mouse model.

The first stage of the study compared the effect of the treatment on the animal's lifespan. The lifespan assessment was performed by Dr Akang Eyo Ekpenyong-Akiba and the data has been published (Ekpenyong-Akiba et al., 2020a). The results did not show significance difference on the average lifespan, however there was a difference in maximum lifespan (**Figure 1.9**). Moreover, when the health of control group started to quickly deteriorate, as measured using clinical frailty scores (**Figure 2.2**), it was still preserved in the treated animals (**Figure 1.9B**). This observation led to analysis of the animals' healthspan.

Healthspan evaluations started with assessment of the potential changes on cognitive functions of the treated animals, since memory loss, cognitive dysfunction and dementia are among disorders associated with aging (Esiri, 2007, Attar et al., 2013, Yang et al., 2017b). Therefore, we used the Barnes maze (Capilla-Gonzalez et al., 2012) to assess the effect of Ibrutinib treatment on long term spatial memory **(Barnes Maze 2.15.2.2**). For additional comparison, wild-type animals, which were, cage mates of the study animals (buddies), were also included in the study. My contribution in this experiment was limited to the analysis of the videos and data analysis from the Recall stage of the experiment. The rest of the data can be found in (Ekpenyong-Akiba, 2018). The experiment was divided into 4 parts: Habituation, Acquisition, Probe Trial and Recall (**Figure 2.4**). Habituation started at the day one of experiment and was aiming at animal's familiarization with the maze and experimental environment. The Acquisition lasted for another five days and focused on the training of the animals to find the escape box. The next stage, Probe Trial started on the day 7 and tested the outcomes of the previous training. The box was taken away from the maze and the number of attempts that the mice poked the target hole with their nose was analysed. The Recall stage was 7 days after Probe Trial (**Figure 2.4**), and the latency, which is the time the mice needed to locate the target hole was recorded and analysed. Detailed description of the

procedure was described above in Materials and Methods section (Barnes Maze). Results revealed no changes in the mean latency between the tested groups: Ibrutinib, vehicle and buddies (**Figure 5.2A**). However, when the data were analysed in the sex-depended manner the significant difference was observed between males from Ibrutinib-treated and vehicle-treated group as well as between buddy group and vehicle-treated group. *ZMPSTE24*$^{-/-}$ males treated with Ibrutinib needed less time than those treated with vehicle to localise the target hole with two-fold difference in the latency. The opposite response was observed in the analysis of females' performance. The mean latency was higher in the buddy group and Ibrutinib-treated females than in mice treated with vehicle. However, the differences were not statistically significant.

The general comparison of all the study animals' performance indicates that the buddies group needed the least time to identify target hole, as expected. This exposed difference in the learning abilities between wild-type and *ZMPSTE24*$^{-/-}$ mice (**Figure 5.2A**). The *ZMPSTE24*$^{-/-}$ progeria model was used for the convenience of a short lifespan, allowing for more accessible experiments. However, it would be necessary to repeat the experiment using wild-type animals to exclude potential impact of genetically modified background of *ZMPSTE24*$^{-/-}$ mice. Our results indicated that age-related impairment of brain functions may be preserved by the usage of BTK-inhibitor Ibrutinib and that the degree of its effectiveness may be sex-specific. Furthermore, it was unclear if the Ibrutinib treatment affected the number of senescent cells *in vivo*. Therefore, the next step of analysis involved biochemistry of the tissues and the relationship between Ibrutinib treatment and the number of senescent cells was tested by comparison of senescence markers expression profiles.

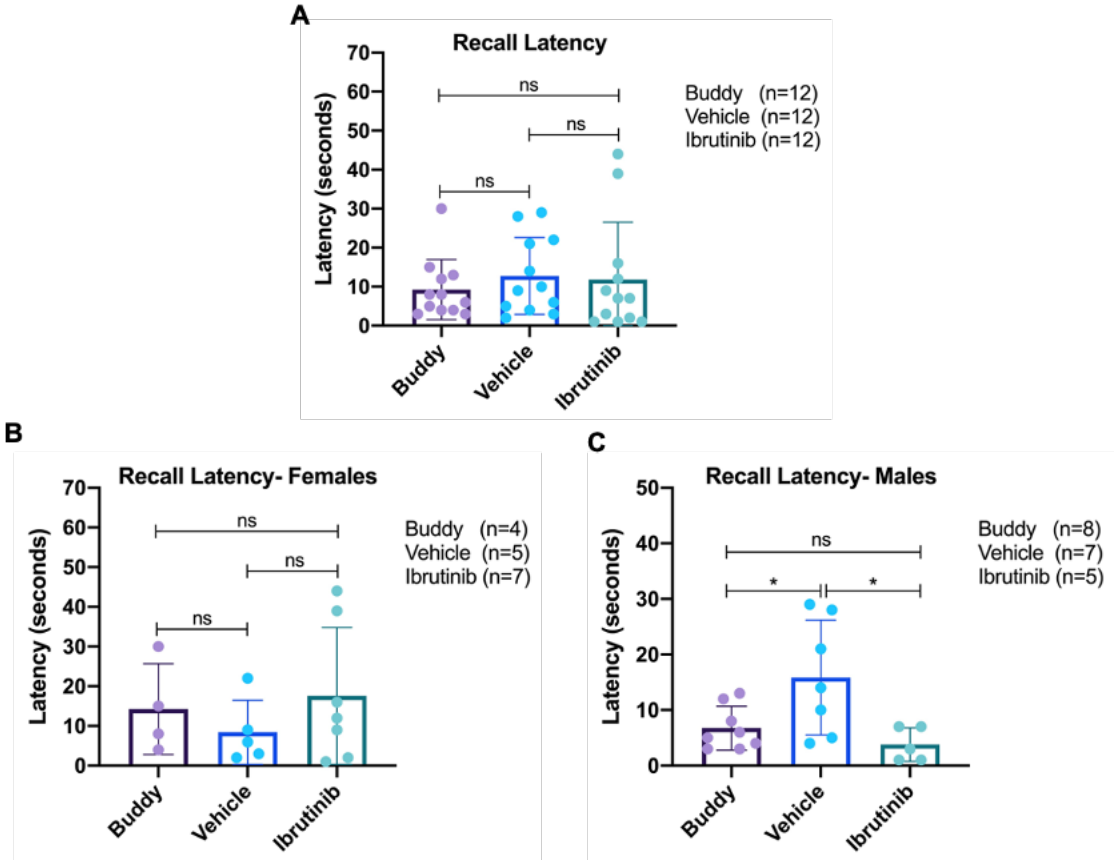

Figure 5.2. The latency analysis during Barnes Maze test- Recall.

Graph represents the results of latency measurements during Recall phase of Barnes Maze test. Latency was the time the animal needed to localise the target hole. Buddy group represents wild type (ZMPSE24$^{+/+}$) n=12, and heterozygous (ZMPSTE24$^{+/-}$) mates of the study animals used as negative control. The two study groups, Ibrutinib n=12 and Vehicle n=12, consists of homozygous (ZMPSTE24$^{-/-}$) mice treated either with Ibrutinib (10mg/kg) or vehicle. [A] Total Recall latency of all study animals. [B] Recall latency of females. [C] Recall latency of males. Results are presented as mean ± SD. Statistical analysis performed using unpaired t-test (p<0.05, ** p<0.01, *** p<0.001, **** p<0.0001). Experiment performed in collaboration with* Dr Akang Eyo Ekpenyong-Akiba.

5.1.1.1 Ibrutinib treatment affects the expression of senescence markers in the brain of progeroid mice.

As the healthspan of animals improved after the treatment of BTK-inhibitor (**Chapter 5, section 5.1.1**), we hypothesized that this could happen due to decreased accumulation of senescent cells, and that the lack of BTK impairs the p53 activity *in vivo.* The expression of the markers was compared in the brain tissues collected from animals used for functional tests. Moreover, animals for biochemistry analysis were chosen based on similar age and the length of the treatment (190-200 days old and ~120 days after the beginning of the treatment).

At first, the mRNA expression of a range of known (p53, p21, p16, IL-1β, IL-6) and yet uncharacterized senescence markers (VPS26A, PLD3, ARMCX3, STX4, B2M, DEP1) were tested using RT-qPCR. Data revealed downregulation of 7 markers when compared with the data from vehicle-treated control group. The Ibrutinib treatment significantly affected mRNA expression of *PLD3, BTK, IL-1β, VPS26A, IL-6, ARMCX3* and *STX4* (**Figure 5.3**). Further, we compared expression profiles of tested markers according to the gender of tested animals. Females analysis revealed significant changes of *ARMCX3, STX4* and *B2M* mRNA level (**Figure 5.4A**). However, due to the low number of females it was impossible to determine statistical significance for all the markers. The analysis of the males' samples showed downregulation of *PLD3* and *BTK* after the treatment with Ibrutinib (**Figure 5.4B**). However, the data presented reflects the results of the pilot study only and higher number of samples should be analysed to confirm these findings. Moreover, expression of tested markers should be compared between wild type and *ZMPSTE24*$^{-/-}$ animals and potential changes that might occur with aging should be tested as well.

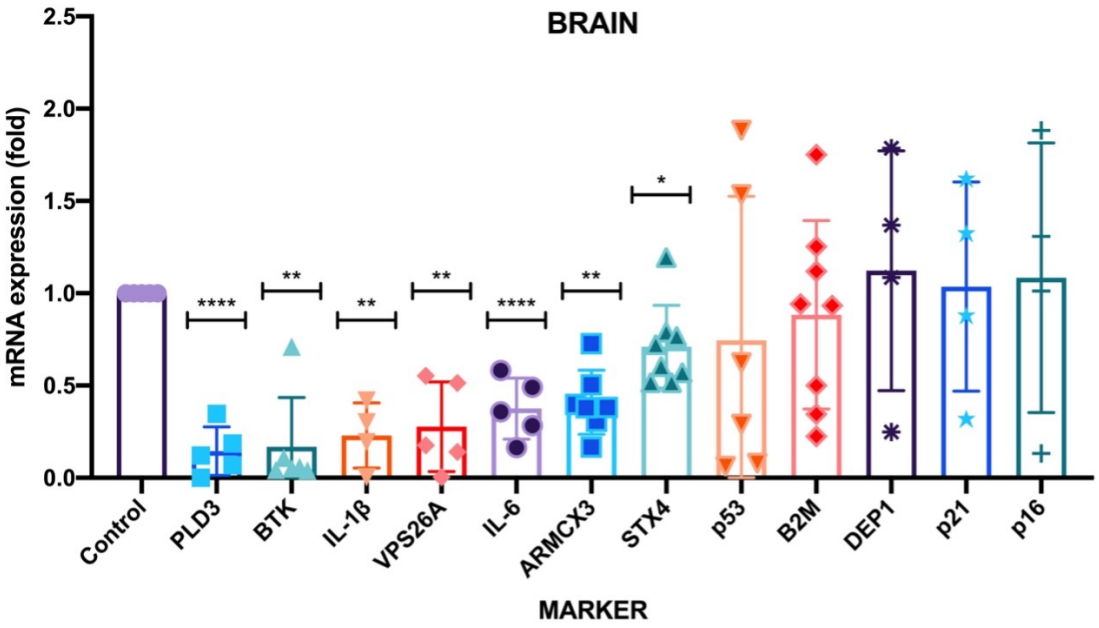

Figure 5.3. QPCR analysis of ZMPSTE24$^{-/-}$ mice brain after the treatment with Ibrutinib.

ZMPSTE24$^{-/-}$ mice were continuously treated with Ibrutinib (10mg/kg) or vehicle twice a week until culled. Data represents RT-qPCR analysis of range of senescence markers in the mice brain. GAPDH was used as internal reference control gene. Data were normalized against vehicle-treated controls. Results are presented as mean ± SD. Statistical analysis performed using unpaired t-test (p<0.05, ** p<0.01, *** p<0.001, **** p<0.0001). n= 4-9.*

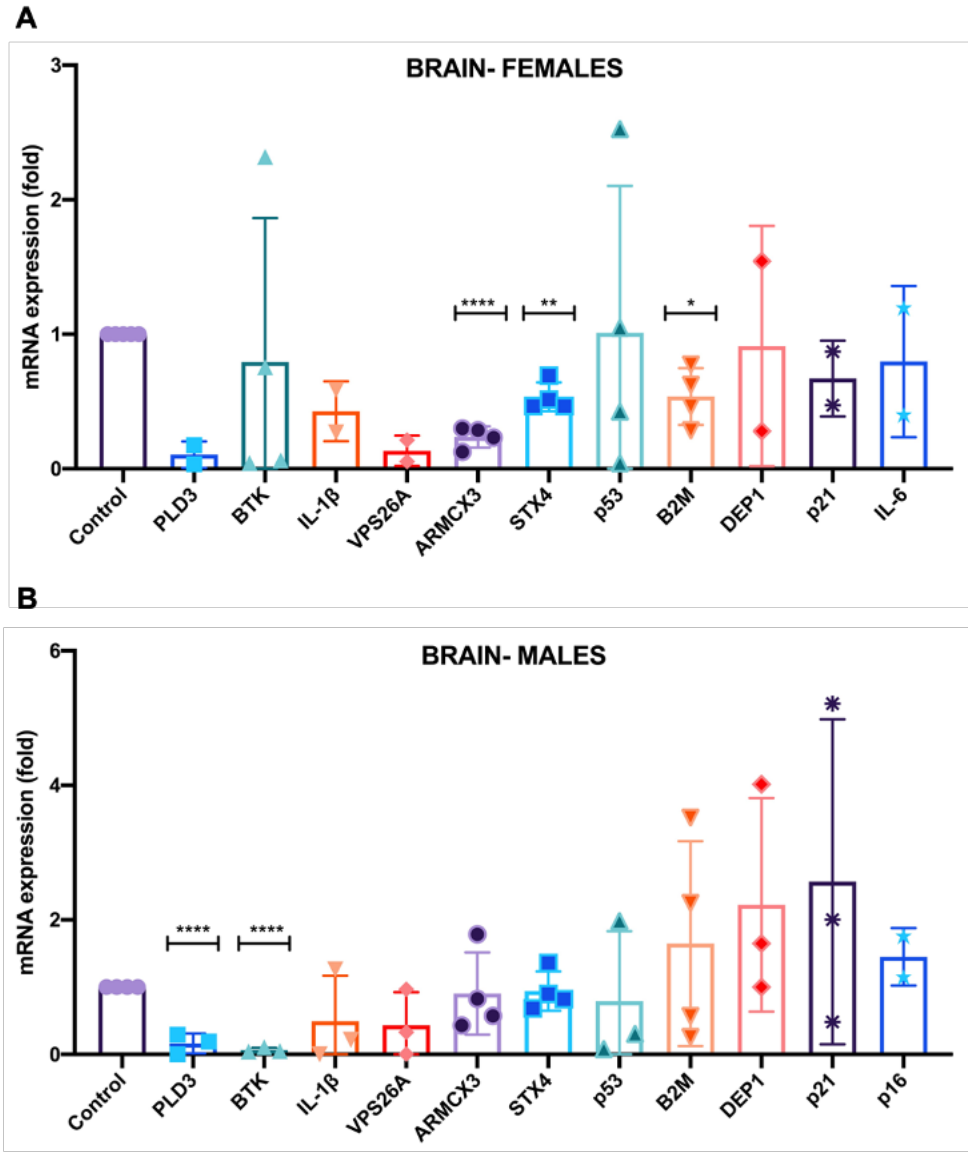

Figure 5.4. QPCR analysis of females and males ZMPSTE24$^{-/-}$ mice brain after the treatment with Ibrutinib.

ZMPSTE24$^{-/-}$ mice were continuously treated with Ibrutinib (10mg/kg) or vehicle twice a week until culled. Data represents sex-depended RT-qPCR analysis of range of senescence markers in the mice brain. GAPDH was used as internal reference control gene. [A] Females data were normalized against vehicle-treated females controls and [B] males against vehicle-treated males' controls. Results are presented as mean ± SD. Statistical analysis performed using unpaired t-test (p<0.05, ** p<0.01, *** p<0.001, **** p<0.0001). Males, n= 3-4, Females, n=2-4*

The reduction in senescent cell accumulation in brains of treated mice was confirmed further by a whole organ SA-β-gal staining, another characteristic feature of cellular senescence. To test its activity after the Ibrutinib-treatment, whole-brain were collected from 2 treated and 2 controls animals. Tissues were fragmented and stained for SA-β-gal activity for 48h as previously described (**Chapter 2, section 2.7**). Data revealed clear changes in the staining between treated and control group. The blue staining was more evident in the vehicle-treated samples than in the Ibrutinib (**Figure 5.5B**), suggesting that Ibrutinib-treatment reduces senescent cell accumulation.

Collected data support initial hypothesis that the BTK inhibition alleviates the senescent phenotype *in vivo*.

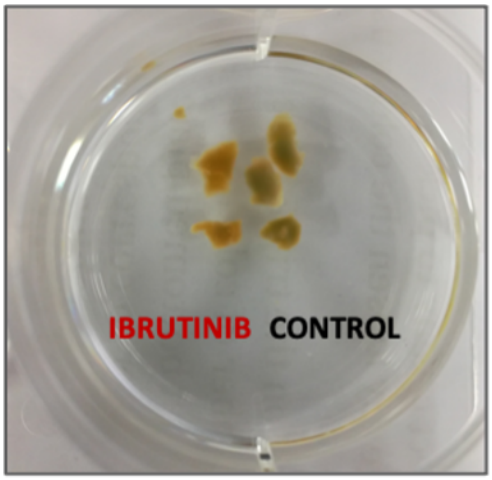

Figure 5.5. SA-β-gal expression after the treatment with Ibrutinib in ZMPSTE24$^{-/-}$ mice brain tissues.

ZMPSTE24$^{-/-}$ mice were continuously treated with Ibrutinib (10mg/kg) or vehicle twice a week. At the end of animals' life, tissues were collected, snap frozen or the whole brain lysates performed. Figure shows representative SA-β-galactosidase staining of the brain fragments of two controls and two Ibrutinib-treated ZMPSTE24$^{-/-}$ mice 70 days after the beginning of treatment.

Next, to investigate further the Ibrutinib effects on mice brain we analysed telomere shortening, one of the most characteristic features of cellular senescence (López-Otín et al., 2013). 10 paraffin blocks of brain samples (5 animals per group) were sent to **Dr D. Jurk** (University of Newcastle) to detect the presence of telomere shortening markers. Telomeres, sequences of DNA that protects the end of chromosomes, are the one of major drivers of senescence. With each cell division, telomeres shorten and if the critical length is reached a DNA damage response (DDR) is activated leading to proliferation arrest and cellular senescence. One of the characteristic features of telomeres damage is the presence of TAF (Telomere associated foci) (Ogrodnik et al., 2017b). The level of TAF increases under condition of chronic inflammation and with age. TAF are established as markers of telomere dysfunction (Kirkland and Tchkonia, 2017, Hewitt et al., 2012) however, it is not clear whether accumulation of TAF with ageing is the result of telomere shortening or random telomeric damage (Hewitt et al., 2012). The evaluation of *ZMPSTE24*$^{-/-}$ mice treated with Ibrutinib showed reduction of senescence markers expression. Therefore, we decided to check if the level of TAF also changed after the treatment and the brain samples were sent for analysis to Newcastle. The analysis focused on the CA1 and CA3 neurons present in hippocampus, as they are linked with autobiographical memory, mental time travel and autonoetic consciousness (Bartsch et al., 2011). The level of TAF were analysed together with γH2A.X, a DNA damage marker (Kinner et al., 2008), both of which accumulate with age (Jurk et al., 2014). Data revealed no change in the mean number of TAF and γH2A.X foci per CA1 and CA3 neurons (**Figure 5.6A-B**) despite BTK inhibition. Moreover, the percentage of TAF negative CA1 neurons was slightly higher in the vehicle group, however the statistical significance was not confirmed **(Figure 5.6C**).

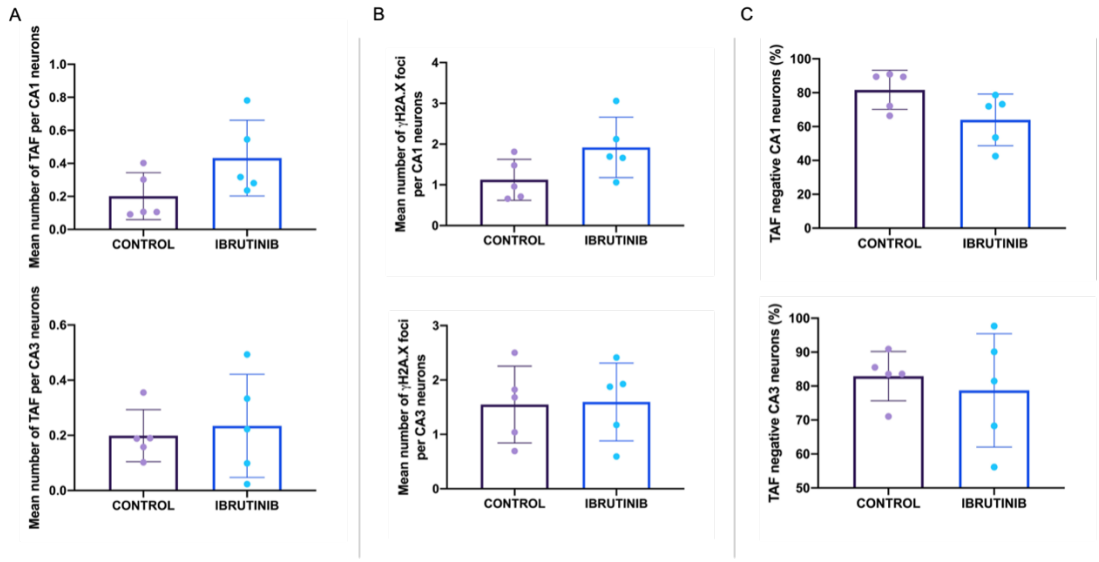

Figure 5.6. Hippocampus analysis for the presence of TAF and γH2A.X.

Analysis of the paraffin-embedded tissues section from 10 ZMPSTE24$^{-/-}$ mice, which were continuously treated with Ibrutinib (10mg/kg) or vehicle twice a week (n=5 mice per group) until culled. At the end of the study tissues were collected and sent to the Institute for Aging and Health, Newcastle University, where immunostaining analysis was performed. [A-B] Data represents mean number of telomeres associated foci (TAF) and γH2A.X in the CA1 and CA3 neurons. [C] The percentage of TAF-negative CA1 and CA3. Results are presented as mean values of ± SD. Statistical analysis performed using unpaired t-test (p<0.05, ** p<0.01, *** p<0.001, **** p<0.0001).*

Data exposed that the blockage of p53 through inhibition of BTK does not prevent neurons from age-related accumulation of damage. However, chronically activated DDR is one of the characteristic features describing the *ZMPSTE24*$^{-/-}$ mouse model (Varela et al., 2005), which could explain the elevated number of TAF and γH2A.X foci. Although the Ibrutinib treatment did not reduce the presence of these senescence-related epigenetic changes, the full senescence-response seems to be affected. These findings reinforce the hypothesis that cellular damage itself may not be sufficient to disrupts the aging-related homeostasis of tissues and that excessive presence of senescent cells may be directly responsible for progression of age-related phenotype.

5.2 The effect of BTK inhibition on muscle.

Muscle is another tissue which deteriorates with age and among the common age-related pathologies are muscle dystrophy or sarcopenia (Munoz-Espin and Serrano, 2014). Sarcopenia is a loss of the muscle mass linked with reduction of its strength and function. The main cause of this pathology are age-related changes in muscle protein synthesis, muscle-fibre distribution and denervation (Siparsky et al., 2014). In this chapter, the *in vivo* effect of BTK inhibition on muscle function was characterized, together with biochemistry evaluations of the senescence markers expression in the tissues of treated *ZMPSTE24*$^{-/-}$ mice.

5.2.1 BTK inhibition attenuates age-related loss of the muscle strength.

In order to investigate the effect of Ibrutinib treatment on the muscle strength we performed the Kondziella's Inverted Screen test (Kondziella, 1964, Deacon, 2013). This test assesses the muscle strength using all four limbs of the animal simultaneously, taking advantage of strength/weight ratio, which is higher in mice than in other rodents, like rats (Deacon, 2013). For example, in mice the support of the body weight can rely only on the usage of fore or hind paws, while in rats it is not that obvious. The detailed explanation of the test assembly was described above (**Chapter 2, section 2.15.2.3**). The study was divided into two phases: pilot and main study. In the pilot study 13 mice, 9 knockdowns (*ZMPSTE24*$^{-/-}$), were treated with 20mg/kg Ibrutinib and 4 young wild-types (*ZMPSTE24*$^{+/+}$) were used as additional untreated controls. The wild-type animals were 5 months old at the beginning of the study. During the main study, 38 *ZMPSTE24*$^{-/-}$ animals were used and 20 of them were treated with 10mg/kg Ibrutinib (oral gavage). The remaining 18 received vehicle. In both studies, the Kondziella test was performed once a week. Animals were assigned a 1-4 score depending on how long were able to hold the grid of inverted screen (**Figure 2.5**). Gained scores were normalized against the weight of the animals.

Results from the pilot study revealed considerable differences between tested groups of animals (**Figure 5.7**). Wild-type animals achieved two-fold higher scores than vehicle-treated *ZMPSTE24*$^{-/-}$. These data confirm age-related decline in the tested animal model.

Next, the outcomes of the Ibrutinib treatment on the muscle strength of *ZMPSTE24*$^{-/-}$ was analysed. At the beginning, till one third of the study, both the treated and control mice showed similar performance. However, with the duration of the treatment, the Ibrutinib cohort began to reach higher scores, comparable to heterozygous performance. The strength of vehicle-treated animals continuously declined and remained at a low level through the whole study (**Figure 5.7A**). Similar results were observed after normalization of data against weight of animals.

Further analysis of the results based on the sex of the animals revealed different responses to the treatment. Wild-type females had the highest scores and were stronger than knockdowns (**Figure 5.7B**). However, the analysis of the Ibrutinib effect was difficult due to the low number of animals. All the tested females had to be culled before the treatment effect was observable. Interpretation of the wild-type males' achievements was not clear due to the high error bars and low number of animals (**Figure 5.7C**). However, the analysis of Ibrutinib-treated males showed considerable improvement of their muscle strength, proportional to the length of the treatment. However, these findings cannot be confronted with the scores gained by vehicle-treated males, again due to the low number of animals. Only one male was treated with a vehicle at that stage and died at the beginning of the pilot study.

In summary, although sex-depended analysis revealed variability of the data, the general results of Ibrutinib treatment on *ZMPSTE24*$^{-/-}$ mice showed improvement in muscle strength over the control cohort of animals. Therefore, a full study, engaging a higher number of animals was performed.

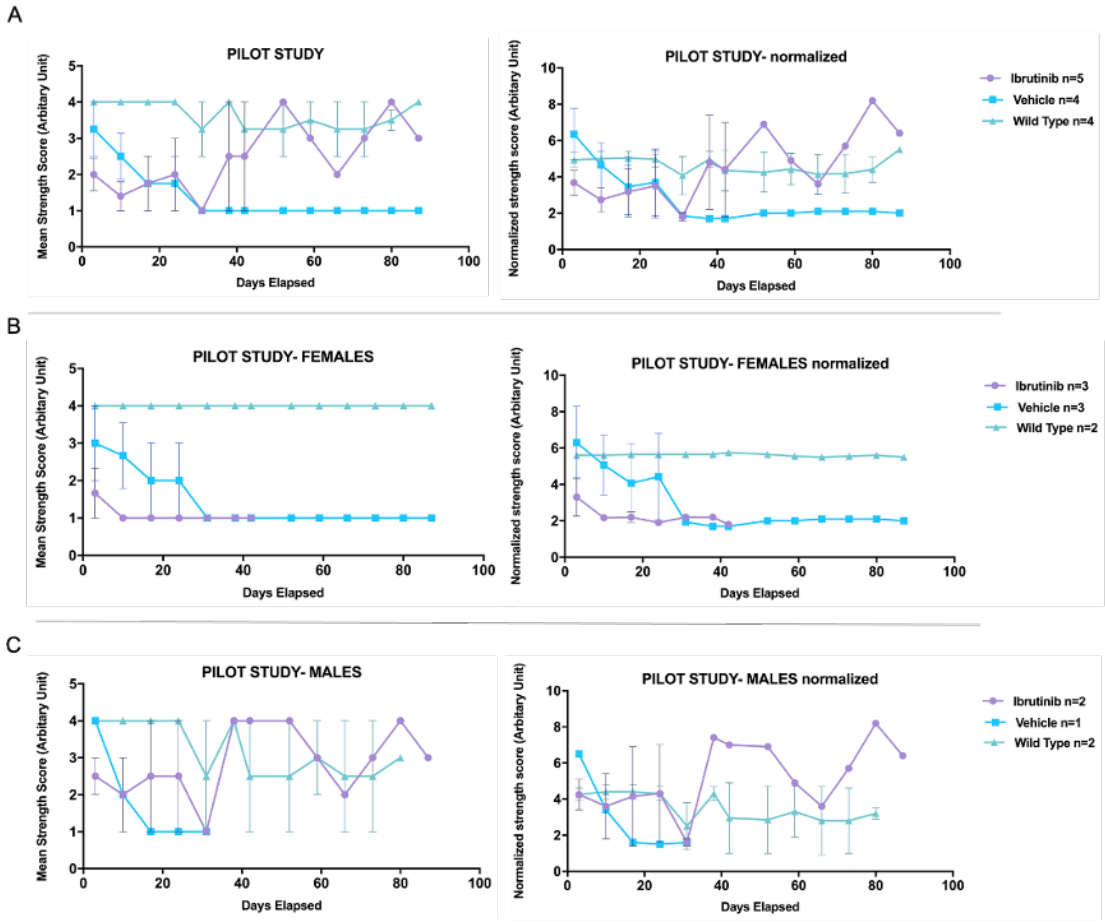

Figure 5.7. Muscle strength analysis- Pilot study.

[A] 9 ZMPSTE24$^{-/-}$ mice, were continuously treated with Ibrutinib (20mg/kg) or vehicle twice a week till the end of animals' life. ZMPSTE24 wild-type and heterozygous mice were used as additional control. The muscle strength measurements were performed once a week for 87 days using Kondziella Inverted Screen test. Additionally, data were normalized against the animals' weight (right panel). [B-C] Sex-depended analysis. Data are presented as mean values ± SD. Experiment performed in collaboration with Dr Akang Eyo Ekpenyong-Akiba.

The main study was performed focusing on *ZMPSTE24*-knockdown mice. 38 animals were used over the duration of the experiment and the dosage of the Ibrutinib was reduced to 10mg/kg. The change of the drug concentration was directed by the desire to reduce potential side effects.

Results exposed no changes in a muscle strength after the treatment with Ibrutinib (**Figure 5.8**). Similar results were observable also in male- and female-specific comparison (**Figure 5.8B,C**). Normalizations against animals' weight did not affected the results and showed the same outcome (**Figure 5.8**). In summary, main study results revealed no changes of the *ZMPSTE24*$^{-/-}$ mice muscle strength after the Ibrutinib treatment.

Taken together, there was a difference in the Ibrutinib effect on the preservation of the muscle strength between pilot and main study. The pilot study revealed a considerable difference between the control and treated mice, however in the main study this trend was lost. This may be due to the reduction of Ibrutinib concentration from 20mg/kg to 10mg/kg. To solidify the findings, another test minimizing element of emotions or behaviour should be used in the future, for example Grip Strength Meter.

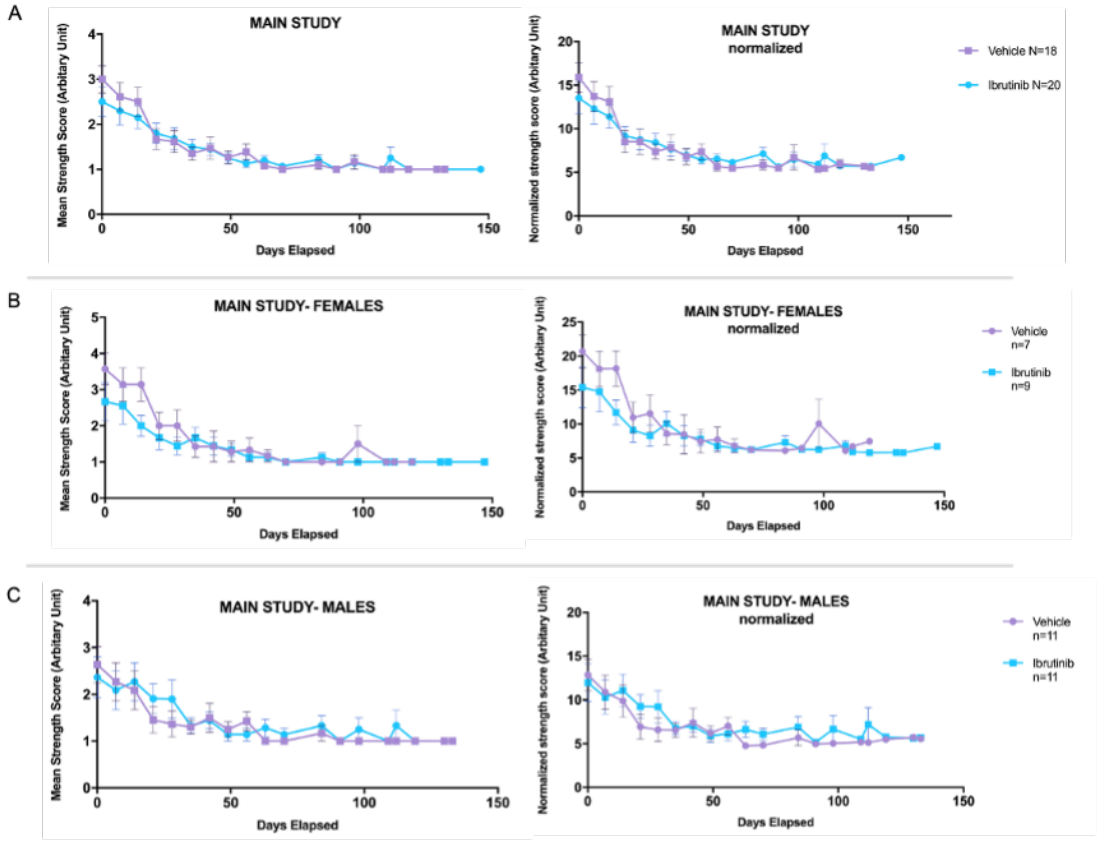

Figure 5.8. Muscle strength analysis- Main study.

[A] 38 ZMPSTE24$^{-/-}$ mice, were continuously treated with Ibrutinib (10mg/kg) or vehicle twice a week till the end of animals' life. The muscle strength measurements were performed once a week for 140 days using Kondziella Inverted Screen test. Additionally, data were normalized against the animals' weight (right panel). [B-C] Sex-depended analysis. Data are presented as mean values ±SD. Experiment performed in collaboration with Dr Akang Eyo Ekpenyong-Akiba.

5.2.2 Biochemical evaluations of Ibrutinib treatment on *ZMPSTE24*$^{-/-}$ mice muscle tissue.

Results from the previous section suggested improvement of the muscle function in *ZMPSTE24*$^{-/-}$ mice after the treatment with 20 mg/kg of Ibrutinib. As we age, skeletal muscle becomes weaker and smaller (Vasilaki et al., 2003) and loss of skeletal muscle mass is one of the main factor of aging. In order to investigate, if the functional improvement was linked to decreased number of senescent cells, we performed analysis of the *Tibialis anterior* (TA), *Gluteus Maximus* (GLUTE) and *Gastrocnemius* muscle (GAS). Muscles were dissected from the animals of similar age and length of the treatment (5-6 months old; 110-120 days of the treatment; Ibrutinib concentration: 10mg/kg).

5.2.2.1 Ibrutinib treatment affects expression of senescence markers in leg skeletal muscles of *ZMPSTE24*$^{-/-}$ mice

In order to test the effect of Ibrutinib on senescence cell accumulation in muscle, qPCR analysis was performed comparing expression of the senescence-related genes between Ibrutinib and vehicle-treated animals. The mRNA level of *BTK*, *p21*, *VPS26A* and *PLD3* was significantly downregulated in TA in the animals treated with Ibrutinib (**Figure 5.9**). *p53* gene expression remained unchanged despite the treatment.

Further, WB evaluations were performed on TA, GAS and GLUTE tissues. The analysis compared expression of senescence markers between three cohorts of *ZMPSTE24*$^{-/-}$ animals: young (2 months of age), old/vehicle (5-6 months old treated with vehicle) and Ibrutinib-treated cohort. TA analysis did not reveal an age-related increase in the BTK expression when comparing data from young and old animals (**Figure 5.10**). Moreover, BTK expression was similar in the animals treated with Ibrutinib compared to vehicle-treated controls. Furthermore, the p53 level was higher in the old animals than in the untreated young controls, confirming the age-related increase of p53 in this mouse

model. Also, analysis revealed a decrease in p53 level after Ibrutinib treatment comparing to vehicle controls.

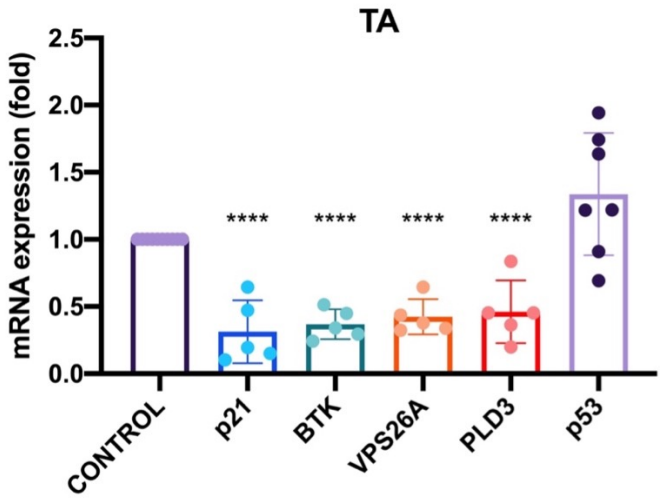

Figure 5.9. Senescence markers mRNA expression analysis of TA.

ZMPSTE24$^{-/-}$ mice were continuously treated with Ibrutinib (10mg/kg) or vehicle twice a week till the end of their life. Data represents RT-qPCR analysis of range of senescence markers in the mice Tibialis anterior (TA) after the Ibrutinib treatment. GAPDH was used as internal reference control gene. Data were normalized against vehicle-treated controls. Results are presented as mean ±SD. Statistical analysis between senescent and control cells performed using unpaired t-test (p<0.05, ** p<0.01, *** p<0.001, **** p<0.0001), n= 5-7.*

Additionally, p16 comparison showed age-related increase in majority of tested samples (**Figure 5.10A**). There was also a decrease in p16 expression when compared Ibrutinib-treated and vehicle group. LAMIN B1 expression profiles indicated no change in the old animals, when compared to controls. Although, results from Ibrutinib treatment group showed slightly increased expression of LAMIN B1 when compared to vehicle controls, the difference was not considerable.

Taken together, analysis of TA tissue revealed changes of senescence markers after the treatment with Ibrutinib.

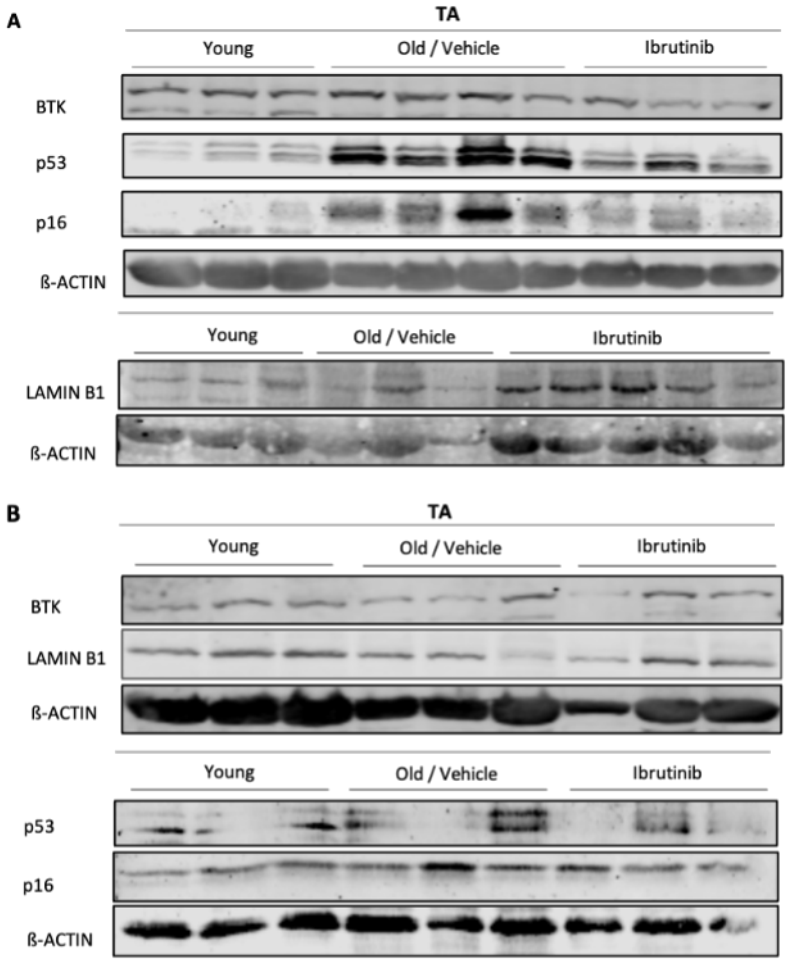

Figure 5.10. Western blot analysis of Tibialis anterior muscle.

ZMPSTE24$^{-/-}$ mice were continuously treated via oral gavage with Ibrutinib (10mg/kg) or vehicle twice a week till the end of their life. At the end of the study Tibialis anterior (TA) muscle was isolated and the whole-tissue lysates performed. [A-B] Western blot showing expression of BTK, p53, LAMIN B1 and between untreated young controls (2 months of age), old/vehicle (5-6 months old treated with vehicle) and Ibrutinib cohort (5-6 months old, treated with Ibrutinib). ß-actin was used as a loading control. n=6-7

Next, we studied the expression of senescence markers in GAS and GLUTE muscle tissues. In GAS, there was no age-related increase in BTK expression and Ibrutinib treatment did not affect it as well **(Figure 5.11**). There was an increase of p53 level when compared old with young animals although p53 expression was quite heterogenous between tested animals. The Ibrutinib treatment also showed a downregulation of p53 level compared to old controls. LAMIN B1 analysis revealed a reduction of its expression in the old mice when compared with young group. There was an increase in LAMIN B1 in animals treated with Ibrutinib (**Figure 5.11**). Although LAMIN B1 analysis were performed only on 3 animals per group, therefore more animals should be added to the study to confirm these findings. GLUTE analysis did not confirm the age-related increase of BTK and its expression was heterogenous between animals. Moreover, treatment with Ibrutinib did not reduce its expression in tested animals (**Figure 5.12**). The analysis of p53 expression revealed an age-related increase only in some of tested animals. p53 analysis revealed also that the differences between Ibrutinib and vehicle-treated animals were quite heterogenous and more animals should be added to the analysis to confirm its expression. LAMIN B1 was reduced in the old vehicle-treated mice when compared with the young controls and comparison of the Ibrutinib-treated group and vehicle controls exposed considerable upregulation of LAMIN B1.

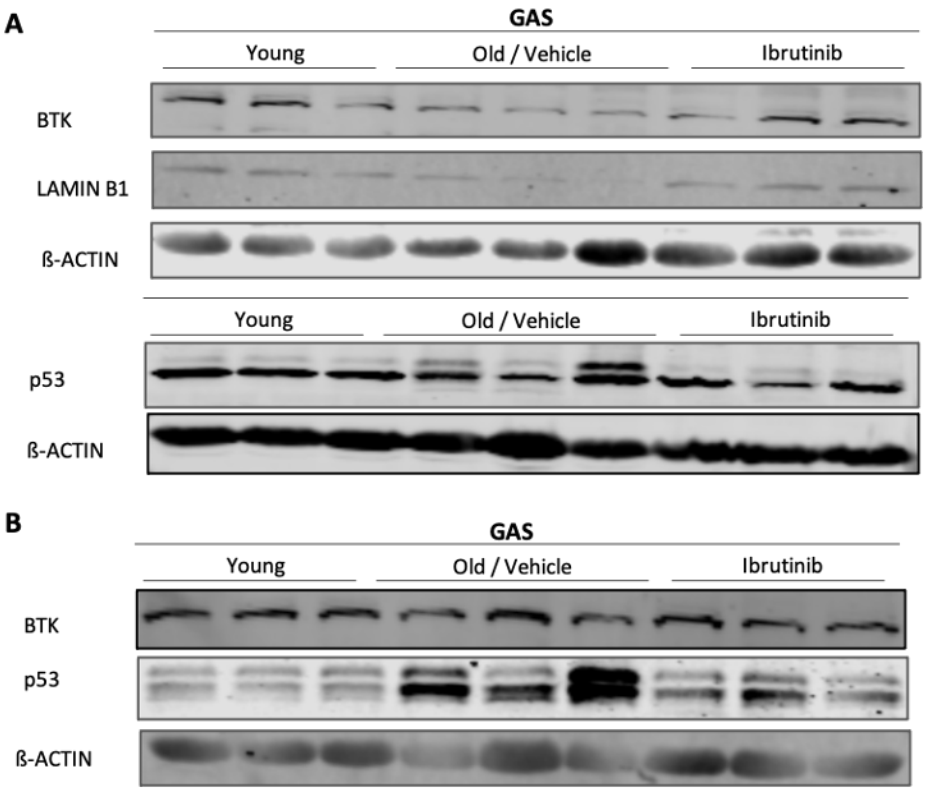

Figure 5.11. Western blot analysis of Gastrocnemius muscle.

ZMPSTE24$^{-/-}$ mice were continuously treated via oral gavage with Ibrutinib (10mg/kg) or vehicle twice a week till the end of their life. At the end of the study Gastrocnemius muscle (GAS) muscle was isolated and the whole-tissue lysates performed. [A] Western blot showing expression of BTK, p53 and LAMIN B1 between untreated young controls (2 months of age), old/vehicle (5-6 months old treated with vehicle) and Ibrutinib cohort (5-6 months old, treated with Ibrutinib). ß-actin was used as a loading control. n=6, only in LAMIN B1 n= 3 animals in each group.

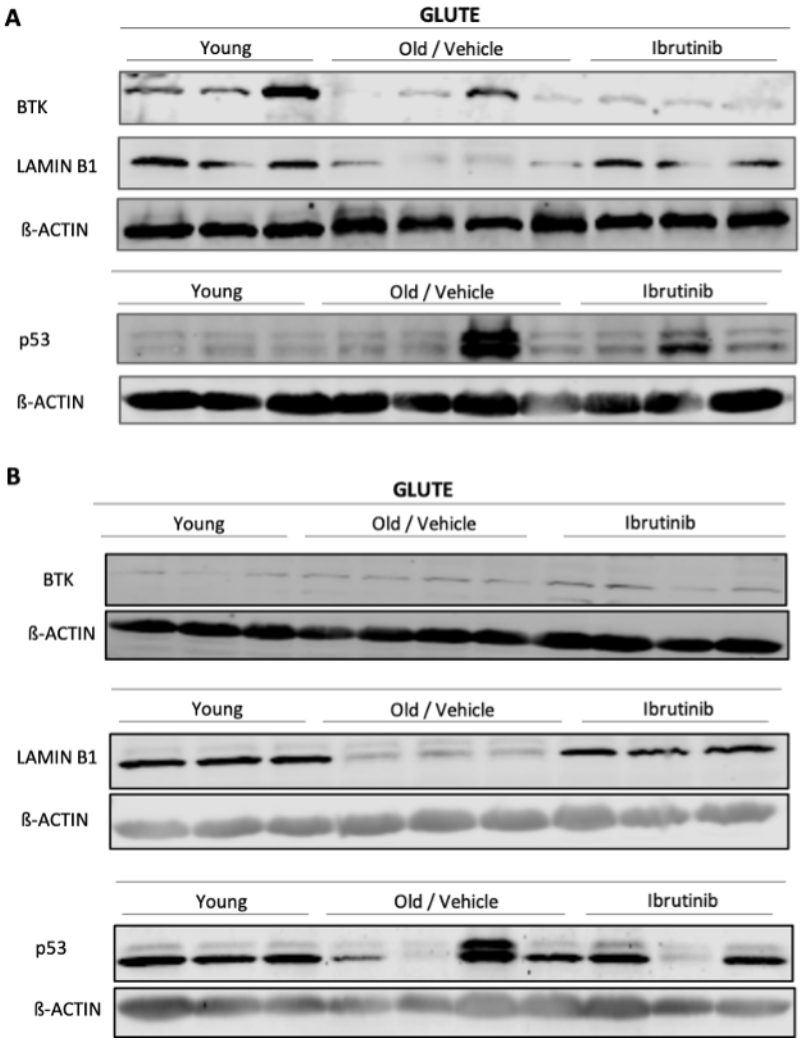

Figure 5.12. Western blot analysis of Gluteus Maximus muscle.

ZMPSTE24$^{-/-}$ mice were continuously treated via oral gavage with Ibrutinib (10mg/kg) or vehicle twice a week till the end of their life. At the end of the study Gluteus Maximus (GLUTE) muscle was isolated and the whole-tissue lysates performed. [A] Representative western blot showing expression of BTK, p53 and LAMIN B1 between untreated young controls (2 months of age), old/vehicle (5-6 months old treated with vehicle) and Ibrutinib cohort (5-6 months old, treated with Ibrutinib). ß-actin was used as a loading control. n=6-7

Taken together, our data support the view that there is an age-dependent accumulation of senescent cells in muscles of *ZMPSTE24*$^{-/-}$ mice, which was reflected by increases of senescent markers in the muscle group tested. Although, in the future more animals should be added into the study. Age-related accumulation of senescent cells could be partially prevented by continuous treatment with Ibrutinib. The strongest effect was observed in the TA, where the expression of majority tested markers of senescence was affected by the treatment, while in the GAS and GLUT only the expression of some of markers was impaired. Our results suggest an heterogenous impact of BTK inhibition on different muscle groups and that BTK might not be increased with ageing in muscle tissue. Although, the changes in BTK protein were not considerable in any muscle of old-untreated or treated mice, the p53 pathway was affected, which was reflected by changes in p53 expression. This is consistent with previous report that Ibrutinib affects BTK activation but not expression (Chu et al., 2019). To further confirm blockage of BTK function, expression level of phosphorylated p53 should be analysed.

5.2.2.2 Morphometric analysis of Tibialis anterior

Disorganization and excessive deposition of collagen is one of the main feature of fibrosis, an age-related disorder (Wynn, 2008). To investigate if Ibrutinib treatment affects the deposition of collagen, IHC sections of TA were prepared and send to De Monfort University for Picrosirius Red Staining and morphometric analysis. Picrosirius Red Staining is a common histological technique used for visualisation of collagen fibres (Lattouf et al., 2014). Results revealed significant reduction in percentage of collagen in the TA samples from mice treated with Ibrutinib when compared with vehicle-treated controls (**Figure 5.13**). Furthermore, morphometric analysis of the fibre size revealed considerable difference in the average (**Figure 5.14C**) and minimum Feret diameter size (**Figure 5.14D**), which were significantly increased in Ibrutinib-treated mice. Moreover, the difference in fibre size was not related to muscle weight, since there were no significant changes in mass in any of the muscle group analysed (**Figure 5.15**).

In summary, these data confirm that Ibrutinib treatment protects skeletal muscle against age-related changes in the *ZMPSTE24*$^{-/-}$ mice, as measured by the reduction in age-associated morphological changes.

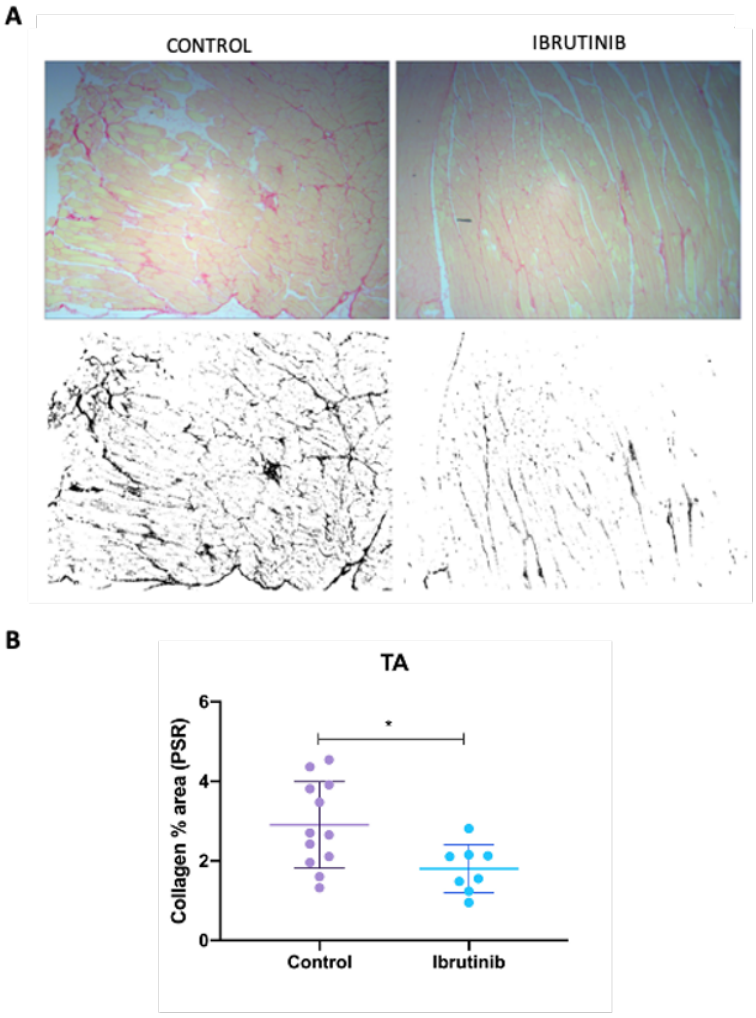

Figure 5.13. Picrosirus red staining of ZMPSTE24$^{-/-}$ mice Tibialis anterior muscle.

ZMPSTE24$^{-/-}$ mice were continuously treated via oral gavage with Ibrutinib (10mg/kg) or vehicle twice a week till the end of their life. At the end of the study Tibialis anterior (TA) muscle was isolated and histological sections prepared. Samples were sent to De Montfort Univeristy where the staining was performed. [A] Representative pictures of the staining. Red colour indicates positive staining. [B] Quantification of the staining presenting mean value of the collagen percentage ±SD, n=10. Statistical analysis performed using unpaired t-test (p<0.05, ** p<0.01, *** p<0.001, **** p<0.0001).*

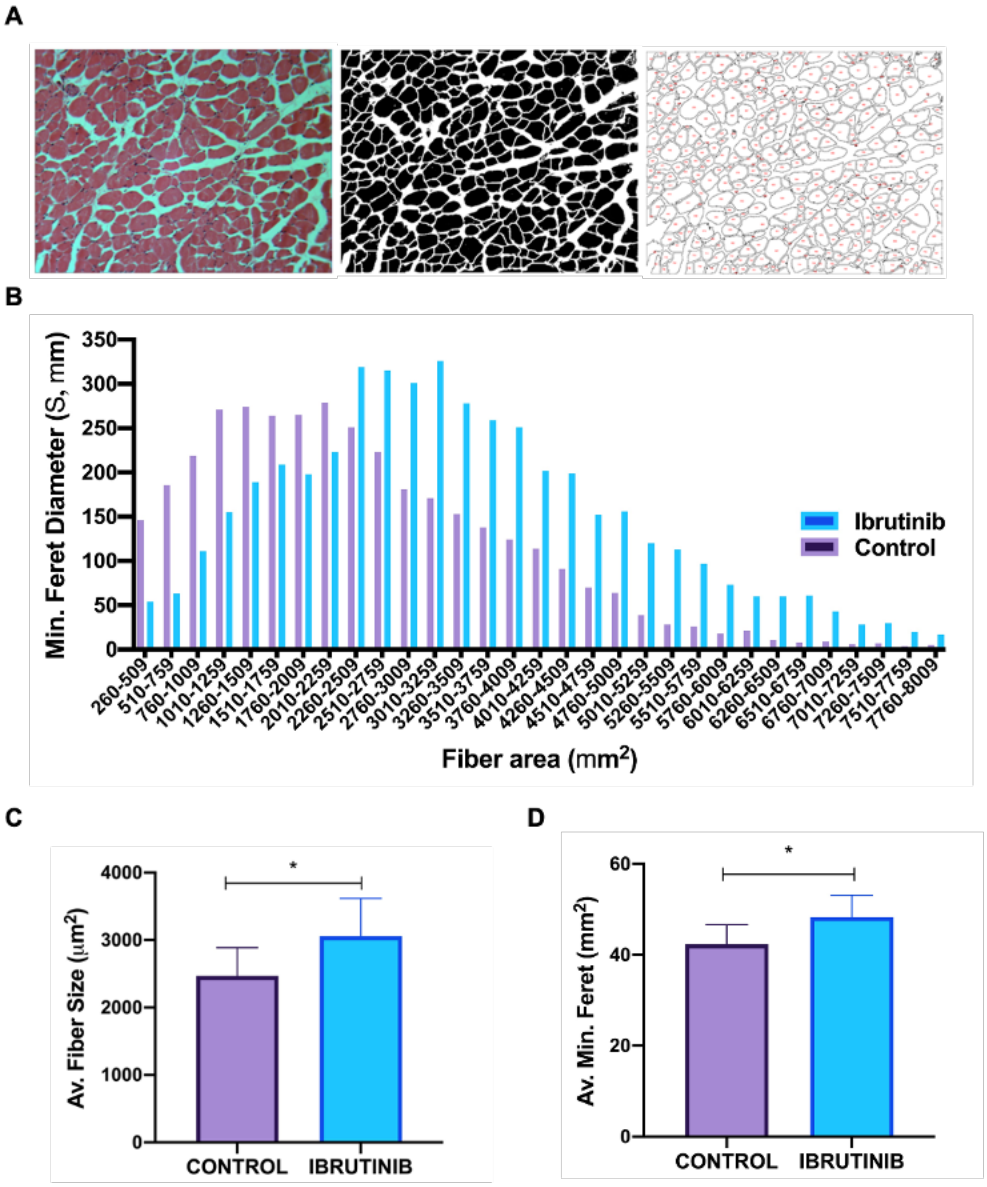

Figure 5.14. Morphometric analysis of Ibrutinib-treated ZMPSTE24$^{-/-}$ TA mice muscle.

[A] Representative images of the staining. Using H&E images, a macro was developed using Fiji (ImageJ) to sequentially (i) subtract background components to minimise noise that could interfere with further analysis; (ii) apply a thresholding filter for fibre border detection; (iii) generate a mask of the muscle fibre borders using the analyse particles function, simultaneously eliminating stray "non-border" signals; and (iv) overlay threshold-delimited nuclei over the border mask, before another analyse particles command was used to measure morphometric variables including "area" and "minimum Feret diameter." as previously described (Sinadinos et al., 2015). n=10 animals per group

A

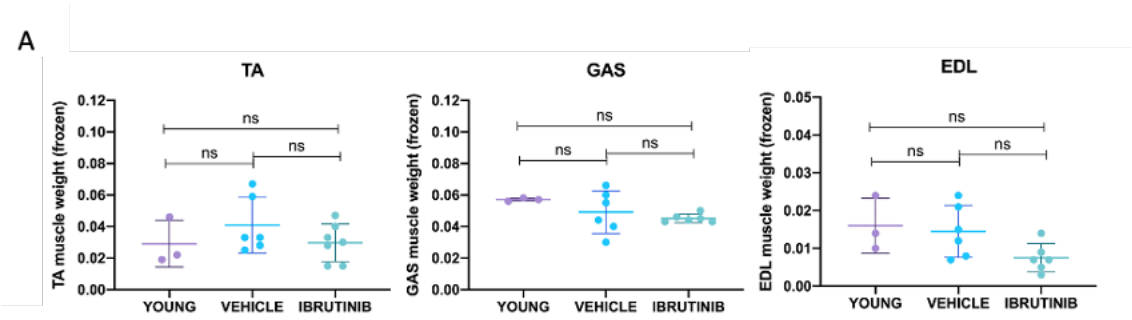

B

CONDITION	BODY WEIGHT (g)	TA WEIGHT (mg)	GAS WEIGHT (mg)	EDL WEIGHT (mg)
YOUNG	20.4±1.1	29.0±1.5	57.0±0.1	16±0.7
OLD/VEHICLE	18.1±1.6	40.8±1.1	49.2±1.4	14.5±0.7
IBRUTINIB	19.0±2.5	29.7±1.2	45.2±0.3	7.5±0.4

Figure 5.15. Comparison of the selected muscle tissues weights.

[A] Comparison of the muscle tissues between young (2 months of age), old (5-6 months old) treated with vehicle (old/vehicle) and Ibrutinib treated ZMPSTE24$^{-/-}$ mice (5-6 months old).[B] Summary table expanded by averages of the whole animal weight from tested groups.

*All treated ZMPSTE24$^{-/-}$ mice in this figure were given 10mg/kg Ibrutinib or vehicle. Tibialis anterior (TA, Gastrocnemius (GAS) and Extensor digitorum longus [EDL] muscles were isolated post-mortem from mice treated for 130±10 days after the beginning of treatment (190±10 days old). Quantification and statistical analysis performed using GraphPad Prism 8. Graph represents mean weight values of selected frozen muscle and error bars show standard deviation. Each dot represents one animal, n=3-5. ns: not significant, *p <0.05; (unpaired t tests).*

5.3 Effect of BTK on *ZMPSTE24*$^{-/-}$ hearts

Progressive destruction of the heart structure and function is one of the aging risks, that leads to cardiovascular disorders (Chiao and Rabinovitch, 2015). Since we observed a reduction in muscle ageing in Ibrutinib-treated mice, we next focused our analysis on the heart. RT-qPCR analysis were performed to assess the levels of senescence markers. Results revealed downregulation of the *BTK* and *p53* gene expression in the heart of *ZMPSTE24*$^{-/-}$ mice treated with Ibrutinib, relative to vehicle-treated controls (**Figure 5.16**). Although, the differences are small and might not reflect a strong biological impact. Expression of *p21* and *IL-1*β was also tested, however results showed no changes in their mRNA level. Some novel markers previously identified in our lab (Althubiti et al., 2014) were also included into the analysis to test their expression. However, there was no difference in *B2M*, *VPS26A* and DEP1 *(PTPRJ)* gene expression between Ibrutinib-treated and control mice (**Figure 5.16**).

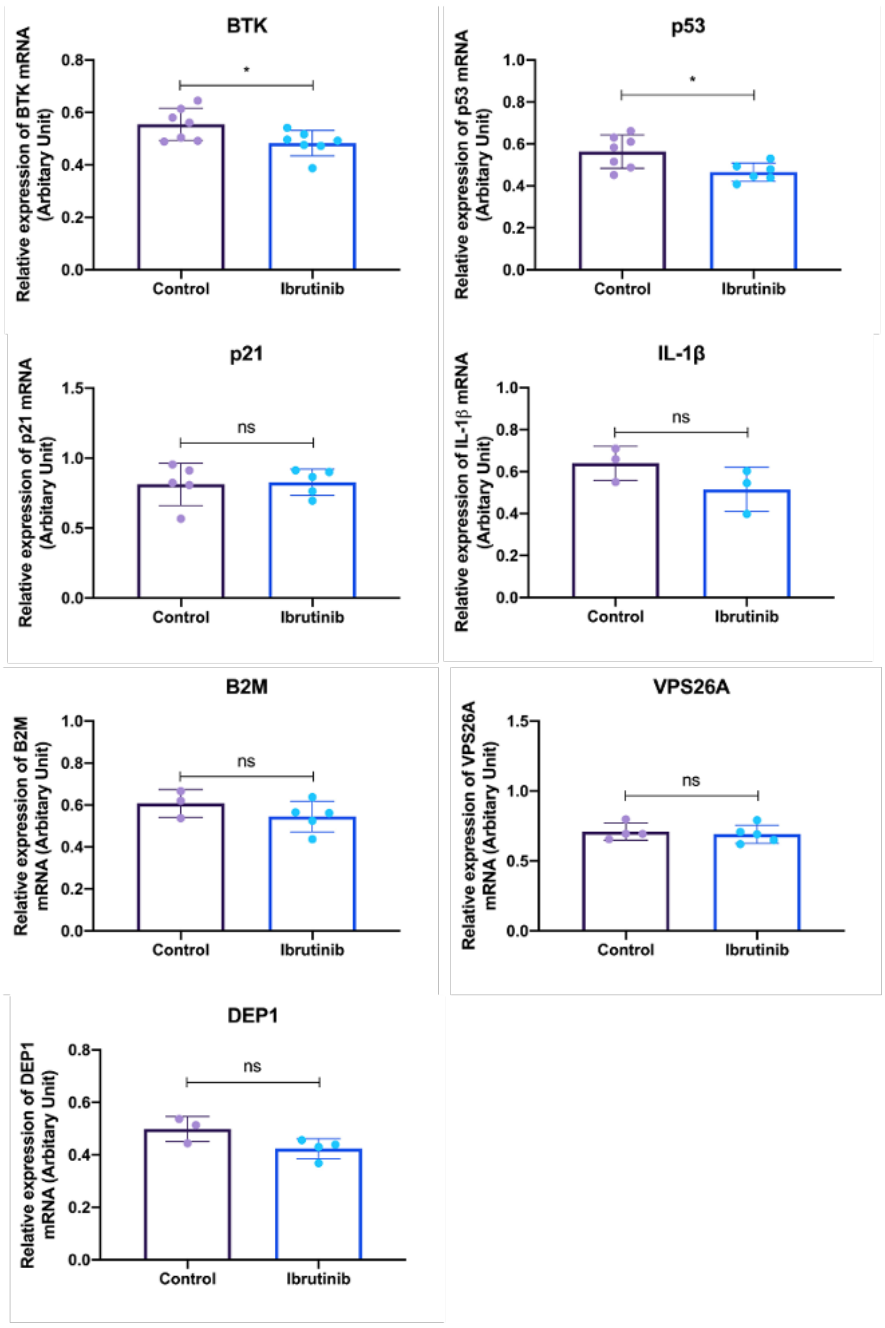

Figure 5.16. QPCR analysis of ZMPSTE24$^{-/-}$ mice heart tissues.

*ZMPSTE24$^{-/-}$ mice were continuously treated with Ibrutinib (10mg/kg) or vehicle twice a week till the end of their life. Data represents RT-qPCR analysis of senescence markers in the mice heart after the Ibrutinib treatment. GAPDH was used as internal reference control gene. Data were normalized against vehicle-treated controls. Results are presented as mean ± SD. Statistical analysis performed using unpaired t-test (ns: not significant, * p<0.05). n= 3-7.*

Next, the fragments of the mice heart tissues were tested for SA-β-Gal expression and data revealed no differences in the staining between control and Ibrutinib group (**Figure 5.17**). The tissues remained unstained despite long incubation time in the staining solution (24h). Experiment was performed twice, albeit it should be repeated with consideration of the protocol adjustments, like longer/shorter fixation time, to exclude the potential technical and manual errors, which could lead to lack of the characteristic blue staining.

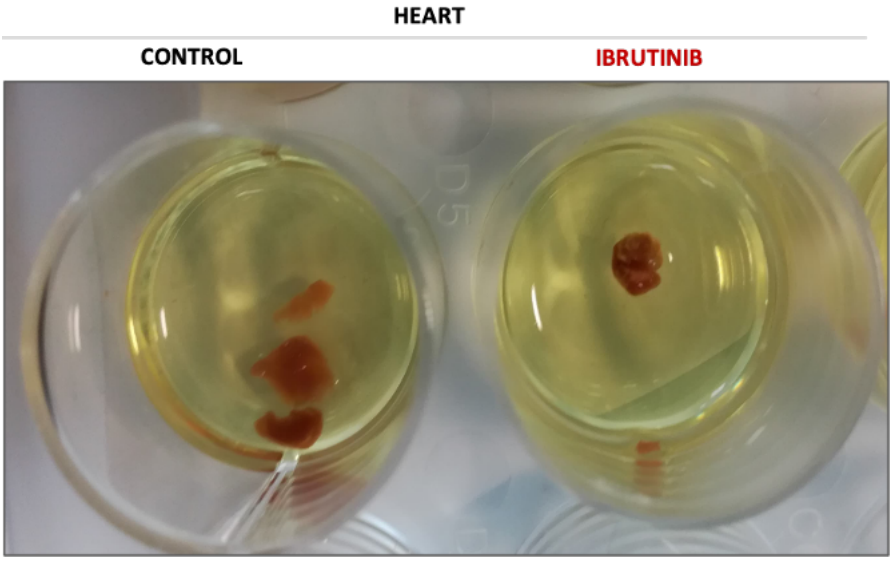

Figure 5.17. SA-β-Gal staining of the heart tissue.

Representative SA-β-galactosidase staining of the heart fragments of two controls and two Ibrutinib-treated Zmpste24$^{-/-}$ mice 110 days after the beginning of treatment. Figure shows results after 24h incubation in the staining solution.

Further, the percentage of the collagen deposition in the heart tissue was compared between treated and untreated mice using Picrosirus Red staining. Data revealed significantly lower abundance of collagen in the Ibrutinib-treated cohort (**Figure 5.18**).

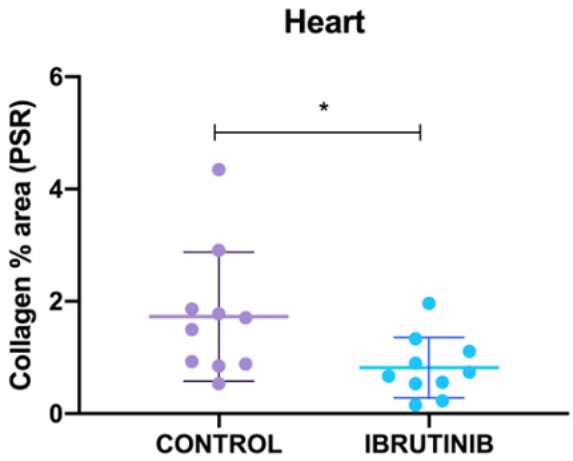

Figure 5.18. Percentage of the collagen deposition in the heart tissues of ZMPSTE24$^{-/-}$ mice.

ZMPSTE24$^{-/-}$ mice were continuously treated via oral gavage with Ibrutinib (10mg/kg) or vehicle twice a week till the end of their life. At the end of the study whole hearts were isolated and histological sections prepared. Samples were sent to De Montfort University where the staining was performed. Figure show the quantification of the staining and graph presents mean value of the collagen percentage ± SD, n=10. Statistical analysis performed using unpaired t-test (p<0.05).*

5.4 BTK inhibition affects expression of senescence markers in kidney

Like other organs, kidneys undergo a variety of structural and physiological changes during aging, that leads to loss of its function (Weinstein and Anderson, 2010, Denic et al., 2016). For instance, decrease of glomerular filtration rate and renal blood flow occurs with age and there is a reduction of renal mass or increase risk of tubulointerstitial fibrosis. All these changes contribute to development of kidney injuries and affects its function. Accumulation of senescent cells occurs in both aging and diseased kidney (Weinstein and Anderson, 2010), therefore, we decided to test if BTK inhibition through Ibrutinib treatment ameliorates kidney ageing.

At first, the mRNA expression of senescence markers was compared. Results exposed statistically significant changes in the mRNA level of *BTK*, and *B2M*, where *BTK* expression was downregulated and *B2M* upregulated in the Ibrutinib-treated mice cohort (**Figure 5.19**). The *p53, p21, IL-6, IL-1*β mRNA expression was similar in both controls and Ibrutinib-treated animals. Next, the gene expression of recently identified novel markers of cellular senescence (Althubiti et al., 2014) was tested. Results exposed significant upregulation of *DEP1* and downregulation of *EBP50* (**Figure 5.20**). Although the upregulation of *DEP1* was statistically significant, the difference seems to not be biologically significant as the difference in the expression of *DEP1* gene level between Ibrutinib-treated and control mice was equal 0.9-fold change. The downregulation of *EBP50* was also lower than 2-fold. *VPS26A, ARMCX3, PLD3* and *STX4* mRNA expression remained unaffected by the treatment.

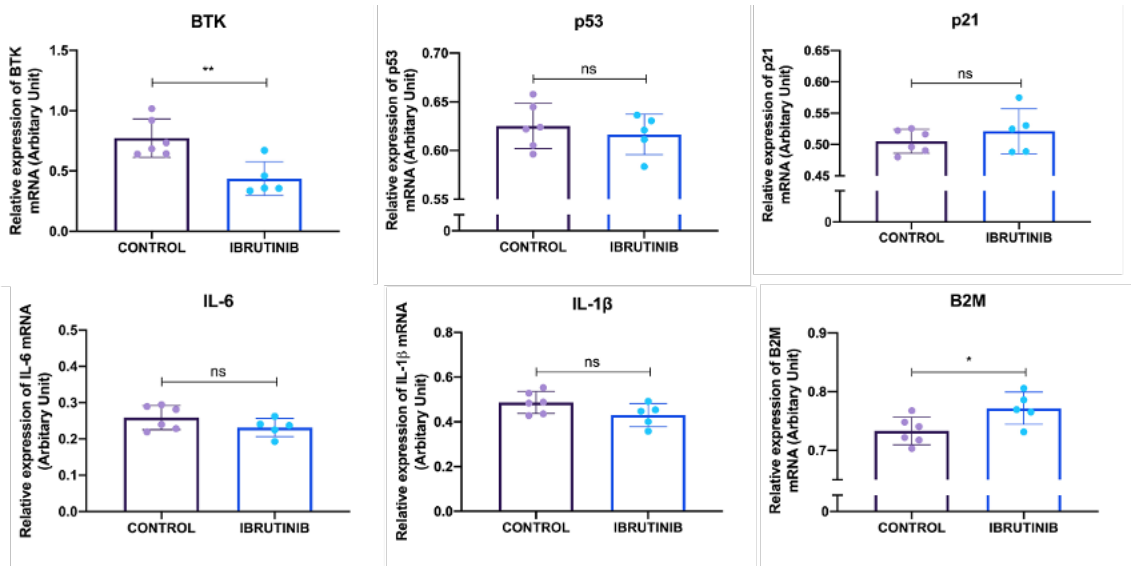

Figure 5.19. mRNA expression of senescence markers in the ZMPSTE24$^{-/-}$ mice kidney tissue.

*ZMPSTE24$^{-/-}$ mice were continuously treated with Ibrutinib (10mg/kg) or vehicle twice a week till the end of their life. Data represents RT-qPCR analysis of senescence markers in the mice kidney after the Ibrutinib treatment. GAPDH was used as internal reference control gene. Data were normalized against vehicle-treated controls. Results are presented as mean ± SD. Statistical analysis performed using unpaired t-test (ns: not significant, * p<0.05, ** p<0.01). n= 5-7.*

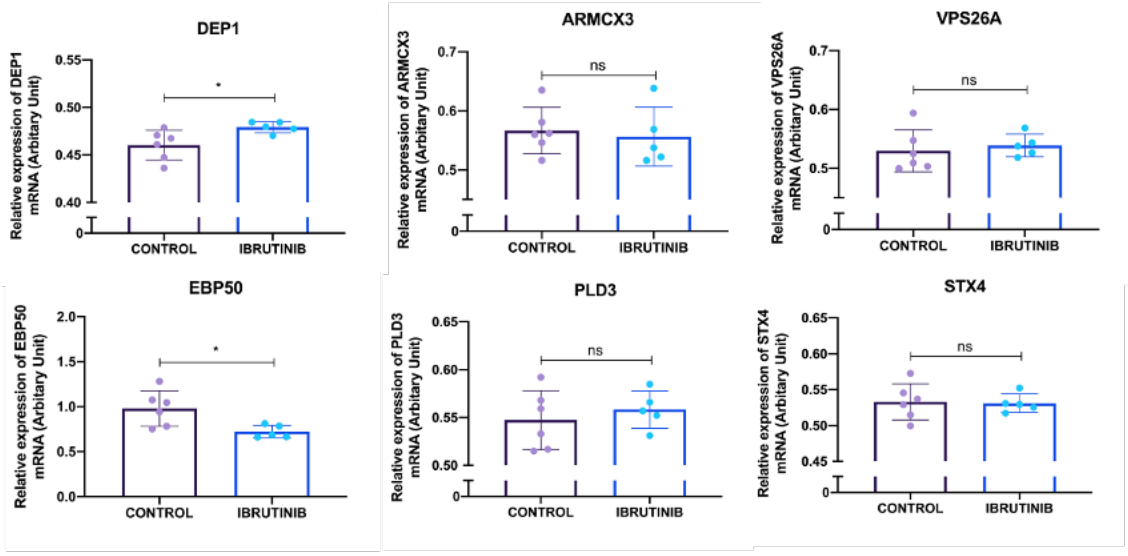

Figure 5.20. Ibrutinib treatment effect on mRNA expression of novel senescence markers in ZMPSTE24$^{-/-}$ mice kidney.

*ZMPSTE24$^{-/-}$ mice were continuously treated with Ibrutinib (10mg/kg) or vehicle twice a week till the end of their life. Data represents RT-qPCR analysis of senescence markers in the mice kidney after the Ibrutinib treatment. GAPDH was used as internal reference control gene. Data were normalized against vehicle-treated controls. Results are presented as mean ± SD. Statistical analysis performed using unpaired t-test (ns: not significant, * p<0.05). n= 5-7.*

Next, tissues were stained for the expression of SA-β-Gal. Results exposed equal level of the staining in both tissues from mice treated with Ibrutinib and vehicle-treated controls (**Figure 5.21**). However, the experiment should be repeated, and protocol adjusted in tissue-specific manner in order to exclude possible technical mistakes, like prolonged incubation in the staining solution, which could cover the potential differences between the tested conditions.

Figure 5.21. SA-β-gal stating of the ZMPSTE24$^{-/-}$ mice kidney tissue.

Representative SA-β-galactosidase staining of the kidney fragments of two controls and two Ibrutinib-treated ZMPSTE24$^{-/-}$ mice 110 days after the beginning of treatment. Figure shows results after 24h incubation in the staining solution.

In summary, our data revealed that Ibrutinib treatment did not affected the expression of senescence markers. To confirm these findings and exclude individuals-related specificity, a higher number of animals should be tested and markers expression should be further confirmed at the protein level.

5.5 The effect of Ibrutinib on the expression of senescence markers in other tissues

Aging-related loss of function is also observable in liver. Gradual alteration of hepatic structure increases the risk of liver diseases (Kim et al., 2015) and contributes to high mortality rate (Sheedfar et al., 2013, Amarapurkar et al., 2007). Cellular senescence has been mainly identified in liver hepatocytes and cholangiocytes and on chronic liver diseases like cirrhosis and fibrosis (Huda et al., 2019). In order to detect if BTK inhibition has a positive impact on the liver function, the expression of senescence markers was tested in the tissues collected from *ZMPSTE24*$^{-/-}$ animals treated with Ibrutinib or vehicle as a control. Analysis started with qPCR, and revealed statistically significant upregulation of *BTK*, *p53* and *B2M* in the livers of animals treated with Ibrutinib (**Figure 5.22**). The *p21, IL-6* and *IL-1*β gene levels remained unaffected by the treatment. Further, the mRNA profiles of novel senescence markers recently identified by our lab (Althubiti et al., 2014) were also tested between the conditions. Results showed statistically significant upregulation of *ARMCX3*, *EBP50* and *STX4* at mRNA level, while the gene expression of *DEP1, VPS26A* and *PLD3* was unaffected by the treatment (**Figure 5.23**). However, it is worth to mention that statistical differences of the data might not reflect their biological relevance, especially that differences in the gene expression are less than 0.2-fold change. Also, there was no difference in the expression of SA-β-Gal between liver tissue fragments isolated from Ibrutinib and vehicle-treated mice (**Figure 5.24**).

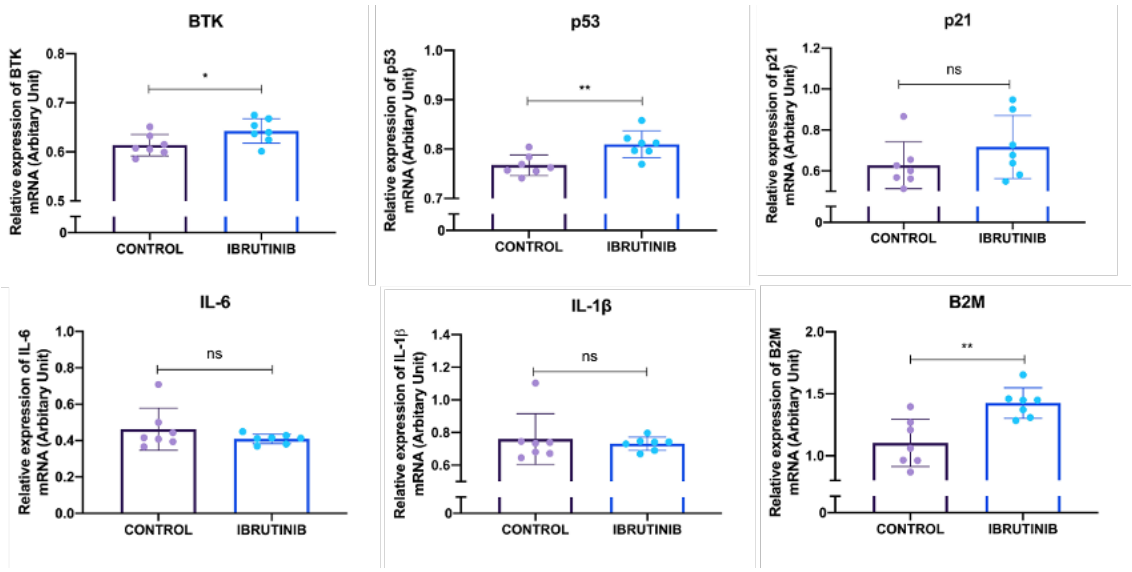

Figure 5.22. Expression of senescence markers after the treatment with Ibrutinib in the ZMPSTE24$^{-/-}$ liver.

*ZMPSTE24$^{-/-}$ mice were continuously treated with Ibrutinib (10mg/kg) or vehicle twice a week till the end of their life. Data represents RT-qPCR analysis of senescence markers in the mice liver after the Ibrutinib treatment. GAPDH was used as internal reference control gene. Data were normalized against vehicle-treated controls. Results are presented as mean ± SD. Statistical analysis performed using unpaired t-test (ns: not significant, * p<0.05, ** p<0.01). n= 5-7.*

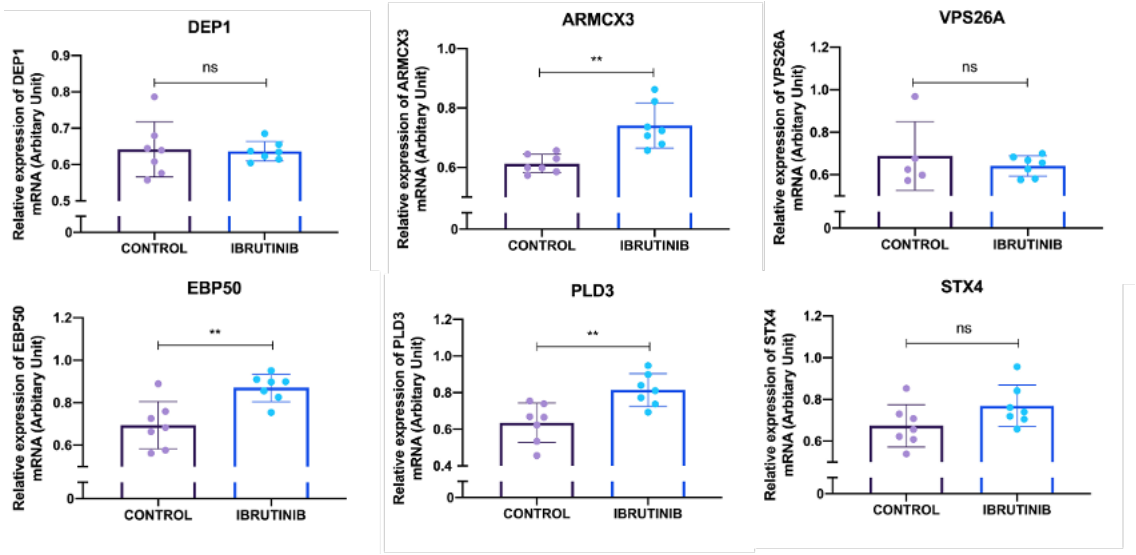

Figure 5.23. mRNA expression of novel senescence markers in liver after Ibrutinib treatment.

*ZMPSTE24-/- mice were continuously treated with Ibrutinib (10mg/kg) or vehicle twice a week till the end of their life. Data represents RT-qPCR analysis of novel senescence markers in the mice liver after the Ibrutinib treatment. GAPDH was used as internal reference control gene. Data were normalized against vehicle-treated controls. Results are presented as mean ± SD. Statistical analysis performed using unpaired t-test (ns: not significant, * p<0.05, ** p<0.01). n= 5-7.*

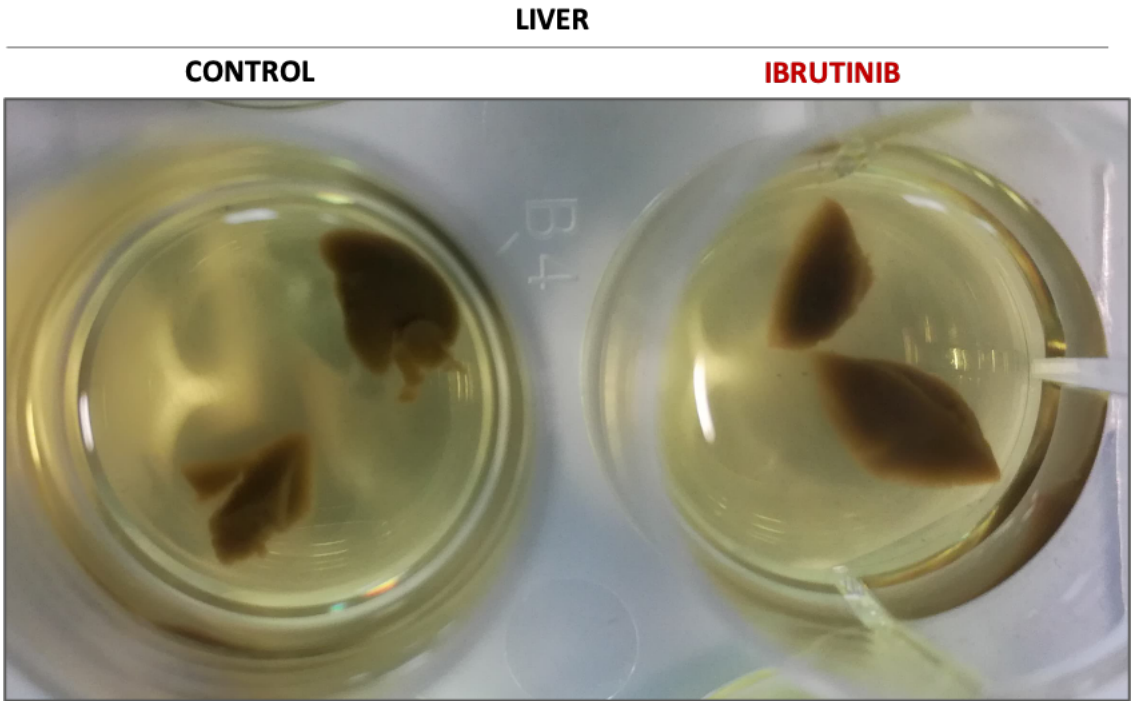

Figure 5.24. SA-β-gal staining of the ZMPSTE24$^{-/-}$ mice liver tissue.

Representative SA-β-galactosidase staining of the kidney fragments of two controls and two Ibrutinib-treated ZMPSTE24$^{-/-}$ mice 110 days after the beginning of treatment. Figure shows results after 24h incubation in the staining solution.

Taken together, the results showed statistically significant diversity in the expression of more than half tested markers. Although, consistency of the data resulted with statistical difference between tested conditions, their actual biological relevance remains unclear. Analysis exposed that for all the tested markers, the expression difference between Ibrutinib-treated and control cohort did not reach 2-fold change. Despite statistical significance, it cannot be assumed that the Ibrutinib treatment considerably affected expression of tested senescence markers.

Additionally, the expression of SA-β-Gal was tested in the fragments of the lung and skin tissues. Results showed no difference in lungs from Ibrutinib and vehicle-treated mice (**Figure 5.25**). However, there was a clear contrast in the back-skin fragments. Fragments isolated from control animals had definite blue colour, while tissues from Ibrutinib-treated mice were barely stained (**Figure 5.26**).

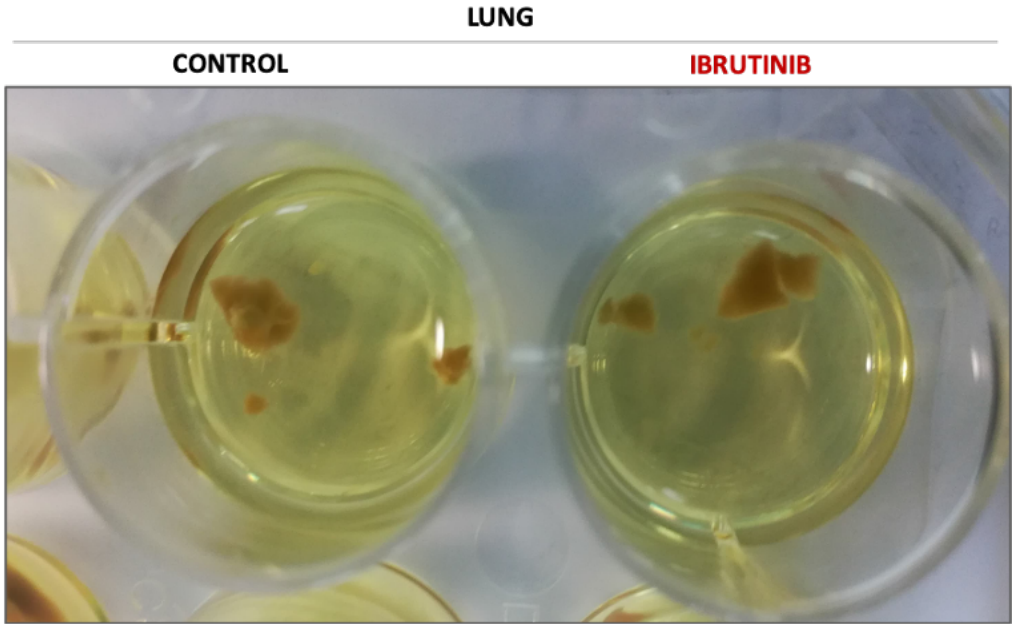

Figure 5.25. Expression of SA-β-gal in the ZMPSTE24$^{-/-}$ mice lung tissue.

Representative SA-β-galactosidase staining of the kidney fragments of two controls and two Ibrutinib-treated ZMPSTE24$^{-/-}$ mice 110 days after the beginning of treatment. Figure shows results after 24h incubation in the staining solution.

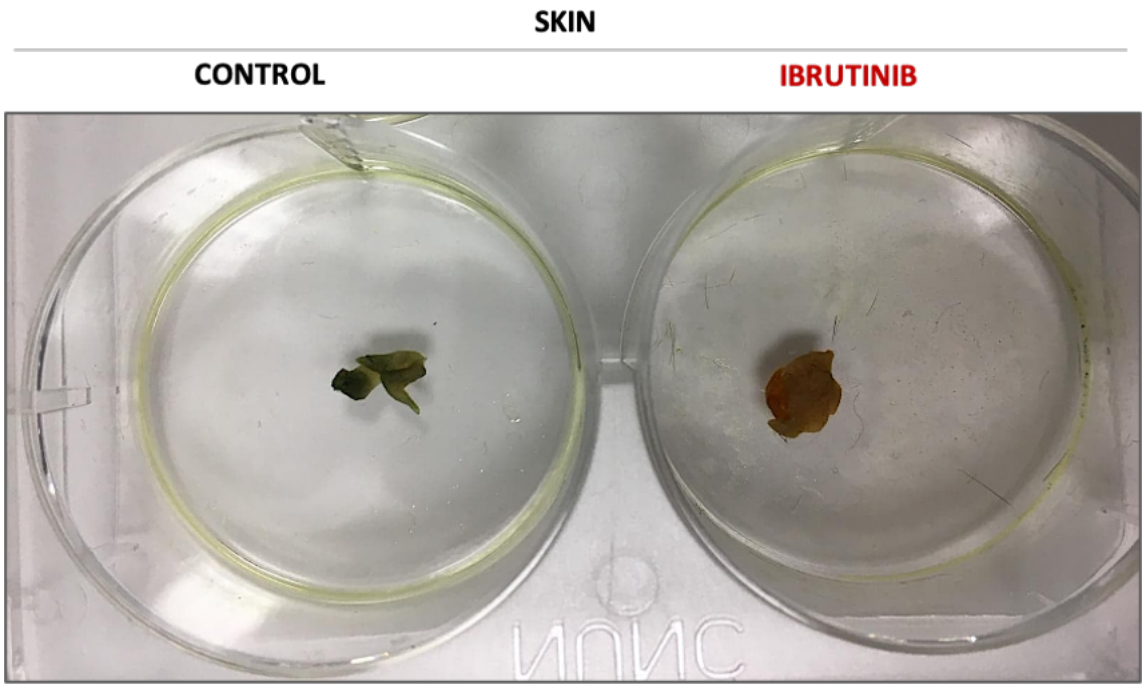

Figure 5.26. Expression of SA-β-gal in the ZMPSTE24$^{-/-}$ mice skin tissue.

Representative SA-β-galactosidase staining of the kidney fragments of two controls and two Ibrutinib-treated ZMPSTE24$^{-/-}$ mice 110 days after the beginning of treatment. Figure shows results after 24h incubation in the staining solution.

In summary, data collected from SA-β-Gal staining exposed differences between some of the tissues, which suggests that the Ibrutinib treatment potentially exhibits a tissue-specific response. However, in order to exclude technical mistakes, results should be repeated considering adjustments to the protocol based on the tissue-specific approach. Each tissue should be approached individually, estimating the most suitable fixation time or incubation in the staining solution. Here, all the tissues were subjected to the same conditions, which could mask potential differences.

Our data show that BTK inhibition by Ibrutinib is tissue- specific. This is consistent with previous finding that Ibrutinib is blocking BTK function which is ambiguous with the interference of BTK protein level (Chu et al., 2019). For additional confirmation of Ibrutinib effectivity we measured p53 level, which should decrease together with BTK inhibition (Althubiti et al., 2016b). However, other kinases blocked by BTK might also interfere with p53 level, therefore for future analysis, the expression level of phosphorylated p53 and also another BTK downstream substrate should be analysed to confirm specificity and effectivity of treatment.

5.6 Discussion

Different strategies have been developed to target and eliminate the burden of senescent cells from the body. One of these strategies, senoblocking, relies on blocking the core pathways responsible for induction and maintenance of cellular senescence, which have been well studied and mostly converge on the p53-p21 and the p16-Rb axes. Manipulation of these pathways could prevent accumulation of senescent cells in the tissues. Based on pharmacological interventions, we showed that continuously disturbing p53 function has an impact on certain ageing features, which was further confirmed using biochemical analysis of tissues and thus we provide the first evidence of the effects of a senoblocking strategy *in vivo*. Our results showed preservation of cognitive brain and skeletal muscle functions. These results support previous findings of senescence-related loss of muscle and brain function. For example, one of the main triggering factors of age-related sarcopenia is senescence of muscle satellite cells (Munoz-Espin and Serrano, 2014). Moreover, different age-related neurodegenerative disorders are accompanied by an increase number of senescent cells (Chinta et al., 2015). Our results suggest that the prevention of senescent cells accumulation might be a good strategy to preserve muscle strength and ameliorate age-related loss of brain function.

The obvious downside of the p53 function disruption (a core tumour suppressor) is the increased risk of tumorigenesis. However, that was not observed during the course of our study. It is important to mention that in tested tissues, such as muscle, the level of p53 was not completely reduced by blocking BTK, which might explain why there is no increase in tumours despite blocking a tumour suppressor pathway. Furthermore, for our study we chose the *ZMPSTE24*$^{-/-}$ progeroid mouse model for a convenience of a short lifespan, that allows for more accessible and faster experiments. However, the short lifespan and genetic background of animals might mask the proper investigation of the tumour development. Therefore, it is important to repeat our study using wild type animals to assess the role of BTK in normal organismal aging. So far, long-term

follow-up clinical studies did not indicate the significant increase in secondary tumours in the patients treated with BTK inhibitors (Walter et al., 2017). Interestingly, mice lacking BTK are severely immunocompromised because of the BTK role in B-cells development, however they develop normally (Kerner et al., 1995, Khan et al., 1995), which is contradictory to the absence of other regulatory kinases upstream of p53 pathway, such as ATM and ATR. Loss of ATM and ATR has been shown to cause embryonic lethality (Daniel et al., 2012, Brown and Baltimore, 2000). Thus, BTK knockdown may only partially inhibit p53 function *in vivo*, thus allowing some of its tumour suppressor functions to continue.

The balance between pro-aging and anti-tumour functions of p53 has been intensively debated. Some reports show that excessive p53 activity would protect against cancer with simultaneous induction of premature aging (Maier et al., 2004, Tyner et al., 2002). However, there are also indications in the literature that increased p53 level prevented cancer without accelerating the aging phenotype if properly controlled (Garcia-Cao et al., 2002). The converse *in vivo* studies of p53 in relation on the lifespan are limited due to the accelerated rate of cancer arising early in p53 knockdown mice (Harvey et al., 1993). The key solution seems to be a proper balance in the level of p53, high enough to stop proliferation of tumours and low enough to not accelerate a premature aging phenotype.

Nevertheless, our studies indicate that continued BTK inhibition via Ibrutinib treatment might preserve muscle and brain function and therefore increase the healthspan of treated animals. Potential mechanism involved could be a reduction in the presence of senescent cells in specific organs, as suggested by our biochemical analysis. That would be consistent with previous reports showing that clearance of senescent cells improves the function of different organs (Kirkland and Tchkonia, 2017, Kirkland and Tchkonia, 2020). However, our data revealed that BTK inhibition had differential effect on tested tissues, which might suggest an heterogenous impact in preserving organ function. That might be linked to tissue-specific levels of BTK expression or other senescence-independent functions of BTK. Moreover, the multiple-target nature of Ibrutinib should be also considered, as Ibrutinib targets a panel of other kinases (e.g., ITK, TEC, BLK)

(Honigberg et al., 2010). Additionally, to further investigate the effect of Ibrutinib treatment it will be interesting to perform tissue- specific mass spec analysis between treated and untreated animals. Analysis should include also comparison of proteins expression profiles between young and old *ZMPSTE24*$^{-/-}$ animals versus young and old wild-type. This should give an indication how *ZMPSTE24*$^{-/-}$ genetic background might affect the response to the drug.

5.6.1 Organ-specific mass spec analysis of *ZMPSTE24*$^{-/-}$ mice treated with Ibrutinib

To further explore the effect of Ibrutinib treatment on the particular tissues using alternative approaches, we performed the pilot mass spec study of the whole-tissue lysates. First, to separate the run samples according to abundance variation and identify run outliers, we prepared the Principal Components Analysis (PCA) plots. All the proteomics analysis were performed with help of Dr Rajinder Singh and Dr Antonella Tabasso-Smith. The first screen of PCA plots, for all the tissues together, did not show separation of the proteins between treated and control groups (**Figure 5.27**). However, when we analysed the tissues separately (**Figure 5.29**, **Figure 5.29**) the differences were noticeable, with the best separation for kidney. This indicates that the greatest difference between Ibrutinib-treated and control animals should be observed in the kidneys (**Figure 5.29**).

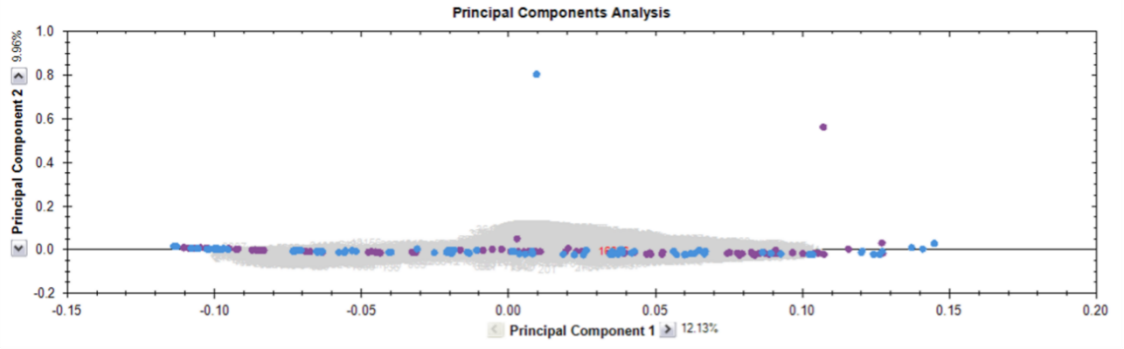

Figure 5.27. The Principal Component Analysis of all the tested tissues.

2 Ibrutinib-treated and 2 control ZMPSTE24$^{-/-}$ mice (each of similar age, approximately 170 days old) were continuously treated via oral gavage with Ibrutinib (10mg/kg) or vehicle twice a week until culled (around 110 days). At the end of the study brain, lung, heart, kidney and liver were isolated and the whole-tissue lysates performed. The Principal Component Analysis (PCA) plots are depicting the two treatment clusters of the experiment. Purple dots represent the controls and blue represents Ibrutinib-treated samples.

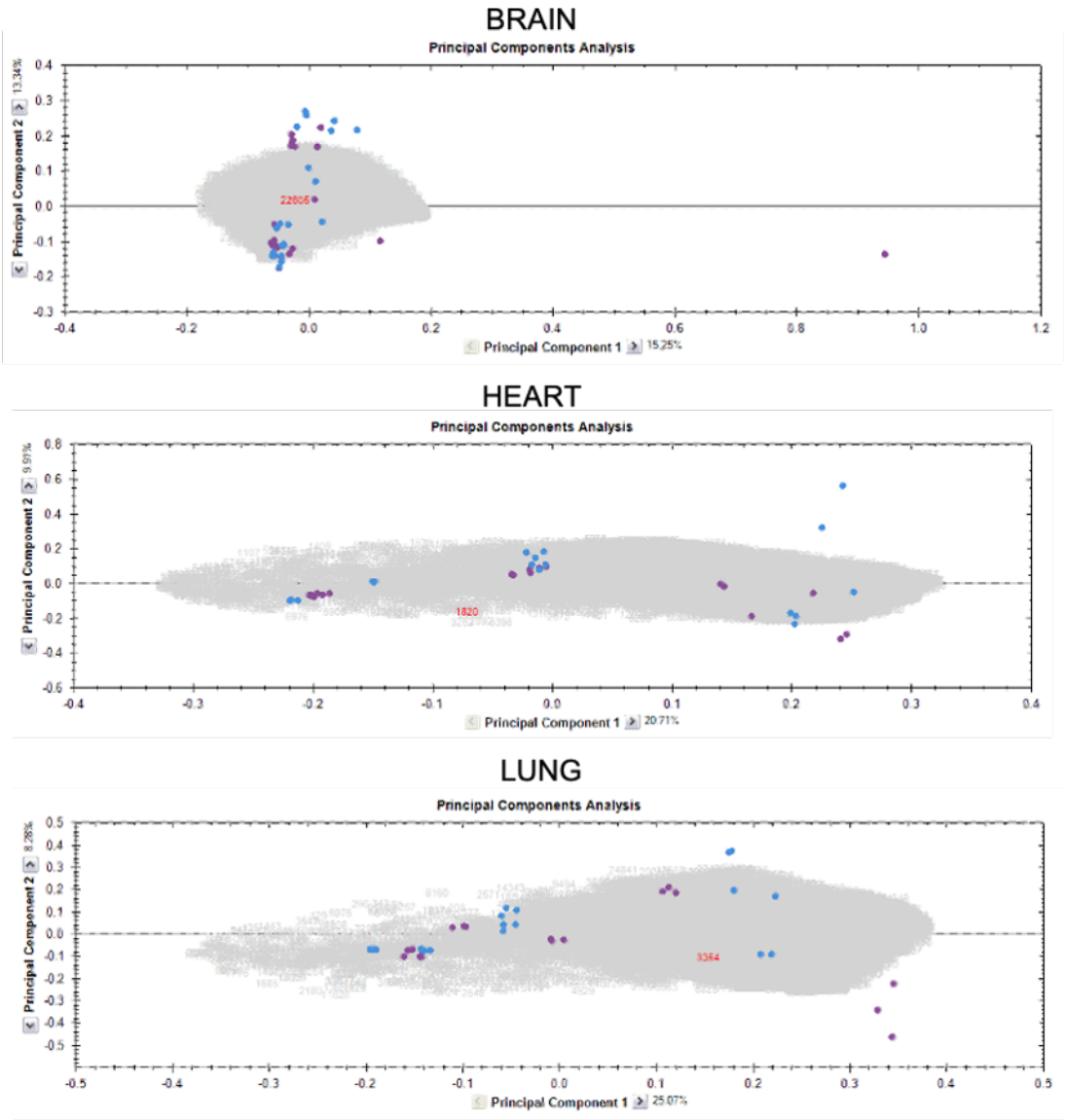

Figure 5.28. The Principal Component Analysis of brain, heart and lung.

2 Ibrutinib-treated and 2 control ZMPSTE24$^{-/-}$ mice (each of similar age, approximately 170 days old) were continuously treated via oral gavage with Ibrutinib (10mg/kg) or vehicle twice a week until culled (for around 110 days). At the end of the study brain, heart and lung were isolated and the whole-tissue lysates performed. The Principal Component Analysis (PCA) plots are depicting the two treatment clusters of the experiment. Purple dots represent the controls and blue represents Ibrutinib-treated samples.

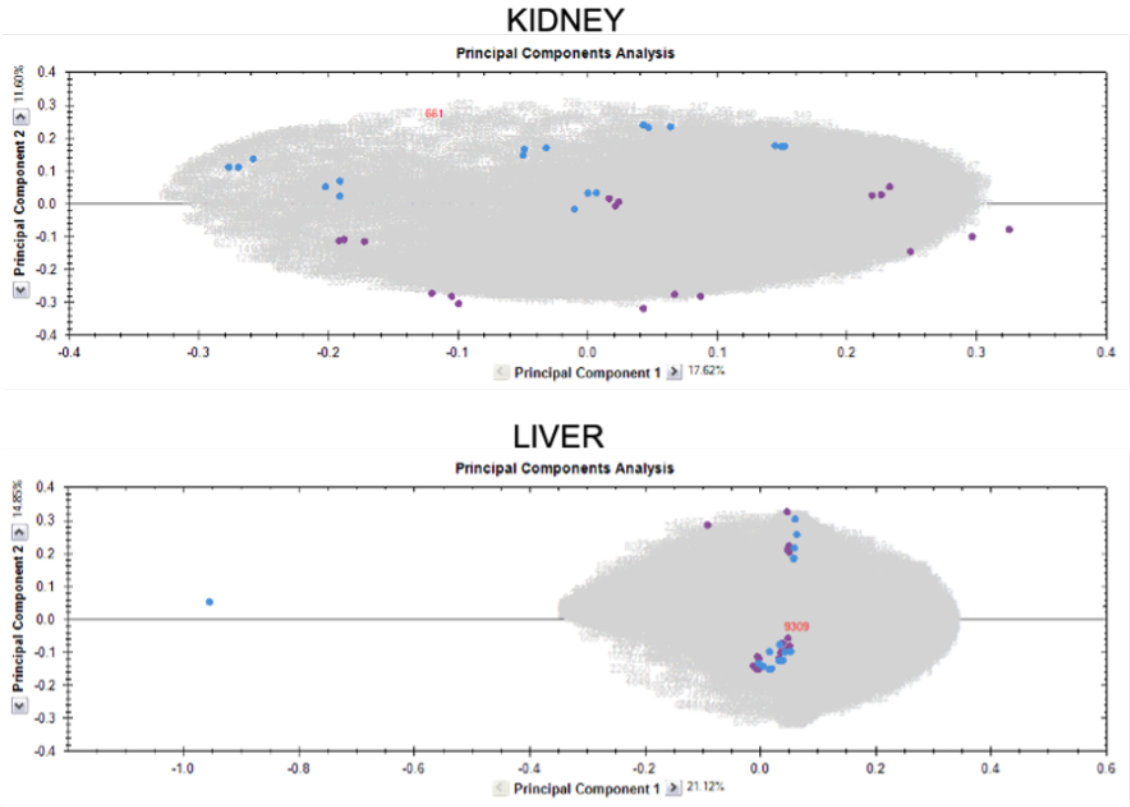

Figure 5.29. The Principal Component Analysis of kidney and liver.

2 Ibrutinib-treated and 2 control ZMPSTE24$^{-/-}$ mice (each of similar age, approximately 170 days old) ZMPSTE24$^{-/-}$ mice were continuously treated via oral gavage with Ibrutinib (10mg/kg) or vehicle twice a week until culled (for around 110 days). At the end of the study kidney and liver were isolated and the whole-tissue lysates performed. The Principal Component Analysis (PCA) plots are depicting the two treatment clusters of the experiment. Purple dots represent the controls and blue represents Ibrutinib-treated samples.

From the total number of proteins affected by the Ibrutinib-treatment, (**Table 9.1-Table 9.9**), 46 were specifically upregulated in Ibrutinib-treated brain, 27 in heart, 22 in kidney, 44 in liver and 11 in lung. In turn, there were 29 downregulated in brain, 13 in heart, 59 in kidney, 31 in liver and 15 in lung (**Figure 5.30**). Moreover, 4 upregulated proteins have been found in all of the tested tissues: Protein disulfide-isomerase (P4hb), Myosin-6 (Myh6), Hydroxyacyl-coenzyme A dehydrogenase mitochondrial (Hadh) and DNA (cytosine-5)-methyltransferase 1 (Dnmt1) (**Table 5.1**).

P4HB is a member of protein disulfide isomerase (PDI) enzyme family responsible for formation, breakdown and rearrangement of protein disulfide bonds in ER. P4HB is generally expressed in a variety of cancer types, such as glioma, lymphoma, ovarian cancer, prostate cancer, renal and lung cancer (Xu et al., 2014a).

MYH6 is a conventional myosin, that hydrolyse ATP to track along actin filaments and microtubules, respectively. Myosin are crucial molecular motor proteins in skeletal muscle that converts chemical energy into mechanical work. Myosin 6 is predominantly expressed in human cardiac atria and it plays a key role in cardiac muscle contraction. Mutations in *MYH6* gene have been linked with cardiac disorders, such as hypertrophic cardiomyopathy (Jiang et al., 2013) . With age, the rate of myosin heavy chain proteins synthesis decreases (Balagopal et al., 1997, Marx et al., 2002). That is thought to be related to age-associated progression of sarcopenia or impaired motor functions. Therefore, upregulation of Myosin 6 might be linked with Ibrutinib beneficial effect in preservation of muscle tissue. However, in here Myosin 6 has been found upregulated in all of the tested tissues, which suggest that its function in aging could be more universal and might not be restricted to single tissue.

Hydroxyacyl-coenzyme A dehydrogenase mitochondrial (HADH) is an enzyme that catalyzes the β-oxidation of fatty acids in mitochondria, which is a crucial process providing energy during time of fasting, severe febrile illness or increased muscular

activity (Popa et al., 2012). Mutations in HADH gene has been linked with disorders, such as hyperinsulininemic hypoglycemia (Velasco et al., 2020). Moreover, decreased level of HADH has been associated with deposition of Alzheimer's vascular amyloid-beta peptide (Frackowiak et al., 2001).

In that context, upregulation of HADH in Ibrutinib-treated mice could suggest positive impact on preservation of tissues-function, including brain. Our data indicate that HADH expression might play a systemic role in aging, as its expression was changed after the treatment with Ibrutinib in all of the tested tissues.

DNA (cytosine-5)-methyltransferase 1 (DNMT1) is DNA methylation enzyme with multiple regulatory features that can control DNA methylation in cells. Its interacting molecules are involved in variety of cellular mechanisms, including chromatin organization, DNA repair and cell-cycle regulation (Svedružić Ž, 2011). DNMT1 has been found elevated in different cancers, such as human hepatocellular carcinomas or in human prostate cancer (Saito et al., 2003, Patra et al., 2002) and drugs that inhibits DNMTs have been widely studied in cancer treatment in vivo and in clinical trials (Xiang et al., 2014, Ma et al., 2018).

Our results identified also 8 proteins that were downregulated by Ibrutinib treatment and shared between all of tested tissues (**Figure 5.30**). Among them, the most interesting in the aging-contexts was Acetyl-CoA acetyltransferase mitochondrial (ACAT1), which is responsible for regulation of cellular cholesterol homeostasis (Shibuya et al., 2015). Importantly, it has been reported that blocking ACAT1 provides multiple beneficial effects on Alzheimer's diseases.

A special mention deserves also mTOR, which has been identified in heart and kidney as one of the most downregulated proteins. mTOR is a key modulator of aging and age-related diseases (Stallone et al., 2019) and linked with BTK through BTK/AKT/mTOR pathway (Hu et al., 2020). Interestingly, previous reports have showed that combination of BTK and mTOR inhibitors had a synergistic anti-tumour effect on Mantle cell lymphoma (Li et al., 2018).

Taken together, mass spectrometry analysis identified couple of interesting proteins that have been related to aging and affected by Ibrutinib treatment. Further analysis should be performed to validate their potential relation with BTK.

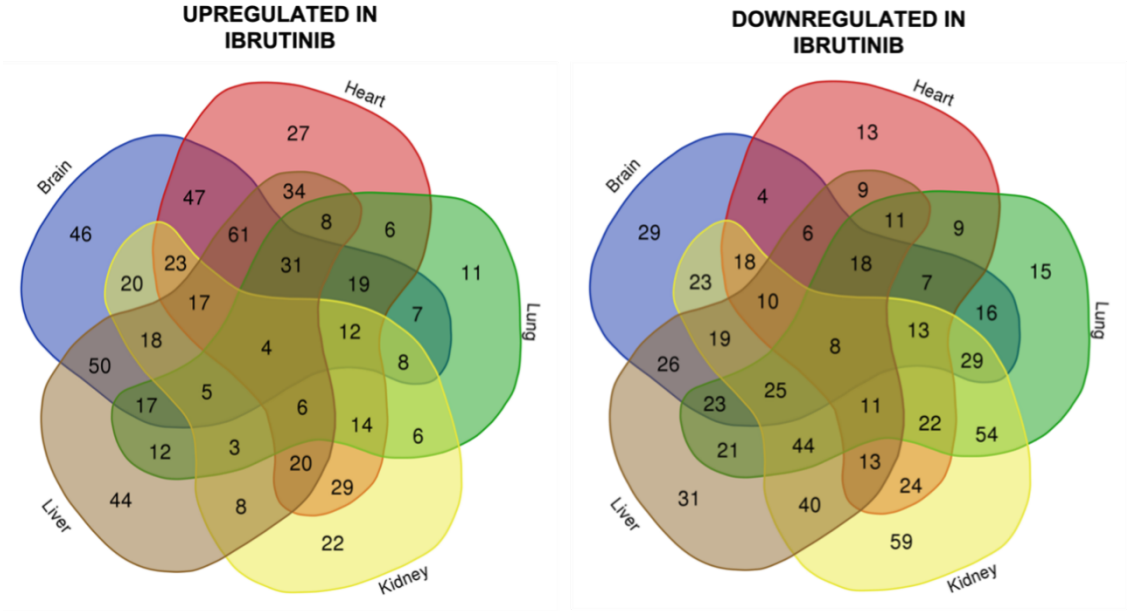

Figure 5.30. The most up and downregulated proteins shared between tested organs.

Venn diagram of the up- and downregulated proteins identified through mass spectrometry screen after the treatment of ZMPST24$^{-/-}$ mice with Ibrutinib. Graph shows relationship of protein between tested organs, Brain, Heart, Lung, Liver and Kidney.

Table 5.1. List of the proteins affected by the Ibrutinib treatment identified by mass spectrometry in each of the tissues tested, brain, heart, lung, kidney and liver.

Name	Level
Protein disulfide-isomerase (P4hb)	Upregulated
Myosin-6 (Myh6)	Upregulated
Hydroxyacyl-coenzyme A dehydrogenase mitochondrial (Hadh)	Upregulated
DNA (cytosine-5)-methyltransferase 1 (Dnmt1)	Upregulated
Neurofascin (Nfasc)	Downregulated
Androgen receptor (Ar)	Downregulated
Nesprin-2 (Syne2)	Downregulated
Succinate--CoA ligase [GDP-forming] subunit beta_ mitochondrial (Suclg2)	Downregulated
Exportin 4 (Xpo4)	Downregulated
Acetyl-CoA acetyltransferase_ mitochondrial (Acat1)	Downregulated
Glycine N-acyltransferase (Glyat)	Downregulated

Furthermore, we decided to assess which biological mechanisms were affected by the Ibrutinib treatment using Reactome online tool. The majority of identified proteins were classified into following mechanisms: immune system, cell cycle, signal transduction, diseases and homeostasis (**Figure 5.31**).

After classification of the identified proteins to their biological functions, we compared which cellular pathways were affected by Ibrutinib treatment. For that purpose, we used the Panther online tool and analysed separately upregulated and downregulated proteins from all of the tested tissues together. Panther analysis revealed a list of downregulated pathways among which few were interesting in the context of aging, such as inflammation mediated by chemokines and cytokines signalling pathway, Parkinson disease and WNT signalling pathway (**Figure 5.32**). However, the same pathways were also detected among the upregulated signalling pathways although with different proportion (**Figure 5.33**). That could be a result of differential effect of Ibrutinib on the proteins belonging to the same pathway. Therefore, further analysis should be taken, depicting which proteins were aligned by Panther tool to signalling pathways of our interests.

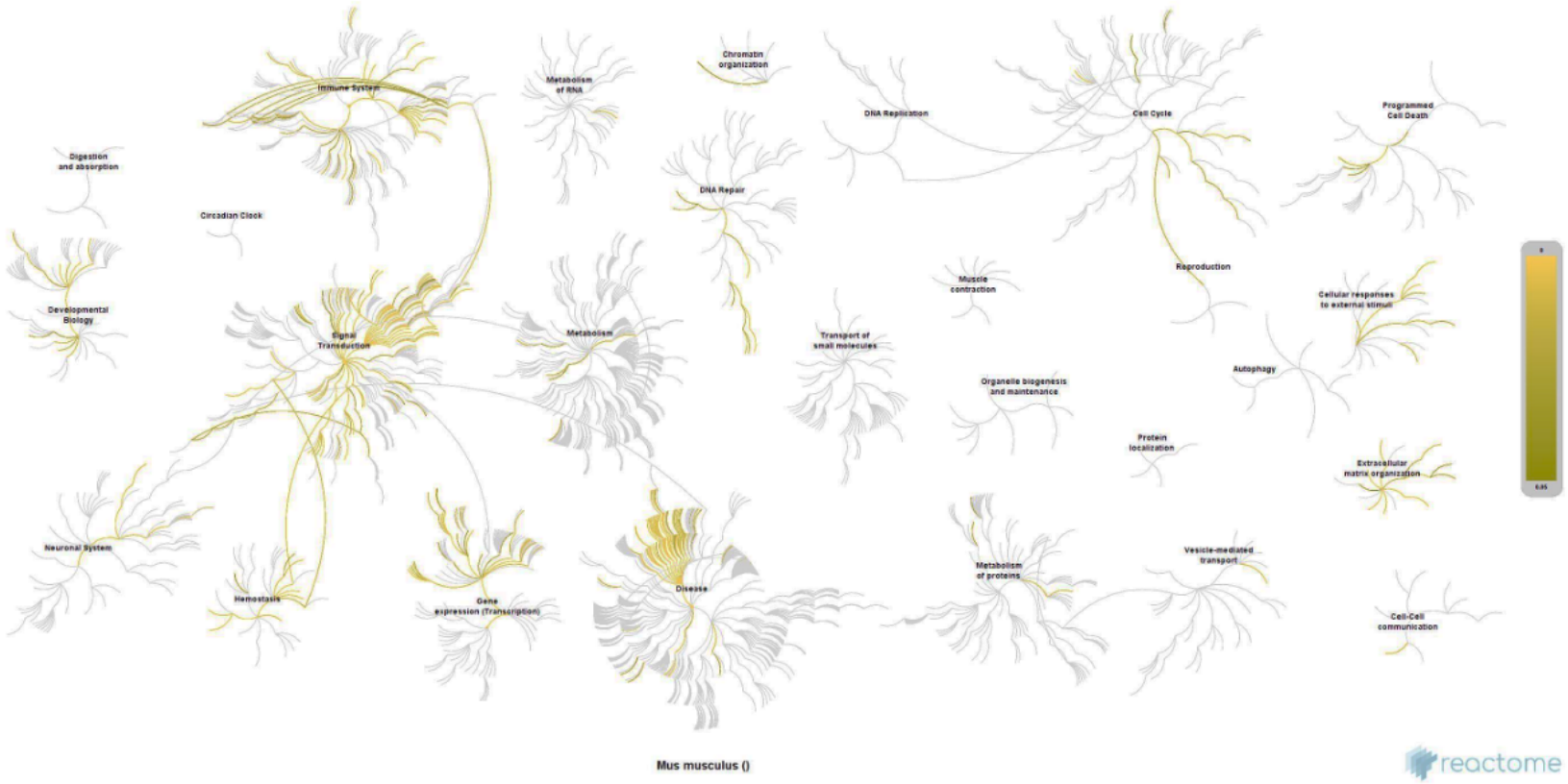

Figure 5.31. The visual representation of detected proteins relation organized into biological pathways and processes.

The entire list of proteins affected by Ibrutinib treatment collected from all the tissues were run through Reactome, a pathway analysing software. The intensity of yellow colour of pathway branches indicates the number of proteins found in the part of the pathway

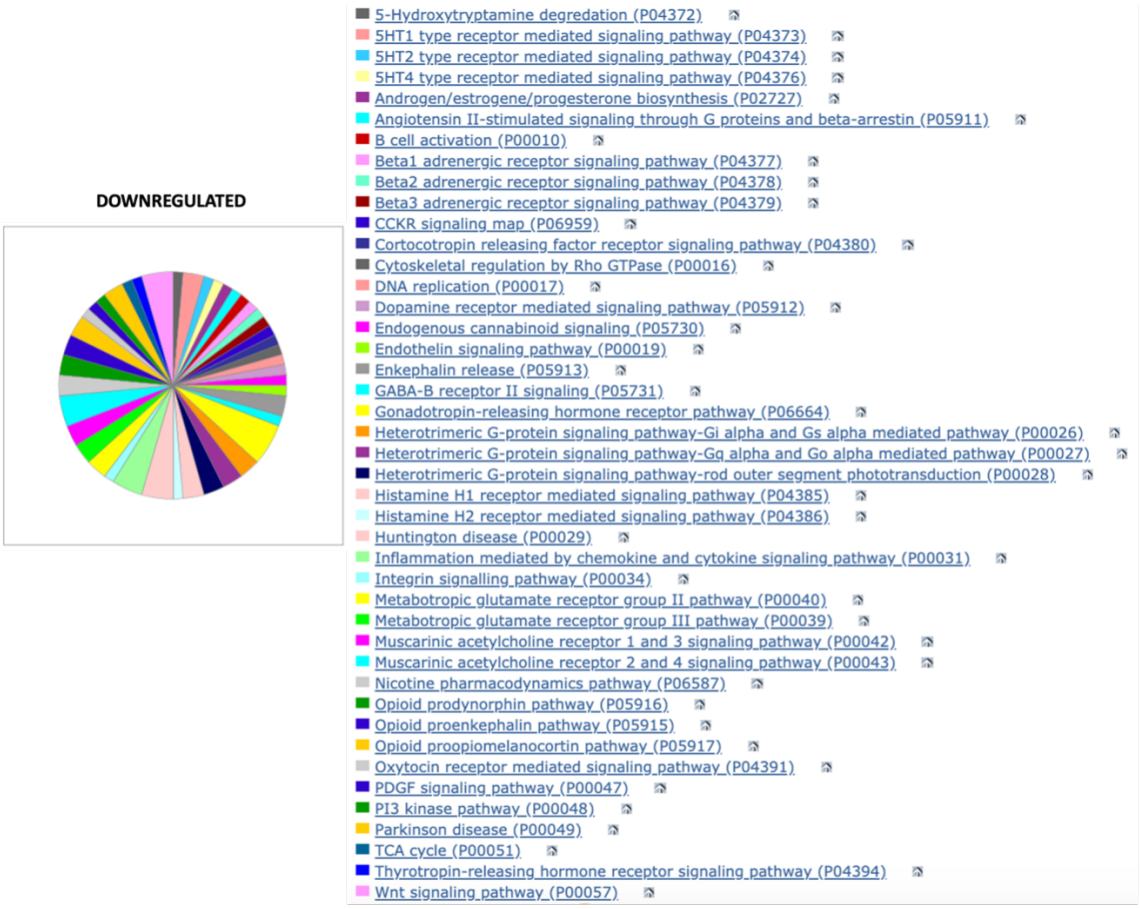

Figure 5.32. PANTHER analysis of proteins found downregulated after the treatment with Ibrutinib.

Graph represents results of PANTHER pathway analysing software of a combined analysis of the entire list of proteins that were found downregulated via mass spectrometry analysis in all of the tested mice tissues, (brain, lung, heart, kidney, liver) after the treatment with Ibrutinib. Proteins were isolated from tissues collected from mice treated with Ibrutinib or control mice treated with vehicle (2 animals per group). A pie chart shows in which pathways the proteins were found to take part in and the proportion of the proteins made up each of the pathway.

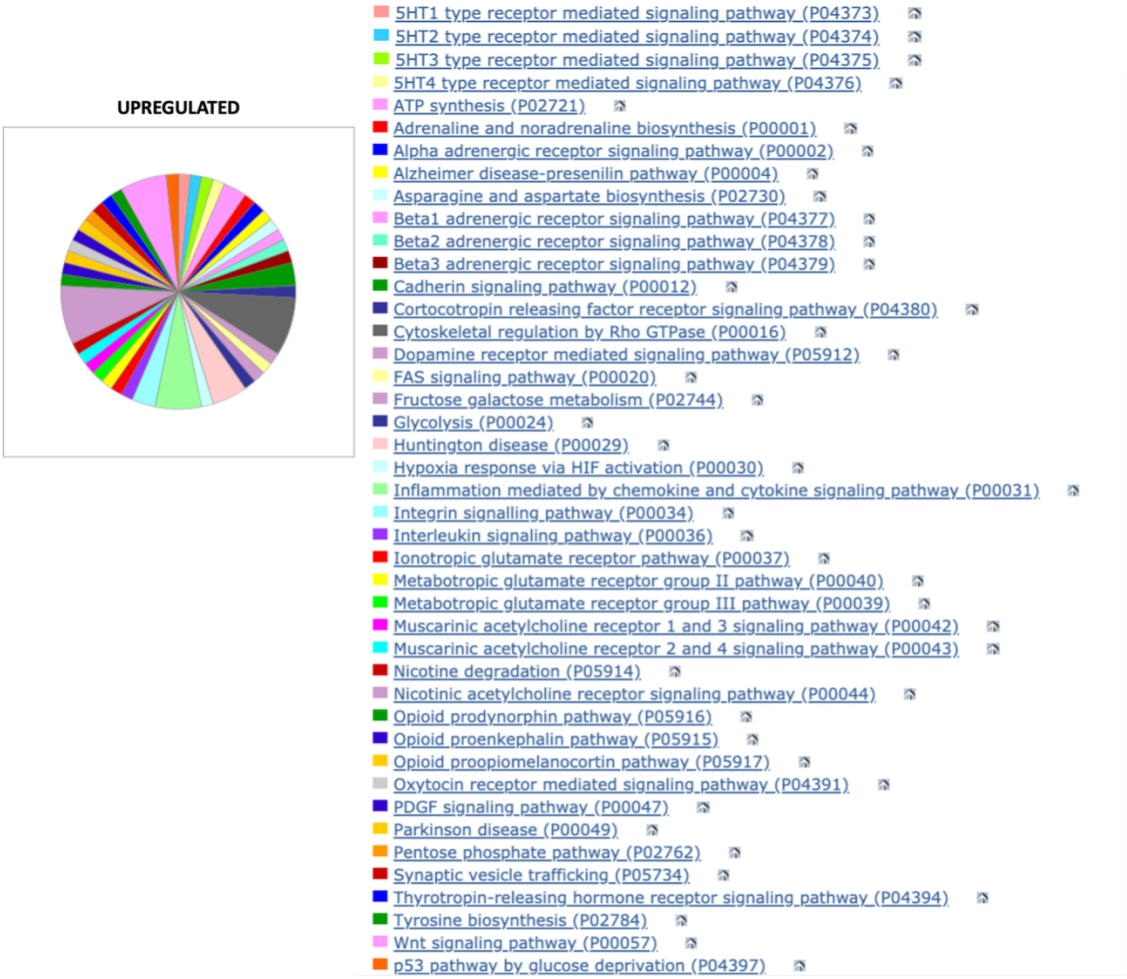

Figure 5.33. PANTHER analysis of proteins found upregulated after the treatment with Ibrutinib.

Graph represents results of PANTHER pathway analysing software of a combined analysis of the entire list of proteins that were found downregulated via mass spectrometry analysis in all of the tested mice tissues, (brain, lung, heart, kidney, liver) after the treatment with Ibrutinib. Proteins were isolated from tissues collected from mice treated with Ibrutinib or control mice treated with vehicle (2 animals per group). A pie chart shows in which pathways the proteins were found to take part in and the proportion of the proteins made up each of the pathway.

The big limitation of this study is the number of samples. Due to the low availability of frozen tissues, we used only 2 animals per condition. Therefore, the differences in the protein expression might be also be related to individual differences of animals tested, which might mask the actual effect of the treatment. Because of that, we have decided to add more animals into the analysis. Moreover, additional limitation of this method is that we performed mass spec analysis on the whole tissues' lysates, which led to identification of vast amount of background, such as housekeeping proteins. Therefore, proteins that could have a potential effect on aging were manually identified and picked (**Table 9.1-Table 9.9**) for further validation. However, despite the fact that there is a low number of biological replicates, we still were able to identify interesting proteins affected by the treatment, such as mTOR or ACAT1 (**Table 9.9**). More animals are recently being added into the analysis so it will be important to confirm findings showed here.

Thus, further studies will be needed to fully evaluate the effect of BTK inhibition on aging. A conditional knockout model that could switch off BTK at different stages in life could be useful to assess the actual impact on aging, especially because the BTK impact on immune system during development might mask the potential differences in the preservation of the healthspan and lifespan. Moreover, it would be interesting to establish a range of dosages of inhibitors beyond the ones that we used. It will be also necessary to use other more specific BTK inhibitors and tests their effect on different aspects of aging and to determine whether the observed effect is maintained. Finally, it would be interesting to test BTK inhibitors in different stages of life, especially when advanced aging is more evident via intermittent patterns or continued treatment.

Taken together, we have presented that BTK inhibition can have positive impact on progeroid mice healthspan and ameliorate certain aging phenotypes. Thus, provide a support for development of future therapeutics that prevents accumulation of senescent cells in certain situations, such as sarcopenia or Alzheimer's disease. However, further experiments are needed to fully understand BTK role in aging and its therapeutic potential in senoblocking strategy.

6 Validation of novel markers of cellular senescence

Proper identification of senescent cells is crucial for further investigation of using them as therapeutic targets to treat diseases and conditions in which accumulation of these cells has been shown to play a role (Munoz-Espin and Serrano, 2014). Lack of specific markers is a first barrier hindering development of such clinical approaches. Currently available markers are characterized by lack of specificity. There is no marker which is entirely specific for senescence state (Campisi and d'Adda di Fagagna, 2007). Therefore, it is necessary to search for novel, more specific markers

In our lab, several proteins preferentially expressed on the surface of senescent cells were identified through mass spectrometry (Althubiti et al., 2014). The screening was performed comparing lysates of a membrane fractions between senescent and proliferating cells. The identified proteins were one of the first indicators of the senescent 'surfaceome'. None of the published proteins had been linked directly to cellular senescence prior to the screening done in our lab. Their presence on the plasma membrane of the senescent cells highlights their potential to act as a target for the elimination of senescent cells from tissues. Three of these proteins, namely VPS26A, EBP50 and PLD3, were investigated in the course of this project and are described here.

Vascular protein sorting-associated protein 26A (VPS26A) is a component of the retromer complex (Gallon and Cullen, 2015, Bugarcic et al., 2011). Together with VPS29 and VPS35, it forms a vacuolar protein sorting trimer responsible for cargo selection, nexin (Snx) sorting, and retrograde transport of proteins to the Golgi apparatus. VPS26A-null mutation in mice embryos leaded to embryonic lethality due to failure in early postimplantation development (Radice et al., 1991). Therefore, a potential role of VPS26A in the development has been tested and VPS26A appeared to be associated with the development of the embryonic ectoderm (Lee et al., 1992). Embryonic ectoderm gives rise to neural-lineage cells (Muhammad et al., 2008). However, despite compelling evidence of the VPS26A association with neural cells in embryonic development, the underlying molecular mechanism remains largely unknown.

Moreover, the retromer complex has been linked with Parkinson's disease (PD) and Alzheimer's disease (AD) (Choi et al., 2018, Tan et al., 2019). However, presented data are contradictory. Shannon et al., 2014 sequenced 70 patients from Mayo Clinic Parkinson's disease cohort for the *VPS29*, *VPS26A/VPS26B* genes and identified mutations that were not common cause of PD (Shannon et al., 2014). It is also worth to mention, that two research groups have previously published that the mutation p.Asp620Asn in VPS35, the other component of the retromer complex, was identified as the genetic determinant of late-onset PD (Vilariño-Güell et al., 2011, Zimprich et al., 2011). However, other studies reported 5 different mutations in VPS26A that might be linked with PD. For example, p.Lys93Glu (c.A277G) in exon 4 has been found in a Canadian female (age of onset= 58) affected by Multiple system atrophy (MSA) (Gustavsson et al., 2015) and 3 people suffering from PD (Shannon et al., 2014). Mutation has been found in highly conserved regions of the VPS26A N-domain, which binds the receptor and promotes its internalization. However, there are no indications that this mutation affects VPS26A function in binding to proteins cargoes. Another mutation, p.Met112Ile (c.336G>C), was found in patients with sporadic PD (Koschmidder et al., 2014) and p.Met112Val (c.334 A>G) was found in patients with atypical PD (Gustavsson et al., 2015). It is thought that both mutations might impair the interaction of VPS26A with other components of the retromer complex. Other mutations have been reported in exon 9, p.Lys296X in patients with atypical parkinsonism Progressive Supranuclear Palsy (Gustavsson et al., 2015) and p.Pro316Ser was found in patient with sporadic PD (Gustavsson et al., 2015), however the effects of exon 9 mutations on retromer function are still unknown (Koschmidder et al., 2014, Gambardella et al., 2016). The exact impact of the above-mentioned mutations still needs to be explored. However, it is important to mention that VPS26A mutations have been found in few tested patients and do not occur frequently in the majority of PD patients.

The potential link between VPS26A with AD is also unclear. The involvement of VPS26A in AD has been suggested because of different lines of evidence. First, down-regulation of *VPS26* caused accumulation of BACE (the β-secretase) , which mediates production of Aβ, the main marker of AD (He et al., 2005, Muhammad et al., 2008). Second,

components of the retromer complex, including VPS35 and VPS26 are deficient in brains of patients with late-onset AD (Scherzer et al., 2004). Third, *in vivo* VSP26 heterozygote knockout (VPS26 +/-) caused hippocampal dysfunction and the knockdown mice do not survive into adulthood (Muhammad et al., 2008). Moreover, reduction of VPS26 caused reduction in VPS35. Therefore, it remains unclear if both or either VPS26 or VPS35 are the key factor responsible for the AD phenotype. Especially, VPS35 deficiency had been found accompanied by VPS26 deficiency (Fuse et al., 2015). Further research should be performed to understand the interconnection function of VPS26 and VPS35 in age-related brain dysfunctions.

It is also worth to mention that another study focused on association of VPS26 variants and AD progression. Samples from 443 patients with sporadic AD have been analysed to detect 8 identified *VSP26A* single nucleotide polymorphisms (SNPs) (Riemenschneider et al., 2007). However, none of them has been associated with disease.

The functional role of VPS26A in intracellular trafficking makes it an interesting target for SASP analysis. Furthermore, its high expression in hippocampus (Muhammad et al., 2008) suggests its therapeutic potential to act as a target in age-related brain dysfunctions. Moreover, computational analysis revealed the presence of a VPS26A extracellular epitope (Althubiti et al., 2014), that could be used for direct- targeting senotherapy. For all that reasons, we have decided to explore the expression level of VPS26A in our senescence models.

Erzin/Radixin/Moesin Binding Protein (EBP50, NHERF1) is another marker identified on the list of proteins preferentially present in senescent cells (Althubiti et al., 2014). EBP50 is a member of the Na+/H+ exchanger regulatory factor (NHERF) family implicated in ion exchange and cancer promotion (Georgescu et al., 2008). Downregulation of EBP50 promoted PC-2 and MiaPaCa-2 pancreatic cancer cells proliferation and accelerated cell cycle progression from G1 to S phase (Ji et al., 2012). Moreover, overexpression of EBP50 in pancreatic cancer cell lines suppressed cell proliferation, promoted cell-cycle arrest at G1 phase and was associated with higher rate of apoptosis in PANC-1 and SW1990 pancreatic cancer cells (Ji et al., 2014). Moreover, another study reported that

EBP50 supresses proliferation of breast cancer MCF-7 cells through decreasing c-Myc expression and its downstream targets, such as cyclin A and E. Interestingly, EBP50 downregulation delayed the c-Myc autophagic lysosomal degradation in breast cancer cell lines, which is consisted with previous reports that EBP50 overexpression promotes autophagy (Liu et al., 2015a). Other studies identified EBP50 as a marker of colorectal cancer (Hayashi et al., 2010). Results revealed that EBP50 undergoes progressive alterations in subcellular localization and its expression during colorectal cancer progression. In normal epithelial cells, EBP50 is localized mainly at the apical plasma membrane. However, that was lost in cancer cells, in which overexpression of NHERF1 had been found in cytoplasm. Moreover, the tumour suppression role of EBP50 has been linked with regulation of β-catenin and PTEN. β-catenin acts as an intracellular signal transducer in the WNT signaling pathway and its overexpression has been found in many cancers (Morin, 1999). NHERF1 deficiency research revealed that β-catenin stabilization and function partially depends on NHERF1 level (Kreimann et al., 2007). Moreover, NHERF1 has been found to directly interact with PTEN, a tumour suppressor frequently disrupted in human cancers (Takahashi et al., 2006).
Although, EBP50 has never been linked with cellular senescence before, its close relation in tumour suppressive role through mediation of cell cycle-arrest highlights evidence for potential cross linkage with cellular senescence. Therefore, it was of extreme interest to validate its expression in our senescence models.

Last but not least is Phospholipase D3 (PLD3) is a member of phospholipase D superfamily of signalling enzymes responsible for vesicle trafficking and conversion of phosphatidylcholine to phosphatidic acid and choline, which has implications for membrane dynamics and cell signalling (Bi et al., 1997, Chen et al., 1997, Brown et al., 2017). PLD3 is a glycoprotein found in the endoplasmatic recitulum (ER) and the lysosome (Osisami et al., 2012, Gonzalez et al., 2018, Nackenoff et al., 2019). It has been found highly expressed in the human and mice brains (Pedersen et al., 1998) but also during myogenesis (Osisami et al., 2012). Similarly, to VPS26A, PLD3 has been found associated with Alzheimer disease (Wang et al., 2015). Using whole-exome sequencing, low-frequence *PLD3* variants, such as Val232Met, have been found enriched in AD

family-based studies (Cruchaga et al., 2014). Moreover, authors reported high expression of *PLD3* mRNA in regions of old mice brains that are vulnerable to age-related pathology, such as hippocampus and cortex. Moreover, *PLD3* expression has been also found at a higher level in the brains of healthy individuals. These might suggest dysregulation of *PLD3* in pathological conditions (Wang et al., 2015). In turn, another study revealed that *PLD3* gene expression was significantly lower in neurons from in AD brains when compared to controls (Xu et al., 2006, Kong et al., 2009). Interestingly, Cruchaga et al. showed that overexpression of PLD3 caused decrease in intracellular amyloid β precursor protein (APP) and two isoforms of Aβ peptide, Aβ40 and Aβ42 (Cruchaga et al., 2014). In turn, PLD3 knockdown caused an increase of Aβ40 and Aβ42. These data indicate that mutations PLD3 may be involved in the regulation of APP processing and mutations in PLD3 genes might be associated with AD risk.
Considering that accumulation of senescent cells in the brain increases the risk for AD (Bhat et al., 2012), the role of PLD3 in cellular senescence seems to be worth investigation.

In order to further validate and characterize these recently identified novel markers of senescence, we used a range *in vitro* and *ex vivo* senescence models, including aged mice tissues and human samples derived from patients suffering for age-related disorders, such as idiopathic pulmonary fibrosis.

6.1 Expression profiles of VPS26A, EBP50, and PLD3 in EJ-based senescence models

Analysis started with comparison of VPS26A, EBP50 and PLD3 expression between senescent and proliferating EJp53, EJp21 and EJp16 cells both at the gene (**Figure 6.1A**) and protein level (

Figure 6.1B). In the EJp16, model of senescence driven by p16 activation, qPCR results indicated a slight increase of *VPS26A* mRNA. In EJp53 and EJp21 cell lines, there was no difference in *VPS26A* mRNA between senescent and proliferating cells (**Figure 6.1A**). Western blot (WB) analysis showed a slight change of VPS26A after senescence induction in EJp53 cell lines although that was not confirmed in the second replicate (**Figure 9.5**). Therefore, VPS26A expression in tested models remains unclear. Experiment should be repeated at least two more times to confirm VPS26A expression profile.

Analysis of EBP50 expression revealed a slight, although not significant increase at the gene level in EJp21 senescent cells but there was no change of EBP50 protein level.

In EJp53 and EJp16 there was no change of EBP50 level at either gene or protein level.

The *PLD3* mRNA level showed upregulation in senescent EJp21 cells. In EJp53, there was no change of *PLD3* between proliferating and senescent cells and a slight upregulation was detected in EJp16 cells. However due to the high error bars the difference was not considered as reliable. WB analysis of PLD3 showed no changes in any of the tested models.

Analysis of the markers revealed no changes in protein level (**Figure 6.1, Figure 9.5**) and results should be repeated to confirm these preliminary findings. qPCR analysis revealed slight upregulation of *PLD3* mRNA level in EJp21 senescent cells when compared to proliferating counterparts and no changes in *VPS26A* mRNA level in tested senescent cell models. EBP50 analysis similarly to PLD3 showed slight upregulation at mRNA level upon senescence induction, although that was not reflected by changes in EBP50 protein. The differences between gene and protein level might suggest the involvement of post-translational modifications that might regulate proteins stabilization or degradation and further tests should be done to confirm it.

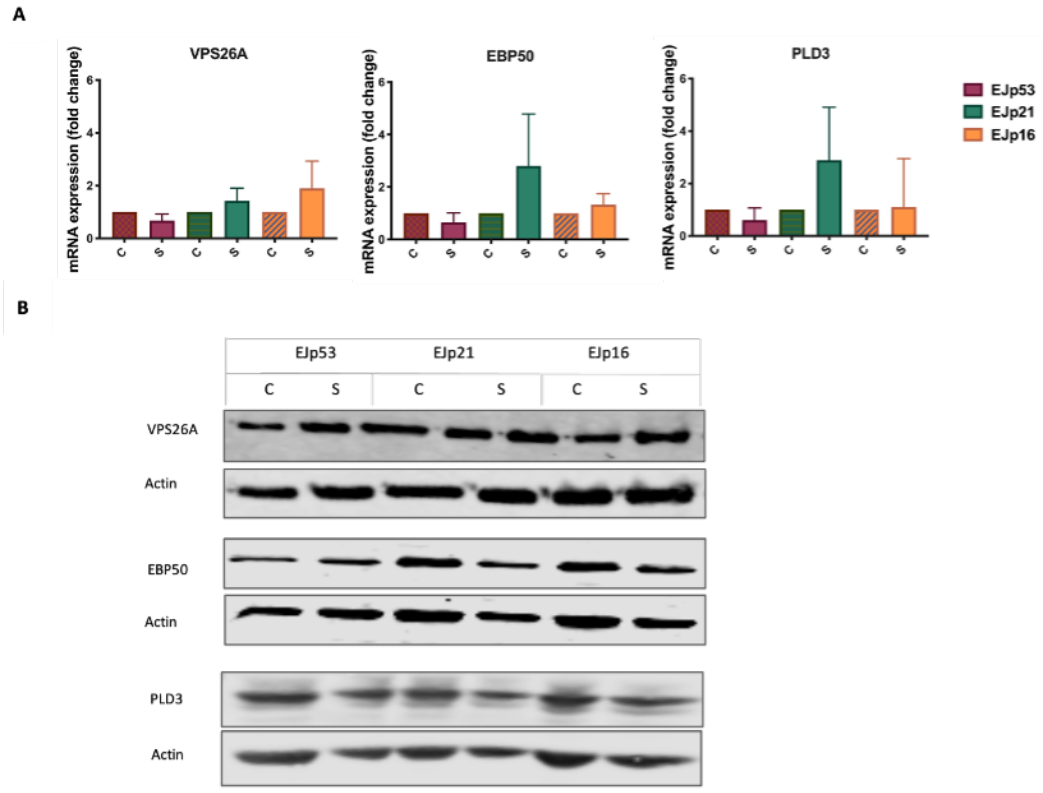

Figure 6.1. Expression of VPS26A, PLD3 and EBP50 in EJ-based cell models

[A] RT-qPCR analysis showing the mRNA expression of VPS26A, EBP50 and PLD3 in EJp53, EJp21 and EJp16 cell lines 4 days after removal of tetracycline. GAPDH was used as internal reference control gene Data were normalized against proliferating controls n=3. Statistical analysis between senescent and control cells performed using paired t-test. [B] Western blot analysis indicating the protein level of VPS26A, EBP50 and PLD3 4 days after removal of tetracycline in corresponding EJ-models, n=2. "S" indicates senescent cells and "C" proliferating controls. (Further blots available in appendix ***Figure 9.5****)*

6.1 Expression profiles of VPS26A, EBP50, and PLD3 in HT1080-p21-9 cell line

To validate expression of novel markers in cells of different origin, the HT1080-p21-9 cell lines was used. After confirmation of senescence induction (**Figure 3.3**), the gene and protein levels of VPS26A, EBP50, and PLD3 were compared between senescent and proliferating cells. Results revealed no changes in VPS26A and EBP50 both at gene and protein level. The expression level of PLD3 showed upregulation of *PLD3* mRNA. Due to unequal loading WB analysis of PLD3 were unclear. To confirm PLD3 expression experiment should be repeated at least two more times (**Figure 6.2, Figure 9.6**).

In summary, there was no change of VPS26A and EBP50 at the protein level after induction of senescence, which indicates that these proteins are not a good senescence marker for the tested cell line.

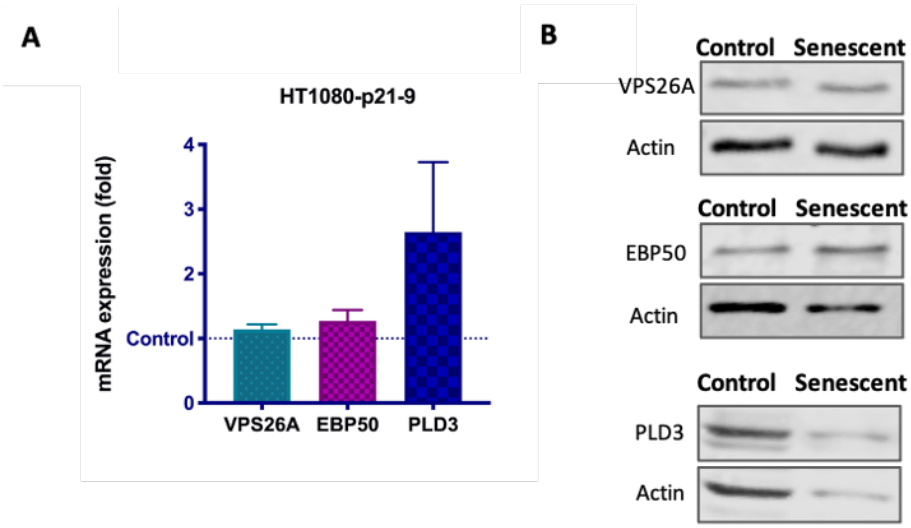

Figure 6.2. The expression profiles of VPS26A, EBP50 and PLD3 in HT1080-p21-9 cell line

*[A] RT-qPCR analysis showing the mRNA expression of VPS26A, EBP50 and PLD3 in HT1080-p21-9 cell line 5 days after addition of IPTG. GAPDH was used as internal reference control gene. Data were normalized against proliferating controls, n=2. Bars represents the mean values ± SD. Statistical analysis performed using paired t-test (ns: not-significant, * p<0.05, ** p<0.01).*

[B] Representative western blot indicating the protein level VPS26A, EBP50 and PLD3 5 days after addition of IPTG. Actin used as loading control, (n=2). Further blots available in appendix ***Figure 9.6***

Comparing both senescence p21-driven systems, EJp21 and HT1080-p21-9, differences in the expression patterns of VPS26A, EBP50, and PLD3 were observed only in qPCR analysis (**Table 6.1**). Results revealed that in both cell lines *VPS26A* mRNA remained unchanged upon senescence induction. Increase of *EBP50* mRNA was detected in EJp21 senescent cells but not in HT1080-p21-9. However, the error bars for *EBP50* expression in EJp21 were quite big, which makes the results less reliable. In turn, there were no changes of EBP50 protein in both cell lines after senescence induction. Analysis of PLD3 expression revealed no changes in in *PLD3* mRNA in senescent EJp21 cells. In HT0180-p21-9 there was increase of *PLD3* mRNA. Importantly, the differences observed in the markers expression might be due to the different origins of the system used. EJp21 is a

human bladder carcinoma cell line with a p53-null mutation, and HT1080-p21-9 human fibrosarcoma cell line with WT p53. Cell-specific factors could be important to favour different cell fates after p21 upregulation. It is possible that cell origin could determine the markers general sensitivity to p21.

In summary, data indicates that none of tested proteins is a suitable marker of cellular senescence in tested cell lines. Analysis should be repeated to confirm possible patterns of expression. Moreover, further validations with wider range of senescence models should be performed to confirm these findings. It is also important to mention that cell lines used in this study are the models of genetically induced senescence. In the future, additional test should involve usage of senescence models that represent more natural conditions.

Table 6.1. Summary of VPS26A, EBP50 and PLD3 expression profiles in tested cell lines.

Table represents the summary of the expression levels of VPS26A, EBP50 and PLD3 at both gene (G) and protein (P) level. The expression of the markers at the gene level was measured using RT-qPCR and at protein level using Western blot (***–:*** *no change;* ***+:*** *upregulation, ?-unclear)*

Cell line	Marker					
	VPS26A		EBP50		PLD3	
	G	P	G	P	G	P
EJp53	-	?	-	-	-	-
EJp21	-	-	+	-	+	-
EJp16	-	-	-	-	-	-
HT1080-p21-9	-	-	-	-	+	?

6.2 Analysis of VPS26A, EBP50 and PLD3 in mice and human tissues

Cellular senescence has been identified as one of the hallmarks of aging (Lopez-Otin et al., 2013). The number of senescent cells increase with age in variety of different tissues. Moreover, abundance of senescent cells has been found at sites of age-related pathologies like renal, cardiac, lung and liver fibrosis (Munoz-Espin and Serrano, 2014, Schafer et al., 2017b, Valentijn et al., 2018). The proper identification of senescent cells is crucial for future therapeutic strategies in amelioration of negative effects of aging and there is an urgent need for recognition of novel markers of cellular senescence. For these reasons, the expression of VPS26A, EBP50 and PLD3 were compared in mice tissues of different age (5 animals per group) to explore if their expression can be linked with biological aging.

6.2.1 Analysis of markers basal expression in human tissues using online databases

At first, the basal expression of VPS26A, EBP50 and PLD3 was screened at the gene and protein level in number of different tissues using the online software **https://gtexportal.org/** and **https://proteinatlas.org/** (Uhlén et al., 2015). Analysis of the markers gene expression were narrowed down to organs commonly impaired by aging, such as brain, heart, kidney and liver. Those tissues were picked by us for further analysis (**Figure 6.3, Figure 6.5, Figure 6.7**). Results of gene expression in the databases revealed some basal expression of novel markers in all of the four tissues. The GTEX database revealed the highest expression of *VPS26A* in brain cerebellum (**Figure 6.3B**), EBP50 *(SLC9A3R1)* in small intestine, liver and kidney cortex (**Figure 6.5B**) and *PLD3* in pituitary and brain (**Figure 6.7B**). The screen of the protein expression of the markers revealed similar findings. According to proteinatlas.org, the expression of VPS26A were scored as medium in the brain cerebellum and cortex and high expression was identified for instance in the small intestine, colon, ovary, spleen and lymph nodes. Screen of the basal protein level of EBP50 also confirmed analysis of the gene expression with medium score in liver and high expression in small intestine, kidney, nasopharynx. High expression of PLD3 protein was shown in the brain, especially in cerebral cortex, lung

and spleen. High expression of VPS26A in brain is consistent with previous reports of VPS26A abundance in mouse brains and in different neuronal cell lines (Bugarcic et al., 2011, Muhammad et al., 2008, Cruchaga et al., 2014).

Interestingly, although the basal gene level of all the markers, VPS26A, EBP50 and PLD3 was identified in heart, that was not confirmed by proteinatlas.org analysis of VPS26A and EBP50 protein level. Only PLD3 were assigned a medium expression score in heart. However, when taking a closer look at the GTEX analysis of the *VPS26A* and *EBP50* gene expressions it can be seen that their expression in heart is low (<50 TPM) when compared with other organs, like brain. This might reflect low or undetectable level of VPS26A and EBP50 proteins in the heart according to proteinatlas.org database.

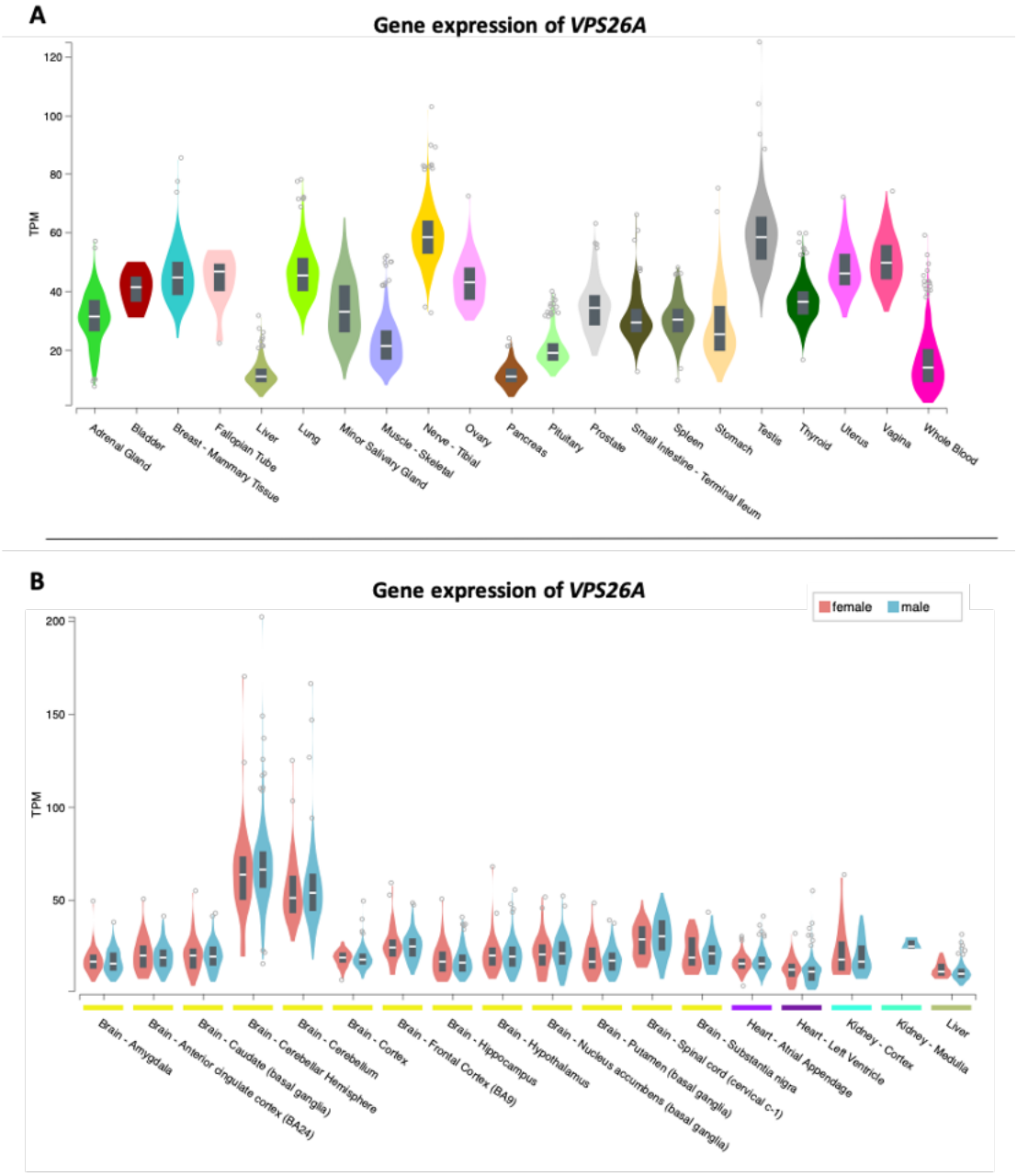

Figure 6.3. Gene expression of VPS26A in different tissues.

[A] Screen of the gene expression of VPS26A across human tissues performed using https://gtexportal.org/. Graphs show abundance of gene in each tissue using transcripts per million value (TPM) as the sum of the TPM values of all its protein-coding transcripts. The threshold level to detect presence of a transcript for a particular gene was set to ≥ 1 TPM. [B] Gtex database results of VPS26A gene expression in brain, heart, kidney and liver including sex difference. Box plots present median and 25th and 75th percentiles. Points are displayed as outliers if they are above or below 1.5 times the interquartile range.

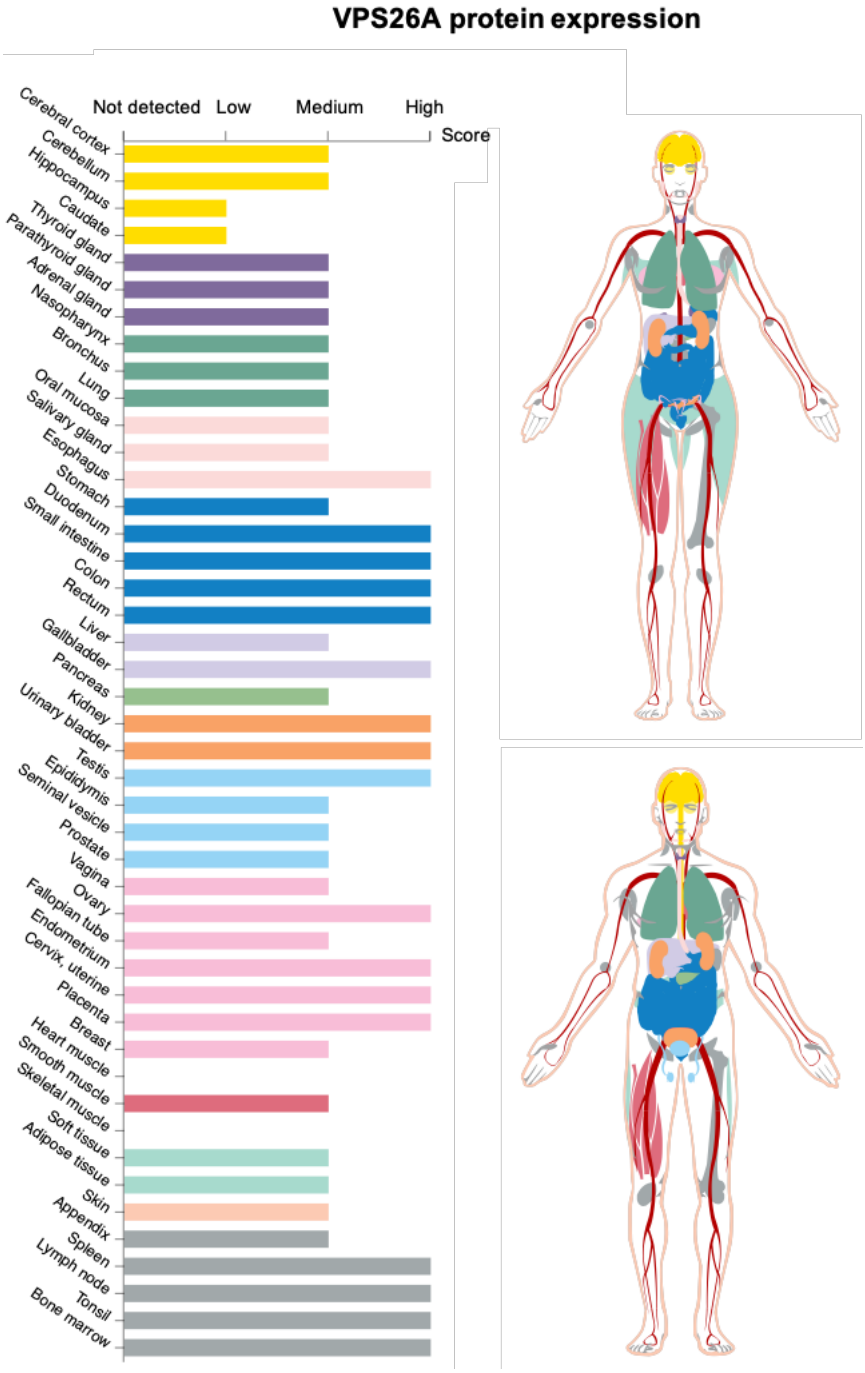

Figure 6.4. Screen of the VPS26A protein expression in different tissues.

Analysis of the VPS26A protein expression shown for 44 tissues using the The Human Protein Atlas version 19.3 and Ensembl version 92.38 database. Expression profiles for proteins in human tissues were scored based on immunohistochemisty using tissue micro arrays. Graphs obtained from proteinatlas.org.

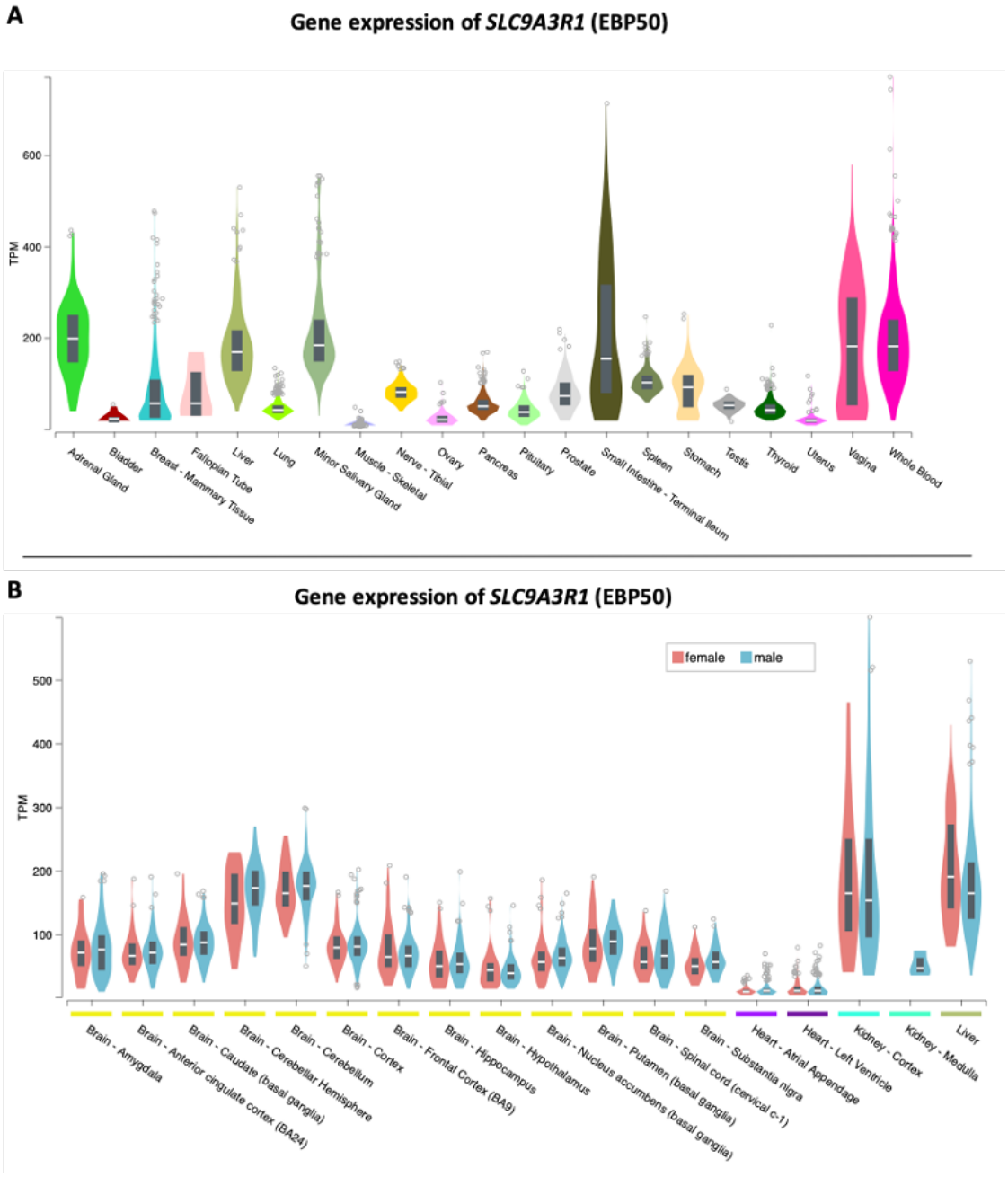

Figure 6.5. Gene expression of EBP50 in different tissues

[A] Screen of the gene expression of SLC9A3R1 (EBP50) across human tissues performed using https://gtexportal.org/. Graphs show abundance of gene in each tissue using transcripts per million value (TPM) as the sum of the TPM values of all its protein-coding transcripts. The threshold level to detect presence of a transcript for a particular gene was set to ≥ 1 TPM. [B] Gtex database results of EBP50 gene expression in brain, heart, kidney and liver including sex differences. Box plots present median and 25th and 75th percentiles. Points are displayed as outliers if they are above or below 1.5 times the interquartile range

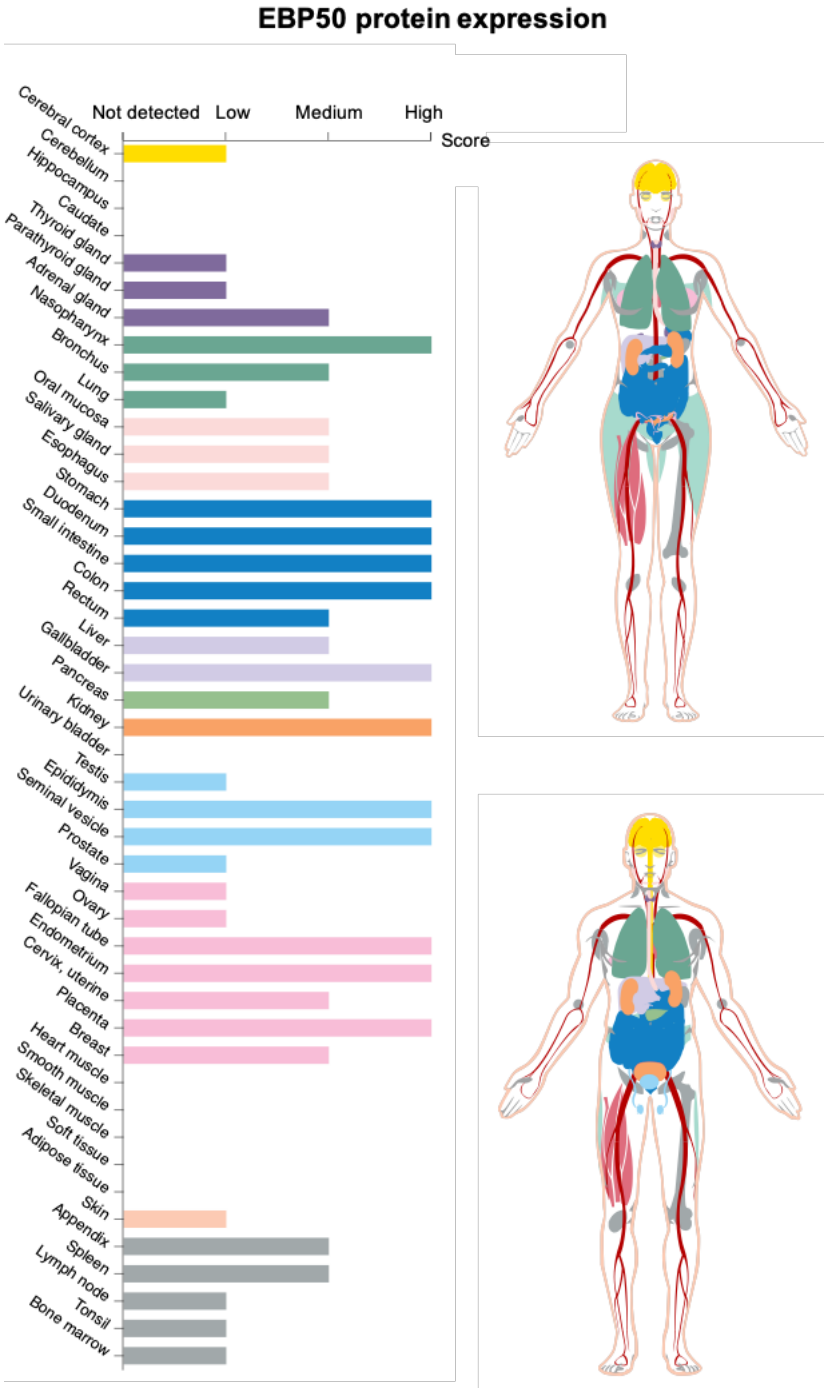

Figure 6.6. Screen of the EBP50 protein expression in different tissues.

Analysis of the EBP50 protein expression shown for 44 tissues using the The Human Protein Atlas version 19.3 and Ensembl version 92.38 database. Expression profiles for proteins in human tissues were scored based on immunohistochemisty using tissue micro arrays. Graphs obtained from proteinatlas.org.

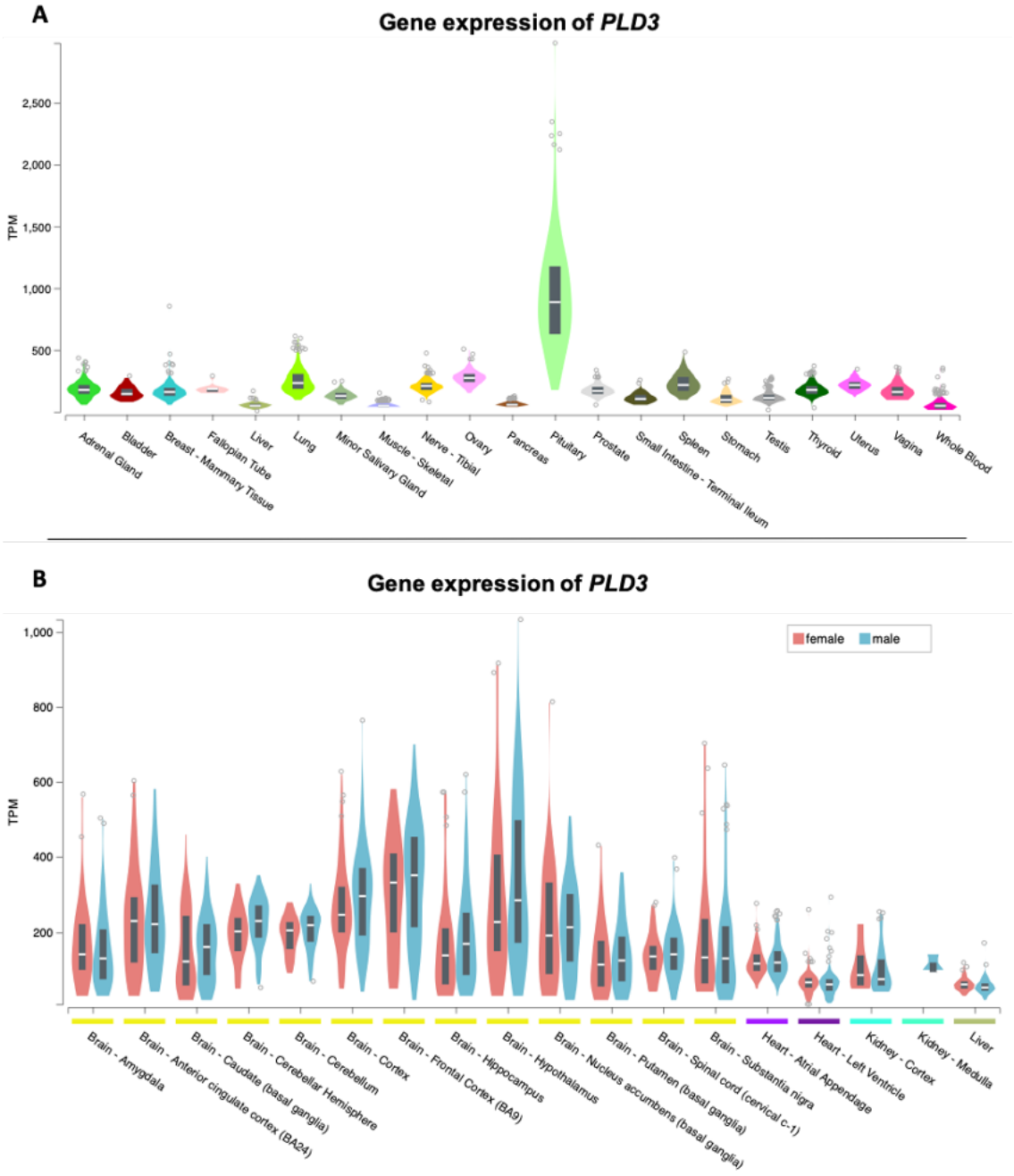

Figure 6.7. Gene expression of PLD3 in different tissues.

[A] Screen of the gene expression of PLD3 across human tissues performed using https://gtexportal.org/. Graphs show abundance of gene in each tissue using transcripts per million value (TPM) as the sum of the TPM values of all its protein-coding transcripts. The threshold level to detect presence of a transcript for a particular gene was set to ≥ 1 TPM. [B] Gtex database results of PLD3 gene expression in brain, heart, kidney and liver including sex differences. Box plots present median and 25th and 75th percentiles. Points are displayed as outliers if they are above or below 1.5 times the interquartile range

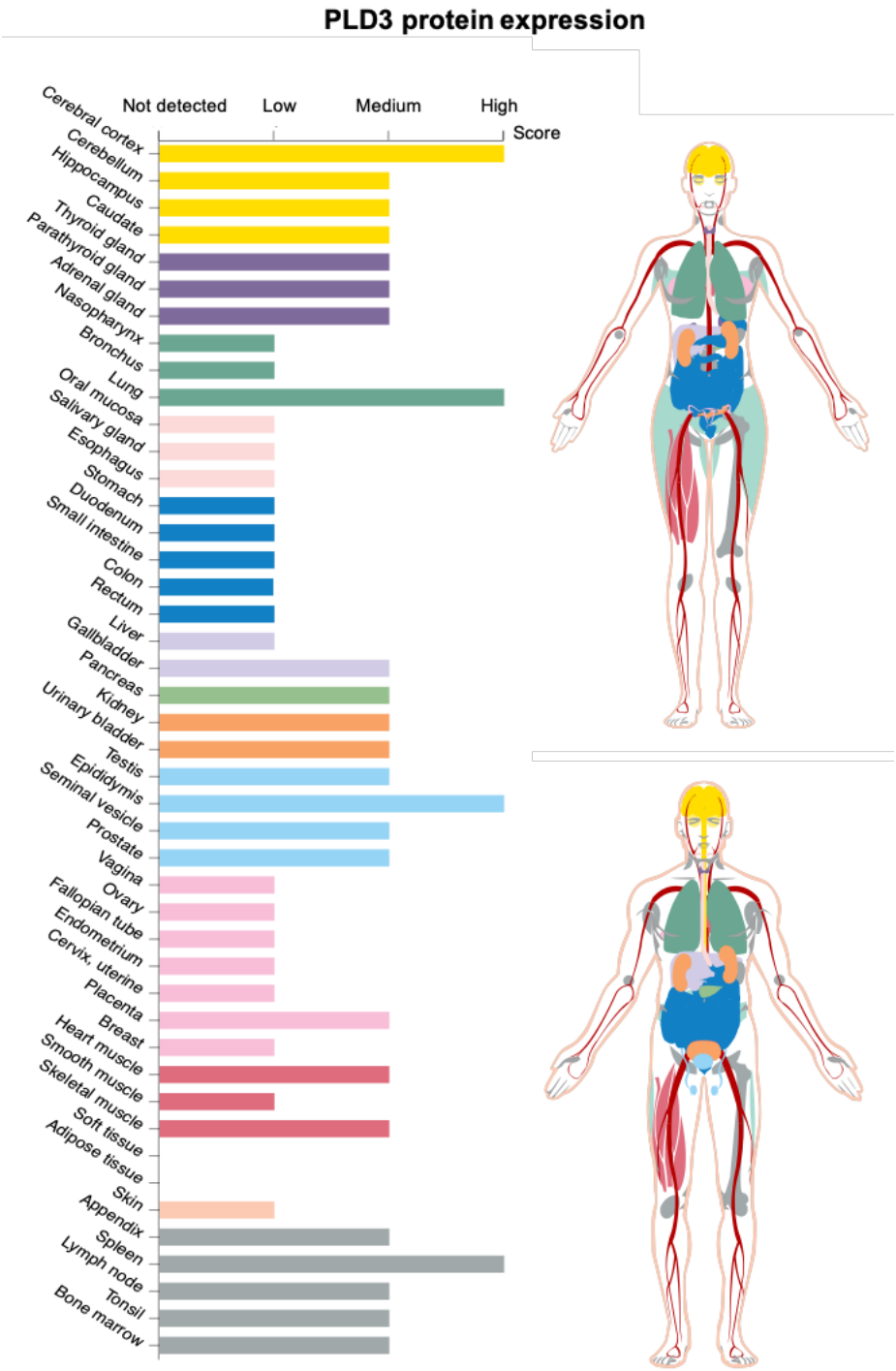

Figure 6.8. Screen of the PLD3 protein expression in different tissues.

Analysis of the PLD3 protein expression shown for 44 tissues using the The Human Protein Atlas version 19.3 and Ensembl version 92.38 database. Expression profiles for proteins in human tissues were scored based on immunohistochemistry using tissue micro arrays. Graphs obtained from proteinatlas.org.

3.1.1. Expression profiles of novel senescence markers in the mice tissues of different ages

Next, to investigate if the expression of markers is changing with age, tissues such as heart, brain and liver were isolated from C57/BL6 wild type animals from a mixed-gender population. The animals were firstly classified into two groups: young and old. The young group consist of maximum 3 months old animals and the old group contained animals were approximately 2-years old (+/- one month). The expression of the markers, VPS26A, EBP50 and PLD3 was compared at gene and protein level.

6.2.1.1 Aging brain: expression profiles of VPS26A, EBP50 and PLD3

At first, the total RNA was extracted from frozen tissues and subjected for RT-qPCR. Whole brain lysates were prepared from fresh tissues and analysed using Western blot. Data were normalized against young counterparts (control) and p16 *(CDKN2A)*, was used as positive control for ageing (**Figure 6.9A**).

VPS26A was slightly decreased at gene level in the aging brain when compared with young controls. Decrease of VPS26A was also observed at the protein level (**Figure 6.9**), although due to low quality of blot that cannot be assumed with certainty. To confirm VPS26A expression, this experiment should be repeated.

EBP50 mRNA analysis revealed significant downregulation in brains of older animals when compared with young, although the EBP50 protein remained unchanged between tested conditions. PLD3 remained unchanged at both protein and gene level **(Figure 6.9B**). Of note, previous reports showed that *PLD3* mRNA was lower in brains of patients suffering for AD than in healthy controls (Blanco-Luquin et al., 2018). However, AD is one of age-related diseases and there might be a chance that tested mice were not exhibiting similar phenotype as Alzheimer diseases or the effect was not strong enough to affect PLD3 expression.

Moreover, the p16 protein level used as positive control did not change with age in the tested individuals (**Figure 6.9**), despite the significant upregulation of its mRNA level in the old group of mice. In summary, validation of the markers in the mice aging brain

revealed no changes of EBP50 and PLD3 with age. Additionally, there was no changes in the positive control. Due to the low number of individuals per group, data are vague. To solidify the findings a larger cohort should be analysed together with region specific Immunohistochemistry.

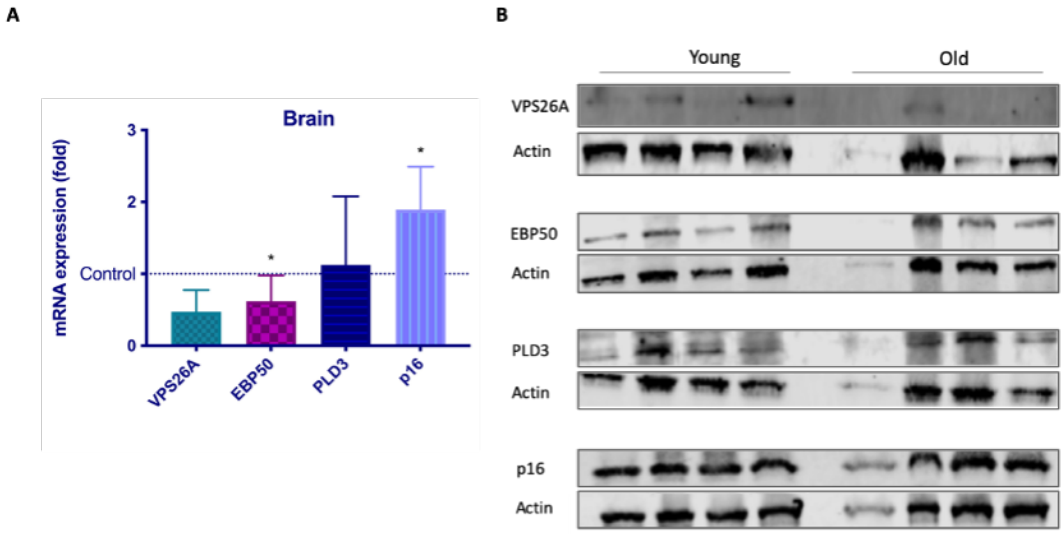

Figure 6.9. Biochemistry analysis of aging brain.

*[A] RT-qPCR results showing fold change mRNA expression of novel markers of the total RNA extracted from brain samples isolated from young (3 months) and old (24 months) wild-type mice (n= 5 animals per group). Data were standardised to reference housekeeping gene GAPDH and normalised against young controls. Bars show mean values and error bars represents standard deviation. Statistical significance determined using unpaired t-test, (ns: not-significant, * p<0.05, ** p<0.01). [B] Representative Western blot of the whole brain lysates isolated from the same animals as in [A] showing VPS26A, PLD3, EBP50, p16 and β-actin as a loading control (50 µg of the protein loaded). n=4 animals per group.*

6.2.1.2 Aging heart: expression profiles of VPS26A, EBP50 and PLD3

Next, the RT-qPCR and WB were performed on aging hearts dissected from the same animals as in 6.2.1.1. Results revealed no changes in VPS26A gene level, and we failed to detect VPS26A protein using western blot. EBP50 level was similar between young and old animals at gene (**Figure 6.10A**) and protein level (**Figure 6.10B**). However, there was a 2-fold upregulation of *PLD3* gene in the old animals compared to the young cohort. PLD3 protein expression analysis was unclear due to low quality of blot (**Figure 6.10**). Moreover, qPCR analysis revealed decreased expression of the p16 gene in the aging hearts of tested animals, and the protein expression of p16 is unclear due to unequal loading (**Figure 6.10**). The difference between gene and protein level might be due to technical mistakes, such as a low concentration of extracted RNA, unequal loading, poor quality of extracted proteins.

According to proteinatlas.org database, the VPS26A and EBP50 were below detectable level in heart. Indeed, we were unable to detect VPS26A level in our model, wherein we could detect EBP50 using commercially available antibodies. The difference might be due to different methods and antibodies used. Proteinatlas.org data were based on the immunohistochemistry analysis of human samples, and we used western blot for detection of our markers. Further, proteinatlas.org screen concentrated on human tissues, while our study focused on mice tissues.

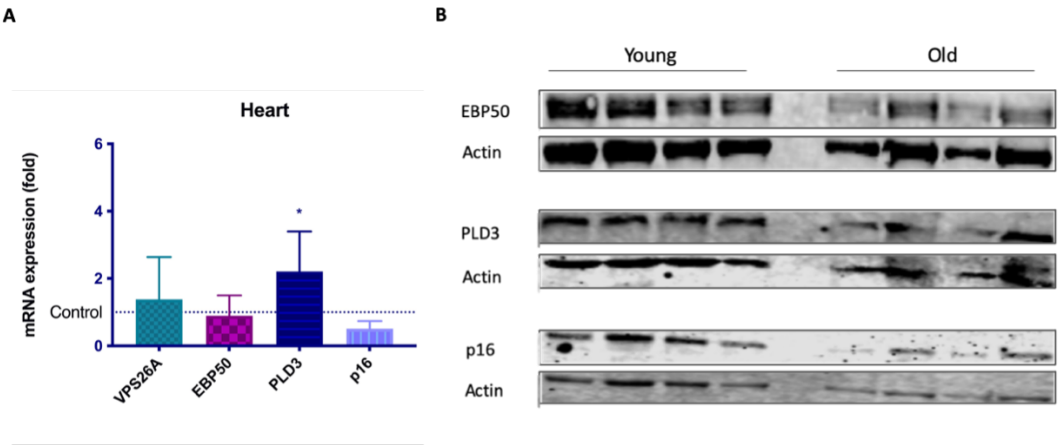

Figure 6.10. Expression of novel markers in the aging heart.

[A] RT-qPCR results showing fold change mRNA expression of novel markers of the total RNA extracted from heart samples isolated from young (3 months) and old (24 months) wild-type mice (n=5 animals per group). Data were standardised to reference housekeeping gene GAPDH and normalised against young controls. Bars show mean values and error bars represents standard deviation. Statistical significance between young and old animals determined using unpaired t-test ($p<0.05$). [B] Representative Western blot of the whole brain lysates isolated from the same animals as in [A] showing EBP50, PLD3, p16 and β-actin (100 μg of the protein loaded) n=4 animals per group.*

6.2.1.3 Aging liver: expression profiles of VPS26A, EBP50 and PLD3

The analysis of the aging liver showed upregulation of the *VPS26A* mRNA level, however no changes in its protein expression (**Figure 6.11**). Moreover, data revealed an increase of PLD3 protein in some, but not all tested animals, despite no changes in the *PLD3* gene level (**Figure 6.11A**). Further, PLD3 data corresponded with the upregulation of positive control, p16 which was higher in old animals at both gene and protein levels.
In turn, EBP50 remained unchanged between tested animals at gene level and due to low quality of WB its protein level was unclear. Of note, previous reports showed that EBP50 is strongly upregulated in liver cancer (Georgescu et al., 2008). It is important to mention that EBP50 function in cancer seems to be closely associated with its cellular localization. Clapéron et al 2012 showed that in 21% of tested cholagiocarinomas and also in normal biliary epithelium, EBP50 was localized at the plasma membrane, whereas in 66% of tumour EBP50 was concentrated in the cytoplasm (Clapéron et al., 2012). Similar changes in EBP50 localization have been reported for other human cancers, such as hepatocellular carcinoma, breast, brain and colon (Stemmer-Rachamimov et al., 2001, Shibata et al., 2003, Georgescu et al., 2008, Hayashi et al., 2010). Therefore, it has been assumed that EBP50 appears to behave as a tumour suppressor when located at the plasma membrane and acts as oncogene when shifts to the cytoplasm. Therefore, it will be extremely interesting to investigate further exact cellular localization of EBP50 in aging tissues.

In summary, there was no difference in protein level of VPS26A in young and old mice in the tested tissues (**Table 6.2**), and PLD3 analysis revealed upregulation in liver, although not in all tested animals.

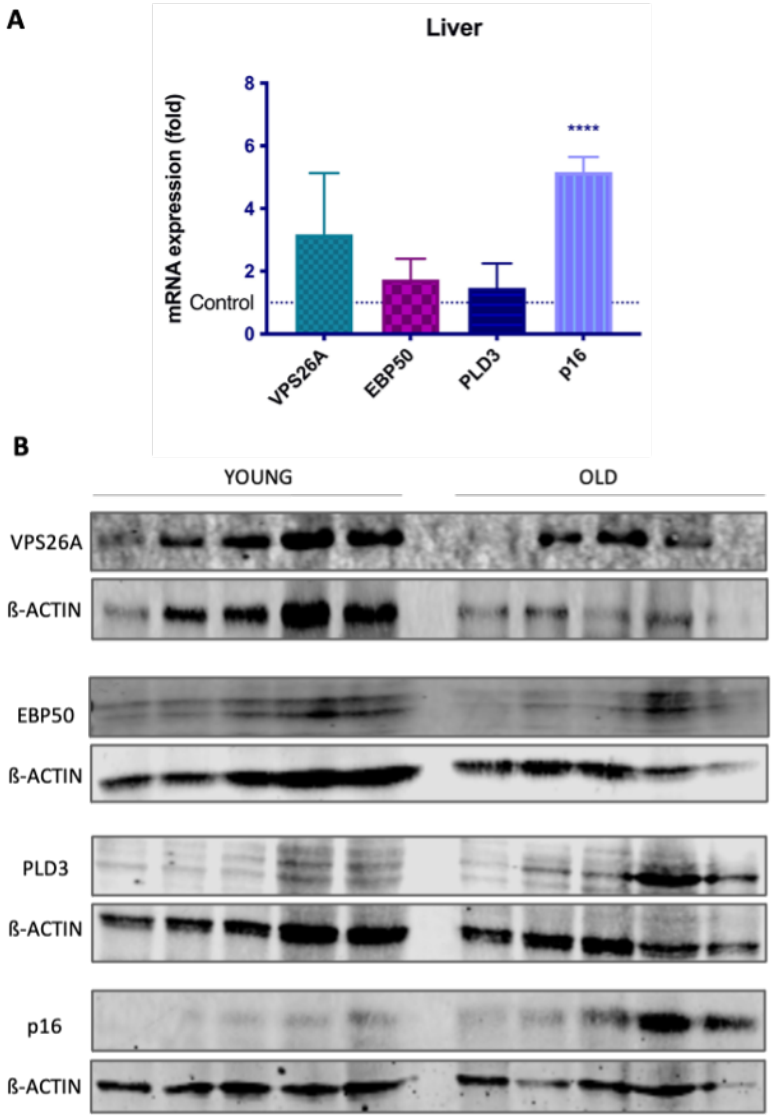

Figure 6.11. VPS26A, PLD3 and EBP50 expression profiles in aging liver.

*[A] RT-qPCR results showing fold change mRNA expression of novel markers of the total RNA extracted from liver samples isolated from young (3 months) and old (24 months) wild-type mice (n=5 animals per group). Data were standardised to reference housekeeping gene GAPDH and normalised against young controls. Bars show mean values and error bars represents standard deviation. Statistical significance determined using unpaired t-test, (ns: not-significant, * p<0.05, ** p<0.01, *** p<0.001, **** p<0.0001). [B] Western blot of the whole brain lysates isolated from the same animals as in [A] showing VPS26A, PLD3, EBP50, p16 and β-actin (50 µg of the protein loaded), n=5 animals per group.*

Taken together, *in vitro* analysis of senescent models showed no changes in PLD3 expression level, however, analysis of aging tissues revealed PLD3 tissue-specific increase when compared to young. Additionally, the analysis of the PLD protein in the aging liver, revealed a similar pattern to the corresponding positive control used, p16. Although, these results are preliminary and more animals should be added into the analysis, they might indicate a diagnostic potential of PLD3 for detection of senescent cells in the aging liver. Similar evaluations should be performed using tissues from human origin and analysis should focus on organ-specific localization of PLD3.

Table 6.2. Summary of VPS26A, EBP50, PLD3 and p16 expression profiles in the mice tissues of different ages.

Table represents the summary of the expression levels of VPS26A, EBP50, PLD3 and p16 at both gene (G) and protein (P) level. The expression of the markers at the gene level was measured using RT-qPCR and at protein level using Western blot. - = no change (FC); + = upregulation; ? = vague/unclear.

Tissue	Marker							
	VPS26A		EBP50		PLD3		p16	
	G	P	G	P	G	P	G	P
Brain	-	?	-	-	-	-	+	-
Heart	-	-	-	-	+	?	-	?
Liver	-	-	-	?	-	+	+	+

6.3 Novel markers and Idiopathic Pulmonary Fibrosis

6.3.1.1 Expression of novel senescence markers in IPF fibroblasts

In the previous sections, the expression of proposed markers of senescence was assessed in mouse aged tissues to verify their diagnostic potential in senescence and ageing. Apart from ageing, senescent cells have been shown to increase in pathologies such as fibrosis (Munoz-Espin and Serrano, 2014, He and Sharpless, 2017). In the current section, the expression of these markers was analysed in Idiopathic Pulmonary Fibrosis (IPF), a senescence-associated disease (Schafer et al., 2017b). The goal was to verify if novel markers can be used for identification, prognosis or as a target in diseases where senescence has a known involvement.

At first, the human samples were collected from **Dr. Katy Roach** from the University of Leicester, Department of Infection, Immunity and Inflammation. Collected samples were divided into two groups: fibroblasts from non-fibrotic controls (NFC) and fibroblasts from Idiopathic Pulmonary Fibrosis (IPF).

Next, increasing passages of NFC and IPF were used to compare expression profiles of novel markers in replicative senescence and in pathological condition of pulmonary fibrosis. Collected fibroblasts were isolated from 4 different patients, 2 controls and 2 IPF. On the day of arrival, fibroblasts were at the following passages (P) NFC1 P:7, NFC2 and IPF1 P:8 and IPF 2 P:6. Cells were cultured in 60mm dishes and passaged when they reached about 70% confluence. Cell counting experiment started when all cells reached P:10. Two of the cell lines, NFC2 and IPF2 were gradually dying with each passage until the passage P:12 after which, rapid decline was observed **(Figure 6.12**). Therefore, NFC2 and IPF2 were excluded from further analysis. NFC1 and IPF1 were chosen for further characteristics, wherein the NFC1 fibroblasts remained viable longer then IPF1.

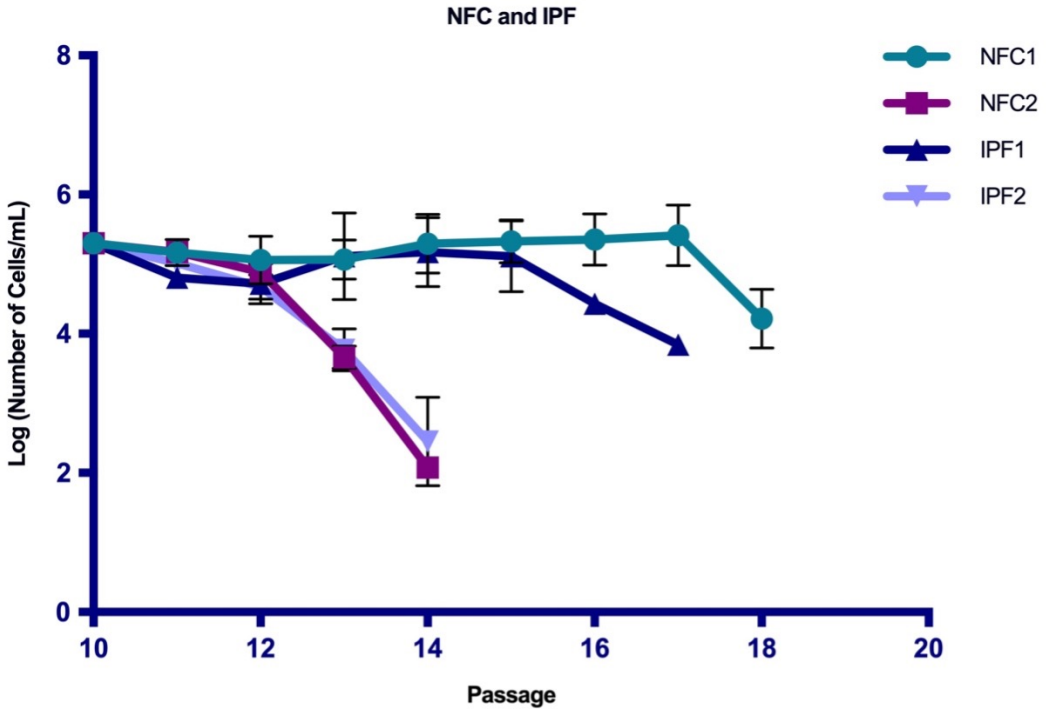

Figure 6.12. Growth curve of NFC and IPF fibroblasts.

Fibroblasts were subjected for prolonged culture in order to induce replicative cellular senescence. Cells were collected from two different patients suffering from Idiopathic Pulmonary Fibrosis (IPF1 and IPF2) and non-fibrotic control isolated from another two different individuals (NFC1 and NFC2) The cells were counted using the T20 automated cell counter to determine their growth curve. Graph represents the logarithm of the number of cells against the passage. Each dot represents mean value and error bars shows standard deviation. Experiment was performed twice each time using two technical replicates.

Next, the expression profiles of already known senescence markers, p53, p21, p16 were compared between low and high passages. RT-qPCR analysis revealed changes in the mRNA expression of the markers. For NFC fibroblasts, the highest increase of *p53* mRNA was observed at the passage 17, when it crossed the two-fold threshold. Similarly, there was an increase of *p53* mRNA level in IPF fibroblasts in old passages, P:16 and P:17 (**Figure 6.13**). p21 mRNA analysis revealed a slight increase in the high passage of NFC (P:18) and IPF (P:16). The upregulation of p16 was observed only in NFC fibroblasts from P:13 till P:18, reaching three-fold increase. However, none of the markers indicated a statistically significant difference in expression between young and old passages.

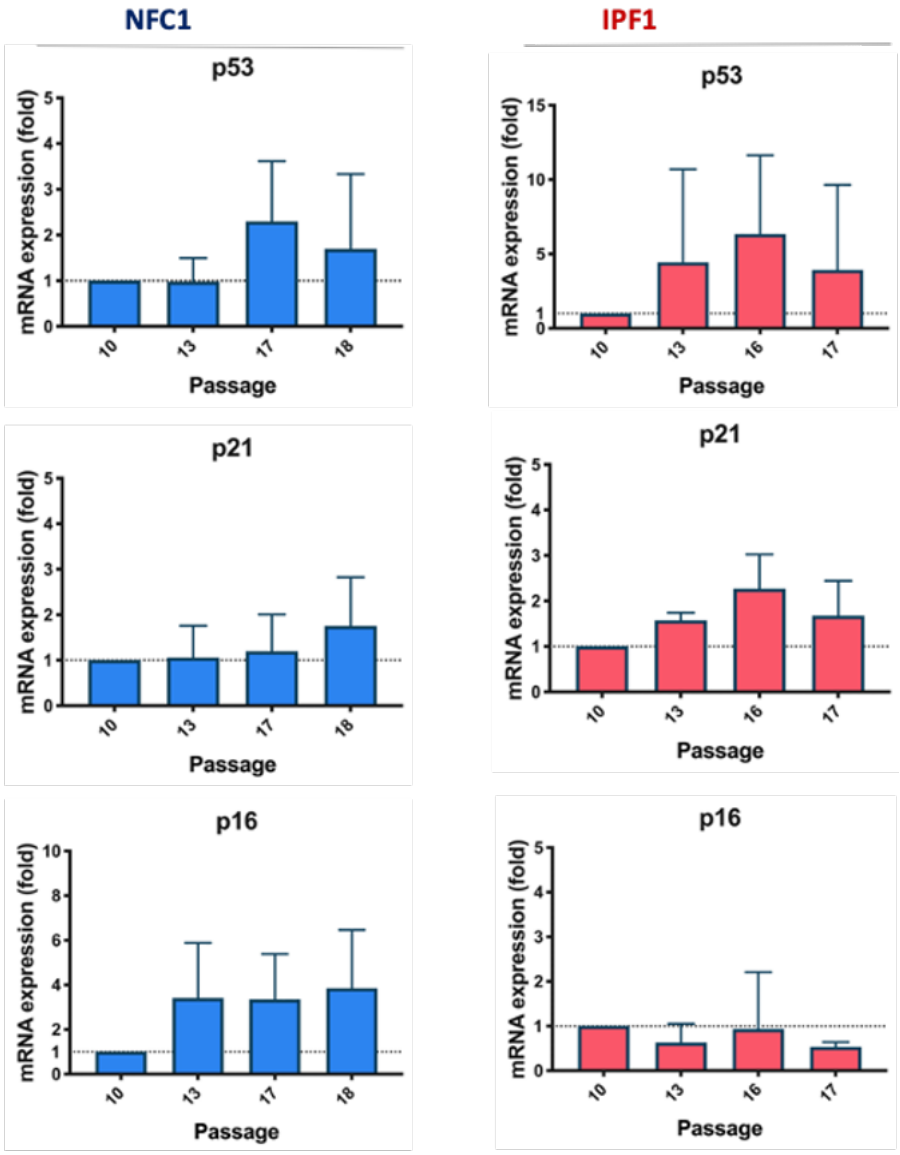

Figure 6.13. qPCR analysis of IPF fibroblasts.

Fibroblasts were subjected to prolonged culture in order to induce replicative cellular senescence. Cells were collected from a patient suffering from Idiopathic Pulmonary Fibrosis (IPF1) and non-fibrotic control (NFC1) and p53, p21 and p16 mRNA expression profiles were compared between increasing passages. Data were standardised to reference housekeeping gene GAPDH and normalized against the lowest available passage (P), P:10. Graphs present a mean value and error bars show standard deviation, n=2.

Despite of the vague results of mRNA expression, the Western blot analysis revealed significant changes in the expression profiles of senescence markers (**Figure 6.13**). There was a clear difference in p53 protein expression between NFC and IPF fibroblasts. More than 10-fold increase of p53 protein was detected at the old passages of NFC fibroblast, while there was only a slight change of p53 protein in IPF samples with less than two-fold increase (**Figure 6.14B**). Interestingly, opposite patterns were observed during p21 analysis. In NFC fibroblasts there was decrease of p21 protein level at the passage 12, 13 and 17 and more than two-fold change increase at P:18 when compared to the P:10. However, presumably due to the high error bars, the difference in p21 expression at P:18 was not significant. In the IPF fibroblasts, significant increase of p21 was observed at P:16. Analysis of p16 expression exposed a high level of p16 protein in NFC samples at the old passages, while in IPF there was smaller, however significant four-fold increase between low and high passage. Similar findings were observed when compared IL-1ß between NFC and IPF samples. IL-1 ß significantly increased in the highest passages of NFC and IPF fibroblasts. Western blot analysis revealed a similar trend of the senescence markers when compared across increasing passages. Analysis of tested passages displayed the highest expression of senescence markers at P:18 in NFC and P:16 of IPF fibroblasts. However, the robust express of majority of p53, p16 and IL-1ß in NFC samples, seems to suggest that control fibroblasts enter senescence faster than IPF.

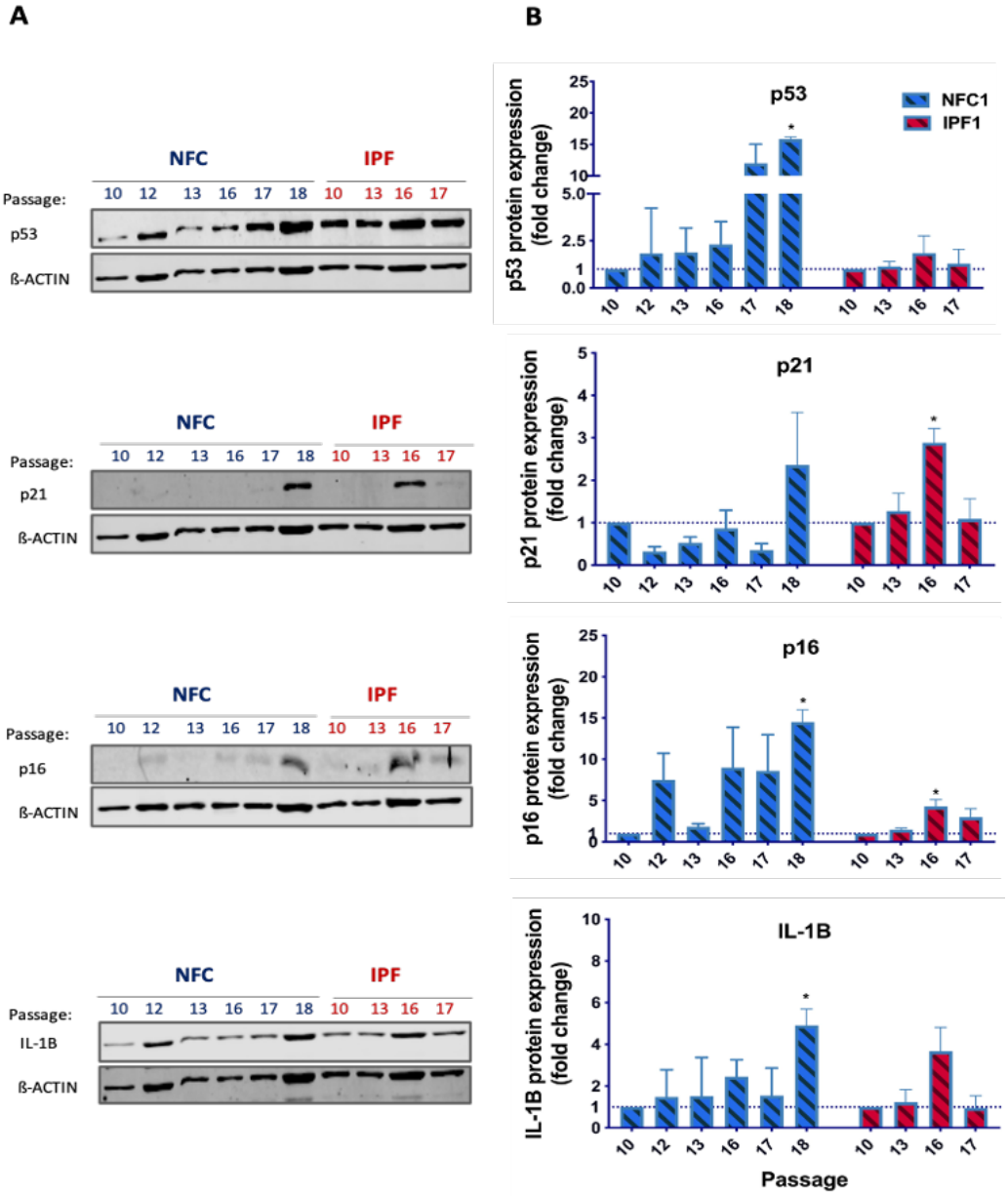

Figure 6.14. Western blot analysis of p53, p21, p16 and IL-1B in IPF fibroblasts.

Fibroblasts were subjected to prolonged culture in order to induce replicative cellular senescence. Cells were collected from a patient suffering from Idiopathic Pulmonary Fibrosis (IPF1) and non-fibrotic control (NFC1) and p53, p21, p16 and IL-1B protein levels were compared between increasing passages and representative Western blots are shown [A]. [B]. Data were standardised to reference housekeeping protein β-actin and normalized against the lowest available passage (P), P:10. Graphs present a mean value and error bars show standard deviation, n=2. See appendix ***Figure 9.7A*** *for further replicates. Statistical significance between each passage in NFC and IPF to corresponding passage 10 estimated used paired t-test (GraphPad Prism 8); * p<0.05, ** p<0.01, *** p<0.001, **** p<0.0001).*

The next step involved comparison of the VPS26A, EBP50 and PLD3 expression profiles across increasing passages of NFC1 and IPF1 (**Figure 6.12**). RT-qPCR analysis revealed more than 2-fold upregulation of *VPS26A* in NFC fibroblasts at P:13, 17 and 18 when compared with the youngest available passage (P:10). However, the difference was not statistically significant. Analysis of IPF samples revealed no changes in *VPS26A* mRNA level when compared to the P:10 (**Figure 6.15**). In NFC samples, the Western blot results were consistent with qPCR data. There was upregulation of VPS26A protein level in P:16 and P:18. However, the results for IPF contradicts the qPCR findings. While our data revealed no changes in mRNA level, there was a vast increase of VPS26A protein level reaching > 10-fold in old passages. The VPS26A data are consistent with the p53 upregulation in NFC samples and p21 in IPF fibroblasts (**Figure 6.14**). Further, there was slight albeit insignificant increase of EBP50 mRNA level in NFC old passages (P:13, P17, P:18). In IPF there was a decrease of EBP50 mRNA level in the P:16, while in the P:13 and P:17 the different was not considerable when compared with P:10. At the protein level, in NFC fibroblast there was a decrease of EBP50 at the P:12 and P:13, however in the oldest passages (P:16, 17 and 18) the EBP50 protein level was at comparable level to the P:10. In the IPF samples, the EBP50 level was decreasing with a peak at P:13. However, in P:16 and P:17 there was only a gentle reduction in EBP50 protein level when compared with P:10 of IPF fibroblasts (**Figure 6.16B**). The mRNA expression profiles of *PLD3* were similar in both NFC and IPF fibroblasts. There was a slight increase of *PLD3* in NFC P:13 and IPF P:13 reaching two-fold in NFC samples. However, in the old passages, the *PLD3* mRNA remained at the similar level as in the young passage. At the protein level, there was no significant difference in PLD3 expression when compared with young passages in both, NFC and IPF samples (**Figure 6.16B**). Taken together, there is no relation between the number of passages and the expression level of PLD3 and EBP50 neither in NFC nor IPF samples. However, VPS26A showed a significant upregulation in the older passages when compared to the young. In NFC fibroblasts VPS26A expression pattern corresponded to expression profiles of positive controls (p53, p21 and p16 and IL-1ß). There was a 5-fold increase of VPS26A at P:18 in NFC samples, while expression of positive controls also was the highest in the same passage. Interestingly, in IPF samples a robust upregulation of VPS26A protein level was observed

at the later passages (P:16-17) reaching more than a ten fold increase compared to IPF P:10. However, the increase in positive controls reached a maximum at P:16 then decreases at P:17. Therefore, it is unclear if VPS26A increase is related to establishment of senescence or pathological condition of IPF and further experiments are essential to determine potential role of VPS26A in IPF.

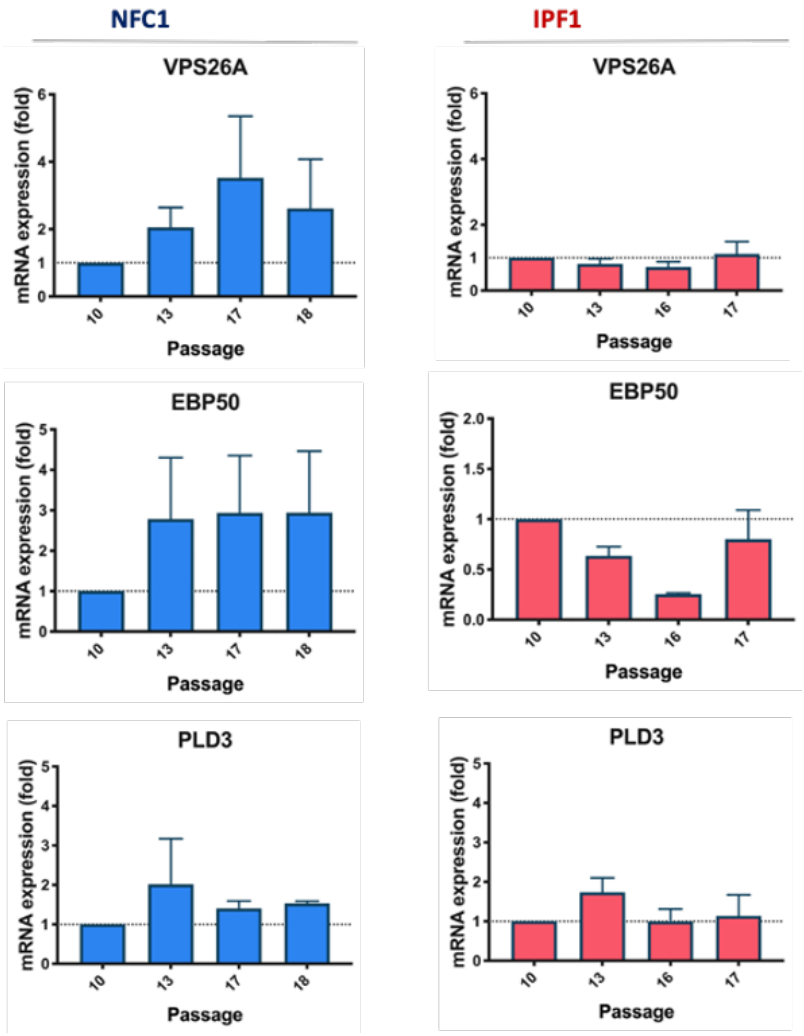

Figure 6.15. qPCR analysis of VPS26A, EBP50 and PLD3 in IPF fibroblasts

Fibroblasts were subjected to prolonged culture in order to induce replicative cellular senescence. Cells were collected from a patient suffering from Idiopathic Pulmonary Fibrosis (IPF1) and non-fibrotic control (NFC1) and VPS26A, EBP50 and PLD3 mRNA expression profiles were compared between increasing passages. Data were standardised to reference housekeeping gene GAPDH and normalized against the lowest available passage (P), P: 10. Graphs present a mean value and error bars show standard deviation, n=2.

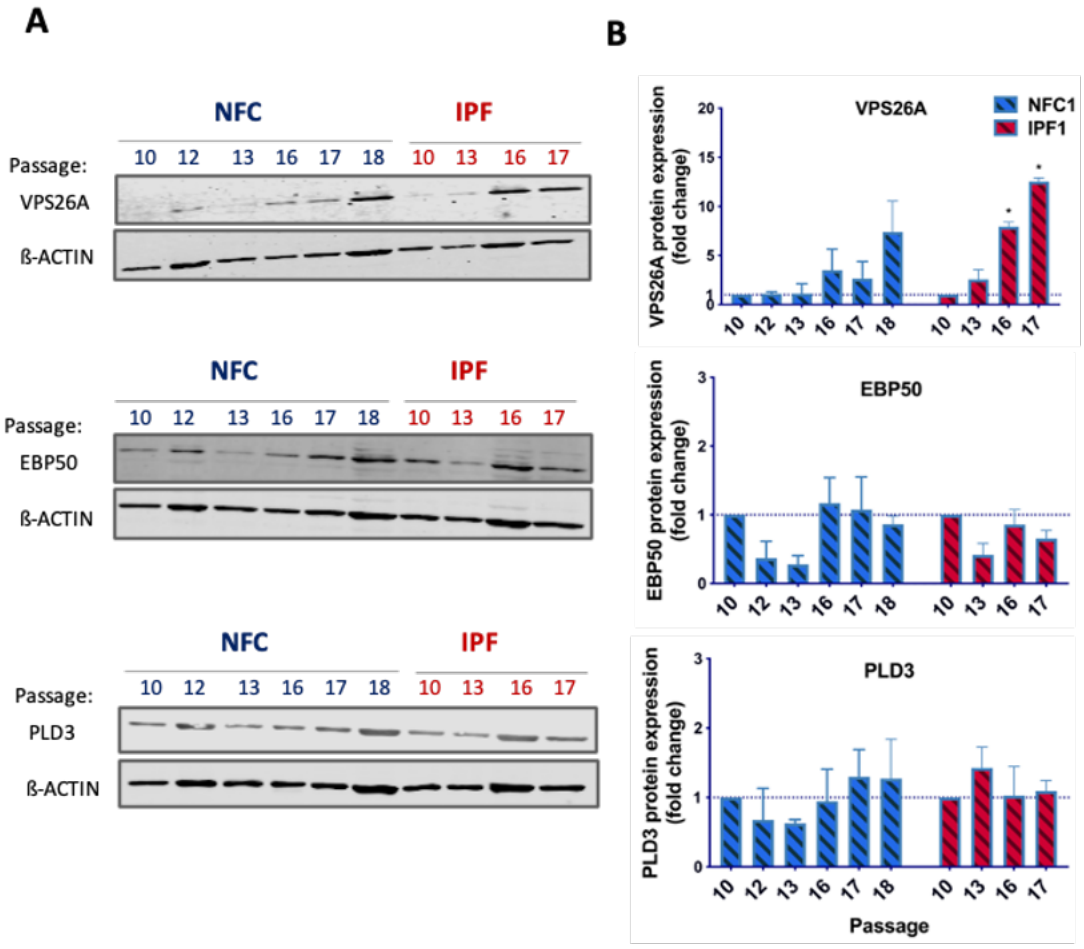

Figure 6.16. Western blot analysis of VPS26A, EBP50 and PLD3 in IPF fibroblasts

Fibroblasts were subjected to prolonged culture in order to induce replicative cellular senescence. Cells were collected from a patient suffering from Idiopathic Pulmonary Fibrosis (IPF1) and non-fibrotic control (NFC1) and VPS26A, EBP50 and PLD3 protein levels were compared between increasing passages and representative Western blots are shown [A]. [B] Data were standardised to reference housekeeping protein β-actin and normalized against the lowest available passage (P), P:10. Graphs present a mean value and error bars show standard deviation, n=2. See appendix ***Figure 9.7B*** *for further replicates Statistical significance estimated used paired t-test (GraphPad Prism 8); * p<0.05, ** p<0.01, *** p<0.001, **** p<0.0001).*

Comparing expression profiles of senescence markers between NFC and IPF fibroblasts it can be seen that the increased protein expression of p53 was only observed in the old passages of the NFC fibroblasts, while in IPF samples it remained unchanged. The expression of p53 downstream targets also depended on the cell line. There was upregulation of p21 level only in the oldest NFC fibroblasts passages tested (P:18). However, in IPF samples the increase was more decent and occurred earlier (P:16). In turn, the expression of p16 was more considerable in NFC fibroblasts in the old passages (≥P:15), while in IPF the increase was minor however significant (P:16). Activation of essential regulators of the cell-cycle, p21 and p16, which serve as markers of senescence, seems to be more definite in NFC fibroblasts than in IPF when subjected to prolonged culture. Also, the *in vitro* lifespan of NFC1 fibroblasts was longer than IPF1 (**Figure 6.12**). Taken into analysis the expression profiles of tested markers, we observed that there was a slight expression of EBP50 across increasing passages of NFC and IPF. PLD3 remained unchanged despite the changing conditions in both cell lines. Only VPS26A protein expression was consistent with the responses of previously established senescence markers. However, it is unclear if that relates to senescence or pathological conditions of IPF.

6.3.2 Expression of novel senescence markers in an *ex vivo* model of IPF

In the next step, our analysis focused on comparison of the expression profiles of novel senescence markers in another laboratory model of IPF, an *ex vivo* tissue model. *Ex vivo* models of human tissues have been already used in pharmacological studies with proven therapeutic relevance, for instance in human prostate cancer (Centenera et al., 2013). A key advantage of using human tissue over studies involving cell culture only is the maintenance of native architecture of the tissue with cell-cell signalling pathways that is lost during isolation of cells. Further, lack of cross-species heterogeneity in tissue responses to injury and drug intervention is another advantage of *ex vivo* tissues models. To analyse expression of our markers, samples were collected from the University of Leicester, Department of Infection, Immunity and Inflammation. Provided samples consisted of total RNA and tissue sections of an *ex vivo* model of human lung fibrogenesis described by (Roach et al., 2018). In this model, induction of fibrosis is triggered via treatment of the tissue sections with TGFβ1, which is one of the central pro-fibrotic growth factors driving lung parenchymal fibrosis (Goodwin and Jenkins, 2009). Together with other growth factors (Nishioka et al., 2013, Inoue et al., 1996), TGFβ1 is responsible for the excessive formation of fibroblast foci and deposition of extracellular matrix (ECM), which are the main characteristics of lung fibrosis (Meiners et al., 2015). The purpose of this study was to investigate if the TGFβ1 treatment would increase the number of senescent cells and investigate the response of VPS26A, EBP50 and PLD3 next to already established senescence markers and compare the responses of tested markers after the TGFβ1 treatment between different laboratory models of IPF, cell lines and *ex-vivo* tissues.

Before collection, healthy areas of human lung parenchyma from lung resection surgery were cut into approximately 2 mm^3 pieces and explanted tissues were cultured for 7 days in following conditions: TGFβ1 (10 ng/ml) or 0.1% DMSO as a negative control. On day 7 tissue was harvested. The expression of the markers in *ex vivo* tissue models were compared to their expression profiles in Idiopathic Pulmonary Fibrosis (IPF) and Non-fibrotic controls (NFC) fibroblasts (passage <4) previously treated with the same conditions. IPF and NFC fibroblasts were also provided by University of Leicester,

Department of Infection, Immunity and Inflammation. NFC and IPF fibroblasts were isolated from 12 patients (6 NFC and 6 IPF) and compared to *ex-vivo* samples collected from 4 different individuals. Firstly, collected total RNA was subjected to RT-PCR and obtained cDNA was used for assessment of the senescent markers' gene expression using qPCR. The panel of senescence markers tested included: p53 *(TP53),* p21 *(CDKN1A),* p16 *(CDKN2A), IL-6, IL-1β, VPS26A,* EBP50 *(SLC9A3R1)* and *PLD3.* p16 was undetectable in all of the samples. Contrary to the initial hypothesis, RT-qPCR results did not confirm overexpression of senescence markers after the treatment with TGFβ1 in either IPF fibroblasts or tissue sections. mRNA fold change was calculated relatively to untreated controls of each tested model. p53 significantly decreased after the incubation with TGFβ1 in NFC and *ex vivo* tissues samples. In IPF results were vague between tested individuals and did not indicate any specific trend (**Figure 6.17**). p21 was detectable only in fibroblasts and results showed no changes between the conditions in both IPF fibroblasts and controls. *IL-6* mRNA expression slightly decreased after the NFC treatment with pro-fibrotic TGFβ1. However, in IPF and *ex vivo* samples there was a slight upregulation, while the difference was significant only in IPF fibroblasts. Different pattern of expression was observed in another inflammation marker, IL-1β. *IL-1β* mRNA level significantly decreased after the treatment of NFC and IPF fibroblasts wherein significant increase was observed in *ex vivo* tissue samples. The upregulation of IL-1 β in *ex vivo* tissue IPF was in accordance with a previously reported analysis of the same IPF model (Roach et al., 2018). The *VPS26A* mRNA decreased after the incubation with TGFβ1 in all of the tested samples and NFC and *ex vivo* tissues the decrease was statistically significant (**Figure 6.18**). Expression of EBP50 remained unchanged in NFC samples, significantly increased in IPF fibroblasts and decreased in *ex vivo* tissue model. *PLD3* results were comparable across the samples. In each of the tested models PLD3 decreased, while similarly to *VSP26A* expression pattern, the difference was significant in NFC and *ex vivo* samples.

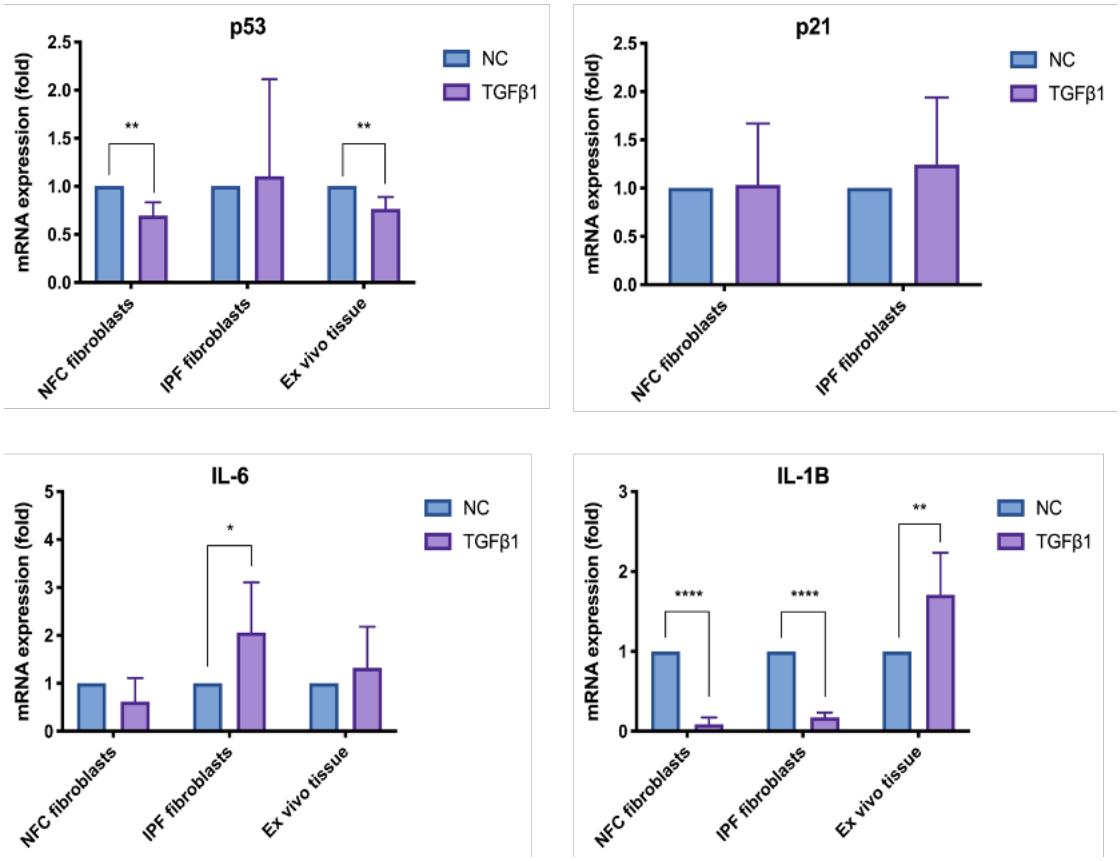

Figure 6.17. Analysis of senescence markers expression profiles between TGFβ1-driven models of IPF.

*Non fibrotic controls (NFC) and Idiopathic Pulmonary Fibrosis (IPF) fibroblasts (samples from 6 patients each group) and ex vivo tissues samples (4 patients) were provided by University of Leicester, Department of Infection, Immunity and Inflammation. Samples were treated for 7 days with 10 ng/ml TGFβ1 or 0.1% DMSO as negative control (NC). Graphs represent qPCR analysis of senescence markers gene expression. Data were standardised to reference housekeeping gene GAPDH and normalized against the untreated controls of each model separately. Graphs present a mean value and error bars show standard deviation, n=2. Statistical significance estimated between NC and TGFβ1 using unpaired t-test ns: not significant, * p<0.05, ** p<0.01, *** p<0.001, **** p<0.0001).*

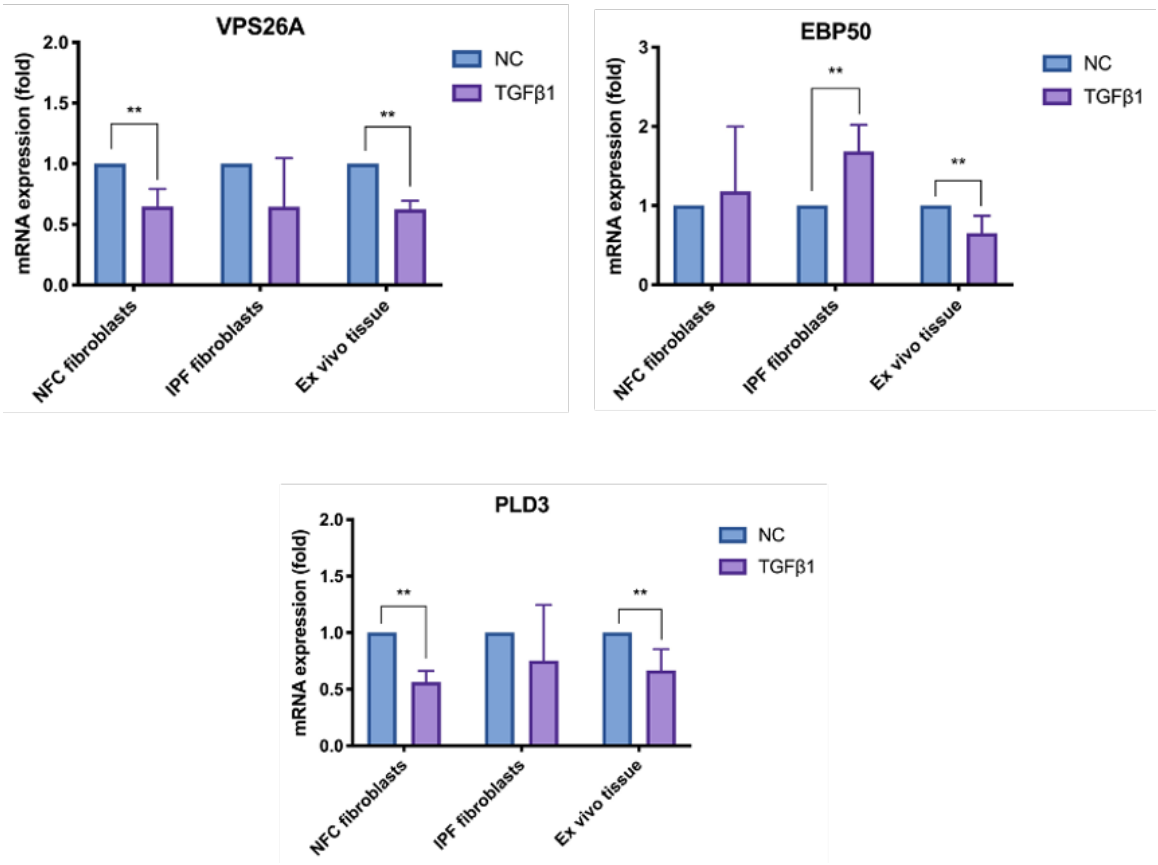

Figure 6.18. Expression profiles of novel senescence markers in TGFβ1-driven models of IPF.

*Non fibrotic controls (NFC) and Idiopathic Pulmonary Fibrosis (IPF) fibroblasts (samples from 6 patients each group) and ex vivo tissues samples (4 patients) were provided by University of Leicester, Department of Infection, Immunity and Inflammation. Samples were treated for 7 days with 10 ng/ml TGFβ1 or 0.1% DMSO as negative control (NC). Graphs represent qPCR analysis of senescence markers gene expression. Data were standardised to reference housekeeping gene GAPDH and normalized against the untreated controls of each model separately. Graphs present a mean value and error bars show standard deviation, n=2. Statistical significance estimated between NC and TGFβ1 using unpaired t-test ns: not significant, * p<0.05, ** p<0.01, *** p<0.001, **** p<0.0001).*

Analysis revealed decreased mRNA expression of the majority of senescence markers tested, thereby rejecting the initial hypothesis that treatment of pro-fibrotic TGFβ1 could accelerate the expression of senescence markers, like p53, p21 or IL-6. Due to the vague results of already established senescence markers, the analysis of VPS26A, EBP50 and PLD3 remains unclear. Albeit results indicated that TGFβ1 treatment had an impact on mRNA level of some of the tested markers, for others mRNA expression was significantly reduced (p53, IL-1β, VPS26A and PLD3). Moreover, there were differences in markers expression between tested models, for example TGFβ1 treatment decreased IL-1β expression in fibroblasts, while it increased in *ex vivo* tissues. The observed differences in the mRNA expression patterns between fibroblasts and *ex vivo* tissues could be linked with distinct baseline mRNA levels of tested markers and heterogenous tissues environment. Importantly, due to limited access to experimental material, the expression of the markers was tested only at the gene level, which might not represent the actual protein abundance in samples. For more precise analysis, first the protein expression profiles of senescence markers like p16, p53, p21, LAMIN B1 should be tested together with analysis of β-galactosidase activity and then analysis should include expression of novel markers. Further, low number of biological replicates was another limitation of the study and the differences between individuals have been reflected by high error bars.

The next step of analysis involved immunohistochemistry analysis of the tissue sections from TGFβ1-driven *ex vivo* model of IPF. Samples were provided by **Dr Katy Roach** from the Infection, immunity & Inflammation Department of University of Leicester, where explanted tissues were cultured for 7 days in following conditions: 0.1% DMSO as a negative control (NC), TGFβ1 (10 ng/ml) or combination of TGFβ1 (10ng/ml) with ICA-17043 (Senicapoc) (100nM). After 7 days of culture tissues were harvested.

Due to the low number of samples, study was limited to the detection of novel markers VPS26A and PLD3, wherein p16 expression was used as positive control. In this experiment, the *ex vivo* tissue samples were treated with ICA-17043 (Senicapoc), a Kca3.1 channel inhibitor which has shown to be effective in treating fibrosis (Schafer et al., 2017b, Roach et al., 2018). The tissues were treated with ICA-17043 in order to test

if the Senicapoc therapy affects expression of senescence markers and if its anti-fibrotic potential could be linked with the reduced onset of senescent cells in the tissue. 6 tissue sections from 2 patients were analysed. Results revealed upregulation of p16 after the TGFβ1 stimulation and downregulation after the treatment with ICA-17043 (**Figure 6.19**). However, there was no difference in VPS26A and PLD3 levels (**Figure 6.20**, **Figure 6.21**).

Presented results of p16 expression revealed a higher number of p16-positive cells after the treatment with TGFβ1, suggesting potential senescence induction, wherein the treatment with ICA-17043 reversed that phenotype. However, additional tests involving analysis of other senescence markers, such as p53, p21, SA-β-gal should be performed to confirm this preliminary finding. Analysis of VPS26A and PLD3 are not very clear due to the high background expression of antibodies. That might be due to technical mistakes and wrong antibody concentration. Therefore, this experiment should be repeated testing lower concentrations of antibodies and compared to the same concentration of isotype control.

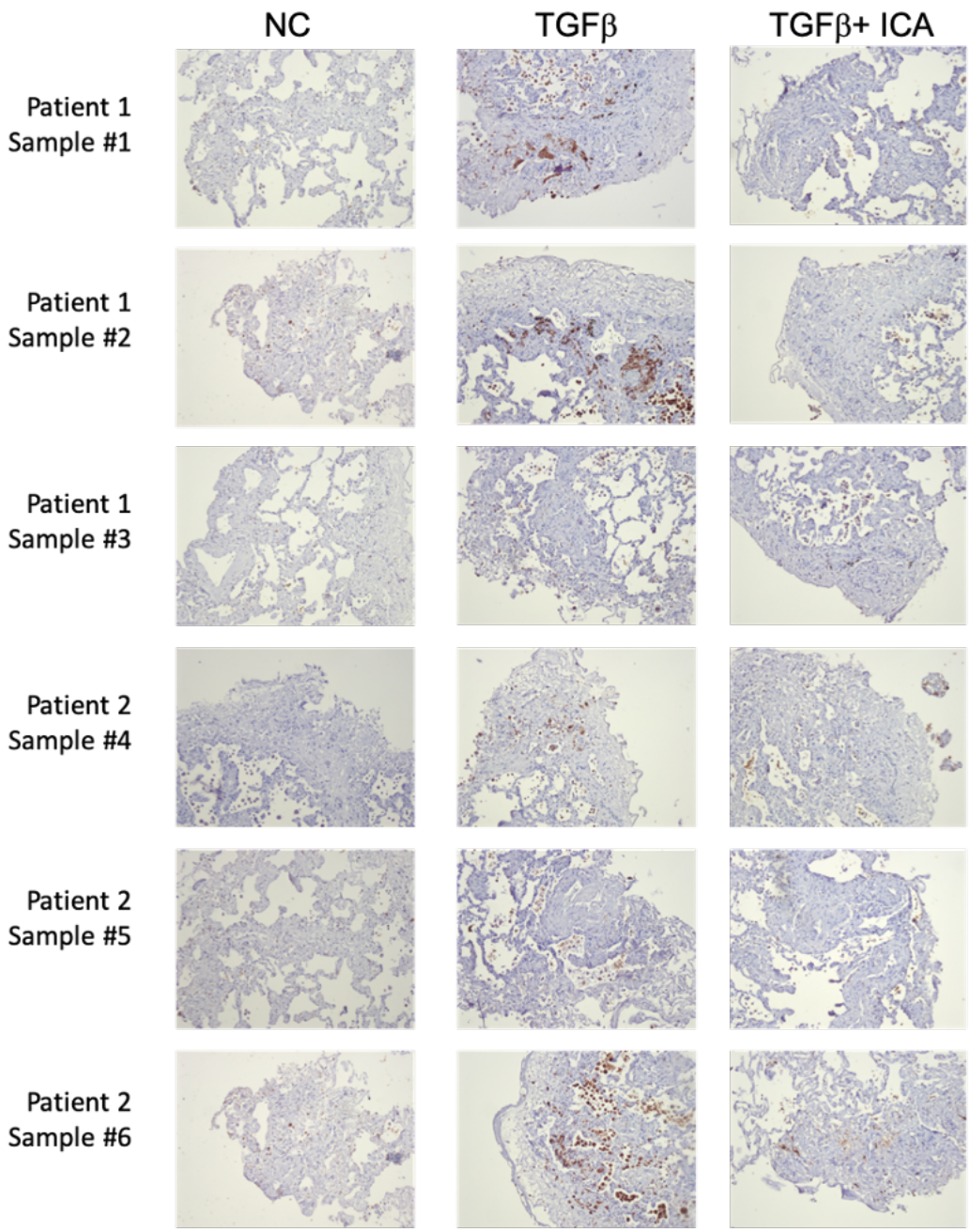

Figure 6.19. Immunohistochemistry analysis of p16 level in TGFβ1-driven ex vivo model of IPF.

The human tissue sections were cultured for 7 days in: 0.1% DMSO as a negative control (NC), TGFβ1 (10 ng/ml) or combination of TGFβ1 (10ng/ml) with ICA-17043 (Senicapoc) (100nM). After 7 days of culture tissues were harvested. Samples were subjected to immunohistochemistry analysis for the presence of p16. Figure presents the representative pictures taken at 10x magnification.

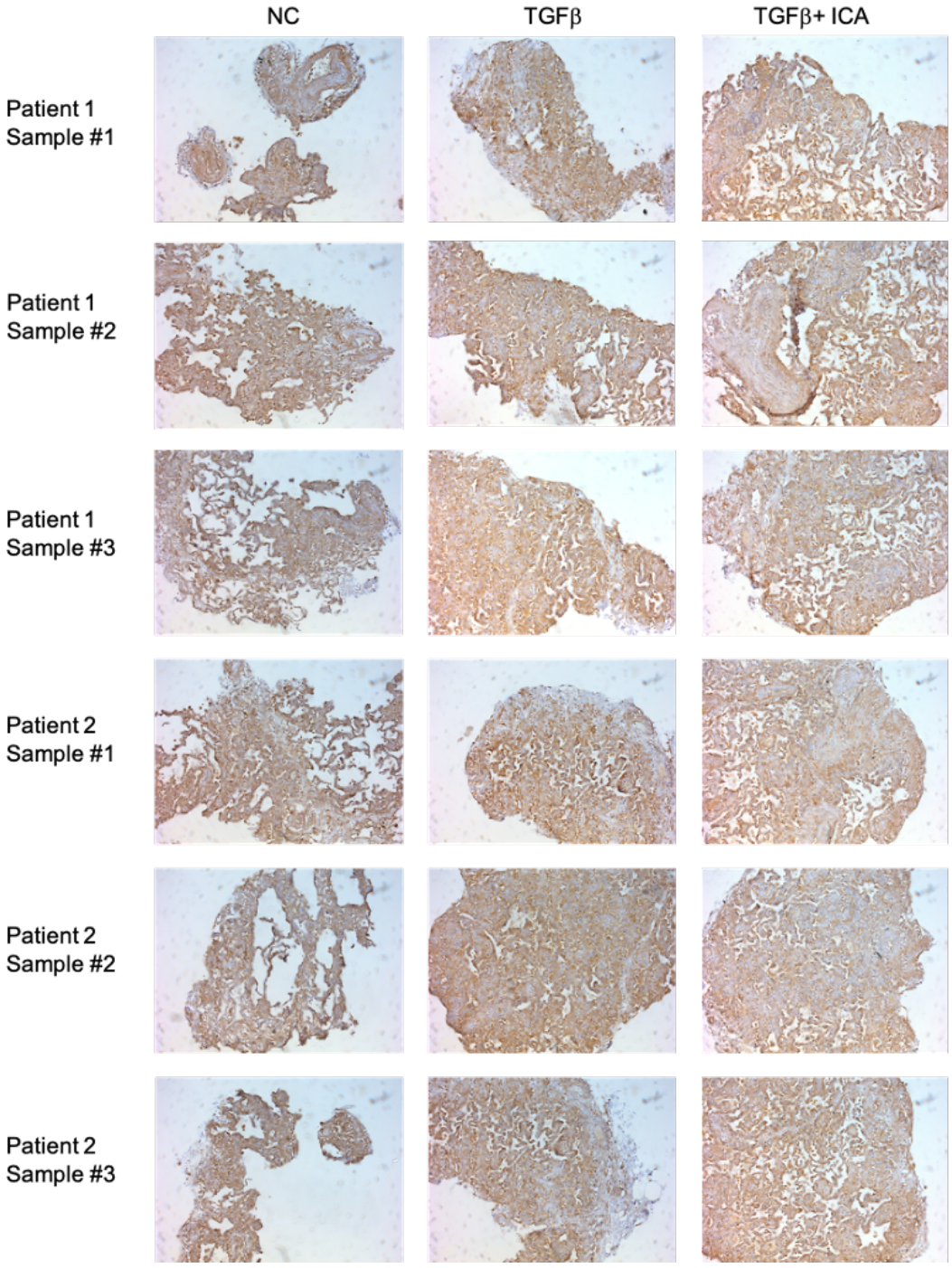

Figure 6.20. Immunohistochemistry analysis of VPS26A level in TGFβ1-driven ex vivo model of IPF.

The human tissue sections were cultured for 7 days in: 0.1% DMSO as a negative control (NC), TGFβ1 (10 ng/ml) or combination of TGFβ1 (10ng/ml) with ICA-17043 (Senicapoc) (100nM). After 7 days of culture tissues were harvested. Samples were subjected to immunohistochemistry analysis for the presence of VPS26A. Figure presents the representative pictures taken at 10x magnification.

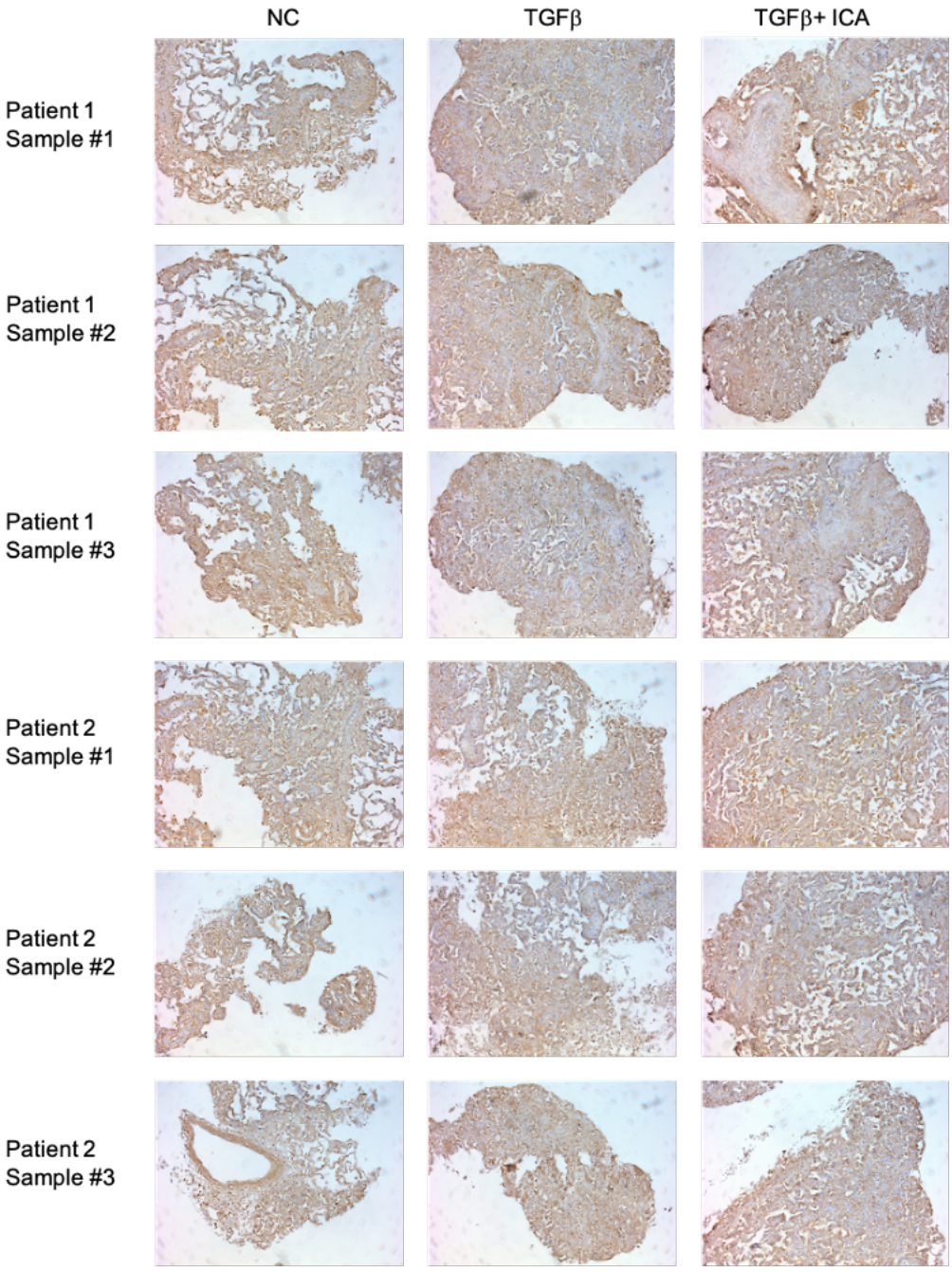

Figure 6.21. Immunohistochemistry analysis of PLD3 level in TGFβ1-driven ex vivo model of IPF.

The human tissue sections were cultured for 7 days in: 0.1% DMSO as a negative control (NC), TGFβ1 (10 ng/ml) or combination of TGFβ1 (10ng/ml) with ICA-17043 (Senicapoc) (100nM). After 7 days of culture tissues were harvested. Samples were subjected to immunohistochemistry analysis for the presence of PLD3. Figure presents the representative pictures taken at 10x magnification.

6.4 Discussion

Three novel markers, namely VPS26A, EBP50 and PLD3, were identified during a mass spectrometry screen of proteins preferentially expressed in the plasma membrane of senescent cells (Althubiti et al., 2014). Here, we further attempted to validate and characterise these novel markers by defining their expression pattern in different senescence models. Results showed that expression of these markers depends on senescence inducing stimuli and is tissue specific, and that none of the tested markers could be considered as universal marker for cellular senescence or aging.

6.4.1 VPS26A and EBP50 are not good markers of senescence

There was no difference in VPS26A levels in majority of tested conditions. This is contrary to what we would have expected as downregulation of VPS26A has been previously showed to be associated with age-related pathologies, such as Alzheimer or Parkinson disease (Gustavsson et al., 2015, Choi et al., 2018). This suggests a negative correlation with brain degeneration however, it is not clear if VPS26A level decreases with age due to age-related brain degeneration and if that is associated with cellular senescence.

VPS26A is a component of retromer complex and it has been shown that its downregulation is associated with the decrease of other core retromer proteins, VPS35 and VPS29 (Ye et al., 2020). VPS26A and VPS35 downregulation has been reported to cause impairment of intercellular trafficking and neuronal dysfunctions (Wang et al., 2014, Gallon and Cullen, 2015, Tang et al., 2015). In theory, impairment of intercellular trafficking could affect the senescence secretome, however that still needs to be tested. The potential role of VPS26A in cellular senescence should be further explored, including analysis of *in vitro* VPS26A knock-down and/or overexpression on senescence-related cell cycle arrest and SASP if cellular models that overexpress VPS26 after senescence can be found.

Results of EBP50 expression pattern also showed no changes after senescence induction *in vitro* and no changes in tested tissues. This is opposite of what was initially expected. EBP50 acts as a tumour suppressor through mediation of cell-cycle arrest. Therefore, it

is likely that EBP50 expression might be associated with cellular senescence. However, in all of the tested senescence models EBP50 protein levels remained unchanged upon senescence induction and its expression was not affected by aging in tested mice tissues. Therefore, EBP50 seems to not be a good senescence marker due to its poor expression upon senescence induction in the models tested.

6.4.2 PLD3 might be a potential marker of aging

PLD3 level remained unchanged upon senescence induction in cellular models of senescence. Although, the upregulation of PLD3 was identified in aging liver but not in brain and heart. Therefore, PLD3 upregulation in aging might be tissue specific and it shows that it could be used as a marker of aging in some but not in all tissues. Therefore, it would be highly beneficial to investigate further the expression of PLD3 in our mice model with a special emphasis on region-specific analysis. Especially that previous reports indicated a high expression of PLD3 in brain regions responsible for memory procession, such as hippocampus and cortex (Cruchaga et al., 2014). In our experiments, lysates were prepared from the whole tissues, and potential region-specific changes could be missed. Therefore, it could be interesting to perform similar analysis and compare region specific expression of PLD3 across more tissues and diseases. Further analysis would be essential to determine expression profiles of PLD3 in aging and cellular senescence, however presented here preliminary findings indicates a potential of PLD3 to serve as marker for identification of aging in certain tissues. Moreover, the upregulation of PLD3 in aging liver suggests that except for being a detection marker, it might play an important function in aging and serve as its effector. Therefore, additional experiments involving conditional *in vivo* blockage of PLD3, which could be regulated during different stages of animal life could be interesting. This would allow for the determination of PLD3 impact on aging through evaluation of lifespan and tissue conditions. Furthermore, PLD3, similarly to VPS26A, is involved in intercellular trafficking (Gonzalez et al., 2018). This makes it an interesting candidate for SASP analysis. Short-term impairment of SASP could be beneficial in the case, where immune system is overloaded by the burden of senescent cells and is not sufficient to clear the excess of senescent cells. In this condition, short-term SASP blockage could be beneficial

to reduce the paracrine functions of senescence and at the same time delay the accumulation of senescent cells within the tissues. However, it is unknown if alterations of PLD3 expression could have such an effect of SASP and the effects of downregulation and overexpression of this marker on senescence features should be investing further.

6.4.3 Future course

Biomarker discovery is important and challenging field in biomedical science research and discovery of senescence markers is still in its infancy. Currently available senescence markers are not reliable due to its unspecific expression. Therefore, identification of new markers that could be used either alone or in combination is crucial. A universal marker of senescence will need to be highly exclusive for the senescent state, but it is unlikely that something like that would have ever be found. However, a set of specific biomarkers for particular senescence-related conditions, tissue or diseases seems like a more rational scenario. A suitable biomarker set should distinguish between senescent and non-senescent cells *in vitro* and *in vivo* and its expression in non-senescent cells should be minimal. Moreover, its expression should be detectable regardless of sample preparation method. For example, usage of SA-β-Gal, one of the main available senescence markers, is limited due to its enzymatic activity and therefore it can be only detected in fresh or frozen samples but not in paraffin embedded tissues.

The list of markers identified in our laboratory might be a base for the search of biomarkers sets specific for particular tissue or age-related disease. Validation of their expression patterns might highlight potential regulators of cellular senescence. Therefore, it is essential to perform overexpression and silencing analysis to investigate whether any of the identified markers might be a crucial effector of senescence induction or regulator of the senescent phenotype, such as cell cycle arrest and SASP. The big advantage of markers identified by our lab is their presence on the plasma membrane of senescent cells. Therefore, except their effector/modulator potential, the membrane markers have the advantage that, apart from being markers, they can be used as targets for targeted senolysis (as discussed in **Chapter 4**). Of note, the

separation of the plasma membrane fraction quite often does not distinguish markers present on the surface with fully or partially extracellular epitopes from those which bound to intercellular part of surface membrane. Moreover, there are also intercellular membrane proteins (i.e. Golgi, endoplasmic reticulum) that should be distinguished from others. Therefore, proper validation and characterisation of potential biomarker function, expression pattern and cellular localisation is crucial to fully explore its biological potential.

There are a few study limitations like lack of a significant number of biological replicates or region-specific immunohistochemistry and these could be further explored in the future. Moreover, further studies will be needed to adequately characterise novel markers of senescence across more tissues and diseases and its role in regulation of senescence' features should be investigated further. Although some of these results are preliminary, they give an indication of the proteins that could be used for identification of aging and present a good starting point for further investigations.

7 Final discussion and conclusion

In recent years, much attention has been paid to targeting cellular senescence due to increasing implications in the pathogenesis of age-related diseases, including cancer. Therefore, the aim of our research was to look for a more specific and efficient ways to target cellular senescence. This research validated a number of chemical senolytics, added another piece of the puzzle for understanding senolytics mechanisms of action and identified new senolytics combinations that exhibit synergistic activity. Validation of chemical senolytics revealed that BCL-X_L inhibitors, such as ABT737 and A1331852 specifically kill senescent cells with functioning p53. These results help to fill the gaps in knowledge and might be especially useful for the choice of the senotherapy in the future. A choice of senotherapy could be dictated by case-to-case assessment of cell-intrinsic senescence pathway activation. Monitoring of p53 level might be important for the specific selection of senolytic treatment. In the future, it would be ideal to generate a senolytics library and the choice of senolytic agent or combination will be made based on the patient-specific characteristic. Especially, that senolytics regime might be synergistic or antagonistic with other fundamental aging processes. Therefore, in the future, before commercialization of senolytics for use in humans, it will be necessary to provide more personal medicine approach, that would be based on blood, urine, biopsies or other tests to determine the best senolytic cocktail for individual. Consideration of senolytics combinations with conventional disease-specific interventions might be also crucial in the future to ameliorate negative functions of aging.

Additionally, senolytics have a great potential to be used as adjuvant therapy during cancer treatment. Treatment with chemotherapeutics that induce p53- dependent senescence in cancer cells could be followed by BCL-X_L- targeting senolytic, such as Navitoclax. This strategy could help to reduce the senescence-dependent resistance of cancer cells for the treatment (Tabasso et al., 2019) and prevents senescent cells from re-fuelling tumour progression via SASP factors. However, it is important to remember that drugs that target anti-apoptotic proteins BCL-X_L, BCL-W and BCL-2, such as

Navitoclax and its analogue ABT737, are toxic for neutrophils and platelets (Cang et al., 2015). This may limit their clinical development and should be carefully consider in future analysis of drug combination proposed in here. A1331852 and 9-hydroxyellipticine are both BCL-X_L inhibitors, albeit working at two different levels, protein and gene. Although, it has been shown that targeting BCL-X_L with single agent is not causing mentioned above side effect (Leverson et al., 2015), it is unknown if double BCL-X_L inhibition would have similar toxic effect on platelets and neutrophils as Navitoclax and ABT737. Additionally, Navitoclax and ABT737 inhibits three anti-apoptotic proteins. In here and other studies (Leverson et al., 2015, Zhu et al., 2016, Kirkland and Tchkonia, 2017, Sharma et al., 2020), specific inhibition of BCL-2 and BCL-X_L has been tested in the context of senolysis and on-target side effects. However, due to lack of specific BCL-W inhibitor, its importance in senescent cells faith decisions remain unknown. Therefore, in the future, it would be also important to validate impact of BCL-W inhibition on survival of senescent cells and if its effectivity might be senescence-inducing pathway dependent.

To fully explore therapeutic potential of A1331852 and its combination with 9-hydroxyellipticine it is essential to perform their *in vivo* validation. It would be essential to define appropriate concentrations and dosages frequency and compare their effectivity to already known senolytics such as Navitoclax or Dasatinib/Quercetin combination. Healthspan and lifespan assessments should be performed using both, progeria and wild-type animals with careful monitoring of side effects.

Another approach proposed by us is the usage of nanoMIPs and ADCs. Both tools are examples of second-generation senolytics that take advantage of senescent cells surfaceome to deliver a cytotoxic compound directly to senescent cells. These results showed that B2M-nanoMIPs preferentially accumulated in the older animals suggesting detection of senescent cells *in vivo*. Our analysis revealed that B2M nanoMIPs preferentially accumulated in approximate localisation of jejunum. At first, we hypothesised that nanoMIPs might accumulate in the kidneys through which they will get cleared from the body. However, our postmortem *ex vivo* analysis of dissected organs, including lungs, kidneys and liver showed no fluorescent signal from any of the

mentioned tissues. Therefore, the exact localisation remains unknown and the presence of other organs cannot be excluded. Moreover, due to heterogenic expression of B2M in different tissues of the body, it is unlikely that B2M would ever be a good therapeutic target, therefore future analysis should focus on validation of others surfaceome markers identified by us (Althubiti et al., 2014) which have extracellular epitope.

Future *in vivo* experiments should involve conjugation of nanoMIPs with a senolytic compound to tests their specificity in senescent cells clearance. Next to nanoMIPs we tested *in vitro* effectivity of ADCs in elimination of senescent cell. ADCs were designed against the same target, B2M and further analysis should be performed to assess the degree of side effects related to B2M background expression and If this is an obstacle for potential therapeutic usage. However, ADCs have a big advantage over nanoMIPs, which has been years of extensive studies on ADCs composition and effectivity in cancer treatment (Chari et al., 2014). Therefore, it would be much easier in the future to repurpose drug delivery tool, which has been extensively studied in another field. Moreover, many ADCs already reached clinical trials and some of them has been already approved for treatment of different cancers starting with Gemtuzumab ozogamicin for the treatment of patients with Acute myeloid leukaemia (AML) developed by Pfizer and approved in 2000 (Chari et al., 2014) and Trastuzumab emtansine (Kadcyla) (Barok et al., 2014) that was approved in 2013 for the treatment of late-stage metastatic breast cancer in HER2-positive patients. In the future B2M-ADCs, or ADCs against other surfaceome target, should be tested *in vivo* using progeria and wild type animals. Moreover, technical aspects such as ADCs stability in circulations should be also considered to make sure that the cytotoxic compound would not be prematurely released. Our results suggests that ADCs could be an efficient approach to bring toxic compound into senescent cells, although not without side effects. In the future, after extensive studies It is likely that this approach could be scaled up and successfully used in human with minimal side effects based on the success of similar approaches in cancer treatment.

The first barrier that slows down transition of second-generation senolytics to clinic is lack of specific marker. In here, we performed validation of three markers VPS26A, PLD3 and EBP50. Among them, VPS26A has known extracellular epitope (Althubiti et al.,

2014) and potentially could serve as a new target for second generation of senolytics. However, our results revealed that VPS26A is not specifically expressed in majority of senescent models tested. Therefore, it is not a good targeting candidate. Delivery of cytotoxic compound through targeting of VPS26A could lead to clearance of senescent and non-senescent cells with the similar rate and intensity causing higher level of damage then benefits.

Another approach tested by us was senoblocking. In here, we showed that continuous BTK inhibition ameliorated certain age-related pathologies, such as cognitive memory and muscle strength, and reduced the number of senescent cells in the tissues. Although, biochemistry analysis revealed that the degree of senescent cells clearance was tissue specific. Of note, continuous treatment of Ibrutinib had no effect on average lifespan of treated animals, but instead there was noticeable improvement of the healthspan, which could be beneficial when applied in humans. One of the recent challenges of anti-aging approaches is not only to increase lifespan but the most importantly to extend the healthspan and delay the onset of aging symptoms. Importantly, there were no increase in tumourigenesis that could be a cause of p53-p21 pathway inhibition. That might be due to degree of p53 inhibition caused by Ibrutinib. Biochemistry analysis of the tissues revealed that p53 was not fully decreased by BTK inhibition via Ibrutinib treatment. Potentially, the degree of p53 inhibition was not sufficient to fully impair its tumour suppressor functions. That is in accordance with long-term follow-up study that have not reported an increase in secondary tumours in patients with leukaemia after the therapy aiming BTK inhibition (Walter et al., 2017). In the future, this experiment should be repeated using wild-type animals. The genetic background of wild-type animals might not be as p53 dependent as in *ZMPSTE24*$^{-/-}$ mice, therefore the effectivity of the treatment might also be less intense. Our results indicates that continuous BTK blockage via Ibrutinib treatment could be potentially beneficial for patients with progeria and other premature syndromes of aging, however further studies will be essential to fully explore the role of BTK in aging and its therapeutic relevance.

Chapter VII: Final discussion and conclusion

Our research contributes to the cellular senescence field by addressing the main issues on senotherapies: lack of a specific therapeutic approach to eliminate senescent cells from the body, and lack of a specific marker that would allow for proper detection and targeting of senescent cells. Since senescence is characterized by a complex phenotype that involves multiple pathways and proteins, it is unlikely that a single compound targeting a single protein will be effective in killing or disrupting all types of senescent cells. For example, Dasatinib is more effective against senescent human primary preadipocytes than Quercetin, but Quercetin is more selective against human endothelial cells (Hickson et al., 2019). Similar differences has been observed in Navitoclax, which is effective against senescent HUVEC and IMR90 cells, although it is not selective for primary senescent preadipocytes (Zhu et al., 2016). Therefore, it is crucial to identify new compounds that could target senescent cells more broadly and at the same time specifically enough to maintain low cytotoxicity. Presented in Chapter 3, our screen of drugs provides important validation and helps to indetify candidates for future investigation, especially considering that potential senolytics were tested here as a single drug and in combination. Moreover, in Chapter 4 we validated second generation of senolytics, a growing field of pro-drugs that could revolutionize the therapeutic market. Approaches presented here acts as representatives of targeted senolytics that recognize surfaceome markers to deliver cytotoxic compounds into senescent cells. In turn, our work on Ibrutinib is an example of a senoblocking strategy that starts in the early stage of life and by continued treatment aims to prevent the accumulation of senescent cells to arise. Last chapter focuses on validation of markers that have been identified in the proteomic screen of proteins selectively present in senescent cells. Depending on the expression patterns and cellular localization, these markers could be used as a target for selective elimination of senescent cells or could act as senescence effector, which could be used as a target for senoblocking or senomorphic strategies. However, our results revealed that markers validated here cannot be used either as a target or effector of cellular senescence due to their ambiguous expression in tested models. If the expression of tested markers were specific for senescent cells, then it would be interesting to take it forward and characterize their role in cellular senescence. Effectors that are responsible for

senescence induction and establishment of cell cycle arrest could be a promising target for senoblocking strategies and a similar research to the BTK data presented in chapter 5 could be performed. If the function of tested marker would be specific for other features of cellular senescence, such as control of SASP, then we could use it as a target for senomorphic strategeis. Nevertheless, unspecific expression of tested markers limited the progression of this side of the project.

The initial concept of this research was to provide instructions for development of second generation of targeted senolytics, which include: validation of the surfaceome marker, characterization of the drug delivery tool and identification of a senescence-specific cytotoxic compound. Combination of all these points would provide a basis for design of second-generation pro-drugs that could be highly specific for senescent cells. In this concept, the pro-drug would have advantage over first-generation senolytics due to a highly specific design. It would recognize specific for the senescent cells surfaceome marker and it would selectively release the drug. To improve specificity even more, a third point of support could be added, such as senescence-specific drug-releasing strategy. Previously published approaches that relies on high level of lysosomal β-galactosidase (Cai et al., 2020, González-Gualda et al., 2020b, Guerrero et al., 2020, Muñoz-Espín et al., 2018a, Thapa et al., 2017a, Xu et al., 2019) seems to be a great candidate, as the drug release is dictated by another specific feature of senescent cells.

Presented here results covered some points of this initial concept (**Figure 7.1**). At first, we provided characteristics of promising drug delivery tool and second, we performed a screen of potential senolytics that could be used as a payload that would be released in senescent cells. Specifically, our results highlight the potential of ADCs that could be conjugated to one of senolytics validated here, such as A1331852 or combination of A1331852 with 9-hydroxyellipticine. To fully cover the initial concept, a senescence-specific target is missing as markers validated here, VPS26A, PLD3 and EBP50 cannot act as a good target, due to their cellular localization and ambiguous expression patterns in senescent models. Therefore, more research should be done to identify a suitable target for the concept of second generation targeted senolytics.

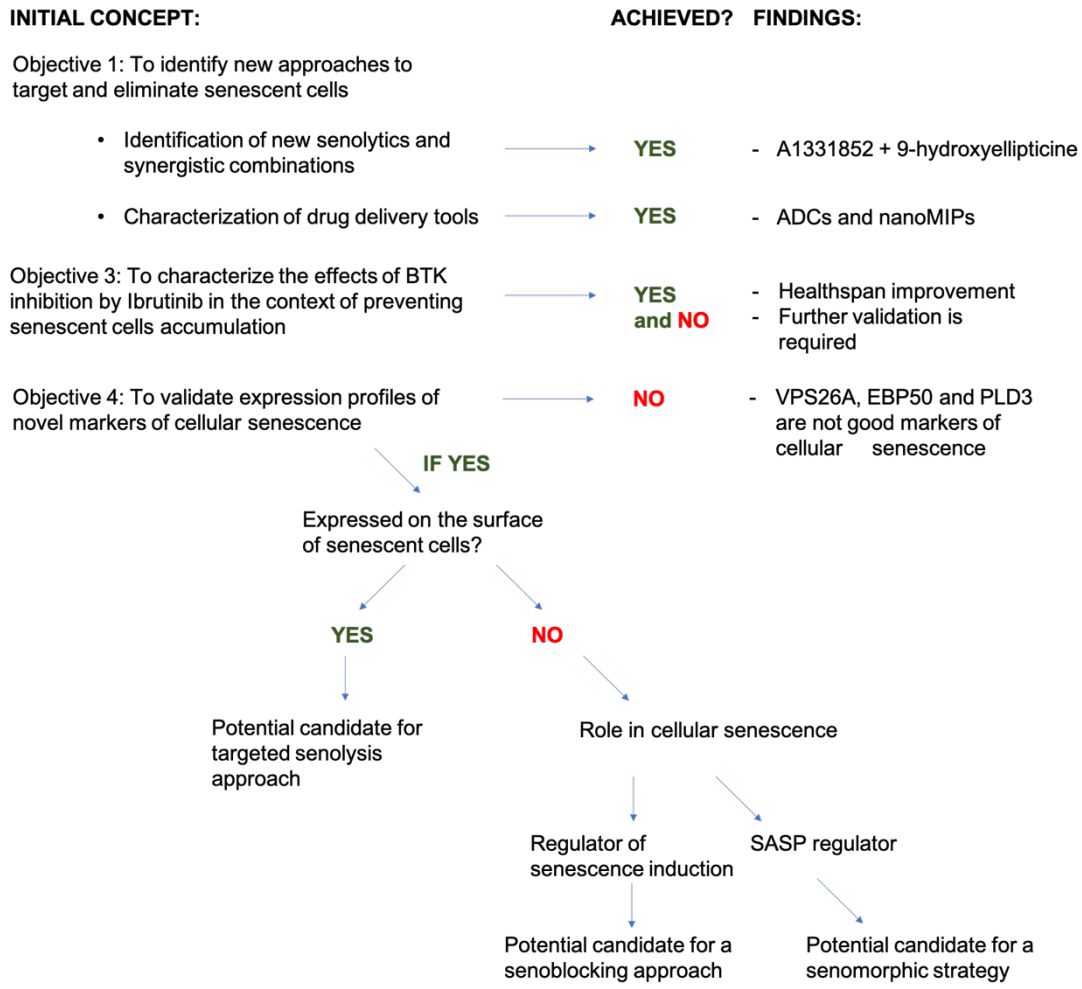

Figure 7.1. Summary of initial concepts and achieved outcomes.

7.1 Conclusion.

Targeting and elimination of senescent cells represents a promising therapeutic strategy due to the increasing implications of cellular senescence in age-related diseases, including cancer. This research validates novel markers of cellular senescence, highlights diagnostic and therapeutic potential of drug delivery tools, such as nanoparticles and antibody drug conjugates that recognize senescent surfaceome markers. Moreover, in this study we show that blocking BTK with Ibrutinib have a beneficial function on progeroid mice healthspan by preservation of certain age-related degeneration and tissue dysfunction. We also propose novel combinations of the drugs, A1331852 and 9-hydroxyellipticine that showed a senolytic activity *in vitro*. This research could be followed up by further characterisation of identified drug combination *in vivo* with biochemistry analysis of senescent markers expression in the tissues to further validate our preliminary findings.

8 Bibliography

AALIPOUR, A. & ADVANI, R. H. 2014. Bruton's tyrosine kinase inhibitors and their clinical potential in the treatment of B-cell malignancies: focus on ibrutinib. *Ther Adv Hematol,* 5**,** 121-33.

ADAMS, B. K., CAI, J., ARMSTRONG, J., HEROLD, M., LU, Y. J., SUN, A., SNYDER, J. P., LIOTTA, D. C., JONES, D. P. & SHOJI, M. 2005. EF24, a novel synthetic curcumin analog, induces apoptosis in cancer cells via a redox-dependent mechanism. *Anti-cancer drugs,* 16**,** 263-275.

ADAMS, P. D. 2007. Remodeling of chromatin structure in senescent cells and its potential impact on tumor suppression and aging. *Gene,* 397**,** 84-93.

AGOSTINI, A., MONDRAGÓN, L., BERNARDOS, A., MARTÍNEZ-MÁÑEZ, R., MARCOS, M. D., SANCENÓN, F., SOTO, J., COSTERO, A., MANGUAN-GARCÍA, C., PERONA, R., MORENO-TORRES, M., APARICIO-SANCHIS, R. & MURGUÍA, J. R. 2012. Targeted cargo delivery in senescent cells using capped mesoporous silica nanoparticles. *Angew Chem Int Ed Engl,* 51**,** 10556-60.

AIRD, D., TENG, T., HUANG, C. L., PAZOLLI, E., BANKA, D., CHEUNG-ONG, K., EIFERT, C., FURMAN, C., WU, Z. J., SEILER, M., BUONAMICI, S., FEKKES, P., KARR, C., PALACINO, J., PARK, E., SMITH, P. G., YU, L., MIZUI, Y., WARMUTH, M., CHICAS, A., CORSON, L. & ZHU, P. 2019. Sensitivity to splicing modulation of BCL2 family genes defines cancer therapeutic strategies for splicing modulators. *Nat Commun,* 10**,** 137.

AKINLEYE, A., CHEN, Y., MUKHI, N., SONG, Y. & LIU, D. 2013. Ibrutinib and novel BTK inhibitors in clinical development. *J Hematol Oncol,* 6**,** 59.

ALAVIAN, K. N., LI, H., COLLIS, L., BONANNI, L., ZENG, L., SACCHETTI, S., LAZROVE, E., NABILI, P., FLAHERTY, B. & GRAHAM, M. 2011. Bcl-x L regulates metabolic efficiency of neurons through interaction with the mitochondrial F 1 FO ATP synthase. *Nature cell biology,* 13**,** 1224-1233.

ALTHUBITI, M., LEZINA, L., CARRERA, S., JUKES-JONES, R., GIBLETT, S. M., ANTONOV, A., BARLEV, N., SALDANHA, G. S., PRITCHARD, C. A., CAIN, K. & MACIP, S. 2014. Characterization of novel markers of senescence and their prognostic potential in cancer. *Cell Death Dis,* 5**,** e1528.

ALTHUBITI, M., RADA, M., SAMUEL, J., ESCORSA, J. M., NAJEEB, H., LEE, K.-G., LAM, K.-P., JONES, G. D. D., BARLEV, N. A. & MACIP, S. 2016a. BTK Modulates p53 Activity to Enhance Apoptotic and Senescent Responses. *Cancer Research,* 76**,** 5405.

ALTHUBITI, M., RADA, M., SAMUEL, J., ESCORSA, J. M., NAJEEB, H., LEE, K. G., LAM, K. P., JONES, G. D., BARLEV, N. A. & MACIP, S. 2016b. BTK Modulates p53 Activity to Enhance Apoptotic and Senescent Responses. *Cancer Res,* 76**,** 5405-14.

AMARAPURKAR, D., KAMANI, P., PATEL, N., GUPTE, P., KUMAR, P., AGAL, S., BAIJAL, R., LALA, S., CHAUDHARY, D. & DESHPANDE, A. 2007. Prevalence of non-alcoholic fatty liver disease: population based study. *Ann Hepatol,* 6**,** 161-3.

AMOR, C., FEUCHT, J., LEIBOLD, J., HO, Y.-J., ZHU, C., ALONSO-CURBELO, D., MANSILLA-SOTO, J., BOYER, J. A., LI, X., GIAVRIDIS, T., KULICK, A., HOULIHAN, S., PEERSCHKE, E., FRIEDMAN, S. L., PONOMAREV, V., PIERSIGILLI, A., SADELAIN, M. & LOWE, S. W. 2020. Senolytic CAR T cells reverse senescence-associated pathologies. *Nature,* 583**,** 127-132.

AOSHIBA, K., TSUJI, T. & NAGAI, A. 2003. Bleomycin induces cellular senescence in alveolar epithelial cells. *European Respiratory Journal,* 22**,** 436-443.

ARTANDI, S. E. & ATTARDI, L. D. 2005. Pathways connecting telomeres and p53 in senescence, apoptosis, and cancer. *Biochem Biophys Res Commun,* 331**,** 881-90.

ASHKENAZI, A., FAIRBROTHER, W. J., LEVERSON, J. D. & SOUERS, A. J. 2017. From basic apoptosis discoveries to advanced selective BCL-2 family inhibitors. *Nature reviews Drug discovery,* 16**,** 273-284.

ATTAR, A., LIU, T., CHAN, W. T., HAYES, J., NEJAD, M., LEI, K. & BITAN, G. 2013. A shortened Barnes maze protocol reveals memory deficits at 4-months of age in the triple-transgenic mouse model of Alzheimer's disease. *PLoS One,* 8**,** e80355.

BAAR, M. P., BRANDT, R. M., PUTAVET, D. A., KLEIN, J. D., DERKS, K. W., BOURGEOIS, B. R., STRYECK, S., RIJKSEN, Y., VAN WILLIGENBURG, H. & FEIJTEL, D. A. 2017. Targeted apoptosis of senescent cells restores tissue homeostasis in response to chemotoxicity and aging. *Cell,* 169**,** 132-147. e16.

BADACHE, A. & HYNES, N. E. 2001. Interleukin 6 inhibits proliferation and, in cooperation with an epidermal growth factor receptor autocrine loop, increases migration of T47D breast cancer cells. *Cancer research,* 61**,** 383-391.

BAHL, R., ARORA, S., NATH, N., MATHUR, M., SHUKLA, N. K. & RALHAN, R. 2000. Novel polymorphism in p21 waf1/cip1 cyclin dependent kinase inhibitor gene: association with human esophageal cancer. *Oncogene,* 19**,** 323-328.

BAKER, D. J., CHILDS, B. G., DURIK, M., WIJERS, M. E., SIEBEN, C. J., ZHONG, J., SALTNESS, R. A., JEGANATHAN, K. B., VERZOSA, G. C., PEZESHKI, A., KHAZAIE, K., MILLER, J. D. & VAN DEURSEN, J. M. 2016. Naturally occurring p16(Ink4a)-positive cells shorten healthy lifespan. *Nature,* 530**,** 184-9.

BAKER, D. J. & PETERSEN, R. C. 2018. Cellular senescence in brain aging and neurodegenerative diseases: evidence and perspectives. *J Clin Invest,* 128**,** 1208-1216.

BAKER, D. J., WIJSHAKE, T., TCHKONIA, T., LEBRASSEUR, N. K., CHILDS, B. G., VAN DE SLUIS, B., KIRKLAND, J. L. & VAN DEURSEN, J. M. 2011. Clearance of p16Ink4a-positive senescent cells delays ageing-associated disorders. *Nature,* 479**,** 232-6.

BALAGOPAL, P., ROOYACKERS, O. E., ADEY, D. B., ADES, P. A. & NAIR, K. S. 1997. Effects of aging on in vivo synthesis of skeletal muscle myosin heavy-chain and sarcoplasmic protein in humans. *American Journal of Physiology-Endocrinology And Metabolism,* 273**,** E790-E800.

BALBÍN, M., HANNON, G. J., PENDÁS, A. M., FERRANDO, A. A., VIZOSO, F., FUEYO, A. & LÓPEZ-OTÍN, C. 1996. Functional analysis of a p21WAF1, CIP1, SDI1 mutant (Arg94→ Trp) identified in a human breast carcinoma Evidence that the mutation impairs the ability of p21 to inhibit cyclin-dependent kinases. *Journal of Biological Chemistry,* 271**,** 15782-15786.

BALLIO, A., CHAIN, E., DE LEO, P., ERLANGER, B., MAURI, M. & TONOLO, A. 1964. Fusicoccin: a new wilting toxin produced by Fusicoccum amygdali Del. *Nature,* 203**,** 297-297.

BARILLE-NION, S., BAH, N., VEQUAUD, E. & JUIN, P. 2012. Regulation of cancer cell survival by BCL2 family members upon prolonged mitotic arrest: opportunities for anticancer therapy. *Anticancer Res,* 32**,** 4225-33.

BARNES, C. A. 1979. Memory deficits associated with senescence: a neurophysiological and behavioral study in the rat. *J Comp Physiol Psychol,* 93**,** 74-104.

BARNES, C. A., NADEL, L. & HONIG, W. K. 1980. Spatial memory deficit in senescent rats. *Can J Psychol,* 34**,** 29-39.

BAROK, M., JOENSUU, H. & ISOLA, J. 2014. Trastuzumab emtansine: mechanisms of action and drug resistance. *Breast cancer research,* 16**,** 1-12.

BARROTT, J. J., ZHU, J. F., SMITH-FRY, K., SUSKO, A. M., NOLLNER, D., BURRELL, L. D., POZNER, A., CAPECCHI, M. R., YAP, J. T., CANNON-ALBRIGHT, L. A., DENG, X. & JONES, K. B. 2017. The Influential Role of BCL2 Family Members in Synovial Sarcomagenesis. *Mol Cancer Res,* 15**,** 1733-1740.

BARTEK, J. & LUKAS, J. 2007. DNA damage checkpoints: from initiation to recovery or adaptation. *Current opinion in cell biology,* 19**,** 238-245.

BARTSCH, T., DÖHRING, J., ROHR, A., JANSEN, O. & DEUSCHL, G. 2011. CA1 neurons in the human hippocampus are critical for autobiographical memory, mental time travel, and autonoetic consciousness. *Proceedings of the National Academy of Sciences,* 108**,** 17562.

BAUM, C. L. & ARPEY, C. J. 2005. Normal cutaneous wound healing: clinical correlation with cellular and molecular events. *Dermatologic surgery,* 31**,** 674-686.

BAUSCH-FLUCK, D., GOLDMANN, U., MULLER, S., VAN OOSTRUM, M., MULLER, M., SCHUBERT, O. T. & WOLLSCHEID, B. 2018. The in silico human surfaceome. *Proc Natl Acad Sci U S A,* 115**,** E10988-E10997.

BAVIK, C., COLEMAN, I., DEAN, J. P., KNUDSEN, B., PLYMATE, S. & NELSON, P. S. 2006. The gene expression program of prostate fibroblast senescence modulates neoplastic epithelial cell proliferation through paracrine mechanisms. *Cancer research,* 66**,** 794-802.

BEAUSÉJOUR, C. M., KRTOLICA, A., GALIMI, F., NARITA, M., LOWE, S. W., YASWEN, P. & CAMPISI, J. 2003. Reversal of human cellular senescence: roles of the p53 and p16 pathways. *Embo j,* 22**,** 4212-22.

BELCHER, C., FAWTHROP, F., BUNNING, R. & DOHERTY, M. 1996. Plasminogen activators and their inhibitors in synovial fluids from normal, osteoarthritis, and rheumatoid arthritis knees. *Annals of the rheumatic diseases,* 55**,** 230-236.

BELINHA, I., AMORIM, M. A., RODRIGUES, P., DE FREITAS, V., MORADAS-FERREIRA, P., MATEUS, N. & COSTA, V. 2007. Quercetin increases oxidative stress resistance and longevity in Saccharomyces cerevisiae. *Journal of agricultural and food chemistry,* 55**,** 2446-2451.

BEN-PORATH, I. & WEINBERG, R. A. 2005. The signals and pathways activating cellular senescence. *Int J Biochem Cell Biol,* 37**,** 961-76.

BERGO, M. O., GAVINO, B., ROSS, J., SCHMIDT, W. K., HONG, C., KENDALL, L. V., MOHR, A., META, M., GENANT, H., JIANG, Y., WISNER, E. R., VAN BRUGGEN, N., CARANO, R. A., MICHAELIS, S., GRIFFEY, S. M. & YOUNG, S. G. 2002a. Zmpste24 deficiency in mice causes spontaneous bone fractures, muscle weakness, and a prelamin A processing defect. *Proc Natl Acad Sci U S A,* 99**,** 13049-54.

BERGO, M. O., GAVINO, B., ROSS, J., SCHMIDT, W. K., HONG, C., KENDALL, L. V., MOHR, A., META, M., GENANT, H., JIANG, Y., WISNER, E. R., VAN BRUGGEN, N., CARANO, R. A. D., MICHAELIS, S., GRIFFEY, S. M. & YOUNG, S. G. 2002b. Zmpste24 deficiency in mice causes spontaneous bone fractures, muscle weakness, and a prelamin A processing defect. *Proceedings of the National Academy of Sciences of the United States of America,* 99**,** 13049-13054.

BERMAN, S. B., CHEN, Y. B., QI, B., MCCAFFERY, J. M., RUCKER, E. B., 3RD, GOEBBELS, S., NAVE, K. A., ARNOLD, B. A., JONAS, E. A., PINEDA, F. J. & HARDWICK, J. M. 2009. Bcl-x L increases mitochondrial fission, fusion, and biomass in neurons. *J Cell Biol,* 184**,** 707-19.

BESANCENOT, R., CHALIGNÉ, R., TONETTI, C., PASQUIER, F., MARTY, C., LÉCLUSE, Y., VAINCHENKER, W., CONSTANTINESCU, S. N. & GIRAUDIER, S. 2010. A senescence-like cell-cycle arrest occurs during megakaryocytic maturation: implications for physiological and pathological megakaryocytic proliferation. *PLoS Biol,* 8**,** e1000476.

BEZERRA, D. P., MILITÃO, G. C. G., DE CASTRO, F. O., PESSOA, C., DE MORAES, M. O., SILVEIRA, E. R., LIMA, M. A. S., ELMIRO, F. J. M. & COSTA-LOTUFO, L. V. 2007. Piplartine induces inhibition of leukemia cell proliferation triggering both apoptosis and necrosis pathways. *Toxicology in vitro,* 21**,** 1-8.

BEZERRA, D. P., PESSOA, C., DE MORAES, M. O., SAKER-NETO, N., SILVEIRA, E. R. & COSTA-LOTUFO, L. V. 2013. Overview of the therapeutic potential of piplartine (piperlongumine). *European Journal of Pharmaceutical Sciences,* 48**,** 453-463.

BHAT, R., CROWE, E. P., BITTO, A., MOH, M., KATSETOS, C. D., GARCIA, F. U., JOHNSON, F. B., TROJANOWSKI, J. Q., SELL, C. & TORRES, C. 2012. Astrocyte senescence as a component of Alzheimer's disease. *PLoS One,* 7**,** e45069.

BI, K., ROTH, M. G. & KTISTAKIS, N. T. 1997. Phosphatidic acid formation by phospholipase D is required for transport from the endoplasmic reticulum to the Golgi complex. *Curr Biol,* 7**,** 301-7.

BLACKBURN, E. H. 1991. Structure and function of telomeres. *Nature,* 350**,** 569-573.

BLACKBURN, E. H. 2001. Switching and signaling at the telomere. *Cell,* 106**,** 661-73.

BLANCO-LUQUIN, I., ALTUNA, M., SÁNCHEZ-RUIZ DE GORDOA, J., URDÁNOZ-CASADO, A., ROLDÁN, M., CÁMARA, M., ZELAYA, V., ERRO, M. E., ECHAVARRI, C. & MENDIOROZ, M. 2018. PLD3 epigenetic changes in the hippocampus of Alzheimer's disease. *Clin Epigenetics,* 10**,** 116.

BLASCO, M. A. 2003. Mammalian telomeres and telomerase: why they matter for cancer and aging. *Eur J Cell Biol,* 82**,** 441-6.

BOISE, L. H., GONZÁLEZ-GARCÍA, M., POSTEMA, C. E., DING, L., LINDSTEN, T., TURKA, L. A., MAO, X., NUÑEZ, G. & THOMPSON, C. B. 1993. bcl-x, a bcl-2-related gene that functions as a dominant regulator of apoptotic cell death. *Cell,* 74**,** 597-608.

BORRAS, C., ABDELAZIZ, K. M., GAMBINI, J., SERNA, E., INGLÉS, M., DE LA FUENTE, M., GARCIA, I., MATHEU, A., SANCHÍS, P. & BELENGUER, A. 2016. Human exceptional longevity: transcriptome from centenarians is distinct from septuagenarians and reveals a role of Bcl-xL in successful aging. *Aging (Albany NY),* 8**,** 3185.

BORRÁS, C., MAS-BARGUES, C., ROMÁN-DOMÍNGUEZ, A., SANZ-ROS, J., GIMENO-MALLENCH, L., INGLÉS, M., GAMBINI, J. & VIÑA, J. 2020. BCL-xL, a Mitochondrial Protein Involved in Successful Aging: From C. elegans to Human Centenarians. *Int J Mol Sci,* 21.

BOULOS, L., PRÉVOST, M., BARBEAU, B., COALLIER, J. & DESJARDINS, R. 1999. LIVE/DEAD BacLight : application of a new rapid staining method for direct enumeration of viable and total bacteria in drinking water. *J Microbiol Methods,* 37**,** 77-86.

BOURGEOIS, B. & MADL, T. 2018. Regulation of cellular senescence via the FOXO4-p53 axis. *FEBS Lett,* 592**,** 2083-2097.

BRADSHAW, J. M. 2010. The Src, Syk, and Tec family kinases: distinct types of molecular switches. *Cell Signal,* 22**,** 1175-84.

BRAIG, M., LEE, S., LODDENKEMPER, C., RUDOLPH, C., PETERS, A. H., SCHLEGELBERGER, B., STEIN, H., DÖRKEN, B., JENUWEIN, T. & SCHMITT, C. A. 2005. Oncogene-induced senescence as an initial barrier in lymphoma development. *Nature,* 436**,** 660-665.

BRIDGER, J. M., FOEGER, N., KILL, I. R. & HERRMANN, H. 2007. The nuclear lamina. Both a structural framework and a platform for genome organization. *Febs j,* 274**,** 1354-61.

BROWN, E. J. & BALTIMORE, D. 2000. ATR disruption leads to chromosomal fragmentation and early embryonic lethality. *Genes Dev,* 14**,** 397-402.

BROWN, H. A., THOMAS, P. G. & LINDSLEY, C. W. 2017. Targeting phospholipase D in cancer, infection and neurodegenerative disorders. *Nat Rev Drug Discov,* 16**,** 351-367.

BRUNET, A., PARK, J., TRAN, H., HU, L. S., HEMMINGS, B. A. & GREENBERG, M. E. 2001. Protein kinase SGK mediates survival signals by phosphorylating the forkhead transcription factor FKHRL1 (FOXO3a). *Molecular and cellular biology,* 21**,** 952-965.

BUGARCIC, A., ZHE, Y., KERR, M. C., GRIFFIN, J., COLLINS, B. M. & TEASDALE, R. D. 2011. Vps26A and Vps26B subunits define distinct retromer complexes. *Traffic,* 12**,** 1759-73.

BURKHOLDER, T., FOLTZ, C., KARLSSON, E., LINTON, C. G. & SMITH, J. M. 2012. Health Evaluation of Experimental Laboratory Mice. *Current protocols in mouse biology,* 2**,** 145-165.

BUSSIAN, T. J., AZIZ, A., MEYER, C. F., SWENSON, B. L., VAN DEURSEN, J. M. & BAKER, D. J. 2018. Clearance of senescent glial cells prevents tau-dependent pathology and cognitive decline. *Nature,* 562**,** 578-582.

CAHU, J. 2013. SASP: roadblock for tissue re-organization. *Aging (Albany NY),* 5**,** 641-2.

CAI, Y., ZHOU, H., ZHU, Y., SUN, Q., JI, Y., XUE, A., WANG, Y., CHEN, W., YU, X., WANG, L., CHEN, H., LI, C., LUO, T. & DENG, H. 2020. Elimination of senescent cells by β-

galactosidase-targeted prodrug attenuates inflammation and restores physical function in aged mice. *Cell Research,* 30**,** 574-589.

CAMPISI, J. 2005. Senescent cells, tumor suppression, and organismal aging: good citizens, bad neighbors. *Cell,* 120**,** 513-22.

CAMPISI, J. 2011. Cellular senescence: putting the paradoxes in perspective. *Curr Opin Genet Dev,* 21**,** 107-12.

CAMPISI, J. & D'ADDA DI FAGAGNA, F. 2007. Cellular senescence: when bad things happen to good cells. *Nature Reviews Molecular Cell Biology,* 8**,** 729.

CANFAROTTA, F., POMA, A., GUERREIRO, A. & PILETSKY, S. 2016a. Solid-phase synthesis of molecularly imprinted nanoparticles. *Nature protocols,* 11**,** 443-455.

CANFAROTTA, F., WATERS, A., SADLER, R., MCGILL, P., GUERREIRO, A., PAPKOVSKY, D., HAUPT, K. & PILETSKY, S. 2016b. Biocompatibility and internalization of molecularly imprinted nanoparticles. *Nano Research,* 9**,** 3463-3477.

CANG, S., IRAGAVARAPU, C., SAVOOJI, J., SONG, Y. & LIU, D. 2015. ABT-199 (venetoclax) and BCL-2 inhibitors in clinical development. *Journal of hematology & oncology,* 8**,** 1-8.

CAPILLA-GONZALEZ, V., GIL-PEROTIN, S., FERRAGUD, A., BONET-PONCE, L., CANALES, J. J. & GARCIA-VERDUGO, J. M. 2012. Exposure to N-ethyl-N-nitrosourea in adult mice alters structural and functional integrity of neurogenic sites. *PLoS One,* 7**,** e29891.

CARRAGHER, L. A., SNELL, K. R., GIBLETT, S. M., ALDRIDGE, V. S., PATEL, B., COOK, S. J., WINTON, D. J., MARAIS, R. & PRITCHARD, C. A. 2010. V600EBraf induces gastrointestinal crypt senescence and promotes tumour progression through enhanced CpG methylation of p16INK4a. *EMBO Mol Med,* 2**,** 458-71.

CASI, G. & NERI, D. 2012. Antibody–drug conjugates: Basic concepts, examples and future perspectives.

CECCHINI, A., RAFFA, V., CANFAROTTA, F., SIGNORE, G., PILETSKY, S., MACDONALD, M. P. & CUSCHIERI, A. 2017a. In vivo recognition of human vascular endothelial growth factor by molecularly imprinted polymers. *Nano letters,* 17**,** 2307-2312.

CECCHINI, A., RAFFA, V., CANFAROTTA, F., SIGNORE, G., PILETSKY, S., MACDONALD, M. P. & CUSCHIERI, A. 2017b. In Vivo Recognition of Human Vascular Endothelial Growth Factor by Molecularly Imprinted Polymers. *Nano letters*.

CENTENERA, M. M., RAJ, G. V., KNUDSEN, K. E., TILLEY, W. D. & BUTLER, L. M. 2013. Ex vivo culture of human prostate tissue and drug development. *Nat Rev Urol,* 10**,** 483-7.

CERTO, M., MOORE, V. D. G., NISHINO, M., WEI, G., KORSMEYER, S., ARMSTRONG, S. A. & LETAI, A. 2006. Mitochondria primed by death signals determine cellular addiction to antiapoptotic BCL-2 family members. *Cancer cell,* 9**,** 351-365.

CHAI, W., SHAY, J. W. & WRIGHT, W. E. 2005. Human telomeres maintain their overhang length at senescence. *Mol Cell Biol,* 25**,** 2158-68.

CHANDRA, T., KIRSCHNER, K., THURET, J. Y., POPE, B. D., RYBA, T., NEWMAN, S., AHMED, K., SAMARAJIWA, S. A., SALAMA, R., CARROLL, T., STARK, R., JANKY, R., NARITA, M., XUE, L., CHICAS, A., NÚÑEZ, S., JANKNECHT, R., HAYASHI-TAKANAKA, Y., WILSON, M. D., MARSHALL, A., ODOM, D. T., BABU, M. M., BAZETT-JONES, D. P., TAVARÉ, S., EDWARDS, P. A., LOWE, S. W., KIMURA, H., GILBERT, D. M. & NARITA, M. 2012. Independence of repressive histone marks and chromatin compaction during senescent heterochromatic layer formation. *Mol Cell,* 47**,** 203-14.

CHANDRASHEKARA, K., POPLI, S. & SHAKARAD, M. 2014. Curcumin enhances parental reproductive lifespan and progeny viability in Drosophila melanogaster. *Age,* 36**,** 9702.

CHANG, B.-D., XUAN, Y., BROUDE, E. V., ZHU, H., SCHOTT, B., FANG, J. & RONINSON, I. B. 1999. Role of p53 and p21waf1/cip1 in senescence-like terminal proliferation arrest induced in human tumor cells by chemotherapeutic drugs. *Oncogene,* 18**,** 4808-4818.

CHANG, B. Y., FRANCESCO, M., DE ROOIJ, M. F. M., MAGADALA, P., STEGGERDA, S. M., HUANG, M. M., KUIL, A., HERMAN, S. E. M., CHANG, S., PALS, S. T., WILSON, W., WIESTNER, A., SPAARGAREN, M., BUGGY, J. J. & ELIAS, L. 2013. Egress of CD19(+)CD5(+) cells into peripheral blood following treatment with the Bruton tyrosine kinase inhibitor ibrutinib in mantle cell lymphoma patients. *Blood,* 122**,** 2412-2424.

CHANG, J., WANG, Y., SHAO, L., LABERGE, R.-M., DEMARIA, M., CAMPISI, J., JANAKIRAMAN, K., SHARPLESS, N. E., DING, S. & FENG, W. 2016a. Clearance of senescent cells by ABT263 rejuvenates aged hematopoietic stem cells in mice. *Nature medicine,* 22**,** 78-83.

CHANG, J., WANG, Y., SHAO, L., LABERGE, R. M., DEMARIA, M., CAMPISI, J., JANAKIRAMAN, K., SHARPLESS, N. E., DING, S., FENG, W., LUO, Y., WANG, X., AYKIN-BURNS, N., KRAGER, K., PONNAPPAN, U., HAUER-JENSEN, M., MENG, A. & ZHOU, D. 2016b. Clearance of senescent cells by ABT263 rejuvenates aged hematopoietic stem cells in mice. *Nat Med,* 22**,** 78-83.

CHARI, R. V., MILLER, M. L. & WIDDISON, W. C. 2014. Antibody-drug conjugates: an emerging concept in cancer therapy. *Angew Chem Int Ed Engl,* 53**,** 3796-827.

CHAUHAN, D., VELANKAR, M., BRAHMANDAM, M., HIDESHIMA, T., PODAR, K., RICHARDSON, P., SCHLOSSMAN, R., GHOBRIAL, I., RAJE, N. & MUNSHI, N. 2007.

A novel Bcl-2/Bcl-X L/Bcl-w inhibitor ABT-737 as therapy in multiple myeloma. *Oncogene,* 26**,** 2374-2380.

CHEN, L., LEE, L., KUDLOW, B. A., DOS SANTOS, H. G., SLETVOLD, O., SHAFEGHATI, Y., BOTHA, E. G., GARG, A., HANSON, N. B., MARTIN, G. M., MIAN, I. S., KENNEDY, B. K. & OSHIMA, J. 2003. LMNA mutations in atypical Werner's syndrome. *The Lancet,* 362**,** 440-445.

CHEN, Q., FISCHER, A., REAGAN, J. D., YAN, L.-J. & AMES, B. N. 1995. Oxidative DNA damage and senescence of human diploid fibroblast cells. *Proceedings of the National Academy of Sciences,* 92**,** 4337-4341.

CHEN, Q. M., LIU, J. & MERRETT, J. B. 2000a. Apoptosis or senescence-like growth arrest: influence of cell-cycle position, p53, p21 and bax in H2O2 response of normal human fibroblasts. *Biochem J,* 347**,** 543-51.

CHEN, Q. M., TU, V. C., CATANIA, J., BURTON, M., TOUSSAINT, O. & DILLEY, T. 2000b. Involvement of Rb family proteins, focal adhesion proteins and protein synthesis in senescent morphogenesis induced by hydrogen peroxide. *J Cell Sci,* 113 (Pt 22)**,** 4087-97.

CHEN, Y. G., SIDDHANTA, A., AUSTIN, C. D., HAMMOND, S. M., SUNG, T. C., FROHMAN, M. A., MORRIS, A. J. & SHIELDS, D. 1997. Phospholipase D stimulates release of nascent secretory vesicles from the trans-Golgi network. *J Cell Biol,* 138**,** 495-504.

CHEN, Z., TROTMAN, L. C., SHAFFER, D., LIN, H.-K., DOTAN, Z. A., NIKI, M., KOUTCHER, J. A., SCHER, H. I., LUDWIG, T. & GERALD, W. 2005. Crucial role of p53-dependent cellular senescence in suppression of Pten-deficient tumorigenesis. *Nature,* 436**,** 725-730.

CHÈNE, P. 2003. Inhibiting the p53–MDM2 interaction: an important target for cancer therapy. *Nature Reviews Cancer,* 3**,** 102-109.

CHIAO, Y. A. & RABINOVITCH, P. S. 2015. The Aging Heart. *Cold Spring Harbor perspectives in medicine,* 5**,** a025148-a025148.

CHIEN, Y., SCUOPPO, C., WANG, X., FANG, X., BALGLEY, B., BOLDEN, J. E., PREMSRIRUT, P., LUO, W., CHICAS, A., LEE, C. S., KOGAN, S. C. & LOWE, S. W. 2011. Control of the senescence-associated secretory phenotype by NF-κB promotes senescence and enhances chemosensitivity. *Genes Dev,* 25**,** 2125-36.

CHILDS, B. G., BAKER, D. J., KIRKLAND, J. L., CAMPISI, J. & VAN DEURSEN, J. M. 2014. Senescence and apoptosis: dueling or complementary cell fates? *EMBO reports,* 15**,** 1139-1153.

CHILDS, B. G., BAKER, D. J., WIJSHAKE, T., CONOVER, C. A., CAMPISI, J. & VAN DEURSEN, J. M. 2016a. Senescent intimal foam cells are deleterious at all stages of atherosclerosis. *Science,* 354**,** 472.

CHILDS, B. G., BAKER, D. J., WIJSHAKE, T., CONOVER, C. A., CAMPISI, J. & VAN DEURSEN, J. M. 2016b. Senescent intimal foam cells are deleterious at all stages of atherosclerosis. *Science,* 354**,** 472-477.

CHILDS, B. G., GLUSCEVIC, M., BAKER, D. J., LABERGE, R.-M., MARQUESS, D., DANANBERG, J. & VAN DEURSEN, J. M. 2017. Senescent cells: an emerging target for diseases of ageing. *Nature reviews Drug discovery,* 16**,** 718.

CHINTA, S. J., WOODS, G., RANE, A., DEMARIA, M., CAMPISI, J. & ANDERSEN, J. K. 2015. Cellular senescence and the aging brain. *Exp Gerontol,* 68**,** 3-7.

CHOI, S. A., KIM, Y. H., PARK, Y. H., YANG, H. J., JEONG, P. S., CHA, J. J., YOON, S. B., KIM, J. S., SONG, B. S., LEE, J. H., SIM, B. W., HUH, J. W., SONG, I. S., LEE, S. R., KIM, M. K., KIM, J. M., BAE, Y. S., IMAKAWA, K., KIM, S. U. & CHANG, K. T. 2018. Novel crosstalk between Vps26a and Nox4 signaling during neurogenesis. *Cell Death Differ*.

CHOU, T.-C. & TALALAY, P. 1984. Quantitative analysis of dose-effect relationships: the combined effects of multiple drugs or enzyme inhibitors. *Advances in enzyme regulation,* 22**,** 27-55.

CHOU, T. C. 2008. Preclinical versus clinical drug combination studies. *Leuk Lymphoma,* 49**,** 2059-80.

CHOU, T. C. 2010. Drug combination studies and their synergy quantification using the Chou-Talalay method. *Cancer Res,* 70**,** 440-6.

CHRISTOFFERSEN, N. R., SHALGI, R., FRANKEL, L. B., LEUCCI, E., LEES, M., KLAUSEN, M., PILPEL, Y., NIELSEN, F. C., OREN, M. & LUND, A. H. 2010. p53-independent upregulation of miR-34a during oncogene-induced senescence represses MYC. *Cell Death Differ,* 17**,** 236-45.

CHU, Y., LEE, S., SHAH, T., YIN, C., BARTH, M., MILES, R. R., AYELLO, J., MORRIS, E., HARRISON, L., VAN DE VEN, C., GALARDY, P., GOLDMAN, S. C., LIM, M. S., HERMISTON, M., MCALLISTER-LUCAS, L. M., GIULINO-ROTH, L., PERKINS, S. L. & CAIRO, M. S. 2019. Ibrutinib significantly inhibited Bruton's tyrosine kinase (BTK) phosphorylation,in-vitro proliferation and enhanced overall survival in a preclinical Burkitt lymphoma (BL) model. *Oncoimmunology,* 8**,** e1512455.

CHUNG, H. Y., CESARI, M., ANTON, S., MARZETTI, E., GIOVANNINI, S., SEO, A. Y., CARTER, C., YU, B. P. & LEEUWENBURGH, C. 2009. Molecular inflammation: underpinnings of aging and age-related diseases. *Ageing research reviews,* 8**,** 18-30.

CHUPRIN, A., GAL, H., BIRON-SHENTAL, T., BIRAN, A., AMIEL, A., ROZENBLATT, S. & KRIZHANOVSKY, V. 2013. Cell fusion induced by ERVWE1 or measles virus causes cellular senescence. *Genes & development,* 27**,** 2356-2366.

CICHOWSKI, K. & HAHN, W. C. 2008. Unexpected pieces to the senescence puzzle. *Cell,* 133**,** 958-61.

CLAPÉRON, A., GUEDJ, N., MERGEY, M., VIGNJEVIC, D., DESBOIS-MOUTHON, C., BOISSAN, M., SAUBAMÉA, B., PARADIS, V., HOUSSET, C. & FOUASSIER, L. 2012. Loss of EBP50 stimulates EGFR activity to induce EMT phenotypic features in biliary cancer cells. *Oncogene,* 31**,** 1376-1388.

CLEMENTS, M. E., CHABER, C. J., LEDBETTER, S. R. & ZUK, A. 2013. Increased cellular senescence and vascular rarefaction exacerbate the progression of kidney fibrosis in aged mice following transient ischemic injury. *PloS one,* 8**,** e70464.

CMIELOVA, J. & REZÁČOVÁ, M. 2011. p21Cip1/Waf1 protein and its function based on a subcellular localization [corrected]. *Journal of cellular biochemistry,* 112**,** 3502.

COLE, G. M., LIM, G. P., YANG, F., TETER, B., BEGUM, A., MA, Q., HARRIS-WHITE, M. E. & FRAUTSCHY, S. A. 2005. Prevention of Alzheimer's disease: Omega-3 fatty acid and phenolic anti-oxidant interventions. *Neurobiology of aging,* 26**,** 133-136.

COLLADO, M., BLASCO, M. A. & SERRANO, M. 2007. Cellular senescence in cancer and aging. *Cell,* 130**,** 223-33.

COLLADO, M., GIL, J., EFEYAN, A., GUERRA, C., SCHUHMACHER, A. J., BARRADAS, M., BENGURIA, A., ZABALLOS, A., FLORES, J. M., BARBACID, M., BEACH, D. & SERRANO, M. 2005. Tumour biology: senescence in premalignant tumours. *Nature,* 436**,** 642.

COLLINS, C. J. & SEDIVY, J. M. 2003. Involvement of the INK4a/Arf gene locus in senescence. *Aging cell,* 2**,** 145-150.

COPPE, J.-P., BOYSEN, M., SUN, C. H., WONG, B. J., KANG, M. K., PARK, N.-H., DESPREZ, P.-Y., CAMPISI, J. & KRTOLICA, A. 2008. A role for fibroblasts in mediating the effects of tobacco-induced epithelial cell growth and invasion. *Molecular Cancer Research,* 6**,** 1085-1098.

COPPÉ, J.-P., KAUSER, K., CAMPISI, J. & BEAUSÉJOUR, C. M. 2006a. Secretion of vascular endothelial growth factor by primary human fibroblasts at senescence. *Journal of Biological Chemistry,* 281**,** 29568-29574.

COPPÉ, J.-P., PATIL, C. K., RODIER, F., SUN, Y., MUÑOZ, D. P., GOLDSTEIN, J., NELSON, P. S., DESPREZ, P.-Y. & CAMPISI, J. 2008. Senescence-associated secretory phenotypes reveal cell-nonautonomous functions of oncogenic RAS and the p53 tumor suppressor. *PLoS biology,* 6**,** 2853-2868.

COPPÉ, J. P., DESPREZ, P. Y., KRTOLICA, A. & CAMPISI, J. 2010. The senescence-associated secretory phenotype: the dark side of tumor suppression. *Annu Rev Pathol,* 5**,** 99-118.

COPPÉ, J. P., KAUSER, K., CAMPISI, J. & BEAUSÉJOUR, C. M. 2006b. Secretion of vascular endothelial growth factor by primary human fibroblasts at senescence. *J Biol Chem,* 281**,** 29568-74.

COPPÉ, J. P., RODIER, F., PATIL, C. K., FREUND, A., DESPREZ, P. Y. & CAMPISI, J. 2011. Tumor suppressor and aging biomarker p16(INK4a) induces cellular senescence without the associated inflammatory secretory phenotype. *J Biol Chem,* 286**,** 36396-403.

COURTOIS-COX, S., JONES, S. L. & CICHOWSKI, K. 2008. Many roads lead to oncogene-induced senescence. *Oncogene,* 27**,** 2801-2809.

CRESCENZI, E., PALUMBO, G. & BRADY, H. J. 2003. Bcl-2 activates a programme of premature senescence in human carcinoma cells. *Biochem J,* 375**,** 263-74.

CRUCHAGA, C., KARCH, C. M., JIN, S. C., BENITEZ, B. A., CAI, Y., GUERREIRO, R., HARARI, O., NORTON, J., BUDDE, J., BERTELSEN, S., JENG, A. T., COOPER, B., SKORUPA, T., CARRELL, D., LEVITCH, D., HSU, S., CHOI, J., RYTEN, M., HARDY, J., RYTEN, M., TRABZUNI, D., WEALE, M. E., RAMASAMY, A., SMITH, C., SASSI, C., BRAS, J., GIBBS, J. R., HERNANDEZ, D. G., LUPTON, M. K., POWELL, J., FORABOSCO, P., RIDGE, P. G., CORCORAN, C. D., TSCHANZ, J. T., NORTON, M. C., MUNGER, R. G., SCHMUTZ, C., LEARY, M., DEMIRCI, F. Y., BAMNE, M. N., WANG, X., LOPEZ, O. L., GANGULI, M., MEDWAY, C., TURTON, J., LORD, J., BRAAE, A., BARBER, I., BROWN, K., PASSMORE, P., CRAIG, D., JOHNSTON, J., MCGUINNESS, B., TODD, S., HEUN, R., KÖLSCH, H., KEHOE, P. G., HOOPER, N. M., VARDY, E. R. L. C., MANN, D. M., PICKERING-BROWN, S., BROWN, K., KALSHEKER, N., LOWE, J., MORGAN, K., DAVID SMITH, A., WILCOCK, G., WARDEN, D., HOLMES, C., PASTOR, P., LORENZO-BETANCOR, O., BRKANAC, Z., SCOTT, E., TOPOL, E., MORGAN, K., ROGAEVA, E., SINGLETON, A. B., HARDY, J., KAMBOH, M. I., ST GEORGE-HYSLOP, P., CAIRNS, N., MORRIS, J. C., KAUWE, J. S. K., GOATE, A. M., CONSORTIUM, U. K. B. E. & THE ALZHEIMER'S RESEARCH, U. K. C. 2014. Rare coding variants in the phospholipase D3 gene confer risk for Alzheimer's disease. *Nature,* 505**,** 550-554.

CUI, H., KONG, Y., XU, M. & ZHANG, H. 2013. Notch3 functions as a tumor suppressor by controlling cellular senescence. *Cancer Res,* 73**,** 3451-9.

CUNLIFFE, D., KIRBY, A. & ALEXANDER, C. 2005. Molecularly imprinted drug delivery systems.

D'ADDA DI FAGAGNA, F., REAPER, P. M., CLAY-FARRACE, L., FIEGLER, H., CARR, P., VON ZGLINICKI, T., SARETZKI, G., CARTER, N. P. & JACKSON, S. P. 2003. A DNA damage checkpoint response in telomere-initiated senescence. *Nature,* 426**,** 194-8.

D'ADDA DI FAGAGNA, F., TEO, S. H. & JACKSON, S. P. 2004. Functional links between telomeres and proteins of the DNA-damage response. *Genes Dev,* 18**,** 1781-99.

DANIEL, J. A., PELLEGRINI, M., LEE, B. S., GUO, Z., FILSUF, D., BELKINA, N. V., YOU, Z., PAULL, T. T., SLECKMAN, B. P., FEIGENBAUM, L. & NUSSENZWEIG, A. 2012. Loss of ATM kinase activity leads to embryonic lethality in mice. *J Cell Biol,* 198**,** 295-304.

DASTE, A., CHAKIBA, C., DOMBLIDES, C., GROSS-GOUPIL, M., QUIVY, A., RAVAUD, A. & SOUBEYRAN, P. 2016. Targeted therapy and elderly people: A review.

DAVAAPIL, H., BROCKES, J. P. & YUN, M. H. 2017. Conserved and novel functions of programmed cellular senescence during vertebrate development. *Development,* 144**,** 106-114.

DAVID, A. V. A., ARULMOLI, R. & PARASURAMAN, S. 2016. Overviews of biological importance of quercetin: a bioactive flavonoid. *Pharmacognosy reviews,* 10**,** 84.

DE KEIZER, P. L., BURGERING, B. M. & DANSEN, T. B. 2011. Forkhead box o as a sensor, mediator, and regulator of redox signaling. *Antioxidants & redox signaling,* 14**,** 1093-1106.

DE KEIZER, P. L., LABERGE, R.-M. & CAMPISI, J. 2010. p53: Pro-aging or pro-longevity? *Aging (Albany NY),* 2**,** 377.

DE LA CUEVA, E., GARCÍA-CAO, I., HERRANZ, M., LÓPEZ, P., GARCÍA-PALENCIA, P., FLORES, J. M., SERRANO, M., FERNÁNDEZ-PIQUERAS, J. & MARTÍN-CABALLERO, J. 2006. Tumorigenic activity of p21Waf1/Cip1 in thymic lymphoma. *Oncogene,* 25**,** 4128-4132.

DEACON, R. M. 2013. Measuring the strength of mice. *J Vis Exp*.

DEBACQ-CHAINIAUX, F., ERUSALIMSKY, J. D., CAMPISI, J. & TOUSSAINT, O. 2009. Protocols to detect senescence-associated beta-galactosidase (SA-βgal) activity, a biomarker of senescent cells in culture and in vivo. *Nature Protocols,* 4**,** 1798-1806.

DECHAT, T., PFLEGHAAR, K., SENGUPTA, K., SHIMI, T., SHUMAKER, D. K., SOLIMANDO, L. & GOLDMAN, R. D. 2008. Nuclear lamins: major factors in the structural organization and function of the nucleus and chromatin. *Genes & development,* 22**,** 832-853.

DEMARIA, M., O'LEARY, M. N., CHANG, J., SHAO, L., LIU, S., ALIMIRAH, F., KOENIG, K., LE, C., MITIN, N. & DEAL, A. M. 2017. Cellular senescence promotes adverse effects of chemotherapy and cancer relapse. *Cancer discovery,* 7**,** 165-176.

DEMARIA, M., OHTANI, N., YOUSSEF, S. A., RODIER, F., TOUSSAINT, W., MITCHELL, J. R., LABERGE, R.-M., VIJG, J., VAN STEEG, H. & DOLLÉ, M. E. 2014a. An essential role

for senescent cells in optimal wound healing through secretion of PDGF-AA. *Developmental cell,* 31**,** 722-733.

DEMARIA, M., OHTANI, N., YOUSSEF, S. A., RODIER, F., TOUSSAINT, W., MITCHELL, J. R., LABERGE, R. M., VIJG, J., VAN STEEG, H., DOLLÉ, M. E., HOEIJMAKERS, J. H., DE BRUIN, A., HARA, E. & CAMPISI, J. 2014b. An essential role for senescent cells in optimal wound healing through secretion of PDGF-AA. *Dev Cell,* 31**,** 722-33.

DEMIDENKO, Z. N., FOJO, T. & BLAGOSKLONNY, M. V. 2005. Complementation of two mutant p53: implications for loss of heterozygosity in cancer. *FEBS Lett,* 579**,** 2231-5.

DENG, J., CARLSON, N., TAKEYAMA, K., DAL CIN, P., SHIPP, M. & LETAI, A. 2007. BH3 profiling identifies three distinct classes of apoptotic blocks to predict response to ABT-737 and conventional chemotherapeutic agents. *Cancer Cell,* 12**,** 171-85.

DENIC, A., GLASSOCK, R. J. & RULE, A. D. 2016. Structural and Functional Changes With the Aging Kidney. *Adv Chronic Kidney Dis,* 23**,** 19-28.

DI LEONARDO, A., LINKE, S. P., CLARKIN, K. & WAHL, G. M. 1994. DNA damage triggers a prolonged p53-dependent G1 arrest and long-term induction of Cip1 in normal human fibroblasts. *Genes & development,* 8**,** 2540-2551.

DI MITRI, D., TOSO, A., CHEN, J. J., SARTI, M., PINTON, S., JOST, T. R., D'ANTUONO, R., MONTANI, E., GARCIA-ESCUDERO, R., GUCCINI, I., DA SILVA-ALVAREZ, S., COLLADO, M., EISENBERGER, M., ZHANG, Z., CATAPANO, C., GRASSI, F. & ALIMONTI, A. 2014. Tumour-infiltrating Gr-1+ myeloid cells antagonize senescence in cancer. *Nature,* 515**,** 134-7.

DIMRI, G. P., LEE, X., BASILE, G., ACOSTA, M., SCOTT, G., ROSKELLEY, C., MEDRANO, E. E., LINSKENS, M., RUBELJ, I. & PEREIRA-SMITH, O. 1995. A biomarker that identifies senescent human cells in culture and in aging skin in vivo. *Proceedings of the National Academy of Sciences of the United States of America,* 92**,** 9363-9367.

DINKOVA-KOSTOVA, A. T., CORY, A. H., BOZAK, R. E., HICKS, R. J. & CORY, J. G. 2007. Bis (2-hydroxybenzylidene) acetone, a potent inducer of the phase 2 response, causes apoptosis in mouse leukemia cells through a p53-independent, caspase-mediated pathway. *Cancer letters,* 245**,** 341-349.

DOKTER, W., UBINK, R., VAN DER LEE, M., VAN DER VLEUTEN, M., VAN ACHTERBERG, T., JACOBS, D., LOOSVELD, E., VAN DEN DOBBELSTEEN, D., EGGING, D., MATTAAR, E., GROOTHUIS, P., BEUSKER, P., COUMANS, R., ELGERSMA, R., MENGE, W., JOOSTEN, J., SPIJKER, H., HUIJBREGTS, T., DE GROOT, V., EPPINK, M., DE ROO, G., VERHEIJDEN, G. & TIMMERS, M. 2014. Preclinical profile of the HER2-targeting ADC SYD983/SYD985: introduction of a new duocarmycin-based linker-drug platform. *Mol Cancer Ther,* 13**,** 2618-29.

DONEHOWER, L. A., HARVEY, M., SLAGLE, B. L., MCARTHUR, M. J., MONTGOMERY, C. A., BUTEL, J. S. & BRADLEY, A. 1992. Mice deficient for p53 are developmentally normal but susceptible to spontaneous tumours. *Nature,* 356**,** 215-221.

DRAYTON, S. & PETERS, G. 2002. Immortalisation and transformation revisited. *Curr Opin Genet Dev,* 12**,** 98-104.

DUTTA, S., RYAN, J., CHEN, T. S., KOUGENTAKIS, C., LETAI, A. & KEATING, A. E. 2015. Potent and specific peptide inhibitors of human pro-survival protein Bcl-xL. *J Mol Biol,* 427**,** 1241-1253.

DZIEGIELEWSKI, J., BAULCH, J. E., GOETZ, W., COLEMAN, M. C., SPITZ, D. R., MURLEY, J. S., GRDINA, D. J. & MORGAN, W. F. 2008. WR-1065, the active metabolite of amifostine, mitigates radiation-induced delayed genomic instability. *Free Radic Biol Med,* 45**,** 1674-81.

EFEYAN, A., ORTEGA-MOLINA, A., VELASCO-MIGUEL, S., HERRANZ, D., VASSILEV, L. T. & SERRANO, M. 2007. Induction of p53-dependent senescence by the MDM2 antagonist nutlin-3a in mouse cells of fibroblast origin. *Cancer Research,* 67**,** 7350-7357.

EGGERT, T., WOLTER, K., JI, J., MA, C., YEVSA, T., KLOTZ, S., MEDINA-ECHEVERZ, J., LONGERICH, T., FORGUES, M., REISINGER, F., HEIKENWALDER, M., WANG, X. W., ZENDER, L. & GRETEN, T. F. 2016. Distinct Functions of Senescence-Associated Immune Responses in Liver Tumor Surveillance and Tumor Progression. *Cancer Cell,* 30**,** 533-547.

EHRLICH, P. 1906. The relationship existing between chemical constitution, distribution and pharmacological action. *Collected Studies on Immunity***,** 441-450.

EIJKELENBOOM, A. & BURGERING, B. M. 2013. FOXOs: signalling integrators for homeostasis maintenance. *Nature reviews Molecular cell biology,* 14**,** 83-97.

EKPENYONG-AKIBA, A. E. 2018. *Novel Approaches for the Identification and Targeted Clearance of Senescent Cells, as a Therapeutic Strategy for Senescence-related and Age-related Diseases.* University of Leicester.

EKPENYONG-AKIBA, A. E., CANFAROTTA, F., ABD H, B., POBLOCKA, M., CASULLERAS, M., CASTILLA-VALLMANYA, L., KOCSIS-FODOR, G., KELLY, M. E., JANUS, J., ALTHUBITI, M., PILETSKA, E., PILETSKY, S. & MACIP, S. 2019. Detecting and targeting senescent cells using molecularly imprinted nanoparticles. *Nanoscale Horizons,* 4**,** 757-768.

EKPENYONG-AKIBA, A. E., POBLOCKA, M., ALTHUBITI, M., RADA, M., JURK, D., GERMANO, S., KOCSIS-FODOR, G., SHI, Y., CANALES, J. J. & MACIP, S. 2020a. Amelioration of age-related brain function decline by Bruton's tyrosine kinase inhibition. *Aging Cell,* 19**,** e13079.

EKPENYONG-AKIBA, A. E., POBLOCKA, M. & MACIP, S. 2020b. Targeted Senolytic Strategies Based on the Senescent Surfaceome. *Senolytics in Disease, Ageing and Longevity.* Springer.

EL-DEIRY, W. S., KERN, S. E., PIETENPOL, J. A., KINZLER, K. W. & VOGELSTEIN, B. 1992. Definition of a consensus binding site for p53. *Nat Genet,* 1**,** 45-9.

ENO, C. O., ECKENRODE, E. F., OLBERDING, K. E., ZHAO, G., WHITE, C. & LI, C. 2012. Distinct roles of mitochondria- and ER-localized Bcl-xL in apoptosis resistance and Ca2+ homeostasis. *Mol Biol Cell,* 23**,** 2605-18.

ERIKSSON, M., BROWN, W. T., GORDON, L. B., GLYNN, M. W., SINGER, J., SCOTT, L., ERDOS, M. R., ROBBINS, C. M., MOSES, T. Y., BERGLUND, P., DUTRA, A., PAK, E., DURKIN, S., CSOKA, A. B., BOEHNKE, M., GLOVER, T. W. & COLLINS, F. S. 2003. Recurrent de novo point mutations in lamin A cause Hutchinson–Gilford progeria syndrome. *Nature,* 423**,** 293.

ESIRI, M. 2007. Ageing and the brain. *The Journal of Pathology,* 211**,** 181-187.

EVERETT, L. A., GLASER, B., BECK, J. C., IDOL, J. R., BUCHS, A., HEYMAN, M., ADAWI, F., HAZANI, E., NASSIR, E., BAXEVANIS, A. D., SHEFFIELD, V. C. & GREEN, E. D. 1997. Pendred syndrome is caused by mutations in a putative sulphate transporter gene (PDS). *Nat Genet,* 17**,** 411-22.

EWALD, J. A., DESOTELLE, J. A., WILDING, G. & JARRARD, D. F. 2010. Therapy-induced senescence in cancer. *J Natl Cancer Inst,* 102**,** 1536-46.

EYMAN, D., DAMODARASAMY, M., PLYMATE, S. R. & REED, M. J. 2009. CCL5 secreted by senescent aged fibroblasts induces proliferation of prostate epithelial cells and expression of genes that modulate angiogenesis. *J Cell Physiol,* 220**,** 376-81.

FAGET, D. V., REN, Q. & STEWART, S. A. 2019. Unmasking senescence: context-dependent effects of SASP in cancer. *Nature Reviews Cancer,* 19**,** 439-453.

FALCICCHIO, M., WARD, J. A., MACIP, S. & DOVESTON, R. G. 2020. Regulation of p53 by the 14-3-3 protein interaction network: new opportunities for drug discovery in cancer. *Cell Death Discovery,* 6**,** 126.

FALSCHLEHNER, C., EMMERICH, C. H., GERLACH, B. & WALCZAK, H. 2007. TRAIL signalling: Decisions between life and death. *The International Journal of Biochemistry & Cell Biology,* 39**,** 1462-1475.

FANG, L., IGARASHI, M., LEUNG, J., SUGRUE, M. M., LEE, S. W. & AARONSON, S. A. 1999. p21Waf1/Cip1/Sdi1 induces permanent growth arrest with markers of replicative senescence in human tumor cells lacking functional p53. *Oncogene,* 18**,** 2789.

FARR, J. N., XU, M., WEIVODA, M. M., MONROE, D. G., FRASER, D. G., ONKEN, J. L., NEGLEY, B. A., SFEIR, J. G., OGRODNIK, M. B., HACHFELD, C. M., LEBRASSEUR, N. K., DRAKE, M. T., PIGNOLO, R. J., PIRTSKHALAVA, T., TCHKONIA, T., OURSLER, M. J., KIRKLAND, J. L. & KHOSLA, S. 2017a. Targeting cellular senescence prevents age-related bone loss in mice. *Nature Medicine,* 23**,** 1072-1079.

FARR, J. N., XU, M., WEIVODA, M. M., MONROE, D. G., FRASER, D. G., ONKEN, J. L., NEGLEY, B. A., SFEIR, J. G., OGRODNIK, M. B., HACHFELD, C. M., LEBRASSEUR, N. K., DRAKE, M. T., PIGNOLO, R. J., PIRTSKHALAVA, T., TCHKONIA, T., OURSLER, M. J., KIRKLAND, J. L. & KHOSLA, S. 2017b. Targeting cellular senescence prevents age-related bone loss in mice. *Nat Med,* 23**,** 1072-1079.

FLORENCE, A. T. & LEE, V. H. L. 2011. Personalised medicines: More tailored drugs, more tailored delivery.

FOIGHT, G. W., RYAN, J. A., GULLA, S. V., LETAI, A. & KEATING, A. E. 2014. Designed BH3 peptides with high affinity and specificity for targeting Mcl-1 in cells. *ACS Chem Biol,* 9**,** 1962-8.

FONG, L. G., NG, J. K., LAMMERDING, J., VICKERS, T. A., META, M., COTÉ, N., GAVINO, B., QIAO, X., CHANG, S. Y. & YOUNG, S. R. 2006. Prelamin A and lamin A appear to be dispensable in the nuclear lamina. *The Journal of clinical investigation,* 116**,** 743-752.

FRACKOWIAK, J., MAZUR-KOLECKA, B., KACZMARSKI, W. & DICKSON, D. 2001. Deposition of Alzheimer's vascular amyloid-beta is associated with decreased expression of brain L-3-hydroxyacyl-coenzyme A dehydrogenase (ERAB). *Brain Res,* 907**,** 44-53.

FRANCESCHI, C., CAPRI, M., MONTI, D., GIUNTA, S., OLIVIERI, F., SEVINI, F., PANOURGIA, M. P., INVIDIA, L., CELANI, L. & SCURTI, M. 2007. Inflammaging and anti-inflammaging: a systemic perspective on aging and longevity emerged from studies in humans. *Mechanisms of ageing and development,* 128**,** 92-105.

FREITAS-RODRÍGUEZ, S., FOLGUERAS, A. R. & LÓPEZ-OTÍN, C. 2017. The role of matrix metalloproteinases in aging: Tissue remodeling and beyond. *Biochimica et Biophysica Acta (BBA) - Molecular Cell Research,* 1864**,** 2015-2025.

FREUND, A., LABERGE, R. M., DEMARIA, M. & CAMPISI, J. 2012. Lamin B1 loss is a senescence-associated biomarker. *Mol Biol Cell,* 23**,** 2066-75.

FREUND, A., PATIL, C. K. & CAMPISI, J. 2011. p38MAPK is a novel DNA damage response-independent regulator of the senescence-associated secretory phenotype. *The EMBO journal,* 30**,** 1536-1548.

FRIPPIAT, C., CHEN, Q. M., ZDANOV, S., MAGALHAES, J.-P., REMACLE, J. & TOUSSAINT, O. 2001. Subcytotoxic H2O2 stress triggers a release of transforming growth

factor-β1, which induces biomarkers of cellular senescence of human diploid fibroblasts. *Journal of Biological Chemistry,* 276**,** 2531-2537.

FUHRMANN-STROISSNIGG, H., LING, Y. Y., ZHAO, J., MCGOWAN, S. J., ZHU, Y., BROOKS, R. W., GRASSI, D., GREGG, S. Q., STRIPAY, J. L. & DORRONSORO, A. 2017a. Identification of HSP90 inhibitors as a novel class of senolytics. *Nature Communications,* 8**,** 1-14.

FUHRMANN-STROISSNIGG, H., LING, Y. Y., ZHAO, J., MCGOWAN, S. J., ZHU, Y., BROOKS, R. W., GRASSI, D., GREGG, S. Q., STRIPAY, J. L., DORRONSORO, A., CORBO, L., TANG, P., BUKATA, C., RING, N., GIACCA, M., LI, X., TCHKONIA, T., KIRKLAND, J. L., NIEDERNHOFER, L. J. & ROBBINS, P. D. 2017b. Identification of HSP90 inhibitors as a novel class of senolytics. *Nature Communications,* 8**,** 422.

FUMAGALLI, M., ROSSIELLO, F., CLERICI, M., BAROZZI, S., CITTARO, D., KAPLUNOV, J. M., BUCCI, G., DOBREVA, M., MATTI, V., BEAUSEJOUR, C. M., HERBIG, U., LONGHESE, M. P. & D'ADDA DI FAGAGNA, F. 2012. Telomeric DNA damage is irreparable and causes persistent DNA-damage-response activation. *Nat Cell Biol,* 14**,** 355-65.

FUSE, A., FURUYA, N., KAKUTA, S., INOSE, A., SATO, M., KOIKE, M., SAIKI, S. & HATTORI, N. 2015. VPS29–VPS35 intermediate of retromer is stable and may be involved in the retromer complex assembly process. *FEBS Letters,* 589**,** 1430-1436.

GALLON, M. & CULLEN, P. J. 2015. Retromer and sorting nexins in endosomal sorting. Portland Press Ltd.

GAMBARDELLA, S., BIAGIONI, F., FERESE, R., BUSCETI, C. L., FRATI, A., NOVELLI, G., RUGGIERI, S. & FORNAI, F. 2016. Vacuolar Protein Sorting Genes in Parkinson's Disease: A Re-appraisal of Mutations Detection Rate and Neurobiology of Disease. *Frontiers in neuroscience,* 10**,** 532-532.

GARCIA-CAO, I., GARCIA-CAO, M., MARTIN-CABALLERO, J., CRIADO, L. M., KLATT, P., FLORES, J. M., WEILL, J. C., BLASCO, M. A. & SERRANO, M. 2002. "Super p53" mice exhibit enhanced DNA damage response, are tumor resistant and age normally. *EMBO J,* 21**,** 6225-35.

GARTEL, A. L. & TYNER, A. L. 2002. The role of the cyclin-dependent kinase inhibitor p21 in apoptosis 1 supported in part by NIH grant R01 DK56283 (to ALT) for the p21 research and Campus Research Board and Illinois Department of Public Health Penny Severns Breast and Cervical Cancer grants (to ALG). 1. *Molecular cancer therapeutics,* 1**,** 639-649.

GAYLE, S. S., SAHNI, J. M., WEBB, B. M., WEBER-BONK, K. L., SHIVELY, M. S., SPINA, R., BAR, E. E., SUMMERS, M. K. & KERI, R. A. 2019. Targeting BCL-xL improves the efficacy of bromodomain and extra-terminal protein inhibitors in triple-negative breast cancer by eliciting the death of senescent cells. *J Biol Chem,* 294**,** 875-886.

GAZDAR, A. F., KURVARI, V., VIRMANI, A., GOLLAHON, L., SAKAGUCHI, M., WESTERFIELD, M., KODAGODA, D., STASNY, V., CUNNINGHAM, H. T., WISTUBA, I. I., TOMLINSON, G., TONK, V., ASHFAQ, R., LEITCH, A. M., MINNA, J. D. & SHAY, J. W. 1998. Characterization of paired tumor and non-tumor cell lines established from patients with breast cancer. *International Journal of Cancer,* 78**,** 766-774.

GÉBLEUX, R. & CASI, G. 2016. Antibody-drug conjugates: Current status and future perspectives.

GEORGAKILAS, A. G., MARTIN, O. A. & BONNER, W. M. 2017. p21: A Two-Faced Genome Guardian. *Trends Mol Med,* 23**,** 310-319.

GEORGAKOPOULOU, E. A., TSIMARATOU, K., EVANGELOU, K., FERNANDEZ MARCOS, P. J., ZOUMPOURLIS, V., TROUGAKOS, I. P., KLETSAS, D., BARTEK, J., SERRANO, M. & GORGOULIS, V. G. 2013. Specific lipofuscin staining as a novel biomarker to detect replicative and stress-induced senescence. A method applicable in cryo-preserved and archival tissues. *Aging (Albany NY),* 5**,** 37-50.

GEORGESCU, M. M., MORALES, F. C., MOLINA, J. R. & HAYASHI, Y. 2008. Roles of NHERF1/EBP50 in cancer. *Curr Mol Med,* 8**,** 459-68.

GONZALEZ, A. C., SCHWEIZER, M., JAGDMANN, S., BERNREUTHER, C., REINHECKEL, T., SAFTIG, P. & DAMME, M. 2018. Unconventional Trafficking of Mammalian Phospholipase D3 to Lysosomes. *Cell Rep,* 22**,** 1040-1053.

GONZÁLEZ-GARCÍA, M., GARCIA, I., DING, L., O'SHEA, S., BOISE, L. H., THOMPSON, C. B. & NÚÑEZ, G. 1995. Bcl-x is expressed in embryonic and postnatal neural tissues and functions to prevent neuronal cell death. *Proceedings of the National Academy of Sciences,* 92**,** 4304-4308.

GONZÁLEZ-GUALDA, E., PÀEZ-RIBES, M., LOZANO-TORRES, B., MACIAS, D., WILSON III, J. R., GONZÁLEZ-LÓPEZ, C., OU, H.-L., MIRÓN-BARROSO, S., ZHANG, Z., LÉRIDA-VISO, A., BLANDEZ, J. F., BERNARDOS, A., SANCENÓN, F., ROVIRA, M., FRUK, L., MARTINS, C. P., SERRANO, M., DOHERTY, G. J., MARTÍNEZ-MÁÑEZ, R. & MUÑOZ-ESPÍN, D. 2020a. Galacto-conjugation of Navitoclax as an efficient strategy to increase senolytic specificity and reduce platelet toxicity. *Aging Cell,* 19**,** e13142.

GONZÁLEZ-GUALDA, E., PÀEZ-RIBES, M., LOZANO-TORRES, B., MACIAS, D., WILSON, J. R., 3RD, GONZÁLEZ-LÓPEZ, C., OU, H. L., MIRÓN-BARROSO, S., ZHANG, Z., LÉRIDA-VISO, A., BLANDEZ, J. F., BERNARDOS, A., SANCENÓN, F., ROVIRA, M., FRUK, L., MARTINS, C. P., SERRANO, M., DOHERTY, G. J., MARTÍNEZ-MÁÑEZ, R. & MUÑOZ-ESPÍN, D. 2020b. Galacto-conjugation of Navitoclax as an efficient strategy to increase senolytic specificity and reduce platelet toxicity. *Aging Cell,* 19**,** e13142.

GOODWIN, A. & JENKINS, G. 2009. Role of integrin-mediated TGFbeta activation in the pathogenesis of pulmonary fibrosis. *Biochem Soc Trans,* 37**,** 849-54.

GORGOULIS, V., ADAMS, P. D., ALIMONTI, A., BENNETT, D. C., BISCHOF, O., BISHOP, C., CAMPISI, J., COLLADO, M., EVANGELOU, K., FERBEYRE, G., GIL, J., HARA, E., KRIZHANOVSKY, V., JURK, D., MAIER, A. B., NARITA, M., NIEDERNHOFER, L., PASSOS, J. F., ROBBINS, P. D., SCHMITT, C. A., SEDIVY, J., VOUGAS, K., VON ZGLINICKI, T., ZHOU, D., SERRANO, M. & DEMARIA, M. 2019. Cellular Senescence: Defining a Path Forward. *Cell,* 179**,** 813-827.

GOWDA, S., DESAI, P. B., KULKARNI, S. S., HULL, V. V., MATH, A. A. K. & VERNEKAR, S. N. 2010. Markers of renal function tests. *North American journal of medical sciences,* 2**,** 170-173.

GRASSILLI, E., PISANO, F., CIALDELLA, A., BONOMO, S., MISSAGLIA, C., CERRITO, M. G., MASIERO, L., IANZANO, L., GIORDANO, F., CICIRELLI, V., NARLOCH, R., D'AMATO, F., NOLI, B., FERRI, G. L., LEONE, B. E., STANTA, G., BONIN, S., HELIN, K., GIOVANNONI, R. & LAVITRANO, M. 2016. A novel oncogenic BTK isoform is overexpressed in colon cancers and required for RAS-mediated transformation. *Oncogene,* 35**,** 4368-78.

GREEN, D. R. & EVAN, G. I. 2002. A matter of life and death. *Cancer Cell,* 1**,** 19-30.

GRIFFITH, J. D., COMEAU, L., ROSENFIELD, S., STANSEL, R. M., BIANCHI, A., MOSS, H. & DE LANGE, T. 1999. Mammalian telomeres end in a large duplex loop. *Cell,* 97**,** 503-14.

GRILL, A. E., SHAHANI, K., KONIAR, B. & PANYAM, J. 2018. Chemopreventive efficacy of curcumin-loaded PLGA microparticles in a transgenic mouse model of HER-2-positive breast cancer. *Drug delivery and translational research,* 8**,** 329-341.

GUERRERO, A., GUIHO, R., HERRANZ, N., UREN, A., WITHERS, D. J., MARTÍNEZ-BARBERA, J. P., TIETZE, L. F. & GIL, J. 2020. Galactose-modified duocarmycin prodrugs as senolytics. *Aging Cell,* 19**,** e13133.

GUERRERO, A., HERRANZ, N., SUN, B., WAGNER, V., GALLAGE, S., GUIHO, R., WOLTER, K., POMBO, J., IRVINE, E. E. & INNES, A. J. 2019a. Cardiac glycosides are broad-spectrum senolytics. *Nature metabolism,* 1**,** 1074-1088.

GUERRERO, A., HERRANZ, N., SUN, B., WAGNER, V., GALLAGE, S., GUIHO, R., WOLTER, K., POMBO, J., IRVINE, E. E., INNES, A. J., BIRCH, J., GLEGOLA, J., MANSHAEI, S., HEIDE, D., DHARMALINGAM, G., HARBIG, J., OLONA, A., BEHMOARAS, J., DAUCH, D., UREN, A. G., ZENDER, L., VERNIA, S., MARTÍNEZ-BARBERA, J. P., HEIKENWALDER, M., WITHERS, D. J. & GIL, J. 2019b. Cardiac glycosides are broad-spectrum senolytics. *Nat Metab,* 1**,** 1074-1088.

GUSTAVSSON, E. K., GUELLA, I., TRINH, J., SZU-TU, C., RAJPUT, A., RAJPUT, A. H., STEELE, J. C., MCKEOWN, M., JEON, B. S., AASLY, J. O. & FARRER, M. J. 2015. Genetic variability of the retromer cargo recognition complex in parkinsonism. *Mov Disord,* 30**,** 580-4.

GUTHOFF, M., WAGNER, R., RANDRIANARISOA, E., HATZIAGELAKI, E., PETER, A., HÄRING, H.-U., FRITSCHE, A. & HEYNE, N. 2017. Soluble urokinase receptor (suPAR) predicts microalbuminuria in patients at risk for type 2 diabetes mellitus. *Scientific reports,* 7**,** 1-7.

HAJMIRZA, A., EMADALI, A., GAUTHIER, A., CASASNOVAS, O., GRESSIN, R. & CALLANAN, M. B. 2018. BET family protein BRD4: An emerging actor in NFκB signaling in inflammation and cancer. *Biomedicines,* 6**,** 16.

HAMPEL, B., MALISAN, F., NIEDEREGGER, H., TESTI, R. & JANSEN-DÜRR, P. 2004. Differential regulation of apoptotic cell death in senescent human cells. *Exp Gerontol,* 39**,** 1713-21.

HANNAH, R., BECK, M., MORAVEC, R. & RISS, T. 2001. CellTiter-Glo™ Luminescent cell viability assay: a sensitive and rapid method for determining cell viability. *Promega Cell Notes,* 2**,** 11-13.

HARBORTH, J., ELBASHIR, S. M., BECHERT, K., TUSCHL, T. & WEBER, K. 2001. Identification of essential genes in cultured mammalian cells using small interfering RNAs. *Journal of cell science,* 114**,** 4557-4565.

HARLEY, C. B., FUTCHER, A. B. & GREIDER, C. W. 1990. Telomeres shorten during ageing of human fibroblasts. *Nature,* 345**,** 458-60.

HARPER, J. W., ADAMI, G. R., WEI, N., KEYOMARSI, K. & ELLEDGE, S. J. 1993. The p21 Cdk-interacting protein Cip1 is a potent inhibitor of G1 cyclin-dependent kinases. *Cell,* 75**,** 805-816.

HARRISON, D. E., STRONG, R., ALLISON, D. B., AMES, B. N., ASTLE, C. M., ATAMNA, H., FERNANDEZ, E., FLURKEY, K., JAVORS, M. A. & NADON, N. L. 2014. Acarbose, 17-α-estradiol, and nordihydroguaiaretic acid extend mouse lifespan preferentially in males. *Aging cell,* 13**,** 273-282.

HARRISON, D. E., STRONG, R., SHARP, Z. D., NELSON, J. F., ASTLE, C. M., FLURKEY, K., NADON, N. L., WILKINSON, J. E., FRENKEL, K. & CARTER, C. S. 2009. Rapamycin fed late in life extends lifespan in genetically heterogeneous mice. *nature,* 460**,** 392-395.

HARVEY, M., MCARTHUR, M. J., MONTGOMERY, C. A., JR., BUTEL, J. S., BRADLEY, A. & DONEHOWER, L. A. 1993. Spontaneous and carcinogen-induced tumorigenesis in p53-deficient mice. *Nat Genet,* 5**,** 225-9.

HATA, A. N., ENGELMAN, J. A. & FABER, A. C. 2015. The BCL2 Family: Key Mediators of the Apoptotic Response to Targeted Anticancer Therapeutics. *Cancer Discov,* 5**,** 475-87.

HAYASHI, Y., MOLINA, J. R., HAMILTON, S. R. & GEORGESCU, M.-M. 2010. NHERF1/EBP50 Is a New Marker in Colorectal Cancer. *Neoplasia,* 12**,** 1013-IN9.

HAYEK, S. S., SEVER, S., KO, Y.-A., TRACHTMAN, H., AWAD, M., WADHWANI, S., ALTINTAS, M. M., WEI, C., HOTTON, A. L. & FRENCH, A. L. 2015. Soluble urokinase receptor and chronic kidney disease. *New England Journal of Medicine,* 373**,** 1916-1925.

HAYFLICK, L. 1965. THE LIMITED IN VITRO LIFETIME OF HUMAN DIPLOID CELL STRAINS. *Exp Cell Res,* 37**,** 614-36.

HAYFLICK, L. & MOORHEAD, P. S. 1961. The serial cultivation of human diploid cell strains. *Exp Cell Res,* 25**,** 585-621.

HE, S. & SHARPLESS, N. E. 2017. Senescence in Health and Disease. *Cell,* 169**,** 1000-1011.

HE, X., LI, F., CHANG, W.-P. & TANG, J. 2005. GGA proteins mediate the recycling pathway of memapsin 2 (BACE). *Journal of Biological Chemistry,* 280**,** 11696-11703.

HE, Y., LI, W., HU, G., SUN, H. & KONG, Q. 2018. Bioactivities of EF24, a novel curcumin analog: a review. *Frontiers in oncology,* 8**,** 614.

HERBIG, U., JOBLING, W. A., CHEN, B. P., CHEN, D. J. & SEDIVY, J. M. 2004. Telomere shortening triggers senescence of human cells through a pathway involving ATM, p53, and p21(CIP1), but not p16(INK4a). *Mol Cell,* 14**,** 501-13.

HERMAN, S. E. M., GORDON, A. L., HERTLEIN, E., RAMANUNNI, A., ZHANG, X., JAGLOWSKI, S., FLYNN, J., JONES, J., BLUM, K. A., BUGGY, J. J., HAMDY, A., JOHNSON, A. J. & BYRD, J. C. 2011. Bruton tyrosine kinase represents a promising therapeutic target for treatment of chronic lymphocytic leukemia and is effectively targeted by PCI-32765. *Blood,* 117**,** 6287-6296.

HERMEKING, H. & BENZINGER, A. 2006. 14-3-3 proteins in cell cycle regulation. *Semin Cancer Biol,* 16**,** 183-92.

HERNANDEZ-SEGURA, A., NEHME, J. & DEMARIA, M. 2018. Hallmarks of Cellular Senescence. *Trends Cell Biol,* 28**,** 436-453.

HERRANZ, N., GALLAGE, S., MELLONE, M., WUESTEFELD, T., KLOTZ, S., HANLEY, C. J., RAGUZ, S., ACOSTA, J. C., INNES, A. J. & BANITO, A. 2015a. mTOR regulates MAPKAPK2 translation to control the senescence-associated secretory phenotype. *Nature cell biology,* 17**,** 1205-1217.

HERRANZ, N., GALLAGE, S., MELLONE, M., WUESTEFELD, T., KLOTZ, S., HANLEY, C. J., RAGUZ, S., ACOSTA, J. C., INNES, A. J., BANITO, A., GEORGILIS, A., MONTOYA, A., WOLTER, K., DHARMALINGAM, G., FAULL, P., CARROLL, T., MARTÍNEZ-BARBERA, J. P., CUTILLAS, P., REISINGER, F., HEIKENWALDER, M., MILLER, R. A., WITHERS, D., ZENDER, L., THOMAS, G. J. & GIL, J. 2015b. mTOR regulates MAPKAPK2 translation to control the senescence-associated secretory phenotype. *Nat Cell Biol,* 17**,** 1205-17.

HEWITT, G., JURK, D., MARQUES, F. D. M., CORREIA-MELO, C., HARDY, T., GACKOWSKA, A., ANDERSON, R., TASCHUK, M., MANN, J. & PASSOS, J. F. 2012. Telomeres are favoured targets of a persistent DNA damage response in ageing and stress-induced senescence. *Nature Communications,* 3**,** 708.

HICKMAN, E. S., MORONI, M. C. & HELIN, K. 2002. The role of p53 and pRB in apoptosis and cancer. *Current opinion in genetics & development,* 12**,** 60-66.

HICKSON, L. J., PRATA, L. G. L., BOBART, S. A., EVANS, T. K., GIORGADZE, N., HASHMI, S. K., HERRMANN, S. M., JENSEN, M. D., JIA, Q. & JORDAN, K. L. 2019. Senolytics decrease senescent cells in humans: Preliminary report from a clinical trial of Dasatinib plus Quercetin in individuals with diabetic kidney disease. *EBioMedicine,* 47**,** 446-456.

HOARE, M., ITO, Y., KANG, T. W., WEEKES, M. P., MATHESON, N. J., PATTEN, D. A., SHETTY, S., PARRY, A. J., MENON, S., SALAMA, R., ANTROBUS, R., TOMIMATSU, K., HOWAT, W., LEHNER, P. J., ZENDER, L. & NARITA, M. 2016. NOTCH1 mediates a switch between two distinct secretomes during senescence. *Nat Cell Biol,* 18**,** 979-92.

HONIGBERG, L. A., SMITH, A. M., SIRISAWAD, M., VERNER, E., LOURY, D., CHANG, B., LI, S., PAN, Z., THAMM, D. H., MILLER, R. A. & BUGGY, J. J. 2010. The Bruton tyrosine kinase inhibitor PCI-32765 blocks B-cell activation and is efficacious in models of autoimmune disease and B-cell malignancy. *Proc Natl Acad Sci U S A,* 107**,** 13075-80.

HOSHINO, Y., KOIDE, H., URAKAMI, T., KANAZAWA, H., KODAMA, T., OKU, N. & SHEA, K. J. 2010. Recognition, neutralization and clearance of target peptides in the blood stream of living mice by molecular imprinted polymer nanoparticles: a plastic antibody. *Journal of the American Chemical Society,* 132**,** 6644-6645.

HSU, B., VISICH, J., LANE, N., LI, L., MITTAL, J., AN, M., LABERGE, R.-M. & DANANBERG, J. 2020. Safety, tolerability, pharmacokinetics, and clinical outcomes following treatment of painful knee osteoarthritis with senolytic molecule UBX0101. *Osteoarthritis and Cartilage,* 28**,** S479-S480.

HU, Y., WEN, Z., LIU, S., CAI, Y., GUO, J., XU, Y., LIN, D., ZHU, J., LI, D. & CHEN, X. 2020. Ibrutinib suppresses intracellular mycobacterium tuberculosis growth by inducing macrophage autophagy. *J Infect,* 80**,** e19-e26.

HUDA, N., LIU, G., HONG, H., YAN, S., KHAMBU, B. & YIN, X. M. 2019. Hepatic senescence, the good and the bad. *World J Gastroenterol,* 25**,** 5069-5081.

HUI, L., ZHENG, Y., YAN, Y., BARGONETTI, J. & FOSTER, D. A. 2006. Mutant p53 in MDA-MB-231 breast cancer cells is stabilized by elevated phospholipase D activity and contributes to survival signals generated by phospholipase D. *Oncogene,* 25**,** 7305-7310.

INOUE, Y., KING, T. E., JR., TINKLE, S. S., DOCKSTADER, K. & NEWMAN, L. S. 1996. Human mast cell basic fibroblast growth factor in pulmonary fibrotic disorders. *Am J Pathol,* 149**,** 2037-54.

ITAHANA, K., CAMPISI, J. & DIMRI, G. P. 2007. Methods to detect biomarkers of cellular senescence: the senescence-associated beta-galactosidase assay. *Methods Mol Biol,* 371**,** 21-31.

ITAHANA, K., ITAHANA, Y. & DIMRI, G. P. 2013. Colorimetric detection of senescence-associated β galactosidase. *Methods Mol Biol,* 965**,** 143-56.

ITO, M., SHICHITA, T., OKADA, M., KOMINE, R., NOGUCHI, Y., YOSHIMURA, A. & MORITA, R. 2015. Bruton's tyrosine kinase is essential for NLRP3 inflammasome activation and contributes to ischaemic brain injury. *Nat Commun,* 6**,** 7360.

IWAKUMA, T., LOZANO, G. & FLORES, E. R. 2005. Li-Fraumeni syndrome: a p53 family affair. *Cell cycle,* 4**,** 865-867.

JANZEN, V., FORKERT, R., FLEMING, H. E., SAITO, Y., WARING, M. T., DOMBKOWSKI, D. M., CHENG, T., DEPINHO, R. A., SHARPLESS, N. E. & SCADDEN, D. T. 2006. Stem-cell ageing modified by the cyclin-dependent kinase inhibitor p16 INK4a. *Nature,* 443**,** 421-426.

JENSON, J. M., RYAN, J. A., GRANT, R. A., LETAI, A. & KEATING, A. E. 2017. Epistatic mutations in PUMA BH3 drive an alternate binding mode to potently and selectively inhibit anti-apoptotic Bfl-1. *Elife,* 6.

JEON, O. H., KIM, C., LABERGE, R. M., DEMARIA, M., RATHOD, S., VASSEROT, A. P., CHUNG, J. W., KIM, D. H., POON, Y., DAVID, N., BAKER, D. J., VAN DEURSEN, J. M., CAMPISI, J. & ELISSEEFF, J. H. 2017. Local clearance of senescent cells attenuates the development of post-traumatic osteoarthritis and creates a pro-regenerative environment. *Nat Med,* 23**,** 775-781.

JI, M., YUAN, L., LV, X., DONG, W. & PENG, X. 2014. EBP50 regulates the apoptosis of pancreatic cancer cells by decreasing the expression levels of Bcl-2. *Exp Ther Med,* 8**,** 919-924.

JI, M. Y., FAN, D. K., LV, X. G., PENG, X. L., LEI, X. F. & DONG, W. G. 2012. The detection of EBP50 expression using quantum dot immunohistochemistry in pancreatic

cancer tissue and down-regulated EBP50 effect on PC-2 cells. *J Mol Histol,* 43**,** 517-26.

JIANG, J., DONG, L., WANG, L., WANG, L., ZHANG, J., CHEN, F., ZHANG, X., HUANG, M., LI, S., MA, W., XU, Q., HUANG, C., FANG, J. & WANG, C. 2016. HER2-targeted antibody drug conjugates for ovarian cancer therapy.

JIANG, J., WAKIMOTO, H., SEIDMAN, J. & SEIDMAN, C. E. 2013. Allele-specific silencing of mutant Myh6 transcripts in mice suppresses hypertrophic cardiomyopathy. *Science,* 342**,** 111-114.

JUN, J.-I. & LAU, L. F. 2010. The matricellular protein CCN1 induces fibroblast senescence and restricts fibrosis in cutaneous wound healing. *Nature Cell Biology,* 12**,** 676-685.

JUN, J.-I. & LAU, L. F. 2017. CCN2 induces cellular senescence in fibroblasts. *Journal of cell communication and signaling,* 11**,** 15-23.

JURK, D., WILSON, C., PASSOS, J. F., OAKLEY, F., CORREIA-MELO, C., GREAVES, L., SARETZKI, G., FOX, C., LAWLESS, C., ANDERSON, R., HEWITT, G., PENDER, S. L., FULLARD, N., NELSON, G., MANN, J., VAN DE SLUIS, B., MANN, D. A. & VON ZGLINICKI, T. 2014. Chronic inflammation induces telomere dysfunction and accelerates ageing in mice. *Nat Commun,* 2**,** 4172.

JUSTICE, J., NAMBIAR, A., TCHKONIA, T., LEBRASSEUR, N., PASCUAL, R., HASHMI, S. & KIRKLAND, J. 2019. Senolytics in idiopathic pulmonary fibrosis: results from a first-in-human, open-label, pilot study. EBioMedicine 40: 554–563.

KALE, J., OSTERLUND, E. J. & ANDREWS, D. W. 2018. BCL-2 family proteins: changing partners in the dance towards death. *Cell Death & Differentiation,* 25**,** 65-80.

KANG, H. T., PARK, J. T., CHOI, K., KIM, Y., CHOI, H. J. C., JUNG, C. W., LEE, Y.-S. & PARK, S. C. 2017. Chemical screening identifies ATM as a target for alleviating senescence. *Nature chemical biology,* 13**,** 616.

KANG, T. W., YEVSA, T., WOLLER, N., HOENICKE, L., WUESTEFELD, T., DAUCH, D., HOHMEYER, A., GEREKE, M., RUDALSKA, R., POTAPOVA, A., IKEN, M., VUCUR, M., WEISS, S., HEIKENWALDER, M., KHAN, S., GIL, J., BRUDER, D., MANNS, M., SCHIRMACHER, P., TACKE, F., OTT, M., LUEDDE, T., LONGERICH, T., KUBICKA, S. & ZENDER, L. 2011. Senescence surveillance of pre-malignant hepatocytes limits liver cancer development. *Nature,* 479**,** 547-51.

KANTARJIAN, H., JABBOUR, E., GRIMLEY, J. & KIRKPATRICK, P. 2006. Dasatinib. Nature Publishing Group.

KARIMIAN, A., AHMADI, Y. & YOUSEFI, B. 2016. Multiple functions of p21 in cell cycle, apoptosis and transcriptional regulation after DNA damage. *DNA Repair (Amst),* 42**,** 63-71.

KASTAN, M. B., ONYEKWERE, O., SIDRANSKY, D., VOGELSTEIN, B. & CRAIG, R. W. 1991. Participation of p53 protein in the cellular response to DNA damage. *Cancer research,* 51**,** 6304-6311.

KE, X. & SHEN, L. 2017. Molecular targeted therapy of cancer: The progress and future prospect.

KEMPE, H., PARAREDA PUJOLRÀS, A. & KEMPE, M. 2015. Molecularly Imprinted Polymer Nanocarriers for Sustained Release of Erythromycin. *Pharmaceutical research,* 32**,** 375-388.

KERNER, J. D., APPLEBY, M. W., MOHR, R. N., CHIEN, S., RAWLINGS, D. J., MALISZEWSKI, C. R., WITTE, O. N. & PERLMUTTER, R. M. 1995. Impaired expansion of mouse B cell progenitors lacking Btk. *Immunity,* 3**,** 301-12.

KESHAVA, C., FRYE, B. L., WOLFF, M. S., MCCANLIES, E. C. & WESTON, A. 2002. Waf-1 (p21) and p53 polymorphisms in breast cancer. *Cancer Epidemiology and Prevention Biomarkers,* 11**,** 127-130.

KHAN, N., SYED, D. N., AHMAD, N. & MUKHTAR, H. 2013. Fisetin: a dietary antioxidant for health promotion. *Antioxidants & redox signaling,* 19**,** 151-162.

KHAN, W. N., ALT, F. W., GERSTEIN, R. M., MALYNN, B. A., LARSSON, I., RATHBUN, G., DAVIDSON, L., MÜLLER, S., KANTOR, A. B., HERZENBERG, L. A. & ET AL. 1995. Defective B cell development and function in Btk-deficient mice. *Immunity,* 3**,** 283-99.

KIM, I. H., KISSELEVA, T. & BRENNER, D. A. 2015. Aging and liver disease. *Curr Opin Gastroenterol,* 31**,** 184-91.

KIM, K. H., CHEN, C. C., MONZON, R. I. & LAU, L. F. 2013. Matricellular protein CCN1 promotes regression of liver fibrosis through induction of cellular senescence in hepatic myofibroblasts. *Mol Cell Biol,* 33**,** 2078-90.

KIM, K. H., WON, J. H., CHENG, N. & LAU, L. F. 2018a. The matricellular protein CCN1 in tissue injury repair. *J Cell Commun Signal,* 12**,** 273-279.

KIM, K. M., NOH, J. H., BODOGAI, M., MARTINDALE, J. L., PANDEY, P. R., YANG, X., BIRAGYN, A., ABDELMOHSEN, K. & GOROSPE, M. 2018b. SCAMP4 enhances the senescent cell secretome. *Genes Dev,* 32**,** 909-914.

KIM, K. M., NOH, J. H., BODOGAI, M., MARTINDALE, J. L., YANG, X., INDIG, F. E., BASU, S. K., OHNUMA, K., MORIMOTO, C., JOHNSON, P. F., BIRAGYN, A., ABDELMOHSEN, K. & GOROSPE, M. 2017. Identification of senescent cell surface targetable protein DPP4. *Genes Dev,* 31**,** 1529-1534.

KIM, S. R., JIANG, K., OGRODNIK, M., CHEN, X., ZHU, X. Y., LOHMEIER, H., AHMED, L., TANG, H., TCHKONIA, T., HICKSON, L. J., KIRKLAND, J. L. & LERMAN, L. O. 2019.

Increased renal cellular senescence in murine high-fat diet: effect of the senolytic drug quercetin. *Transl Res,* 213**,** 112-123.

KIM, W. Y. & SHARPLESS, N. E. 2006. The regulation of INK4/ARF in cancer and aging. *Cell,* 127**,** 265-275.

KIM, Y., SHAROV, A. A., MCDOLE, K., CHENG, M., HAO, H., FAN, C.-M., GAIANO, N., KO, M. S. & ZHENG, Y. 2011. Mouse B-type lamins are required for proper organogenesis but not by embryonic stem cells. *Science,* 334**,** 1706-1710.

KINNER, A., WU, W., STAUDT, C. & ILIAKIS, G. 2008. Gamma-H2AX in recognition and signaling of DNA double-strand breaks in the context of chromatin. *Nucleic Acids Res,* 36**,** 5678-94.

KIRKLAND, J. L., STOUT, M. B. & SIERRA, F. 2016. Resilience in aging mice. *Journals of Gerontology Series A: Biomedical Sciences and Medical Sciences,* 71**,** 1407-1414.

KIRKLAND, J. L. & TCHKONIA, T. 2017. Cellular Senescence: A Translational Perspective. *EBioMedicine,* 21**,** 21-28.

KIRKLAND, J. L. & TCHKONIA, T. 2020. Senolytic drugs: from discovery to translation. *Journal of internal medicine*.

KLINAKIS, A., LOBRY, C., ABDEL-WAHAB, O., OH, P., HAENO, H., BUONAMICI, S., VAN DE WALLE, I., CATHELIN, S., TRIMARCHI, T., ARALDI, E., LIU, C., IBRAHIM, S., BERAN, M., ZAVADIL, J., EFSTRATIADIS, A., TAGHON, T., MICHOR, F., LEVINE, R. L. & AIFANTIS, I. 2011. A novel tumour-suppressor function for the Notch pathway in myeloid leukaemia. *Nature,* 473**,** 230-3.

KOKABEE, L., WANG, X., SEVINSKY, C. J., WANG, W. L., CHEU, L., CHITTUR, S. V., KARIMIPOOR, M., TENNISWOOD, M. & CONKLIN, D. S. 2015. Bruton's tyrosine kinase is a potential therapeutic target in prostate cancer. *Cancer Biol Ther,* 16**,** 1604-15.

KOLODYCH, S., MICHEL, C., DELACROIX, S., KONIEV, O., EHKIRCH, A., EBEROVA, J., CIANFÉRANI, S., RENOUX, B., KREZEL, W., POINOT, P., MULLER, C. D., PAPOT, S. & WAGNER, A. 2017. Development and evaluation of β-galactosidase-sensitive antibody-drug conjugates.

KONDO, S., BARNA, B. P., KONDO, Y., TANAKA, Y., CASEY, G., LIU, J., MORIMURA, T., KAAKAJI, R., PETERSON, J. W. & WERBEL, B. 1996. WAF1/CIP1 increases the susceptibility of p53 non-functional malignant glioma cells to cisplatin-induced apoptosis. *Oncogene,* 13**,** 1279-1285.

KONDZIELLA, W. 1964. [a New Method for the Measurement of Muscle Relaxation in White Mice]. *Arch Int Pharmacodyn Ther,* 152**,** 277-84.

KONG, W., MOU, X., LIU, Q., CHEN, Z., VANDERBURG, C. R., ROGERS, J. T. & HUANG, X. 2009. Independent component analysis of Alzheimer's DNA microarray gene expression data. *Molecular neurodegeneration,* 4**,** 5.

KORNS, D. R., FRASCH, S. C., FERNANDEZ-BOYANAPALLI, R., HENSON, P. M. & BRATTON, D. L. 2011. Modulation of macrophage efferocytosis in inflammation. *Frontiers in immunology,* 2**,** 57.

KOSCHMIDDER, E., MOLLENHAUER, B., KASTEN, M., KLEIN, C. & LOHMANN, K. 2014. Mutations in VPS26A are not a frequent cause of Parkinson's disease. *Neurobiology of Aging,* 35**,** 1512. e1-1512. e2.

KRAJEWSKA, M., MAI, J., ZAPATA, J., ASHWELL, K. W., SCHENDEL, S., REED, J. & KRAJEWSKI, S. 2002. Dynamics of expression of apoptosis-regulatory proteins Bid, Bcl-2, Bcl-X, Bax and Bak during development of murine nervous system. *Cell Death & Differentiation,* 9**,** 145-157.

KREIMANN, E. L., MORALES, F. C., DE ORBETA-CRUZ, J., TAKAHASHI, Y., ADAMS, H., LIU, T. J., MCCREA, P. D. & GEORGESCU, M. M. 2007. Cortical stabilization of β-catenin contributes to NHERF1/EBP50 tumor suppressor function. *Oncogene,* 26**,** 5290-5299.

KRISHNAMURTHY, J., RAMSEY, M. R., LIGON, K. L., TORRICE, C., KOH, A., BONNER-WEIR, S. & SHARPLESS, N. E. 2006. p16 INK4a induces an age-dependent decline in islet regenerative potential. *Nature,* 443**,** 453-457.

KRISHNAMURTHY, J., TORRICE, C., RAMSEY, M. R., KOVALEV, G. I., AL-REGAIEY, K., SU, L. & SHARPLESS, N. E. 2004. Ink4a/Arf expression is a biomarker of aging. *J Clin Invest,* 114**,** 1299-307.

KRIZHANOVSKY, V., YON, M., DICKINS, R. A., HEARN, S., SIMON, J., MIETHING, C., YEE, H., ZENDER, L. & LOWE, S. W. 2008. Senescence of activated stellate cells limits liver fibrosis. *Cell,* 134**,** 657-67.

KROHNE, G. & BENAVENTE, R. 1986. The nuclear lamins. A multigene family of proteins in evolution and differentiation. *Exp Cell Res,* 162**,** 1-10.

KRTOLICA, A., PARRINELLO, S., LOCKETT, S., DESPREZ, P. Y. & CAMPISI, J. 2001. Senescent fibroblasts promote epithelial cell growth and tumorigenesis: a link between cancer and aging. *Proc Natl Acad Sci U S A,* 98**,** 12072-7.

KUILMAN, T., MICHALOGLOU, C., MOOI, W. J. & PEEPER, D. S. 2010. The essence of senescence. *Genes Dev,* 24**,** 2463-79.

KUILMAN, T. & PEEPER, D. S. 2009. Senescence-messaging secretome: SMS-ing cellular stress. *Nature Reviews Cancer,* 9**,** 81-94.

KUMAR, A., WHITE, J., JAMES CHRISTIE, R., DIMASI, N. & GAO, C. 2017. Chapter Twelve - Antibody-Drug Conjugates. *In:* GOODNOW, R. A. (ed.). Academic Press.

LABERGE, R.-M., SUN, Y., ORJALO, A. V., PATIL, C. K., FREUND, A., ZHOU, L., CURRAN, S. C., DAVALOS, A. R., WILSON-EDELL, K. A. & LIU, S. 2015a. MTOR regulates the pro-tumorigenic senescence-associated secretory phenotype by promoting IL1A translation. *Nature cell biology,* 17**,** 1049-1061.

LABERGE, R. M., SUN, Y., ORJALO, A. V., PATIL, C. K., FREUND, A., ZHOU, L., CURRAN, S. C., DAVALOS, A. R., WILSON-EDELL, K. A., LIU, S., LIMBAD, C., DEMARIA, M., LI, P., HUBBARD, G. B., IKENO, Y., JAVORS, M., DESPREZ, P. Y., BENZ, C. C., KAPAHI, P., NELSON, P. S. & CAMPISI, J. 2015b. MTOR regulates the pro-tumorigenic senescence-associated secretory phenotype by promoting IL1A translation. *Nat Cell Biol,* 17**,** 1049-61.

LABERGE, R. M., ZHOU, L., SARANTOS, M. R., RODIER, F., FREUND, A., DE KEIZER, P. L., LIU, S., DEMARIA, M., CONG, Y. S. & KAPAHI, P. 2012. Glucocorticoids suppress selected components of the senescence-associated secretory phenotype. *Aging cell,* 11**,** 569-578.

LALL, R. K., ADHAMI, V. M. & MUKHTAR, H. 2016. Dietary flavonoid fisetin for cancer prevention and treatment. *Molecular nutrition & food research,* 60**,** 1396-1405.

LANE, D. P. 1992. Cancer. p53, guardian of the genome. *Nature,* 358**,** 15-6.

LATTOUF, R., YOUNES, R., LUTOMSKI, D., NAAMAN, N., GODEAU, G., SENNI, K. & CHANGOTADE, S. 2014. Picrosirius red staining: a useful tool to appraise collagen networks in normal and pathological tissues. *Journal of Histochemistry & Cytochemistry,* 62**,** 751-758.

LAZZERINI DENCHI, E., ATTWOOLL, C., PASINI, D. & HELIN, K. 2005. Deregulated E2F activity induces hyperplasia and senescence-like features in the mouse pituitary gland. *Mol Cell Biol,* 25**,** 2660-72.

LEE, B. Y., HAN, J. A., IM, J. S., MORRONE, A., JOHUNG, K., GOODWIN, E. C., KLEIJER, W. J., DIMAIO, D. & HWANG, E. S. 2006. Senescence-associated beta-galactosidase is lysosomal beta-galactosidase. *Aging Cell,* 5**,** 187-95.

LEE, H. W., LEE, S. H., LEE, H. W., RYU, Y. W., KWON, M. H. & KIM, Y. S. 2005. Homomeric and heteromeric interactions of the extracellular domains of death receptors and death decoy receptors. *Biochem Biophys Res Commun,* 330**,** 1205-12.

LEE, J. J., RADICE, G., PERKINS, C. P. & COSTANTINI, F. 1992. Identification and characterization of a novel, evolutionarily conserved gene disrupted by the murine H beta 58 embryonic lethal transgene insertion. *Development,* 115**,** 277-288.

LEHMANN, M., KORFEI, M., MUTZE, K., KLEE, S., SKRONSKA-WASEK, W., ALSAFADI, H. N., OTA, C., COSTA, R., SCHILLER, H. B. & LINDNER, M. 2017. Senolytic drugs target alveolar epithelial cell function and attenuate experimental lung fibrosis ex vivo. *European Respiratory Journal,* 50.

LEVERSON, J. D., PHILLIPS, D. C., MITTEN, M. J., BOGHAERT, E. R., DIAZ, D., TAHIR, S. K., BELMONT, L. D., NIMMER, P., XIAO, Y. & MA, X. M. 2015. Exploiting selective BCL-2 family inhibitors to dissect cell survival dependencies and define improved strategies for cancer therapy. *Science translational medicine,* 7**,** 279ra40-279ra40.

LEWIS-MCDOUGALL, F. C., RUCHAYA, P. J., DOMENJO-VILA, E., SHIN TEOH, T., PRATA, L., COTTLE, B. J., CLARK, J. E., PUNJABI, P. P., AWAD, W. & TORELLA, D. 2019. Aged-senescent cells contribute to impaired heart regeneration. *Aging Cell,* 18**,** e12931.

LI, H., ALAVIAN, K. N., LAZROVE, E., MEHTA, N., JONES, A., ZHANG, P., LICZNERSKI, P., GRAHAM, M., UO, T. & GUO, J. 2013. A Bcl-x L–Drp1 complex regulates synaptic vesicle membrane dynamics during endocytosis. *Nature cell biology,* 15**,** 773-785.

LI, H., CHEN, Y., JONES, A. F., SANGER, R. H., COLLIS, L. P., FLANNERY, R., MCNAY, E. C., YU, T., SCHWARZENBACHER, R. & BOSSY, B. 2008. Bcl-xL induces Drp1-dependent synapse formation in cultured hippocampal neurons. *Proceedings of the National Academy of Sciences,* 105**,** 2169-2174.

LI, J., CHEN, J. & KIRSNER, R. 2007. Pathophysiology of acute wound healing. *Clinics in dermatology,* 25**,** 9-18.

LI, J., WANG, X., XIE, Y., YING, Z., LIU, W., PING, L., ZHANG, C., PAN, Z., DING, N., SONG, Y. & ZHU, J. 2018. The mTOR kinase inhibitor everolimus synergistically enhances the anti-tumor effect of the Bruton's tyrosine kinase (BTK) inhibitor PLS-123 on Mantle cell lymphoma. *Int J Cancer,* 142**,** 202-213.

LI, W., HE, Y., ZHANG, R., ZHENG, G. & ZHOU, D. 2019a. The curcumin analog EF24 is a novel senolytic agent. *Aging (Albany NY),* 11**,** 771.

LI, W., HE, Y., ZHANG, R., ZHENG, G. & ZHOU, D. 2019b. The curcumin analog EF24 is a novel senolytic agent. *Aging (Albany NY),* 11**,** 771-782.

LI, Y., UPADHYAY, S., BHUIYAN, M. & SARKAR, F. H. 1999. Induction of apoptosis in breast cancer cells MDA-MB-231 by genistein. *Oncogene,* 18**,** 3166-3172.

LIAO, V. H.-C., YU, C.-W., CHU, Y.-J., LI, W.-H., HSIEH, Y.-C. & WANG, T.-T. 2011. Curcumin-mediated lifespan extension in Caenorhabditis elegans. *Mechanisms of ageing and development,* 132**,** 480-487.

LIM, H., PARK, H. & KIM, H. P. 2015. Effects of flavonoids on senescence-associated secretory phenotype formation from bleomycin-induced senescence in BJ fibroblasts. *Biochemical pharmacology,* 96**,** 337-348.

LIN, F. & WORMAN, H. J. 1993. Structural organization of the human gene encoding nuclear lamin A and nuclear lamin C. *Journal of Biological Chemistry,* 268**,** 16321-16326.

LIN, P. J. C., WILLIAMS, W. P., LUU, Y., MOLDAY, R. S., ORLOWSKI, J. & NUMATA, M. 2005. Secretory carrier membrane proteins interact and regulate trafficking of the organellar (Na⁺,K⁺)/H⁺ exchanger NHE7. *Journal of Cell Science,* 118**,** 1885-1897.

LINCET, H., POULAIN, L., REMY, J., DESLANDES, E., DUIGOU, F., GAUDUCHON, P. & STAEDEL, C. 2000. The p21cip1/waf1 cyclin-dependent kinase inhibitor enhances the cytotoxic effect of cisplatin in human ovarian carcinoma cells. *Cancer letters,* 161**,** 17-26.

LINDQVIST, L. M., HEINLEIN, M., HUANG, D. C. & VAUX, D. L. 2014. Prosurvival Bcl-2 family members affect autophagy only indirectly, by inhibiting Bax and Bak. *Proceedings of the National Academy of Sciences,* 111**,** 8512-8517.

LINDQVIST, L. M. & VAUX, D. L. 2014. BCL2 and related prosurvival proteins require BAK1 and BAX to affect autophagy. *Autophagy,* 10**,** 1474-1475.

LINDVALL, J. M., BLOMBERG, K. E. M., BERGLÖF, A., YANG, Q., SMITH, C. I. E. & ISLAM, T. C. 2004. Gene expression profile of B cells from Xid mice and Btk knockout mice. *European Journal of Immunology,* 34**,** 1981-1991.

LIU, H., MA, Y., HE, H.-W., WANG, J.-P., JIANG, J.-D. & SHAO, R.-G. 2015a. SLC9A3R1 stimulates autophagy via BECN1 stabilization in breast cancer cells. *Autophagy,* 11**,** 2323-2334.

LIU, J., YANG, J.-R., HE, Y.-N., CAI, G.-Y., ZHANG, J.-G., LIN, L.-R., ZHAN, J., ZHANG, J.-H. & XIAO, H.-S. 2012. Accelerated senescence of renal tubular epithelial cells is associated with disease progression of patients with immunoglobulin A (IgA) nephropathy. *Translational Research,* 159**,** 454-463.

LIU, S., UPPAL, H., DEMARIA, M., DESPREZ, P.-Y., CAMPISI, J. & KAPAHI, P. 2015b. Simvastatin suppresses breast cancer cell proliferation induced by senescent cells. *Scientific reports,* 5**,** 1-11.

LIU, X., WANG, Y., ZHANG, X., GAO, Z., ZHANG, S., SHI, P., ZHANG, X., SONG, L., HENDRICKSON, H., ZHOU, D. & ZHENG, G. 2018. Senolytic activity of piperlongumine analogues: Synthesis and biological evaluation. *Bioorg Med Chem,* 26**,** 3925-3938.

LO NIGRO, C., MACAGNO, M., SANGIOLO, D., BERTOLACCINI, L., AGLIETTA, M. & MERLANO, M. C. 2019. NK-mediated antibody-dependent cell-mediated cytotoxicity in solid tumors: biological evidence and clinical perspectives. *Ann Transl Med,* 7**,** 105.

LOPEZ-OTIN, C., BLASCO, M. A., PARTRIDGE, L., SERRANO, M. & KROEMER, G. 2013. The hallmarks of aging. *Cell,* 153**,** 1194-217.

LÓPEZ-OTÍN, C., BLASCO, M. A., PARTRIDGE, L., SERRANO, M. & KROEMER, G. 2013. The hallmarks of aging. *Cell,* 153**,** 1194-1217.

LULIŃSKI, P. 2017. Molecularly imprinted polymers based drug delivery devices: a way to application in modern pharmacotherapy. A review.

LUNDBERG, A. S., HAHN, W. C., GUPTA, P. & WEINBERG, R. A. 2000. Genes involved in senescence and immortalization. *Curr Opin Cell Biol,* 12**,** 705-9.

MA, H. S., WANG, E. L., XU, W. F., YAMADA, S., YOSHIMOTO, K., QIAN, Z. R., SHI, L., LIU, L. L. & LI, X. H. 2018. Overexpression of DNA (Cytosine-5)-Methyltransferase 1 (DNMT1) And DNA (Cytosine-5)-Methyltransferase 3A (DNMT3A) Is Associated with Aggressive Behavior and Hypermethylation of Tumor Suppressor Genes in Human Pituitary Adenomas. *Med Sci Monit,* 24**,** 4841-4850.

MACIP, S., IGARASHI, M., BERGGREN, P., YU, J., LEE, S. W. & AARONSON, S. A. 2003. Influence of induced reactive oxygen species in p53-mediated cell fate decisions. *Molecular and cellular biology,* 23**,** 8576-8585.

MACIP, S., IGARASHI, M., FANG, L., CHEN, A., PAN, Z. Q., LEE, S. W. & AARONSON, S. A. 2002. Inhibition of p21-mediated ROS accumulation can rescue p21-induced senescence. *EMBO J,* 21**,** 2180-8.

MADSEN, S. D., RUSSELL, K. C., TUCKER, H. A., GLOWACKI, J., BUNNELL, B. A. & O'CONNOR, K. C. 2017. Decoy TRAIL receptor CD264: a cell surface marker of cellular aging for human bone marrow-derived mesenchymal stem cells. *Stem Cell Res Ther,* 8**,** 201.

MAECKER, H. T., TODD, S. C. & LEVY, S. 1997. The tetraspanin superfamily: molecular facilitators. *The FASEB Journal,* 11**,** 428-442.

MAIER, B., GLUBA, W., BERNIER, B., TURNER, T., MOHAMMAD, K., GUISE, T., SUTHERLAND, A., THORNER, M. & SCRABLE, H. 2004. Modulation of mammalian life span by the short isoform of p53. *Genes Dev,* 18**,** 306-19.

MALAQUIN, N., MARTINEZ, A. & RODIER, F. 2016. Keeping the senescence secretome under control: Molecular reins on the senescence-associated secretory phenotype. *Exp Gerontol,* 82**,** 39-49.

MALKIN, D., LI, F. P., STRONG, L. C., FRAUMENI, J. F., NELSON, C. E., KIM, D. H., KASSEL, J., GRYKA, M. A., BISCHOFF, F. Z. & TAINSKY, M. A. 1990. Germ line p53 mutations in a familial syndrome of breast cancer, sarcomas, and other neoplasms. *science,* 250**,** 1233-1238.

MARKOWSKI, D. N., THIES, H. W., GOTTLIEB, A., WENK, H., WISCHNEWSKY, M. & BULLERDIEK, J. 2013. HMGA2 expression in white adipose tissue linking cellular senescence with diabetes. *Genes & nutrition,* 8**,** 449-456.

MARTINS, R., LITHGOW, G. J. & LINK, W. 2016. Long live FOXO: unraveling the role of FOXO proteins in aging and longevity. *Aging cell,* 15**,** 196-207.

MARUTHUR, N. M., TSENG, E., HUTFLESS, S., WILSON, L. M., SUAREZ-CUERVO, C., BERGER, Z., CHU, Y., IYOHA, E., SEGAL, J. B. & BOLEN, S. 2016. Diabetes medications as monotherapy or metformin-based combination therapy for type 2 diabetes: a systematic review and meta-analysis. *Annals of internal medicine,* 164**,** 740-751.

MARX, J. O., KRAEMER, W. J., NINDL, B. C. & LARSSON, L. 2002. Effects of Aging on Human Skeletal Muscle Myosin Heavy-Chain mRNA Content and Protein Isoform Expression. *The Journals of Gerontology: Series A,* 57**,** B232-B238.

MASGRAS, I., CARRERA, S., DE VERDIER, P. J., BRENNAN, P., MAJID, A., MAKHTAR, W., TULCHINSKY, E., JONES, G. D., RONINSON, I. B. & MACIP, S. 2012. Reactive oxygen species and mitochondrial sensitivity to oxidative stress determine induction of cancer cell death by p21. *J Biol Chem,* 287**,** 9845-54.

MASSO-VALLES, D., JAUSET, T. & SOUCEK, L. 2016. Ibrutinib repurposing: from B-cell malignancies to solid tumors. *Oncoscience,* 3**,** 147-8.

MCDUFF, F. K. & TURNER, S. D. 2011. Jailbreak: oncogene-induced senescence and its evasion. *Cell Signal,* 23**,** 6-13.

MCEACHERN, M. J., KRAUSKOPF, A. & BLACKBURN, E. H. 2000. Telomeres and their control. *Annu Rev Genet,* 34**,** 331-358.

MCGILL, M. R. 2016. The past and present of serum aminotransferases and the future of liver injury biomarkers. *EXCLI journal,* 15**,** 817-828.

MCHUGH, D. & GIL, J. 2018. Senescence and aging: Causes, consequences, and therapeutic avenues. *J Cell Biol,* 217**,** 65-77.

MEINERS, S., EICKELBERG, O. & KÖNIGSHOFF, M. 2015. Hallmarks of the ageing lung. *Eur Respir J,* 45**,** 807-27.

MENG, X.-M., NIKOLIC-PATERSON, D. J. & LAN, H. Y. 2016. TGF-β: the master regulator of fibrosis. *Nature Reviews Nephrology,* 12**,** 325.

MERCER, K., GIBLETT, S., GREEN, S., LLOYD, D., DAROCHA DIAS, S., PLUMB, M., MARAIS, R. & PRITCHARD, C. 2005. Expression of endogenous oncogenic V600EB-raf induces proliferation and developmental defects in mice and transformation of primary fibroblasts. *Cancer Res,* 65**,** 11493-500.

MEYER, K., HODWIN, B., RAMANUJAM, D., ENGELHARDT, S. & SARIKAS, A. 2016. Essential role for premature senescence of myofibroblasts in myocardial fibrosis. *Journal of the american college of cardiology,* 67**,** 2018-2028.

MICHALOGLOU, C., VREDEVELD, L. C., SOENGAS, M. S., DENOYELLE, C., KUILMAN, T., VAN DER HORST, C. M., MAJOOR, D. M., SHAY, J. W., MOOI, W. J. & PEEPER, D. S. 2005. BRAF E600-associated senescence-like cell cycle arrest of human naevi. *Nature,* 436**,** 720-724.

MIJIT, M., CARACCIOLO, V., MELILLO, A., AMICARELLI, F. & GIORDANO, A. 2020. Role of p53 in the Regulation of Cellular Senescence. *Biomolecules,* 10**,** 420.

MIKAWA, R., SUZUKI, Y., BASKORO, H., KANAYAMA, K., SUGIMOTO, K., SATO, T. & SUGIMOTO, M. 2018. Elimination of p19ARF-expressing cells protects against pulmonary emphysema in mice. *Aging cell,* 17**,** e12827.

MINAMINO, T., ORIMO, M., SHIMIZU, I., KUNIEDA, T., YOKOYAMA, M., ITO, T., NOJIMA, A., NABETANI, A., OIKE, Y. & MATSUBARA, H. 2009. A crucial role for adipose tissue p53 in the regulation of insulin resistance. *Nature medicine,* 15**,** 1082-1087.

MIRZAYANS, R., ANDRAIS, B. & MURRAY, D. 2017. Impact of Premature Senescence on Radiosensitivity Measured by High Throughput Cell-Based Assays. *Int J Mol Sci,* 18.

MOISEEVA, O., DESCHÊNES-SIMARD, X., ST-GERMAIN, E., IGELMANN, S., HUOT, G., CADAR, A. E., BOURDEAU, V., POLLAK, M. N. & FERBEYRE, G. 2013. Metformin inhibits the senescence-associated secretory phenotype by interfering with IKK/NF-κ B activation. *Aging cell,* 12**,** 489-498.

MOLOFSKY, A., SLUTSKY, S., JOSEPH, N., HE, S., PARDAL, R., KRISHNAMURTHY, J., SHARPLESS, N. & MORRISON, S. 2006. Declines in forebrain progenitor function and neurogenesis during aging are partially caused by increasing Ink4a expression. *Nature,* 443**,** 448-452.

MONCSEK, A., AL-SURAIH, M. S., TRUSSONI, C. E., O'HARA, S. P., SPLINTER, P. L., ZUBER, C., PATSENKER, E., VALLI, P. V., FINGAS, C. D. & WEBER, A. 2018. Targeting senescent cholangiocytes and activated fibroblasts with B-cell lymphoma-extra large inhibitors ameliorates fibrosis in multidrug resistance 2 gene knockout (Mdr2−/−) mice. *Hepatology,* 67**,** 247-259.

MORIN, P. J. 1999. β-catenin signaling and cancer. *Bioessays,* 21**,** 1021-1030.

MUHAMMAD, A., FLORES, I., ZHANG, H., YU, R., STANISZEWSKI, A., PLANEL, E., HERMAN, M., HO, L., KREBER, R. & HONIG, L. S. 2008. Retromer deficiency observed in Alzheimer's disease causes hippocampal dysfunction, neurodegeneration, and Aβ accumulation. *Proceedings of the National Academy of Sciences,* 105**,** 7327-7332.

MUÑOZ-ESPÍN, D., CAÑAMERO, M., MARAVER, A., GÓMEZ-LÓPEZ, G., CONTRERAS, J., MURILLO-CUESTA, S., RODRÍGUEZ-BAEZA, A., VARELA-NIETO, I., RUBERTE, J., COLLADO, M. & SERRANO, M. 2013. Programmed cell senescence during mammalian embryonic development. *Cell,* 155**,** 1104-18.

MUÑOZ-ESPIN, D. & DEMARIA, M. 2020. *Senolytics in Disease, Ageing and Longevity*, Springer.

MUNOZ-ESPIN, D., ROVIRA, M., GALIANA, I., GIMENEZ, C., LOZANO-TORRES, B., PAEZ-RIBES, M., LLANOS, S., CHAIB, S., MUNOZ-MARTIN, M., UCERO, A. C., GARAULET, G., MULERO, F., DANN, S. G., VANARSDALE, T., SHIELDS, D. J., BERNARDOS, A., MURGUIA, J. R., MARTINEZ-MANEZ, R. & SERRANO, M. 2018. A versatile drug delivery system targeting senescent cells. *EMBO Mol Med*.

MUÑOZ-ESPÍN, D., ROVIRA, M., GALIANA, I., GIMÉNEZ, C., LOZANO-TORRES, B., PAEZ-RIBES, M., LLANOS, S., CHAIB, S., MUÑOZ-MARTÍN, M., UCERO, A. C., GARAULET, G., MULERO, F., DANN, S. G., VANARSDALE, T., SHIELDS, D. J., BERNARDOS, A., MURGUÍA, J. R., MARTÍNEZ-MÁÑEZ, R. & SERRANO, M. 2018a. A versatile drug delivery system targeting senescent cells. *EMBO Molecular Medicine,* 10**,** e9355.

MUÑOZ-ESPÍN, D., ROVIRA, M., GALIANA, I., GIMÉNEZ, C., LOZANO-TORRES, B., PAEZ-RIBES, M., LLANOS, S., CHAIB, S., MUÑOZ-MARTÍN, M., UCERO, A. C., GARAULET, G., MULERO, F., DANN, S. G., VANARSDALE, T., SHIELDS, D. J., BERNARDOS, A., MURGUÍA, J. R., MARTÍNEZ-MÁÑEZ, R. & SERRANO, M. 2018b. A versatile drug delivery system targeting senescent cells. *EMBO Mol Med,* 10.

MUNOZ-ESPIN, D. & SERRANO, M. 2014. Cellular senescence: from physiology to pathology. *Nat Rev Mol Cell Biol,* 15**,** 482-96.

NACKENOFF, A. G., HOHMAN, T. J., NEUNER, S. M., AKERS, C. S., WEITZEL, N. C., SHOSTAK, A., FERGUSON, S., BENNETT, D. A., SCHNEIDER, J. A. & JEFFERSON, A. L. 2019. PLD3 is a neuronal lysosomal phospholipase D associated with β-amyloid plaques and cognitive function in Alzheimer's disease. *bioRxiv***,** 746222.

NAN-PING, W. & HODES, R. J. 2000. The Role of Telomerase Expression and Telomere Length Maintenance in Human and Mouse. *Journal of Clinical Immunology,* 20**,** 257-267.

NARITA, M., NÛNEZ, S., HEARD, E., NARITA, M., LIN, A. W., HEARN, S. A., SPECTOR, D. L., HANNON, G. J. & LOWE, S. W. 2003. Rb-mediated heterochromatin formation and silencing of E2F target genes during cellular senescence. *Cell,* 113**,** 703-16.

NICOLAS, M., WOLFER, A., RAJ, K., KUMMER, J. A., MILL, P., VAN NOORT, M., HUI, C. C., CLEVERS, H., DOTTO, G. P. & RADTKE, F. 2003. Notch1 functions as a tumor suppressor in mouse skin. *Nat Genet,* 33**,** 416-21.

NISHIO, K., INOUE, A., QIAO, S., KONDO, H. & MIMURA, A. 2001. Senescence and cytoskeleton: overproduction of vimentin induces senescent-like morphology in human fibroblasts. *Histochem Cell Biol,* 116**,** 321-7.

NISHIOKA, Y., AZUMA, M., KISHI, M. & AONO, Y. 2013. Targeting platelet-derived growth factor as a therapeutic approach in pulmonary fibrosis. *J Med Invest,* 60**,** 175-83.

NOGUEIRA, V., PARK, Y., CHEN, C. C., XU, P. Z., CHEN, M. L., TONIC, I., UNTERMAN, T. & HAY, N. 2008. Akt determines replicative senescence and oxidative or oncogenic premature senescence and sensitizes cells to oxidative apoptosis. *Cancer Cell,* 14**,** 458-70.

NOREN HOOTEN, N., MARTIN-MONTALVO, A., DLUZEN, D. F., ZHANG, Y., BERNIER, M., ZONDERMAN, A. B., BECKER, K. G., GOROSPE, M., DE CABO, R. & EVANS, M. K. 2016. Metformin-mediated increase in DICER1 regulates microRNA expression and cellular senescence. *Aging cell,* 15**,** 572-581.

NYBLOM, H., BJÖRNSSON, E., SIMRÉN, M., ALDENBORG, F., ALMER, S. & OLSSON, R. 2006. The AST/ALT ratio as an indicator of cirrhosis in patients with PBC. *Liver International,* 26**,** 840-845.

ODA, A., IKEDA, Y., OCHS, H. D., DRUKER, B. J., OZAKI, K., HANDA, M., ARIGA, T., SAKIYAMA, Y., WITTE, O. N. & WAHL, M. I. 2000. Rapid tyrosine phosphorylation and activation of Bruton's tyrosine/Tec kinases in platelets induced by collagen binding or CD32 cross-linking. *Blood,* 95**,** 1663-70.

OGRODNIK, M., MIWA, S., TCHKONIA, T., TINIAKOS, D., WILSON, C. L., LAHAT, A., DAY, C. P., BURT, A., PALMER, A., ANSTEE, Q. M., GRELLSCHEID, S. N., HOEIJMAKERS, J. H. J., BARNHOORN, S., MANN, D. A., BIRD, T. G., VERMEIJ, W. P., KIRKLAND, J. L., PASSOS, J. F., VON ZGLINICKI, T. & JURK, D. 2017a. Cellular senescence drives age-dependent hepatic steatosis. *Nature Communications,* 8**,** 15691.

OGRODNIK, M., MIWA, S., TCHKONIA, T., TINIAKOS, D., WILSON, C. L., LAHAT, A., DAY, C. P., BURT, A., PALMER, A., ANSTEE, Q. M., GRELLSCHEID, S. N., HOEIJMAKERS, J. H. J., BARNHOORN, S., MANN, D. A., BIRD, T. G., VERMEIJ, W. P., KIRKLAND, J. L., PASSOS, J. F., VON ZGLINICKI, T. & JURK, D. 2017b. Cellular senescence drives age-dependent hepatic steatosis. *Nature Communications,* 8**,** 15691.

OGRODNIK, M., ZHU, Y., LANGHI, L. G. P., TCHKONIA, T., KRÜGER, P., FIELDER, E., VICTORELLI, S., RUSWHANDI, R. A., GIORGADZE, N., PIRTSKHALAVA, T., PODGORNI, O., ENIKOLOPOV, G., JOHNSON, K. O., XU, M., INMAN, C., PALMER, A. K., SCHAFER, M., WEIGL, M., IKENO, Y., BURNS, T. C., PASSOS, J. F., VON ZGLINICKI, T., KIRKLAND, J. L. & JURK, D. 2019. Obesity-Induced Cellular

Senescence Drives Anxiety and Impairs Neurogenesis. *Cell Metabolism,* 29**,** 1061-1077.e8.

OHKOSHI, S., YANO, M. & MATSUDA, Y. 2015. Oncogenic role of p21 in hepatocarcinogenesis suggests a new treatment strategy. *World journal of gastroenterology,* 21**,** 12150-12156.

OLTERSDORF, T., ELMORE, S. W., SHOEMAKER, A. R., ARMSTRONG, R. C., AUGERI, D. J., BELLI, B. A., BRUNCKO, M., DECKWERTH, T. L., DINGES, J. & HAJDUK, P. J. 2005. An inhibitor of Bcl-2 family proteins induces regression of solid tumours. *Nature,* 435**,** 677-681.

ORMEROD, M. G. & IMRIE, P. R. 1990. Flow cytometry. *Animal Cell Culture.* Springer.

OSISAMI, M., ALI, W. & FROHMAN, M. A. 2012. A role for phospholipase D3 in myotube formation. *PLoS One,* 7**,** e33341.

OUBAHA, M., MILOUDI, K., DEJDA, A., GUBER, V., MAWAMBO, G., GERMAIN, M.-A., BOURDEL, G., POPOVIC, N., REZENDE, F. A. & KAUFMAN, R. J. 2016. Senescence-associated secretory phenotype contributes to pathological angiogenesis in retinopathy. *Science translational medicine,* 8**,** 362ra144-362ra144.

OZSVARI, B., NUTTALL, J. R., SOTGIA, F. & LISANTI, M. P. 2018. Azithromycin and Roxithromycin define a new family of "senolytic" drugs that target senescent human fibroblasts. *Aging (Albany NY),* 10**,** 3294-3307.

PAEZ-RIBES, M., GONZÁLEZ-GUALDA, E., DOHERTY, G. J. & MUÑOZ-ESPÍN, D. 2019. Targeting senescent cells in translational medicine. *EMBO Molecular Medicine,* 11**,** e10234.

PAL, H. C., PEARLMAN, R. L. & AFAQ, F. 2016. Fisetin and its role in chronic diseases. *Anti-inflammatory Nutraceuticals and Chronic Diseases.* Springer.

PAL SINGH, S., DAMMEIJER, F. & HENDRIKS, R. W. 2018. Role of Bruton's tyrosine kinase in B cells and malignancies. *Molecular Cancer,* 17**,** 57.

PALMER, A. K., XU, M., ZHU, Y., PIRTSKHALAVA, T., WEIVODA, M. M., HACHFELD, C. M., PRATA, L. G., VAN DIJK, T. H., VERKADE, E., CASACLANG-VERZOSA, G., JOHNSON, K. O., CUBRO, H., DOORNEBAL, E. J., OGRODNIK, M., JURK, D., JENSEN, M. D., CHINI, E. N., MILLER, J. D., MATVEYENKO, A., STOUT, M. B., SCHAFER, M. J., WHITE, T. A., HICKSON, L. J., DEMARIA, M., GAROVIC, V., GRANDE, J., ARRIAGA, E. A., KUIPERS, F., VON ZGLINICKI, T., LEBRASSEUR, N. K., CAMPISI, J., TCHKONIA, T. & KIRKLAND, J. L. 2019. Targeting senescent cells alleviates obesity-induced metabolic dysfunction. *Aging Cell,* 18**,** e12950.

PAN, G., NI, J., YU, G.-L., WEI, Y.-F. & DIXIT, V. M. 1998. TRUNDD, a new member of the TRAIL receptor family that antagonizes TRAIL signalling. *FEBS Letters,* 424**,** 41-45.

PAN, J., LI, D., XU, Y., ZHANG, J., WANG, Y., CHEN, M., LIN, S., HUANG, L., CHUNG, E. J. & CITRIN, D. E. 2017. Inhibition of Bcl-2/xl with ABT-263 selectively kills senescent type II pneumocytes and reverses persistent pulmonary fibrosis induced by ionizing radiation in mice. *International Journal of Radiation Oncology* Biology* Physics,* 99**,** 353-361.

PANCHE, A. N., DIWAN, A. D. & CHANDRA, S. R. 2016. Flavonoids: an overview. *J Nutr Sci,* 5**,** e47.

PARIKH, P., BRITT, R. D., JR., MANLOVE, L. J., WICHER, S. A., ROESLER, A., RAVIX, J., TESKE, J., THOMPSON, M. A., SIECK, G. C., KIRKLAND, J. L., LEBRASSEUR, N., TSCHUMPERLIN, D. J., PABELICK, C. M. & PRAKASH, Y. S. 2019. Hyperoxia-induced Cellular Senescence in Fetal Airway Smooth Muscle Cells. *Am J Respir Cell Mol Biol,* 61**,** 51-60.

PARK, H., WAHL, M. I., AFAR, D. E., TURCK, C. W., RAWLINGS, D. J., TAM, C., SCHARENBERG, A. M., KINET, J. P. & WITTE, O. N. 1996. Regulation of Btk function by a major autophosphorylation site within the SH3 domain. *Immunity,* 4**,** 515-25.

PARKS, D. E. & WEIGLE, W. O. 1980. Current perspectives on the cellular mechanisms of immunologic tolerance. *Clin Exp Immunol,* 39**,** 257-62.

PARRINELLO, S., COPPE, J.-P., KRTOLICA, A. & CAMPISI, J. 2005. Stromal-epithelial interactions in aging and cancer: senescent fibroblasts alter epithelial cell differentiation. *Journal of cell science,* 118**,** 485-496.

PATRA, S. K., PATRA, A., ZHAO, H. & DAHIYA, R. 2002. DNA methyltransferase and demethylase in human prostate cancer. *Molecular Carcinogenesis,* 33**,** 163-171.

PATTINGRE, S., TASSA, A., QU, X., GARUTI, R., LIANG, X. H., MIZUSHIMA, N., PACKER, M., SCHNEIDER, M. D. & LEVINE, B. 2005. Bcl-2 antiapoptotic proteins inhibit Beclin 1-dependent autophagy. *Cell,* 122**,** 927-939.

PAULIAH, M., ZANGANEH, S., ERFANZADEH, M. & HO, J. Q. 2018. Chapter 10 - Tumor-Targeted Therapy. *In:* MAHMOUDI, M. & LAURENT, S. (eds.). Elsevier.

PEDERSEN, K. M., FINSEN, B., CELIS, J. E. & JENSEN, N. A. 1998. Expression of a novel murine phospholipase D homolog coincides with late neuronal development in the forebrain. *J Biol Chem,* 273**,** 31494-504.

PELLEGRINI, G., DELLAMBRA, E., PATERNA, P., GOLISANO, O., TRAVERSO, C. E., RAMA, P., LACAL, P. & DE LUCA, M. 2004. Telomerase activity is sufficient to bypass replicative senescence in human limbal and conjunctival but not corneal keratinocytes. *Eur J Cell Biol,* 83**,** 691-700.

PELLOW, S., CHOPIN, P., FILE, S. E. & BRILEY, M. 1985. Validation of open : closed arm entries in an elevated plus-maze as a measure of anxiety in the rat. *Journal of Neuroscience Methods,* 14**,** 149-167.

PENDÁS, A. M., ZHOU, Z., CADIÑANOS, J., FREIJE, J. M. P., WANG, J., HULTENBY, K., ASTUDILLO, A., WERNERSON, A., RODRÍGUEZ, F., TRYGGVASON, K. & LÓPEZ-OTÍN, C. 2002. Defective prelamin A processing and muscular and adipocyte alterations in Zmpste24 metalloproteinase–deficient mice. *Nature Genetics,* 31**,** 94-99.

PEREZ, H. L., CARDARELLI, P. M., DESHPANDE, S., GANGWAR, S., SCHROEDER, G. M., VITE, G. D. & BORZILLERI, R. M. 2014. Antibody–drug conjugates: current status and future directions.

PERNA, G., IANNONE, G., ALCIATI, A. & CALDIROLA, D. 2016. Are anxiety disorders associated with accelerated aging? A focus on neuroprogression. *Neural Plasticity,* 2016.

PERRI, F., PISCONTI, S. & DELLA VITTORIA SCARPATI, G. 2016. P53 mutations and cancer: a tight linkage. *Ann Transl Med,* 4**,** 522.

PICALLOS-RABINA, P., DA SILVA-ÁLVAREZ, S., ANTELO-IGLESIAS, L., TRIANA-MARTÍNEZ, F. & COLLADO, M. 2020. Senotherapy of Cancer. *Senolytics in Disease, Ageing and Longevity.* Springer.

PILETSKY, S. A., TURNER, N. W. & LAITENBERGER, P. 2006. Molecularly imprinted polymers in clinical diagnostics--future potential and existing problems. *Medical engineering & physics,* 28**,** 971-977.

PISKA, K., GUNIA-KRZYŻAK, A., KOCZURKIEWICZ, P., WÓJCIK-PSZCZOŁA, K. & PĘKALA, E. 2018. Piperlongumine (piplartine) as a lead compound for anticancer agents–Synthesis and properties of analogues: A mini-review. *European journal of medicinal chemistry,* 156**,** 13-20.

PŁOTKA-WASYLKA, J., SZCZEPAŃSKA, N., DE LA GUARDIA, M. & NAMIEŚNIK, J. 2015. Miniaturized solid-phase extraction techniques. *TrAC Trends in Analytical Chemistry,* 73**,** 19-38.

PLUQUET, O., NORTH, S., BHOUMIK, A., DIMAS, K., RONAI, Z. E. & HAINAUT, P. 2003. The cytoprotective aminothiol WR1065 activates p53 through a non-genotoxic signaling pathway involving c-Jun N-terminal kinase. *Journal of Biological Chemistry,* 278**,** 11879-11887.

POPA, F. I., PERLINI, S., TEOFOLI, F., DEGANI, D., FUNGHINI, S., LA MARCA, G., RINALDO, P., VINCENZI, M., ANTONIAZZI, F., BONER, A. & CAMILOT, M. 2012. 3-hydroxyacyl-coenzyme a dehydrogenase deficiency: identification of a new

mutation causing hyperinsulinemic hypoketotic hypoglycemia, altered organic acids and acylcarnitines concentrations. *JIMD Rep,* 2**,** 71-7.

PORTER, D. C., FARMAKI, E., ALTILIA, S., SCHOOLS, G. P., WEST, D. K., CHEN, M., CHANG, B. D., PUZYREV, A. T., LIM, C. U., ROKOW-KITTELL, R., FRIEDHOFF, L. T., PAPAVASSILIOU, A. G., KALURUPALLE, S., HURTEAU, G., SHI, J., BARAN, P. S., GYORFFY, B., WENTLAND, M. P., BROUDE, E. V., KIARIS, H. & RONINSON, I. B. 2012. Cyclin-dependent kinase 8 mediates chemotherapy-induced tumor-promoting paracrine activities. *Proc Natl Acad Sci U S A,* 109**,** 13799-804.

POWELL, B. L., VAN STAVEREN, I. L., ROOSKEN, P., GRIEU, F., BERNS, E. M. & IACOPETTA, B. 2002. Associations between common polymorphisms in TP53 and p21WAF1/Cip1 and phenotypic features of breast cancer. *Carcinogenesis,* 23**,** 311-315.

PUOCI, F., CIRILLO, G., CURCIO, M., PARISI, O. I., IEMMA, F. & PICCI, N. 2011. Molecularly imprinted polymers in drug delivery: state of art and future perspectives. *Expert opinion on drug delivery,* 8**,** 1379-1393.

QIAN, Y. & CHEN, X. 2013. Senescence regulation by the p53 protein family. *Methods in molecular biology (Clifton, N.J.),* 965**,** 37-61.

RADA, M., ALTHUBITI, M., EKPENYONG-AKIBA, A. E., LEE, K. G., LAM, K. P., FEDOROVA, O., BARLEV, N. A. & MACIP, S. 2017. BTK blocks the inhibitory effects of MDM2 on p53 activity. *Oncotarget,* 8**,** 106639-106647.

RADA, M., BARLEV, N. & MACIP, S. 2018a. BTK modulates p73 activity to induce apoptosis independently of p53. *Cell Death Discovery,* 4**,** 95.

RADA, M., BARLEV, N. & MACIP, S. 2018b. BTK: a two-faced effector in cancer and tumour suppression. *Cell Death & Disease,* 9**,** 1064.

RADICE, G., LEE, J. J. & COSTANTINI, F. 1991. H beta 58, an insertional mutation affecting early postimplantation development of the mouse embryo. *Development,* 111**,** 801-11.

RALHAN, R., AGARWAL, S., MATHUR, M., WASYLYK, B. & SRIVASTAVA, A. 2000. Association between polymorphism in p21Waf1/Cip1 cyclin-dependent kinase inhibitor gene and human oral cancer. *Clinical cancer research,* 6**,** 2440-2447.

RANGARAJAN, A., TALORA, C., OKUYAMA, R., NICOLAS, M., MAMMUCARI, C., OH, H., ASTER, J. C., KRISHNA, S., METZGER, D., CHAMBON, P., MIELE, L., AGUET, M., RADTKE, F. & DOTTO, G. P. 2001. Notch signaling is a direct determinant of keratinocyte growth arrest and entry into differentiation. *Embo j,* 20**,** 3427-36.

RAUSER, C. L., MUELLER, L. D. & ROSE, M. R. 2006. The evolution of late life. *Ageing research reviews,* 5**,** 14-32.

RAWLINGS, D. J., SCHARENBERG, A. M., PARK, H., WAHL, M. I., LIN, S., KATO, R. M., FLUCKIGER, A.-C., WITTE, O. N. & KINET, J.-P. 1996. Activation of BTK by a Phosphorylation Mechanism Initiated by SRC Family Kinases. *Science,* 271**,** 822.

RAYESS, H., WANG, M. B. & SRIVATSAN, E. S. 2012. Cellular senescence and tumor suppressor gene p16. *International journal of cancer,* 130**,** 1715-1725.

REBBAA, A., ZHENG, X., CHOU, P. M. & MIRKIN, B. L. 2003. Caspase inhibition switches doxorubicin-induced apoptosis to senescence. *Oncogene,* 22**,** 2805-2811.

REDDY, S. & COMAI, L. 2012. Lamin A, farnesylation and aging. *Exp Cell Res,* 318**,** 1-7.

RIEMENSCHNEIDER, M., SCHOEPFER-WENDELS, A., FRIEDRICH, P., KONTA, L., LAWS, S. M., MUELLER, J. C., KURZ, A. & FÖRSTL, H. 2007. No association of Vacuolar protein sorting 26 polymorphisms with Alzheimer's disease. *Neurobiology of Aging,* 28**,** 883-884.

RISTOW, M. & SCHMEISSER, S. 2011. Extending life span by increasing oxidative stress. *Free radical biology and medicine,* 51**,** 327-336.

RITSCHKA, B., STORER, M., MAS, A., HEINZMANN, F., ORTELLS, M. C., MORTON, J. P., SANSOM, O. J., ZENDER, L. & KEYES, W. M. 2017. The senescence-associated secretory phenotype induces cellular plasticity and tissue regeneration. *Genes & development,* 31**,** 172-183.

RIVLIN, N., BROSH, R., OREN, M. & ROTTER, V. 2011. Mutations in the p53 Tumor Suppressor Gene: Important Milestones at the Various Steps of Tumorigenesis. *Genes Cancer,* 2**,** 466-74.

ROACH, K. M., SUTCLIFFE, A., MATTHEWS, L., ELLIOTT, G., NEWBY, C., AMRANI, Y. & BRADDING, P. 2018. A model of human lung fibrogenesis for the assessment of anti-fibrotic strategies in idiopathic pulmonary fibrosis. *Sci Rep,* 8**,** 342.

RODIER, F. & CAMPISI, J. 2011a. Four faces of cellular senescence. *The Journal of cell biology,* 192**,** 547-556.

RODIER, F. & CAMPISI, J. 2011b. Four faces of cellular senescence. *J Cell Biol,* 192**,** 547-56.

RODIER, F., KIM, S. H., NIJJAR, T., YASWEN, P. & CAMPISI, J. 2005. Cancer and aging: the importance of telomeres in genome maintenance. *Int J Biochem Cell Biol,* 37**,** 977-90.

RODIER, F., MUÑOZ, D. P., TEACHENOR, R., CHU, V., LE, O., BHAUMIK, D., COPPÉ, J. P., CAMPEAU, E., BEAUSÉJOUR, C. M., KIM, S. H., DAVALOS, A. R. & CAMPISI, J. 2011. DNA-SCARS: distinct nuclear structures that sustain damage-induced senescence growth arrest and inflammatory cytokine secretion. *J Cell Sci,* 124**,** 68-81.

ROMAGOSA, C., SIMONETTI, S., LÓPEZ-VICENTE, L., MAZO, A., LLEONART, M. E., CASTELLVI, J. & RAMON Y CAJAL, S. 2011. p16Ink4a overexpression in cancer: a tumor suppressor gene associated with senescence and high-grade tumors. *Oncogene,* 30**,** 2087-2097.

ROOS, C. M., ZHANG, B., PALMER, A. K., OGRODNIK, M. B., PIRTSKHALAVA, T., THALJI, N. M., HAGLER, M., JURK, D., SMITH, L. A., CASACLANG-VERZOSA, G., ZHU, Y., SCHAFER, M. J., TCHKONIA, T., KIRKLAND, J. L. & MILLER, J. D. 2016. Chronic senolytic treatment alleviates established vasomotor dysfunction in aged or atherosclerotic mice. *Aging Cell,* 15**,** 973-977.

RUFINI, A., TUCCI, P., CELARDO, I. & MELINO, G. 2013. Senescence and aging: the critical roles of p53. *Oncogene,* 32**,** 5129-5143.

RYAN, J. & LETAI, A. 2013. BH3 profiling in whole cells by fluorimeter or FACS. *Methods,* 61**,** 156-64.

SADELAIN, M., RIVIÈRE, I. & RIDDELL, S. 2017. Therapeutic T cell engineering. *Nature,* 545**,** 423-431.

SAFFREY, M. J. 2014. Aging of the mammalian gastrointestinal tract: a complex organ system. *Age (Dordrecht, Netherlands),* 36**,** 9603-9603.

SAITO, Y., KANAI, Y., NAKAGAWA, T., SAKAMOTO, M., SAITO, H., ISHII, H. & HIROHASHI, S. 2003. Increased protein expression of DNA methyltransferase (DNMT) 1 is significantly correlated with the malignant potential and poor prognosis of human hepatocellular carcinomas. *International Journal of Cancer,* 105**,** 527-532.

SALAMA, R., SADAIE, M., HOARE, M. & NARITA, M. 2014. Cellular senescence and its effector programs. *Genes Dev,* 28**,** 99-114.

SAMARAWEERA, L., ADOMAKO, A., RODRIGUEZ-GABIN, A. & MCDAID, H. M. 2017. A novel indication for panobinostat as a senolytic drug in NSCLC and HNSCC. *Scientific reports,* 7**,** 1-11.

SANZ, C., BENET, I., RICHARD, C., BADIA, B., ANDREU, E. J., PROSPER, F. & FERNÁNDEZ-LUNA, J. L. 2001. Antiapoptotic protein Bcl-xL is up-regulated during megakaryocytic differentiation of CD34+ progenitors but is absent from senescent megakaryocytes. *Experimental hematology,* 29**,** 728-735.

SARETZKI, G. 2010. Cellular senescence in the development and treatment of cancer. *Current pharmaceutical design,* 16**,** 79-100.

SARKISIAN, C. J., KEISTER, B. A., STAIRS, D. B., BOXER, R. B., MOODY, S. E. & CHODOSH, L. A. 2007. Dose-dependent oncogene-induced senescence in vivo and its evasion during mammary tumorigenesis. *Nature Cell Biology,* 9**,** 493-505.

SCHAFER, M. J., WHITE, T. A., IIJIMA, K., HAAK, A. J., LIGRESTI, G., ATKINSON, E. J., OBERG, A. L., BIRCH, J., SALMONOWICZ, H. & ZHU, Y. 2017a. Cellular senescence mediates fibrotic pulmonary disease. *Nature communications,* 8**,** 1-11.

SCHAFER, M. J., WHITE, T. A., IIJIMA, K., HAAK, A. J., LIGRESTI, G., ATKINSON, E. J., OBERG, A. L., BIRCH, J., SALMONOWICZ, H., ZHU, Y., MAZULA, D. L., BROOKS, R. W., FUHRMANN-STROISSNIGG, H., PIRTSKHALAVA, T., PRAKASH, Y. S., TCHKONIA, T., ROBBINS, P. D., AUBRY, M. C., PASSOS, J. F., KIRKLAND, J. L., TSCHUMPERLIN, D. J., KITA, H. & LEBRASSEUR, N. K. 2017b. Cellular senescence mediates fibrotic pulmonary disease. *Nat Commun,* 8**,** 14532.

SCHERZER, C. R., OFFE, K., GEARING, M., REES, H. D., FANG, G., HEILMAN, C. J., SCHALLER, C., BUJO, H., LEVEY, A. I. & LAH, J. J. 2004. Loss of apolipoprotein E receptor LR11 in Alzheimer disease. *Arch Neurol,* 61**,** 1200-5.

SCHMITT, C. A., FRIDMAN, J. S., YANG, M., LEE, S., BARANOV, E., HOFFMAN, R. M. & LOWE, S. W. 2002. A senescence program controlled by p53 and p16INK4a contributes to the outcome of cancer therapy. *Cell,* 109**,** 335-346.

SCHMITT, E., BEAUCHEMIN, M. & BERTRAND, R. 2007. Nuclear colocalization and interaction between bcl-xL and cdk1(cdc2) during G2/M cell-cycle checkpoint. *Oncogene,* 26**,** 5851-5865.

SCHULIGA, M., JAFFAR, J., HARRIS, T., KNIGHT, D. A., WESTALL, G. & STEWART, A. G. 2017. The fibrogenic actions of lung fibroblast-derived urokinase: a potential drug target in IPF. *Scientific reports,* 7**,** 1-11.

SELLERGREN, B. & ALLENDER, C. J. 2005. Molecularly imprinted polymers: A bridge to advanced drug delivery. *Advanced Drug Delivery Reviews,* 57**,** 1733-1741.

SELUANOV, A., GORBUNOVA, V., FALCOVITZ, A., SIGAL, A., MILYAVSKY, M., ZURER, I., SHOHAT, G., GOLDFINGER, N. & ROTTER, V. 2001. Change of the death pathway in senescent human fibroblasts in response to DNA damage is caused by an inability to stabilize p53. *Mol Cell Biol,* 21**,** 1552-64.

SELVENDIRAN, K., KUPPUSAMY, M. L., BRATASZ, A., TONG, L., RIVERA, B. K., RINK, C., SEN, C. K., KALAI, T., HIDEG, K. & KUPPUSAMY, P. 2009. Inhibition of vascular smooth-muscle cell proliferation and arterial restenosis by HO-3867, a novel synthetic curcuminoid, through up-regulation of PTEN expression. *Journal of Pharmacology and Experimental Therapeutics,* 329**,** 959-966.

SENGUPTA, S. & SASISEKHARAN, R. 2007. Exploiting nanotechnology to target cancer. *British journal of cancer,* 96**,** 1315-1319.

SEOANE, J., LE, H.-V., SHEN, L., ANDERSON, S. A. & MASSAGUÉ, J. 2004. Integration of Smad and forkhead pathways in the control of neuroepithelial and glioblastoma cell proliferation. *Cell,* 117**,** 211-223.

SERGIEV, P., DONTSOVA, O. & BEREZKIN, G. 2015. Theories of aging: an ever-evolving field. *Acta Naturae (англоязычная версия),* 7.

SERRANO, M. 2017. Understanding aging. *New England Journal of Medicine,* 376**,** 1083-1085.

SERRANO, M. & BLASCO, M. A. 2001. Putting the stress on senescence. *Curr Opin Cell Biol,* 13**,** 748-53.

SERRANO, M., LIN, A. W., MCCURRACH, M. E., BEACH, D. & LOWE, S. W. 1997. Oncogenic ras provokes premature cell senescence associated with accumulation of p53 and p16INK4a. *Cell,* 88**,** 593-602.

SHAMAS-DIN, A., KALE, J., LEBER, B. & ANDREWS, D. W. 2013. Mechanisms of action of Bcl-2 family proteins. *Cold Spring Harbor perspectives in biology,* 5**,** a008714.

SHANNON, B., SOTO-ORTOLAZA, A., RAYAPROLU, S., CANNON, H. D., LABBÉ, C., BENITEZ, B. A., CHOI, J., LYNCH, T., BOCZARSKA-JEDYNAK, M., OPALA, G., KRYGOWSKA-WAJS, A., BARCIKOWSKA, M., VAN GERPEN, J. A., UITTI, R. J., SPRINGER, W., CRUCHAGA, C., WSZOLEK, Z. K. & ROSS, O. A. 2014. Genetic variation of the retromer subunits VPS26A/B-VPS29 in Parkinson's disease. *Neurobiology of Aging,* 35**,** 1958.e1-1958.e2.

SHARMA, A. K., ROBERTS, R. L., BENSON JR, R. D., PIERCE, J. L., YU, K., HAMRICK, M. W. & MCGEE-LAWRENCE, M. E. 2020. The Senolytic Drug Navitoclax (ABT-263) Causes Trabecular Bone Loss and Impaired Osteoprogenitor Function in Aged Mice. *Frontiers in Cell and Developmental Biology,* 8**,** 354.

SHARMA, O. 1976. Antioxidant activity of curcumin and related compounds. *Biochemical pharmacology,* 25**,** 1811-1812.

SHARPLESS, N. E. & SHERR, C. J. 2015. Forging a signature of in vivo senescence. *Nature reviews.Cancer,* 15**,** 397-408.

SHAW, T. J. & MARTIN, P. 2016. Wound repair: a showcase for cell plasticity and migration. *Current opinion in cell biology,* 42**,** 29-37.

SHAY, J. W., PEREIRA-SMITH, O. M. & WRIGHT, W. E. 1991. A role for both RB and p53 in the regulation of human cellular senescence. *Experimental Cell Research,* 196**,** 33-39.

SHEEDFAR, F., DI BIASE, S., KOONEN, D. & VINCIGUERRA, M. 2013. Liver diseases and aging: friends or foes? *Aging Cell,* 12**,** 950-4.

SHER, Y.-P. & HUNG, M.-C. 2013. Blood AST, ALT and UREA/BUN Level Analysis. *Bio-protocol,* 3**,** e931.

SHERR, C. J. 2012. Ink4-Arf locus in cancer and aging. *Wiley Interdiscip Rev Dev Biol,* 1**,** 731-41.

SHIBATA, T., CHUMA, M., KOKUBU, A., SAKAMOTO, M. & HIROHASHI, S. 2003. EBP50, a β-catenin–associating protein, enhances Wnt signaling and is over-expressed in hepatocellular carcinoma. *Hepatology,* 38**,** 178-186.

SHIBUYA, Y., CHANG, C. C. & CHANG, T. Y. 2015. ACAT1/SOAT1 as a therapeutic target for Alzheimer's disease. *Future Med Chem,* 7**,** 2451-67.

SHIMIZU, I. & MINAMINO, T. 2019. Cellular senescence in cardiac diseases. *Journal of Cardiology,* 74**,** 313-319.

SHINOHARA, M., KOGA, T., OKAMOTO, K., SAKAGUCHI, S., ARAI, K., YASUDA, H., TAKAI, T., KODAMA, T., MORIO, T., GEHA, R. S., KITAMURA, D., KUROSAKI, T., ELLMEIER, W. & TAKAYANAGI, H. 2008. Tyrosine kinases Btk and Tec regulate osteoclast differentiation by linking RANK and ITAM signals. *Cell,* 132**,** 794-806.

SHKRETA, L., MICHELLE, L., TOUTANT, J., TREMBLAY, M. L. & CHABOT, B. 2011. The DNA damage response pathway regulates the alternative splicing of the apoptotic mediator Bcl-x. *Journal of Biological Chemistry,* 286**,** 331-340.

SHOBA, G., JOY, D., JOSEPH, T., MAJEED, M., RAJENDRAN, R. & SRINIVAS, P. S. 1998. Influence of piperine on the pharmacokinetics of curcumin in animals and human volunteers. *Planta Med,* 64**,** 353-6.

SIEVERS, E. L. & SENTER, P. D. 2013. Antibody-drug conjugates in cancer therapy. *Annual Review of Medicine,* 64**,** 15-29.

SIKORA, E., ARENDT, T., BENNETT, M. & NARITA, M. 2011. Impact of cellular senescence signature on ageing research.

SIMBOECK, E. & DI CROCE, L. 2013. p16INK4a in cellular senescence. *Aging (Albany NY),* 5**,** 590-1.

SINADINOS, A., YOUNG, C. N., AL-KHALIDI, R., TETI, A., KALINSKI, P., MOHAMAD, S., FLORIOT, L., HENRY, T., TOZZI, G., JIANG, T., WURTZ, O., LEFEBVRE, A., SHUGAY, M., TONG, J., VAUDRY, D., ARKLE, S., DOREGO, J. C. & GÓRECKI, D. C. 2015. P2RX7 purinoceptor: a therapeutic target for ameliorating the symptoms of duchenne muscular dystrophy. *PLoS Med,* 12**,** e1001888.

SINGH, A., NAIDU, P. S. & KULKARNI, S. K. 2003. Reversal of aging and chronic ethanol-induced cognitive dysfunction by quercetin a bioflavonoid. *Free radical research,* 37**,** 1245-1252.

SIPARSKY, P. N., KIRKENDALL, D. T. & GARRETT, W. E., JR. 2014. Muscle changes in aging: understanding sarcopenia. *Sports Health,* 6**,** 36-40.

SMITH, H. A. & KANG, Y. 2013. The metastasis-promoting roles of tumor-associated immune cells. *Journal of Molecular Medicine,* 91**,** 411-429.

SMITH, H. W. & MARSHALL, C. J. 2010. Regulation of cell signalling by uPAR. *Nature reviews Molecular cell biology,* 11**,** 23-36.

SOLÁROVÁ, Z., MOJŽIŠ, J. & SOLÁR, P. 2015. Hsp90 inhibitor as a sensitizer of cancer cells to different therapies. *International journal of oncology,* 46**,** 907-926.

SRIVASTAVA, S., ZOU, Z., PIROLLO, K., BLATTNER, W. & CHANG, E. H. 1990. Germ-line transmission of a mutated p53 gene in a cancer-prone family with Li–Fraumeni syndrome. *Nature,* 348**,** 747-749.

ST SAUVER, J. L., BOYD, C. M., GROSSARDT, B. R., BOBO, W. V., RUTTEN, L. J. F., ROGER, V. L., EBBERT, J. O., THERNEAU, T. M., YAWN, B. P. & ROCCA, W. A. 2015. Risk of developing multimorbidity across all ages in an historical cohort study: differences by sex and ethnicity. *BMJ open,* 5.

STALLONE, G., INFANTE, B., PRISCIANDARO, C. & GRANDALIANO, G. 2019. mTOR and Aging: An Old Fashioned Dress. *Int J Mol Sci,* 20.

STEIN, G. H., DRULLINGER, L. F., SOULARD, A. & DULIĆ, V. 1999. Differential roles for cyclin-dependent kinase inhibitors p21 and p16 in the mechanisms of senescence and differentiation in human fibroblasts. *Molecular and cellular biology,* 19**,** 2109-2117.

STEMMER-RACHAMIMOV, A. O., WIEDERHOLD, T., NIELSEN, G. P., JAMES, M., PINNEY-MICHALOWSKI, D., ROY, J. E., COHEN, W. A., RAMESH, V. & LOUIS, D. N. 2001. NHE-RF, a merlin-interacting protein, is primarily expressed in luminal epithelia, proliferative endometrium, and estrogen receptor-positive breast carcinomas. *The American journal of pathology,* 158**,** 57-62.

STEWART, S. A., BEN-PORATH, I., CAREY, V. J., O'CONNOR, B. F., HAHN, W. C. & WEINBERG, R. A. 2003. Erosion of the telomeric single-strand overhang at replicative senescence. *Nature Genetics,* 33**,** 492-496.

STORER, M., MAS, A., ROBERT-MORENO, A., PECORARO, M., ORTELLS, M. C., DI GIACOMO, V., YOSEF, R., PILPEL, N., KRIZHANOVSKY, V., SHARPE, J. & KEYES, W. M. 2013. Senescence is a developmental mechanism that contributes to embryonic growth and patterning. *Cell,* 155**,** 1119-30.

STROHL, W. R. & STROHL, L. M. 2012. 15 - Antibody-drug conjugates. *In:* STROHL, W. R. & STROHL, L. M. (eds.) *Therapeutic Antibody Engineering.* Woodhead Publishing.

SUGRUE, M. M., SHIN, D. Y., LEE, S. W. & AARONSON, S. A. 1997a. Wild-type p53 triggers a rapid senescence program in human tumor cells lacking functional p53. *Proceedings of the National Academy of Sciences of the United States of America,* 94**,** 9648-9653.

SUGRUE, M. M., SHIN, D. Y., LEE, S. W. & AARONSON, S. A. 1997b. Wild-type p53 triggers a rapid senescence program in human tumor cells lacking functional p53. *Proceedings of the National Academy of Sciences,* 94**,** 9648-9653.

SUNDARRAJ, K., RAGHUNATH, A. & PERUMAL, E. 2018. A review on the chemotherapeutic potential of fisetin: In vitro evidences. *Biomedicine & Pharmacotherapy,* 97**,** 928-940.

SVEDRUŽIĆ Ž, M. 2011. Dnmt1 structure and function. *Prog Mol Biol Transl Sci,* 101**,** 221-54.

SWANSON, E. C., MANNING, B., ZHANG, H. & LAWRENCE, J. B. 2013. Higher-order unfolding of satellite heterochromatin is a consistent and early event in cell senescence. *J Cell Biol,* 203**,** 929-42.

SYED, Y. Y. 2020. Zanubrutinib: first approval. *Drugs***,** 1-7.

TABASSO, A. F. S., JONES, D. J. L., JONES, G. D. D. & MACIP, S. 2019. Radiotherapy-Induced Senescence and its Effects on Responses to Treatment. *Clin Oncol (R Coll Radiol),* 31**,** 283-289.

TAGSCHERER, K. E., FASSL, A., CAMPOS, B., FARHADI, M., KRAEMER, A., BÖCK, B., MACHER-GOEPPINGER, S., RADLWIMMER, B., WIESTLER, O. & HEROLD-MENDE, C. 2008. Apoptosis-based treatment of glioblastomas with ABT-737, a novel small molecule inhibitor of Bcl-2 family proteins. *Oncogene,* 27**,** 6646-6656.

TAHIR, S. K., YANG, X., ANDERSON, M. G., MORGAN-LAPPE, S. E., SARTHY, A. V., CHEN, J., WARNER, R. B., NG, S. C., FESIK, S. W., ELMORE, S. W., ROSENBERG, S. H. & TSE, C. 2007. Influence of Bcl-2 family members on the cellular response of small-cell lung cancer cell lines to ABT-737. *Cancer Res,* 67**,** 1176-83.

TAKAHASHI, A., OHTANI, N. & HARA, E. 2007. Irreversibility of cellular senescence: dual roles of p16INK4a/Rb-pathway in cell cycle control. *Cell Div,* 2**,** 10.

TAKAHASHI, Y., MORALES, F. C., KREIMANN, E. L. & GEORGESCU, M. M. 2006. PTEN tumor suppressor associates with NHERF proteins to attenuate PDGF receptor signaling. *Embo j,* 25**,** 910-20.

TAKANO, K., TATEBE, J., WASHIZAWA, N. & MORITA, T. 2018. Curcumin inhibits age-related vascular changes in aged mice fed a high-fat diet. *Nutrients,* 10**,** 1476.

TAMVAKOPOULOS, C., DIMAS, K., SOFIANOS, Z. D., HATZIANTONIOU, S., HAN, Z., LIU, Z.-L., WYCHE, J. H. & PANTAZIS, P. 2007. Metabolism and anticancer activity of the curcumin analogue, dimethoxycurcumin. *Clinical Cancer Research,* 13**,** 1269-1277.

TAN, M., LI, J., MA, F., ZHANG, X., ZHAO, Q. & CAO, X. 2019. PLD3 Rare Variants Identified in Late-Onset Alzheimer's Disease Affect Amyloid-beta Levels in Cellular Model. *Front Neurosci,* 13**,** 116.

TANG, F.-L., LIU, W., HU, J.-X., ERION, J. R., YE, J., MEI, L. & XIONG, W.-C. 2015. VPS35 deficiency or mutation causes dopaminergic neuronal loss by impairing mitochondrial fusion and function. *Cell reports,* 12**,** 1631-1643.

TANIGUCHI, K., KOHSAKA, H., INOUE, N., TERADA, Y., ITO, H., HIROKAWA, K. & MIYASAKA, N. 1999. Induction of the p16INK4a senescence gene as a new therapeutic strategy for the treatment of rheumatoid arthritis. *Nat Med,* 5**,** 760-7.

TASDEMIR, N., BANITO, A., ROE, J.-S., ALONSO-CURBELO, D., CAMIOLO, M., TSCHAHARGANEH, D. F., HUANG, C.-H., AKSOY, O., BOLDEN, J. E. & CHEN, C.-C. 2016. BRD4 connects enhancer remodeling to senescence immune surveillance. *Cancer discovery,* 6**,** 612-629.

TCHKONIA, T. & KIRKLAND, J. L. 2018. Aging, Cell Senescence, and Chronic Disease: Emerging Therapeutic Strategies. *Jama,* 320**,** 1319-1320.

TCHKONIA, T., MORBECK, D. E., VON ZGLINICKI, T., VAN DEURSEN, J., LUSTGARTEN, J., SCRABLE, H., KHOSLA, S., JENSEN, M. D. & KIRKLAND, J. L. 2010. Fat tissue, aging, and cellular senescence. *Aging cell,* 9**,** 667-684.

TEPPER, C. G., SELDIN, M. F. & MUDRYJ, M. 2000. Fas-mediated apoptosis of proliferating, transiently growth-arrested, and senescent normal human fibroblasts. *Exp Cell Res,* 260**,** 9-19.

TERMAN, A. & BRUNK, U. T. 2004. Lipofuscin. *Int J Biochem Cell Biol,* 36**,** 1400-4.

THAPA, R. K., NGUYEN, H. T., JEONG, J.-H., KIM, J. R., CHOI, H.-G., YONG, C. S. & KIM, J. O. 2017a. Progressive slowdown/prevention of cellular senescence by CD9-targeted delivery of rapamycin using lactose-wrapped calcium carbonate nanoparticles. *Scientific reports,* 7**,** 1-11.

THAPA, R. K., NGUYEN, H. T., JEONG, J. H., KIM, J. R., CHOI, H. G., YONG, C. S. & KIM, J. O. 2017b. Progressive slowdown/prevention of cellular senescence by CD9-targeted delivery of rapamycin using lactose-wrapped calcium carbonate nanoparticles. *Sci Rep,* 7**,** 43299.

THOMAS, A., TEICHER, B. A. & HASSAN, R. 2016. Antibody–drug conjugates for cancer therapy. *The Lancet Oncology,* 17**,** e254-e262.

THOMAS, J. D., SIDERAS, P., SMITH, C. I., VORECHOVSKÝ, I., CHAPMAN, V. & PAUL, W. E. 1993. Colocalization of X-linked agammaglobulinemia and X-linked immunodeficiency genes. *Science,* 261**,** 355-8.

TIAN, Y., LI, H., QIU, T., DAI, J., ZHANG, Y., CHEN, J. & CAI, H. 2019. Loss of PTEN induces lung fibrosis via alveolar epithelial cell senescence depending on NF-κB activation. *Aging cell,* 18**,** e12858.

TIEPPO, A., WHITE, C. J., PAINE, A. C., VOYLES, M. L., MCBRIDE, M. K. & BYRNE, M. E. 2012. Sustained in vivo release from imprinted therapeutic contact lenses.

TISATO, V., VOLTAN, R., GONELLI, A., SECCHIERO, P. & ZAULI, G. 2017. MDM2/X inhibitors under clinical evaluation: perspectives for the management of hematological malignancies and pediatric cancer. *Journal of hematology & oncology,* 10**,** 133.

TOUFEKTCHAN, E. & TOLEDO, F. 2018. The Guardian of the Genome Revisited: p53 Downregulates Genes Required for Telomere Maintenance, DNA Repair, and Centromere Structure. *Cancers (Basel),* 10.

TOUSSAINT, O., MEDRANO, E. E. & VON ZGLINICKI, T. 2000. Cellular and molecular mechanisms of stress-induced premature senescence (SIPS) of human diploid fibroblasts and melanocytes. *Exp Gerontol,* 35**,** 927-45.

TRAIL, P. A., DUBOWCHIK, G. M. & LOWINGER, T. B. 2018. Antibody drug conjugates for treatment of breast cancer: Novel targets and diverse approaches in ADC design.

TRAIL, P. A., WILLNER, D., LASCH, S. J., HENDERSON, A. J., HOFSTEAD, S., CASAZZA, A. M., FIRESTONE, R. A., HELLSTROM, I. & HELLSTROM, K. E. 1993. Cure of xenografted human carcinomas by BR96-doxorubicin immunoconjugates. *Science (New York, N.Y.),* 261**,** 212-215.

TRAN, H., BRUNET, A., GRENIER, J. M., DATTA, S. R., FORNACE, A. J., DISTEFANO, P. S., CHIANG, L. W. & GREENBERG, M. E. 2002. DNA repair pathway stimulated by the forkhead transcription factor FOXO3a through the Gadd45 protein. *Science,* 296**,** 530-534.

TREIT, D., MENARD, J. & ROYAN, C. 1993. Anxiogenic stimuli in the elevated plus-maze. *Pharmacology Biochemistry and Behavior,* 44**,** 463-469.

TRIANA-MARTÍNEZ, F., PICALLOS-RABINA, P., DA SILVA-ÁLVAREZ, S., PIETROCOLA, F., LLANOS, S., RODILLA, V., SOPRANO, E., PEDROSA, P., FERREIRÓS, A. & BARRADAS, M. 2019a. Identification and characterization of Cardiac Glycosides as senolytic compounds. *Nature communications,* 10**,** 1-12.

TRIANA-MARTÍNEZ, F., PICALLOS-RABINA, P., DA SILVA-ÁLVAREZ, S., PIETROCOLA, F., LLANOS, S., RODILLA, V., SOPRANO, E., PEDROSA, P., FERREIRÓS, A., BARRADAS, M., HERNÁNDEZ-GONZÁLEZ, F., LALINDE, M., PRATS, N., BERNADÓ, C., GONZÁLEZ, P., GÓMEZ, M., IKONOMOPOULOU, M. P., FERNÁNDEZ-MARCOS, P. J., GARCÍA-CABALLERO, T., DEL PINO, P., ARRIBAS, J., VIDAL, A., GONZÁLEZ-BARCIA, M., SERRANO, M., LOZA, M. I., DOMÍNGUEZ, E. & COLLADO, M. 2019b.

Identification and characterization of Cardiac Glycosides as senolytic compounds. *Nature Communications,* 10**,** 4731.

TSE, C., SHOEMAKER, A. R., ADICKES, J., ANDERSON, M. G., CHEN, J., JIN, S., JOHNSON, E. F., MARSH, K. C., MITTEN, M. J. & NIMMER, P. 2008. ABT-263: a potent and orally bioavailable Bcl-2 family inhibitor. *Cancer research,* 68**,** 3421-3428.

TSUKADA, S., SAFFRAN, D. C., RAWLINGS, D. J., PAROLINI, O., ALLEN, R. C., KLISAK, I., SPARKES, R. S., KUBAGAWA, H., MOHANDAS, T., QUAN, S. & ET AL. 1993. Deficient expression of a B cell cytoplasmic tyrosine kinase in human X-linked agammaglobulinemia. *Cell,* 72**,** 279-90.

TYAGI, N., ARORA, S., DESHMUKH, S. K., SINGH, S., MARIMUTHU, S. & SINGH, A. P. 2016. Exploiting Nanotechnology for the Development of MicroRNA-Based Cancer Therapeutics. *Journal of biomedical nanotechnology,* 12**,** 28-42.

TYNER, S. D., VENKATACHALAM, S., CHOI, J., JONES, S., GHEBRANIOUS, N., IGELMANN, H., LU, X., SORON, G., COOPER, B., BRAYTON, C., PARK, S. H., THOMPSON, T., KARSENTY, G., BRADLEY, A. & DONEHOWER, L. A. 2002. p53 mutant mice that display early ageing-associated phenotypes. *Nature,* 415**,** 45-53.

UHLÉN, M., FAGERBERG, L., HALLSTRÖM, B. M., LINDSKOG, C., OKSVOLD, P., MARDINOGLU, A., SIVERTSSON, Å., KAMPF, C., SJÖSTEDT, E., ASPLUND, A., OLSSON, I., EDLUND, K., LUNDBERG, E., NAVANI, S., SZIGYARTO, C. A., ODEBERG, J., DJUREINOVIC, D., TAKANEN, J. O., HOBER, S., ALM, T., EDQVIST, P. H., BERLING, H., TEGEL, H., MULDER, J., ROCKBERG, J., NILSSON, P., SCHWENK, J. M., HAMSTEN, M., VON FEILITZEN, K., FORSBERG, M., PERSSON, L., JOHANSSON, F., ZWAHLEN, M., VON HEIJNE, G., NIELSEN, J. & PONTÉN, F. 2015. Proteomics. Tissue-based map of the human proteome. *Science,* 347**,** 1260419.

VALENTIJN, F. A., FALKE, L. L., NGUYEN, T. Q. & GOLDSCHMEDING, R. 2018. Cellular senescence in the aging and diseased kidney. *Journal of cell communication and signaling,* 12**,** 69-82.

VAN DER LEE, M. M., GROOTHUIS, P. G., UBINK, R., VAN DER VLEUTEN, M. A., VAN ACHTERBERG, T. A., LOOSVELD, E. M., DAMMING, D., JACOBS, D. C., ROUWETTE, M., EGGING, D. F., VAN DEN DOBBELSTEEN, D., BEUSKER, P. H., GOEDINGS, P., VERHEIJDEN, G. F., LEMMENS, J. M., TIMMERS, M. & DOKTER, W. H. 2015. The Preclinical Profile of the Duocarmycin-Based HER2-Targeting ADC SYD985 Predicts for Clinical Benefit in Low HER2-Expressing Breast Cancers. *Mol Cancer Ther,* 14**,** 692-703.

VARELA, I., CADIÑANOS, J., PENDÁS, A. M., GUTIÉRREZ-FERNÁNDEZ, A., FOLGUERAS, A. R., SÁNCHEZ, L. M., ZHOU, Z., RODRÍGUEZ, F. J., STEWART, C. L., VEGA, J. A., TRYGGVASON, K., FREIJE, J. M. P. & LÓPEZ-OTÍN, C. 2005. Accelerated ageing in mice deficient in Zmpste24 protease is linked to p53 signalling activation. *Nature,* 437**,** 564.

VASAPOLLO, G., SOLE, R. D., MERGOLA, L., LAZZOI, M. R., SCARDINO, A., SCORRANO, S. & MELE, G. 2011a. Molecularly imprinted polymers: present and future prospective. *Int J Mol Sci,* 12**,** 5908-45.

VASAPOLLO, G., SOLE, R. D., MERGOLA, L., LAZZOI, M. R., SCARDINO, A., SCORRANO, S. & MELE, G. 2011b. Molecularly imprinted polymers: present and future prospective. *International journal of molecular sciences,* 12**,** 5908-5945.

VASILAKI, A., IWANEJKO, L. M., MCARDLE, F., BROOME, C. S., JACKSON, M. J. & MCARDLE, A. 2003. Skeletal muscles of aged male mice fail to adapt following contractile activity. *Biochem Soc Trans,* 31**,** 455-6.

VELASCO, K., ST-LOUIS, J. L., HOVLAND, H. N., THOMPSON, N., OTTESEN, Å., CHOI, M. H., PEDERSEN, L., NJØLSTAD, P. R., ARNESEN, T., FJELD, K., AUKRUST, I., MYKLEBUST, L. M. & MOLVEN, A. 2020. Functional evaluation of 16 SCHAD missense variants: Only amino acid substitutions causing congenital hyperinsulinism of infancy lead to loss-of-function phenotypes in vitro. *J Inherit Metab Dis*.

VELNAR, T., BAILEY, T. & SMRKOLJ, V. 2009. The wound healing process: an overview of the cellular and molecular mechanisms. *Journal of International Medical Research,* 37**,** 1528-1542.

VENTURA, A., KIRSCH, D. G., MCLAUGHLIN, M. E., TUVESON, D. A., GRIMM, J., LINTAULT, L., NEWMAN, J., RECZEK, E. E., WEISSLEDER, R. & JACKS, T. 2007. Restoration of p53 function leads to tumour regression in vivo. *Nature,* 445**,** 661-665.

VERGNES, L., PÉTERFY, M., BERGO, M. O., YOUNG, S. G. & REUE, K. 2004. Lamin B1 is required for mouse development and nuclear integrity. *Proceedings of the National Academy of Sciences,* 101**,** 10428-10433.

VETRIE, D., VOŘECHOVSKÝ, I., SIDERAS, P., HOLLAND, J., DAVIES, A., FLINTER, F., HAMMARSTRÖM, L., KINNON, C., LEVINSKY, R., BOBROW, M., SMITH, C. I. E. & BENTLEY, D. R. 1993. The gene involved in X-linked agammaglobulinaemia is a member of the src family of protein-tyrosine kinases. *Nature,* 361**,** 226.

VILARIÑO-GÜELL, C., WIDER, C., ROSS, OWEN A., DACHSEL, JUSTUS C., KACHERGUS, JENNIFER M., LINCOLN, SARAH J., SOTO-ORTOLAZA, ALEXANDRA I., COBB, STEPHANIE A., WILHOITE, GREGGORY J., BACON, JUSTIN A., BEHROUZ, B., MELROSE, HEATHER L., HENTATI, E., PUSCHMANN, A., EVANS, DANIEL M., CONIBEAR, E., WASSERMAN, WYETH W., AASLY, JAN O., BURKHARD, PIERRE R., DJALDETTI, R., GHIKA, J., HENTATI, F., KRYGOWSKA-WAJS, A., LYNCH, T., MELAMED, E., RAJPUT, A., RAJPUT, ALI H., SOLIDA, A., WU, R.-M., UITTI, RYAN J., WSZOLEK, ZBIGNIEW K., VINGERHOETS, F. & FARRER, MATTHEW J. 2011. VPS35 Mutations in Parkinson Disease. *The American Journal of Human Genetics,* 89**,** 162-167.

VILLIARD, É., DENIS, J.-F., HASHEMI, F. S., IGELMANN, S., FERBEYRE, G. & ROY, S. 2017. Senescence gives insights into the morphogenetic evolution of anamniotes. *Biology Open,* 6**,** 891-896.

VOGLER, M., HAMALI, H. A., BAMPTON, E. T., DINSDALE, D., SUN, X.-M., DYER, M. J., GOODALL, A. H. & COHEN, G. M. 2011. Platelet toxicity induced by the BCL2-inhibitor ABT-263, a novel anti-cancer agent. *Toxicology,* 2**,** 108.

VOGT, M., HAGGBLOM, C., YEARGIN, J., CHRISTIANSEN-WEBER, T. & HAAS, M. 1998. Independent induction of senescence by p16INK4a and p21CIP1 in spontaneously immortalized human fibroblasts. *Cell Growth Differ,* 9**,** 139-46.

VOIGT, J., CHRISTENSEN, J. & SHASTRI, V. P. 2014. Differential uptake of nanoparticles by endothelial cells through polyelectrolytes with affinity for caveolae. *Proceedings of the National Academy of Sciences of the United States of America,* 111**,** 2942-2947.

WAKITA, M., TAKAHASHI, A., SANO, O., LOO, T. M., IMAI, Y., NARUKAWA, M., IWATA, H., MATSUDAIRA, T., KAWAMOTO, S., OHTANI, N., YOSHIMORI, T. & HARA, E. 2020. A BET family protein degrader provokes senolysis by targeting NHEJ and autophagy in senescent cells. *Nature Communications,* 11**,** 1935.

WALTER, H. S. & AHMED, S. 2017. Targeted therapies in cancer. *Surgery (Oxford)*.

WALTER, H. S., JAYNE, S., RULE, S. A., CARTRON, G., MORSCHHAUSER, F., MACIP, S., KARLIN, L., JONES, C., HERBAUX, C., QUITTET, P., SHAH, N., HUTCHINSON, C. V., FEGAN, C., YANG, Y., MITRA, S., SALLES, G. & DYER, M. J. S. 2017. Long-term follow-up of patients with CLL treated with the selective Bruton's tyrosine kinase inhibitor ONO/GS-4059. *Blood,* 129**,** 2808-2810.

WANG, B., KOHLI, J. & DEMARIA, M. 2020. Senescent Cells in Cancer Therapy: Friends or Foes? *Trends in Cancer*.

WANG, C., JURK, D., MADDICK, M., NELSON, G., MARTIN-RUIZ, C. & VON ZGLINICKI, T. 2009. DNA damage response and cellular senescence in tissues of aging mice. *Aging Cell,* 8**,** 311-23.

WANG, E. 1985. Are cross-bridging structures involved in the bundle formation of intermediate filaments and the decrease in locomotion that accompany cell aging? *The Journal of cell biology,* 100**,** 1466-1473.

WANG, E. & GUNDERSEN, D. 1984. Increased organization of cytoskeleton accompanying the aging of human fibroblasts in vitro. *Exp Cell Res,* 154**,** 191-202.

WANG, J., YU, J. T. & TAN, L. 2015. PLD3 in Alzheimer's disease. *Mol Neurobiol,* 51**,** 480-6.

WANG, J. C. & BENNETT, M. 2012. Aging and atherosclerosis: mechanisms, functional consequences, and potential therapeutics for cellular senescence. *Circ Res,* 111**,** 245-59.

WANG, R., SUNCHU, B. & PEREZ, V. I. 2017a. Rapamycin and the inhibition of the secretory phenotype. *Exp Gerontol,* 94**,** 89-92.

WANG, R., YU, Z., SUNCHU, B., SHOAF, J., DANG, I., ZHAO, S., CAPLES, K., BRADLEY, L., BEAVER, L. M., HO, E., LÖHR, C. V. & PEREZ, V. I. 2017b. Rapamycin inhibits the secretory phenotype of senescent cells by a Nrf2-independent mechanism. *Aging Cell,* 16**,** 564-574.

WANG, S., TAN, K. L., AGOSTO, M. A., XIONG, B., YAMAMOTO, S., SANDOVAL, H., JAISWAL, M., BAYAT, V., ZHANG, K. & CHARNG, W.-L. 2014. The retromer complex is required for rhodopsin recycling and its loss leads to photoreceptor degeneration. *PLoS Biol,* 12**,** e1001847.

WANG, Y., CHANG, J., LIU, X., ZHANG, X., ZHANG, S., ZHANG, X., ZHOU, D. & ZHENG, G. 2016a. Discovery of piperlongumine as a potential novel lead for the development of senolytic agents. *Aging (Albany NY),* 8**,** 2915-2926.

WANG, Y., CHANG, J., LIU, X., ZHANG, X., ZHANG, S., ZHANG, X., ZHOU, D. & ZHENG, G. 2016b. Discovery of piperlongumine as a potential novel lead for the development of senolytic agents. *Aging (Albany NY),* 8**,** 2915.

WANG, Z., WEI, D. & XIAO, H. 2013. Methods of cellular senescence induction using oxidative stress. *Methods Mol Biol,* 1048**,** 135-44.

WEI, L., SU, Y. K., LIN, C. M., CHAO, T. Y., HUANG, S. P., HUYNH, T. T., JAN, H. J., WHANG-PENG, J., CHIOU, J. F., WU, A. T. & HSIAO, M. 2016. Preclinical investigation of ibrutinib, a Bruton's kinase tyrosine (Btk) inhibitor, in suppressing glioma tumorigenesis and stem cell phenotypes. *Oncotarget,* 7**,** 69961-69975.

WEINSTEIN, J. R. & ANDERSON, S. 2010. The aging kidney: physiological changes. *Adv Chronic Kidney Dis,* 17**,** 302-7.

WELDON, C., DACANAY, J. G., GOKHALE, V., BODDUPALLY, P. V. L., BEHM-ANSMANT, I., BURLEY, G. A., BRANLANT, C., HURLEY, L. H., DOMINGUEZ, C. & EPERON, I. C. 2018. Specific G-quadruplex ligands modulate the alternative splicing of Bcl-X. *Nucleic Acids Res,* 46**,** 886-896.

WHITE, M. C., HOLMAN, D. M., BOEHM, J. E., PEIPINS, L. A., GROSSMAN, M. & HENLEY, S. J. 2014. Age and cancer risk: a potentially modifiable relationship. *Am J Prev Med,* 46**,** S7-15.

WHITEHEAD, J. C., HILDEBRAND, B. A., SUN, M., ROCKWOOD, M. R., ROSE, R. A., ROCKWOOD, K. & HOWLETT, S. E. 2014. A clinical frailty index in aging mice:

comparisons with frailty index data in humans. *J Gerontol A Biol Sci Med Sci,* 69**,** 621-32.

WHITESELL, L. & LINDQUIST, S. L. 2005. HSP90 and the chaperoning of cancer. *Nature Reviews Cancer,* 5**,** 761-772.

WILEY, C. D., SCHAUM, N., ALIMIRAH, F., LOPEZ-DOMINGUEZ, J. A., ORJALO, A. V., SCOTT, G., DESPREZ, P.-Y., BENZ, C., DAVALOS, A. R. & CAMPISI, J. 2018. Small-molecule MDM2 antagonists attenuate the senescence-associated secretory phenotype. *Scientific reports,* 8**,** 1-9.

WILKINSON, H. N. & HARDMAN, M. J. 2017. The role of estrogen in cutaneous ageing and repair. *Maturitas,* 103**,** 60-64.

WILKINSON, H. N. & HARDMAN, M. J. 2020. Senescence in Wound Repair: Emerging Strategies to Target Chronic Healing Wounds. *Front Cell Dev Biol,* 8**,** 773.

WILLIAMS, G. C. 1957. Pleiotropy, natural selection, and the evolution of senescence. *evolution***,** 398-411.

WISNIEWSKI, J. R., ZOUGMAN, A., NAGARAJ, N. & MANN, M. 2009. Universal sample preparation method for proteome analysis. *Nat Methods,* 6**,** 359-62.

WITZIG, T. E. & INWARDS, D. 2019. Acalabrutinib for mantle cell lymphoma. *blood,* 133**,** 2570-2574.

WOLSTEIN, J. M., LEE, D. H., MICHAUD, J., BUOT, V., STEFANCHIK, B. & PLOTKIN, M. D. 2010. INK4a knockout mice exhibit increased fibrosis under normal conditions and in response to unilateral ureteral obstruction. *American Journal of Physiology-Renal Physiology,* 299**,** F1486-F1495.

WORMAN, H. J., ÖSTLUND, C. & WANG, Y. 2010. Diseases of the nuclear envelope. *Cold Spring Harbor perspectives in biology,* 2**,** a000760.

WRIGHT, W. E. & SHAY, J. W. 2000. Telomere dynamics in cancer progression and prevention: fundamental differences in human and mouse telomere biology. *Nature Medicine,* 6**,** 849-851.

WU, T., RAYNER, C. K. & HOROWITZ, M. 2016. Incretins. *In:* HERZIG, S. (ed.) *Metabolic Control.* Cham: Springer International Publishing.

WYNN, T. A. 2008. Cellular and molecular mechanisms of fibrosis. *The Journal of pathology,* 214**,** 199-210.

XIANG, Y., MA, N., WANG, D., ZHANG, Y., ZHOU, J., WU, G., ZHAO, R., HUANG, H., WANG, X. & QIAO, Y. 2014. MiR-152 and miR-185 co-contribute to ovarian cancer cells cisplatin sensitivity by targeting DNMT1 directly: a novel epigenetic therapy independent of decitabine. *Oncogene,* 33**,** 378-386.

XIE, J., CHEN, Y., HU, C., PAN, Q., WANG, B., LI, X., GENG, J. & XU, B. 2017. Premature senescence of cardiac fibroblasts and atrial fibrosis in patients with atrial fibrillation. *Oncotarget,* 8**,** 57981-57990.

XU, M., PIRTSKHALAVA, T., FARR, J. N., WEIGAND, B. M., PALMER, A. K., WEIVODA, M. M., INMAN, C. L., OGRODNIK, M. B., HACHFELD, C. M. & FRASER, D. G. 2018. Senolytics improve physical function and increase lifespan in old age. *Nature medicine,* 24**,** 1246-1256.

XU, M., TCHKONIA, T., DING, H., OGRODNIK, M., LUBBERS, E. R., PIRTSKHALAVA, T., WHITE, T. A., JOHNSON, K. O., STOUT, M. B. & MEZERA, V. 2015. JAK inhibition alleviates the cellular senescence-associated secretory phenotype and frailty in old age. *Proceedings of the National Academy of Sciences,* 112**,** E6301-E6310.

XU, P.-T., LI, Y.-J., QIN, X.-J., SCHERZER, C. R., XU, H., SCHMECHEL, D. E., HULETTE, C. M., ERVIN, J., GULLANS, S. R. & HAINES, J. 2006. Differences in apolipoprotein E3/3 and E4/4 allele-specific gene expression in hippocampus in Alzheimer disease. *Neurobiology of disease,* 21**,** 256-275.

XU, S., SANKAR, S. & NEAMATI, N. 2014a. Protein disulfide isomerase: a promising target for cancer therapy. *Drug discovery today,* 19**,** 222-240.

XU, T., CAI, Y., ZHONG, X., ZHANG, L., ZHENG, D., GAO, Z., PAN, X., WANG, F., CHEN, M. & YANG, Z. 2019. beta-Galactosidase instructed supramolecular hydrogelation for selective identification and removal of senescent cells. *Chem Commun (Camb)*.

XU, Y., LI, N., XIANG, R. & SUN, P. 2014b. Emerging roles of the p38 MAPK and PI3K/AKT/mTOR pathways in oncogene-induced senescence. *Trends Biochem Sci,* 39**,** 268-76.

XUE, W., ZENDER, L., MIETHING, C., DICKINS, R. A., HERNANDO, E., KRIZHANOVSKY, V., CORDON-CARDO, C. & LOWE, S. W. 2007. Senescence and tumour clearance is triggered by p53 restoration in murine liver carcinomas. *Nature,* 445**,** 656-660.

YANAI, H., SHTEINBERG, A., PORAT, Z., BUDOVSKY, A., BRAIMAN, A., ZEISCHE, R. & FRAIFELD, V. E. 2015. Cellular senescence-like features of lung fibroblasts derived from idiopathic pulmonary fibrosis patients. *Aging (Albany NY),* 7**,** 664.

YANG, F., TUXHORN, J. A., RESSLER, S. J., MCALHANY, S. J., DANG, T. D. & ROWLEY, D. R. 2005. Stromal expression of connective tissue growth factor promotes angiogenesis and prostate cancer tumorigenesis. *Cancer research,* 65**,** 8887-8895.

YANG, G., ROSEN, D. G., ZHANG, Z., BAST, R. C., JR., MILLS, G. B., COLACINO, J. A., MERCADO-URIBE, I. & LIU, J. 2006. The chemokine growth-regulated oncogene

1 (Gro-1) links RAS signaling to the senescence of stromal fibroblasts and ovarian tumorigenesis. *Proc Natl Acad Sci U S A,* 103**,** 16472-7.

YANG, H.-Y., WEN, Y.-Y., CHEN, C.-H., LOZANO, G. & LEE, M.-H. 2003. 14-3-3σ positively regulates p53 and suppresses tumor growth. *Molecular and cellular biology,* 23**,** 7096-7107.

YANG, L., ZHENG, Z., QIAN, C., WU, J., LIU, Y., GUO, S., LI, G., LIU, M., WANG, X. & KAPLAN, D. L. 2017a. Curcumin-functionalized silk biomaterials for anti-aging utility. *Journal of colloid and interface science,* 496**,** 66-77.

YANG, Z., JUN, H., CHOI, C. I., YOO, K. H., CHO, C. H., HUSSAINI, S. M. Q., SIMMONS, A. J., KIM, S., VAN DEURSEN, J. M., BAKER, D. J. & JANG, M. H. 2017b. Age-related decline in BubR1 impairs adult hippocampal neurogenesis. *Aging Cell,* 16**,** 598-601.

YE, H., OJELADE, S. A., LI-KROEGER, D., ZUO, Z., WANG, L., LI, Y., GU, J. Y., TEPASS, U., RODAL, A. A. & BELLEN, H. J. 2020. Retromer subunit, VPS29, regulates synaptic transmission and is required for endolysosomal function in the aging brain. *Elife,* 9**,** e51977.

YOSEF, R., PILPEL, N., TOKARSKY-AMIEL, R., BIRAN, A., OVADYA, Y., COHEN, S., VADAI, E., DASSA, L., SHAHAR, E. & CONDIOTTI, R. 2016a. Directed elimination of senescent cells by inhibition of BCL-W and BCL-XL. *Nature communications,* 7**,** 1-11.

YOSEF, R., PILPEL, N., TOKARSKY-AMIEL, R., BIRAN, A., OVADYA, Y., COHEN, S., VADAI, E., DASSA, L., SHAHAR, E., CONDIOTTI, R., BEN-PORATH, I. & KRIZHANOVSKY, V. 2016b. Directed elimination of senescent cells by inhibition of BCL-W and BCL-XL. *Nat Commun,* 7**,** 11190.

YOULE, R. J. & STRASSER, A. 2008. The BCL-2 protein family: opposing activities that mediate cell death. *Nature reviews Molecular cell biology,* 9**,** 47-59.

YOUNG, A. & MCNAUGHT, C.-E. 2011. The physiology of wound healing. *Surgery (Oxford),* 29**,** 475-479.

YOUNG, A. R., NARITA, M. & NARITA, M. 2013. Cell senescence as both a dynamic and a static phenotype. *Methods Mol Biol,* 965**,** 1-13.

YOUSEFZADEH, M. J., ZHU, Y., MCGOWAN, S. J., ANGELINI, L., FUHRMANN-STROISSNIGG, H., XU, M., LING, Y. Y., MELOS, K. I., PIRTSKHALAVA, T. & INMAN, C. L. 2018. Fisetin is a senotherapeutic that extends health and lifespan. *EBioMedicine,* 36**,** 18-28.

YU, Q. & YUN, M. H. 2020. Interconnection Between Cellular Senescence, Regeneration and Ageing in Salamanders. *Senolytics in Disease, Ageing and Longevity.* Springer.

ZENG, X. & RAO, M. 2007. Human embryonic stem cells: long term stability, absence of senescence and a potential cell source for neural replacement. *Neuroscience,* 145**,** 1348-1358.

ZHANG, P., KISHIMOTO, Y., GRAMMATIKAKIS, I., GOTTIMUKKALA, K., CUTLER, R. G., ZHANG, S., ABDELMOHSEN, K., BOHR, V. A., SEN, J. M. & GOROSPE, M. 2019. Senolytic therapy alleviates Aβ-associated oligodendrocyte progenitor cell senescence and cognitive deficits in an Alzheimer's disease model. *Nature neuroscience,* 22**,** 719-728.

ZHANG, X., ZHANG, S., LIU, X., WANG, Y., CHANG, J., ZHANG, X., MACKINTOSH, S. G., TACKETT, A. J., HE, Y. & LV, D. 2018. Oxidation resistance 1 is a novel senolytic target. *Aging cell,* 17**,** e12780.

ZHONG, J., RAO, X., DEIULIIS, J., BRAUNSTEIN, Z., NARULA, V., HAZEY, J., MIKAMI, D., NEEDLEMAN, B., SATOSKAR, A. R. & RAJAGOPALAN, S. 2013. A Potential Role for Dendritic Cell/Macrophage-Expressing DPP4 in Obesity-Induced Visceral Inflammation. *Diabetes,* 62**,** 149.

ZHU, C., ZHANG, L., ZHENG, Y., XU, J., SONG, J., ROLFE, B. E. & CAMPBELL, J. H. 2011. Effects of estrogen on stress-induced premature senescence of vascular smooth muscle cells: a novel mechanism for the "time window theory" of menopausal hormone therapy. *Atherosclerosis,* 215**,** 294-300.

ZHU, F., LI, Y., ZHANG, J., PIAO, C., LIU, T., LI, H.-H. & DU, J. 2013. Senescent cardiac fibroblast is critical for cardiac fibrosis after myocardial infarction. *PloS one,* 8**,** e74535.

ZHU, Y., DOORNEBAL, E. J., PIRTSKHALAVA, T., GIORGADZE, N., WENTWORTH, M., FUHRMANN-STROISSNIGG, H., NIEDERNHOFER, L. J., ROBBINS, P. D., TCHKONIA, T. & KIRKLAND, J. L. 2017a. New agents that target senescent cells: the flavone, fisetin, and the BCL-X(L) inhibitors, A1331852 and A1155463. *Aging (Albany NY),* 9**,** 955-963.

ZHU, Y., DOORNEBAL, E. J., PIRTSKHALAVA, T., GIORGADZE, N., WENTWORTH, M., FUHRMANN-STROISSNIGG, H., NIEDERNHOFER, L. J., ROBBINS, P. D., TCHKONIA, T. & KIRKLAND, J. L. 2017b. New agents that target senescent cells: the flavone, fisetin, and the BCL-XL inhibitors, A1331852 and A1155463. *Aging (Albany NY),* 9**,** 955.

ZHU, Y., TCHKONIA, T., FUHRMANN-STROISSNIGG, H., DAI, H. M., LING, Y. Y., STOUT, M. B., PIRTSKHALAVA, T., GIORGADZE, N., JOHNSON, K. O. & GILES, C. B. 2016. Identification of a novel senolytic agent, navitoclax, targeting the Bcl-2 family of anti-apoptotic factors. *Aging cell,* 15**,** 428-435.

ZHU, Y., TCHKONIA, T., PIRTSKHALAVA, T., GOWER, A. C., DING, H., GIORGADZE, N., PALMER, A. K., IKENO, Y., HUBBARD, G. B. & LENBURG, M. 2015a. The Achilles'

heel of senescent cells: from transcriptome to senolytic drugs. *Aging cell,* 14**,** 644-658.

ZHU, Y., TCHKONIA, T., PIRTSKHALAVA, T., GOWER, A. C., DING, H., GIORGADZE, N., PALMER, A. K., IKENO, Y., HUBBARD, G. B., LENBURG, M., O'HARA, S. P., LARUSSO, N. F., MILLER, J. D., ROOS, C. M., VERZOSA, G. C., LEBRASSEUR, N. K., WREN, J. D., FARR, J. N., KHOSLA, S., STOUT, M. B., MCGOWAN, S. J., FUHRMANN-STROISSNIGG, H., GURKAR, A. U., ZHAO, J., COLANGELO, D., DORRONSORO, A., LING, Y. Y., BARGHOUTHY, A. S., NAVARRO, D. C., SANO, T., ROBBINS, P. D., NIEDERNHOFER, L. J. & KIRKLAND, J. L. 2015b. The Achilles' heel of senescent cells: from transcriptome to senolytic drugs. *Aging Cell,* 14**,** 644-58.

ZIMPRICH, A., BENET-PAGÈS, A., STRUHAL, W., GRAF, E., ECK, S. H., OFFMAN, M. N., HAUBENBERGER, D., SPIELBERGER, S., SCHULTE, E. C. & LICHTNER, P. 2011. A mutation in VPS35, encoding a subunit of the retromer complex, causes late-onset Parkinson disease. *The American Journal of Human Genetics,* 89**,** 168-175.

ZOLOT, R. S., BASU, S. & MILLION, R. P. 2013. Antibody–drug conjugates. *Nature Reviews Drug Discovery,* 12**,** 259-260.

ZUCHA, M. A., WU, A. T., LEE, W. H., WANG, L. S., LIN, W. W., YUAN, C. C. & YEH, C. T. 2015. Bruton's tyrosine kinase (Btk) inhibitor ibrutinib suppresses stem-like traits in ovarian cancer. *Oncotarget,* 6**,** 13255-68.

9 Appendix

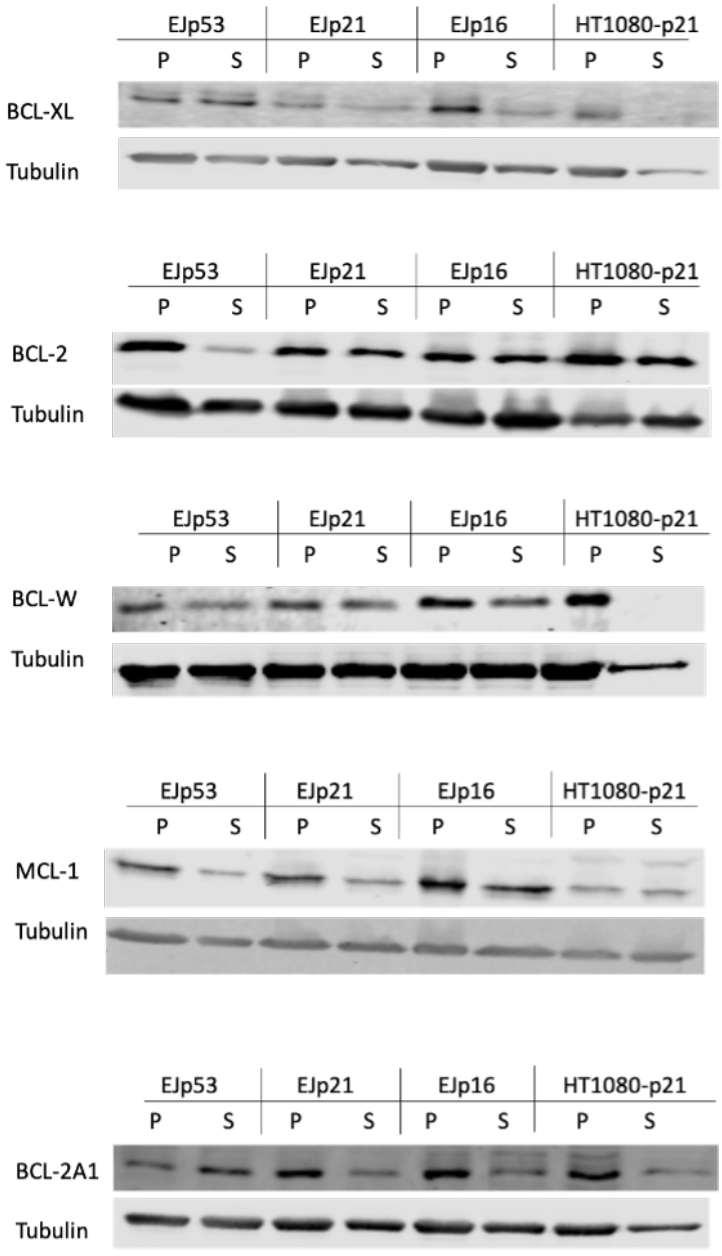

Figure 9.1. Expression of anti-apoptotic members of BCL-2 family in senescent models.

Western blot analysis showing protein level of anti-apoptotic BCL-2 family members in EJp53, EJp21, EJp16 and HT1080-p21 proliferating and senescent cells (5 days after induction). Tubulin was used loading control.

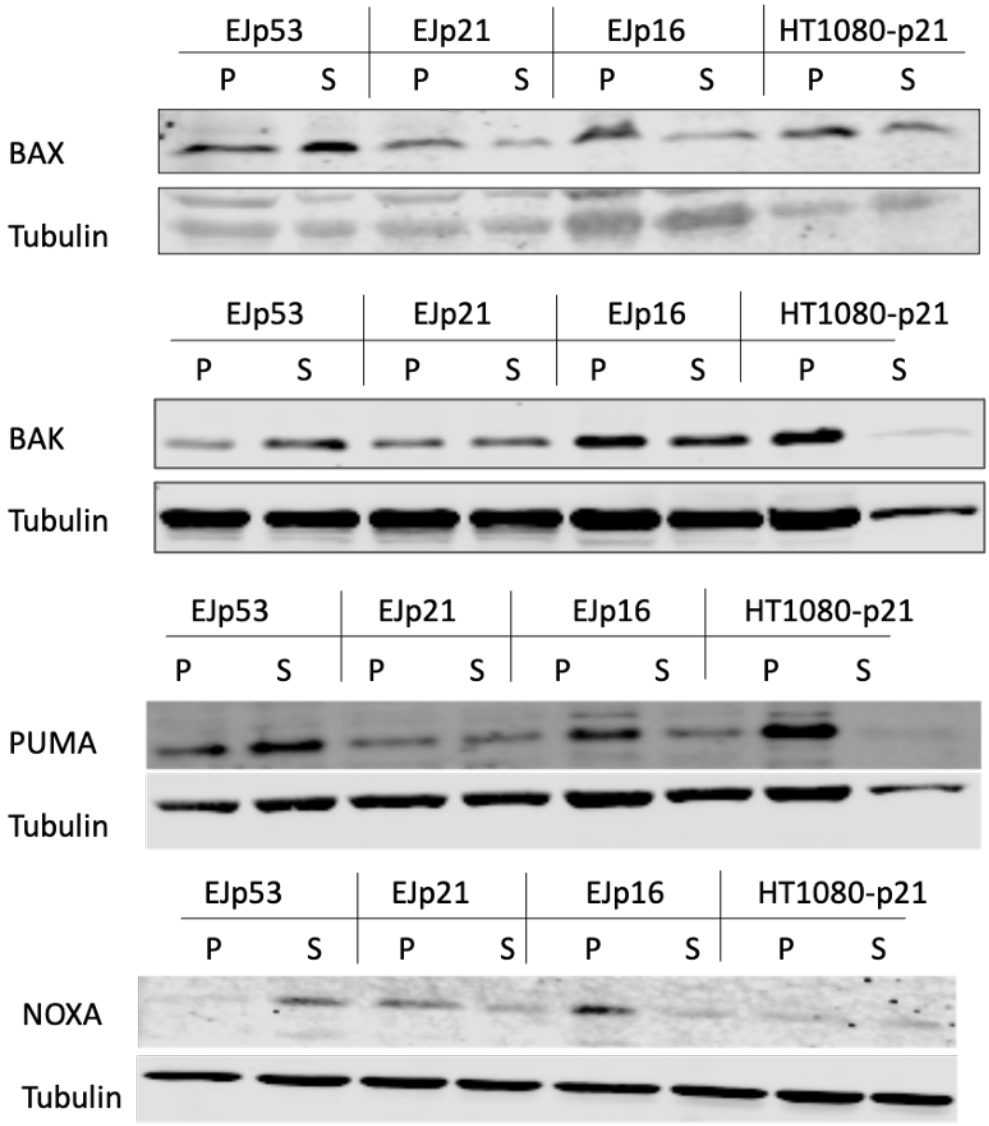

Figure 9.2. Expression of pro-apoptotic members of BCL-2 family in senescent models.

Western blot analysis showing protein level of anti-apoptotic BCL-2 family members in EJp53, EJp21, EJp16 and HT1080-p21 proliferating and senescent cells (5 days after induction). Tubulin was used loading control.

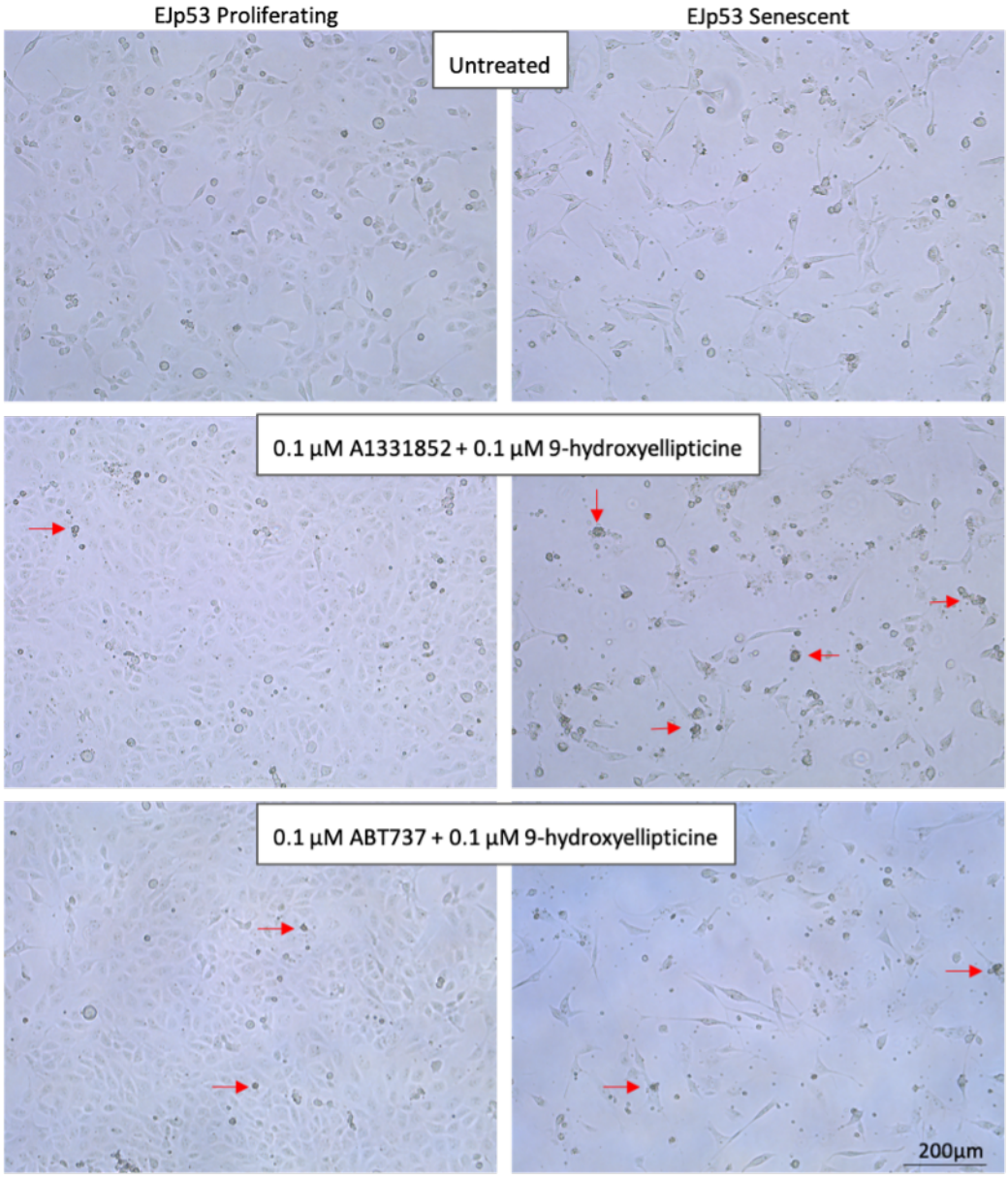

Figure 9.3. Presence of dead cells after combination of 9-hydroxyellipticine with A1331852 or ABT737 in EJp53 cell line.

5 days after senescence induction, EJp53 proliferating (left) and senescent cells (right) were treated with 0.1 µM of A1331852 (BCL-X_L inhibitor) and 0.1 µM 9-hydroxyellipticine (BCL-X splicing regulator) (middle) or ABT737 (BCL-2, BCL-2 and BCL-X_L inhibitor) (bottom) for 8 hours and the presence of dead cells was visually determined using Leica DMi1 microscope with Leica MC170 HD camera (10x magnification. Red arrows show examples of dead cells. Untreated cells were used as negative control (top).

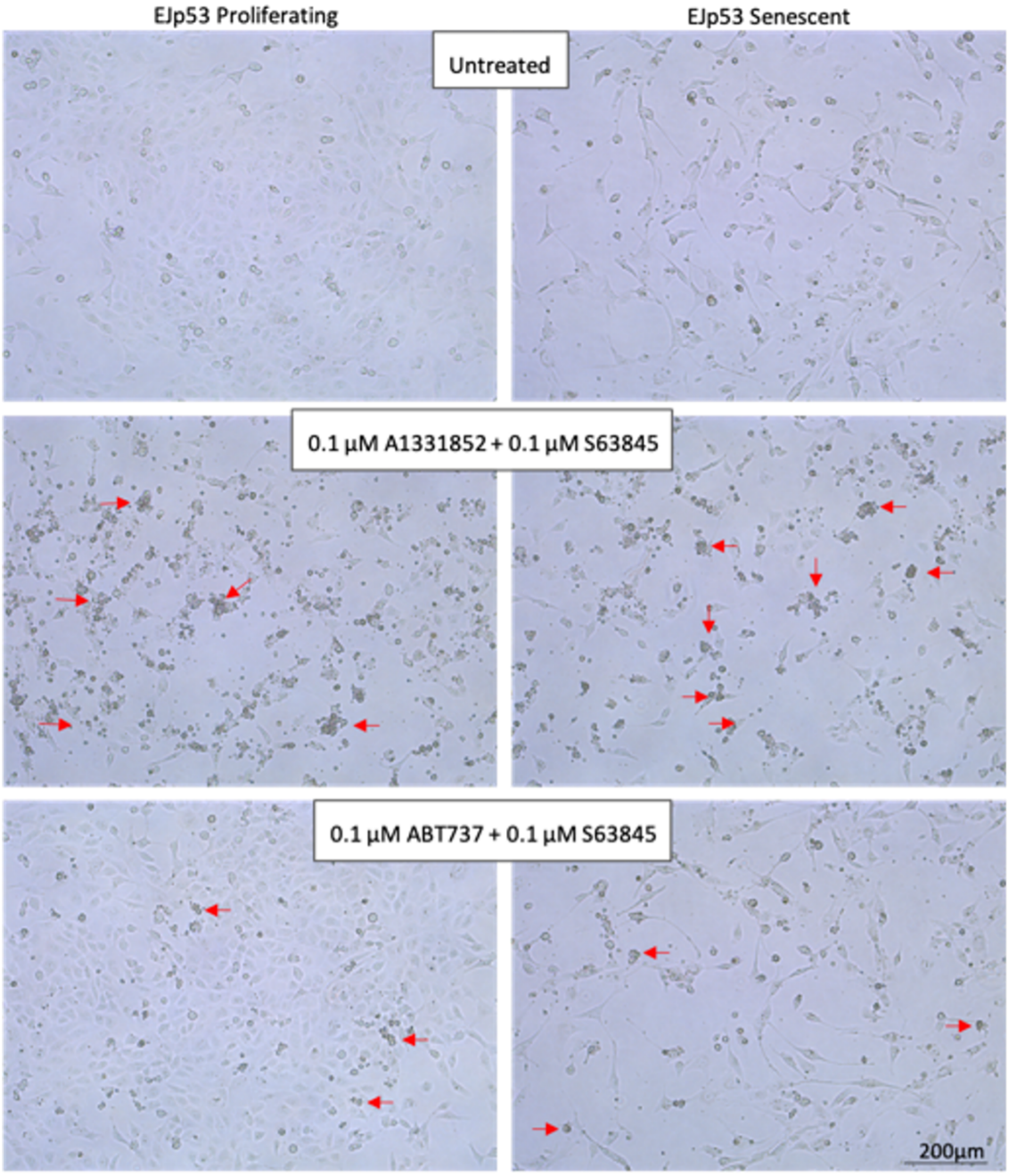

Figure 9.4. Presence of dead cells after combination of S63845 with A1331852 or ABT737 in EJp53 cell line.

5 days after senescence induction, EJp53 proliferating (left) and senescent cells (right) were treated with 0.1 µM of A1331852 (BCL-X_L inhibitor) and 0.1 µM S63845 (BCL-X splicing regulator) (middle) or ABT737 (BCL-2, BCL-2 and BCL-X_L inhibitor) (bottom) for 8 hours and the presence of dead cells was visually determined using Leica DMi1 microscope with Leica MC170 HD camera. (10x magnification. Red arrows show examples of dead cells. Untreated cells were used as negative control (top)

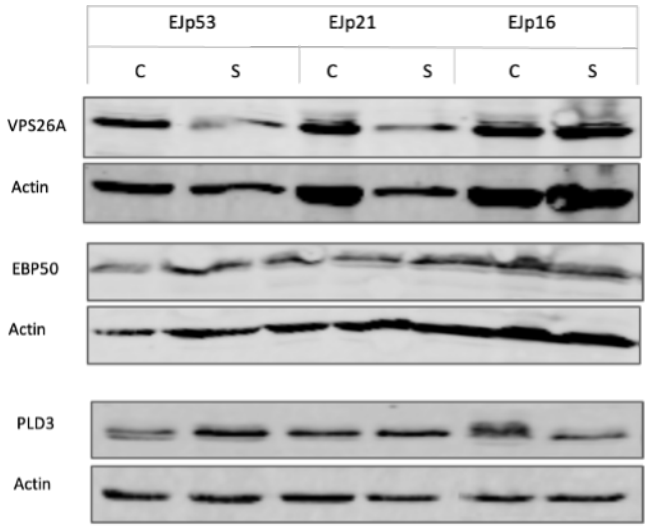

Figure 9.5. Expression of VPS26A, PLD3 and EBP50 in EJ-based cell models, other replicates.

Second replicate of western blot analysis indicating the protein level of p53, p21 and p16 4 days after removal of tetracycline in corresponding EJ-models. "S" indicates senescent cells and "C" proliferating controls.

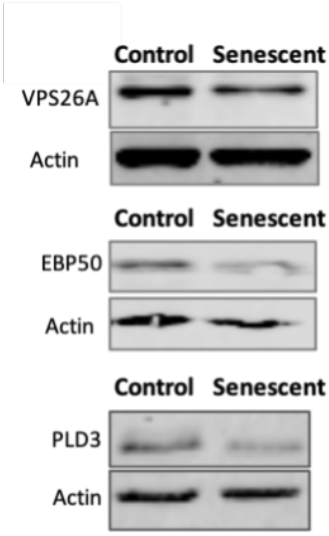

Figure 9.6. The expression profiles of VPS26A, EBP50 and PLD3 in HT1080-p21-9 cell line, other replicates.

Western blot analysis indicating the protein level of VPS26A, EBP50 and PLD3 5 days after addition of IPTG. Actin used as loading control.

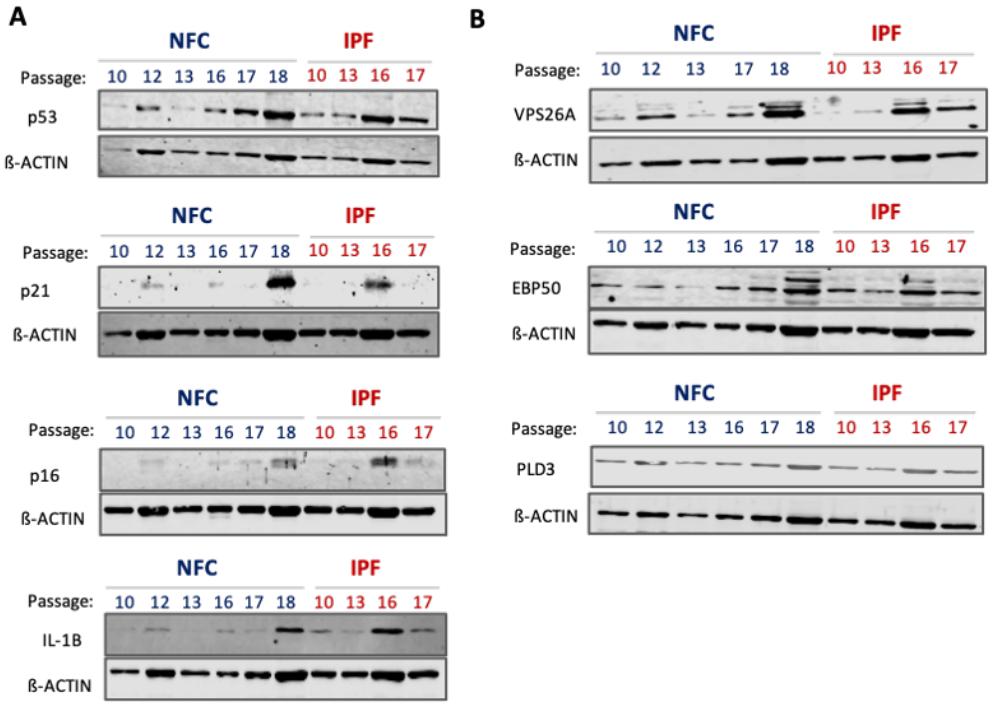

Figure 9.7. Western blot analysis of VPS26A, EBP50 and PLD3 in IPF fibroblasts, second replicate.

Fibroblasts were subjected to prolonged culture in order to induce replicative cellular senescence. Cells were collected from a patient suffering from Idiopathic Pulmonary Fibrosis (IPF1) and non-fibrotic control (NFC1). [A] p53, p21, p16, IL-1ß and [B] VPS26A, EBP50 and PLD3 protein levels were compared between increasing passages. Data were standardised to reference housekeeping protein β-actin and normalized against the lowest available passage (P), P:10

Table 9.1. List of the proteins downregulated in the brains of Ibrutinib-treated animals when compared to controls.

Proteins selected based on the max fold change values (>2-fold)

Max fold change	Name
Infinity	Synemin OS=Mus musculus GN=Synm PE=1 SV=2
Infinity	Nucleoside diphosphate kinase (Fragment) OS=Mus musculus GN=Nme2 PE=2 SV=1
Infinity	Inositol 1_4_5-trisphosphate receptor type 1 OS=Mus musculus GN=Itpr1 PE=1 SV=2
Infinity	Kinesin-like protein KIF27 OS=Mus musculus GN=Kif27 PE=1 SV=1
Infinity	Cell division control protein 6 homolog OS=Mus musculus GN=Cdc6 PE=1 SV=1
Infinity	Unconventional myosin-IXb OS=Mus musculus GN=Myo9b PE=1 SV=2
Infinity	Tankyrase 1 binding protein 1 OS=Mus musculus GN=Tnks1bp1 PE=2 SV=1
Infinity	NADH dehydrogenase [ubiquinone] 1 beta subcomplex subunit 8_ mitochondrial OS=Mus musculus GN=Ndufb8 PE=1 SV=1
Infinity	Amphiphysin OS=Mus musculus GN=Amph PE=1 SV=1
Infinity	Cysteine and glycine-rich protein 1 OS=Mus musculus GN=Csrp1 PE=1 SV=3
Infinity	Paraneoplastic antigen-like protein 5 OS=Mus musculus GN=Pnma5 PE=1 SV=2
Infinity	Leucine-rich repeats and immunoglobulin-like domains protein 3 OS=Mus musculus GN=Lrig3 PE=1 SV=1
Infinity	Histone-lysine N-methyltransferase ASH1L OS=Mus musculus GN=Ash1l PE=1 SV=3
Infinity	Cell adhesion molecule 3 OS=Mus musculus GN=Cadm3 PE=1 SV=1
Infinity	Calmodulin-1 OS=Mus musculus GN=Calm1 PE=1 SV=1

2135.65	Heat shock 70 kDa protein 12A OS=Mus musculus GN=Hspa12a PE=1 SV=1
439.16	GC-rich sequence DNA-binding factor 2 OS=Mus musculus GN=Gcfc2 PE=1 SV=2
104.53	Ubiquitin carboxyl-terminal hydrolase 5 (Fragment) OS=Mus musculus GN=Usp5 PE=1 SV=1
39.34	Alpha-1_4 glucan phosphorylase OS=Mus musculus GN=Pygl PE=2 SV=1
24.12	DNA-dependent protein kinase catalytic subunit OS=Mus musculus GN=Prkdc PE=1 SV=3
19.33	MKIAA0864 protein (Fragment) OS=Mus musculus GN=Mprip PE=2 SV=1
16.80	Dimethylaniline monooxygenase [N-oxide-forming] 5 OS=Mus musculus GN=Fmo5 PE=1 SV=4
16.50	E3 ubiquitin-protein ligase Itchy OS=Mus musculus GN=Itch PE=1 SV=2
14.48	Stathmin (Fragment) OS=Mus musculus GN=Stmn1 PE=1 SV=1
13.08	Septin-14 OS=Mus musculus GN=Sept14 PE=1 SV=3
12.55	Nebulin-related-anchoring protein OS=Mus musculus GN=Nrap PE=1 SV=3
12.49	Uncharacterized protein OS=Mus musculus GN=Emilin2 PE=2 SV=1
10.98	Delta(3_5)-Delta(2_4)-dienoyl-CoA isomerase_ mitochondrial OS=Mus musculus GN=Ech1 PE=1 SV=1
9.84	Protein bassoon OS=Mus musculus GN=Bsn PE=1 SV=4
9.16	Alpha-internexin OS=Mus musculus GN=Ina PE=1 SV=3
9.11	Eukaryotic translation initiation factor 4 gamma 2 OS=Mus musculus GN=Eif4g2 PE=1 SV=2
7.77	D-beta-hydroxybutyrate dehydrogenase_ mitochondrial OS=Mus musculus GN=Bdh1 PE=1 SV=2
7.23	Alpha-methylacyl-CoA racemase OS=Mus musculus GN=Amacr PE=1 SV=4

7.17	Testis-expressed protein 15 OS=Mus musculus GN=Tex15 PE=2 SV=1
7.07	Phosphatidylinositol 3-kinase_ catalytic_ alpha polypeptide_ isoform CRA_a OS=Mus musculus GN=Pik3ca PE=1 SV=1
7.02	Tubulin beta-1 chain OS=Mus musculus GN=Tubb1 PE=1 SV=1
6.59	Sarcoplasmic/endoplasmic reticulum calcium ATPase 3 OS=Mus musculus GN=Atp2a3 PE=1 SV=3
6.24	Peroxiredoxin-1 OS=Mus musculus GN=Prdx1 PE=1 SV=1
5.66	Cytochrome c oxidase subunit 5B_ mitochondrial OS=Mus musculus GN=Cox5b PE=1 SV=1
5.34	Cadherin EGF LAG seven-pass G-type receptor 1 OS=Mus musculus GN=Celsr1 PE=1 SV=3
4.93	Mitochondrial pyruvate carrier 1 OS=Mus musculus GN=Mpc1 PE=1 SV=1
4.90	ADP-ribosylation factor 5 OS=Mus musculus GN=Arf5 PE=1 SV=2
4.87	Uncharacterized protein (Fragment) OS=Mus musculus GN=Acaa1b PE=2 SV=1
4.83	Alpha-actinin-1 OS=Mus musculus GN=Actn1 PE=1 SV=1
4.51	Uncharacterized protein OS=Mus musculus GN=Cyb5b PE=2 SV=1
4.45	Long-chain-fatty-acid--CoA ligase 5 OS=Mus musculus GN=Acsl5 PE=1 SV=1
4.39	Microtubule-associated protein tau OS=Mus musculus GN=Mapt PE=1 SV=3
4.37	DNA topoisomerase 2-beta OS=Mus musculus GN=Top2b PE=1 SV=2
4.28	Zinc finger protein 292 OS=Mus musculus GN=Zfp292 PE=1 SV=2
4.08	14-3-3 protein epsilon OS=Mus musculus GN=Ywhae PE=1 SV=1
3.94	Voltage-dependent anion-selective channel protein 3 OS=Mus musculus GN=Vdac3 PE=1 SV=1
3.85	Myosin-9 OS=Mus musculus GN=Myh9 PE=1 SV=4
3.62	Carbonic anhydrase 2 OS=Mus musculus GN=Ca2 PE=1 SV=4
3.62	Annexin (Fragment) OS=Mus musculus GN=Anxa2 PE=1 SV=1

3.40	Carboxylesterase 1F OS=Mus musculus GN=Ces1f PE=1 SV=1
3.36	Dynein heavy chain 8_ axonemal OS=Mus musculus GN=Dnah8 PE=1 SV=2
3.27	NACHT and WD repeat domain-containing protein 2 OS=Mus musculus GN=Nwd2 PE=1 SV=2
3.16	CAP-Gly domain-containing linker protein 1 (Fragment) OS=Mus musculus GN=Clip1 PE=1 SV=1
3.03	Uncharacterized protein OS=Mus musculus GN=Akr1a1 PE=2 SV=1
2.92	ATP synthase subunit e_ mitochondrial OS=Mus musculus GN=Atp5i PE=1 SV=2
2.91	Striated muscle-specific serine/threonine-protein kinase OS=Mus musculus GN=Speg PE=1 SV=2
2.83	Tripartite motif-containing 61 OS=Mus musculus GN=Trim61 PE=2 SV=1
2.76	Enoyl-CoA delta isomerase 1_ mitochondrial OS=Mus musculus GN=Eci1 PE=1 SV=2
2.74	Spectrin alpha chain_ erythrocytic 1 OS=Mus musculus GN=Spta1 PE=1 SV=3
2.63	Tensin-2 OS=Mus musculus GN=Tns2 PE=1 SV=1
2.55	Unconventional myosin-Va OS=Mus musculus GN=Myo5a PE=1 SV=1
2.46	Rab GDP dissociation inhibitor alpha OS=Mus musculus GN=Gdi1 PE=1 SV=3
2.46	AP-1 complex subunit beta-1 OS=Mus musculus GN=Ap1b1 PE=1 SV=2
2.45	Uncharacterized protein KIAA1109 OS=Mus musculus GN=Kiaa1109 PE=1 SV=4
2.44	Choline dehydrogenase_ mitochondrial OS=Mus musculus GN=Chdh PE=1 SV=1
2.44	Cytochrome P450 2C37 OS=Mus musculus GN=Cyp2c37 PE=1 SV=2
2.43	AP-2 complex subunit alpha-2 OS=Mus musculus GN=Ap2a2 PE=1 SV=2
2.41	Dystonin OS=Mus musculus GN=Dst PE=1 SV=2

2.38	Pyruvate kinase PKLR OS=Mus musculus GN=Pklr PE=1 SV=1
2.32	Kinesin-1 heavy chain OS=Mus musculus GN=Kif5b PE=1 SV=3
2.30	Guanine nucleotide-binding protein G(t) subunit alpha-1 OS=Mus musculus GN=Gnat1 PE=1 SV=3
2.30	Bifunctional epoxide hydrolase 2 OS=Mus musculus GN=Ephx2 PE=1 SV=2
2.29	17-beta-hydroxysteroid dehydrogenase type 6 OS=Mus musculus GN=Hsd17b6 PE=1 SV=1
2.24	Carboxylic ester hydrolase OS=Mus musculus GN=Ces1g PE=1 SV=1
2.24	3-hydroxyisobutyrate dehydrogenase_ mitochondrial OS=Mus musculus GN=Hibadh PE=1 SV=1
2.18	Serine/threonine-protein phosphatase 2A 65 kDa regulatory subunit A alpha isoform OS=Mus musculus GN=Ppp2r1a PE=1 SV=3
2.18	HEAT repeat-containing protein 5A OS=Mus musculus GN=Heatr5a PE=1 SV=2
2.16	Myosin-8 OS=Mus musculus GN=Myh8 PE=2 SV=2
2.15	Myelin-associated glycoprotein OS=Mus musculus GN=Mag PE=1 SV=1
2.12	Integrator complex subunit 4 OS=Mus musculus GN=Ints4 PE=1 SV=1
2.12	Gamma-soluble NSF attachment protein (Fragment) OS=Mus musculus GN=Napg PE=1 SV=1
2.11	Histone H4 OS=Mus musculus GN=Hist1h4a PE=1 SV=2
2.11	Cytochrome P450 4B1 (Fragment) OS=Mus musculus GN=Cyp4b1 PE=1 SV=1
2.11	NADH dehydrogenase [ubiquinone] iron-sulfur protein 3_ mitochondrial OS=Mus musculus GN=Ndufs3 PE=1 SV=2
2.08	Histidine triad nucleotide binding protein 2 OS=Mus musculus GN=Hint2 PE=1 SV=1
2.03	Collagen alpha-1(VII) chain OS=Mus musculus GN=Col7a1 PE=1 SV=3

Table 9.2. List of the proteins upregulated in the hearts of Ibrutinib-treated animals when compared to controls.

Proteins selected based on the max fold change values (>2-fold)

Max fold change	Name
Infinity	Microtubule-associated protein tau OS=Mus musculus GN=Mapt PE=1 SV=3
Infinity	Quinone oxidoreductase-like protein 2 OS=Mus musculus PE=1 SV=1
Infinity	Leucine-rich repeat-containing protein 9 OS=Mus musculus GN=Lrrc9 PE=1 SV=1
Infinity	14-3-3 protein epsilon OS=Mus musculus GN=Ywhae PE=1 SV=1
Infinity	40S ribosomal protein S2 OS=Mus musculus GN=Rps2 PE=1 SV=3
Infinity	Kynurenine/alpha-aminoadipate aminotransferase_ mitochondrial OS=Mus musculus GN=Aadat PE=1 SV=1
Infinity	Synaptotagmin II OS=Mus musculus GN=Syt2 PE=1 SV=1
Infinity	Visinin-like protein 1 OS=Mus musculus GN=Vsnl1 PE=2 SV=1
Infinity	Uncharacterized protein OS=Mus musculus GN=Afg3l2 PE=2 SV=1
Infinity	Endophilin-A1 OS=Mus musculus GN=Sh3gl2 PE=1 SV=1
Infinity	RIKEN cDNA 4932415D10 gene OS=Mus musculus GN=4932415D10Rik PE=4 SV=1
Infinity	Rai1 protein OS=Mus musculus GN=Rai1 PE=2 SV=1
Infinity	Actin_ cytoplasmic 1 OS=Mus musculus GN=Actb PE=1 SV=1
Infinity	Transitional endoplasmic reticulum ATPase OS=Mus musculus GN=Vcp PE=1 SV=4
Infinity	Kynurenine 3-monooxygenase OS=Mus musculus GN=Kmo PE=1 SV=1
Infinity	Ribosomal protein L4 OS=Mus musculus GN=Rpl4 PE=1 SV=1
Infinity	E3 ubiquitin-protein ligase LRSAM1 OS=Mus musculus GN=Lrsam1 PE=1 SV=1

Infinity	Anion exchange protein (Fragment) OS=Mus musculus GN=Slc4a4 PE=2 SV=1
Infinity	V-type proton ATPase subunit D OS=Mus musculus GN=Atp6v1d PE=1 SV=1
Infinity	Carboxylic ester hydrolase OS=Mus musculus GN=Ces1g PE=1 SV=1
Infinity	Dedicator of cytokinesis protein 4 OS=Mus musculus GN=Dock4 PE=1 SV=1
Infinity	Utrophin OS=Mus musculus GN=Utrn PE=1 SV=1
Infinity	Inorganic pyrophosphatase 2_ mitochondrial OS=Mus musculus GN=Ppa2 PE=1 SV=1
Infinity	Cingulin-like protein 1 OS=Mus musculus GN=Cgnl1 PE=1 SV=2
Infinity	Intersectin-1 OS=Mus musculus GN=Itsn1 PE=1 SV=1
Infinity	Uncharacterized protein OS=Mus musculus GN=Emilin2 PE=2 SV=1
Infinity	Calmodulin-1 OS=Mus musculus GN=Calm1 PE=1 SV=1
Infinity	Guanine nucleotide-binding protein G(I)/G(S)/G(T) subunit beta-2 OS=Mus musculus GN=Gnb2 PE=1 SV=1
Infinity	Apolipoprotein E OS=Mus musculus GN=Apoe PE=1 SV=2
Infinity	Acetyl-coenzyme A synthetase OS=Mus musculus GN=Acss1 PE=2 SV=1
Infinity	Putative adenosylhomocysteinase 3 OS=Mus musculus GN=Ahcyl2 PE=1 SV=1
Infinity	Glutathione S-transferase P 1 OS=Mus musculus GN=Gstp1 PE=1 SV=2
Infinity	Cytochrome c_ somatic OS=Mus musculus GN=Cycs PE=1 SV=2
Infinity	Integrator complex subunit 4 OS=Mus musculus GN=Ints4 PE=1 SV=1
2401071.79	Isocitrate dehydrogenase [NAD] subunit_ mitochondrial OS=Mus musculus GN=Idh3b PE=1 SV=1
174.85	Excitatory amino acid transporter 1 OS=Mus musculus GN=Slc1a3 PE=1 SV=2

142.13	Dihydropyrimidinase-related protein 1 OS=Mus musculus GN=Crmp1 PE=1 SV=1
106.64	Uncharacterized protein OS=Mus musculus GN=Atp6v1b2 PE=2 SV=1
61.24	60S acidic ribosomal protein P0 OS=Mus musculus GN=Rplp0 PE=1 SV=3
42.39	Cytochrome P450 2A5 OS=Mus musculus GN=Cyp2a5 PE=2 SV=1
33.69	Vesicle-associated membrane protein 2 OS=Mus musculus GN=Vamp2 PE=1 SV=1
32.24	Uncharacterized protein OS=Mus musculus GN=Vnn1 PE=2 SV=1
30.39	Arginase-1 OS=Mus musculus GN=Arg1 PE=1 SV=1
30.33	Dynein heavy chain 8_ axonemal OS=Mus musculus GN=Dnah8 PE=1 SV=2
19.95	Flavin-containing monooxygenase OS=Mus musculus GN=Fmo4 PE=2 SV=1
18.54	SH3 domain-binding protein 5 OS=Mus musculus GN=Sh3bp5 PE=1 SV=3
16.87	Anoctamin-1 (Fragment) OS=Mus musculus GN=Ano1 PE=1 SV=1
15.44	Dynein_ axonemal_ heavy chain 7A OS=Mus musculus GN=Dnah7a PE=1 SV=2
12.51	Syp protein (Fragment) OS=Mus musculus GN=Syp PE=2 SV=1
10.71	Guanine nucleotide-binding protein G(o) subunit alpha OS=Mus musculus GN=Gnao1 PE=1 SV=3
9.26	Cofilin-1 OS=Mus musculus GN=Cfl1 PE=1 SV=3
9.02	Pyruvate kinase PKLR OS=Mus musculus GN=Pklr PE=1 SV=1
7.95	Uncharacterized protein OS=Mus musculus GN=Mroh8 PE=2 SV=1
7.79	Acyl-CoA dehydrogenase family member 9_ mitochondrial OS=Mus musculus GN=Acad9 PE=1 SV=2
7.73	Ellis-van Creveld syndrome protein homolog OS=Mus musculus GN=Evc PE=1 SV=1

6.94	Ribosomal protein L14 OS=Mus musculus GN=Rpl14-ps1 PE=2 SV=1
6.89	Dynein_ axonemal_ heavy chain 9 OS=Mus musculus GN=Dnah9 PE=1 SV=1
6.63	Alpha-enolase OS=Mus musculus GN=Eno1 PE=1 SV=3
6.43	Serine/threonine-protein phosphatase 2A 65 kDa regulatory subunit A alpha isoform OS=Mus musculus GN=Ppp2r1a PE=1 SV=3
6.38	GTP:AMP phosphotransferase AK3_ mitochondrial OS=Mus musculus GN=Ak3 PE=1 SV=3
6.32	Myosin-9 OS=Mus musculus GN=Myh9 PE=1 SV=4
6.09	Cytochrome c oxidase subunit 5B_ mitochondrial OS=Mus musculus GN=Cox5b PE=1 SV=1
5.86	Fructose-bisphosphate aldolase B OS=Mus musculus GN=Aldob PE=1 SV=3
5.64	Sodium/potassium-transporting ATPase subunit alpha-3 OS=Mus musculus GN=Atp1a3 PE=1 SV=1
5.49	Helicase with zinc finger domain 2 OS=Mus musculus GN=Helz2 PE=1 SV=1
4.96	Pregnancy-specific glycoprotein 29 OS=Mus musculus GN=Psg29 PE=2 SV=1
4.68	Protein unc-13 homolog B OS=Mus musculus GN=Unc13b PE=1 SV=1
4.64	Activated CDC42 kinase 1 OS=Mus musculus GN=Tnk2 PE=1 SV=1
4.44	Succinate-CoA ligase subunit beta (Fragment) OS=Mus musculus GN=Sucla2 PE=2 SV=1
4.44	Uncharacterized protein OS=Mus musculus GN=Akr1a1 PE=2 SV=1
4.32	Alpha-actinin-1 OS=Mus musculus GN=Actn1 PE=1 SV=1
4.23	Alpha-aminoadipic semialdehyde dehydrogenase OS=Mus musculus GN=Aldh7a1 PE=1 SV=4
4.20	DNA replication complex GINS protein PSF2 OS=Mus musculus GN=Gins2 PE=1 SV=1

4.09	Methylcrotonoyl-Coenzyme A carboxylase 2 (Beta) OS=Mus musculus GN=Mccc2 PE=1 SV=1
4.07	Glycine N-acyltransferase-like protein Keg1 OS=Mus musculus GN=Keg1 PE=1 SV=1
4.05	Tenascin-R OS=Mus musculus GN=Tnr PE=1 SV=2
3.97	Cytochrome P450 4B1 (Fragment) OS=Mus musculus GN=Cyp4b1 PE=1 SV=1
3.93	Microtubule-associated protein 1A OS=Mus musculus GN=Map1a PE=1 SV=2
3.89	Pericentrin OS=Mus musculus GN=Pcnt PE=1 SV=2
3.81	Synaptosomal-associated protein 25 OS=Mus musculus GN=Snap25 PE=1 SV=1
3.75	Zinc finger protein 292 OS=Mus musculus GN=Zfp292 PE=1 SV=2
3.71	Acetylcholinesterase collagenic tail peptide OS=Mus musculus GN=Colq PE=1 SV=1
3.69	DNA polymerase zeta catalytic subunit OS=Mus musculus GN=Rev3l PE=1 SV=3
3.68	Transient receptor potential cation channel_ subfamily M_ member 3 OS=Mus musculus GN=Trpm3 PE=1 SV=1
3.61	Protocadherin Fat 4 OS=Mus musculus GN=Fat4 PE=1 SV=2
3.52	Protein sidekick-2 OS=Mus musculus GN=Sdk2 PE=1 SV=1
3.43	Mitochondrial amidoxime reducing component 2 OS=Mus musculus GN=Marc2 PE=1 SV=1
3.43	ATP synthase F(0) complex subunit B1_ mitochondrial OS=Mus musculus GN=Atp5f1 PE=1 SV=1
3.42	Heterogeneous nuclear ribonucleoprotein A2/B1 OS=Mus musculus GN=Hnrnpa2b1 PE=2 SV=1
3.40	Kinesin-like protein KIF15 OS=Mus musculus GN=Kif15 PE=1 SV=1
3.33	Serum paraoxonase/arylesterase 1 OS=Mus musculus GN=Pon1 PE=1 SV=2

3.30	Cytochrome P450 2F2 OS=Mus musculus GN=Cyp2f2 PE=1 SV=1
3.13	Midasin OS=Mus musculus GN=Mdn1 PE=1 SV=1
3.12	Neural cell adhesion molecule 1 OS=Mus musculus GN=Ncam1 PE=1 SV=3
3.11	Glucose-6-phosphate isomerase OS=Mus musculus GN=Gpi PE=1 SV=4
3.09	Potassium-transporting ATPase alpha chain 2 OS=Mus musculus GN=Atp12a PE=1 SV=3
2.89	Ogdhl protein OS=Mus musculus GN=Ogdhl PE=2 SV=1
2.86	Citron Rho-interacting kinase OS=Mus musculus GN=Cit PE=1 SV=3
2.86	Clathrin coat assembly protein AP180 OS=Mus musculus GN=Snap91 PE=1 SV=2
2.82	Creatine kinase S-type_ mitochondrial OS=Mus musculus GN=Ckmt2 PE=1 SV=1
2.81	RAS-related C3 botulinum substrate 1 OS=Mus musculus GN=Rac1 PE=1 SV=1
2.80	Calcium/calmodulin-dependent protein kinase type II subunit alpha OS=Mus musculus GN=Camk2a PE=1 SV=2
2.78	UDP-glucuronosyltransferase 2B17 OS=Mus musculus GN=Ugt2b17 PE=1 SV=1
2.76	Unconventional myosin-Va OS=Mus musculus GN=Myo5a PE=1 SV=1
2.69	L-lactate dehydrogenase B chain OS=Mus musculus GN=Ldhb PE=1 SV=2
2.67	3-hydroxyisobutyrate dehydrogenase_ mitochondrial OS=Mus musculus GN=Hibadh PE=1 SV=1
2.66	ATP synthase protein 8 OS=Mus musculus musculus GN=ATP8 PE=3 SV=1
2.63	Tubulin beta-5 chain OS=Mus musculus GN=Tubb5 PE=1 SV=1
2.57	40S ribosomal protein S3 OS=Mus musculus GN=Rps3 PE=1 SV=1

2.56	UDP-glucuronosyltransferase 2A3 OS=Mus musculus GN=Ugt2a3 PE=1 SV=1
2.54	Medium-chain specific acyl-CoA dehydrogenase_ mitochondrial OS=Mus musculus GN=Acadm PE=1 SV=1
2.47	Versican core protein OS=Mus musculus GN=Vcan PE=1 SV=2
2.47	Xin actin-binding repeat-containing protein 2 OS=Mus musculus GN=Xirp2 PE=1 SV=1
2.46	Methylmalonyl-CoA mutase_ mitochondrial OS=Mus musculus GN=Mut PE=1 SV=2
2.41	StAR-related lipid transfer protein 9 OS=Mus musculus GN=Stard9 PE=1 SV=2
2.41	Centrosomal protein of 162 kDa OS=Mus musculus GN=Cep162 PE=1 SV=2
2.35	Thioredoxin-dependent peroxide reductase_ mitochondrial OS=Mus musculus GN=Prdx3 PE=1 SV=1
2.35	NAD-dependent protein deacetylase sirtuin-2 OS=Mus musculus GN=Sirt2 PE=1 SV=2
2.34	Striated muscle-specific serine/threonine-protein kinase OS=Mus musculus GN=Speg PE=1 SV=2
2.33	78 kDa glucose-regulated protein OS=Mus musculus GN=Hspa5 PE=1 SV=3
2.33	Cytochrome b5 OS=Mus musculus GN=Cyb5a PE=1 SV=2
2.29	AHNAK nucleoprotein (desmoyokin) OS=Mus musculus GN=Ahnak PE=1 SV=1
2.28	Transketolase OS=Mus musculus GN=Tkt PE=1 SV=1
2.25	Elongation factor 1-alpha 1 OS=Mus musculus GN=Eef1a1 PE=1 SV=3
2.24	Heat shock 70 kDa protein 1B OS=Mus musculus GN=Hspa1b PE=1 SV=3
2.23	Ras-related protein Rab-3A OS=Mus musculus GN=Rab3a PE=1 SV=1

2.22	Uricase OS=Mus musculus GN=Uox PE=1 SV=2
2.21	Bifunctional epoxide hydrolase 2 OS=Mus musculus GN=Ephx2 PE=1 SV=2
2.20	NADH dehydrogenase [ubiquinone] 1 alpha subcomplex subunit 9_ mitochondrial OS=Mus musculus GN=Ndufa9 PE=1 SV=1
2.15	Coiled-coil domain-containing protein 88B OS=Mus musculus GN=Ccdc88b PE=1 SV=2
2.11	Amine oxidase [flavin-containing] B OS=Mus musculus GN=Maob PE=1 SV=4
2.11	Histone-lysine N-methyltransferase 2C OS=Mus musculus GN=Kmt2c PE=1 SV=2
2.08	NADH dehydrogenase [ubiquinone] 1 alpha subcomplex subunit 10_ mitochondrial OS=Mus musculus GN=Ndufa10 PE=1 SV=1
2.06	Septin-14 OS=Mus musculus GN=Sept14 PE=1 SV=3
2.06	Limbic system-associated membrane protein OS=Mus musculus GN=Lsamp PE=1 SV=1
2.05	Structural maintenance of chromosomes flexible hinge domain-containing protein 1 OS=Mus musculus GN=Smchd1 PE=1 SV=2
2.05	DNA topoisomerase 2-beta OS=Mus musculus GN=Top2b PE=1 SV=2
2.00	Uncharacterized protein KIAA1109 OS=Mus musculus GN=Kiaa1109 PE=1 SV=4

Table 9.3. List of the proteins downregulated in the hearts of Ibrutinib-treated animals when compared to controls.

Proteins selected based on the max fold change values (>2-fold)

Max fold change	Name
Infinity	UDP-glucuronosyltransferase 1-2 OS=Mus musculus GN=Ugt1a2 PE=1 SV=1
Infinity	Dual specificity protein phosphatase 23 OS=Mus musculus GN=Dusp23 PE=2 SV=1 OS=Thanatephorus cucumeris (strain AG1-IB / isolate 7/3/14) GN=RSOLAG1IB_09263 PE=4 SV=1
Infinity	Nucleoside diphosphate kinase (Fragment) OS=Mus musculus GN=Nme2 PE=2 SV=1
Infinity	RAB39_ member RAS oncogene family OS=Mus musculus GN=Rab39 PE=2 SV=1
Infinity	Peroxiredoxin-6 OS=Mus musculus GN=Prdx6 PE=1 SV=3
Infinity	Superoxide dismutase [Cu-Zn] OS=Mus musculus GN=Sod1 PE=1 SV=2
Infinity	Tensin-2 OS=Mus musculus GN=Tns2 PE=1 SV=1
Infinity	Histone-lysine N-methyltransferase 2A OS=Mus musculus GN=Kmt2a PE=1 SV=3
Infinity	Solute carrier family 12 member 1 OS=Mus musculus GN=Slc12a1 PE=1 SV=1
Infinity	Exportin 4 [Mus musculus] OS=Lepeophtheirus salmonis GN=Xpo4 PE=4 SV=1
Infinity	Sulfotransferase OS=Mus musculus GN=Hs3st3b1 PE=2 SV=1
Infinity	Laminin receptor (Fragment) OS=Mus musculus GN=Rpsa PE=2 SV=1
Infinity	ATP synthase subunit e_ mitochondrial OS=Mus musculus GN=Atp5i PE=1 SV=2
Infinity	ADP-ribosylation factor 5 OS=Mus musculus GN=Arf5 PE=1 SV=2

Infinity	Triple functional domain protein OS=Mus musculus GN=Trio PE=1 SV=3
Infinity	Serine--pyruvate aminotransferase_ mitochondrial OS=Mus musculus GN=Agxt PE=1 SV=3
Infinity	MKIAA1087 protein (Fragment) OS=Mus musculus GN=mKIAA1087 PE=2 SV=1
Infinity	60S ribosomal protein L13 OS=Mus musculus GN=Rpl13 PE=1 SV=3
Infinity	Beta-synuclein OS=Mus musculus GN=Sncb PE=1 SV=1
Infinity	Uncharacterized protein OS=Mus musculus GN=Bphl PE=2 SV=1
Infinity	Mitochondrial amidoxime-reducing component 1 OS=Mus musculus GN=Marc1 PE=1 SV=1
Infinity	E3 ubiquitin-protein ligase HECTD1 OS=Mus musculus GN=Hectd1 PE=1 SV=2
Infinity	Glutaredoxin-related protein 5_ mitochondrial OS=Mus musculus GN=Glrx5 PE=1 SV=1
Infinity	Adrenodoxin_ mitochondrial OS=Mus musculus GN=Fdx1 PE=1 SV=1
Infinity	Dimethylaniline monooxygenase [N-oxide-forming] 5 OS=Mus musculus GN=Fmo5 PE=1 SV=4
Infinity	Enoyl-CoA hydratase domain-containing protein 2_ mitochondrial OS=Mus musculus GN=Echdc2 PE=1 SV=2
Infinity	Cadherin-16 OS=Mus musculus GN=Cdh16 PE=1 SV=1
194.15	Isocitrate dehydrogenase [NAD] subunit gamma 1_ mitochondrial OS=Mus musculus GN=Idh3g PE=1 SV=1
164.68	Eukaryotic translation initiation factor 4 gamma 2 OS=Mus musculus GN=Eif4g2 PE=1 SV=2
46.63	Polyamine-modulated factor 1-binding protein 1 OS=Mus musculus GN=Pmfbp1 PE=2 SV=1
39.52	Sodium/potassium-transporting ATPase subunit gamma OS=Mus musculus GN=Fxyd2 PE=1 SV=2

26.63	Heat shock-related 70 kDa protein 2 OS=Mus musculus GN=Hspa2 PE=1 SV=2
23.81	Phosphoglycerate kinase 1 OS=Mus musculus GN=Pgk1 PE=1 SV=4
23.20	Histone H2B (Fragment) OS=Mus musculus GN=Hist1h2bj PE=2 SV=1
19.82	Coiled-coil domain-containing protein 57 OS=Mus musculus GN=Ccdc57 PE=1 SV=1
19.39	CD81 antigen OS=Mus musculus GN=Cd81 PE=1 SV=2
14.08	Homeobox protein cut-like 1 OS=Mus musculus GN=Cux1 PE=1 SV=3
13.06	Aminopeptidase N OS=Mus musculus GN=Anpep PE=1 SV=4
10.56	Lymphocyte antigen 6 complex_ locus H_ isoform CRA_a OS=Mus musculus GN=Ly6h PE=1 SV=1
9.90	Vacuolar protein sorting 13D OS=Mus musculus GN=Vps13d PE=1 SV=1
9.11	AP-2 complex subunit mu OS=Mus musculus GN=Ap2m1 PE=1 SV=1
8.42	Spectrin beta chain_ erythrocytic OS=Mus musculus GN=Sptb PE=1 SV=4
7.99	Myosin_ heavy polypeptide 13_ skeletal muscle OS=Mus musculus GN=Myh13 PE=1 SV=1
7.95	3-mercaptopyruvate sulfurtransferase OS=Mus musculus GN=Mpst PE=1 SV=3
7.35	Calreticulin OS=Mus musculus GN=Calr PE=1 SV=1
6.89	Triosephosphate isomerase OS=Mus musculus GN=Tpi1 PE=1 SV=4
6.55	Down syndrome cell adhesion molecule homolog OS=Mus musculus GN=Dscam PE=1 SV=1
6.31	Septin-11 OS=Mus musculus GN=Sept11 PE=1 SV=1
6.27	Uncharacterized protein (Fragment) OS=Mus musculus GN=Pmpcb PE=2 SV=1
6.16	Nephrocystin-3 [Mus musculus] OS=Rhizoctonia solani GN=RSOLAG22IIIB_12418 PE=4 SV=1

5.87	Plasma membrane calcium-transporting ATPase 1 OS=Mus musculus GN=Atp2b1 PE=1 SV=1
5.41	Heat shock protein HSP 90-beta OS=Mus musculus GN=Hsp90ab1 PE=1 SV=3
5.22	Guanine nucleotide-binding protein G(I)/G(S)/G(O) subunit gamma-2 OS=Mus musculus GN=Gng2 PE=1 SV=2
5.08	Ezrin OS=Mus musculus GN=Ezr PE=1 SV=3
5.05	G-protein coupled receptor 98 OS=Mus musculus GN=Gpr98 PE=2 SV=1
4.74	14-3-3 protein beta/alpha OS=Mus musculus GN=Ywhab PE=1 SV=3
4.69	Cytochrome P450 2E1 OS=Mus musculus GN=Cyp2e1 PE=1 SV=1
4.34	14-3-3 protein gamma subtype OS=Mus musculus GN=Ywhag PE=1 SV=1
4.08	Peroxiredoxin-1 OS=Mus musculus GN=Prdx1 PE=1 SV=1
3.87	Alpha-aminoadipic semialdehyde synthase_ mitochondrial OS=Mus musculus GN=Aass PE=1 SV=1
3.79	Calcium-transporting ATPase OS=Mus musculus GN=Atp2b3 PE=1 SV=1
3.76	Endoplasmin OS=Mus musculus GN=Hsp90b1 PE=1 SV=2
3.71	Actin_ alpha cardiac muscle 1 OS=Mus musculus GN=Actc1 PE=1 SV=1
3.62	Persulfide dioxygenase ETHE1_ mitochondrial OS=Mus musculus GN=Ethe1 PE=1 SV=2
3.54	Syntaxin-1B OS=Mus musculus GN=Stx1b PE=1 SV=1
3.39	Coiled-coil domain containing 108 OS=Mus musculus GN=Cfap65 PE=2 SV=1
3.24	Advanced glycosylation end product-specific receptor variant 2 OS=Mus musculus GN=Ager PE=2 SV=1
3.18	Neuron navigator 2 OS=Mus musculus GN=Nav2 PE=1 SV=1
3.00	Syntaxin-1A OS=Mus musculus GN=Stx1a PE=1 SV=1
2.58	Adenomatosis polyposis coli OS=Mus musculus GN=Apc PE=1 SV=1

2.52	Duox2 protein OS=Mus musculus GN=Duox2 PE=2 SV=1
2.52	Septin-5 OS=Mus musculus GN=Sept5 PE=1 SV=2
2.46	Fibrous sheath-interacting protein 2 OS=Mus musculus GN=Fsip2 PE=1 SV=3
2.36	Alpha-methylacyl-CoA racemase OS=Mus musculus GN=Amacr PE=1 SV=4
2.31	Aldehyde dehydrogenase OS=Mus musculus GN=Aldh3a2 PE=1 SV=1
2.29	Phosphatidylinositol phosphatase PTPRQ OS=Mus musculus GN=Ptprq PE=1 SV=1
2.26	MKIAA0830 protein (Fragment) OS=Mus musculus GN=Endod1 PE=2 SV=1
2.20	Nuclear receptor corepressor 1 OS=Mus musculus GN=Ncor1 PE=1 SV=1
2.14	Tyrosine-protein phosphatase non-receptor type 13 OS=Mus musculus GN=Ptpn13 PE=1 SV=2
2.14	Kinesin-1 heavy chain OS=Mus musculus GN=Kif5b PE=1 SV=3
2.12	Calcium-transporting ATPase OS=Mus musculus GN=Atp2b4 PE=2 SV=2
2.09	Sodium- and chloride-dependent GABA transporter 3 OS=Mus musculus GN=Slc6a11 PE=1 SV=2
2.05	Heat shock protein HSP 90-alpha OS=Mus musculus GN=Hsp90aa1 PE=1 SV=4
2.05	Annexin (Fragment) OS=Mus musculus GN=Anxa2 PE=1 SV=1
2.03	Neurofascin OS=Mus musculus GN=Nfasc PE=1 SV=1
2.03	Predicted gene 11639 OS=Mus musculus GN=Gm11639 PE=4 SV=1

Table 9.4. List of the proteins upregulated in the kidneys of Ibrutinib-treated animals when compared to controls.

Proteins selected based on the max fold change values (>2-fold)

Max fold change	Name
Infinity	Myosin Vb_ isoform CRA_a OS=Mus musculus GN=Myo5b PE=1 SV=1
Infinity	Profilin-1 OS=Mus musculus GN=Pfn1 PE=1 SV=2
Infinity	Dysferlin OS=Mus musculus GN=Dysf PE=1 SV=1
Infinity	Immunoglobulin-like and fibronectin type III domain-containing protein 1 OS=Mus musculus GN=Igfn1 PE=1 SV=3
Infinity	Peptidyl-prolyl cis-trans isomerase B OS=Mus musculus GN=Ppib PE=1 SV=2
34.37	Kinesin-1 heavy chain OS=Mus musculus GN=Kif5b PE=1 SV=3
33.89	Gamma-tubulin complex component 6 OS=Mus musculus GN=Tubgcp6 PE=1 SV=1
31.27	UDP-glucuronosyltransferase 1-2 OS=Mus musculus GN=Ugt1a2 PE=1 SV=1
23.17	Laminin subunit alpha-3 OS=Mus musculus GN=Lama3 PE=1 SV=4
19.61	Uncharacterized protein (Fragment) OS=Mus musculus GN=Pmpcb PE=2 SV=1
15.00	Fibrous sheath-interacting protein 2 OS=Mus musculus GN=Fsip2 PE=1 SV=3
13.09	RIKEN cDNA 2900041A09_ isoform CRA_a OS=Mus musculus GN=Tppp PE=1 SV=1
10.30	Cytochrome P450 2C29 OS=Mus musculus GN=Cyp2c29 PE=1 SV=2
9.54	Uncharacterized protein OS=Mus musculus GN=Cyb5b PE=2 SV=1
8.84	Pre-mRNA-processing-splicing factor 8 OS=Mus musculus GN=Prpf8 PE=1 SV=2

8.19	Phosphatidylinositol 3-kinase_ catalytic_ alpha polypeptide_ isoform CRA_a OS=Mus musculus GN=Pik3ca PE=1 SV=1
7.00	Nephrocystin-3 [Mus musculus] OS=Rhizoctonia solani GN=RSOLAG22IIIB_12418 PE=4 SV=1
6.63	60S acidic ribosomal protein P0 OS=Mus musculus GN=Rplp0 PE=1 SV=3
6.02	CDGSH iron-sulfur domain-containing protein 1 OS=Mus musculus GN=Cisd1 PE=1 SV=1
5.92	Histone-lysine N-methyltransferase 2C OS=Mus musculus GN=Kmt2c PE=1 SV=2
5.86	Protein RRP5 homolog OS=Mus musculus GN=Pdcd11 PE=1 SV=2
5.54	Phosphatidylinositol 4_5-bisphosphate 3-kinase catalytic subunit delta isoform OS=Mus musculus GN=Pik3cd PE=1 SV=1
5.48	Ras-related protein Rab-10 OS=Mus musculus GN=Rab10 PE=1 SV=1
4.98	Dimethylaniline monooxygenase [N-oxide-forming] 3 OS=Mus musculus GN=Fmo3 PE=1 SV=1
4.42	Lipoxygenase homology domain-containing protein 1 OS=Mus musculus GN=Loxhd1 PE=2 SV=1
4.21	Uncharacterized protein OS=Mus musculus GN=Vnn1 PE=2 SV=1
4.02	Histone H2B (Fragment) OS=Mus musculus GN=Hist1h2bj PE=2 SV=1
3.87	Microtubule-associated serine/threonine-protein kinase 4 (Fragment) OS=Mus musculus GN=Mast4 PE=1 SV=1
3.82	Creatine kinase U-type_ mitochondrial OS=Mus musculus GN=Ckmt1 PE=1 SV=1
3.76	Myosin light chain 3 OS=Mus musculus GN=Myl3 PE=1 SV=4
3.49	HEAT repeat-containing protein 5A OS=Mus musculus GN=Heatr5a PE=1 SV=2
3.43	Cytoplasmic dynein 1 heavy chain 1 OS=Mus musculus GN=Dync1h1 PE=1 SV=2
3.41	Dystonin OS=Mus musculus GN=Dst PE=1 SV=2
3.40	AP-2 complex subunit beta OS=Mus musculus GN=Ap2b1 PE=1 SV=1

3.35	Sodium- and chloride-dependent GABA transporter 3 OS=Mus musculus GN=Slc6a11 PE=1 SV=2
3.33	Mitochondrial pyruvate carrier 1 OS=Mus musculus GN=Mpc1 PE=1 SV=1
3.18	Lysine-specific demethylase 6B OS=Mus musculus GN=Kdm6b PE=1 SV=1
3.13	Electron transfer flavoprotein-ubiquinone oxidoreductase_ mitochondrial OS=Mus musculus GN=Etfdh PE=1 SV=1
3.12	Predicted gene 11639 OS=Mus musculus GN=Gm11639 PE=4 SV=1
3.08	NADH dehydrogenase [ubiquinone] flavoprotein 2_ mitochondrial OS=Mus musculus GN=Ndufv2 PE=1 SV=2
3.04	Spectrin beta chain OS=Mus musculus GN=Sptbn2 PE=1 SV=1
3.01	Pyruvate kinase PKM OS=Mus musculus GN=Pkm PE=1 SV=4
2.94	Serine/threonine-protein phosphatase 6 regulatory ankyrin repeat subunit C OS=Mus musculus GN=Ankrd52 PE=1 SV=1
2.90	Gamma-soluble NSF attachment protein (Fragment) OS=Mus musculus GN=Napg PE=1 SV=1
2.85	Myelin basic protein OS=Mus musculus GN=Mbp PE=1 SV=2
2.83	Serine hydroxymethyltransferase OS=Mus musculus GN=Shmt2 PE=1 SV=1
2.82	UDP-glucuronosyltransferase 1-9 OS=Mus musculus GN=Ugt1a9 PE=1 SV=3
2.79	Long-chain-fatty-acid--CoA ligase 1 OS=Mus musculus GN=Acsl1 PE=1 SV=2
2.78	Dihydropyrimidinase-related protein 1 OS=Mus musculus GN=Crmp1 PE=1 SV=1
2.75	Glutamine synthetase OS=Mus musculus GN=Glul PE=1 SV=6
2.73	Plectin OS=Mus musculus GN=Plec PE=1 SV=3
2.73	Beta-actin-like protein 2 OS=Mus musculus GN=Actbl2 PE=1 SV=1
2.72	Hemicentin-2 OS=Mus musculus GN=Hmcn2 PE=1 SV=1
2.71	AP-1 complex subunit beta-1 OS=Mus musculus GN=Ap1b1 PE=1 SV=2

2.69	Fumarylacetoacetate hydrolase domain-containing protein 2A OS=Mus musculus GN=Fahd2 PE=1 SV=1
2.68	Myosin-8 OS=Mus musculus GN=Myh8 PE=2 SV=2
2.67	Annexin A5 OS=Mus musculus GN=Anxa5 PE=1 SV=1
2.62	Ryanodine receptor 2 OS=Mus musculus GN=Ryr2 PE=1 SV=1
2.58	ATP synthase subunit gamma_ mitochondrial OS=Mus musculus GN=Atp5c1 PE=1 SV=1
2.55	3-ketoacyl-CoA thiolase A_ peroxisomal OS=Mus musculus GN=Acaa1a PE=1 SV=1
2.47	L-lactate dehydrogenase A chain OS=Mus musculus GN=Ldha PE=1 SV=3
2.44	Cadherin EGF LAG seven-pass G-type receptor 1 OS=Mus musculus GN=Celsr1 PE=1 SV=3
2.44	Collagen_ type VI_ alpha 3 OS=Mus musculus GN=Col6a3 PE=1 SV=1
2.40	V-type proton ATPase subunit H OS=Mus musculus GN=Atp6v1h PE=1 SV=1
2.37	Alcohol dehydrogenase 1 OS=Saccharomyces cerevisiae (strain ATCC 204508 / S288c) GN=ADH1 PE=1 SV=5
2.29	Prohibitin-2 OS=Mus musculus GN=Phb2 PE=1 SV=1
2.21	Carbamoyl-phosphate synthase [ammonia]_ mitochondrial OS=Mus musculus GN=Cps1 PE=1 SV=2
2.19	Dedicator of cytokinesis protein 1 OS=Mus musculus GN=Dock1 PE=1 SV=3
2.17	ATP synthase protein 8 OS=Mus musculus musculus GN=ATP8 PE=3 SV=1
2.14	Syntaxin-1B OS=Mus musculus GN=Stx1b PE=1 SV=1
2.14	Endophilin-A1 OS=Mus musculus GN=Sh3gl2 PE=1 SV=1
2.12	Uncharacterized protein (Fragment) OS=Mus musculus GN=Eif4enif1 PE=2 SV=1
2.07	Coiled-coil domain-containing protein 88B OS=Mus musculus GN=Ccdc88b PE=1 SV=2

2.05	ATP synthase subunit beta_ mitochondrial OS=Mus musculus GN=Atp5b PE=1 SV=2
2.05	Rootletin OS=Mus musculus GN=Crocc PE=1 SV=2
2.03	Myosin-14 OS=Mus musculus GN=Myh14 PE=1 SV=1
2.00	Alpha-internexin OS=Mus musculus GN=Ina PE=1 SV=3

Table 9.5. List of the proteins downregulated in the hearts of Ibrutinib-treated animals when compared to controls.

Proteins selected based on the max fold change values (>2-fold)

Max fold change	Name
Infinity	Agmatinase_ mitochondrial OS=Mus musculus GN=Agmat PE=1 SV=1
Infinity	DIS3 mitotic control homolog (S. cerevisiae) OS=Mus musculus GN=Dis3 PE=2 SV=1
Infinity	V-type proton ATPase subunit E 2 OS=Mus musculus GN=Atp6v1e2 PE=1 SV=1
Infinity	Dual specificity protein phosphatase 23 OS=Mus musculus GN=Dusp23 PE=2 SV=1 OS=Thanatephorus cucumeris (strain AG1-IB / isolate 7/3/14) GN=RSOLAG1IB_09263 PE=4 SV=1
Infinity	Ryanodine receptor 1 OS=Mus musculus GN=Ryr1 PE=1 SV=1
Infinity	14-3-3 protein epsilon OS=Mus musculus GN=Ywhae PE=1 SV=1
Infinity	Poly [ADP-ribose] polymerase 14 OS=Mus musculus GN=Parp14 PE=1 SV=3
Infinity	Uncharacterized protein OS=Mus musculus GN=Mroh8 PE=2 SV=1
Infinity	GC-rich sequence DNA-binding factor 2 OS=Mus musculus GN=Gcfc2 PE=1 SV=2
Infinity	Chromodomain-helicase-DNA-binding protein 1 OS=Mus musculus GN=Chd1 PE=1 SV=3
Infinity	Activated CDC42 kinase 1 OS=Mus musculus GN=Tnk2 PE=1 SV=1
Infinity	MKIAA0830 protein (Fragment) OS=Mus musculus GN=Endod1 PE=2 SV=1
Infinity	Actin_ alpha cardiac muscle 1 OS=Mus musculus GN=Actc1 PE=1 SV=1
Infinity	Protein bassoon OS=Mus musculus GN=Bsn PE=1 SV=4
Infinity	Calcium channel_ voltage-dependent_ T type_ alpha 1G subunit OS=Mus musculus GN=Cacna1g PE=1 SV=1
Infinity	Myopalladin OS=Mus musculus GN=Mypn PE=1 SV=2

Infinity	Signal-regulatory protein alpha_ isoform CRA_b OS=Mus musculus GN=Sirpa PE=1 SV=1
Infinity	Synaptogyrin-3 OS=Mus musculus GN=Syngr3 PE=1 SV=1
Infinity	Neurofilament light polypeptide OS=Mus musculus GN=Nefl PE=1 SV=5
Infinity	SWI/SNF-related matrix-associated actin-dependent regulator of chromatin subfamily A member 5 OS=Mus musculus GN=Smarca5 PE=1 SV=1
Infinity	Cysteine and glycine-rich protein 1 OS=Mus musculus GN=Csrp1 PE=1 SV=3
Infinity	Adnp protein (Fragment) OS=Mus musculus GN=Adnp PE=2 SV=1
Infinity	Cell adhesion molecule-related/down-regulated by oncogenes OS=Mus musculus GN=Cdon PE=1 SV=2
Infinity	Lymphocyte antigen 6 complex_ locus H_ isoform CRA_a OS=Mus musculus GN=Ly6h PE=1 SV=1
Infinity	Left-right dynein OS=Mus musculus GN=Dnah11 PE=2 SV=1
Infinity	Dynein_ axonemal_ heavy chain 7A OS=Mus musculus GN=Dnah7a PE=1 SV=2
Infinity	Dimethylaniline monooxygenase [N-oxide-forming] 5 OS=Mus musculus GN=Fmo5 PE=1 SV=4
2853.41	Alpha-1_4 glucan phosphorylase OS=Mus musculus GN=Pygl PE=2 SV=1
293.28	Aminopeptidase N OS=Mus musculus GN=Anpep PE=1 SV=4
179.17	V-type proton ATPase subunit D OS=Mus musculus GN=Atp6v1d PE=1 SV=1
105.23	Kinesin-like protein KIF21A OS=Mus musculus GN=Kif21a PE=1 SV=2 OS=Thanatephorus cucumeris (strain AG1-IB / isolate 7/3/14) GN=RSOLAG1IB_05566 PE=3 SV=1
84.51	Probable phospholipid-transporting ATPase IIA OS=Mus musculus GN=Atp9a PE=1 SV=3
66.10	Vesicle-associated membrane protein 2 OS=Mus musculus GN=Vamp2 PE=1 SV=1
61.40	Probable helicase senataxin OS=Mus musculus GN=Setx PE=1 SV=1
60.02	Gamma-aminobutyraldehyde dehydrogenase OS=Mus musculus GN=Aldh9a1 PE=2 SV=1

51.04	Methylmalonyl-CoA mutase_ mitochondrial OS=Mus musculus GN=Mut PE=1 SV=2
46.84	Elongation factor 1-alpha 1 OS=Mus musculus GN=Eef1a1 PE=1 SV=3
45.89	Krt78 protein (Fragment) OS=Mus musculus GN=Krt78 PE=2 SV=1
31.91	E3 ubiquitin-protein ligase HECTD1 OS=Mus musculus GN=Hectd1 PE=1 SV=2
31.57	Centrosome-associated protein CEP250 OS=Mus musculus GN=Cep250 PE=1 SV=2
29.06	Eukaryotic translation initiation factor 4 gamma 2 OS=Mus musculus GN=Eif4g2 PE=1 SV=2
29.03	Visinin-like protein 1 OS=Mus musculus GN=Vsnl1 PE=2 SV=1
24.92	Dedicator of cytokinesis protein 4 OS=Mus musculus GN=Dock4 PE=1 SV=1
22.58	Transformation/transcription domain-associated protein OS=Mus musculus GN=Trrap PE=1 SV=2
20.39	Uncharacterized protein (Fragment) OS=Mus musculus GN=Acaa1b PE=2 SV=1
19.87	Zinc finger protein 292 OS=Mus musculus GN=Zfp292 PE=1 SV=2
19.35	Guanine nucleotide-binding protein G(i) subunit alpha-1 OS=Mus musculus GN=Gnai1 PE=1 SV=1
18.26	Phosphatidylinositol phosphatase PTPRQ OS=Mus musculus GN=Ptprq PE=1 SV=1
17.38	Heterogeneous nuclear ribonucleoprotein A2/B1 OS=Mus musculus GN=Hnrnpa2b1 PE=2 SV=1
17.13	Microtubule-associated protein RP/EB family member 2 (Fragment) OS=Mus musculus GN=Mapre2 PE=1 SV=1
17.05	Dynein heavy chain 3_ axonemal OS=Mus musculus GN=Dnah3 PE=1 SV=2
14.96	Leucine-rich repeat-containing protein 9 OS=Mus musculus GN=Lrrc9 PE=1 SV=1
14.87	Calcium-transporting ATPase OS=Mus musculus GN=Atp2b3 PE=1 SV=1
14.75	Pregnancy-specific glycoprotein 29 OS=Mus musculus GN=Psg29 PE=2 SV=1

14.67	Intersectin-1 OS=Mus musculus GN=Itsn1 PE=1 SV=1
14.57	Uncharacterized protein OS=Mus musculus GN=Afg3l2 PE=2 SV=1
13.91	E3 ubiquitin-protein ligase RNF213 OS=Mus musculus GN=Rnf213 PE=1 SV=1
12.00	Synemin OS=Mus musculus GN=Synm PE=1 SV=2
11.66	Androgen receptor OS=Mus musculus GN=Ar PE=1 SV=1
10.78	Cytochrome P450 4B1 (Fragment) OS=Mus musculus GN=Cyp4b1 PE=1 SV=1
10.07	Microtubule-associated protein 1B OS=Mus musculus GN=Map1b PE=1 SV=2
9.27	Cingulin-like protein 1 OS=Mus musculus GN=Cgnl1 PE=1 SV=2
8.82	NADH dehydrogenase (Ubiquinone) 1 alpha subcomplex_ 8 OS=Mus musculus GN=Ndufa8 PE=2 SV=1
8.77	Filamin-C OS=Mus musculus GN=Flnc PE=1 SV=3
8.67	Serum paraoxonase/arylesterase 1 OS=Mus musculus GN=Pon1 PE=1 SV=2
8.60	Ninein OS=Mus musculus GN=Nin PE=1 SV=1
8.59	AP-2 complex subunit mu OS=Mus musculus GN=Ap2m1 PE=1 SV=1
8.59	2-hydroxyacyl-CoA lyase 1 OS=Mus musculus GN=Hacl1 PE=1 SV=2
8.47	40S ribosomal protein S2 OS=Mus musculus GN=Rps2 PE=1 SV=3
8.42	Eukaryotic peptide chain release factor GTP-binding subunit ERF3A OS=Mus musculus GN=Gspt1 PE=1 SV=2
8.40	Microtubule-associated protein tau OS=Mus musculus GN=Mapt PE=1 SV=3
8.28	Angiopoietin-4 OS=Mus musculus GN=Angpt4 PE=1 SV=1
8.03	Talin-1 OS=Mus musculus GN=Tln1 PE=1 SV=2
7.85	Cytochrome c_ somatic OS=Mus musculus GN=Cycs PE=1 SV=2
7.64	Unconventional myosin-Va OS=Mus musculus GN=Myo5a PE=1 SV=1
7.38	DNA replication complex GINS protein PSF2 OS=Mus musculus GN=Gins2 PE=1 SV=1
7.02	Myosin-9 OS=Mus musculus GN=Myh9 PE=1 SV=4

6.90	Polycystic kidney and hepatic disease 1 OS=Mus musculus GN=Pkhd1 PE=1 SV=1
6.76	DNA polymerase zeta catalytic subunit OS=Mus musculus GN=Rev3l PE=1 SV=3
6.61	Breast cancer type 2 susceptibility protein homolog OS=Mus musculus GN=Brca2 PE=1 SV=2
6.39	Carnitine O-palmitoyltransferase 2_ mitochondrial OS=Mus musculus GN=Cpt2 PE=1 SV=2
6.27	Spermatogenesis- and oogenesis-specific basic helix-loop-helix-containing protein 2 OS=Mus musculus GN=Sohlh2 PE=1 SV=2
6.15	Adrenodoxin_ mitochondrial OS=Mus musculus GN=Fdx1 PE=1 SV=1
5.84	Heat shock protein HSP 90-beta OS=Mus musculus GN=Hsp90ab1 PE=1 SV=3
5.83	Ribosomal protein L14 OS=Mus musculus GN=Rpl14-ps1 PE=2 SV=1
5.82	Rab GDP dissociation inhibitor alpha OS=Mus musculus GN=Gdi1 PE=1 SV=3
5.81	Kinesin-like protein KIF27 OS=Mus musculus GN=Kif27 PE=1 SV=1
5.74	Carbonic anhydrase 2 OS=Mus musculus GN=Ca2 PE=1 SV=4
5.70	Calcium/calmodulin-dependent protein kinase type II subunit alpha OS=Mus musculus GN=Camk2a PE=1 SV=2
5.61	Coiled-coil domain-containing protein 57 OS=Mus musculus GN=Ccdc57 PE=1 SV=1
5.35	Nuclear mitotic apparatus protein 1 OS=Mus musculus GN=Numa1 PE=1 SV=1
5.18	Choline dehydrogenase_ mitochondrial OS=Mus musculus GN=Chdh PE=1 SV=1
5.14	Collagen alpha-1(VII) chain OS=Mus musculus GN=Col7a1 PE=1 SV=3
4.93	Cordon-bleu OS=Mus musculus GN=Cobl PE=2 SV=1
4.90	4F2 cell-surface antigen heavy chain OS=Mus musculus GN=Slc3a2 PE=1 SV=1
4.86	Triosephosphate isomerase OS=Mus musculus GN=Tpi1 PE=1 SV=4

4.79	Spectrin beta chain_ erythrocytic OS=Mus musculus GN=Sptb PE=1 SV=4
4.62	Serine--pyruvate aminotransferase_ mitochondrial OS=Mus musculus GN=Agxt PE=1 SV=3
4.53	Guanine nucleotide-binding protein G(I)/G(S)/G(T) subunit beta-1 OS=Mus musculus GN=Gnb1 PE=1 SV=3
4.50	Calretinin OS=Mus musculus GN=Calb2 PE=1 SV=3
4.45	Potassium-transporting ATPase alpha chain 2 OS=Mus musculus GN=Atp12a PE=1 SV=3
4.41	Laminin receptor (Fragment) OS=Mus musculus GN=Rpsa PE=2 SV=1
4.38	Sarcoplasmic/endoplasmic reticulum calcium ATPase 3 OS=Mus musculus GN=Atp2a3 PE=1 SV=3
4.35	Uncharacterized protein OS=Mus musculus GN=Akr1a1 PE=2 SV=1
4.34	Heat shock-related 70 kDa protein 2 OS=Mus musculus GN=Hspa2 PE=1 SV=2
4.30	Beta-globin OS=Mus musculus GN=Hbbt1 PE=3 SV=1
4.27	Tubulin alpha chain (Fragment) OS=Mus musculus GN=Tuba4a PE=1 SV=1
4.25	MKIAA0864 protein (Fragment) OS=Mus musculus GN=Mprip PE=2 SV=1
4.18	Helicase with zinc finger domain 2 OS=Mus musculus GN=Helz2 PE=1 SV=1
4.04	Transitional endoplasmic reticulum ATPase OS=Mus musculus GN=Vcp PE=1 SV=4
3.97	Telomerase reverse transcriptase OS=Mus musculus GN=Tert PE=1 SV=1
3.94	Arginase-1 OS=Mus musculus GN=Arg1 PE=1 SV=1
3.85	Syntaxin-1A OS=Mus musculus GN=Stx1a PE=1 SV=1
3.81	Cytochrome P450 2F2 OS=Mus musculus GN=Cyp2f2 PE=1 SV=1
3.80	AP-2 complex subunit alpha-2 OS=Mus musculus GN=Ap2a2 PE=1 SV=2
3.78	Uricase OS=Mus musculus GN=Uox PE=1 SV=2
3.69	Dystrophin OS=Mus musculus GN=Dmd PE=1 SV=3
3.69	ATPase family AAA domain-containing protein 3 OS=Mus musculus GN=Atad3 PE=1 SV=1

3.62	Sodium/potassium-transporting ATPase subunit alpha-4 OS=Mus musculus GN=Atp1a4 PE=1 SV=3
3.59	Limbic system-associated membrane protein OS=Mus musculus GN=Lsamp PE=1 SV=1
3.53	Neuromodulin OS=Mus musculus GN=Gap43 PE=1 SV=1
3.49	Roquin-1 OS=Mus musculus GN=Rc3h1 PE=1 SV=1
3.43	Calcium-binding mitochondrial carrier protein Aralar1 OS=Mus musculus GN=Slc25a12 PE=1 SV=1
3.38	10 kDa heat shock protein_ mitochondrial OS=Mus musculus GN=Hspe1 PE=1 SV=2
3.36	AHNAK nucleoprotein (desmoyokin) OS=Mus musculus GN=Ahnak PE=1 SV=1
3.35	Inositol 1_4_5-trisphosphate receptor type 2 OS=Mus musculus GN=Itpr2 PE=1 SV=4
3.24	Succinate-CoA ligase subunit beta (Fragment) OS=Mus musculus GN=Sucla2 PE=2 SV=1
3.24	Alpha-methylacyl-CoA racemase OS=Mus musculus GN=Amacr PE=1 SV=4
3.23	NADH dehydrogenase [ubiquinone] 1 alpha subcomplex subunit 10_ mitochondrial OS=Mus musculus GN=Ndufa10 PE=1 SV=1
3.20	Tubulin alpha-1A chain OS=Mus musculus GN=Tuba1a PE=1 SV=1
3.16	Sideroflexin-1 OS=Mus musculus GN=Sfxn1 PE=1 SV=3
3.15	Ras-related protein Rab-3A OS=Mus musculus GN=Rab3a PE=1 SV=1
3.15	Corticosteroid 11-beta-dehydrogenase isozyme 1 OS=Mus musculus GN=Hsd11b1 PE=1 SV=3
3.12	Glutathione S-transferase P 1 OS=Mus musculus GN=Gstp1 PE=1 SV=2
3.07	Testis-expressed protein 15 OS=Mus musculus GN=Tex15 PE=2 SV=1
3.06	Stathmin (Fragment) OS=Mus musculus GN=Stmn1 PE=1 SV=1
3.04	Dynein_ axonemal_ heavy chain 10 OS=Mus musculus GN=Dnah10 PE=1 SV=2
3.00	Uncharacterized protein OS=Mus musculus GN=D830013H23Rik PE=2 SV=1

2.99	E3 ubiquitin-protein ligase HERC2 OS=Mus musculus GN=Herc2 PE=1 SV=3
2.98	Fructose-bisphosphate aldolase A OS=Mus musculus GN=Aldoa PE=1 SV=2
2.95	MKIAA4169 protein (Fragment) OS=Mus musculus GN=Sept3 PE=2 SV=1
2.94	Centrosomal protein of 290 kDa OS=Mus musculus GN=Cep290 PE=1 SV=2
2.91	Malate dehydrogenase_ cytoplasmic OS=Mus musculus GN=Mdh1 PE=1 SV=3
2.78	Pyruvate kinase PKLR OS=Mus musculus GN=Pklr PE=1 SV=1
2.77	Predicted gene 20425 OS=Mus musculus GN=Gm20425 PE=4 SV=1
2.76	Peptidyl-prolyl cis-trans isomerase A OS=Mus musculus GN=Ppia PE=1 SV=2
2.74	Alanine aminotransferase 2 OS=Mus musculus GN=Gpt2 PE=1 SV=1
2.74	Guanine nucleotide-binding protein G(o) subunit alpha OS=Mus musculus GN=Gnao1 PE=1 SV=3
2.73	Isovaleryl-CoA dehydrogenase_ mitochondrial OS=Mus musculus GN=Ivd PE=1 SV=1
2.72	Uncharacterized protein OS=Mus musculus GN=Atp6v1b2 PE=2 SV=1
2.69	Beta-synuclein OS=Mus musculus GN=Sncb PE=1 SV=1
2.64	Cyp27a1 protein OS=Mus musculus GN=Cyp27a1 PE=2 SV=1
2.62	Anion exchange protein (Fragment) OS=Mus musculus GN=Slc4a4 PE=2 SV=1
2.61	Midasin OS=Mus musculus GN=Mdn1 PE=1 SV=1
2.60	Alpha-actinin-1 OS=Mus musculus GN=Actn1 PE=1 SV=1
2.58	Kinesin-like protein KIF15 OS=Mus musculus GN=Kif15 PE=1 SV=1
2.53	Myelin-oligodendrocyte glycoprotein OS=Mus musculus GN=Mog PE=1 SV=1
2.52	14-3-3 protein gamma subtype OS=Mus musculus GN=Ywhag PE=1 SV=1
2.51	Aldehyde dehydrogenase X_ mitochondrial OS=Mus musculus GN=Aldh1b1 PE=1 SV=1
2.51	Leucine-rich repeats and immunoglobulin-like domains protein 3 OS=Mus musculus GN=Lrig3 PE=1 SV=1
2.51	Flavin-containing monooxygenase OS=Mus musculus GN=Fmo4 PE=2 SV=1

2.51	Striated muscle-specific serine/threonine-protein kinase OS=Mus musculus GN=Speg PE=1 SV=2
2.50	Prolow-density lipoprotein receptor-related protein 1 OS=Mus musculus GN=Lrp1 PE=1 SV=1
2.50	Synaptotagmin-1 OS=Mus musculus GN=Syt1 PE=1 SV=1
2.48	3-mercaptopyruvate sulfurtransferase OS=Mus musculus GN=Mpst PE=1 SV=3
2.48	Cytochrome P450 2A5 OS=Mus musculus GN=Cyp2a5 PE=2 SV=1
2.47	Neuroplastin OS=Mus musculus GN=Nptn PE=1 SV=3
2.46	Isocitrate dehydrogenase [NAD] subunit_ mitochondrial OS=Mus musculus GN=Idh3b PE=1 SV=1
2.43	Tenascin-R OS=Mus musculus GN=Tnr PE=1 SV=2
2.41	NADH dehydrogenase [ubiquinone] iron-sulfur protein 2_ mitochondrial OS=Mus musculus GN=Ndufs2 PE=1 SV=1
2.39	Protein unc-13 homolog B OS=Mus musculus GN=Unc13b PE=1 SV=1
2.38	UDP-glucuronosyltransferase 2B17 OS=Mus musculus GN=Ugt2b17 PE=1 SV=1
2.37	Tensin-2 OS=Mus musculus GN=Tns2 PE=1 SV=1
2.36	D-beta-hydroxybutyrate dehydrogenase_ mitochondrial OS=Mus musculus GN=Bdh1 PE=1 SV=2
2.34	E3 ubiquitin-protein ligase LRSAM1 OS=Mus musculus GN=Lrsam1 PE=1 SV=1
2.34	Myosin_ heavy polypeptide 13_ skeletal muscle OS=Mus musculus GN=Myh13 PE=1 SV=1
2.30	Dihydropyrimidinase-related protein 2 OS=Mus musculus GN=Dpysl2 PE=1 SV=2
2.29	Mitochondrial amidoxime reducing component 2 OS=Mus musculus GN=Marc2 PE=1 SV=1
2.29	ATPase_ H+ transporting_ lysosomal V1 subunit B1 OS=Mus musculus GN=Atp6v1b1 PE=2 SV=1

2.29	Carboxylic ester hydrolase OS=Mus musculus GN=Ces1g PE=1 SV=1
2.29	Ezrin OS=Mus musculus GN=Ezr PE=1 SV=3
2.28	Polyamine-modulated factor 1-binding protein 1 OS=Mus musculus GN=Pmfbp1 PE=2 SV=1
2.27	Centromere protein F OS=Mus musculus GN=Cenpf PE=1 SV=1
2.27	ProSAAS OS=Mus musculus GN=Pcsk1n PE=1 SV=2
2.26	Rab GDP dissociation inhibitor OS=Mus musculus GN=Gdi2 PE=2 SV=1
2.26	Actin_ alpha skeletal muscle OS=Mus musculus GN=Acta1 PE=1 SV=1
2.24	Gamma-enolase OS=Mus musculus GN=Eno2 PE=1 SV=2
2.23	Casein kinase II subunit alpha' (Fragment) OS=Mus musculus GN=Csnk2a2 PE=1 SV=1
2.23	SH3 domain-binding protein 5 OS=Mus musculus GN=Sh3bp5 PE=1 SV=3
2.22	Utrophin OS=Mus musculus GN=Utrn PE=1 SV=1
2.21	Excitatory amino acid transporter 2 OS=Mus musculus GN=Slc1a2 PE=1 SV=1
2.20	N-myc downstream regulated gene 1 OS=Mus musculus GN=Ndrg1 PE=2 SV=1
2.17	Neurofascin OS=Mus musculus GN=Nfasc PE=1 SV=1
2.16	Integrator complex subunit 4 OS=Mus musculus GN=Ints4 PE=1 SV=1
2.16	V-type proton ATPase 116 kDa subunit a isoform 1 OS=Mus musculus GN=Atp6v0a1 PE=1 SV=3
2.15	Protein sidekick-2 OS=Mus musculus GN=Sdk2 PE=1 SV=1
2.14	Phosphoglycerate kinase 1 OS=Mus musculus GN=Pgk1 PE=1 SV=4
2.12	Serine/threonine-protein phosphatase 2A 65 kDa regulatory subunit A alpha isoform OS=Mus musculus GN=Ppp2r1a PE=1 SV=3
2.12	Protein NDRG2 OS=Mus musculus GN=Ndrg2 PE=1 SV=1
2.11	Microtubule-associated protein 1A OS=Mus musculus GN=Map1a PE=1 SV=2
2.10	78 kDa glucose-regulated protein OS=Mus musculus GN=Hspa5 PE=1 SV=3

2.09	Histidine triad nucleotide binding protein 2 OS=Mus musculus GN=Hint2 PE=1 SV=1
2.09	Isocitrate dehydrogenase [NAD] subunit gamma 1_ mitochondrial OS=Mus musculus GN=Idh3g PE=1 SV=1
2.08	Clathrin heavy chain 1 OS=Mus musculus GN=Cltc PE=1 SV=3
2.08	Acyl-CoA dehydrogenase family member 9_ mitochondrial OS=Mus musculus GN=Acad9 PE=1 SV=2
2.05	Septin-14 OS=Mus musculus GN=Sept14 PE=1 SV=3
2.03	Glycine N-acyltransferase-like protein Keg1 OS=Mus musculus GN=Keg1 PE=1 SV=1
2.03	Exportin 4 [Mus musculus] OS=Lepeophtheirus salmonis GN=Xpo4 PE=4 SV=1
2.02	Sulfotransferase OS=Mus musculus GN=Hs3st3b1 PE=2 SV=1
2.02	Guanine nucleotide-binding protein G(I)/G(S)/G(T) subunit beta-2 OS=Mus musculus GN=Gnb2 PE=1 SV=1
2.01	Guanine nucleotide-binding protein G(I)/G(S)/G(O) subunit gamma-2 OS=Mus musculus GN=Gng2 PE=1 SV=2
2.01	ATP synthase subunit e_ mitochondrial OS=Mus musculus GN=Atp5i PE=1 SV=2

Table 9.6. List of the proteins upregulated in the livers of Ibrutinib-treated animals when compared to controls.

Proteins selected based on the max fold change values (>2-fold)

Max fold change	Name
Infinity	DIS3 mitotic control homolog (S. cerevisiae) OS=Mus musculus GN=Dis3 PE=2 SV=1
Infinity	Dystonin OS=Mus musculus GN=Dst PE=1 SV=2
Infinity	Tubulin beta-1 chain OS=Mus musculus GN=Tubb1 PE=1 SV=1
Infinity	GC-rich sequence DNA-binding factor 2 OS=Mus musculus GN=Gcfc2 PE=1 SV=2
Infinity	Gamma-aminobutyraldehyde dehydrogenase OS=Mus musculus GN=Aldh9a1 PE=2 SV=1
Infinity	Chromodomain-helicase-DNA-binding protein 1 OS=Mus musculus GN=Chd1 PE=1 SV=3
Infinity	ProSAAS OS=Mus musculus GN=Pcsk1n PE=1 SV=2
Infinity	CAP-Gly domain-containing linker protein 1 OS=Mus musculus GN=Clip1 PE=1 SV=1
Infinity	Copper-transporting ATPase 1 OS=Mus musculus GN=Atp7a PE=1 SV=1
Infinity	Macrophage migration inhibitory factor OS=Mus musculus GN=Mif PE=1 SV=2
Infinity	Lysine-specific demethylase 3A OS=Mus musculus GN=Kdm3a PE=1 SV=1
Infinity	Tyrosine-protein phosphatase non-receptor type 13 OS=Mus musculus GN=Ptpn13 PE=1 SV=2
Infinity	E3 ubiquitin-protein ligase Itchy OS=Mus musculus GN=Itch PE=1 SV=2
Infinity	Amphiphysin OS=Mus musculus GN=Amph PE=1 SV=1
Infinity	Paraneoplastic antigen-like protein 5 OS=Mus musculus GN=Pnma5 PE=1 SV=2
Infinity	Triple functional domain protein OS=Mus musculus GN=Trio PE=1 SV=3

Infinity	Ryanodine receptor 3 OS=Mus musculus GN=Ryr3 PE=1 SV=1
Infinity	Histone-lysine N-methyltransferase ASH1L OS=Mus musculus GN=Ash1l PE=1 SV=3
Infinity	Cell adhesion molecule 3 OS=Mus musculus GN=Cadm3 PE=1 SV=1
Infinity	Calmodulin-1 OS=Mus musculus GN=Calm1 PE=1 SV=1
Infinity	Microtubule-associated protein 1B OS=Mus musculus GN=Map1b PE=1 SV=2
3929.8	Cysteine and glycine-rich protein 1 OS=Mus musculus GN=Csrp1 PE=1 SV=3
51.5	Neurofilament light polypeptide OS=Mus musculus GN=Nefl PE=1 SV=5
45.0	Leukemia inhibitory factor receptor OS=Mus musculus GN=Lifr PE=1 SV=1
34.8	UDP-glucuronosyltransferase 1-2 OS=Mus musculus GN=Ugt1a2 PE=1 SV=1
29.0	Synaptic vesicle glycoprotein 2A OS=Mus musculus GN=Sv2a PE=1 SV=1
24.6	Nebulin-related-anchoring protein OS=Mus musculus GN=Nrap PE=1 SV=3
17.9	Annexin (Fragment) OS=Mus musculus GN=Anxa2 PE=1 SV=1
16.7	Filamin-C OS=Mus musculus GN=Flnc PE=1 SV=3
14.7	Poly [ADP-ribose] polymerase 14 OS=Mus musculus GN=Parp14 PE=1 SV=3
14.1	CAP-Gly domain-containing linker protein 1 (Fragment) OS=Mus musculus GN=Clip1 PE=1 SV=1
13.2	40S ribosomal protein S2 OS=Mus musculus GN=Rps2 PE=1 SV=3
12.5	Myosin Vb_ isoform CRA_a OS=Mus musculus GN=Myo5b PE=1 SV=1
12.0	V-type proton ATPase subunit D OS=Mus musculus GN=Atp6v1d PE=1 SV=1
11.6	Myosin-8 OS=Mus musculus GN=Myh8 PE=2 SV=2
10.8	Signal-regulatory protein alpha_ isoform CRA_b OS=Mus musculus GN=Sirpa PE=1 SV=1
10.8	Hemicentin-2 OS=Mus musculus GN=Hmcn2 PE=1 SV=1

10.0	L-lactate dehydrogenase B chain OS=Mus musculus GN=Ldhb PE=1 SV=2
9.5	Synaptogyrin-3 OS=Mus musculus GN=Syngr3 PE=1 SV=1
8.8	Dynein heavy chain 3_ axonemal OS=Mus musculus GN=Dnah3 PE=1 SV=2
8.0	Dystrophin OS=Mus musculus GN=Dmd PE=1 SV=3
7.0	Actin_ cytoplasmic 1 OS=Mus musculus GN=Actb PE=1 SV=1
6.9	DNA (cytosine-5)-methyltransferase 1 OS=Mus musculus GN=Dnmt1 PE=1 SV=5
6.8	Protein RRP5 homolog OS=Mus musculus GN=Pdcd11 PE=1 SV=2
6.3	Histone-lysine N-methyltransferase 2C OS=Mus musculus GN=Kmt2c PE=1 SV=2
5.7	14-3-3 protein epsilon OS=Mus musculus GN=Ywhae PE=1 SV=1
5.5	AP-2 complex subunit mu OS=Mus musculus GN=Ap2m1 PE=1 SV=1
5.4	Neuroplastin OS=Mus musculus GN=Nptn PE=1 SV=3
5.1	Lymphocyte antigen 6 complex_ locus H_ isoform CRA_a OS=Mus musculus GN=Ly6h PE=1 SV=1
5.0	Neuron navigator 2 OS=Mus musculus GN=Nav2 PE=1 SV=1
4.9	Beta-enolase OS=Mus musculus GN=Eno3 PE=1 SV=3
4.7	Cytochrome c oxidase subunit 5B_ mitochondrial OS=Mus musculus GN=Cox5b PE=1 SV=1
4.3	Tubulin beta-4A chain OS=Mus musculus GN=Tubb4a PE=1 SV=3
4.1	Septin-14 OS=Mus musculus GN=Sept14 PE=1 SV=3
4.1	Transient receptor potential cation channel_ subfamily M_ member 3 OS=Mus musculus GN=Trpm3 PE=1 SV=1
4.1	Leucine-rich repeat-containing protein 9 OS=Mus musculus GN=Lrrc9 PE=1 SV=1
4.0	SH3 domain-binding protein 5 OS=Mus musculus GN=Sh3bp5 PE=1 SV=3
3.9	Pyruvate kinase PKLR OS=Mus musculus GN=Pklr PE=1 SV=1
3.8	Transitional endoplasmic reticulum ATPase OS=Mus musculus GN=Vcp PE=1 SV=4
3.8	Septin-11 OS=Mus musculus GN=Sept11 PE=1 SV=1

3.7	Activated CDC42 kinase 1 OS=Mus musculus GN=Tnk2 PE=1 SV=1
3.6	Septin-5 OS=Mus musculus GN=Sept5 PE=1 SV=2
3.4	Dimethylaniline monooxygenase [N-oxide-forming] 3 OS=Mus musculus GN=Fmo3 PE=1 SV=1
3.2	NACHT and WD repeat domain-containing protein 2 OS=Mus musculus GN=Nwd2 PE=1 SV=2
3.2	Dihydropyrimidinase-related protein 1 OS=Mus musculus GN=Crmp1 PE=1 SV=1
3.1	Phosphoglycerate kinase 1 OS=Mus musculus GN=Pgk1 PE=1 SV=4
3.0	FAST kinase domain-containing protein 1_ mitochondrial OS=Mus musculus GN=Fastkd1 PE=2 SV=1
3.0	Elongation factor 1-alpha 2 OS=Mus musculus GN=Eef1a2 PE=1 SV=1
2.9	Uncharacterized protein OS=Mus musculus GN=Mroh8 PE=2 SV=1
2.9	E3 ubiquitin-protein ligase HECTD1 OS=Mus musculus GN=Hectd1 PE=1 SV=2
2.8	Synemin OS=Mus musculus GN=Synm PE=1 SV=2
2.8	Limbic system-associated membrane protein OS=Mus musculus GN=Lsamp PE=1 SV=1
2.8	Calcium-transporting ATPase OS=Mus musculus GN=Atp2b3 PE=1 SV=1
2.7	Proline-rich transmembrane protein 2 OS=Mus musculus GN=Prrt2 PE=1 SV=1
2.6	NADH dehydrogenase [ubiquinone] flavoprotein 2_ mitochondrial OS=Mus musculus GN=Ndufv2 PE=1 SV=2
2.6	Cytosolic acyl coenzyme A thioester hydrolase OS=Mus musculus GN=Acot7 PE=1 SV=1
2.6	Ninein OS=Mus musculus GN=Nin PE=1 SV=1
2.5	Laminin receptor (Fragment) OS=Mus musculus GN=Rpsa PE=2 SV=1
2.4	Myosin_ heavy polypeptide 13_ skeletal muscle OS=Mus musculus GN=Myh13 PE=1 SV=1
2.4	Uncharacterized protein OS=Mus musculus GN=Akr1a1 PE=2 SV=1

2.4	Choline dehydrogenase_ mitochondrial OS=Mus musculus GN=Chdh PE=1 SV=1
2.4	Casein kinase II subunit alpha' (Fragment) OS=Mus musculus GN=Csnk2a2 PE=1 SV=1
2.4	RAB39_ member RAS oncogene family OS=Mus musculus GN=Rab39 PE=2 SV=1
2.3	Serine/threonine-protein phosphatase 2A 65 kDa regulatory subunit A alpha isoform OS=Mus musculus GN=Ppp2r1a PE=1 SV=3
2.3	Dynein_ axonemal_ heavy chain 6 OS=Mus musculus GN=Dnah6 PE=1 SV=1
2.3	AP-2 complex subunit alpha-2 OS=Mus musculus GN=Ap2a2 PE=1 SV=2
2.2	Potassium-transporting ATPase alpha chain 1 OS=Mus musculus GN=Atp4a PE=1 SV=3
2.2	Myopalladin OS=Mus musculus GN=Mypn PE=1 SV=2
2.2	Heat shock protein HSP 90-beta OS=Mus musculus GN=Hsp90ab1 PE=1 SV=3
2.2	Syntaxin-1B OS=Mus musculus GN=Stx1b PE=1 SV=1
2.1	Testis-expressed protein 15 OS=Mus musculus GN=Tex15 PE=2 SV=1
2.1	ATP synthase subunit e_ mitochondrial OS=Mus musculus GN=Atp5i PE=1 SV=2
2.1	Carboxylic ester hydrolase OS=Mus musculus GN=Ces1g PE=1 SV=1
2.1	Annexin A5 OS=Mus musculus GN=Anxa5 PE=1 SV=1

Table 9.7. List of the proteins downregulated in the livers of Ibrutinib-treated animals when compared to controls.

Proteins selected based on the max fold change values (>2-fold)

Max fold change	Name
Infinity	Kinesin-like protein KIF21A OS=Mus musculus GN=Kif21a PE=1 SV=2 OS=Thanatephorus cucumeris (strain AG1-IB / isolate 7/3/14) GN=RSOLAG1IB_05566 PE=3 SV=1
Infinity	Spermatogenesis- and oogenesis-specific basic helix-loop-helix-containing protein 2 OS=Mus musculus GN=Sohlh2 PE=1 SV=2
Infinity	Ubiquitin carboxyl-terminal hydrolase 5 (Fragment) OS=Mus musculus GN=Usp5 PE=1 SV=1
Infinity	Stathmin (Fragment) OS=Mus musculus GN=Stmn1 PE=1 SV=1
Infinity	Inositol 1_4_5-trisphosphate receptor type 1 OS=Mus musculus GN=Itpr1 PE=1 SV=2
Infinity	Guanine nucleotide-binding protein G(z) subunit alpha OS=Mus musculus GN=Gnaz PE=1 SV=4
Infinity	Transmembrane protein 205 (Fragment) OS=Mus musculus GN=Tmem205 PE=1 SV=1
Infinity	Dihydropteridine reductase OS=Mus musculus GN=Qdpr PE=1 SV=1
Infinity	C230096C10Rik protein OS=Mus musculus GN=Emc1 PE=2 SV=1
Infinity	Dysferlin OS=Mus musculus GN=Dysf PE=1 SV=1
Infinity	Rai1 protein OS=Mus musculus GN=Rai1 PE=2 SV=1
Infinity	Phosphatidylinositol 3-kinase_ catalytic_ alpha polypeptide_ isoform CRA_a OS=Mus musculus GN=Pik3ca PE=1 SV=1
Infinity	Midasin OS=Mus musculus GN=Mdn1 PE=1 SV=1
Infinity	Tetratricopeptide repeat protein 21B OS=Mus musculus GN=Ttc21b PE=1 SV=1
Infinity	Left-right dynein OS=Mus musculus GN=Dnah11 PE=2 SV=1
Infinity	Pre-mRNA-processing-splicing factor 8 OS=Mus musculus GN=Prpf8 PE=1 SV=2
Infinity	Neurofibromin OS=Mus musculus GN=Nf1 PE=1 SV=1

Infinity	Eukaryotic peptide chain release factor GTP-binding subunit ERF3A OS=Mus musculus GN=Gspt1 PE=1 SV=2
Infinity	Replicase polyprotein 1ab OS=Murine coronavirus (strain 2) GN=rep PE=3 SV=1
20693.58	Adnp protein (Fragment) OS=Mus musculus GN=Adnp PE=2 SV=1
1936.11	Nuclear mitotic apparatus protein 1 OS=Mus musculus GN=Numa1 PE=1 SV=1
118.73	Aminopeptidase N OS=Mus musculus GN=Anpep PE=1 SV=4
36.07	Protein NDRG2 OS=Mus musculus GN=Ndrg2 PE=1 SV=1
26.42	Cell adhesion molecule-related/down-regulated by oncogenes OS=Mus musculus GN=Cdon PE=1 SV=2
21.61	Uncharacterized protein (Fragment) OS=Mus musculus GN=Acaa1b PE=2 SV=1
16.64	Creatine kinase S-type_ mitochondrial OS=Mus musculus GN=Ckmt2 PE=1 SV=1
14.11	Uncharacterized protein OS=Mus musculus GN=Vnn1 PE=2 SV=1
13.80	GTP:AMP phosphotransferase AK3_ mitochondrial OS=Mus musculus GN=Ak3 PE=1 SV=3
10.94	Xin actin-binding repeat-containing protein 2 OS=Mus musculus GN=Xirp2 PE=1 SV=1
10.62	SWI/SNF-related matrix-associated actin-dependent regulator of chromatin subfamily A member 5 OS=Mus musculus GN=Smarca5 PE=1 SV=1
10.15	Predicted gene 20425 OS=Mus musculus GN=Gm20425 PE=4 SV=1
9.68	Calretinin OS=Mus musculus GN=Calb2 PE=1 SV=3
9.23	Long-chain-fatty-acid--CoA ligase 5 OS=Mus musculus GN=Acsl5 PE=1 SV=1
8.46	Uncharacterized protein OS=Mus musculus GN=Emilin2 PE=2 SV=1
8.12	Sodium/potassium-transporting ATPase subunit gamma OS=Mus musculus GN=Fxyd2 PE=1 SV=2
7.71	Guanine nucleotide-binding protein G(i) subunit alpha-1 OS=Mus musculus GN=Gnai1 PE=1 SV=1
7.64	Dynein_ axonemal_ heavy chain 7A OS=Mus musculus GN=Dnah7a PE=1 SV=2
7.34	Breast cancer type 2 susceptibility protein homolog OS=Mus musculus GN=Brca2 PE=1 SV=2

6.58	E3 ubiquitin-protein ligase LRSAM1 OS=Mus musculus GN=Lrsam1 PE=1 SV=1
6.38	Neural cell adhesion molecule 1 OS=Mus musculus GN=Ncam1 PE=1 SV=3
6.27	Glutaredoxin-related protein 5_ mitochondrial OS=Mus musculus GN=Glrx5 PE=1 SV=1
5.88	Peptidyl-prolyl cis-trans isomerase B OS=Mus musculus GN=Ppib PE=1 SV=2
5.76	Gamma-soluble NSF attachment protein (Fragment) OS=Mus musculus GN=Napg PE=1 SV=1
5.75	Acetyl-coenzyme A synthetase OS=Mus musculus GN=Acss1 PE=2 SV=1
5.74	Alpha-internexin OS=Mus musculus GN=Ina PE=1 SV=3
3.56	Mitochondrial pyruvate carrier 1 OS=Mus musculus GN=Mpc1 PE=1 SV=1
3.51	Androgen receptor OS=Mus musculus GN=Ar PE=1 SV=1
3.38	Beta-soluble NSF attachment protein OS=Mus musculus GN=Napb PE=1 SV=2
3.15	Sarcoplasmic/endoplasmic reticulum calcium ATPase 3 OS=Mus musculus GN=Atp2a3 PE=1 SV=3
3.14	Myelin-associated glycoprotein OS=Mus musculus GN=Mag PE=1 SV=1
3.02	Dynein_ axonemal_ heavy chain 9 OS=Mus musculus GN=Dnah9 PE=1 SV=1
2.97	Isocitrate dehydrogenase [NAD] subunit gamma 1_ mitochondrial OS=Mus musculus GN=Idh3g PE=1 SV=1
2.96	Transformation/transcription domain-associated protein OS=Mus musculus GN=Trrap PE=1 SV=2
2.77	Alpha-1_4 glucan phosphorylase OS=Mus musculus GN=Pygl PE=2 SV=1
2.74	Delta(3_5)-Delta(2_4)-dienoyl-CoA isomerase_ mitochondrial OS=Mus musculus GN=Ech1 PE=1 SV=1
2.73	Agmatinase_ mitochondrial OS=Mus musculus GN=Agmat PE=1 SV=1
2.73	Centrosome-associated protein CEP250 OS=Mus musculus GN=Cep250 PE=1 SV=2
2.64	Guanine nucleotide-binding protein G(o) subunit alpha OS=Mus musculus GN=Gnao1 PE=1 SV=3
2.64	Dedicator of cytokinesis protein 4 OS=Mus musculus GN=Dock4 PE=1 SV=1
2.56	Dynein heavy chain 17_ axonemal OS=Mus musculus GN=Dnah17 PE=1 SV=2

2.53	StAR-related lipid transfer protein 9 OS=Mus musculus GN=Stard9 PE=1 SV=2
2.48	Uncharacterized protein (Fragment) OS=Mus musculus GN=Pmpcb PE=2 SV=1
2.45	Carboxylesterase 3A OS=Mus musculus GN=Ces3a PE=1 SV=2
2.42	Ryanodine receptor 1 OS=Mus musculus GN=Ryr1 PE=1 SV=1
2.39	Creatine kinase U-type_ mitochondrial OS=Mus musculus GN=Ckmt1 PE=1 SV=1
2.38	Microtubule-associated serine/threonine-protein kinase 4 (Fragment) OS=Mus musculus GN=Mast4 PE=1 SV=1
2.38	Uncharacterized protein OS=Mus musculus GN=Atp6v1b2 PE=2 SV=1
2.32	Guanine nucleotide-binding protein G(I)/G(S)/G(T) subunit beta-2 OS=Mus musculus GN=Gnb2 PE=1 SV=1
2.24	Histone H2B (Fragment) OS=Mus musculus GN=Hist1h2bj PE=2 SV=1
2.21	Dynein heavy chain 8_ axonemal OS=Mus musculus GN=Dnah8 PE=1 SV=2
2.21	Lipoxygenase homology domain-containing protein 1 OS=Mus musculus GN=Loxhd1 PE=2 SV=1
2.15	Cingulin-like protein 1 OS=Mus musculus GN=Cgnl1 PE=1 SV=2
2.13	Heterogeneous nuclear ribonucleoprotein A2/B1 OS=Mus musculus GN=Hnrnpa2b1 PE=2 SV=1
2.05	Cytochrome P450 2F2 OS=Mus musculus GN=Cyp2f2 PE=1 SV=1
2.04	Probable phospholipid-transporting ATPase IIA OS=Mus musculus GN=Atp9a PE=1 SV=3
2.02	Laminin subunit beta-3 OS=Mus musculus GN=Lamb3 PE=1 SV=2
2.00	ATP synthase protein 8 OS=Mus musculus musculus GN=ATP8 PE=3 SV=1

Table 9.8. List of the proteins upregulated in the lungs of Ibrutinib-treated animals when compared to controls.

Proteins selected based on the max fold change values (>2-fold)

Max fold change	Name
Infinity	Calcium-binding mitochondrial carrier protein Aralar1 OS=Mus musculus GN=Slc25a12 PE=1 SV=1
Infinity	CD81 antigen OS=Mus musculus GN=Cd81 PE=1 SV=2
Infinity	Myelin-associated glycoprotein OS=Mus musculus GN=Mag PE=1 SV=1
Infinity	Methylmalonyl-CoA mutase_ mitochondrial OS=Mus musculus GN=Mut PE=1 SV=2
Infinity	Uncharacterized protein OS=Mus musculus GN=Mroh8 PE=2 SV=1
Infinity	Tensin-2 OS=Mus musculus GN=Tns2 PE=1 SV=1
Infinity	Dihydropyrimidinase-related protein 1 OS=Mus musculus GN=Crmp1 PE=1 SV=1
Infinity	RAS-related C3 botulinum substrate 1 OS=Mus musculus GN=Rac1 PE=1 SV=1
Infinity	Succinate-CoA ligase subunit beta (Fragment) OS=Mus musculus GN=Sucla2 PE=2 SV=1
Infinity	Leucine-rich repeats and immunoglobulin-like domains protein 3 OS=Mus musculus GN=Lrig3 PE=1 SV=1
Infinity	AP-2 complex subunit mu OS=Mus musculus GN=Ap2m1 PE=1 SV=1
Infinity	Angiopoietin-4 OS=Mus musculus GN=Angpt4 PE=1 SV=1
Infinity	Casein kinase II subunit alpha' (Fragment) OS=Mus musculus GN=Csnk2a2 PE=1 SV=1
Infinity	Serum paraoxonase/arylesterase 1 OS=Mus musculus GN=Pon1 PE=1 SV=2
Infinity	Low-density lipoprotein receptor-related protein 2 OS=Mus musculus GN=Lrp2 PE=1 SV=1
Infinity	Protein sidekick-2 OS=Mus musculus GN=Sdk2 PE=1 SV=1

Infinity	Guanine nucleotide-binding protein G(I)/G(S)/G(T) subunit beta-1 OS=Mus musculus GN=Gnb1 PE=1 SV=3
Infinity	Tubulin alpha chain (Fragment) OS=Mus musculus GN=Tuba4a PE=1 SV=1
Infinity	Microtubule-associated protein RP/EB family member 2 (Fragment) OS=Mus musculus GN=Mapre2 PE=1 SV=1
Infinity	Heat shock protein HSP 90-alpha OS=Mus musculus GN=Hsp90aa1 PE=1 SV=4
Infinity	V-type proton ATPase subunit G OS=Mus musculus GN=Atp6v1g2 PE=1 SV=1
Infinity	Vesicle-associated membrane protein 2 OS=Mus musculus GN=Vamp2 PE=1 SV=1
Infinity	Pregnancy-specific glycoprotein 29 OS=Mus musculus GN=Psg29 PE=2 SV=1
Infinity	Cytochrome P450 2E1 OS=Mus musculus GN=Cyp2e1 PE=1 SV=1
Infinity	Dynein_ axonemal_ heavy chain 7A OS=Mus musculus GN=Dnah7a PE=1 SV=2
Infinity	Ras-related protein Rab-3A OS=Mus musculus GN=Rab3a PE=1 SV=1
Infinity	Cytochrome b-c1 complex subunit Rieske_ mitochondrial OS=Mus musculus GN=Uqcrfs1 PE=1 SV=1
Infinity	Cytochrome c_ somatic OS=Mus musculus GN=Cycs PE=1 SV=2
23.93	Glutaredoxin-related protein 5_ mitochondrial OS=Mus musculus GN=Glrx5 PE=1 SV=1
22.52	Peroxisomal sarcosine oxidase OS=Mus musculus GN=Pipox PE=1 SV=1
13.40	Polyamine-modulated factor 1-binding protein 1 OS=Mus musculus GN=Pmfbp1 PE=2 SV=1
12.70	Cytochrome P450 2C29 OS=Mus musculus GN=Cyp2c29 PE=1 SV=2
11.99	Poly [ADP-ribose] polymerase 14 OS=Mus musculus GN=Parp14 PE=1 SV=3
8.38	Carboxylesterase 1F OS=Mus musculus GN=Ces1f PE=1 SV=1

7.63	Creatine kinase S-type_ mitochondrial OS=Mus musculus GN=Ckmt2 PE=1 SV=1
7.53	Tenascin-R OS=Mus musculus GN=Tnr PE=1 SV=2
7.39	Glutathione S-transferase Mu 1 OS=Mus musculus GN=Gstm1 PE=1 SV=2
5.48	Alpha-aminoadipic semialdehyde dehydrogenase OS=Mus musculus GN=Aldh7a1 PE=1 SV=4
5.30	Ankyrin-3 (Fragment) OS=Mus musculus GN=Ank3 PE=1 SV=1
4.74	Mitochondrial amidoxime reducing component 2 OS=Mus musculus GN=Marc2 PE=1 SV=1
4.55	Uncharacterized protein OS=Mus musculus GN=Afg3l2 PE=2 SV=1
4.39	Alpha-synuclein OS=Mus musculus GN=Snca PE=1 SV=2
4.08	Dimethylaniline monooxygenase [N-oxide-forming] 5 OS=Mus musculus GN=Fmo5 PE=1 SV=4
3.94	Protein unc-13 homolog B OS=Mus musculus GN=Unc13b PE=1 SV=1
3.85	Cordon-bleu OS=Mus musculus GN=Cobl PE=2 SV=1
3.77	Alpha-aminoadipic semialdehyde synthase_ mitochondrial OS=Mus musculus GN=Aass PE=1 SV=1
3.30	Pleckstrin homology-like domain family B member 1 OS=Mus musculus GN=Phldb1 PE=1 SV=1
3.14	V-type proton ATPase subunit E 1 OS=Mus musculus GN=Atp6v1e1 PE=1 SV=2
3.10	Calretinin OS=Mus musculus GN=Calb2 PE=1 SV=3
3.05	Aldehyde dehydrogenase X_ mitochondrial OS=Mus musculus GN=Aldh1b1 PE=1 SV=1
2.95	NADH dehydrogenase [ubiquinone] 1 alpha subcomplex subunit 6 OS=Mus musculus GN=Ndufa6 PE=1 SV=1
2.87	Uncharacterized protein OS=Mus musculus GN=Cyb5b PE=2 SV=1
2.83	StAR-related lipid transfer protein 9 OS=Mus musculus GN=Stard9 PE=1 SV=2
2.79	Ribosomal protein L4 OS=Mus musculus GN=Rpl4 PE=1 SV=1

2.73	Peroxiredoxin-6 OS=Mus musculus GN=Prdx6 PE=1 SV=3
2.66	Glycine amidinotransferase_ mitochondrial OS=Mus musculus GN=Gatm PE=1 SV=1
2.61	Serine/threonine-protein kinase mTOR OS=Mus musculus GN=Mtor PE=1 SV=2
2.59	Creatine kinase B-type OS=Mus musculus GN=Ckb PE=1 SV=1
2.59	ATP-dependent 6-phosphofructokinase_ muscle type OS=Mus musculus GN=Pfkm PE=1 SV=3
2.57	Protocadherin Fat 4 OS=Mus musculus GN=Fat4 PE=1 SV=2
2.55	Very long-chain acyl-CoA synthetase OS=Mus musculus GN=Slc27a2 PE=1 SV=2
2.52	Anion exchange protein (Fragment) OS=Mus musculus GN=Slc4a4 PE=2 SV=1
2.42	Dynein_ axonemal_ heavy chain 10 OS=Mus musculus GN=Dnah10 PE=1 SV=2
2.37	Visinin-like protein 1 OS=Mus musculus GN=Vsnl1 PE=2 SV=1
2.36	Non-specific lipid-transfer protein OS=Mus musculus GN=Scp2 PE=1 SV=3
2.35	Catalase OS=Mus musculus GN=Cat PE=1 SV=4
2.34	Aldehyde dehydrogenase OS=Mus musculus GN=Aldh3a2 PE=1 SV=1
2.29	Myosin regulatory light chain 2_ ventricular/cardiac muscle isoform OS=Mus musculus GN=Myl2 PE=1 SV=3
2.25	Flavin-containing monooxygenase OS=Mus musculus GN=Fmo4 PE=2 SV=1
2.20	Calcium-binding mitochondrial carrier protein Aralar2 OS=Mus musculus GN=Slc25a13 PE=1 SV=1
2.18	NADH dehydrogenase [ubiquinone] iron-sulfur protein 3_ mitochondrial OS=Mus musculus GN=Ndufs3 PE=1 SV=2
2.15	Fructose-bisphosphate aldolase A OS=Mus musculus GN=Aldoa PE=1 SV=2
2.14	14-3-3 protein zeta/delta OS=Mus musculus GN=Ywhaz PE=1 SV=1
2.13	FAT atypical cadherin 1 OS=Mus musculus GN=Fat1 PE=1 SV=2

2.11	3-mercaptopyruvate sulfurtransferase OS=Mus musculus GN=Mpst PE=1 SV=3
2.03	Collagen_ type VI_ alpha 3 OS=Mus musculus GN=Col6a3 PE=1 SV=1
2.03	Microtubule-actin cross-linking factor 1 OS=Mus musculus GN=Macf1 PE=1 SV=2
2.00	GTP:AMP phosphotransferase AK3_ mitochondrial OS=Mus musculus GN=Ak3 PE=1 SV=3

Table 9.9. List of the proteins downregulated in the lungs of Ibrutinib-treated animals when compared to controls.

Proteins selected based on the max fold change values (>2-fold)

Max fold change	Name
Infinity	Agmatinase_ mitochondrial OS=Mus musculus GN=Agmat PE=1 SV=1
Infinity	Zinc finger protein 292 OS=Mus musculus GN=Zfp292 PE=1 SV=2
Infinity	Quinone oxidoreductase-like protein 2 OS=Mus musculus PE=1 SV=1
Infinity	Unconventional myosin-Va OS=Mus musculus GN=Myo5a PE=1 SV=1
Infinity	Cytochrome P450 2A5 OS=Mus musculus GN=Cyp2a5 PE=2 SV=1
Infinity	Cytochrome b-c1 complex subunit 7 OS=Mus musculus GN=Uqcrb PE=1 SV=3
Infinity	Roquin-1 OS=Mus musculus GN=Rc3h1 PE=1 SV=1
Infinity	Striated muscle-specific serine/threonine-protein kinase OS=Mus musculus GN=Speg PE=1 SV=2
Infinity	Ubiquitin carboxyl-terminal hydrolase 25 OS=Mus musculus GN=Usp25 PE=1 SV=2
Infinity	Myosin-9 OS=Mus musculus GN=Myh9 PE=1 SV=4
Infinity	Filamin-C OS=Mus musculus GN=Flnc PE=1 SV=3
Infinity	NACHT and WD repeat domain-containing protein 2 OS=Mus musculus GN=Nwd2 PE=1 SV=2
Infinity	Coiled-coil domain-containing protein 88B OS=Mus musculus GN=Ccdc88b PE=1 SV=2
Infinity	Sorting nexin-29 OS=Mus musculus GN=Snx29 PE=1 SV=2
Infinity	NADH dehydrogenase [ubiquinone] 1 alpha subcomplex subunit 10_ mitochondrial OS=Mus musculus GN=Ndufa10 PE=1 SV=1
Infinity	Septin-14 OS=Mus musculus GN=Sept14 PE=1 SV=3
Infinity	Serine/threonine-protein phosphatase 2A catalytic subunit beta isoform OS=Mus musculus GN=Ppp2cb PE=1 SV=1
Infinity	Cyp27a1 protein OS=Mus musculus GN=Cyp27a1 PE=2 SV=1

Infinity	Peroxiredoxin-1 OS=Mus musculus GN=Prdx1 PE=1 SV=1
Infinity	E3 ubiquitin-protein ligase LRSAM1 OS=Mus musculus GN=Lrsam1 PE=1 SV=1
Infinity	Succinate dehydrogenase [ubiquinone] iron-sulfur subunit_ mitochondrial OS=Mus musculus GN=Sdhb PE=1 SV=1
Infinity	Ribosomal protein L14 OS=Mus musculus GN=Rpl14-ps1 PE=2 SV=1
Infinity	Phosphatidylinositol 4_5-bisphosphate 3-kinase catalytic subunit delta isoform OS=Mus musculus GN=Pik3cd PE=1 SV=1
Infinity	V-type proton ATPase 116 kDa subunit a isoform 1 OS=Mus musculus GN=Atp6v0a1 PE=1 SV=3
Infinity	Isocitrate dehydrogenase [NAD] subunit gamma 1_ mitochondrial OS=Mus musculus GN=Idh3g PE=1 SV=1
Infinity	Intersectin-1 OS=Mus musculus GN=Itsn1 PE=1 SV=1
Infinity	Kinesin-1 heavy chain OS=Mus musculus GN=Kif5b PE=1 SV=3
Infinity	Cytosolic acyl coenzyme A thioester hydrolase OS=Mus musculus GN=Acot7 PE=1 SV=1
Infinity	Cytoskeleton-associated protein 5 OS=Mus musculus GN=Ckap5 PE=1 SV=1
Infinity	Histidine triad nucleotide binding protein 2 OS=Mus musculus GN=Hint2 PE=1 SV=1
Infinity	Triosephosphate isomerase OS=Mus musculus GN=Tpi1 PE=1 SV=4
Infinity	Uncharacterized protein OS=Mus musculus GN=Vnn1 PE=2 SV=1
Infinity	Versican core protein OS=Mus musculus GN=Vcan PE=1 SV=2
Infinity	17-beta-hydroxysteroid dehydrogenase type 6 OS=Mus musculus GN=Hsd17b6 PE=1 SV=1
Infinity	E3 ubiquitin-protein ligase HECTD1 OS=Mus musculus GN=Hectd1 PE=1 SV=2
Infinity	Anoctamin-1 (Fragment) OS=Mus musculus GN=Ano1 PE=1 SV=1
Infinity	Carnitine O-palmitoyltransferase 2_ mitochondrial OS=Mus musculus GN=Cpt2 PE=1 SV=2
Infinity	Cadherin-16 OS=Mus musculus GN=Cdh16 PE=1 SV=1

150.69	Citron Rho-interacting kinase OS=Mus musculus GN=Cit PE=1 SV=3
35.63	ATPase_ H+ transporting_ lysosomal V1 subunit B1 OS=Mus musculus GN=Atp6v1b1 PE=2 SV=1
33.91	Neurofascin OS=Mus musculus GN=Nfasc PE=1 SV=1
16.87	Myosin_ heavy polypeptide 13_ skeletal muscle OS=Mus musculus GN=Myh13 PE=1 SV=1
13.00	NADH dehydrogenase [ubiquinone] 1 alpha subcomplex subunit 13 OS=Mus musculus GN=Ndufa13 PE=1 SV=3
11.37	Homeobox protein cut-like 1 OS=Mus musculus GN=Cux1 PE=1 SV=3
11.19	2-oxoisovalerate dehydrogenase subunit alpha_ mitochondrial OS=Mus musculus GN=Bckdha PE=1 SV=1
10.61	Beta-synuclein OS=Mus musculus GN=Sncb PE=1 SV=1
10.51	14-3-3 protein beta/alpha OS=Mus musculus GN=Ywhab PE=1 SV=3
10.02	Superoxide dismutase [Mn]_ mitochondrial OS=Mus musculus GN=Sod2 PE=1 SV=3
8.58	Androgen receptor OS=Mus musculus GN=Ar PE=1 SV=1
8.46	Cadherin EGF LAG seven-pass G-type receptor 1 OS=Mus musculus GN=Celsr1 PE=1 SV=3
7.79	NADH dehydrogenase [ubiquinone] 1 alpha subcomplex subunit 12 OS=Mus musculus GN=Ndufa12 PE=1 SV=2
7.62	Phosphatidylethanolamine-binding protein 1 OS=Mus musculus GN=Pebp1 PE=1 SV=3
7.58	Spectrin beta chain_ erythrocytic OS=Mus musculus GN=Sptb PE=1 SV=4
7.36	CAP-Gly domain-containing linker protein 1 (Fragment) OS=Mus musculus GN=Clip1 PE=1 SV=1
6.49	Probable helicase senataxin OS=Mus musculus GN=Setx PE=1 SV=1
6.45	Pericentrin OS=Mus musculus GN=Pcnt PE=1 SV=2
6.07	Creatine kinase U-type_ mitochondrial OS=Mus musculus GN=Ckmt1 PE=1 SV=1

5.99	Proline dehydrogenase 1_ mitochondrial OS=Mus musculus GN=Prodh PE=1 SV=2
5.92	Actin_ alpha skeletal muscle OS=Mus musculus GN=Acta1 PE=1 SV=1
5.36	G-protein coupled receptor 98 OS=Mus musculus GN=Gpr98 PE=2 SV=1
5.26	Septin-5 OS=Mus musculus GN=Sept5 PE=1 SV=2
5.21	Structural maintenance of chromosomes flexible hinge domain-containing protein 1 OS=Mus musculus GN=Smchd1 PE=1 SV=2
5.02	NADH dehydrogenase (Ubiquinone) 1 alpha subcomplex_ 8 OS=Mus musculus GN=Ndufa8 PE=2 SV=1
4.99	Spermatogenesis- and oogenesis-specific basic helix-loop-helix-containing protein 2 OS=Mus musculus GN=Sohlh2 PE=1 SV=2
4.91	Pyruvate kinase PKLR OS=Mus musculus GN=Pklr PE=1 SV=1
4.83	Microtubule-associated protein tau OS=Mus musculus GN=Mapt PE=1 SV=3
4.80	Calcium/calmodulin-dependent protein kinase type II subunit alpha OS=Mus musculus GN=Camk2a PE=1 SV=2
4.74	Septin-7 OS=Mus musculus GN=Sept7 PE=1 SV=2
4.64	ATP synthase subunit delta_ mitochondrial OS=Mus musculus GN=Atp5d PE=1 SV=1
4.55	Centromere protein F OS=Mus musculus GN=Cenpf PE=1 SV=1
4.51	Neuromodulin OS=Mus musculus GN=Gap43 PE=1 SV=1
4.40	Cell cycle exit and neuronal differentiation protein 1 OS=Mus musculus GN=Cend1 PE=1 SV=1
3.93	A-kinase anchor protein 9 OS=Mus musculus GN=Akap9 PE=1 SV=2
3.92	Dedicator of cytokinesis protein 1 OS=Mus musculus GN=Dock1 PE=1 SV=3
3.83	Uncharacterized protein (Fragment) OS=Mus musculus GN=Pmpcb PE=2 SV=1
3.75	Argininosuccinate synthase OS=Mus musculus GN=Ass1 PE=1 SV=1
3.75	Krt78 protein (Fragment) OS=Mus musculus GN=Krt78 PE=2 SV=1

3.73	DDB1- and CUL4-associated factor 1 OS=Mus musculus GN=Dcaf1 PE=1 SV=4
3.62	UDP-glucuronosyltransferase 2A3 OS=Mus musculus GN=Ugt2a3 PE=1 SV=1
3.58	NADH-cytochrome b5 reductase 3 OS=Mus musculus GN=Cyb5r3 PE=1 SV=3
3.51	Down syndrome cell adhesion molecule homolog OS=Mus musculus GN=Dscam PE=1 SV=1
3.51	Transient receptor potential cation channel_ subfamily M_ member 3 OS=Mus musculus GN=Trpm3 PE=1 SV=1
3.47	Carboxylic ester hydrolase OS=Mus musculus GN=Ces1g PE=1 SV=1
3.44	V-type proton ATPase catalytic subunit A OS=Mus musculus GN=Atp6v1a PE=1 SV=2
3.40	Uncharacterized protein KIAA1109 OS=Mus musculus GN=Kiaa1109 PE=1 SV=4
3.37	Annexin A5 OS=Mus musculus GN=Anxa5 PE=1 SV=1
3.24	2-oxoglutarate dehydrogenase_ mitochondrial OS=Mus musculus GN=Ogdh PE=1 SV=3
3.17	Glyceraldehyde-3-phosphate dehydrogenase_ testis-specific OS=Mus musculus GN=Gapdhs PE=1 SV=1
3.15	Thioredoxin-dependent peroxide reductase_ mitochondrial OS=Mus musculus GN=Prdx3 PE=1 SV=1
3.12	Titin (Fragment) OS=Mus musculus GN=Ttn PE=1 SV=1
2.97	Bile acyl-CoA synthetase OS=Mus musculus GN=Slc27a5 PE=1 SV=2
2.94	ATP-binding cassette sub-family A member 13 OS=Mus musculus GN=Abca13 PE=2 SV=1
2.93	Uncharacterized protein OS=Mus musculus GN=Bphl PE=2 SV=1
2.89	Protein/nucleic acid deglycase DJ-1 OS=Mus musculus GN=Park7 PE=1 SV=1
2.86	78 kDa glucose-regulated protein OS=Mus musculus GN=Hspa5 PE=1 SV=3

2.85	Limbic system-associated membrane protein OS=Mus musculus GN=Lsamp PE=1 SV=1
2.85	MKIAA4169 protein (Fragment) OS=Mus musculus GN=Sept3 PE=2 SV=1
2.84	Synapsin-1 OS=Mus musculus GN=Syn1 PE=1 SV=2
2.78	Ellis-van Creveld syndrome protein homolog OS=Mus musculus GN=Evc PE=1 SV=1
2.77	Histone H2B (Fragment) OS=Mus musculus GN=Hist1h2bj PE=2 SV=1
2.74	Acyl-CoA dehydrogenase family member 9_ mitochondrial OS=Mus musculus GN=Acad9 PE=1 SV=2
2.63	NAD-dependent protein deacetylase sirtuin-2 OS=Mus musculus GN=Sirt2 PE=1 SV=2
2.59	Peroxisomal multifunctional enzyme type 2 OS=Mus musculus GN=Hsd17b4 PE=1 SV=3
2.57	Fumarate hydratase_ mitochondrial OS=Mus musculus GN=Fh PE=1 SV=3
2.56	Syntaxin-1B OS=Mus musculus GN=Stx1b PE=1 SV=1
2.55	Glyceraldehyde-3-phosphate dehydrogenase OS=Mus musculus GN=Gapdh PE=1 SV=2
2.53	Brain acid soluble protein 1 OS=Mus musculus GN=Basp1 PE=1 SV=3
2.52	E3 ubiquitin-protein ligase RNF213 OS=Mus musculus GN=Rnf213 PE=1 SV=1
2.50	Enoyl-CoA delta isomerase 1_ mitochondrial OS=Mus musculus GN=Eci1 PE=1 SV=2
2.47	Vacuolar protein sorting 13D OS=Mus musculus GN=Vps13d PE=1 SV=1
2.45	ATP synthase F(0) complex subunit B1_ mitochondrial OS=Mus musculus GN=Atp5f1 PE=1 SV=1
2.44	Tubulin alpha-1A chain OS=Mus musculus GN=Tuba1a PE=1 SV=1
2.43	Trifunctional enzyme subunit alpha_ mitochondrial OS=Mus musculus GN=Hadha PE=1 SV=1
2.41	Excitatory amino acid transporter 1 OS=Mus musculus GN=Slc1a3 PE=1 SV=2

2.40	L-lactate dehydrogenase B chain OS=Mus musculus GN=Ldhb PE=1 SV=2
2.38	Delta-1-pyrroline-5-carboxylate dehydrogenase_ mitochondrial OS=Mus musculus GN=Aldh4a1 PE=1 SV=3
2.36	Succinate dehydrogenase [ubiquinone] flavoprotein subunit_ mitochondrial OS=Mus musculus GN=Sdha PE=1 SV=1
2.36	Heat shock cognate 71 kDa protein OS=Mus musculus GN=Hspa8 PE=1 SV=1
2.32	Uncharacterized protein (Fragment) OS=Mus musculus GN=Myo1d PE=2 SV=1
2.31	60S ribosomal protein L13 OS=Mus musculus GN=Rpl13 PE=1 SV=3
2.26	Serine/threonine-protein phosphatase 2A 65 kDa regulatory subunit A alpha isoform OS=Mus musculus GN=Ppp2r1a PE=1 SV=3
2.25	Cytochrome b-c1 complex subunit 2_ mitochondrial OS=Mus musculus GN=Uqcrc2 PE=1 SV=1
2.25	Aconitate hydratase_ mitochondrial OS=Mus musculus GN=Aco2 PE=1 SV=1
2.24	Myelin-oligodendrocyte glycoprotein OS=Mus musculus GN=Mog PE=1 SV=1
2.23	Ras-related protein Rab-10 OS=Mus musculus GN=Rab10 PE=1 SV=1
2.20	Ras-related protein Rab-1A OS=Mus musculus GN=Rab1A PE=1 SV=3
2.20	Pyruvate dehydrogenase E1 component subunit beta_ mitochondrial OS=Mus musculus GN=Pdhb PE=1 SV=1
2.19	ES1 protein homolog_ mitochondrial OS=Mus musculus GN=D10Jhu81e PE=1 SV=1
2.18	Isocitrate dehydrogenase [NAD] subunit alpha_ mitochondrial OS=Mus musculus GN=Idh3a PE=1 SV=1
2.16	Helicase with zinc finger domain 2 OS=Mus musculus GN=Helz2 PE=1 SV=1
2.14	Cytochrome c oxidase subunit NDUFA4 OS=Mus musculus GN=Ndufa4 PE=1 SV=2
2.12	Centrosomal protein of 290 kDa OS=Mus musculus GN=Cep290 PE=1 SV=2

2.12	Bifunctional epoxide hydrolase 2 OS=Mus musculus GN=Ephx2 PE=1 SV=2
2.12	Nephrocystin-3 [Mus musculus] OS=Rhizoctonia solani GN=RSOLAG22IIIB_12418 PE=4 SV=1
2.12	Endophilin-A1 OS=Mus musculus GN=Sh3gl2 PE=1 SV=1
2.08	Tenascin XB OS=Mus musculus GN=Tnxb PE=1 SV=1
2.08	Heat shock-related 70 kDa protein 2 OS=Mus musculus GN=Hspa2 PE=1 SV=2
2.05	Cytochrome b-c1 complex subunit 1_ mitochondrial OS=Mus musculus GN=Uqcrc1 PE=1 SV=2
2.04	2-hydroxyacyl-CoA lyase 1 OS=Mus musculus GN=Hacl1 PE=1 SV=2
2.04	Plasma membrane calcium-transporting ATPase 2 OS=Mus musculus GN=Atp2b2 PE=1 SV=2
2.04	Long-chain-fatty-acid--CoA ligase 5 OS=Mus musculus GN=Acsl5 PE=1 SV=1
2.01	Trifunctional enzyme subunit beta_ mitochondrial OS=Mus musculus GN=Hadhb PE=1 SV=1
2.01	Pyrethroid hydrolase Ces2a OS=Mus musculus GN=Ces2a PE=1 SV=1
2.01	Coiled-coil domain containing 108 OS=Mus musculus GN=Cfap65 PE=2 SV=1